IAEA-TECDOC-2031

IAEA TECDOC SERIES

IAEA-TECDOC-2031

Advancing the State of the Practice in Uncertainty and Sensitivity Methodologies for Severe Accident Analysis in Water Cooled Reactors of PWR and SMR Types

Final Report of a Coordinated Research Project

IAEA
International Atomic Energy Agency

ADVANCING THE STATE OF THE PRACTICE IN UNCERTAINTY AND SENSITIVITY METHODOLOGIES FOR SEVERE ACCIDENT ANALYSIS IN WATER COOLED REACTORS OF PWR AND SMR TYPES

The following States are Members of the International Atomic Energy Agency:

AFGHANISTAN
ALBANIA
ALGERIA
ANGOLA
ANTIGUA AND BARBUDA
ARGENTINA
ARMENIA
AUSTRALIA
AUSTRIA
AZERBAIJAN
BAHAMAS
BAHRAIN
BANGLADESH
BARBADOS
BELARUS
BELGIUM
BELIZE
BENIN
BOLIVIA, PLURINATIONAL STATE OF
BOSNIA AND HERZEGOVINA
BOTSWANA
BRAZIL
BRUNEI DARUSSALAM
BULGARIA
BURKINA FASO
BURUNDI
CABO VERDE
CAMBODIA
CAMEROON
CANADA
CENTRAL AFRICAN REPUBLIC
CHAD
CHILE
CHINA
COLOMBIA
COMOROS
CONGO
COSTA RICA
CÔTE D'IVOIRE
CROATIA
CUBA
CYPRUS
CZECH REPUBLIC
DEMOCRATIC REPUBLIC OF THE CONGO
DENMARK
DJIBOUTI
DOMINICA
DOMINICAN REPUBLIC
ECUADOR
EGYPT
EL SALVADOR
ERITREA
ESTONIA
ESWATINI
ETHIOPIA
FIJI
FINLAND
FRANCE
GABON
GAMBIA
GEORGIA
GERMANY
GHANA
GREECE
GRENADA
GUATEMALA
GUINEA
GUYANA
HAITI
HOLY SEE
HONDURAS
HUNGARY
ICELAND
INDIA
INDONESIA
IRAN, ISLAMIC REPUBLIC OF
IRAQ
IRELAND
ISRAEL
ITALY
JAMAICA
JAPAN
JORDAN
KAZAKHSTAN
KENYA
KOREA, REPUBLIC OF
KUWAIT
KYRGYZSTAN
LAO PEOPLE'S DEMOCRATIC REPUBLIC
LATVIA
LEBANON
LESOTHO
LIBERIA
LIBYA
LIECHTENSTEIN
LITHUANIA
LUXEMBOURG
MADAGASCAR
MALAWI
MALAYSIA
MALI
MALTA
MARSHALL ISLANDS
MAURITANIA
MAURITIUS
MEXICO
MONACO
MONGOLIA
MONTENEGRO
MOROCCO
MOZAMBIQUE
MYANMAR
NAMIBIA
NEPAL
NETHERLANDS
NEW ZEALAND
NICARAGUA
NIGER
NIGERIA
NORTH MACEDONIA
NORWAY
OMAN
PAKISTAN
PALAU
PANAMA
PAPUA NEW GUINEA
PARAGUAY
PERU
PHILIPPINES
POLAND
PORTUGAL
QATAR
REPUBLIC OF MOLDOVA
ROMANIA
RUSSIAN FEDERATION
RWANDA
SAINT KITTS AND NEVIS
SAINT LUCIA
SAINT VINCENT AND THE GRENADINES
SAMOA
SAN MARINO
SAUDI ARABIA
SENEGAL
SERBIA
SEYCHELLES
SIERRA LEONE
SINGAPORE
SLOVAKIA
SLOVENIA
SOUTH AFRICA
SPAIN
SRI LANKA
SUDAN
SWEDEN
SWITZERLAND
SYRIAN ARAB REPUBLIC
TAJIKISTAN
THAILAND
TOGO
TONGA
TRINIDAD AND TOBAGO
TUNISIA
TÜRKİYE
TURKMENISTAN
UGANDA
UKRAINE
UNITED ARAB EMIRATES
UNITED KINGDOM OF GREAT BRITAIN AND NORTHERN IRELAND
UNITED REPUBLIC OF TANZANIA
UNITED STATES OF AMERICA
URUGUAY
UZBEKISTAN
VANUATU
VENEZUELA, BOLIVARIAN REPUBLIC OF
VIET NAM
YEMEN
ZAMBIA
ZIMBABWE

The Agency's Statute was approved on 23 October 1956 by the Conference on the Statute of the IAEA held at United Nations Headquarters, New York; it entered into force on 29 July 1957. The Headquarters of the Agency are situated in Vienna. Its principal objective is "to accelerate and enlarge the contribution of atomic energy to peace, health and prosperity throughout the world".

IAEA-TECDOC-2031

ADVANCING THE STATE OF THE PRACTICE IN UNCERTAINTY AND SENSITIVITY METHODOLOGIES FOR SEVERE ACCIDENT ANALYSIS IN WATER COOLED REACTORS OF PWR AND SMR TYPES

FINAL REPORT OF A COORDINATED RESEARCH PROJECT

INTERNATIONAL ATOMIC ENERGY AGENCY
VIENNA, 2023

COPYRIGHT NOTICE

All IAEA scientific and technical publications are protected by the terms of the Universal Copyright Convention as adopted in 1952 (Berne) and as revised in 1972 (Paris). The copyright has since been extended by the World Intellectual Property Organization (Geneva) to include electronic and virtual intellectual property. Permission to use whole or parts of texts contained in IAEA publications in printed or electronic form must be obtained and is usually subject to royalty agreements. Proposals for non-commercial reproductions and translations are welcomed and considered on a case-by-case basis. Enquiries should be addressed to the IAEA Publishing Section at:

Marketing and Sales Unit, Publishing Section
International Atomic Energy Agency
Vienna International Centre
PO Box 100
1400 Vienna, Austria
fax: +43 1 26007 22529
tel.: +43 1 2600 22417
email: sales.publications@iaea.org
www.iaea.org/publications

For further information on this publication, please contact:

Nuclear Power Technology Development Section
International Atomic Energy Agency
Vienna International Centre
PO Box 100
1400 Vienna, Austria
Email: Official.Mail@iaea.org

© IAEA, 2023

Printed by the IAEA in Austria
November 2023

IAEA Library Cataloguing in Publication Data

Names: International Atomic Energy Agency.
Title: Advancing the state of the practice in uncertainty and sensitivity methodologies for severe accident analysis in water cooled reactors of PWR and SMR types / International Atomic Energy Agency.
Description: Vienna : International Atomic Energy Agency, 2023. | Series: IAEA TECDOC series, ISSN 1011-4289 ; no. 2031 | Includes bibliographical references.
Identifiers: IAEAL 23-01636 | ISBN 978-92-0-152423-2 (paperback : alk. paper) |
ISBN 978-92-0-152523-9 (pdf)
Subjects: LCSH: Water cooled reactors — Safety measures. | Pressurized water reactors — Safety measures. | Nuclear reactor accidents.

FOREWORD

In 2019 the IAEA launched a coordinated research project entitled Advancing the State of Practice in Uncertainty and Sensitivity Methodologies for Severe Accident Analysis in Water Cooled Reactors. By bringing together experts from Member States with relevant technologies, the primary objectives of the coordinated research project were to advance the understanding and characterization of sources of uncertainties and their effects on the key figure of merit predictions in severe accident codes for water cooled reactors; improve capabilities and expertise in Member States to perform state of the art uncertainty and sensitivity analysis with severe accident codes; and support relevant research by graduate students. The participating Member State organizations contributed to two major exercises: the Quench-06 test application uncertainty exercise and the plant application uncertainty exercise. The latter was divided into five subtasks addressing existing reactor lines: boiling water reactors, pressurized water reactors (including small modular reactor designs), pressurized heavy water reactors, and water cooled, water moderated power reactors. This publication presents the contributions from eight individual organizations from seven Member States describing the uncertainty and sensitivity methods used for severe accident analysis in pressurized water reactors and in integral pressurized water reactors, a type of small modular reactor.

The IAEA acknowledges the efforts and assistance provided by the contributors listed at the end of this publication. The IAEA officer responsible for this publication was T. Jevremovic of the Division of Nuclear Power.

EDITORIAL NOTE

This publication has been prepared from the original material as submitted by the contributors and has not been edited by the editorial staff of the IAEA. The views expressed remain the responsibility of the contributors and do not necessarily represent the views of the IAEA or its Member States.

Guidance and recommendations provided here in relation to identified good practices represent expert opinion but are not made on the basis of a consensus of all Member States.

Neither the IAEA nor its Member States assume any responsibility for consequences which may arise from the use of this publication. This publication does not address questions of responsibility, legal or otherwise, for acts or omissions on the part of any person.

The use of particular designations of countries or territories does not imply any judgement by the publisher, the IAEA, as to the legal status of such countries or territories, of their authorities and institutions or of the delimitation of their boundaries.

The mention of names of specific companies or products (whether or not indicated as registered) does not imply any intention to infringe proprietary rights, nor should it be construed as an endorsement or recommendation on the part of the IAEA.

The authors are responsible for having obtained the necessary permission for the IAEA to reproduce, translate or use material from sources already protected by copyrights.

The IAEA has no responsibility for the persistence or accuracy of URLs for external or third party Internet web sites referred to in this publication and does not guarantee that any content on such web sites is, or will remain, accurate or appropriate.

Contents

1. INTRODUCTION

1.1. BACKGROUND

Since the accident at Three Mile Island Unit 2 (TMI-2), severe accident codes have been developed to address the significant lack of understanding of what happened during that accident. The degraded core accident at TMI-2 that reached conditions more severe than design basis accidents prompted new initiatives and subsequent revaluation of regulatory processes. The 2011 Fukushima accident stressed the necessity to extend the focus of international research and development efforts also to containment phenomena impacting the source term to the environment (including aerosol and core melt behavior in the containment, risk of combustible gas mixtures, and other associated phenomena). In the decades following the TMI-2 accident the codes were used largely in what is commonly termed a deterministic mode where single representative accidents were modelled to represent classes of accidents such as unrecovered large and small break loss of coolant accidents (LOCA's) or station blackout (SBO). During this time the analyses performed with these tools were computationally intensive calculations carried out on much slower computers with much lower memory in comparison to nowadays modern computational platforms. Uncertainty in the operative physics/phenomena and the stochastic aspects of accident conditions in these types of analyses was known to exist but onerous to quantify. For this reason, the deterministic analyses were often biased conservatively in hopes of producing a bounding calculation result which could be compared to the requirements such as for example public exposure limits. As the severe accident codes improved in robustness and runtime efficiency in years to come, and as computational platforms significantly increased in speed, sampling-based uncertainty studies began to emerge using sampling methodologies embodied in statistical tools. These tools allowed the uncertainties in an analysis to be expressed in terms of variability in the code input and boundary conditions that could be propagated through the severe accident analysis producing an ensemble of answers from which probability distributions instead of single realization point values. In this way a likelihood distribution of accident figures of merit (FOM) is obtained that give indications of mean values, central tendencies and dispersion in the answers. Nowadays, the codes are significantly more robust and computational platforms are vastly faster in execution including massively parallel computational resources with thousands of individually addressable processors, sampling-based for these selected accident sequences uncertainty methods are eased within reach of severe accident analysis efforts.

The International Atomic Energy Agency (IAEA) Coordinated Research Project (CRP) on Advancing the State-Of-Practice in Uncertainty and Sensitivity Methodologies for Severe Accident Analysis in Water Cooled Reactors (WCRs) in 2019. By bringing together the experts from the IAEA Member States with relevant technologies, the primary objectives of this CRP were to advance the understanding and characterization of sources of uncertainties and their effects on the key figure-of-merit predictions in severe accident codes for water cooled reactors, improve capabilities and expertise in Member States to perform state-of-the-art uncertainty and sensitivity analysis with severe accidents codes, and support graduate students relevant research. Knowing that the severe accident codes embody complex multi-disciplinary physics spanning a variety of phenomena, they can often be outside of the users' range of experience and competency. Equally, the code users could be unsure about the correctness or accuracy of their nuclear power plant (NPP) accident analyses and/or not aware of the importance or impact of uncertainty and variability on predicted code results. The Technical Meeting on the Status and Evaluation of Severe Accident Simulation Codes for Water Cooled Reactors held in October 2017, as a response to the Member

States interests in information exchange on the current status of severe accident simulation and modelling codes and tools for WCRs and as a response to the request from the Technical Working Groups on Advanced Technologies for light water cooled reactors (LWRs) and heavy water cooled reactors (HWRs) to address the status of these codes and outline associated uncertainties, pointed to a need to initiate this CRP.

The IAEA organizes CRP to facilitate the co-operation on research and development, including the development and validation of computer codes for design and safety analysis of NPPs, to bring together the experts from the Member States with WCRs technologies experienced in developing and using the severe accident codes to further advance the state-of-knowledge on uncertainty propagation in severe accident simulation and modelling analyses. The newly developed knowledge is shared with developing Member States through various activities: support of their graduate students, participation in training workshops, and participation in the exercises. The CRP is specifically aimed at improving the state of practice in severe accident analyses by examining and characterizing the impact of uncertainty and variability on severe accident simulation and modelling. Various widely used severe accident codes such as MELCOR, MAAP, ASTEC to mention just a few, are used to evaluate model form uncertainty by benchmarking them against each other.

1.2. OBJECTIVE

The objectives of this CRP were to bring together the current state-of-knowledge on uncertainty propagation in severe accident analyses that has been accumulated by experienced analysts with the aim of increasing the sophistication and competency of the practitioners in this field as follows:

- Achieve significant improvement in sophistication and quality of severe accident analyses performed by the participants from Member States with well-developed knowledge, adequate simulation capabilities (both software and hardware) and long years of relevant practice;
- Enable objective peer review of the benchmark studies with various codes by the participating Member States and thus lead to new knowledge and sharing of research results relevant to evaluation of uncertainties in severe accident analyses;
- Foster national excellence and international cooperation through an exercise to elevate the capability and sophistication of global severe accident code users;
- Promote sharing of newly developed knowledge and contribute to capacity building in developing countries.

The participating Member State organizations contributed to two major exercises named: Quench6 test application uncertainty exercise and plant application uncertainty exercise that was divided into five subtasks addressing the existing reactor lines: boiling water reactors (BWRs), pressurized water reactors (PWRs) inclusive of small modular reactor (SMRs) designs, pressurized heavy water reactors (PHWRs), and water-water energetic reactors (VVERs). This publication provides the contributions from eight individual institutions from seven Member States describing their utilized uncertainty and sensitivity methods for severe accidents analysis in PWRs of large size and in SMR of integral PWR (iPWR) type.

The objective of this publication is to therefore highlight the results of the analysis developed under the CRP plant application task applicable to PWRs and SMR. The plant application exercise is aimed at consolidating existing experience in development of a strong technical basis for establishing uncertainty and sensitivity methodologies in severe accident analyses that has been accumulated by experienced analysts with the aim to increase sophistication and competency of the practitioners in this field. The insights gained from the plant application exercise lead towards newly generated knowledge to be referred on the uncertainty and sensitivity analysis and methods for severe accident codes with the intent of capturing the best practices and lessons learned.

1.3. SCOPE

The scope of this publication is the PWR and SMR (iPWR) plant application exercise performed by the CRP participants in support of addressing improvement in sophistication and quality of severe accident analyses with various codes that generated new knowledge relevant to evaluation of uncertainties and sensitivity analysis of severe accident simulation and modelling. The CRP exercises are developed as per flow diagram shown in Fig. 1 indicating five TECDOC publications, each addressing a specific plant application exercise and outlining relevant research technical results with lessons learned and best practices:

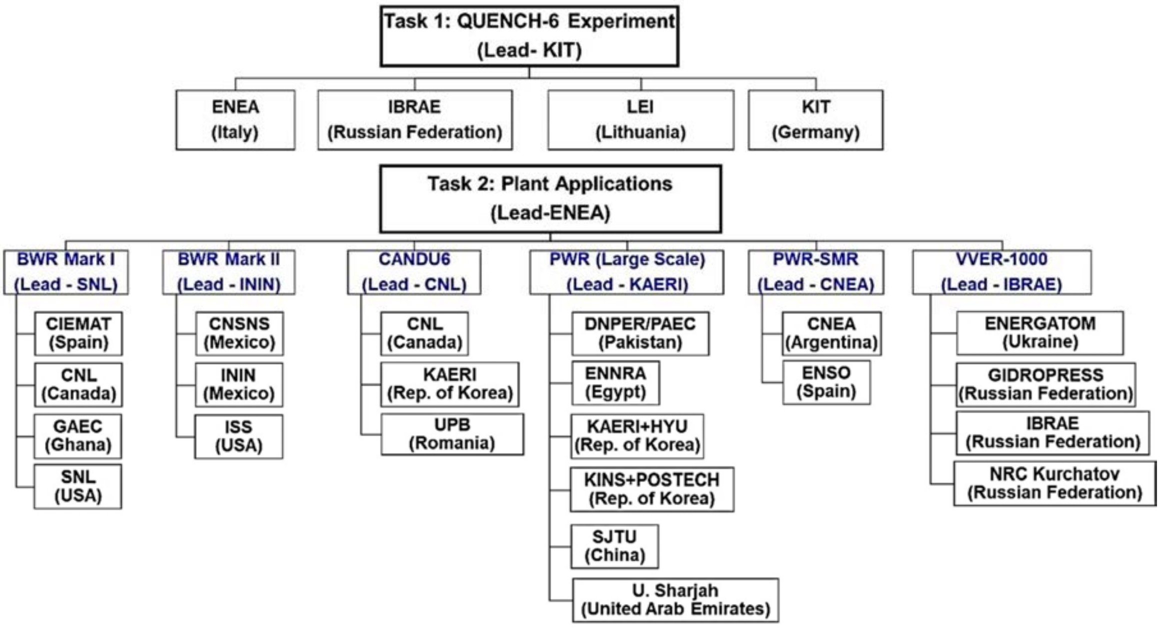

FIG. 1. CRP tasks and participants (refer to Abbreviations for the organizations full names).

Participating organizations in this exercise and contributors to this publication were:

— Directorate of Nuclear Power Engineering-Reactor (DNPER), Pakistan Atomic Energy Commission (PAEC, Pakistan);
— Egyptian Nuclear and Radiological Regulatory Authority (ENRRA, Egypt);
— Korea Atomic Energy Research Institute (KAERI, Republic of Korea);
— Korea Institute of Nuclear Safety (KINS, Republic of Korea);
— Shanghai Jiao Tong University (SJTU, China);
— University of Sharjah (UoS, United Arab Emirates (UAE));
— National Atomic Energy Commission (CNEA, Argentina);

— Energy Software (ENSO, Spain).

1.4. STRUCTURE

This publication is structured such to provide the readers with a logical progression from the general background and detailed information regarding calculations and benchmark results to summary and main conclusions. The participating organizations employed their own calculation framework for the uncertainty and sensitivity analyses, covering six types of PWRs, ACP1000, KWU-PWR1300, OPR1000, APR1400, CNP600, and SMR, six different severe accident analysis codes, four representative accident scenarios, and two accident progression phases (in-vessel only and in-/ex-vessel). Following this introductory section, Section 2 provides an overview of analysis performed by the participating organizations, scope of the analysis, codes used, and results obtained. Section 3 summarizes participating organizations' results, comparisons and conclusions.

2. PWR AND SMR APPLICATIONS

2.1. ANALYSIS SCOPE AND FRAMEWORK

Main frameworks for the uncertainty anal sensitivity analysis, which were employed by the participating organizations are summarized in Tables 1 and 2. As indicated in Table 1, this plant application exercise described in this section was based on six types of large PWRs, ACP1000, KWU-PWR1300, OPR1000, APR1400, CNP600, and iPWR, six different severe accident simulation codes, MELCOR, MAAP5, ATHLET, 3KEYMASTER, RELAP5, and RELAP/SCDAPSIM), four reference scenarios, LBLOCA, SBLOCA, SBO, and STSBO, and two accident progression phases (in-vessel only and in-/ex-vessel both).

TABLE 1. SCOPE AND REFERENCE PLANTS WITH MODELED SCENARIOS

PWR type	Participating organization	Reference plant	Reference scenario (scope)	Severe accident code	Framework of analysis
Large-scale PWR	DNPER/PAEC (Pakistan)	ACP1000 (K-2)	SBO (in-/ex-vessel)	MELCOR1.8.6	Regulatory review support
	ENRRA (Egypt)	KWU-PWR1300	LBLOCA w/o SCRAM (in-vessel)	ATHLET & SCALE6.3	Regulatory review support
	KAERI+HYU (Republic of Korea)	OPR1000	STSBO (in-/ex-vessel)	MELCOR2.2 & MAAP5	SAM & Level 2 PSA support
	KINS+SNU (Republic of Korea)	APR1400	SBO (in-vessel & reactor cavity)	MELCOR2.2 & COOLAP2	Regulatory/safety review support
	SJTU (China)	CNP600	SBO (in-/ex-vessel)	MELCOR1.8.5	SAM support
	University of Sharjah (UAE)	APR1400	SBO (in-vessel, early phase fuel temperature response)	RELAP5/NESTLE-based 3Keymaster simulator (using SCALE6.1)	Reactor design and simulation
SMR (iPWR)	CNEA (Argentina)	CAREM (iPWR)	SBLOCA (in-vessel)	MELCOR1.8.6	SAM support
	ENSO (Spain)		SBO (in-vessel)	RELAP/SCDAPSIM/MOD3.5	SAM support

LBLOCA: large break loss of coolant accident; PSA: probabilistic safety assessment; SAM: severe accident management/mitigation; SBLOCA: small break loss of coolant accident; SCRAM: safety control rod axe man; STSBO: short-term SBO

Table 2 summarizes the analysis methods per participating organization. The uncertainty quantification methods include Monte Carlo method and simple random sampling (SRS), Latin hypercube sampling (LHS), low rank approximation (LRA), and singular value decomposition/unscented transform (SVD/UT).

The sensitivity methods applied to this exercise include: generalized perturbation theory-based deterministic method, Pearson, Spearman, and Kendall correlation coefficients, partial correlation coefficient (PCC) or partial rank correlation coefficient (PRCC), standardized rank correlation coefficient (SRRC), and principal component analysis/parameter space analysis (PCA/PSA) based method.

The uncertainty quantification tools applied are either based on in-house developed ones or DAKOTA and IUA (integrated uncertainty analysis).

TABLE 2. ANALYSIS METHODS

PWR type	Participating organization	Uncertainty quantification method	Uncertainty quantification tool	Sensitivity analysis method
Large-scale PWR	DNPER/PAEC (Pakistan)	Monte-Carlo method (SRS): N = 2,548	DST (MATLAB – based, In-house)	Pearson, Spearman, and Kendall correlation coefficients
	ENRRA (Egypt)	SVD/UT and LRA approach (SRS: N = 150, multivariate sampling)	PYTHON (In-house)	Generalized perturbation theory-based deterministic method
	KAERI+HYU (Republic of Korea)	SRS: N = 200	DAKOTA (MELCOR) / MOSAIQUE (MAAP5, In-house)	Pearson and Spearman correlation coefficients, and PRCC/SRRC
	KINS+SNU (Republic of Korea)	LHS: N = 300	DAKOTA + In-house	One-at-a-time parametric sensitivity ananlysis
	SJTU (China)	LHS: N = 120	MATLAB (In-house) + SPSS (statistical package for the social sciences)	Pearson and Spearman correlation coefficients, and PCC/PRCC
	University of Sharjah (UAE)	SRS: N = 120 (perturbation of the parameter space)	DAKOTA + ROMUSE (In-house)	PSA/Principal component analysis-based sensitivity method
SMR (iPWR)	CNEA (Argentina)	SRS: N = 59 (one-side Wilks tolerance limit, 95%/95%)	DAKOTA	Pearson and Spearman coefficients
	ENSO (Spain)	Monte Carlo method (SRS) and Wilks approach	IUA	Pearson, Spearman, and Kendall correlation coefficients

The main points of interest where each participating organization intended to answer through relevant plant application exercises are described in Table 3.

TABLE 3. MAIN POINTS IN THE ANALYSIS

Reactor type	Participating organization	Main points of interest
Large-scale PWR	DNPER/PAEC (Pakistan)	Exploring how to revise the base analysis using best estimated parameters / conditions with uncertainty analysis
	ENRRA (Egypt)	Demonstration of a proposed method to reduce the computational time required by the sampling-based uncertainty quantification method in calculating uncertainty
	KAERI+HYU (Republic of Korea)	Difference of the severe accident related uncertainty analysis results predicted from the two severe accident codes (MELCOR/MAAP5) and the influence of relevant SAMs
	KINS+SNU (Republic of Korea)	Assessment of uncertainty related to the long-term corium coolability in containment in a severe accident scenario when various SAM actions were applied
	SJTU (China)	Assessment of uncertainty addressed in the hydrogen source term uncertainty quantification, and the influence of relevant SAMs
	University of Sharjah (UAE)	Demonstration of a proposed PSA based uncertainty quantification method to rate the importance of contributing parameters in the early phase of severe accident
SMR (iPWR)	CNEA (Argentina)	Determination of the time available for human actions and severe accident management/mitigation guideline (SAMG) initiation in case of severe accident
	ENSO (Spain)	Demonstration of the RELAP/SCDAPSIM capability to carry out a best estimate plus uncertainty (BEPU) calculation in a severe accident scenario

Relevant FOMs are defined in Table 4, and the code input parameters and relevant probability distribution functions (PDFs) for the uncertainty and sensitivity analyses, which might affect the defined FOMs, are proposed by each participant, as shown in Table 5.

TABLE 4. PROPOSED MAIN FOMs

Institution	FOMs
DNPER/PAEC (Pakistan)	1) time to core uncovery, 2) reactor pressure vessel (RPV) failure time, 3) in-vessel H_2 generation, 4) ex-vessel $H_2/CO/CO_2$ generation, 5) CsI release into the environment, 6) Cs release into the environment, 7) containment breach time, 8) activity release into the environment: (**10 FOMs**)
ENRRA (Egypt)	1) peak cladding temperature (PCT): (**1 FOM**)
KAERI+HYU (Republic of Korea)	1) Time to core uncovery/damage, 2) time to the RPV lower head failure, 3) time to the reactor building (containment) failure, 4) generation of H_2/CO in the in-/ex-vessel, 5) fission products (Cs) release into the environment: (**7 FOMs**)
KINS+SNU (Republic of Korea)	1) containment pressure, 2) depth of cavity concrete ablation, 3) generation of H_2/CO in the in-/ex-vessel: (**3 FOMs**)
SJTU (China)	1) generation of H_2 in the in-/ex-vessel: (**2 FOMs**)
University of Sharjah (UAE)	1) early phase fuel temperature (in-vessel): (**1 FOM**)
CNEA (Argentina)	1) core uncovery time, 2) onset of core degradation, 3) core relocation time to the RPV lower plenum: (**3 FOMs**)
ENSO (Spain)	1) oxidation time > 0.1% of the nominal power, 2) time T_{cladding} > 1,477K, 3) time fuel rupture, 4) time debris formation, 5) time core slumping, 6) time creep rupture occurs, 7) cumulative H_2, 8) T_{cladding} when fuel rupture, 9) cumulative fission products, 10) cumulative fission products soluble: (**10 FOMs**)

TABLE 5. INPUT PARAMETERS AND RELEVANT PDFs

<table>
<tr><th>Institution</th><th colspan="2">Source: code manual, literature survey, expert Judgment, and parametric analysis</th></tr>
<tr><td>DNPER/PAEC (Pakistan)</td><td colspan="2">MELCOR1.8.6 (26 parameters) (PDF type: triangular, log-triangular, normal, lognormal, uniform, log-uniform, beta, discrete): 1) Core melt progression (in-vessel) (17), 2) H_2 combustion in containment (1), 3) Aerosol/fission products release and transport (in-/ex-vessel) (7), 4) Heat transfer to concrete walls (containment) (1)</td></tr>
<tr><td>ENRRA (Egypt)</td><td colspan="2">ATHLET + SCALE6.3 (one parameter: coolant void reactivity): 1) Reactivities at different coolant densities (in-vessel) (14 multivariate Gaussian PDFs)</td></tr>
<tr><td rowspan="2">KAERI+HYU (Republic of Korea)</td><td>MELCOR2.2 (26 parameters): 1) Core melt progression (in-vessel) (20), 2) Molten core-concrete interactions (MCCI) in reactor cavity (ix-vessel) (3), 3) H_2 combustion (containment) (1), 4) Fission products release and transport (in-/ex-vessel) (2), 5) Heat transfer to concrete walls (1)</td><td>MAAP5.05 (29 parameters): 1) Core melt progression (in-vessel) (18), 2) MCCI in reactor cavity (ex-vessel) (3), 3) H_2 combustion (containment) (2), 4) Fission products release and transport (in-/ex-vessel) (5), 5) Heat transfer to passive heat sinks (1)</td></tr>
<tr><td colspan="2">PDF type: Triangular, log-triangular, normal, lognormal, uniform, log-uniform, beta, discrete</td></tr>
<tr><td>KINS+SNU (Republic of Korea)</td><td colspan="2">MELCOR2.2/COOLAP2 (13 parameters) (PDF type: triangular, normal, lognormal, uniform): 1) MELCOR2.2 : Core melt progression (in-vessel) (5 parameters); 2) COOLAP2: MCCI in reactor cavity (ex-vessel) (8 parameters)</td></tr>
<tr><td>SJTU (China)</td><td colspan="2">MELCOR1.8.5 (18 parameters) (PDF type: normal, uniform, triangular): 1) Thermal power (1); Core melt progression (in-vessel) (17)</td></tr>
<tr><td>University of Sharjah (UAE)</td><td colspan="2">3KEYMASTER simulator (44 parameters) (PDF type: normal): 1) 44 groups SCALE covariance library for the cross-sections affecting on the fuel early phase fuel temperature</td></tr>
<tr><td>CNEA (Argentina)</td><td colspan="2">MELCOR1.8.6 (11 parameters) (PDF type: uniform, normal, lognormal): 1) Physical models, integrity criteria, and core relocation models (In-vessel) (10), 2) Accident management (1)</td></tr>
<tr><td>ENSO (Spain)</td><td colspan="2">RELAP/SCDAPSIM/MOD3.5 (20 parameters) (PDF type: uniform, normal, lognormal): 1) Physical models, boundary and initial conditions, material properties, and code correlations (in-vessel) (17), 2) Safety systems (3)</td></tr>
</table>

The foregoing situation indicates that the conventional benchmark study, which has been focused on common target plant and reference scenarios, but different predictions from different severe accidents tools, was not feasible for this exersice. Accordingly, all participating organizations employed their own uncertainty and sensitivity analysis framework. Severe accidents and relevant supporting analysis codes (such as thermal hydraulics and neutronics) utilized by participating organizations are described in Section 2.2. The key contributions of each participating organizations are described in Section 2.3.

2.2. SEVERE ACCIDENT CODES

2.2.1. MELCOR Code

MELCOR [1–4], being developed by the SNL (Sandia National Laboratories), is the integral system-level code for simulating various severe accident scenarios including the release an transports of fission products in LWRs and other nuclear facilities. For the purpose, the code employs several dedicated code packages, together modelling important plant systems/structures and coupling interactions between them. Flexible nodalization of the reactor coolant system (RCS) and containment employed the code allows not only the simulation of entire severe accident sequences for different kinds of reactors such as PWRs, BWRs, and VVERs, leading to the release and transport of fission products within these systems, but also the simulation of experimental facilities with different geometries. Flexible control functions employed by the code also allows for the simulation of various plant and auxiliary systems.

The code was at first developed for fast-running severe accident analyses as required for PSA, with various functions for performing relevant sensitivity and uncertainty analyses. The recent versions of the code employ various improved functions and models, not only for best-estimate analysis but for assessing the effect of mitigation measures being carried out as part of SAM strategy. The exchange of relevant information including code uncertainties is made by the user group meetings (MUGs). As of June 2019, the latest version released is the MELCOR 2.2.

2.2.2. MAAP Code

MAAP (Modular Accident Analysis Program) [1, 5], being managed by the EPRI (Electric Power Research Institute), is an industry standard integral systems code for analysing plant-level severe accidents including fission products. In mid of the 1990s MAAP4 was issued and thereafter it was greatly extended to evaluate more flexibly the response of advanced LWRs as well as current designs, including mitigation measures being taken as part of SAM. Major improvements include refined reactor core and RPV lower plenum models, a generalized node and junction containment model, and models to represent features of advanced LWR designs including passive safety features.

Due to the fast-running algorithms and parametric models employed by the code, the code is being widely used by utilities for the PSA Level 2 analysis, but the fixed nodalization for the RCS of standard LWRs limits its application to relevant experiments with different geometries. The code is being used in some of the more recent international standard problems (ISPs), from which received information about code deficiencies and user effects. As of June 2019, the latest version released is the MAAP5.05.

2.2.3. ATHLET Code

ATHLET [6], being managed by the GRS (Gesellschaft fur Anlagen-und Reaktorsicherheit, Germany), is a mechanistically-based system code developed to simulate the design basis and some beyond design basis accidents (BDBAs) of LWRs. Whereas, its follow-up version, ATHLET-CD [1, 7], includes core degradation parts to simulate the in-vessel severe accident phenomena: its ATHLET part includes the thermal-hydraulics of the primary system, reactor control systems, neutron kinetics, thermal behavior of the structures, and non-condensable gases. Its core damage part simulates relevant core degradation in case of a severe accident.

2.2.4. RELAP/SCDAPSIM Code

RELAP (Reactor Excursion and Leak Analysis Program) [1, 8], being developed at the INL (Idaho National Laboratory), is a best estimate simulation code for analysing both transient and LOCAs. To solve the thermal hydraulics of reactor in real time and economically calculate system transients, the code solves nonhomogeneous and non-equilibrium models for two-phase systems, using fast and partially-implicit numerical scheme. The code also employs several component models to simulate general systems and validate experimental works as well as modelling multi-phase flow of fluids in piping networks. With the option for time-varying conditions, the code calculates thermal-hydraulics of the reactor in steady-state or transient conditions including accidents, but containment and related components are not included in the code. By the reason, the code is being benchmarked and used by numerous organizations including utilities and regulators. As of June 2019, the latest version released is the RELAP 7.

RELAP/SCDAPSIM (Severe Core Damage Analysis Package SIMulator) [9], being developed by the Innovative Systems Software as part of the international SCDAP Development and Training Program, employs various versions of RELAP such as SCDAP/RELAP5/MOD3.2 models developed for severe accident analysis [10] and RELAP/MOD3.3 [8] models for best-estimate system analysis. Its latest version MOD3.5 is currently being used for the validation of experimental facilities such as PHEBUS [11] and QUENCH [12, 13] as well as user training.

2.2.5. SCALE and NESTLE codes

SCALE (Comprehensive Modelling and Simulation Suite for Nuclear Safety Analysis and Design) [14, 15], being developed by the ORNL (Oak Ridge National Laboratory), is a neutronics code solving neutron transport equation to compute the forward and adjoint fluxes involved in the sensitivity calculations. The two functional modules employed by the code, TSAR and TSURFER, are used to calculate the covariance matrices. TSAR calculates sensitivities for reactivity coefficients responses (or eigenvalue difference) and creates sensitivity files used by TSURFER. Then, TSURFER computes the correlated uncertainties between different states (e.g., different coolant densities and fuel temperatures).

NESTLE [16] is a two-energy neutronics code for calculating the neutron flux and the relevant reactor power in real time. The code obtains the corresponding results by calculating steady state thermal-hydraulics at the current time-step, then solving nodal diffusion equations in a full two-group form at the end of time-step. The nodal expansion method is used to solve the diffusion equations.

2.2.6. 3KEYMASTER Code

3KETMASTER [17], developed by the Western Service Corporation, is a simulator that simulates the power plant in real time, with a graphical visualization. The simulator employs various functions capable of performing reactor start-up/shutdown and emergency operations for user training as well as of calculating reactor power transients. For the thermal-hydraulics and neutronics analyses, the code environment can adapt and embed the relevant codes like RELAP5 and NESTLE within it.

2.2.7. COOLAP Code

COOLAP [18], being developed by POSTECH (Pohang University of Science and Technology), is a lumped parametric code for evaluating the coolability of molten core debris discharged into the reactor cavity during the late phase of severe accidents in LWRs. In case of the pre-flooded reactor cavity, the molten core could break up in the water pool in the cavity, accumulate on the cavity floor, and forms a particulate debris bed. The continuous lump of the melt may be less coolable than particles and can cause the MCCI. To solve such a problem, the code employs the simplified physical models of corium jet breakup during fuel-coolant interactions, corium particle sedimentation, particle debris bed formation, and debris bed heat transfer and dryout heat flux.

2.3. CONTRIBUTION OF THE MEMBER STATES

This section summarizes overall contributions from eight participating organizations from seven Member States. Each contribution is presented in the same way describing the motivations and objectives, description of the relevant plant, description of the accident scenario and used computational codes, plant modelling, methodologies used to assess the uncertainties and sensitivity analysis, and the summary results outlining as well lessons learned and best practices.

2.3.1. Directorate of Nuclear Power Engineering-Reactor (DNPER)

The DNPER contributed to the accident analysis applied to ACP1000 plant type. Description of the plant specifics, accident scenarios analysed, applied models and approaches, and summary of the results are provided in the following sections.

2.3.1.1. Motivation and objectives

One of the key problems related to severe accident uncertainty analysis is the large computational time requirement by using different statistical sampling methods for computation. This problem can be solved by introducing uncertainty analysis techniques to achieve the uncertainty along with the confidence level that may be acceptable in simulations which cover the maximum spectrum of uncertain ranges along with the parameters affects the FOMs of interest. By introducing such sampling techniques, the sample inputs population size reduces considerably with acceptable confidence level in the output spectrum of results. The FOMs for these analyses are:

- RPV water level;
- RPV failure;
- In-vessel hydrogen generation;
- Ex-vessel hydrogen generation;
- Radionuclide/aerosol production during SBO;
- Containment failure;
- Radioactivity release to the environment.

2.3.1.2. Description of the relevant plant

K-2 Nuclear Power Plant (ACP1000) ((CNPE), 2019) is comprised of three loop PWR nuclear steam supply system (NSSS) and related auxiliary facilities. The highlight of design is inclusion of passive safety systems which results in high reliability of engineered safety features and improvement in economics. The reactor core consists of standard PWR fuel assemblies with three different fuel enrichments. The detailed description of design parameters of the K-2 is presented in Table 6.

The site of K-2 is located on the coastline of the Arabian Sea near Karachi city in the Sindh Province of Pakistan. The site of K-2 is about 1.5 km in the North-West of existing Karachi NPP Unit-1 (K-1).

2.3.1.3. Accident scenarios and severe accident codes

The current study is performed to analyse the transient behaviour of K-2, considering the SBO accident scenario. The current model contains of detailed primary and secondary loop modelling. The containment and cavity control volumes are also incorporated. The safety injection system, containment spray system and auxiliary feed water system are also modelled for detailed analysis. The analytical work focuses on the uncertainty quantification during SBO scenario which is classified as a beyond design basis accident.

The MELCOR code, version 1.8.6 [2, 3] was used (the code is described in Section 2.2.1).

TABLE 6. K-2 NPP DESIGN PARAMETERS

Parameter	Unit	Value
Unit power output	MWe	1,100
Reactor thermal power	MWt	3,050
Pressurizer pressure	MPa	15.5
Reactor coolant system flow rate	m^3/h	68,520
Number of fuel assemblies	–	177
Fuel rods per assembly	–	264
Fuel rod pitch	cm	1.26
Fuel rod outer diameter	cm	0.95
Cladding thickness	cm	0.057
RCS inlet temperature	ºC	291.5
Average temperature rise in core	ºC	39.3
RCS average temperature	ºC	311
Steam generators operating pressure	MPa (abs)	6.8
Main steam flow rate	kg/s	1,700
Containment design pressure	MPa (abs)	0.52

2.3.1.4. Plant modelling and nodalization

A complete nodalization of K-2 is presented in Figs. 2–5. The nodalization includes detailed discretization of all important components of the primary & secondary side and core.

The primary system of the NPP is divided into 41 control volumes in which 11 control volumes for RPV and 30 control volumes are used for the primary loop. The core and lower head plenum are modelled using 04 rings radially and 14 nodes axially. First 08 axial nodes are used to model RPV lower head, lower head plenum, support structures and core support plate. Six axial nodes are used to model the core. The secondary side is modelled using 39 control volumes which include the control volumes for steam generators, turbine, feed-water source and piping, while the containment is modelled using eight control volumes.

The plant is assumed to be operated steady state at full power. The main design parameters of the plant are at the nominal value as shown in Table 6. The sequence of accident is initiated as induced transient and accident scenario; the following basic assumptions are made:

- Steady state analysis starts at –2,000 s;
- At 0.0 seconds, loss of power occurs, which leads to reactor scram, reactor coolant pumps trip;

turbine trip, and loss of main feed water as well as auxiliary feed water;
- Diesel driven auxiliary feed water pumps are unavailable;
- Emergency diesel generators and alternate AC are assumed to be unavailable;
- Pressurizer relief valves are unavailable due to station blackout and its safety valves are available;
- Relief valves of secondary system are unavailable due to station blackout and its safety valves are available;
- One train of dedicated pressure relief valves are opened by operator manually when outlet core temperature reaches 650°C in this accident;
- Availability of accumulators is confirmed;
- Unavailability of safety injection system is considered;
- Unavailability of containment spray system and recirculation system are considered;
- Unavailability of cavity flooding system is considered.

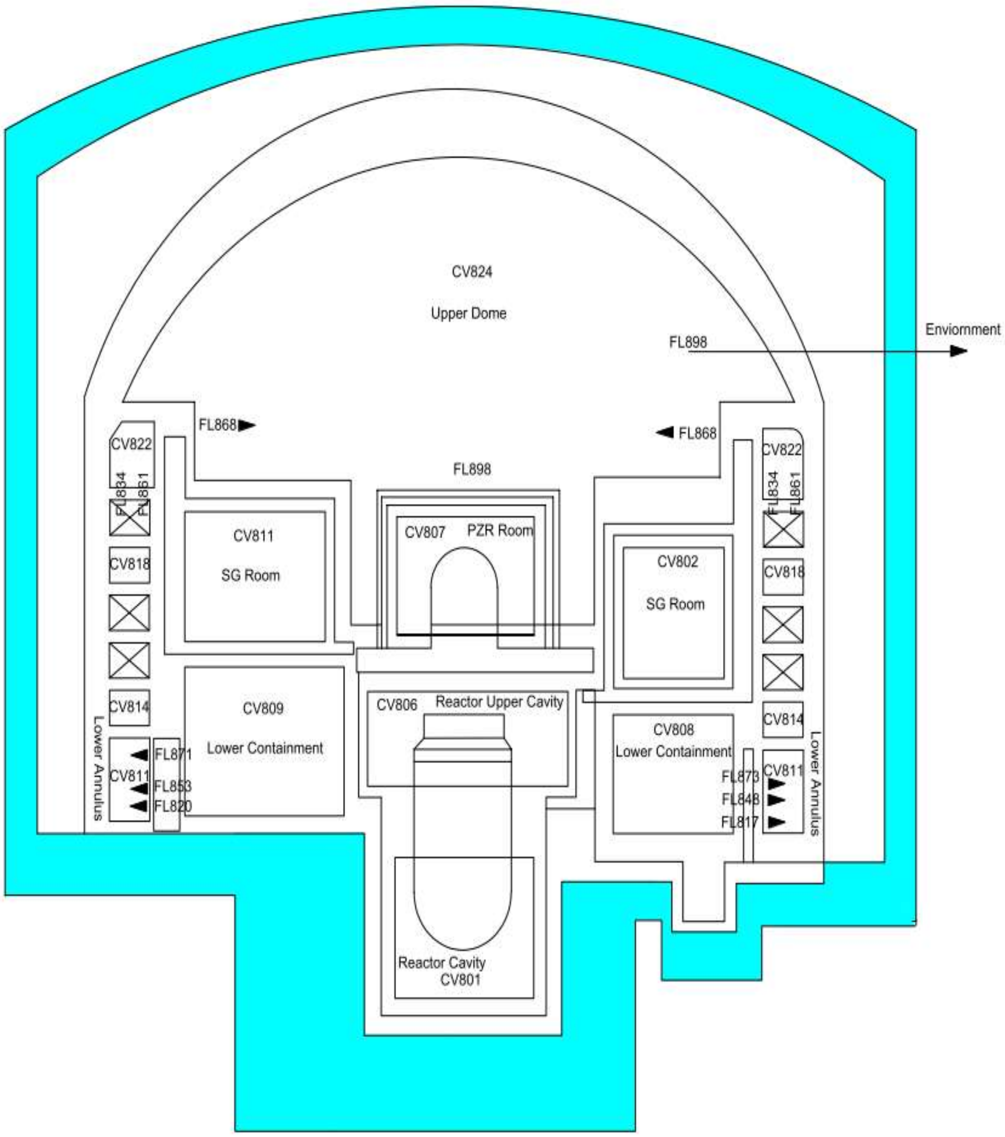

FIG. 2. K-2 NPP containment nodalization.

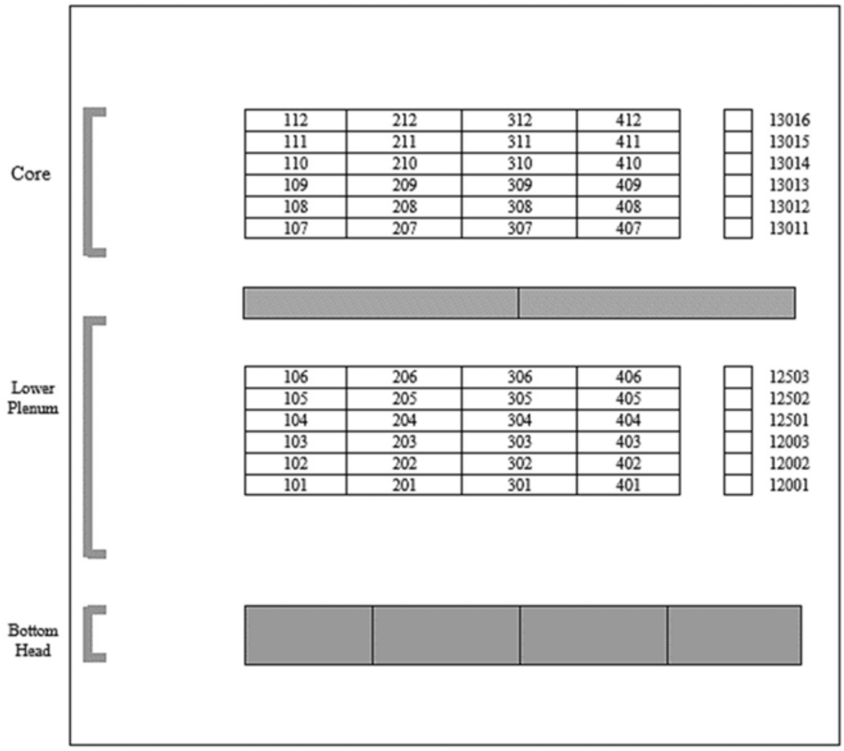

FIG. 3. K-2 NPP core axial nodalization.

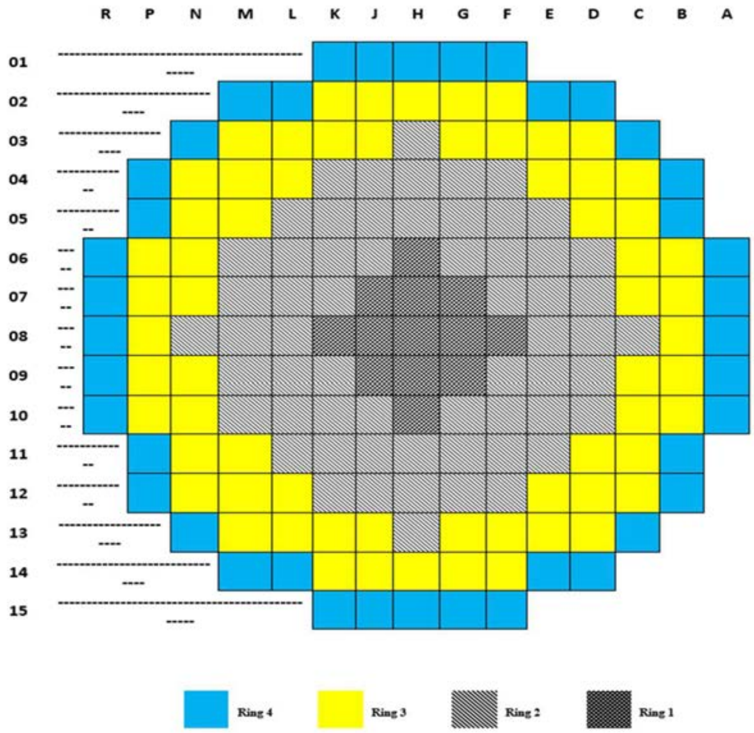

FIG. 4. K-2 NPP core radial nodalization.

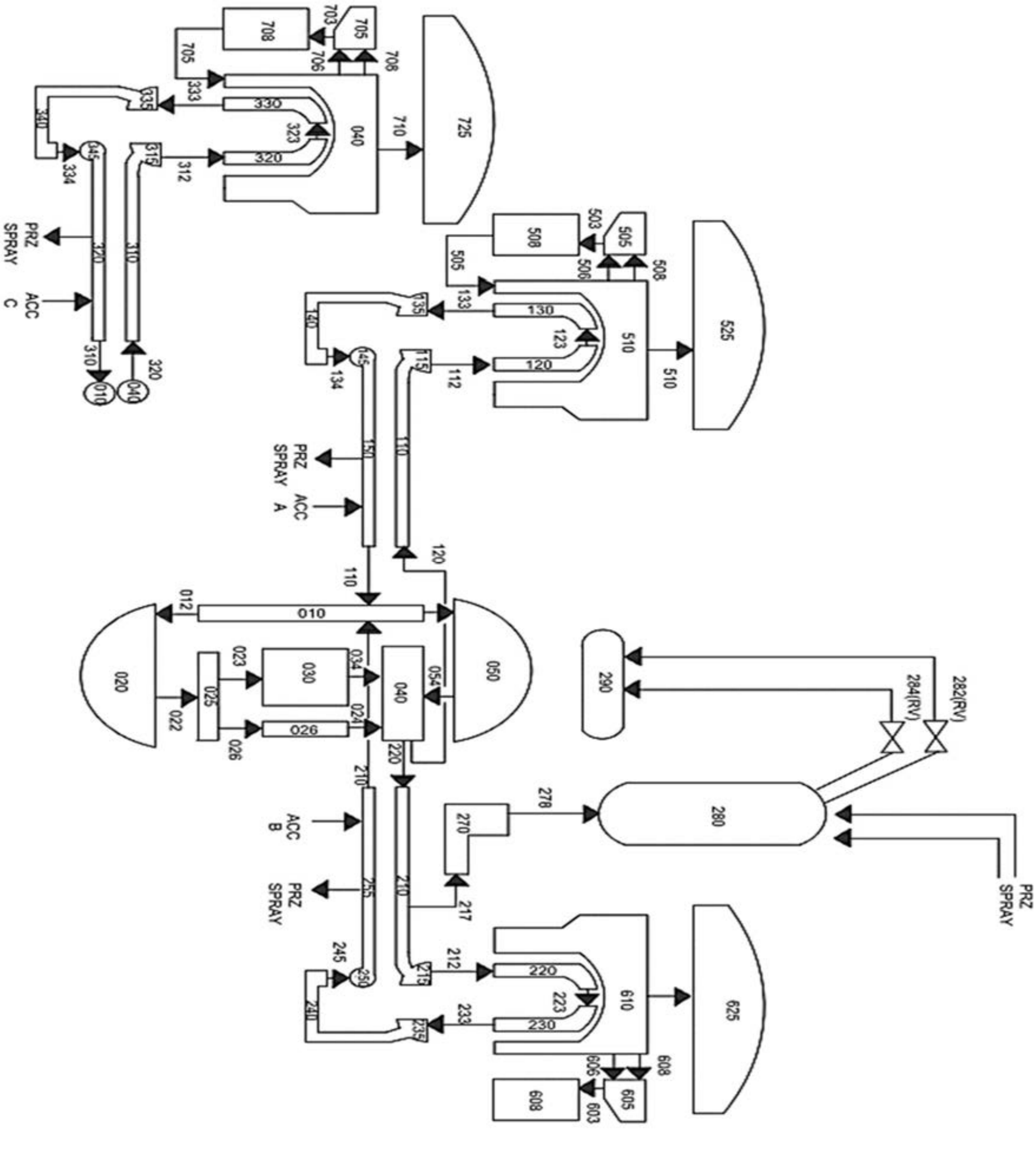

FIG. 5. K-2 NPP primary system nodalization.

2.3.1.5. Methodologies and tools for uncertainty and sensitivity analyses

Several methodologies have been developed so far to estimate the effect of uncertainties and sensitivities on severe accident analysis. These include statistical sampling methods as well as deterministic approach using sandwich formula. The computation of uncertainty analysis using Monte Carlo technique is assumed to be a much dependable being sampling based. Although this method is relatively a simple method but it requires more computational time because it requires extensive executions to sample the multi parameter space. Generally, in first step uncertainty analysis is performed and then proceed to sensitivity calculations which is different to deterministic safety analysis.

Advantages and disadvantages: For quantification method Monte Carlo sampling is mostly used. This technique is assumed to be a more dependable being sampling based and it can be made applicable to any computer code. The number of executions required to be performed depend upon the sample size. It is considered to be acceptable in uncertainty quantification method. Using Wilks formula [19], the 95% probability and 95% confidence level were selected as the requirement of the licensing. The size of a random sample *(N)* can be calculated using Wilks formula with the probability that most of the sample is greater than a given percentile (α) as;

$$1 - \alpha^N - N(1-\alpha)\alpha^{N-1} \geq \beta \tag{1}$$

where β is the confidence level. Monte Carlo sampling method deals with non-parametric and non-asymptotic i.e., probability distributions of outputs and sample size are independent to achieve the desired level of confidence.

Pearson correlation describes the linear correlation between the two variables and its value is limited between −1 and +1. If the resultant correlation *(r)* is negative it means that an increment of x variable leads to a reduction in y variable. Similarly, if the resultant correlation is positive it means that an increment of x variable leads to an increment in y variable. If the resultant is zero, there is no correlation between the two variables. The simplified Pearson correlation between two variables x and y can be expressed as:

$$r = \frac{\sum_{i=1}^{n}(x_i - x_m)(y_i - y_m)}{\sqrt{\sum_{i=1}^{n}(x_i - x_m)^2 \sum_{i=1}^{n}(y_i - y_m)^2}} \tag{2}$$

Spearman correlation [20] is a measure of monotonic correlation between two variables. R_i and S_i are ranks of randomly chosen input parameter values and simulation results. Ranks are assigned in ascending order. For matching values an average rank should be assigned. If absolute value of ρ_s is less than critical value (R), there exists no correlation. Critical value $\bar{R}$ is a function of sample size N and confidence level:

$$\rho_S = \frac{\sum_{i=1}^{N}(R_i - \bar{R})(S_i - \bar{S})}{\sqrt{\sum_{i=1}^{N}(R_i - \bar{R})^2 \sum_{i=1}^{N}(S_i - \bar{S})^2}} \tag{3}$$

$$\bar{R} = \bar{S} = \frac{N+1}{2}$$

Kendall correlation [20] in which T is a measure of coherence between two variables and τ is a measure of disorder; x_i and y_i are randomly chosen input parameter values and simulation results respectively:

$$\tau = \frac{T}{\max T}. \tag{4}$$

$$T = \sum_{1 \leq i \leq j \leq N}^{N} sign(x_j - x_i) \times sign(y_j - y_i)$$

$$\max T = \frac{N(N-1)}{2}$$

Uncertainty and sensitivity calculation scheme and DNPER statistical tool: it is an interface code developed indigenously by Severe Accident Analysis Division and is based on MATLAB (Programing & Numeric

Computing Platform for Data Analysis, Model and Algorithm Development). It focuses on the main hurdle i.e. reduction in large computational time while performing the uncertainty analysis. Computing considering uncertainty parameters, computational time is a prime issue. As shown in Fig. 6, this issue is overcome by developing an indigenous code that reduces computational time from months to days.

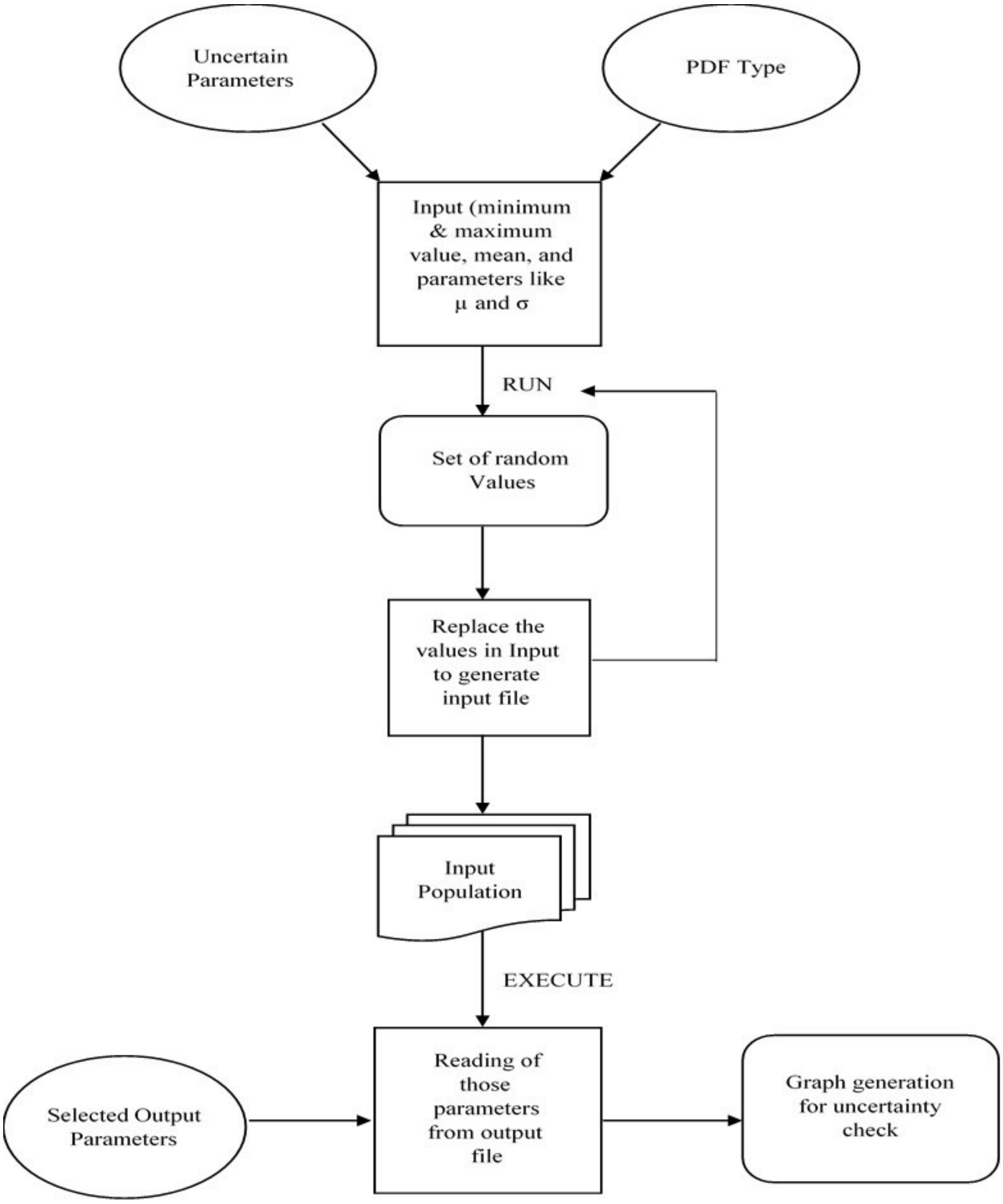

FIG. 6. Flow chart of the K-2 NPP uncertainty and sensitivity calculation scheme.

The estimation of the uncertainty in the final analysis results by using the best estimate model is considered utmost requirement. During power operation of a plant, limiting transients can be handled efficiently while the key parameters like peak fuel clad temperature etc. are known with great confidence. The operators can deploy some conservative technique to enhance the plant operational cycle and plant availability. Hence, plant operational cost may be reduced by using more confident results.

Uncertain parameters and related probability distribution: through engineering judgement and experience, 26 uncertain parameters have been selected with 95% probability and 95% confidence level resulting sample size as 2,548. Each uncertain parameter [21–25] has its lower and upper bound and follows a specific probability distribution function as given in Table 7. In order to obtain the best estimate value, random values need to be selected over the given range for each parameter. The statistical tool generates the random values of all uncertain parameters from their respective PDFs spectra as per requirement depending on pre-calculated sample size. Hence, a large number of files is thus generated for preparation for MELCOR input data set. These generated data sets are used to prepare unique MELCOR input by replacing their relevant default values. Hence in this way, required input population sets is properly generated.

TABLE 7. K-2 NPP MODEL PARAMETERS AND PDFs FOR THE UNCERTAINTY ANALYSIS (MELCOR, 26)

Parameter	**Range**	**Default Value**	**Detail**	**Probability Distribution**
		MELCOR model parameters for core melt progression		
PORDP	0.1 – 0.5	0.4	Particulate debris porosity for the given cells of all cells	Lognormal, μ = -0.85, σ = 0.32
DHYPD	0 – 0.06 (in LP region) 0.002 – 0.05 (in core region)	0.002 (in LP region) 0.01 (in core region)	Equivalent diameter of particulate debris. For calculation of total debris surface area this parameter is used. In debris quench model this diameter has prime importance for determination diameter of debris falling from the core to the lower plenum. The best estimate values for shallow pools are not applicable, following best estimate values is used for deep pool condition. (perhaps not correct for shallow pools)	Lognormal, μ = -3.68, σ = 0.5 (in LP region), Lognormal, μ = -4.34, σ = 0.58 (in core region)
VFALL	0.01 – 1.0	0.01	Velocity of falling debris. This parameter deals the falling debris velocity used in quench model as mentioned in code. The loss of heat of debris to surrounding water in the lower plenum has been defined in MELCOR and it is considered in each radial ring after failure of the core support plate. The best estimate values for shallow pools are not applicable, following best estimate values is used for deep pool condition. (perhaps not correct for shallow pools)	Uniform
HDBH2O	200 – 2000	2000	Heat transfer coefficient from in-vessel falling debris to pool. The best estimate values for shallow pools are not applicable, following best estimate values is used for deep pool condition. (perhaps not correct for shallow pools)	Uniform

TABLE 7. K-2 NPP MODEL PARAMETERS AND PDFs FOR THE UNCERTAINTY ANALYSIS (MELCOR, 26) (Cont.)

Parameter	**Range**	**Default Value**	**Detail**	**Probability Distribution**
		MELCOR model parameters for core melt progression		
COR_CHT	2000 – 22000 (UO_2 + Zr + ZrO_2), 500 – 8000 (Steel + Steel Oxide + Poison)	7500 (UO_2 + Zr + ZrO_2), 2500 (Steel + Steel Oxide + Poison)	This parameter deals heat transfer coefficients as candling. For molten core material modelling this parameter used for heat transfer coefficient as refreezing in the candling model. To determine the impact on overall melt progression default values with sensitivity studies are considered to produce plausible simulations for relocation phenomena.	Lognormal, μ = 9.04, σ = 0.63 (UO_2 + Zr + ZrO_2) Lognormal, μ = 7.9, σ = 0.83 (Steel + Steel Oxide + Poison)
FUOZR	0.0 – 0.5	0.2	This parameter deals with local fractional dissolution of UO_2 in molten zirconium. The default value assumes that the molten metallic cladding will incorporate adjacent UO2 fuel material so that 20% by mass of the total melt is dissolved fuel.	Triangular, Mode = 0.2
FCELR & FCELA	0.02 – 0.18	0.1	Radioactive exchange factor for radiation heat transfer outward radially (FCELR) and upward axially (FCELA) encounter with the cell boundary and to the next adjacent cell.	Normal, Mean: 0.1, σ: 0.0375
HDBPN	100 – 1000	100	This parameter deals with coefficient of heat transfer for debris to penetration structures. The default value used but it needs to be changed in full range during sensitivity studies to estimate its role on lower head failure after excessive heat transfer.	Uniform
TPFAIL	1273.15 – 1686.15	1273.15	This parameter deals with the temperature at which lower head penetration fails. It is an approximate value for transition of plastic behaviour of steel (Lower bound: MELCOR default, upper bound: melting point for Inconel600)	Uniform
SC1020	100 – 1000 (Solid), 10 – 100 (Liquid)	300 (Solid), 10 (Liquid)	This parameter deals relocation of molten material and solid particulate from ring to ring and used in relocation model in radial direction.	Uniform
SC1030_2	9.1232×10-2 – 9.2148×10-2	9.17×10^{-2}	*dT/dz* model, time constant for average flow	Uniform
SC1030_4	8.8286–8.9174	8.873	*dT/dz* model characteristic time. When this model is considered active it is the time for temperature to average control volume hydrodynamic for calculation of volume temperature	Uniform
SC1131-2	2,100–2,540	2,400	This parameter deals with holdup of molten material. These coefficients are used to define either oxide shell can hold the molten material. (2) is referred to the maximum zirconium dioxide temperature for hold up of molten Zr.	Beta, α = 3.83, β = 3.00

TABLE 7. K-2 NPP MODEL PARAMETERS AND PDFs FOR THE UNCERTAINTY ANALYSIS (MELCOR, 26) (Cont.)

Parameter	**Range**	**Default Value**	**Detail**	**Probability Distribution**
MELCOR model parameters for core melt progression				
SC1132-1	–	2,500	This parameter deals with failure of core component. It shows the temperature at which Zr is melted and candled so represents the failure temperature of fuel. (1) refers to the max temperature up to which fuel rods (oxidized) can stand stable in the absence of un-oxidized Zirconium in the cladding.	Normal distribution, Mean = 2479, Σ= 83
SC1141-2	0.1–2.0	1	This parameter deals with candling parameter for core melt breakthrough. It is used for calculating the crust and oxide shell holdup of molten materials. (2) refers to the maximum value of the melt flow rate after breakthrough per unit width.	Log triangular, Mode = 0.2
SC1601-4	0.16–0.20	0.18	This parameter deals with creep rupture of vessel steel in Larson-Miller model.(4) refers to the total strain assumed to cause failure.	Uniform
SC3200-1	0.9–1.1	1	This parameter deals with decay heat curve as multiplier as ANS equation for decay heat.	Uniform
MELCOR model parameters for hydrogen combustion				
XH2IGN	0.03–0.09	0.1	H_2 mole fraction limit for ignition without igniters. This parameter used to specify the uncertainty in lower flammability limit for the direction of propagation from the ignition source for downward, horizontal and upward directions	Discrete, 0.03 = 0.33, 0.06 = 0.33, 0.09 = 0.33
CHI,	1.0–5.0	1	This parameter deals with aerosol dynamic shape factor. It is the ratio of the forces of the non-spherical particle to the resistance of a sphere of same volume and same velocity. The default value used as 1.0 means a perfect sphere.	Scaled Beta, α = 1.00, β = 5.00
FSLIP	1.2–1.3	1.257	Particle slip factor in Cunningham slip correction. The default value is 1.257	Beta, p = 4, q = 4
STICK	0.5–1.0	1	Particle sticking coefficient with default value of unity	Beta biased to 1, p = 2.5, q = 1
FTHERM	2.2–2.5	2.25	Factor in Thermal Accommodation Coefficient	Uniform
TKGOP	0.006–0.06	0.05	Gas/Aerosol Particle thermal conductivity ratio	log uniform
TURBDS	0.00075–0.00125	0.001	Turbulent energy dissipation density with default value of 0.001	uniform
XHTFCL	1.0–2.0	1.4	Deals with scaling factor for atmospheric heat transfer	Triangular, Mode = 1.4

2.3.1.6. Results

The first part of this study deals with the analysis of steady state conditions of the plant operating at nominal power 3,050 MW_t. The steady state analysis is performed for 2,000 seconds. The primary side as well as secondary side parameters i.e., temperature, pressure and coolant flow are analysed.

<u>*Reference case results:*</u> as shown in Fig. 7 (a), the steady flow rate of 22,500 m^3/hr is expected for single loop. RCS pressure is given in Fig. 7 (b) that shows the steady pressure of about 15.5 MPa. Figure 6 (c) shows the steady state steam flow rate of 567 Kg/s in one steam generator. The steady state pressure achieved in steam generator secondary side is about 6.8 MPa which is shown in Fig. 6 (d). Figure 6 (e) gives the core inlet/exit temperature of the coolant which is about 565 K and 602 K, respectively. Figure 6 (a) and (b) show the temperature profile for two radial rings contains five axial levels of core; since the core is divided into four radial rings.

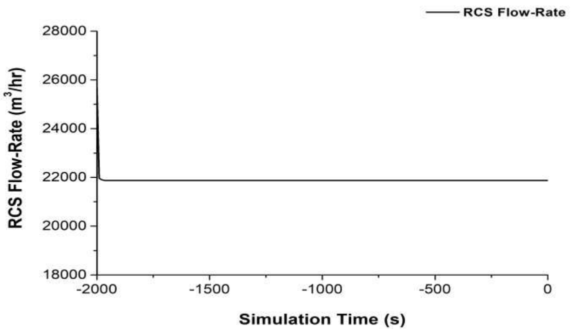

(a) RCS flow rate

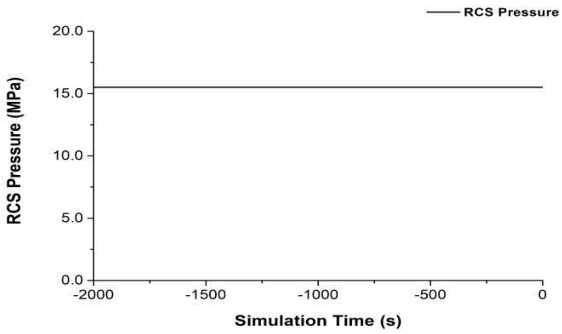

(b) RCS pressure

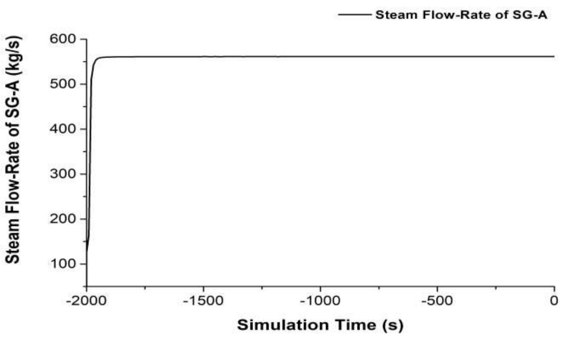

(c) Steam flow rate from steam generator

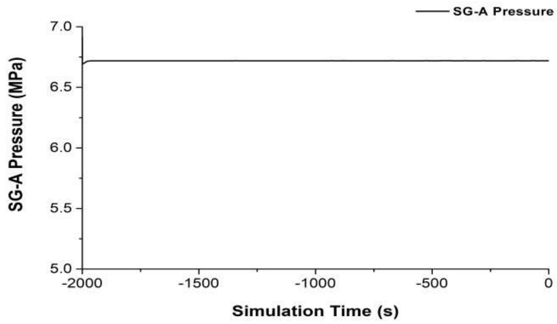

(d) Steam generator pressure

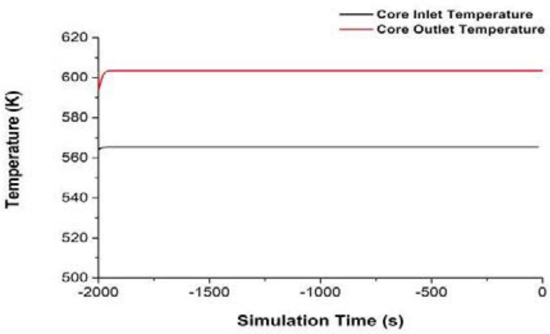

(e) Core inlet & outlet temperature

FIG. 7. K-2 NPP results for steady state analysis.

The postulated transient sequence begins with station black out that causes loss of cooling as forced convection not available in reactor coolant system resulting ultimately resulting in loss of primary and secondary side water inventory. To remove the decay heat present in primary cooling system natural convection is the only way. This mode has lesser capability to remove this remaining larger fraction of decay heat causing ultimately increase of core heat up and loss of water inventory. Time sequence of the main events is presented in Table 8.

TABLE 8. K-2 NPP: TIME SEQUENCE OF MAIN EVENTS

SBO (for hydrogen control measures)	
Parameters	**Unit value**
Station blackout	0
Reactor shutdown	0
Secondary side safety valve open	10
Steam generator depletion	4,840
Core uncover	6,648
Core outlet temperature > 650°C	7,690
Dedicated pressure relief valves opened manually	7,690
Core dry out	7,756
Accumulators' actuation	8,100
Accumulators' stoppage	9,120
Cladding oxidation	12,170

Inadequate core cooling may result in core melt after a severe accident. The upper core region becomes uncovered as the water in the RPV becomes dry out. Steam formed in the upper region will cool this section but it may not provide adequate cooling. This phenomenon will lead to over heat up of the fuel rods along with their cladding material in the uncovered part of the core. The fuel cladding Zr will be oxidized more and more because of this increased temperature which will result in production of hydrogen in excess. The oxidation process being exothermic in nature will result in further temperature increase and more steam-cladding reaction in the uncovered region of the core. This amplified temperature will also boost the heat transfer quantity to other components and structural materials inside RPV through the process of convection, conduction and radiation. Solid structural materials may become in molten and liquefaction form and will result in molten material relocation towards the bottom of the core region.

Molten materials may settle down and may form some type of blockages resulting in the significant changes in the steam flow paths inside RPV. Eventually, release of volatile fission products will start during downwards relocating. During core heat up, hydrogen is mainly produced by oxidation of Zr cladding which is highly exothermic reaction. At temperatures above 1,300 °C this reaction accelerates the heating up of the fuel rod materials. Figure 8 presents the results of hydrogen generation for the case study. The in-vessel hydrogen generation for the base case is shown in Fig. 8 (c). It shows hydrogen generation through Zr oxidation and stainless steel oxidation along with total hydrogen generation. Molten material will flow down the fuel rods gradually to relatively cooler lower core region and will block the channels between the fuel rods. At this situation if the pressure in RCS is lower, the corium will flow below the vessel towards the cavity otherwise it will be ejected violently and will dispersed. The consequences of these two scenarios on the containment may be different in nature. Core water level and RCS pressure are given in Figs. 8 (d) and (e), respectively.

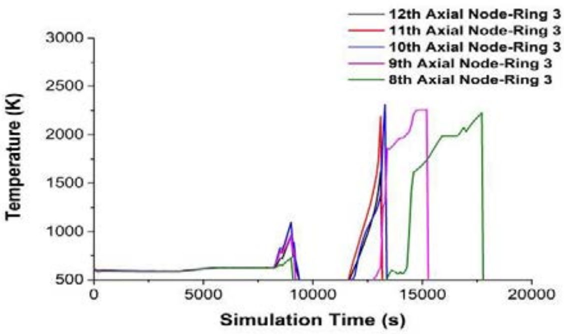

(a) Core axial temperature profile in Ring-3

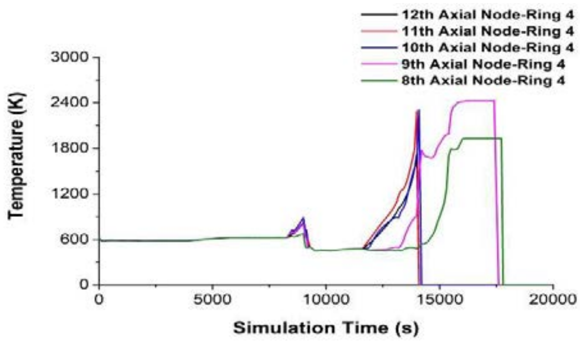

(b) Core axial temperature profile in Ring-4

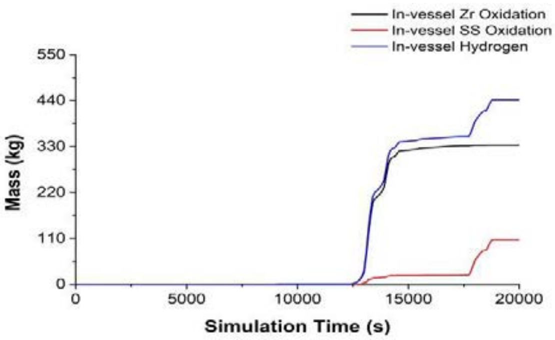

(c) In-vessel hydrogen generation

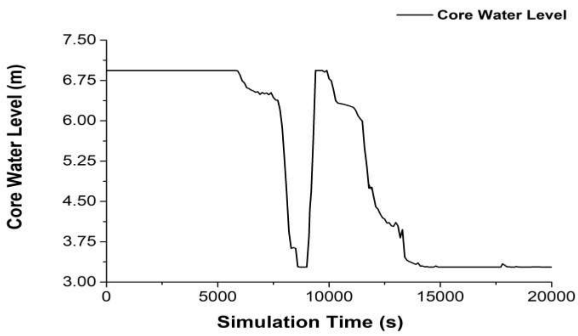

(d) Core water level

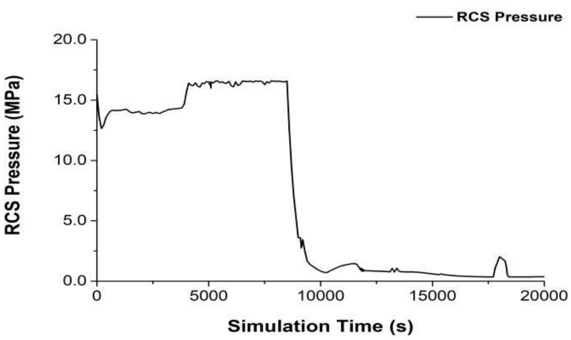

(e) RCS pressure

FIG. 8. K-2 NPP analysis results for reference case.

Uncertainty analysis: in this section the results of statistical analysis of the uncertainty and their comparison with the base case are documented and discussed to define the importance of each selected parameter in consideration with its statistical convergence. Figure 9 shows histograms of some of the random samples generated from probability distributions functions given in Table 7.

The predicted RCS pressure trends for the 2,548 simulations produced are presented in Fig.10 (a). It can be observed that in all the cases the pressure converges to the median value initially. The sudden drop in pressure between 2.2 and 2.6 h predicted for all cases is due to the activation of dedicated depressurization system. When outlet core temperature reaches 650 °C in the total loss of multiple safety functions failure accident, one train of dedicated pressure relief valves is opened by operator manually. Because of the intentional depressurization by the dedicated pressure relief valves, borated water in accumulator is injected into RPV, which stops the core meltdown process temporarily. But the core continues to meltdown again after the accumulator becomes dry.

RPV water level drop leads to heat up of the fuel rods and their cladding in the dry region of the core. The predicted RPV water level for each simulation is shown in Fig. 10 (b). This figure describes that the core uncover time falls in band spectrum from 2.2 to 3.2 hours as water level reaches the top of active fuel height. The water level loss rate shows a decrease as the water level lowers to the end of the core. This is the result of lesser water availability for steam generation and retention of higher fraction decay heat increased as loss of cooling present in the system. Between 3.1 and 3.5 hours' duration, there is sudden decrease in the inventory of the core water. At this point control rod melting occurs and their slumping results in badly damaging of Zr clad from the upper core region towards lower core plate regions. As highly energetic molten core reaches to lower core plate a rapid boiling starts and remaining amount of water replenish in a short interval of time. Comparison of average value of for RPV water level and base case results show that water in RPV drains at about 15 minutes early in case of base case as compared to averaged value of uncertainties.

The reactor core begins to be exposed and there is exothermic zirconium-water reaction occur between fuel cladding and steam, as shown in Fig. 10 (c). Since the active safety injection system is not available, there is no continuous cooling water injection after draining off of the accumulator. This leads to gradual heating of and boiling in the primary loop and makes the reactor core exposed again. A range of 350–850 kg of hydrogen generated during in-vessel phenomenon. Comparison of averaged case and base case is represented shows that base case over predicted the hydrogen generation.

The Lower head failure caused due to unavailability of cavity injection system occurs at a range of 3.52–10.66 h. Average value for RPV breach time calculated from uncertainties is 4.98 h while for base case its value is 4.76 h. Its averaged value suggests that there is about 15 minutes more for safety measures as compared to base case. The molten core enters the reactor cavity and leads to interaction with the concrete base mat of reactor cavity which results in corrosion of the base mat and continuous release of hydrogen, as shown in Fig. 9 (d). In cavity amount of 850–1,300 kg hydrogen is generated. Comparison of averaged case and base case show that base case slightly under predicted the hydrogen generation. Total hydrogen generated during SBO case has generated the mass in the range of 1,200–2,150 kg in about 70 h of occurring of this accident as shown in Fig.10 (e). Comparison between averaged and base case results for total hydrogen generated show that base case over predicted the hydrogen generation. When corium dumps to reactor cavity floor and spreads onto the cavity floor. Corium transfers heat to the cavity floor and then molten core-concrete interaction occurs. After being heated by the melt, the concrete is first dehydrated (steam is released), then decomposed (releases water vapour and carbon dioxide) and melted. The rate at which gas is generated during the interaction of the molten corium with the concrete depends on the heat flow rate and the type of concrete. MCCI generates aerosols, which affect the release of radioactive material. The range of maximum Cs and radionuclides generated as a result of this postulated accident are predicted about 18 to 25 kg with a mean value of 20 kg having standard deviation of ±0.019 and of CsI is about 40 to 65 kg with a mean value of 51 kg and a standard deviation of ±0.06 as shown in Figs. 10 (f) and (g), respectively.

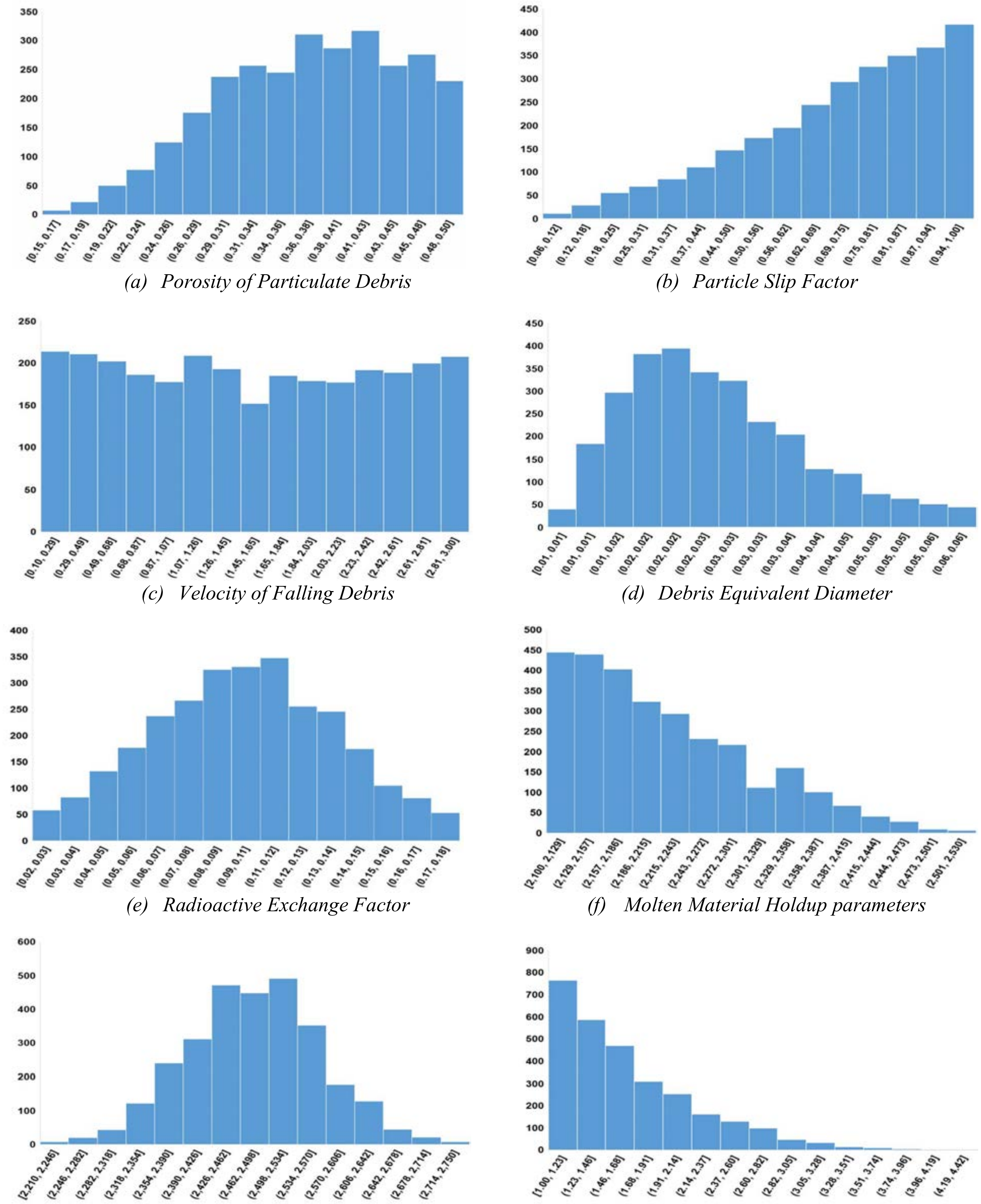

(a) Porosity of Particulate Debris

(b) Particle Slip Factor

(c) Velocity of Falling Debris

(d) Debris Equivalent Diameter

(e) Radioactive Exchange Factor

(f) Molten Material Holdup parameters

(g) Core Component Failure Parameters

(h) Aerosol Dynamic shape Factor

FIG. 9. Histograms for probability distribution functions of uncertain parameter inputs for K-2 NPP.

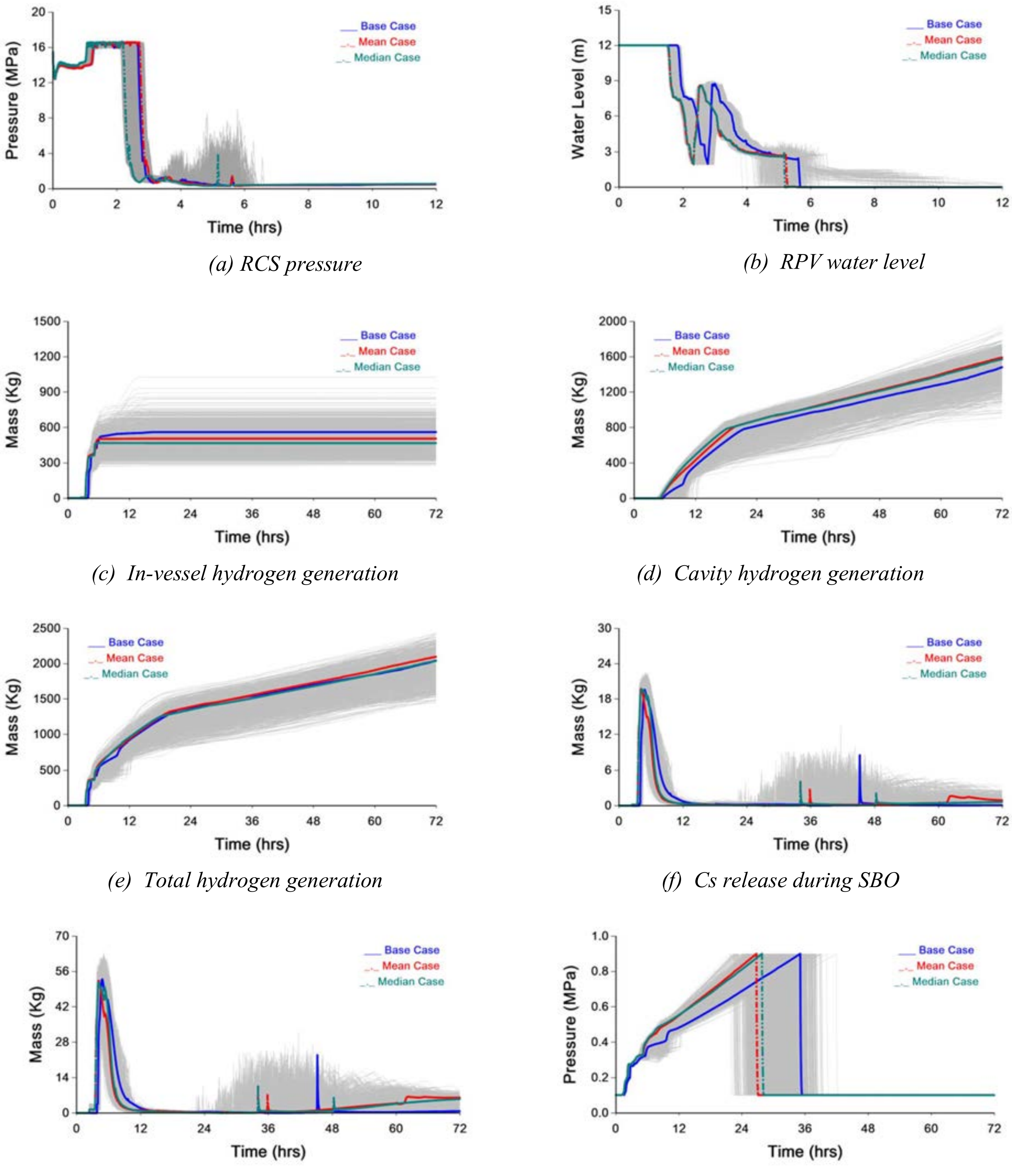

(a) RCS pressure *(b) RPV water level*

(c) In-vessel hydrogen generation *(d) Cavity hydrogen generation*

(e) Total hydrogen generation *(f) Cs release during SBO*

(g) CsI release during SBO *(h) Containment pressure*

FIG. 10. Uncertainty analysis results for K-2 NPP case study.

Sensitivity analysis: Pearson, Spearman and Kendall correlation coefficient were chosen to identify the more impactful uncertain parameters for relevant FOMs. Those uncertain parameters which provide least meaningful information were excluded. On the basis of sensitivity analysis key contributors having stronger correlation with each relevant FOMs are summarized in Table 9. Final ranking of those inputs are determined by weighting equally the relevant correlation coefficients.

The following is explanation about the key contributors to relevant FOMs: core uncovery time (FOM 1) is related to the decay heat power and radiative exchange between fuel cells used as primary model parameters. RPV lower head failure (FOM 2) is related to reactor coolant change and accident progression during in-vessel phenomenon as basic model parameters. In-vessel hydrogen generation (FOM 3) is mainly related to the in-vessel cladding oxidation. Ex-vessel hydrogen generation (FOM 4), ex-vessel CO production (FOM 5) and ex-vessel CO_2 production (FOM 6) are mainly related to concrete ablation caused by molten core concrete interaction affected by molten corium of in-vessel entered into the reactor cavity. CsI release (FOM 7), Cs release (FOM 8), containment breach (FOM 9) and activity release to environment (FOM 10) are mainly dependent on the time of RPV break as generation of more fission fragments occurred due to ex-vessel phenomenon and caused more activity release to the environment.

TABLE 9. KEY CONTRIBUTORS TO RELEVANT FOMs IN MELCOR 1.8.6 FOR K-2 NPP CASE STUDY

FOMs	Rank 1	Rank 2	Rank 3	Rank 4	Rank 5
FOM 1	SC3200_1 (–0.70)	FCEL (+0.1)	HDBPN (+0.1)	SC1020_1 (+0.1)	TPFAIL (+0.1)
FOM 2	SC3200_1 (–0.70)	FCEL (-0.12)	SC1141_2 (+0.12)	HDBPN (-0.1)	SC1020_2 (+0.1)
FOM 3	HDBPN (-0.4)	DHYPD (-0.2)	SC1131_2 (+0.17)	TPFAIL (+0.16)	SC1141_2 (+0.10)
FOM 4	SC3200_1 (+0.55)	HDBPN (-0.2)	DHYPD (+0.18)	SC1141_2 (-0.10)	FCEL (+0.09)
FOM 5	SC3200_1 (+0.58)	HDBPN (-0.2)	DHYPD (+0.16)	FCEL (+0.1)	SC1141_2 (-0.10)
FOM 6	SC3200_1 (+0.70)	DHYPD (+0.12)	FCEL (+0.12)	SC1141_2 (-0.10)	SC1131_2 (+0.09)
FOM 7	SC1141_2 (-0.30)	DHYPD (+0.18))	SC3200_1 (–0.15)	SC1131_2 (+0.12)	-
FOM 8	FCEL (+0.45)	DHYPD (+0.33)	-	-	-
FOM 9	SC3200_1 (-0.9)	DHYPD (+0.12)	-	-	-
FOM 10	SC3200_1 (+0.7)	HDBPN (+0.11)	-	-	-

— *Core uncovery time (FOM 1):* main parameter which affects the core uncovery time is SC3200_1 having very strong negative correlation about less than –0.7. This parameter is the multiplier for ANS decay heat curve. Core heating and dry out before the core degradation mainly deals with this parameter and observed as the highest value of importance. Strong negative correlation of SC3200_1 indicates that the larger decay heat which leads to the faster boiling and uncovery of coolant. Parameters of minor effects on this FOM are FCELR/FCELA, HDBPN, SC1020_2, TPFAIL and SC1141_2 having magnitude of measure is about 0.1. The important analysis results for FOM 1 are shown in Fig. 10.

— *RPV failure time (FOM 2):* main parameter which affect the RPV failure is SC3200_1 having very strong negative correlation about less than –0.7. This parameter deals as multiplier of decay heat having strong negative correlation indicates that the larger decay heat which leads to the faster boiling, uncovery of coolant and ultimately RPV failure. Magnitude of the relevant parameters are relatively lower than those of SC3200_1, radioactive exchange factor form the cell boundary to the next adjacent cell for radiation radially outward (FCELR) and axially upward (FCELA), Heat transfer coefficient from debris to penetration structures (HDBPN) as larger HDBPN results strong heat transfer and early RPV failure, Radial relocation model parameter (SC1020_2) deals with relocation of both molten material and solid particulate debris from ring to ring as higher SC1020_2 causing delay in relocation of molten corium to the lower head, Failure temperature of the penetrations (TPFAIL) causing positive correlation as higher its value determines early RPV failure. Core melt breakthrough candling parameter (SC1141_2) with positive correlation and core component failure parameter (SC1131_2) deals with the temperatures used in extended failure criteria for fuel after the Zr has melted and candled with negative correlation related to FOM 2. The important analysis results for FOM 2 are shown in Fig. 11.

— *In-vessel H_2 generation (FOM 3):* main parameter which affects the in-vessel hydrogen generation is HDBPN having strong negative correlation about less than –0.4. This parameter deals with heat transfer coefficient from debris to penetration structures to determine their possible impact on lower failure by head heat transfer. DHYPD parameter is the second contributor that deals particulate debris equivalent diameters in core region with negative correlation of –0.2 magnitude. Higher value of DHYPD leading to decrease in-vessel hydrogen generation due to reduction in area-to-volume ratio. Magnitude of the relevant parameters having positive correlation are; core component failure parameter (SC1131_2) deals with the temperatures used in extended failure criteria for fuel after the Zr has melted and candled ranked at third contributor of +0.17 magnitude and failure temperature of the penetrations (TPFAIL) causing positive correlation of +0.16 magnitude. Parameters of minor positive effects on this FOM are radial relocation model parameters (SC1020_1), core melt breakthrough candling parameters (SC1141_2) and core component failure parameters (SC1132_1) having magnitude of measure is about 0.1. The important analysis results for FOM 3 are shown in Fig. 10.
— *Ex-vessel H_2, generation (FOM 4):* main parameter which affects the ex-vessel H_2, CO and CO_2 generation is SC3200_1 having strong positive correlation about greater than +0.5. This parameter is the multiplier for ANS decay heat curve. This sensitivity coefficient affects the heat transfer mechanism condition of in-vessel molten corium when injected in reactor cavity. Magnitude of the relevant parameters are relatively lower than those of SC3200_1. Particulate debris equivalent diameter (DHYPD) used in calculating total debris surface area, this diameter is of particular importance from the core to the lower plenum in the falling debris quench model having positive magnitude of +0.18 for these FOMs ranked at second important parameter. Radioactive exchange factor for radiation form the cell boundary to the next adjacent cell radially outward (FCELR) and axially upward (FCELA) has positive magnitude +0.1 for these FOMs. HDBPN having strong negative correlation which is less than –0.2 deals with heat transfer coefficient from debris to penetration structures to determine their impact on lower head heat transfer and failure while core melt breakthrough candling parameter (SC1141_2) with negative correlation of –0.1 magnitude. The important analysis results for FOM 4, FOM 5 and FOM 6 are shown in Fig. 11.
— *Ex-vessel CO and CO_2 generation (FOM 5 and FOM 6):* the main parameter which affects the ex-vessel, CO and CO_2 generation is SC3200_1 having strong positive correlation about greater than +0.5. Particulate debris equivalent diameter (DHYPD), this diameter is of particular importance from the core to the lower plenum in the falling debris quench model having positive magnitude of +0.18 for these FOMs is ranked at second important parameter. Radioactive exchange factor for radiation form the cell boundary to the next adjacent cell radially outward (FCELR) and axially upward (FCELA) has positive magnitude +0.1 for these FOMs. HDBPN having strong negative correlation which is less than –0.2 deals with heat transfer coefficient from debris to penetration structures to determine their impact on lower head heat transfer and failure while core melt breakthrough candling parameter (SC1141_2) with negative correlation of –0.1 magnitude. The important analysis results for FOM 5 and FOM 6 are shown in Fig. 11.

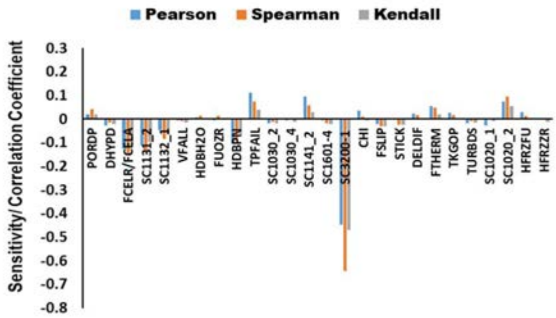

(a) Core uncovery (FOM1)

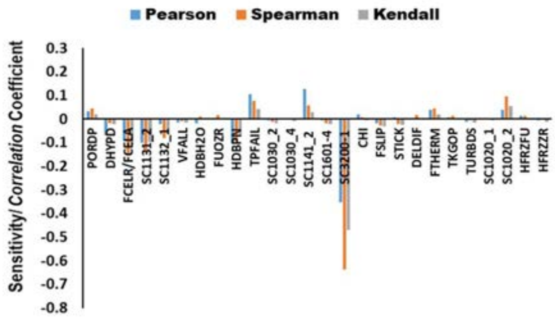

(b) RPV failure time (FOM2)

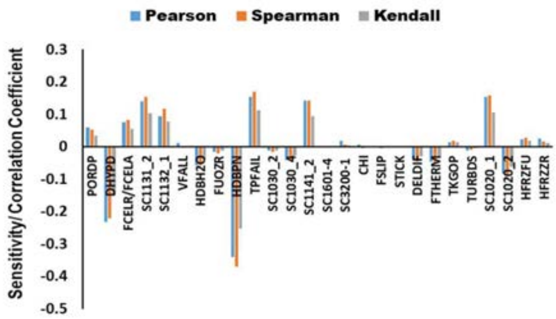

(c) In-vessel H_2 generation (FOM3)

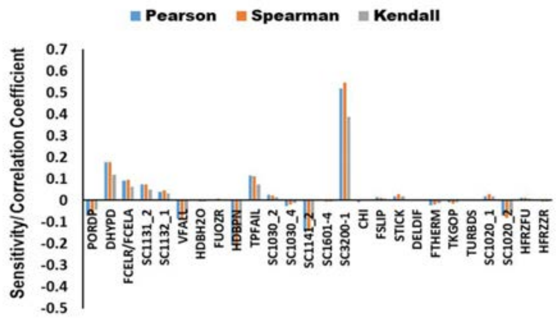

(d) Ex-vessel H_2 generation (FOM4)

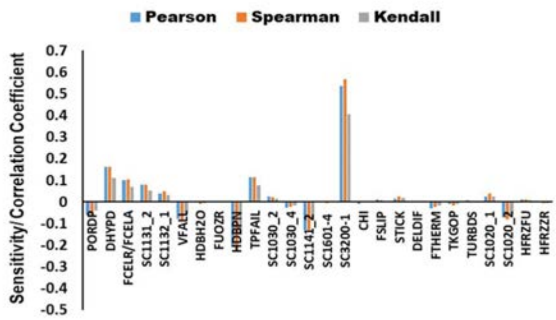

(e) Ex-vessel CO generation (FOM5)

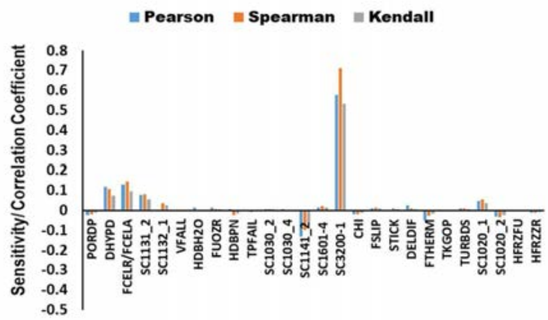

(f) Ex-vessel CO_2 generation (FOM6)

FIG. 11. Dependency of FOMs 1–6 on selected parameters for K-2 NPP case study.

— *CsI release to the environment (FOM 7):* main parameter which affects the CSI release to the environment is SC1141_2 having strong negative correlation about less than –0.3. This parameter deals with core melt breakthrough candling parameter. Magnitude of the parameters are relatively lesser than those of SC1141_2. The DHYPD used for debris surface area, this diameter is used in quench model for calculating the falling debris to lower plenum from core having positive magnitude of +0.18 for this FOM ranked at second important parameter. SC3200_1 have negative correlation about less than –0.15 is the multiplier for ANS decay heat curve and affects the heat transfer mechanism for corium when entered in reactor cavity ranked at third main parameter. Core component failure parameter (SC1131_2) deals with the temperatures at which failure criteria for fuel after the Zirconium has melted and candled ranked at fourth contributor of +0.12 magnitude on this FOM. The important analysis results for FOM7 are shown in Fig. 12.

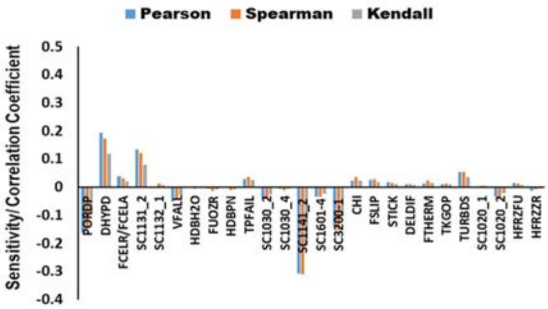

(g) CsI generation (FOM7)

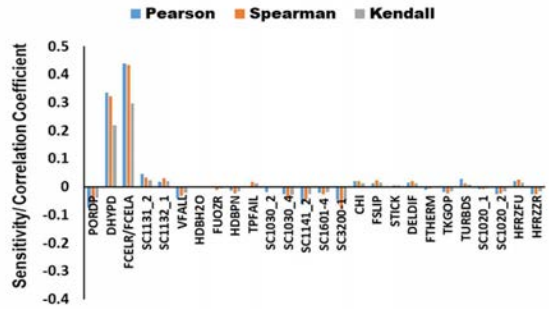

(h) Cs generation (FOM8)

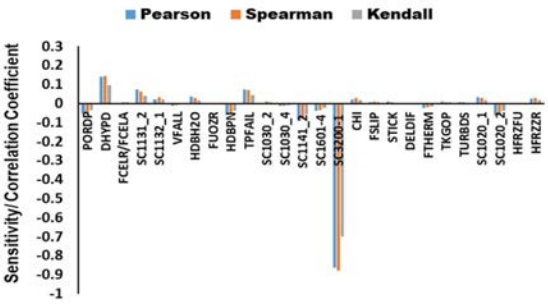

(i) Containment breach time (FOM9)

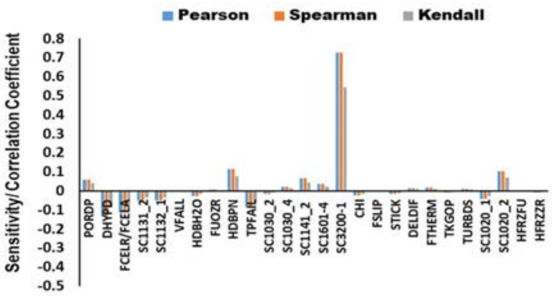

(j) Activity release to environment (FOM10)

FIG. 12. Dependency of FOMs 7–10 on selected parameters for K-2 NPP case study.

— *Cs release to the environment (FOM 8):* main parameter which affects the release to environment is FCELR/FCELA having strong positive correlation about greater than +0.45. This parameter deals as radioactive exchange factor for radiation form the cell boundary to the next adjacent cell radially outward (FCELR) and axially upward (FCELA). Particulate debris equivalent diameter (DHYPD) used in calculating total debris surface area, this diameter is of particular importance from the core to the lower plenum in the falling debris quench model having positive magnitude of +0.33 for this FOM ranked at second most important parameter. The important analysis results for FOM 8 are shown in Fig. 12.

— *Containment breach time (FOM 9):* main parameter which affects containment breach time is SC3200_1 having strong negative correlation about less than –0.9. This parameter used as multiplier of decay heat having strong negative correlation indicates that the larger decay heat which leads to the faster boiling, uncovery of coolant and ultimately containment failure. Magnitude of the relevant parameter is relatively lower than those of SC3200_1. Particulate debris equivalent diameter (DHYPD) used in calculating total debris surface area, this diameter is of particular importance from the core to the lower plenum in the falling debris quench model having positive magnitude of +0.12 for this FOM. The important analysis results for FOM 9 are shown in Fig. 12.

— *Activity release to environment (FOM 10):* main parameter which affects activity release to environment is SC3200_1 having strong positive correlation about greater than +0.7. This parameter used as multiplier of decay heat having strong negative correlation indicates that the larger decay heat which leads to the faster boiling, uncovery of coolant and ultimately containment failure causing release of activity in the environment. HDBPN having positive correlation greater than +0.11 deals with heat transfer coefficient from debris to penetration structures and to determine their impact on heat transfer to lower head of reactor pressure vessel and its failure. It has been ranked at second most important parameter for this FOM. The important analysis results for FOM 10 are shown in Fig. 12.

2.3.1.7. Summary and conclusions

Uncertain parameters were sampled randomly to produce 2,548 MELCOR simulations to identify the range of their predicted variations. The spectra of FOM provide more appropriate safety threshold as compared to conservative model and assumptions. Potential improvements attain from the behaviour of FOMs were identified to improve the accident scenario timing such as lower head failure of RPV etc. Such improvements provide better understanding and accuracy for severe accident analysis and management.

<u>Main sources of uncertainty resulting from the analysis</u>: behaviours of uncertain parameters are different for each FOM. Ranking of uncertain parameters provides the range of effect on particular FOM. SC3200_1 having strong correlation and act as main contributors to mostly FOMs. This parameter deals as multiplier of decay heat and indicates that the larger decay heat which leads to the faster boiling, uncovery of coolant and ultimately containment failure causing release of activity in the environment.

<u>Lesson learned and best practices</u>: magnitude of variances is assessed for the results of FOMs during uncertainty and sensitivity analysis. Numerical imprecision anticipation in reactor pressure vessel damage helps to identify a complete spectrum of identifications in potential barrier damage. The best estimated model and values with uncertainty treatment in comparison with worst case scenarios, assumptions and values provide much better understating of safety and regulatory limits for severe accidents. Most of the parameters selected for uncertainty/sensitivity analysis showed a very nominal/negligible impact on the FOMs, in future work these parameters can be omitted and detail analysis can be made for higher impacting parameters only.

2.3.2. Egyptian Nuclear and Radiological Regulatory Authority (ENRRA)

The ENRRA based the accident analysis using the German-type PWR plant of 1,300 MWe. Description of this plant specifics, accident scenarios analysed, applied models and approaches, and summary of the results are provided in the following sections.

2.3.2.1. Motivation and objectives

It was necessary to develop methods to quantify the uncertainty during normal and accident conditions [6, 26] following the recommendations from the IAEA to apply uncertainty and sensitivity analysis when using best-estimated codes (BEPU) (IAEA, 2002). In this study, one of the most important issues that face the regulatory bodies when performing uncertainty analysis for nuclear reactor parameters under accident conditions is addressed. This problem arises from the long computational time the statistical sampling method takes in calculating the uncertainty. The problem is addressed by introducing an algorithm called the unscented transform which uses the LRA. The sigma points that are generated by the combination of these algorithms are representative of the probability distribution as a whole. An uncertainty analysis generally takes one of two approaches. First is the deterministic technique which computes sensitivity coefficients for a response and uses adjoint-based perturbation theory to determine sensitivity coefficients, these sensitivities are multiplied by the covariance matrices to calculate the uncertainties (sandwich formula). The perturbation theory is categorized into two types: the classical and the generalized perturbation theories (Gandini, 1967).

Statistical random sampling is the second approach. In this technique, all input data is perturbed simultaneously, in order to determine the total uncertainty in every output response as a result of all input data uncertainties. Two main methods can be distinguished: SRS and stratified sampling (such as LHS), [27]. The Sobol method can be used to deduce sensitivity coefficients, however, it requires a huge number of simulation runs to get a full set of sensitivity coefficients [28]. Even if the sampling-based uncertainty analysis is relatively straightforward, it is computationally expensive because calculations have to be repeated *N*-times, where the sample size "*N*" depends on the confidence level, the minimum acceptable level of precision, etc., [29].

A primary objective is to reduce the calculation time that is required by statistical techniques to calculate uncertainty during the accident with the required accuracy. In the current work, a novel method has been established to decrease the computational time by using the unscented transform algorithm and SVD. The unscented transform and SVD algorithms are integrated to generate a minimal set of precisely selected sample points that entirely capture the real mean and covariance of the input variables although the detailed probability distribution is not estimated. This technique is named SVD/UT. Further reducing computation time is achieved using the LRA by revealing the active subspace and by reducing the order of the covariance matrix [30], which is referred to as the LRA/UT method. While the LRA has been used in nuclear engineering before, it has been separately implemented. This work combines the LRA technique with the unscented transform algorithm in order to further reduce computation time during accident conditions in nuclear power plants. For the purpose of verifying this method, the uncertainties calculated by the unscented transform algorithm based on SVD and LRA/UT are compared with that calculated using normal random sampling.

The purpose of this study is to quantify the uncertainty in LBLOCA in PWRs without control rod insertion, thus termed by regulatory bodies as beyond design basis accidents. A significant negative reactivity coefficient is observed during the LBLOCA. This is caused by the large void fraction produced by the rapid cooling in the primary coolant. As a result of the large negative reactivity of the anticipated transient without scram, even if no control rods were inserted, the reactor would still be shut down safely. As a result, the variables of uncertainty are the reactivity coefficients of the coolant density, and the variables of response are the peak temperatures of the clad during the accident.

The uncertainty associated with the reactivity coefficients of coolant density has a variety of reasons, such as nuclear data uncertainty and approximations used in the numerical methods. Among the sources of uncertainty, only nuclear data is taken into account. Since nuclear data have quite different sensitivities for lower and higher densities of coolant, the degree of uncertainty of the reactivity coefficient varies with coolant density. In addition, the uncertainties for different coolant densities are correlated; because the uncertainty source is the same (nuclear data). In order to perform a realistic analysis, not only the variance, but also the covariance of the reactivity coefficients of coolant density should be considered. Therefore, the SCALE 6.2 code is used to calculate the means and relative covariance matrix of the coolant density reactivities, to consider uncertainties of nuclear data [15]. The thermal-hydraulic calculations are performed by using the ATHLET code [6] in calculating the peak cladding temperatures, this is done by entering reactivity coefficients as input tables.

2.3.2.2. *Description of the relevant plant*

The uncertainties are quantified for the German-type PWR of 1,300 MWe (KWU-PWR) plant as shown in Table 10.

TABLE 10. DESIGN CHARACTERISTICS OF GERMAN-TYPE PWR POWER PLANT (KWU-PWR)

Parameter	**Value**
Primary system	
Number of coolant loops	4
Core flow rate	18.8 t/s
Coolant pressure	15.8 MPa
Coolant inlet temperature	292 °C
Coolant outlet temperature	326 °C
Soluble poison in coolant	Boric acid
Reactor power	
Plant thermal efficiency	32.8 %
Thermal	3780 MWt
Electric	1300 MWe
Secondary system	
Steam pressure	6.4 MPa
Steam temperature	285 °C
Reactor core	
Fuel type	UO_2
^{235}U fuel enrichment	3.5–4.5 wt.%
Cladding material	Zircaloy-4
Equivalent core diameter	3.6 m
Active core height	3.9 m
Number of fuel assemblies	193
Fuel rod array	16x16
Number of fuel rods per fuel assembly	236
Number of control rods per fuel assembly	236
Absorber material	Ag, In, Cd and B_4C
Fuel rod	
Fuel rod pitch	1.43 cm
Cladding outer radius	0.528 cm
Cladding thickness	2.0×10^{-4} cm
Fuel rod radius	0.455 cm

2.3.2.3. *Accident scenarios and severe accidents code*

The goal of this study is to quantify the uncertainty that occurs during a LBLOCA scenario without control rod insertion, which is classified as beyond design basis accidents by the regulatory body. Because of the rapid depression in primary coolant during the LBLOCA, the reactivity coefficients are remarkably negative (due to the large void fraction). The thermal hydraulics calculations are carried out using the ATHLET code, while the input reactivities and correlation matrices are calculated using the SCALE 6.2 code [9].

The in-house code, developed at Nagoya University in Japan, is used to carry out uncertainty and sensitivity analyses. In addition, we have developed a Python script to calculate reactivities perturbed values by using normal random, SVD/UT, and LRA/UT sampling, also used to combine different calculations, generating and running *N*-size ATHLET inputs files, reading and extracting the results, execute interpolation, and analyzing uncertainty and sensitivity.

2.3.2.4. Plant modelling and nodalization

In the thermal hydraulics simulation, the break is assumed to be in the cold leg of one loop (loop-2) whereas the other three circuits are lumped together as one intact loop (loop-1) as shown Fig. 13.

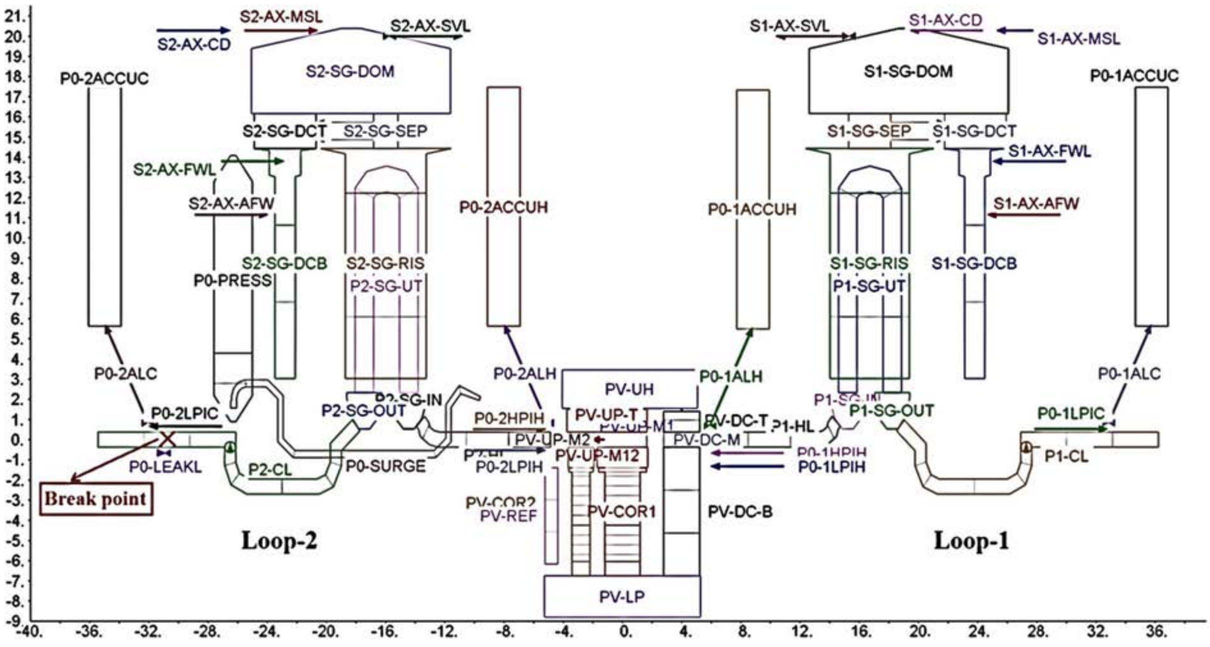

FIG. 13. ATHLET nodalization of KWU-PWR.

The LBLOCA scenario is as follows: after 60 s of steady state, an accident scenario assumes a large break in the cold leg (having a cross-section area of 0.11 m^2). As soon as the primary pressure reaches 13.2 MPa, the scram signal is activated, resulting in the stoppage of the main and auxiliary feed water pumps. In this study, the external reactivity is assumed to be zero, based on the assumption that either there is no scram signal is activated or the control rods are all stuck over the reactor core. After the primary circuit pressure falls to about 10.03 MPa, the high-pressure injection system automatically gets activated. When the pressure drops to about 2.5 MPa, the accumulators are turned on, thereafter, the low-pressure injection systems are activated at 1.07 MPa.

LBLOCA without control rod insertion is an important scenario, since the large negative reactivity coefficient insures a safe shut down of the nuclear reactor regardless of whether the control rods are inserted. Therefore, the coolant density reactivities are the input variables with uncertainty while the peak cladding temperatures are the response variables (FOM).

2.3.2.5. Uncertainty and sensitivity analysis methodology

Uncertainty analysis methodology: in the estimation of uncertainty, Monte Carlo approaches are considered the most reliable technique, which can be used for any code. The calculations should be performed *N* times, where *N* represents the sample size. Wilks estimator can be used to determine the minimum size of a random sample where the probability that the sample maximum is greater than a particular α-percentile is calculated as follows [12, 13]:

$$1-\alpha^N-N(1-\alpha)\alpha^{N-1}\beta \tag{5}$$

where β is the confidence level. Wilks's formula is used only for motivation, to indicate that a minimum sample size of *N* is used to achieve the acceptance level of precision. In order to obtain more reliable results, more runs are necessary, resulting in longer processing times. Thus, an advanced method had to be applied to reduce the computational time. The unscented transform method dramatically reduced the amount of time spent on processing. The main idea is to reduce the computational time by decreasing the number of input data points needed to represent the actual mean and covariance. There are only *2L+1* inputs that need to be replicated, where *L* is the dimensions/size of the input data.

Unscented transformations are used to compute the statistics of random variables subject to a nonlinear transformation [31]. It has the advantage of being able to handle linear and non-linear systems [15, 16]. Unscented transformation generates a set of sigma points that represent the entire probability distribution.

The steps involved in the unscented transformation are described as follows:

— *Compute set of sigma points*

There are *2L+1* sigma points, where *L* indicates the input data dimension. Consider the random input variable $\boldsymbol{x}$ (L-dimension) that has a mean $\overline{\boldsymbol{xx}}$ and a covariance matrix $\boldsymbol{A}$, thus, matrix $\boldsymbol{\mathcal{X}}$ of *2L+1* sigma vectors $\boldsymbol{\mathcal{X}}_i$ is formed as follows:

$$\begin{gathered}\boldsymbol{\mathcal{X}}_0=\overline{\boldsymbol{xx}}\\ \boldsymbol{\mathcal{X}}_i=\overline{\boldsymbol{xx}}+(\sqrt{(L+\lambda)\boldsymbol{A}_{xx}})_i \qquad for\ i=1,\dots,L\\ \boldsymbol{\mathcal{X}}_i=\overline{\boldsymbol{xx}}-\left(\sqrt{(L+\lambda)\boldsymbol{A}_{xx}}\right)_{i-L}\ for\ i=L+1,\dots,2L,\end{gathered} \tag{6}$$

where λ is the scaling parameter (which indicates how far from the mean we should select the sigma points). As the parameter λ increases, the input value perturbations increase, resulting in a wider range of output variations. The SVD can be used to obtain the square root of matrix $\boldsymbol{A}$. The vector $(\sqrt{(L+\lambda)\boldsymbol{A}})_i$ represents the *i*-th vector of the matrix $\sqrt{\mathbf{A}}$ multiplied by γ, where γ= $\sqrt{L+\lambda}$.

— *Assign weights to each sigma point*

Sigma points' weights are computed as follows:

$$\omega_0 = \frac{\lambda}{L+\lambda} \tag{7}$$

$$\omega_i = \frac{1}{2(L+\lambda)}, \quad for\ i = 1, \ldots, 2L,$$

There is a different equation for the mean weight ω_0 than for the rest of the sigma points, where the summation of all the weights equals one ($\sum \omega_i = 1$). When $\lambda = \frac{1}{2}$, all weights are of the same value, these weights are used in this study.

— *Sigma points transformation and calculates mean and covariance*

These sigma points are then mapped to a target distribution by transmitting $\boldsymbol{\mathcal{X}}$ over a non-linear transformation,

$$\mathcal{Y}_i = f(\mathcal{X}_i), \qquad i = 0, \ldots, 2L \tag{8}$$

Following the non-linear transformation, you can calculate the mean and covariance of the results as follows:

$$\overline{\boldsymbol{y}} = \sum_{i=0}^{2L} \omega_i \mathcal{Y}_i$$
$$\boldsymbol{A_{yy}} = \sum_{i=0}^{2L} \omega_i (\mathcal{Y}_i - \overline{y\boldsymbol{y}})(\mathcal{Y}_i - \overline{y\boldsymbol{y}})^T \tag{9}$$

where $\overline{\boldsymbol{y}}$ and $\boldsymbol{A_{yy}}$ present the results mean and covariance matrix, respectively. Figure 14 shows the block diagram of the unscented transform algorithm.

The SVD that is used to obtain the matrix square root $\sqrt{\mathbf{A}}$ enables us in reducing the order of the covariance matrix, and results in an additional decrease in the sample size [32].

The main idea of SVD is that the covariance matrix can be described by its singular vectors. Furthermore, the SVD is more numerically robust in the unscented transformation than the Cholesky decomposition [33].

The singular value decomposition of a matrix $\boldsymbol{A}$ is:

$$\boldsymbol{A} = \boldsymbol{UU}\Sigma\Sigma\boldsymbol{VV}^T = \boldsymbol{UU}\Sigma\Sigma^{1/2}\Sigma\Sigma^{1/2}\boldsymbol{VV}^T \tag{10}$$

where $\boldsymbol{U}$ (eigenvectors of $\boldsymbol{AA}^T$) and $\boldsymbol{V}$ (eigenvectors of $\boldsymbol{A}^T\boldsymbol{A}$) form the basis for the column and row space of matrix $\boldsymbol{A}$, respectively, while the $\boldsymbol{\Sigma}$ is the diagonal matrix whose elements represent the singular values as shown in Fig. 15 [19, 20].

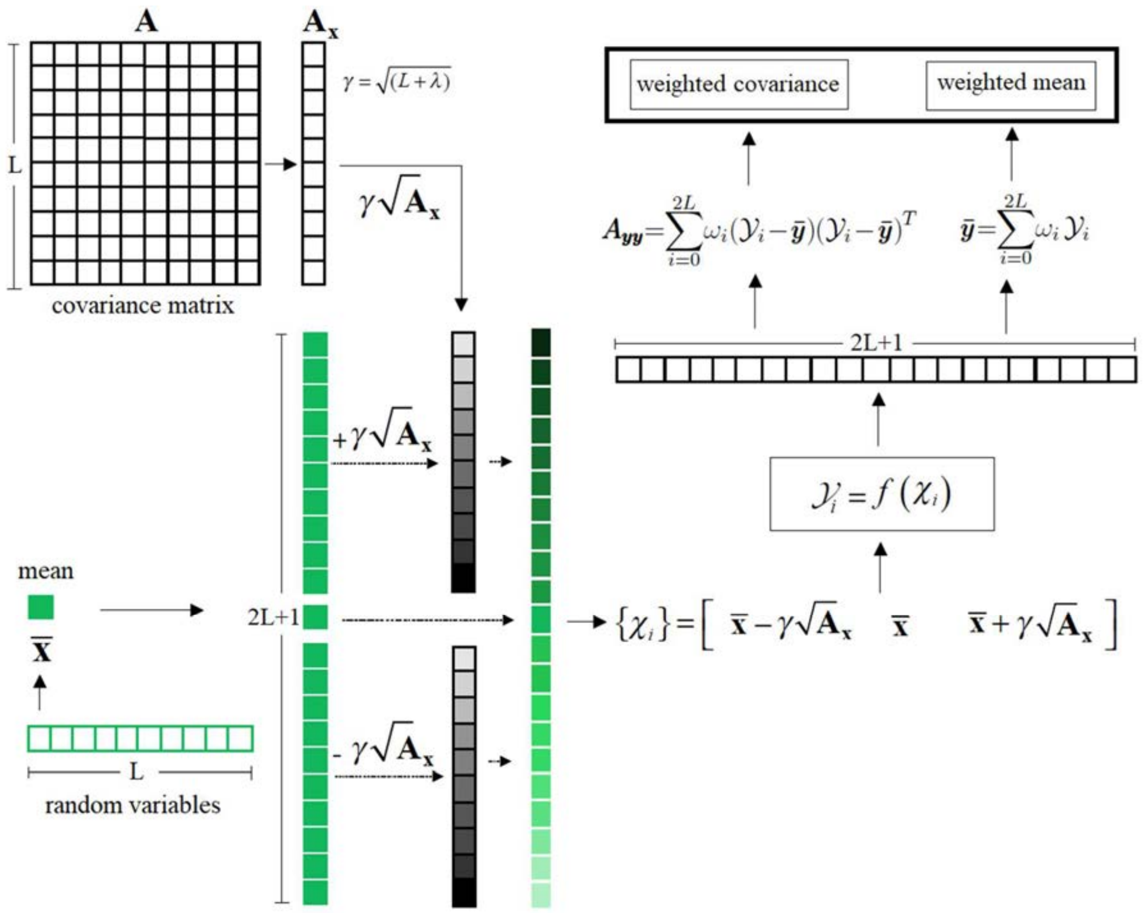

FIG. 14. Block diagram of the unscented transform algorithm.

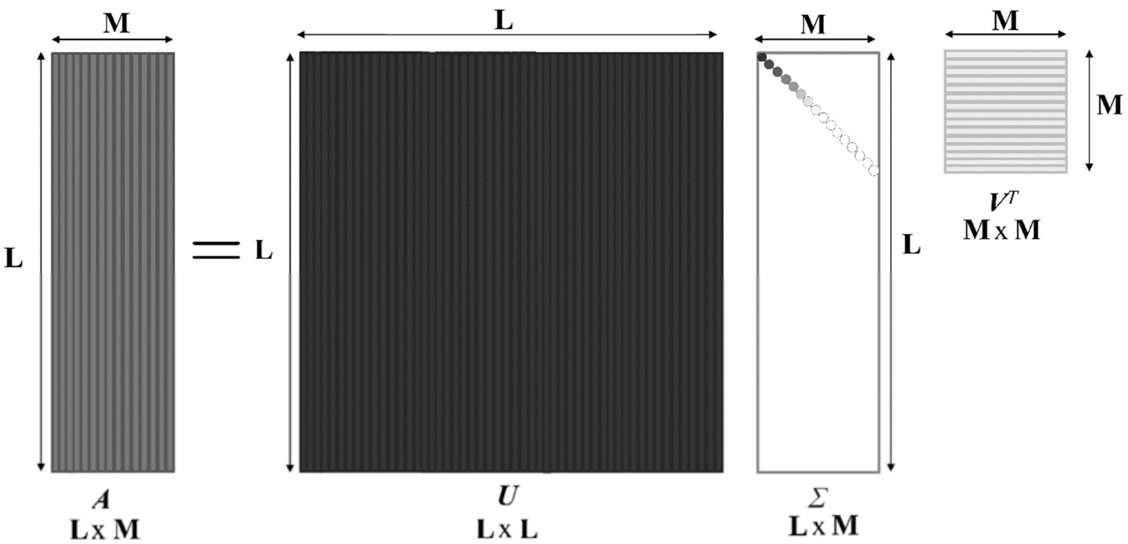

*FIG. 15. Graphical depiction of SVD of a matrix **A**.*

The diagonal elements of the matrix $\mathbf{\Sigma}$ are ordered so that $\sigma_{ii} > \sigma_{jj}$ for all $I < j$.

$$\boldsymbol{\Sigma} = \begin{pmatrix} \sigma_{11} & 0 & 0 & \cdots & 0 \\ 0 & \sigma_{22} & 0 & \cdots & 0 \\ 0 & 0 & \sigma_{33} & \cdots & 0 \\ \vdots & \vdots & \vdots & \ddots & 0 \\ 0 & 0 & 0 & 0 & \sigma_{mm} \end{pmatrix} \tag{11}$$

By multiplying $\boldsymbol{x}$ with $\mathbf{V}^{\mathrm{T}}$, the vector $\boldsymbol{x}$ will be projected on the row space, after which it is scaled by $\boldsymbol{\Sigma}$ along the coordinate axes, and finally rotated to the column space when multiplied by $\mathbf{U}$. The SVD decomposes any matrix into three transformations: a projected $\mathbf{V}^{\mathrm{T}}$, a scaling $\boldsymbol{\Sigma}$, and a second rotation $\mathbf{U}$, as represented in Fig. 16.

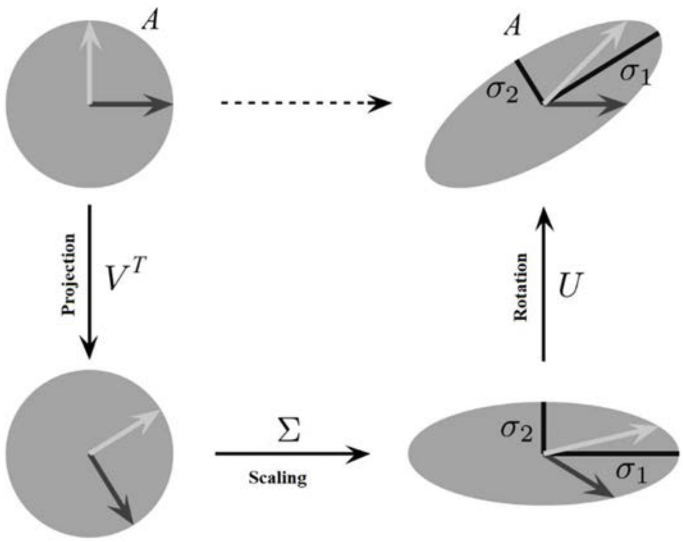

*FIG. 16. Transformations of matrix **A** by SVD.*

Due to the symmetry of the covariance matrix $\boldsymbol{\Sigma}$, the singular value decomposition can be defined as

$$\boldsymbol{A} = \boldsymbol{V}\boldsymbol{\Sigma}\boldsymbol{V}^T = \boldsymbol{V}\boldsymbol{\Sigma}^{1/2}\boldsymbol{\Sigma}^{1/2}\boldsymbol{V}^T \tag{12}$$

Accordingly, the matrix square root can be written as follows:

$$\begin{aligned} \sqrt{A\boldsymbol{A}} &= V\boldsymbol{V}\boldsymbol{\Sigma}\Sigma^{1/2} \\ \sqrt{A\boldsymbol{A}}^T &= \Sigma\boldsymbol{\Sigma}^{1/2}V\boldsymbol{V}^T \end{aligned} \tag{13}$$

The truncated SVD is one of the most effective techniques for reducing the computational cost, it can reduce the problem dimension by predicting the important degrees of freedom and calculating the basis of the active sub-space depending on its singular values [21, 22].

The $\boldsymbol{A}$ matrix in Eq. (10) can be expressed as the sum of the outer products of the $\boldsymbol{U}$ columns and the $\boldsymbol{V}^T$ rows, factorized by the singular values σ [34]:

$$A_{ij} = \sum_{g=1}^{r} \sigma_{gg} U_{ig} V_{jg}, \tag{14}$$

In this case, the number of non-zero singular values equals *r*. For some models, the number of degrees of freedom is large, thus the solution of Eq. (14) may be computationally expensive. Thanks to the robust correlation between input data, we can detect important degrees of freedom and reduce the input dimensions with satisfactory accuracy [30]. This method is called LRA and is described in Fig. 17. If truncating to *k*-active sub-space ($k < r$), thereafter, Eq. (14) can be minimized to:

$$(A_k)_{ij} = \sum_{g=1}^{k} \sigma_{gg} U_{ig} V_{jg}, \tag{15}$$

where σ_{gg} with higher order than *k* are neglected (i.e., $g > k$). The inputs dimensions are decreased to *k*, thereby the dimensions in Eq. () and Eq. (11) are *k* instead of *L* as follows:

$$\begin{aligned} \mathcal{X}_0 &= \overline{\boldsymbol{x}\boldsymbol{x}} \\ \mathcal{X}_i &= \overline{x\boldsymbol{x}} + (\sqrt{(k+\lambda)A_k\boldsymbol{A}_k})_i \qquad for\ i = 1, \dots, k \\ \mathcal{X}_i &= \overline{\boldsymbol{x}} - \left(\sqrt{(k+\lambda)A_k\boldsymbol{A}_k}\right)_{i-k} \quad for\ i = k+1, \dots, 2k \end{aligned} \tag{16}$$

$$\begin{aligned} \omega_0 &= \frac{\lambda}{k+\lambda} \\ \omega_i &= \frac{\lambda}{2(k+\lambda)}, \qquad for\ i = 1, \dots, 2k \end{aligned} \tag{17}$$

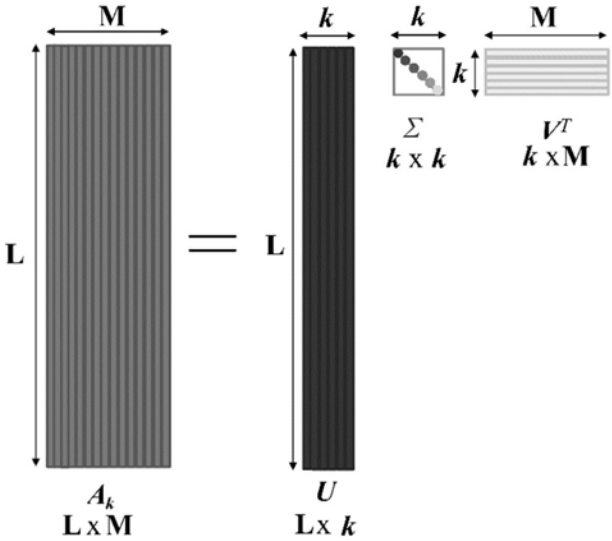

FIG. 17. Graphical representation of LRA matrix $\boldsymbol{A}_k$.

$\boldsymbol{A}_k$ is an approximation of the matrix $\boldsymbol{A}$; in order to evaluate the variance value expressed by the first k-spaces, one needs to compute the truncation coefficient as follows

$$E_k = \frac{\sum_{g=1}^{k} \sigma_{gg}}{\sum_{g=1}^{r} \sigma_{gg}} \tag{18}$$

To apply the SVD-UT and LRA-UT algorithms; it is necessary to calculate the mean and covariance matrix between the input parameters. Since uncertainties are calculated during the LBLOCA characterized by remarkable negative reactivity coefficients due to the large void fraction produced. Accordingly, the input parameters are the coolant density reactivities. TSAR and TSURFER modules of SCALE 6.2 are used to compute the input covariance matrix [6]. The correlations between different reactivities are also defined by:

$$corr(\rho_i, \rho_j) = \frac{cov(\rho_i, \rho_j)}{\sigma_{\rho_i}\sigma_{\rho_j}} = \frac{cov(\rho_i, \rho_j)}{\sqrt{var(\rho_i)var(\rho_j)}} \quad , \tag{19}$$

where ρ_i are the coolant density reactivity $\frac{\Delta k}{k}$, σ is the standard deviation, $var(\rho)$ is the variance, and $cov(\rho_i, \rho_j)$ the reactivity relative covariance matrix is calculated by the following sandwich formula [35]:

$$cov(\rho_i, \rho_j) = \sigma^2_{\rho_i,\rho_j} = \boldsymbol{ss}(\rho_i) \cdot V\boldsymbol{V} \cdot ss(\rho_j)^T, \tag{20}$$

where $\boldsymbol{V}$ is the covariance matrix and $\boldsymbol{s}$ is the sensitivity of reactivity coefficients (eigenvalue-difference) defined by [6]:

$$s_{i,j,g}(\rho) = \frac{\frac{1}{k_2} \cdot ss_{i,j,g}(k_2) - \frac{1}{k_1} \cdot ss_{i,j,g}(k_1)}{\rho_{1\to 2}} \tag{21}$$

$ss_{i,j,g}(k_1)$ and $ss_{i,j,g}(k_2)$ are the cross-section sensitivity coefficients of the k_{eff} (in nuclide i, reaction j, energy-group g) for two different coolant densities or fuel temperatures (calculated from a TSUNAMI module, where state 1 is the nominal state).

<u>Uncertainty and sensitivity calculation scheme and relevant tool</u>: following is the description of the overall calculation steps summarized in Fig. 18:

— TSUNAMI module is used to compute k_{eff} sensitivity coefficients for 14 states (14 coolant densities), after that TSAR module was used to calculate sensitivities of reactivities responses, then TSURFER module was used to calculate the correlated matrix. Multivariate sampling is used to generate N-size samples for normal random sampling. For SVD/UT sampling, the SVD algorithm will be used to compute the singular vectors of covariance matrix $\boldsymbol{A}$, generating $2L+1$ sigma samples. Otherwise, the LRA/UT is applied to truncate the k-active subspace and reduce the sample size to $2k+1$ sigma points.
— The reactivities are then entered as input parameters into the ATHLET code to compute the results.

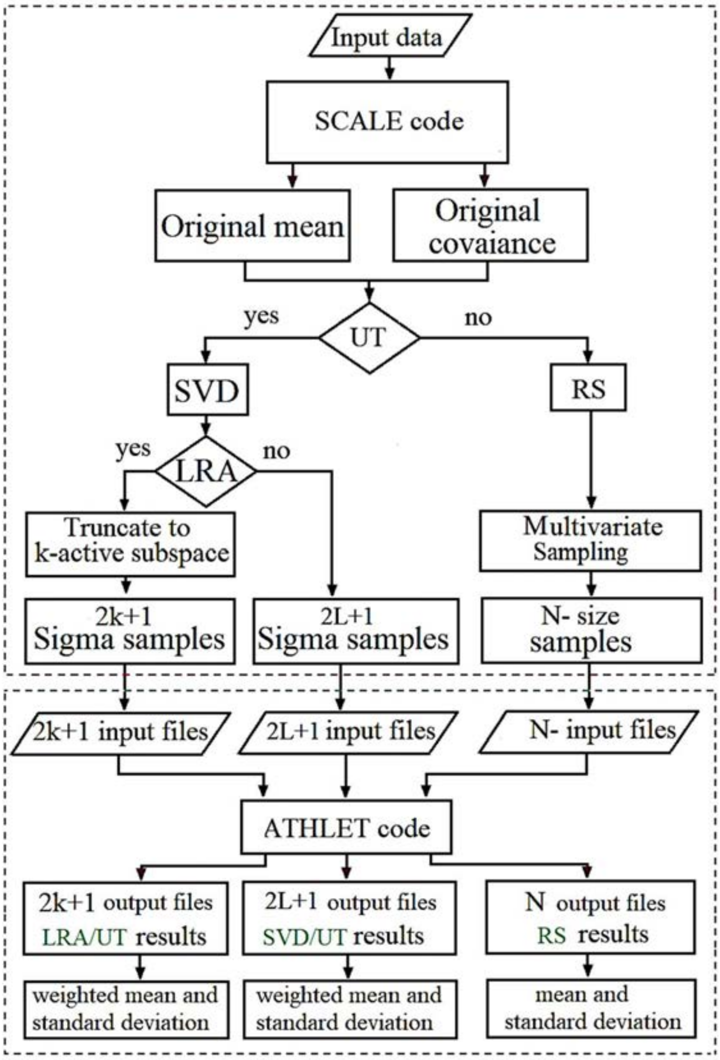

FIG. 18. Calculation steps applied to the three sampling algorithms.

<u>Uncertain parameters and related probability distributions:</u> the input uncertainty parameters are the reactivity coefficients of the coolant density, and the output response parameters (FOM) are the peak cladding temperatures during the accident. The PDFs have the multivariate Gaussian/normal distributions defined as:

$$P(x;\overline{x},\Sigma) = \frac{1}{(2\pi)^{\frac{n}{2}}|\Sigma|^{\frac{1}{2}}}\exp\left(\frac{1}{2}(x-\overline{x})^T\Sigma^{-1}(x-\overline{x})\right), \tag{22}$$

where x is the distributed Gaussian with mean $\overline{x}$ and covariance matrix Σ have given in the SCALE nuclear data covariance library. It is possible to generate a set of random dependent variables by using a vector of random independent numbers with average *0* and mean *1* based on the multivariate normal distribution using the following formula:

$$G\boldsymbol{G}(\overline{\boldsymbol{xx}},A)\boldsymbol{A}) = A\boldsymbol{A}^{1/2}G(0,1)\boldsymbol{G}(0,1) + \overline{\boldsymbol{xx}}, \tag{23}$$

where $\boldsymbol{G}(\overline{\boldsymbol{x}}, A)\boldsymbol{A})$ is a vector of random dependent variables with absolute covariance $\boldsymbol{A}$, $\boldsymbol{G}(0,1)$ is a *N*-vector of random independent variables, where *N* is the sample size, and $\overline{\boldsymbol{x}}$ is a vector of average values.

The square root of $\boldsymbol{A}$ can be solved using the SVD. The covariance is normally given as relative covariance so to use Eq. (23) we can instead generate a vector of perturbation factors which are essentially just a vector of dependent variables with relative covariance $\boldsymbol{A}_r$ where all of the average values are equal to 1.

$$Q\boldsymbol{Q} = A\boldsymbol{A}_r^{1/2}G(0,1)\boldsymbol{G}(0,1) + [1.0,1.0,1.0,\ldots1.0]^T \tag{24}$$

The perturbation factors $\boldsymbol{Q}$ can then be multiplied by a vector of average values to create a vector of random dependent variables centered on those average values.

$$G\boldsymbol{G}(\overline{\boldsymbol{x}\boldsymbol{x}}, A)\boldsymbol{A}) = Q\boldsymbol{Q} \cdot \overline{x\boldsymbol{x}} \tag{25}$$

In this study, there are fourteen values for the moderator density reactivities are considered. There are four values that demonstrate expansions in coolant densities (from 10% to 40% increase in the coolant density). Though ten values represent the contraction (from 10% to 99% decrease in the coolant densities).

2.3.2.6. Results

<u>*Reference case results*</u>: the total core power and pressure calculated by the ATHLET code are shown in Fig. 19. Due to the break in the cold leg, the pressure suddenly falls at 60 s, resulting in a rapid decline in the core power because of the negative coolant density reactivities. Figure 20 illustrates the reactivity components due to the coolant density, Doppler effect, boron, and total reactivities.

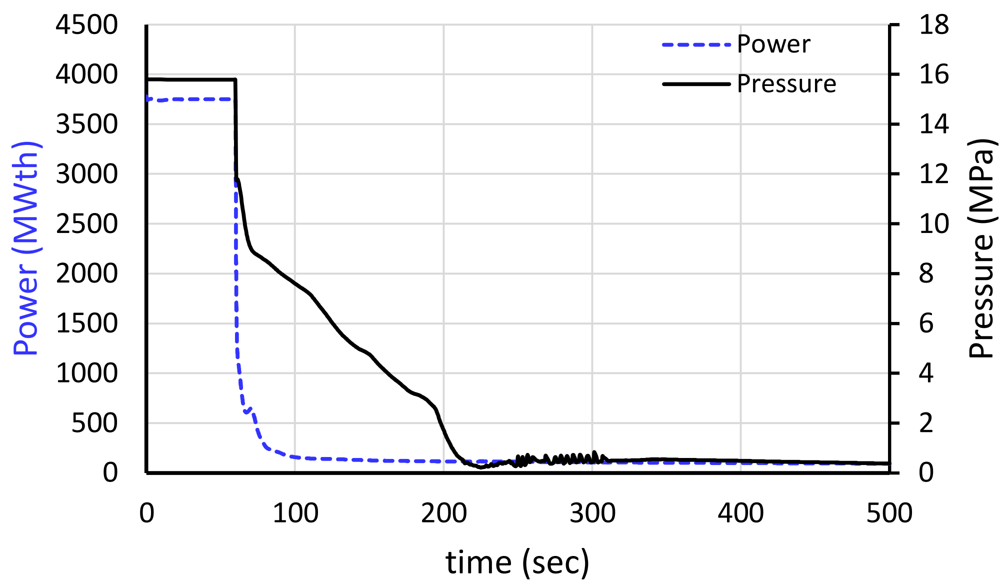

FIG. 19. Total power (MWt) generated in the core and pressure (MPa).

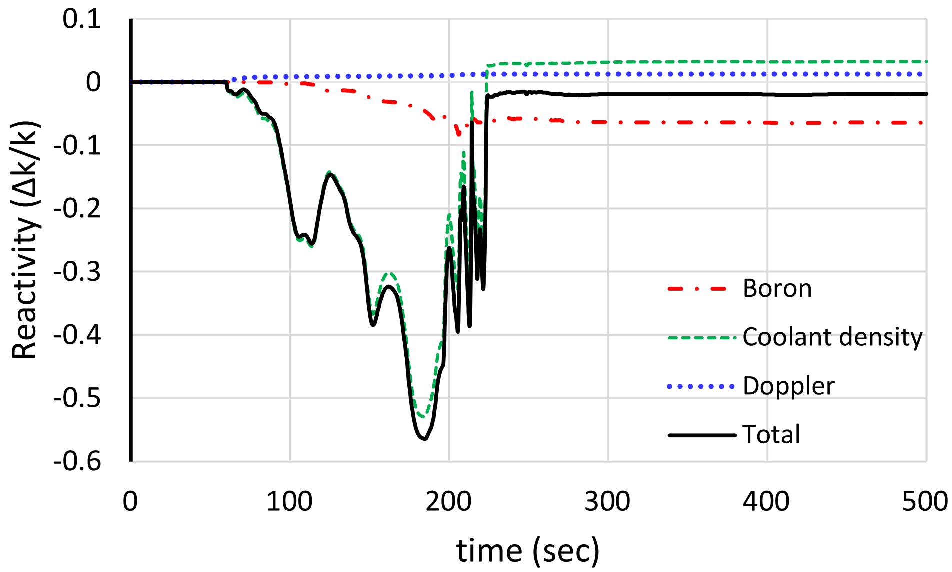

FIG. 20. Reactivity contributions in the core ($\frac{\Delta k}{k}$).

In the initial stage, the fuel temperature decreases due to a rapid decrease in core power as shown in Fig. 21. The scram signal is activated when the pressure falls to 13.2 MPa (0.5 s later), accordingly, the core power increases slightly (see Fig. 18 for power shoulder at 65 s) due to the increment of the coolant density. The coolant density increases because of the reversal of the coolant flow through the broken loop following the stoppage of the main pump. Figure 22 displays the core coolant's average density and the mass flow rate at the junction between the cold leg of the broken loop and the core's coolant inlet.

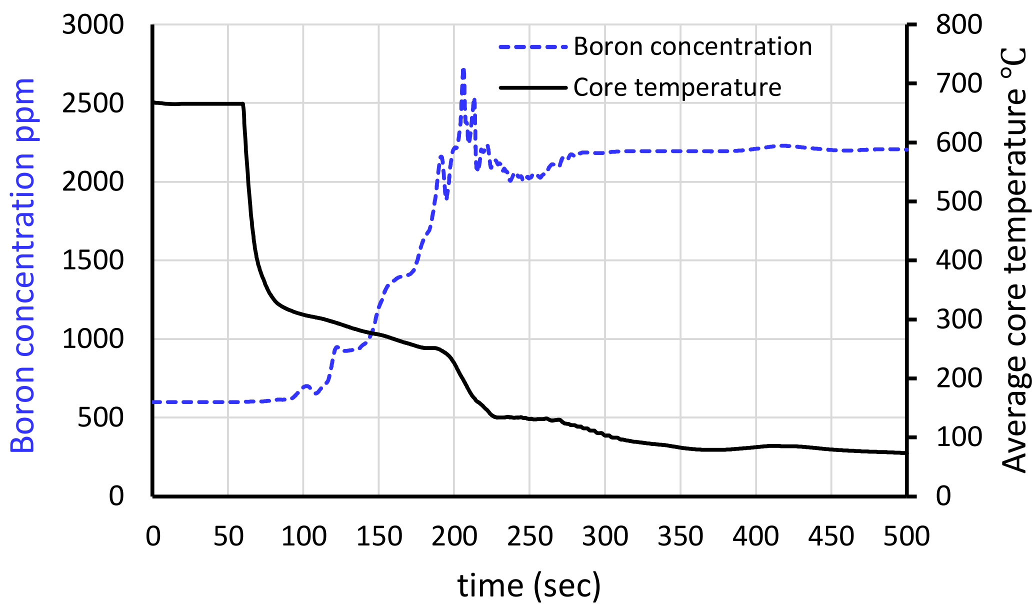

FIG. 21. Boron mass fraction (ppm) and average fuel temperature (°C).

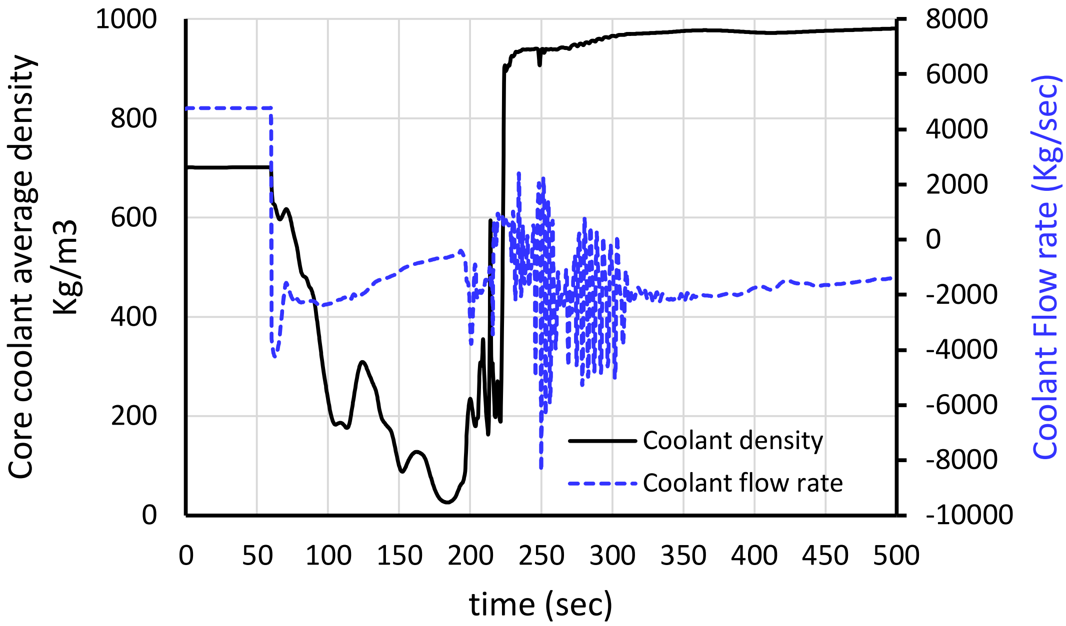

FIG. 22. Average coolant density and mass flow-rate in the cold leg of the broken loop.

When the pressure in the primary circuit drops to 10.03 MPa at 66 s, consequently, the high-pressure injection system is activated causing the boron concentration to increase as can be seen in Fig. 20 leading to an increase in boron reactivity. More negative reactivity is inserted as a result of decreased coolant density, which is much greater than the Doppler positive reactivity. In accordance with the expectations, the total negative reactivity coefficient comes mainly from the coolant density reactivity, due to the loss of coolant, which reaches about -0.53 $\frac{\Delta k}{k}$ at 180 s. At 190 s, the accumulator is automatically activated when the core pressure drops to 2.5 MPa, adding 2,200 ppm of borated water (as seen in Fig. 20) leading to an increment of the negative reactivity coefficients. On the other hand, the negative coolant density reactivity decreases due to coolant recovery as a result of accumulators. Finally, the primary core pressure drops to 1.07 MPa and the LPI signal is activated at 205 s.

<u>Uncertainty estimation of input parameters</u>: the input reactivities and covariance matrices are calculated using the SCALE 6.2 code, with a nominal coolant density of 700 kg/m^3. The ^{235}U enrichment in the typical PWR fuel cell is 4.5% ^{235}U. The ENDF/B-VII.1 nuclear data is used in the calculation (252 energy-groups). In this study, the model has a dimension of 14, four values demonstrate expansions in coolant densities (from 10% to 40% increase in the coolant density). Though ten values represent the contraction (from 10% to 99% decrease in the coolant densities). Figure 23 demonstrates the uncertainty in reactivity coefficients (represented by the relative standard deviation, for a 40% expansion in coolant density, the uncertainty is 2.36% $\frac{\Delta\rho}{\rho}$ and it increases as the coolant density decreases, the maximum uncertainty is about 6.11% $\frac{\Delta\rho}{\rho}$ for a 99% decrease in coolant density. The main contributor to this uncertainty is the ^{238}U inelastic cross-section, which is about 5.09% $\frac{\Delta\rho}{\rho}$ for a 99% decline in the coolant density [36]. The reactivities correlation matrix is illustrated in Fig. 24 where the correlation between the different reactivity coefficients is strongly positive.

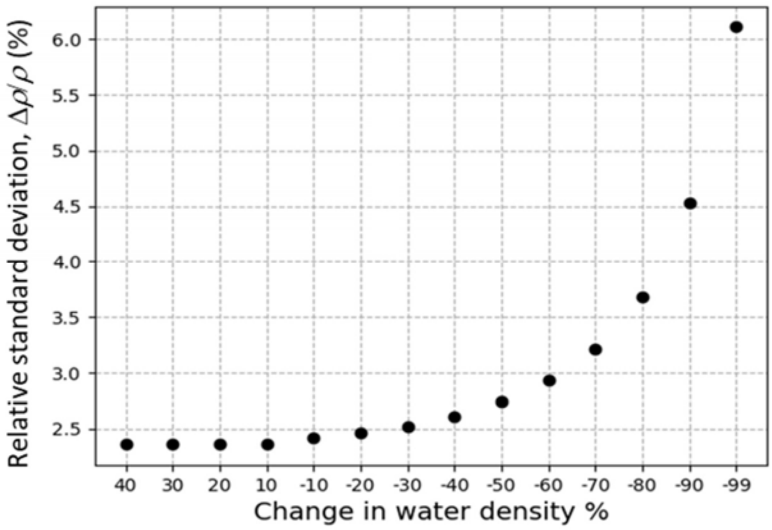

FIG. 23. Relative standard deviation of reactivity as a function of water density change.

Three different methodologies are used to compute uncertainties, normal random sampling and SVD/UT, and the LRA/UT techniques. For the normal random sampling, the sample size is 150 to assure a 98% confidence interval with a 95% probability (based on Wilks formula). For the SVD/UT technique, the number of sigma points is $N = (2n+1) = 2\times14+1 = 29$, where n is the model's dimensions. Finally, for the LRA/UT algorithm, the truncation coefficient is calculated to identify the k-active subspace and decide the sigma points as illustrated in Fig. 24. The first two singular-values demonstrate 99.82% of the model behavior, thus, the dimension can be reduced to only two where the number of sigma points drops to $N = (2k+1) = 2\times2+1 = 5$.

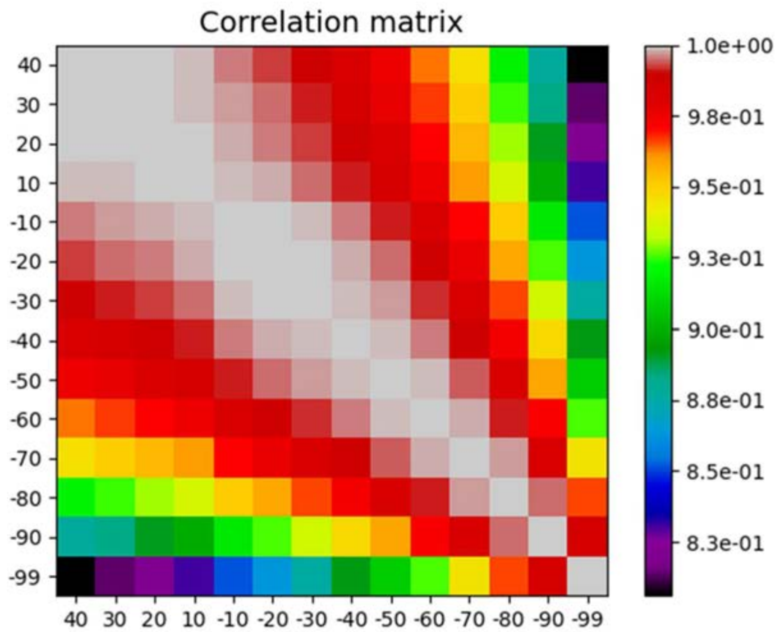

FIG. 24. Reactivity correlation matrix.

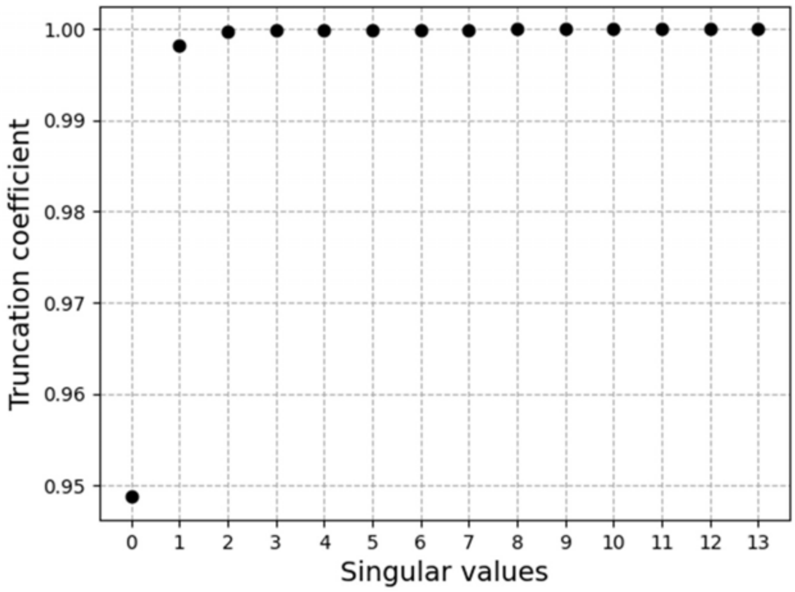

FIG. 25. Truncation coefficient.

The differences between the input mean and sample mean of the coolant density reactivity coefficients using random sampling (refer to the random sampling as the reference value), SVD/UT, and LRA/UT sampling techniques are shown in Fig. 26. For random sampling method, the differences have the order of −5 and dropped to −17 and −16, when using the SVD/UT and LRA/UT sampling, respectively.

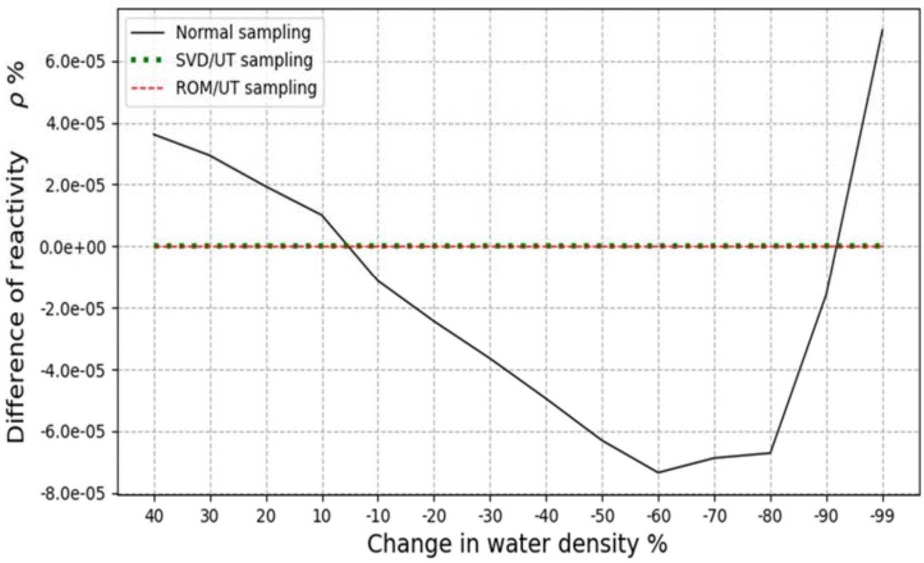

FIG. 26. Difference between the input and sample means of coolant density reactivity.

Figure 27 (a) represents the input relative covariance matrix; the relative covariance between 40% reactivities is about 5.57×10^{-4}, and it increases with decreasing the coolant density reaching 3.74×10^{-3} between −99% reactivities. Figures 27 (b)–(d) explain the relative difference between the input and sample covariance matrices using RS, SVD/UT, and LRA/UT sampling, respectively. All three methods are able to reproduce the input covariance matrix accurately, but the differences are approximately −2 for random sampling and it drops to −5 for SVD/UT sampling. By applying the LRA to the singular value matrix, the differences reach orders of −3.

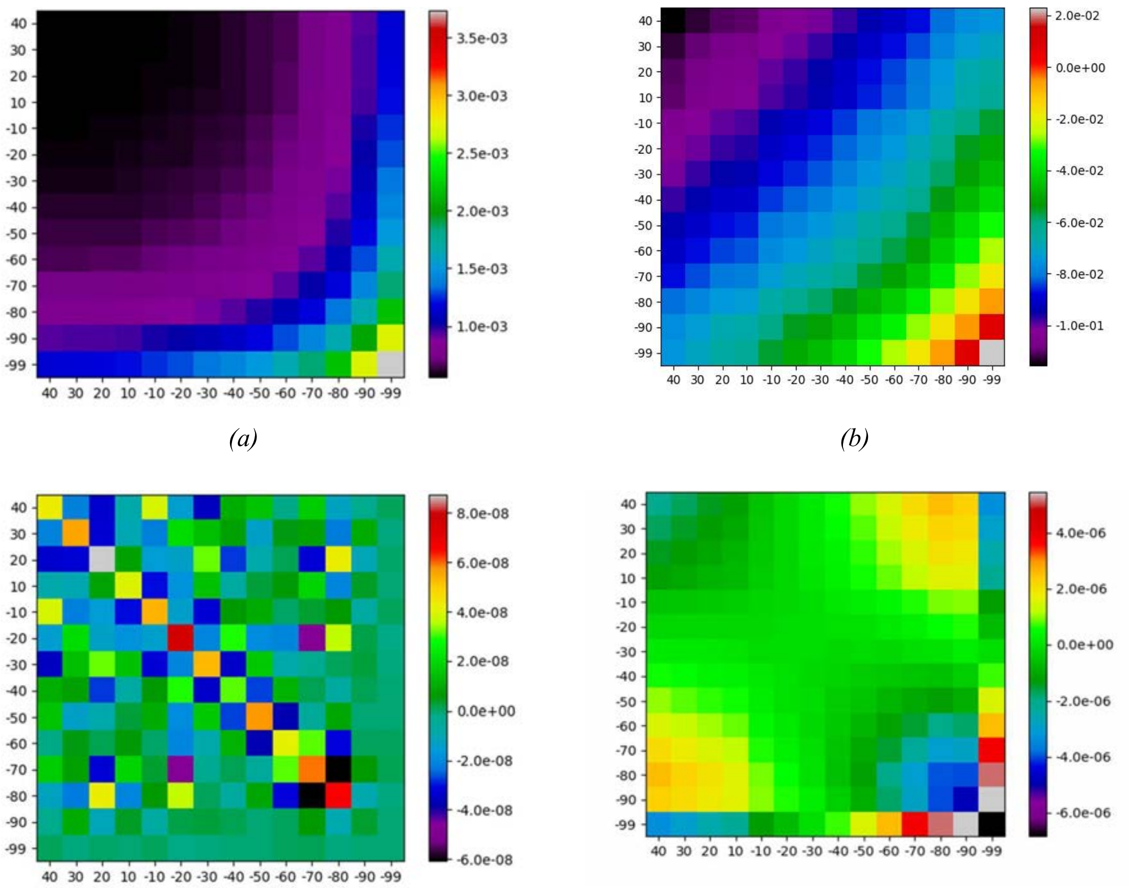

(a) *(b)*

(c) *(d)*

FIG. 27. Relative difference between input and reproduced covariance matrices of reactivity: (a) relative covariance, (b) normal random sampling, (c) SVD/UT sampling, (d) LRA/UT sampling.

The PDFs for reactivities generated by the three sampling techniques due to a 99% drop and 20% expansion in coolant density are illustrated in Fig. 28 (a)–(f). Figure 27 is interesting and informative; the PDFs generated by random sampling are roughly symmetric as illustrated in Figs. 28 (a) and (b). Though, the PDFs of the SVD/UT and LRA/UT techniques are asymmetric because the sigma points generated by SVD depend on the singular values of the matrix Σ. The scaling parameters γ and/or λ used in tells how much the sigma points are far from the mean. For the SVD/UT, $\gamma = \sqrt{(n + \lambda)} = \sqrt{(14 + 1/2)}$, while for the LRA/UT which truncated to two active subspace k=2 has $\gamma = \sqrt{(k + \lambda)} = \sqrt{(2 + 1/2)}$. As the value of γ and/or λ parameters decreased as there is a smaller perturbation of input values, which results in the uncertainty estimation over a narrow range of output variations, and the perturbation factors become closer to the mean.

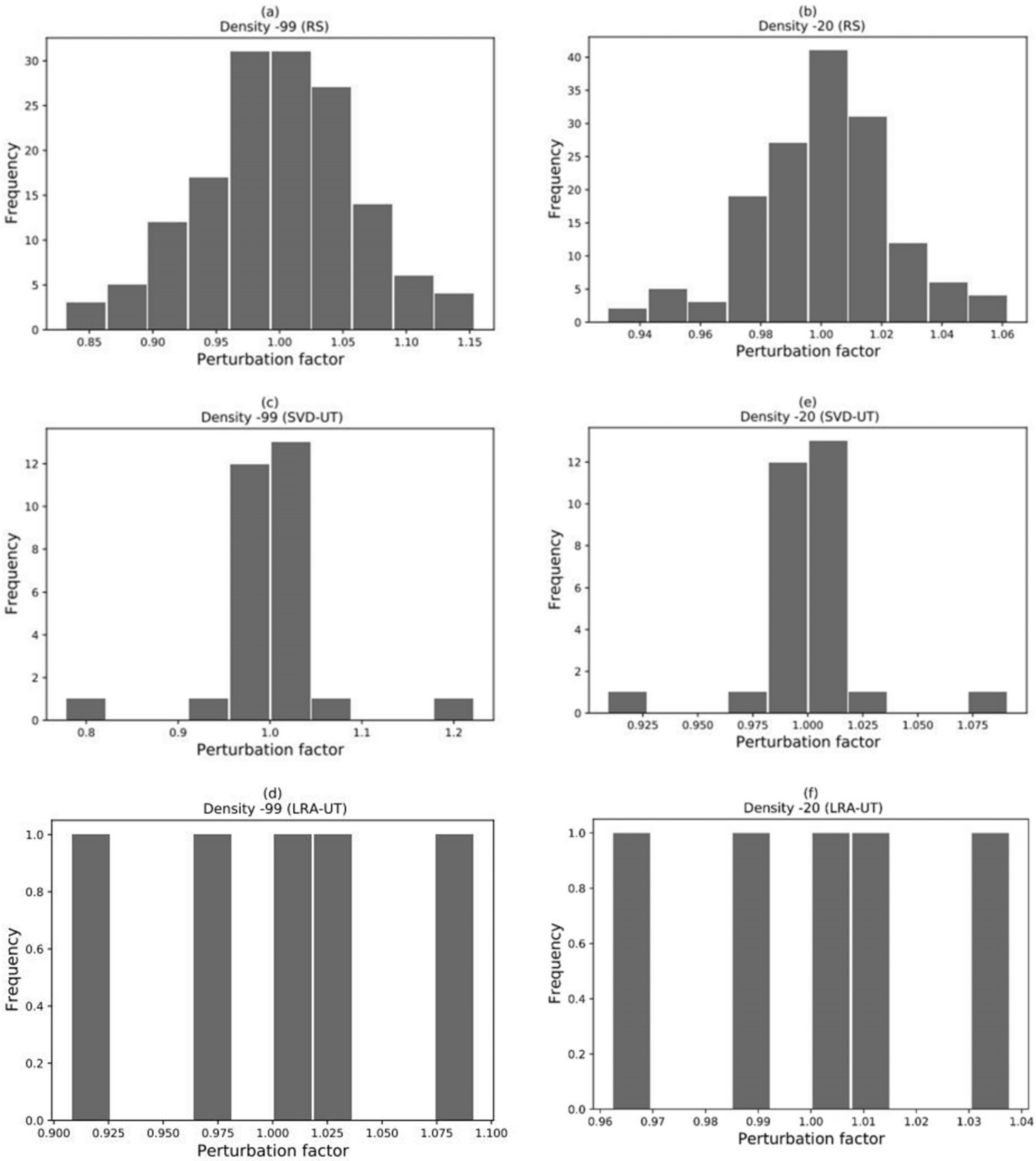

FIG. 28. Probability density functions.

<u>Uncertainty estimation of output response</u>: for random sampling, about 16 h and 29 minutes are required to execute 150 ATHLET code runs. For, SVD/UT sampling where the sample size is 29, the computational time is dramatically reduced to 3 h and 16 minutes. Moreover, when the LRA/UT sampling is applied, the calculation time is drastically reduced to 36 minutes where only 5 runs are needed. In Fig. 29, the peak cladding temperatures evaluated by the ATHLET code are compared with the mean values calculated using the three methodologies during 500 s.

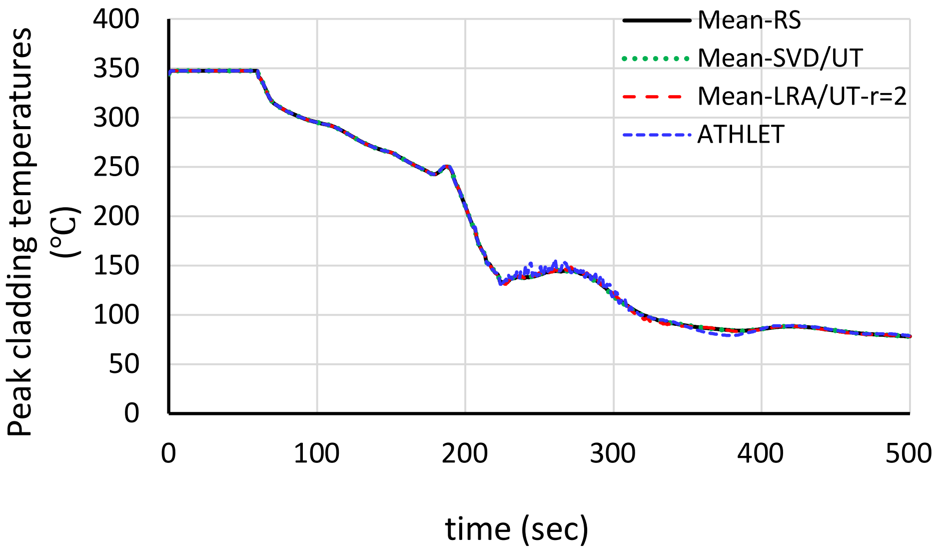

FIG. 29. Average peak cladding temperatures (°C).

As can be seen, around 350 s, there are differences in the cladding temperatures calculated by the ATHLET code and the three sampling logarithms. The uncertainties in the peak cladding temperature for the three different techniques are compared in Fig. 30. Until 180 s, the uncertainties are nearly zero, then increase and oscillate around 3% because of the slight fluctuation in peak cladding temperatures. Thereafter, the uncertainties increase to about 5.5% when applying the random sampling and about 6.2% for SVD/UT, while applying the LRA/UT sampling decreased to 5.2%. It is important to note that for the SVD/UT and LRA/UT sampling, the scaling parameter λ is the main factor causing the differences. The smaller value of γ results in uncertainty estimation over a narrow range of output variations.

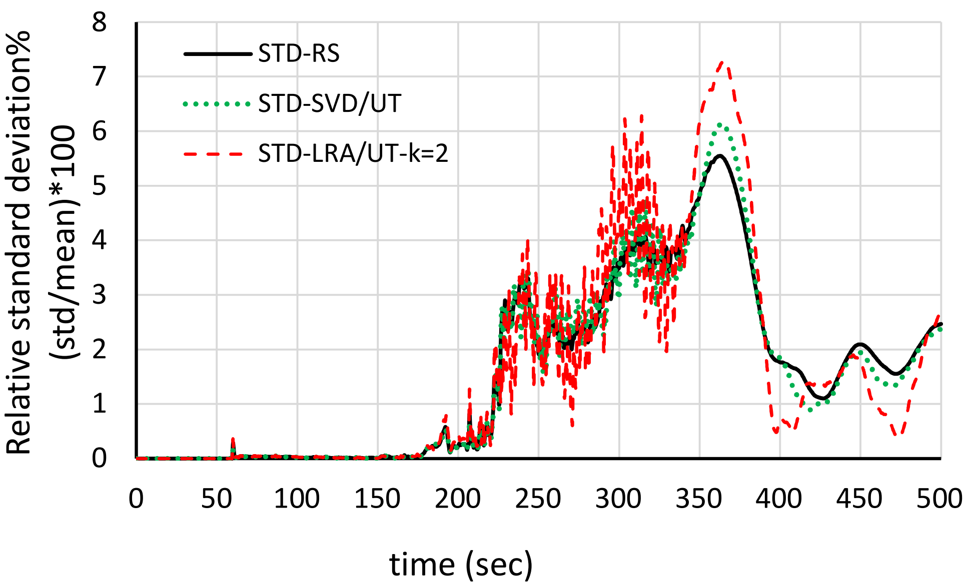

FIG. 30. Relative standard deviation in the peak cladding.

2.3.2.7. Summary and conclusions

In this study, we introduced an advanced method for calculating uncertainty during accident conditions that reduces the computation time required by statistical sampling methods. First, the SVD/UT sampling was used to generate a precisely selected sample set. By using the LRA technique, the active sub-space was revealed, and the computational time was significantly reduced. In order to evaluate the efficiency of LRA/UT and SVD/UT algorithms, normal sampling results were compared with both. An estimation of the uncertainty was done for the KWU-PWR1300 during large break LOCA without the insertion of control rods, where uncertainties are calculated for the peak cladding temperature due to perturbations in the coolant density reactivities. In conclusion, it can be said that all three methods are able to reproduce the input covariance matrix accurately, but the differences are approximately −2 for random sampling and it drops to −5 for SVD/UT sampling. By applying the LRA to the singular value matrix, the differences reach orders of −3. For random sampling, about 16 h and 29 minutes are required to execute 150 ATHLET code runs. For, SVD/UT sampling where the sample size is 29, the computational time is dramatically reduced to 3 h and 16 minutes. Moreover, when the LRA/UT sampling is applied, the calculation time is drastically reduced to 36 minutes where only 5 runs are needed.

Main sources of uncertainty resulting from the analysis: LBLOCA without control rod insertion is an important scenario, since the large negative reactivity coefficient insures a safe shut down of the nuclear reactor regardless of whether the control rods are inserted. Therefore, the coolant density reactivities are the input variables with uncertainty while the peak cladding temperatures are the response variables (FOM).

Lesson learned and best practices: the inconsistencies between LRA/UT, SVD/UT, and RS techniques maybe because of the non-linearity of the calculation model where the mean may be slightly biased. In addition, for the SVD/UT and LRA/UT sampling, the scaling parameter λ is the main factor causing the differences.

2.3.3. Korea Atomic Energy Research Institute (KAERI)

The KAERI based the accident analysis using as a reference plant the OPR1000. Description of this plant specifics, accident scenarios analysed, applied models and approaches, and summary of the results are provided in the following sections.

2.3.3.1. Motivation and objectives

In the Republic of Korea, severe accident uncertainty analyses have been carried out in the context of Level 2 PSA and SAM and assessment of severe accidents related design requirements, with the MELCOR [1] and MAAP [2] codes for PWRs and the MAAP-ISAAC (Integrated Severe Accident Analysis Code for CANDU) code for pressurized heavy water reactors (PHWR: CANDU-6) [3]. Meanwhile, the Republic of Korea revised its Nuclear Safety Act in June 2015, to strengthen the legal framework behind the current SAM strategy. The new Nuclear Safety Act requires applicants to file an Accident Management Program including the dedicated SAM measures to obtain an operating license with the following stated safety and performance goals [4]:

— The equivalent performance goals (objectives) for operating plants are to satisfy a core damage frequency (CDF) of 1.0×10^{-4}/ry and a large early release frequency (LERF) of 1.0×10^{-5}/ry, but the performance goals less than one order of magnitude (CDF of 1.0×10^{-5}/ry and LERF of 1.0×10^{-6}/ry) to be applied to the APR1400 (Advanced Power Reactor 1,400 MWe) follow-up designs [5];

— For each plant, the sum of the frequencies of the accident scenarios in which the amount of radionuclide ^{137}Cs release exceeds 100 TBq should be less than 1.0×10^{-6}/ry.

Among them, the LERF and ^{137}Cs criteria are in the realm of severe accidents and relevant radiological source terms analyses, but the currently available severe accident integral analysis codes include many uncertain models and parameters that should be more clearly understood. Accordingly, the uncertainty and relevant sensitivity for those parameters analyses could be a plausible way to assess and ensure the confidence and credibility of the estimated performance goals (i.e., LERF and ^{137}Cs criteria).

The objective of the present study is to explore best practice approaches for the uncertainty and sensitivity analyses, through characterizing uncertainties addressed in various model inputs of the currently available severe accident codes and identifying relevant key contributors influencing the FOMs of interest.

For the purpose, the OPR1000 (Optimized Power Reactor 1,000 MWe) [6, 7] was selected as the reference plant and a STSBO accident was chosen as the reference scenario, which is one of the risk-relevant accidents of NPPs [8] as took place at the Fukushima Daiichi NPPs in 2011. MELCOR2.2 [1] and MAAP5.05 [2], were used to investigate respective prediction capability for the results of interest, which could differ due to their different modelling schemes for relevant phenomena [9]. Two plant-specific accident mitigation measures were additionally considered to investigate their influence on the FOMs of interest, consequently so as to provide technical support for the plant-specific SAM and Level 2 PSA.

2.3.3.2. Description of the relevant plant

The reference plant, OPR1000 [7], is the first standard two loop PWR plant in the Republic of Korea and the primary loop includes the RPV, two reactor coolant loops, each containing one steam generator (SG), one hot leg, two cold legs, two reactor coolant pumps (RCPs), and a pressurizer placed in one of the hot legs.

The steam generators located at a higher elevation than the RPV for natural circulation provide an interface between the RCS (primary) and the main feedwater/steam system (secondary). The steam generators and the four RCPs are symmetrically arranged.

The safety injection system (SIS) or emergency core cooling system (ECCS) provisioned for long-term core cooling in the event of a LOCA is designed to supply sufficient cooling sources to preclude fuel melting and to remove the heat generated in the reactor core for an extended period of time following the LOCA.

A schematic diagram of the primary system and relevant SISs is shown in Fig. 31 and the major design parameters utilized in this study are summarized in Table 11.

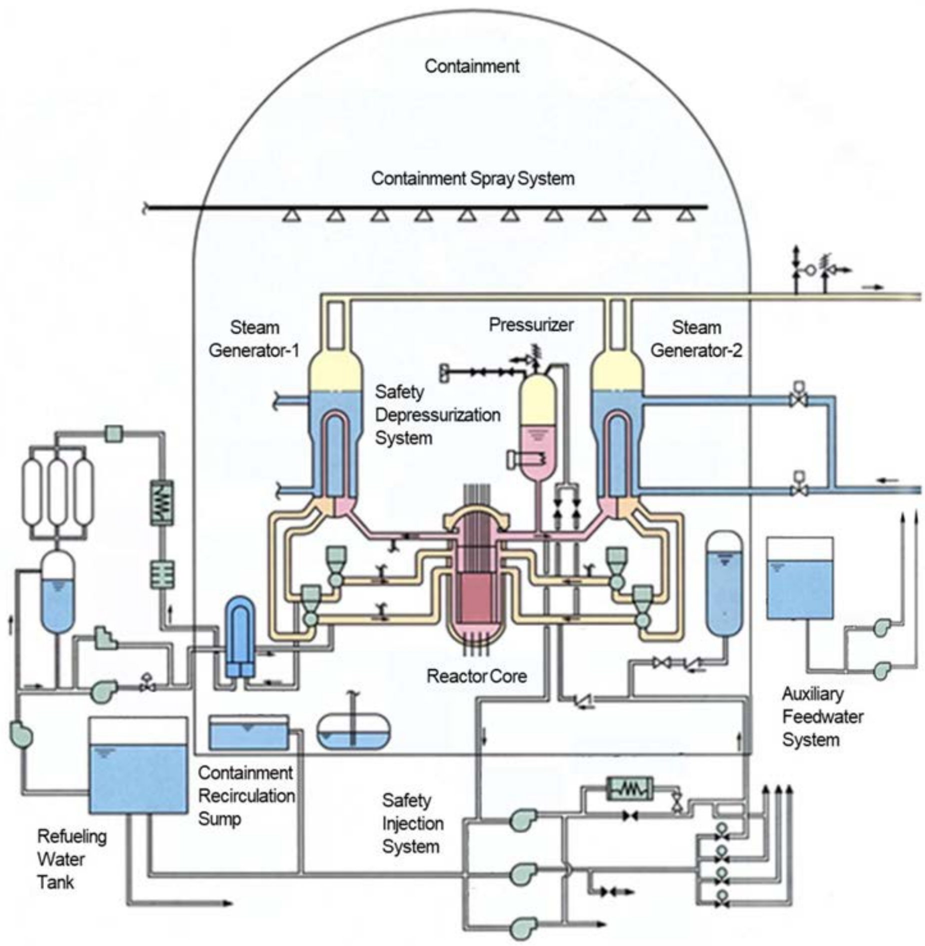

FIG. 31. Schematic diagram of the OPR1000 primary and safety systems [7].

TABLE 11. DESIGN PARAMETERS OF THE OPR1000 [7]

Category	**Plant parameter**	**Design value**
Power	Reactor thermal power	2,815 MWt
	Power plant output (net)	1,000 MWe
Reactor core	Equivalent diameter / active height	3.12 m / 3.81 m
	Fuel material / number of assemblies	UO_2 / 177
	Fuel enrichment at equilibrium core	4 (Batch Average) w.t%
	Material of the cladding tube	Optimized ZIRLO
	Rod array of a fuel assembly	Square 16×16
	Average discharge fuel burnup	54.1
	Control rod absorber material	B_4C or Inconel slug
Reactor coolant system	Number of coolant loops / core flow rate	2 (two RCPs per loop) / 15.3 t/s
	RCS operating pressure	15.5 MPa(a)
	RCS inlet / outlet temperatures	296°C / 327°C
	Soluble poison in coolant	Boric acid
Reactor pressure vessel	Cylindrical shell inner diameter / thickness	4,120 mm / 205 mm
	Height of the vessel (inner)	14,642 mm
	Base lower head composition	SA508, Grade 3, Class 1
	Design pressure / temperature	17.2 MPa(a) / 343.3°C

TABLE 11. DESIGN PARAMETERS OF THE OPR1000 [7] (Cont.)

Category	Plant parameter	Design value
Steam supply system	Steam pressure / temperature	7.4 MPa / 294.4°C
	Steam generator type / tube material	Vertical U-tube / Inconel 600
	Steam flow rate at nominal condition	790 kg/s (per steam generator)
Material of major components	Hot leg pipe / RPV lower head	Carbon steel
	Pressurizer surge line	Stainless steel (SS-316)
Reactor (containment) building	Free volume / design leak rate	7.72×10^4 m^3 / 0.1–0.2% vol/day
	Design / operating pressure	0.494 MPa / 0.1 MPa
	Composition of the reactor cavity	Basaltic concrete
	Dimension of the cavity wall	Axial: 4.57 m / radial: 2.6 m

2.3.3.3. *Accident scenarios and severe accident codes*

The reference accident scenario, STSBO, is a core damage sequence induced by a complete loss of all onsite and offsite AC powers. As a result, all safety-related systems being driven by the AC power are not available in this scenario. According to the OPR1000 Level 1 PSA [10], the accident sequence results in a CDF of 2.69×10^{-6}/ry, taking up 9.4% of the OPR1000 internal events CDF. Three reference cases are selected for the present study, as described in Table 12: a base case scenario and two mitigation scenarios (cases 1 & 2) for investigating the influence of relevant SAM measures [11], using mobile equipment provisioned for the emergency situation after the Fukushima Daiichi NPPs accident [12].

TABLE 12. OPR1000 REFERENCE SCENARIOS[1]

<table>
<tr><th>Base case</th><th>Case 1
(Water injection into RCS: SAG-3)</th><th>Case 2
(Water injection into SG: SAG-1)</th></tr>
<tr><td rowspan="4">・ Loss of offsite AC power and EDG without AC power recovery;
・ TDAFW, MDAFW, HPSI, and LPSI pumps are not available, but all SITs are available;
・ The RCP seal keeps its integrity;
・ Hydrogen control is made only by PARs, but not hydrogen ignitors.</td><td colspan="2">・ Manual operation of a 1 MW mobile EDG at 4 h after the beginning of the accident to run relevant mobile pumps provisioned to cope with accidents like the SBO
・ Manual open of 2 SDS valves at the SAMG entrance condition to depressurize the RCS (i.e., when the CET > 923.15 K) (SAG-2);
・ Manual stop of four SITs for preventing the inflow of N_2 into the RCS at their set-point (i.e., the pressurizer pressure of 1.196 MPa).</td></tr>
<tr><td>–</td><td>・ Manual close of 2 SDS valves in the primary side after stopping the SIT injection</td></tr>
<tr><td>–</td><td>・ Manual open of 2 ADVs of at 4 h after the SBO to inject external water into the steam generator</td></tr>
<tr><td>・ Manual injection of external cooling water into the RCS (EWI) at 4 h with a mobile pump</td><td>・ Manual injection of external cooling water into the SG (EWI) with a relevant mobile pump</td></tr>
</table>

[1] AC: alternating current; ADV: atmospheric dump valve; CET: core exit temperature; EDG: emergency diesel generator; EWI: emergency/external water injection; MDAFW: motor-driven auxiliary feedwater; PAR: passive autocatalytic recombiner; SAG: severe accident guideline; SDS: safety depressurization system; SIT: safety injection tank; TDAFW: turbine-driven auxiliary feedwater.

MELCOR2.2 and MAAP5.05 (described in Section 2.2) are used to compare their prediction capability for the results of interest.

2.3.3.4. Plant modelling and nodalization

To take into account the integral responses of severe accident progressions over the reactor and containment, the OPR1000 nodalization model included all safety-relevant plant structure, systems and components (SSCs) [1, 13].

<u>RCS primary and secondary loops</u>: main components of the RCS primary and secondary loops (circuits) employed for this study are as follows:

- RCS primary circuit includes the RPV, the reactor core, and two RCS loops: one with pressurizer and the other without. Each loop includes its own hot and cold legs, steam generator, and RCP. The primary circuit also includes dedicated SISs such as four passive SITs, HPSI, and LPSI systems. The RCS loop B is the same as the RCS loop A, except that the pressurizer is placed in the loop A;
- Pressurizer includes a surge line and dedicated safety valves (three pressurizer safety valves (PSVs) and two SDS valves), whose opening and closing are automatically according to their set-points or can be made manually by the operator wherever required. The steam and water discharged from these safety valves are released into the refueling water storage tank (RWST);

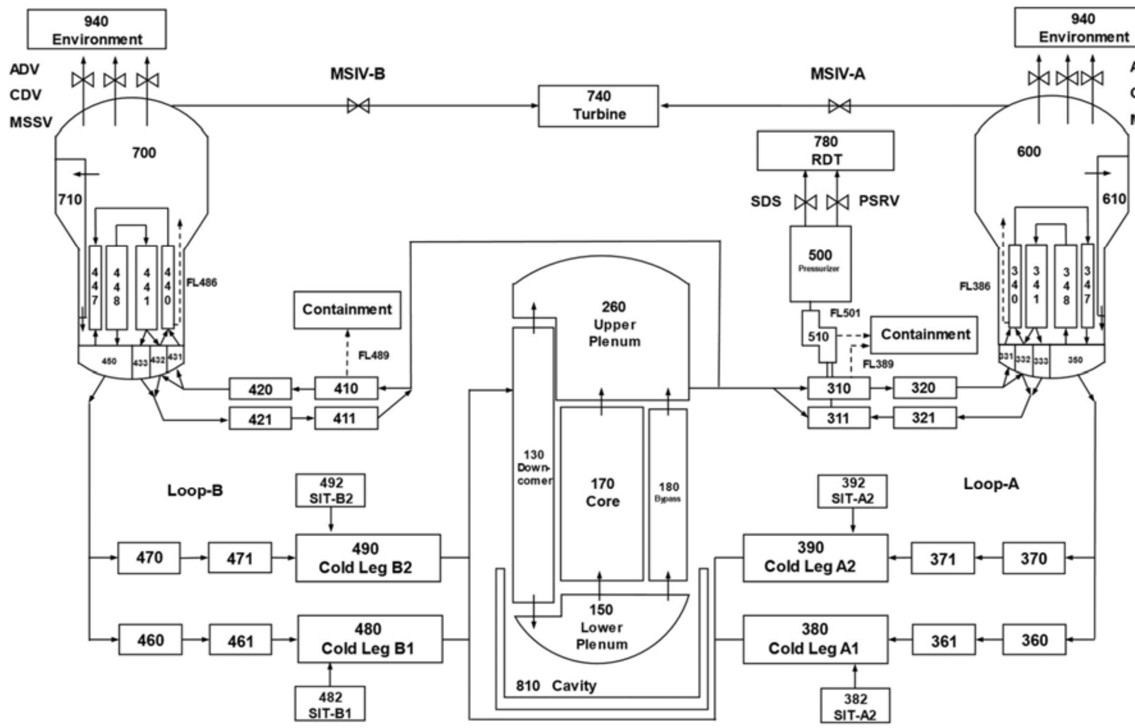

FIG. 32. MELCOR nodalization of the OPR1000 RCS loop and RPV.

- In MELCOR, the hot leg was additionally split into upper and lower nodes to consider a counter-current natural circulation expected in the primary coolant loop (between hot leg and steam generator), as shown in Fig. 32;

- Steam generator secondary loop includes main steam lines with relevant MSSVs and ADVs and the external atmosphere, which providing a flow path to make bypass the steam through the ADVs or containment rupture/leakage;
- In MELCOR, the steam generator inlet plenum are split into the following three regions to model natural circulation of the primary loop in more detail: a hotter fluid region, a mixed fluid region and a colder fluid region, as shown in Fig. 32.
- In MELCOR, the SG U-tubes were also subdivided into two regions to simulate relevant thermal behavior in more detail: an up-flowing zone leading to hotter tubes and a down-flowing zone where relevant tubes become colder, as shown in Fig. 32;
- The primary and secondary loops are not defined by the user in the case of MAAP5, and thus a standard MAAP5 nodalization scheme [2] was used for the present study.

Reactor core and RPV: the core region was divided into 8 radial rings and 16 axial sections in MELCOR, as shown in Fig. 33 (a), of which the active fuel region takes up sections 6–15 and the core support plate is the 5th axial section. The RPV includes a lower plenum, a downcomer and core bypass, and an upper plenum region. The lower head wall was subdivided into 12 segments and 4 nodes across the wall. Relating to MAAP5, the core region was divided into 7 radial rings and 13 axial sections, as shown in Fig. 33 (b), of which the active fuel region is placed in sections 3–12. The lower head wall was subdivided into 25 segments and 5 nodes across the wall.

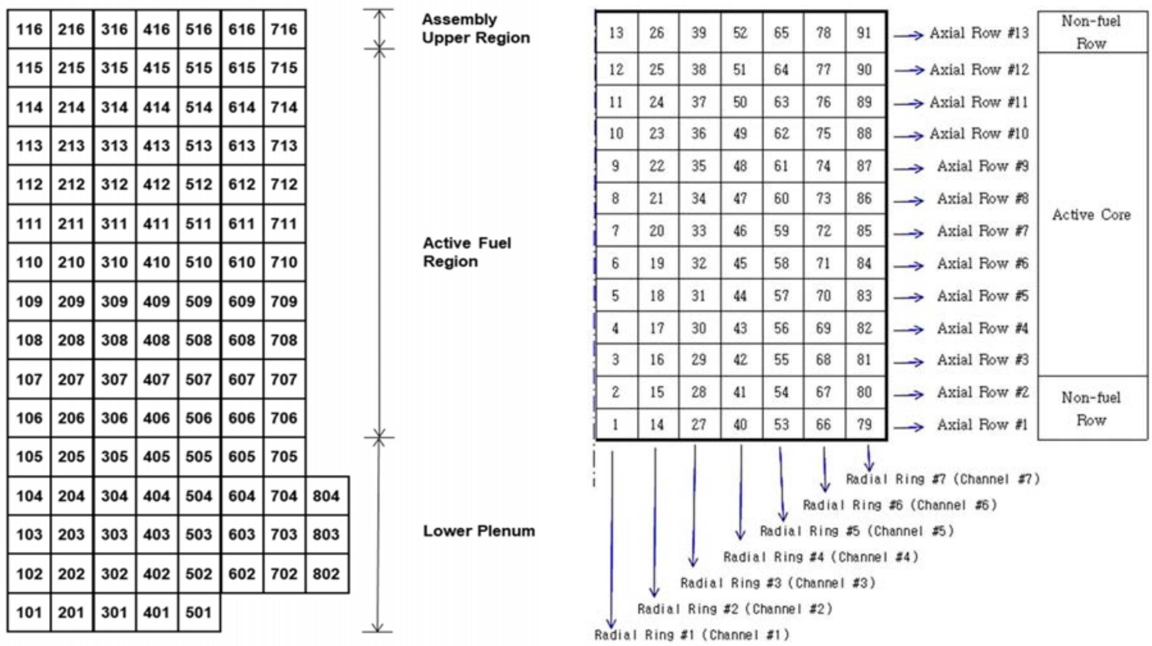

(a) *(b)*

FIG. 33.Nodalization of the OPR1000 reactor core: (a) MELCOR, (b) MAAP5 [2].

Reactor/containment building: the containment was divided into 19 compartments in MELCOR and 6 compartments in MAAP5, as shown in Fig. 34. This is because MAAP5 is less sensitive to the number of compartments [2]. The arrangement of 21 PARs and additional ignitors installed to mitigate hydrogen risk are also shown in the corresponding figures.

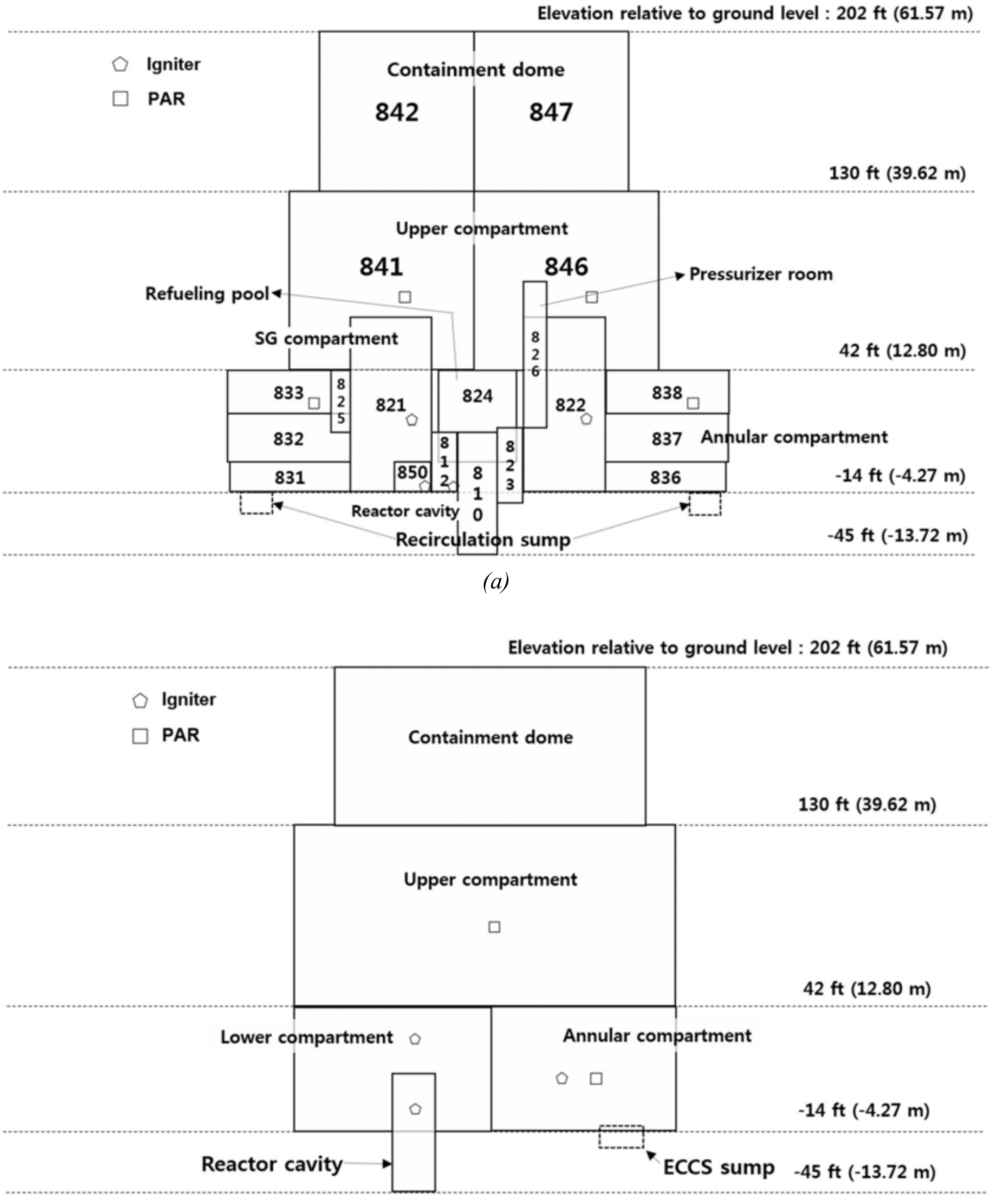

FIG. 34. Nodalization of the OPR1000 reactor building: (a) MELCOR, (b) MAAP5.

Major modelling assumptions: additional modelling assumptions and failure criteria used for the present study are as follows; otherwise the code default values known as the currently available best estimates are used:

— Failure of the RPV lower head: a melting point of the tube welding material (1273.15 K) was applied for the penetration tube failure (a criterion for temperature) and Larson-Miller parametric model (its failure is made by a total strain) (MELCOR/MAAP5) was applied for the lower head wall creep rupture, assuming the initial break size 0.01 m^2;
— Containment fails when exceeding its pressure of 0.9632 MPa, assuming the initial break size 0.1 m^2 in the upper compartment. The failure pressure was taken from the high-confidence low-probability of failure (HCLPF) performance estimated for the OPR1000 [14];
— Conditions for counter-current natural circulation in the primary loop and and relevant flow through the hot leg and steam generator [15, 16] are given in Tables 13 and 14, respectively;
— Initial inventories of in-core fission products are taken from the ORIGEN code calculation [17] for the end of cycle (EOC);
— PSV opens and closes when the RCS pressure exceeds its set-points of 17.24 and 14.1 MPa, respectively and the SIT injection is automatically made when the RCS pressure exceeds 4.3 MPa;
— MSSV opens and closes when the steam generator pressures its set-points of 8.91 and 8.6 MPa, respectively;
— PARs run when the hydrogen concentration reached 2.0 vol.% and stops when it is below 0.5 vol.%;
— EWI rate into the steam generator or RCS was taken from the utility document [18], as shown in Table 15.

TABLE 13. CONDITIONS FOR THE COUNTER-CURRENT NATURAL CIRCULATION

	Natural circulation-driving conditions
MELCOR	Starts when a superheat of the hot leg fluid exceeds 10 K and when its void fraction exceeds 0.95.
MAAP5	Starts when the RPV upper plenum fluid temperature exceeds that of the steam generator inlet plenum and when a void fraction of the steam generator outlet plenum fluid exceeds 1.
Common	Stops when failing the RCS pressure boundary or when the PSVs are stuck opened.

TABLE 14. RELEVANT COUNTER-CURRENT FLOW

	Partition of fluids in each region
MELCOR	· Ratio of cold and hot fluids in the hot leg: 50 / 50 · Ratio of cold, mixing, and hot fluids in the steam generator inlet plenum: 5 / 90 / 5 · Ratio of cold and hot fluid in the steam generator tubes: 65 / 35
MAAP5	· Proposed default values

TABLE 15. EMERGENCY WATER INJECTION RATE

RCS pressure (MPa)	**Injection rate (kg/min)**	
	RCS	**Steam generator**
0.101	0.8497	0.3258
0.591	0.7478	0.2464
1.082	0.5992	0.1547
1.278	0.4911	0.0989
1.533	0.0	

2.3.3.5. Methodologies and tools for uncertainty and sensitivity analyses

<u>*Uncertainty analysis methodology*</u>: the main purpose is to characterize uncertainties of inputs addressed in the relevant codes and uncertainties being addressed in the process of code prediction (i.e., FOMs). For the

purpose, the Monte Carlo sampling approach being widely utilized in the realm of thermal-hydraulic and severe accident analyses, was employed in this study, and relevant processes for the quantification of the uncertainties are shown in Fig. 35.

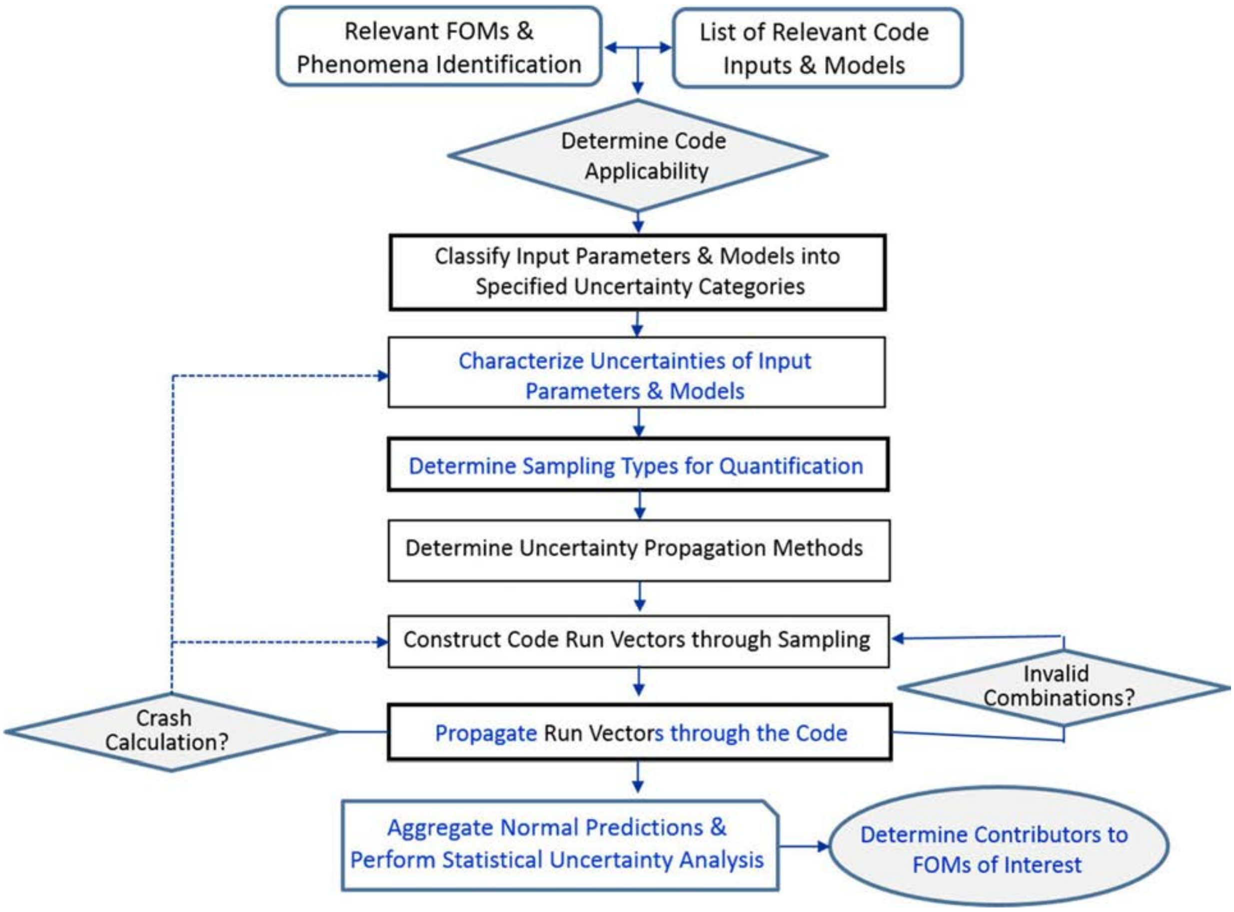

FIG. 35. Key processes for the OPR1000 severe accident uncertainty analysis.

Sensitivity analysis methodology: the sensitivity/correlation/importance analyses have been employed to provide a sound guidance for improving the state of knowledge of models and input parameters, which are considered in relevant computational codes and/or to reduce uncertainties being addressed inherently in the process of code prediction. If a sufficient number of samples are available as implemented by a statistical approaches like the Monte Carlo simulations, the following probabilistic approaches could be used in identifying the influence of input parameters on the FOMs of interest [19–21]:

— Correlation-based sensitivity analysis: Pearson, Spearman, and Kendall correlations;
— Regression-based sensitivity analysis: PCC, PRCC, SRC, and SRRC. For reference, the coefficient of determination R^2 [22], which is estimated for the formulated regression model, gives a good measure to determine whether the formulated regression model is sufficient or not.

Since the forgoing sensitivity measures are easy to intuitively understand, they are widely used in many science and engineering fields. In case that the relationship between inputs and relevant responses is highly complex, the nonlinear regression approaches could be more flexible, but may still require a greater of lesser assumptions on the functional forms of the formulated regression models [23, 24]. Thus, this study explored a suite of sensitivity coefficients, i.e., Pearson/Spearman correlation coefficients and PRCC/SRRC, for a better coverage of potential relations between the uncertainty inputs and relevant FOMs.

Table 16 summarizes the four sensitivity measures and relevant applicability.

TABLE 16. SENSITIVITY/CORRELATION MEASURES OF INTEREST

Sensitivity measures	Comments
Pearson correlation coefficient	· This is a measure to identify a linear relationship between the two variables, which is obtained by dividing their covariance by the product of relevant standard deviations.
Spearman correlation coefficient	· This is used to identify a monotonic strength between the two variables. The coefficient uses ranks in ascending order instead of the simulation results, i.e., non-parametric measure.
PCC / PRCC	· The PCC is used to identify a linear relationship between any two variables among *n* variables in multivariate correlation analysis. The coefficient is often to avoid masking effects of correlations between any two variables while removing the effect of the rest. The PRCC is the corresponding non-parametric rank correlation measure, which is often used to improve the PCC.
SRC / SRRC	· This is coefficients of a multiple regression model where relevant data for the response variable and input variables have been standardized so that their variances are equal to 1. The SRRC is the corresponding non-parametric rank correlation measure, which is often used to improve the SRC.
Degree of correlation and importance (r) [25]	· For $\|r\| \leq 1$, if $\|r\| \geq 0.7$, high correlation between two variables; if $0.3 \leq \|r\| <0.7$, modera te correlation; if $0.3<\|r\|<0$, low correlation.

<u>*Uncertainty and sensitivity calculation scheme and relevant tool*</u>: two software tools dedicated for the uncertainty and sensitivity analysis, as shown in Fig. 36, were utilized in this study: SNAP/DAKOTA for MELCOR [26, 27] and an in-house code MOSAIQUE for MAAP5. Relating to SNAP/DAKOTA, the symbolic nuclear analysis package (SNAP) environment [26] provides a graphical user interface (GUI) to simply create the code input files and to visualize relevant results. For the uncertainty analysis, the SNAP also provides an additional plugin program DAKOTA (Design Analysis Kit for Optimization and Terascale Applications) [27]. Using the DAKOTA plugin, the users can create the random samples or the Latin hypercube samples and combine them into the input data set for calculation of the specified code.

MOSAIQUE (Module for SAmpling Input and QUantifying Estimator) [28] can also create the random samples or the Latin hypercube samples to carry out the relevant uncertainty analysis, and then combine them into the input data set for calculation of the specified code. Similar to DAKOTA, MOSAIQUE also provides the relevant GUI to simplify the creation of code input files and to visualize relevant code results, and for a few sensitivity and correlation analyses.

<u>*FOMs*</u>: as summarized in Table 17, the FOMs chosen for the present study include the timings of key events expected in the entire phases of accident progressions, the generation of combustible gas, and the environmental release fraction of fission product Cs.

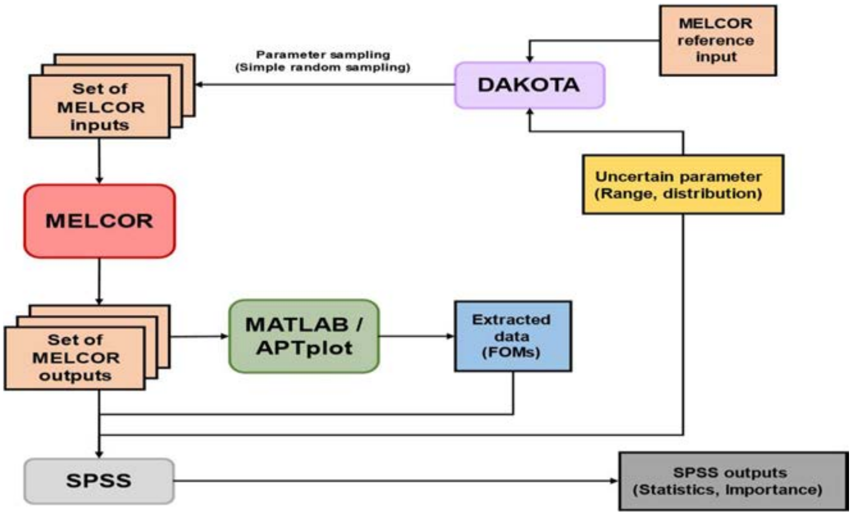

DAKOTA (MELCOR)

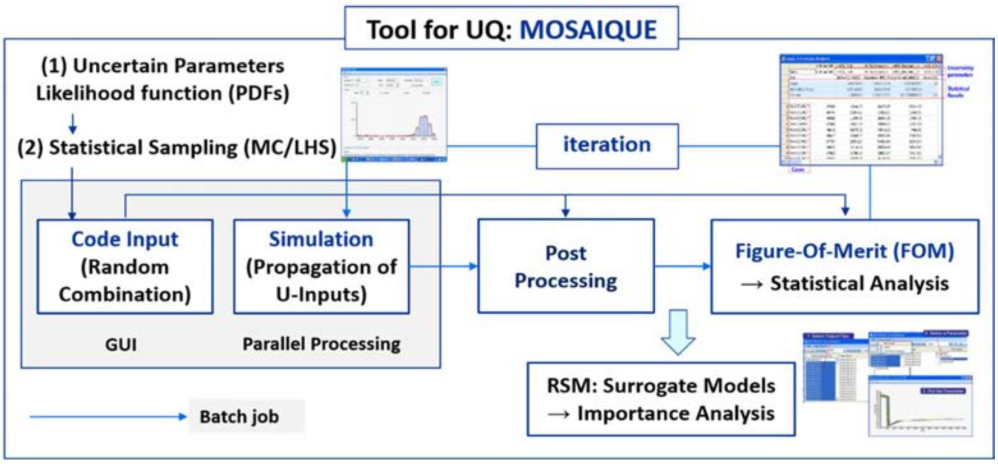

MOSAIQUE (MAAP5)

FIG. 36. Uncertainty and sensitivity tools employed for the present study and relevant analysis processes.

TABLE 17. FOMs VARIABLES EMPLOYED BY MELCOR AND MAAP5

FOMs	Definition	MELCOR	MAAP5
FOM 1	Core (top of the active fuel) uncover time	RN10001	IEVNT49
FOM 2	RPV lower head (penetration/creep) failure time	COR0001	IEVNT3
FOM 3	Reactor/containment building failure time (rupture)	CFVALU863	IEVNT104
FOM 4	Mass of hydrogen generated by the in-vessel Zr/steel oxidation before the RPV failure	COR-DMH2-TOT	MH2CR
FOM 5	Mass of hydrogen generated by the ex-vessel MCCI after the RPV failure	CAV-MEX-H2.10	MH2CBT
FOM 6	Mass of carbon monoxide (CO) generated by the ex-vessel MCCI after the RPV failure	CAV-MEX-CO.10	MCOCBT
FOM 7	Environmental release fraction of fission product Cs through the containment leakage/ rupture or damaged steam generator tube (the ratio of its initial inventory)	RN1-TYCLT-x-2.ty	FCSRELT

Uncertainty inputs and relevant probability distributions: one of the key challenges being encountered in quantifying the uncertainty of the FOM of interest is to specify properly relevant uncertain inputs used for the analysis, their best estimate values and ranges (e.g., lower and upper bound), and relevant probability distributions. In the case of MELCOR, all uncertainty inputs employed are model parameters, as summarized in Table 18, but MAAP5 included a few inputs for the selection between different physical models or correlations during the accident progression, as shown in Table 19. The MELCOR inputs and relevant PDFs were selected based on the code manual [1], previous studies including the US SOARCA (State of Art Reactor Consequence Analysis) [24, 29–31], engineering judgements, and parametric sensitivity study. The MAAP5 uncertainty inputs were also selected in a similar way, based on the relevant code manual [2], previous studies [32–35], and parametric sensitivity study [36]. For most uncertainty inputs employed for the study, the code default values were adopted as the corresponding best estimate values. When there are no preferences to justify, uniform distribution was assigned, by which all possible values between lower and upper bounds are equally distributed. In the case of MAAP5, most uncertainty inputs were assumed to have a triangular PDF [36], since there is currently no information to judge that another PDF is better.

Sampling and propagation of uncertain inputs: one of another challenges encountered in applying statistical methods such as the Monte Carlo sampling is to determine the appropriate_sample size [20, 37]. For example, when the crude Monte Carlo sampling (SRS) method is employed, data points for the uncertainty analysis are independently sampled from the relevant PDF and new sample data are generated independently from the previously generated ones. If possible, the number of the random samples should be enough to ensure that the analysis results well represent their full space of the population, including their mean and variance. There seem be no currently accepted criteria on how many samples are required for ensuring more robust results. Even with a significantly smaller number of samples, there are approaches ensuring a robust sampling of distributions in a large range of conditions. For instance, Wilks formula [38, 39] allows us to specify the minimum sample size at the desired confidence and tolerance level for the analysis results. For instance, when applying the 2nd order Wilks formula, a minimum sample size of 93 is enough for the one-sided tolerance limit of 95%/95%. For the two-sided tolerance interval of 95%/95% at the 2nd order, the minimum sample size is given as N=198. However, the formula could be applied to the completely random and independent samples, but not suitable for the LHS samples and in the case of code crashes.

The studies related to LHS (or stratified MCS) [37] show that LHS sample size (N) might give a reasonable convergence of the statistical estimators (such as mean and standard deviation) for the model response and can adequately identify relevant sensitive input parameters: N=(4/3)k for time-consuming computer models employing k uncertain input variables; otherwise N=2k~5k. However, there might be cases where statistical values estimated from the LHS do not converge more quickly than the SRS as the size of samples increases, depending greatly upon a complexity of the code as well as the number of relevant input parameters employed for the uncertainty analysis. While samples generated by the LHS algorithm are completely random in nature, as is required by the Wilks formula [38], the approach seems be better than the SRS approach in case that low probability-high consequence tails exist in the input PDFs. By the forgoing reason, the present study employed the SRS method, considering a possibility of code crashes that may take place relating to settings of the sampled input parameters. Also, considering the current situation in which the order of hours per sample calculation is required to simulate all the phases of severe accidents, the SRS sample of N=200 was primarily tested to obtain relevant insights into the analysis results of interest. All relevant uncertainty inputs were assumed to be mutually independent and uncorrelated in the present study.

TABLE 18. OPR1000 UNCERTAINTY INPUTS AND RELEVANT PDFs (MELCOR, 26)

Category	Parameter	Range	Default value	Description	PDF
Decay heat	SC3200_1	0.9 – 1.1	1.0	Multiplier for the American Nuclear Society (ANS) decay heat equation.	Uniform
In-vessel core melt progression	PORDP	0.1 – 0.5	0.4	Porosity of particulate debris in the core and lower plenum	Lognormal: μ = -0.85, σ =0.32
	DHYPD (m)	0.01 – 0.06 (lower plenum region)	0.002 (lower plenum region)	Particulate core debris equivalent diameter used in calculating the total debris surface area	Lognormal: μ = -3.68, σ = 0.5
		0.002 – 0.05 (core region)	0.01 (core region)		Lognormal: μ = -4.34, σ =0.58
	VFALL (m/s)	0.01 – 1.0	0.01	Velocity of falling debris to calculate the quenching heat transfer of the falling debris	Uniform
	HDBH2O (W/m^2/K)	200 – 2,000	2,000	Heat transfer coefficient between in-vessel falling debris and the RPV lower plenum pool	Uniform
	COR_CHT (W/m^2/K)	2,000 – 22,000 (UO_2-Zr-ZrO_2)	7,500 (UO_2-Zr-ZrO_2)	Candling heat transfer coefficients to specify the heat transfer between the molten corium and the core structure	Lognormal: μ = 9.04, σ = 0.63
		500 – 8000 (steel/ steel oxide/poison)	2500 (steel/steel oxide/poison)		Lognormal: μ = 7.9, σ = 0.83
	FUOZR	0.0 – 0.5	0.2	Fractional local dissolution of UO_2 in molten Zr	Triangular (mode = 0.2)
	FCELR & FCELA	0.02 – 0.18	0.1	The coefficient for radiation heat transfer, radially outward (FCELR) and axially upward (FCELA) between each core cells	Normal: μ = 0.1, σ = 0.0375
	HDBPN (W/m^2/K)	100 – 1,000	100	Heat transfer coefficient from debris to penetration structures	Uniform
	TPFAIL (K)	1,273.15 –1,686.15	1,273.15	The criteria temperature of the penetrations or the lower head for the RPV failure. The default value is an approximate value for the transition to plastic behavior for steel. (lower bound: MELCOR Default, Upper bound: Melting point for Inconel 600)	Uniform
	SC1020_1 (s)	100 – 1,000 (Solid)	300 (Solid)	Radial relocation model parameters used to control the operation of the routines that relocate both solid particulate debris (RDSTC) and molten material (RDMTC) from ring to ring	Uniform
	SC1020_2 (s)	10 - 100 (Liquid)	10 (Liquid)		

TABLE 18. OPR1000 UNCERTAINTY INPUTS AND RELEVANT PDFs (MELCOR, 26) (CONT.)

Category	Parameter	Range	Default value	Description	PDF
	SC1131_2 (K)	2,100 – 2,540	2,400	Molten material holdup parameter. (2) refers to the maximum temperature of ZrO_2 that can hold up molten Zr in cladding.	Beta (scaled): α = 3.83, β = 3.00
	SC1132_1 (K)	–	2,500	Core component failure parameters. (1) refers to the temperature to which oxidized fuel rods which have no any un-oxidized Zr can stand.	Normal: μ = 2479, σ = 83
	SC1141_2 (kg/m-s)	0.1 – 2.0	1.0	Core melt breakthrough candling parameters to control the candling model. (2) refers to its maximum flow rate per unit width to axial direction after a breakthrough.	Log-triangular (mode = 0.2)
	SC1601_4	0.16 – 0.20	0.18	Larson-Miller creep-rupture parameters for vessel steel. (4) refers to the total strain assumed to cause failure.	Uniform
Ex-vessel core melt progression	XHTFCL	1.0 – 2.0	1.4	The coefficient for heat transfer between atmosphere and concrete walls	Triangular (mode = 1.4)
	HTRBOT	0.9 – 2.0	1.0	Multiplier in the standard CORCON-mod3 model for heat transfer between the bottom surface and the debris	Triangular (mode = 0.85)
	HTRSIDE	0.9 – 2.0	1.0	Multiplier in the standard CORCON-mod3 model for heat transfer between the radial surface and the debris	Triangular (mode = 300)
	COND.CRUST	1.0 – 5.0	1.0	Multiplier for the conductivity in a solid (crust) sublayer in contact with water	Uniform
Hydrogen combustion	XH2IGN	0.03 – 0.09	0.1	H_2 mole fraction limit for ignition without igniters (hydrogen ignition criteria), which is used specify the uncertainty in propagation from the ignition source.	Discrete: 0.04 = 0.33, 0.06 = 0.33, 0.09 = 0.33
Fission products release and transport	CHI	1.0 – 5.0	1.0	Aerosol dynamic shape factor, whose value of 1.0 means a perfect sphere.	Beta (scaled): α = 1.0, β = 5.0
	CHEMFORM	0.0 – 1.0	0.8	Fraction of a total Cs remaining in the fuel that used to create Cs_2MoO_4, with the remainder as CsOH	Beta: α = 9, β = 3

TABLE 19. OPR1000 UNCERTAINTY INPUTS AND RELEVANT PDFs (MAAP5, 29)

Category	Parameter	Range	Default	Description	PDF
Decay heat	IANSI	1 – 6	1	Flag to select the type of American National Standards Institute (ANSI) decay heat models	Uniform
In-vessel core melt progression	FAOX	1 – 2	1	Multiplier for the outer surface area of fuel cladding for oxidation by steam ingression after the rupture of the cladding	Triangular (mode = 1)
	FPEEL	0.01 – 1	–	Fraction of the ZrO_2 layer that peels off during the re-flooding of core. Larger value increase cladding oxidation during re-flooding.	Loguniform
	FACT	0.1 – 0.5	0.3	Multiplier to specify flow area and hydraulic diameter of the collapsed intact fuel nodes. Larger value leads to a reduced hydraulic diameter.	Triangular (mode = 0.3)
	TCLMAX (K)	2,300 – 2,700	2,500	Rupture temperature of the fuel clad. Higher value delays the rupture and reduces clad oxidation because MAAP assumes the oxidation occurs on both the inner and the outer surfaces when the clad ruptures.	Triangular (mode = 2500)
	FGBYPA	0 – 1	1	Flag for flow not diverted to bypass channel increasing likelihood of oxidation	Triangular (mode = 1)
	FFRICR	0.1 – 1.0	0.1	Friction coefficient to specify a gas flow in axial direction between the core and the upper plenum	Triangular (mode = 0.1)
	FFRICX	0.1 – 1.0	0.25	Friction coefficient for the cross-flow used to characterize natural circulation gas flow in the in-vessel	Triangular (mode = 0.25)
	FWHL	0.05 – 0.15	0.115	Correlation coefficient for hot leg natural circulation flow rate	Triangular (mode = 0.115)
	FAOUT	0.1 – 0.5	0.5	Steam generator tubes fraction carrying ‘‘out” flow in the hot leg natural circulation model	Triangular (mode = 0.5)
	HTSTAG (W/m^2-K)	425 – 2500	850	Heat transfer coefficient of the steam generator primary side in a stagnant water pool without forced or natural circulation	Triangular (mode = 850)
	LMCOL0 /1 /2 /3	48 – 54	53	Larger value leads to the core maintaining rod bundle geometry for a longer time and increases clad oxidation.	Triangular (mode = 53)
	FCRDR	0 – 0.3	0.1	Fraction of a critical mass of molten corium, below which all the remaining core materials are discharged onto the lower plenum.	Triangular (mode = 0.1)
	VFCRCO	0.3 – 0.4	0.35	Porosity of a collapsed core region.	Triangular (mode = 0.35)
	FGPOOL	0.5 – 1	0.738	Geometric factor defining the in-core molten pool height, then used in conjunction with the pool's mass to determine if the side crust will fail	Triangular (mode = 0.738)
	XLFALS (m)	0.01 – 0.1	0.03	Width of the failure opening to define the sideward relocation to the RPV lower head, when the side crust of in-core corium pool has failed.	Triangular (mode = 0.03)

TABLE 19. OPR1000 UNCERTAINTY INPUTS AND RELEVANT PDFs (MAAP5, 29) (CONT.)

Category	Parameter	Range	Default	Description	PDF
In-vessel core melt progression	FMOVE	1.0 – 5.0	1.0	Scalar variable controlling the relocation of solid U-Zr-O embedded in liquid U-Zr-O. This parameter affects the composition of molten pools and the debris in the lower head. 1.0 = no solid material is embedded; otherwise, (FMOVE-1.0) kg of solid material is embedded in every kg of liquid material.	Triangular (mode = 1.0)
	IOXIDHT	0 – 2	1	Heat transfer correlation between the oxidic corium pool of the RPV lower plenum and surrounding solid crust	Uniform
	SCALH	0.8 – 1.2	1.0	Scale factor for various heat transfer coefficients, including those between containment gas and concrete walls.	Triangular (mode = 1.0)
Ex-vessel core melt progression	ECM	0.70 – 0.99	0.85	Emissivity of molten corium surfaces	Triangular (mode = 0.85)
	HTFB (W/m^2-K)	100 – 400	300	Heat transfer by a film boiling accounting for heat conduction through the steam layer above corium pool	Triangular (mode = 300)
	IKCMOXIDE	0 – 1	1	Flag for the thermal conductivity of corium used in water ingression model. =0, use average thermal conductivity for oxides and metals; =1, use thermal conductivity for oxides only	Uniform
Hydrogen combustion	TAUTO (K)	750 – 1,200	983	Auto-ignition temperature for burning combustible gas like H_2 & CO	Triangular (mode = 983)
	TJBRN (K)	900 – 1,900	1,060	Temperature of hydrogen jet entering a non-inerted compartment	Triangular (mode = 1060)
Fission products release and transport	FPRAT	-6 – -4	–	Fission product release correlation: 4 for CORSOR-O if 4.5≥|X|≥3.5; 5 for ORNL-BOOTH if 5.5≥|X|≥4.5; 6 for CORSOR-M and CORSOR-O if 6.5>|X|>5.5	Uniform
	FVPREV	0.1 – 2.0	1.0	Multiplier for the vapor pressure of CsI & CsOH participating in re-vaporization	Triangular (mode = 1.0)
	FCSIVP	0.1 – 5	1.0	Multiplier of CsI vapour pressure for vapour-aerosol equilibrium	Triangular (mode = 1.0)
	FCSHVP	0.01 – 1.0	0.1	Multiplier of CsOH vapour pressure for vapour-aerosol equilibrium	Triangular (mode = 0.1)
	FCS2MOO4	0.6667 – 0.75	0.7	Fraction of a total Cs remaining in the fuel that used to create Cs_2MoO_4, with the remainder as CsI	Triangular (mode = 0.7)

2.3.3.6. *Results*

Steady-state analysis results: the stead-sate analysis was performed to determine the initial conditions of plant for ensuring the input models developed used for the transient analysis. With the prepared MELCOR and MAAP5 input models, the calculation was carried out until 500 s for some plant parameters, including reactor thermal power, and thermal-hydraulic parameters (pressure, temperature, and flow) in the RCS and steam generator secondary sides. According to the results shown in Table 20, the estimated parameters are within an error of no more than 2% for MELCOR and 1% for MAAP5, compared to the corresponding OPR1000 design values [40]. This indicates that the respective input models are in a relatively good agreement with the design values.

TABLE 20. OPR1000 STEADY STATE RESULTS

Plant parameters	Expected	Relative error (%)	
		MELCOR	MAAP5
Total thermal power (MWt)	2,815	0.0	
Pressurizer/RCS pressure (MPa)	15.50	- 0.05	- 0.003
Coolant temperature in the core inlet (K)	568.8	+ 0.81	- 0.0007
Coolant temperature in the core outlet (K)	600.3	+ 0.53	+ 0.0003
Total primary flow rate (kg/s)	15,305	**+1.78**	-0.00002
SG secondary pressure (MPa)	7.375	- 0.07	+ 0.0012
Steam flow rate per SG (kg/s)	801.4	**+ 0.977**	
Containment pressure (MPa)	0.1	+0.1	

Reference case analysis results: the code run for the transient analysis was carried out until 72 h after the STSBO. Tables 21 and 22 summarize timings of the key events predicted by MELCOR and MAAP5, the amount of combustible gas (H_2, CO) generated in the in- and ex-vessel, and the environmental release of fission product Cs, respectively.

The analysis results for each reference case are discussed as follows:

— *MELCOR predictions (shown in Figs. 37–45)*: the base case results shows that, due to a continuous boiling in the core region and insufficient heat removal through the steam generator secondary side, the water level of the reactor core and RPV dropped below the top of active fuel at approximately 2.09 h (i.e., core uncover) after the initiation of the accident (FOM 1). Shortly after, the CET reached the SAMG entrance point at approximately 2.42 h. Then after, the inflow of the hot steam and gas into the hot leg from the reactor core by natural circulation heated up the hot leg nozzle and, as a result, the hot leg ruptured at 3.22 h. Thereafter, the primary side pressure reached the SIT injection set-point, but the lower head ruptured at approximately 6.77 h (FOM 2). Since no subsequent actions for the reactor cavity flooding were taken in the base case scenario, molten debris discharged through the lower head rupture led to MCCI in the cavity. After failing the RCS pressure boundary, the containment pressure increased up to its rupture point, due to the continuous release of the steam from the core to the containment and non-condensable generated by the ex-vessel MCCI.

  For reference, Fig. 40 shows that the reactor cavity wall is gradually ablated after 24 h. This is just because the decay heat generated from molten corium accumulated in the cavity completely depleted the cavity water at approximately 24 h. After all, the containment building failed at approximately 47.94 h (FOM 3), but the reactor cavity maintained its integrity since the depth ablated by the MCCI did not exceed a design thickness of 4.57 m. In the base case, hydrogens of 573.0 and 658.0 kg (FOMs 4 & 5) were generated in the in-vessel before the RCS pressure boundary fails, and by the MCCI in the ex-vessel cavity, respectively. CO gas of 972 kg was generated by the MCCI during 72 h after the initiation of the accident (FOM 6) and Cs of 5.71% was released through the damaged containment into the environment (FOM 7).

Case 1 is the mitigation strategy injecting manually the external (emergency) water into the primary side with the mobile pump at the SAMG entrance point. For the measure, the operator manually opens the SDS valves to drop the RCS pressure at approximately 2.42 h after the ignition of the accident and so that the SIT water is passively injected into the RCS. Consequently, the dedicated mitigation action, delayed greatly the subsequent accident progressions, compared to the base case and the hot leg and RPV lower head kept their integrity (FOM 2). Whereas the containment (FOM 3) failed slightly faster than the base case because the steam released from the core into the containment was much more than that of the base case. Also, the combustible gases generated in both in- and ex-vessel (FOMs 4–6) and the Cs release into the environment (FOM 7) were greatly reduced, compared to the base case.

TABLE 21. KEY EVENT TIMINGS [IN HOURS]

Events	**MELCOR**			**MAAP5**		
	Base case	**Case 1**	**Case 2**	**Base case**	**Case 1**	**Case 2**
Reactor trip				0.0		
Open of MSSV		0.01			0.02	
Dryout of SGs		1.02			1.14	
Open of PSV		1.39			0.96	
Core uncover (**FOM 1**)		2.09			1.93	
SAMG entry		2.42			2.40	
Clad oxidation	2.45	2.49	–		2.18	
SDS valves open	n.a.	2.42	2.42	n.a.	2.40	2.40
Cladding failure	2.49	3.56	–	2.47	2.46	2.46
Hot leg rupture	3.21	–	–	3.73	–	–
SIT injection	3.22	2.48	2.48	3.75	2.59	2.59
Two ADVs open	n.a.	n.a	4.0	n.a.	n.a	4.0
EWI (RCS, SG)	n.a.	4.00	4.03	n.a.	5.02	4.05
SIT injection stop	3.32	2.54	7.77	3.78	15.44	4.11
Support plate fail	6.07	–	–	6.61	–	–
RPV lower head failure (**FOM 2**)	6.77	–	–	7.98	–	–
Reactor building failure (**FOM 3**)	47.94	44.40	–	44.44	37.68	–

Case 2 is the mitigation strategy depressurizing the RCS using the SDS valves as in Case 1, but they are closed manually at the RCS pressure of 1.196 MPa in Case 2. As a result, the SIT injection was continued longer compared to Case 1. Following operator action made for the external water injection into the SG, the RCS pressure boundary (FOM 2) and the containment (FOM 3) kept their integrity in Case 2. Also, no combustible gases (FOMs 4–6) were not generated and no Cs (FOM 7) was not released in Case 2. This means that Case 2 is much more effective mitigation strategy for the STSBO accident, compared to Case 1.

TABLE 22. COMBUSTIBLE GASES AND Cs RELEASE

FOMs	MELCOR			MAAP5		
	Base case	Case 1	Case 2	Base case	Case 1	Case 2
FOM 4 (kg)	573	226	–	616	26	–
FOM 5 (kg)	658	–	–	2,020	–	–
FOM 6 (kg)	972	–	–	4,579	–	–
FOM 7 (–)	0.057	3.6×10^{-4}	–	0.107	–	–

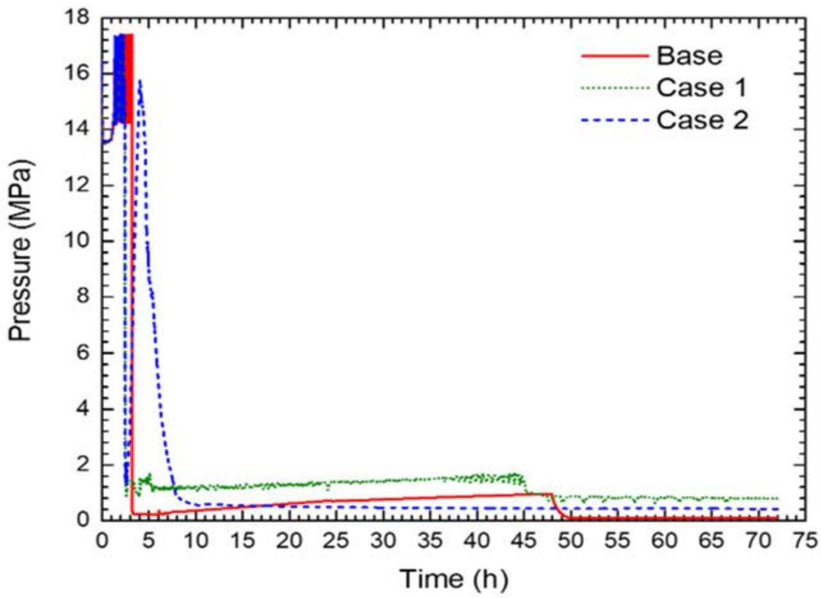

FIG. 37. MELCOR results: RCS pressure.

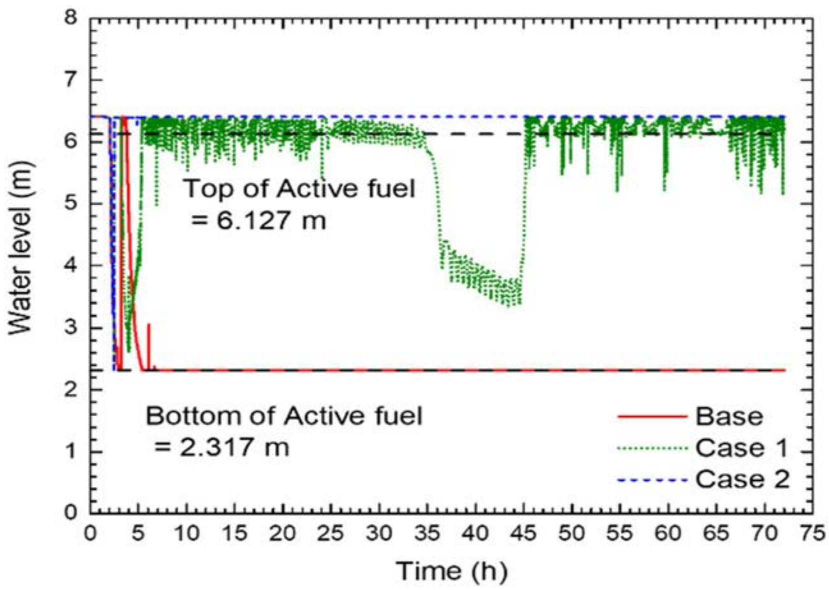

FIG. 38. MELCOR results: RPV/core water level.

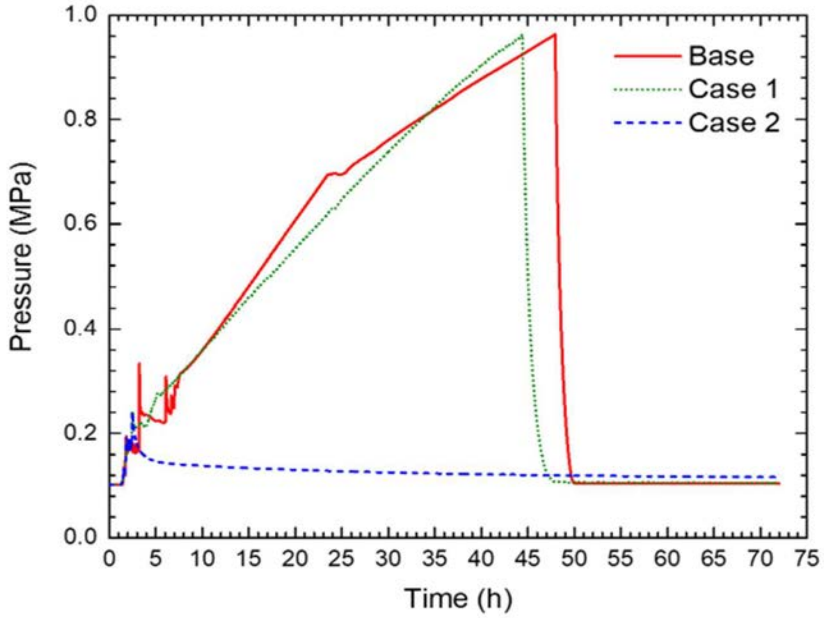

FIG. 39. MELCOR results: containment pressure.

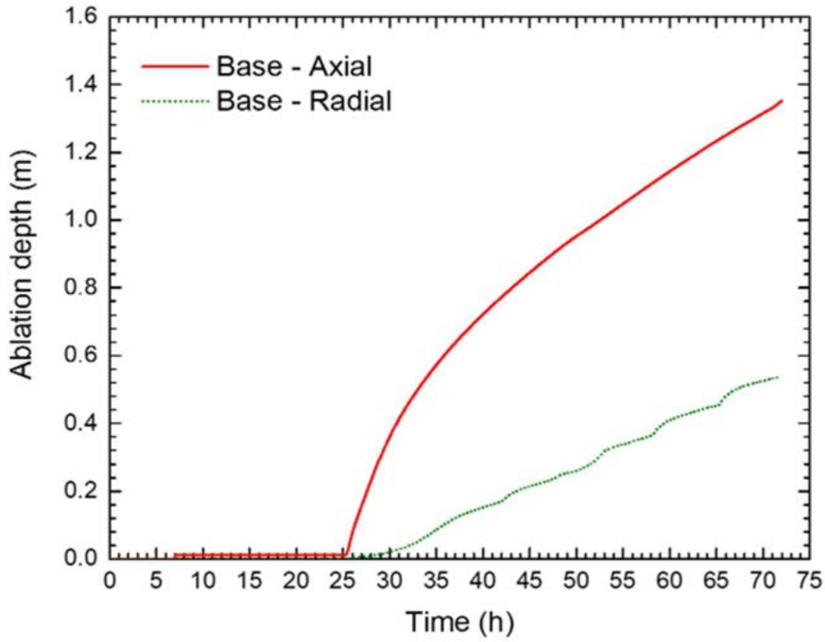

FIG. 40. MELCOR results: concrete erosion by MCCI.

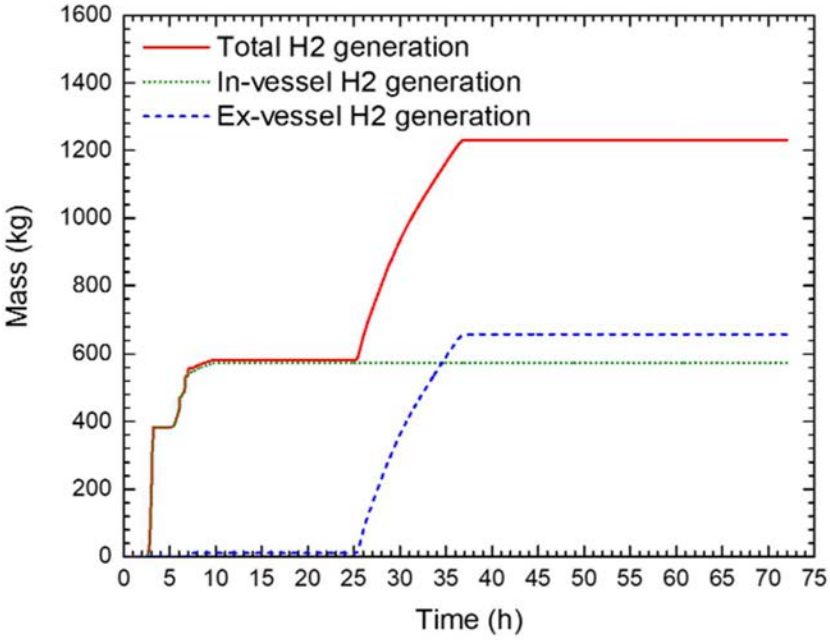

FIG. 41. MELCOR results: in-/ex-vessel H_2 generation (base case).

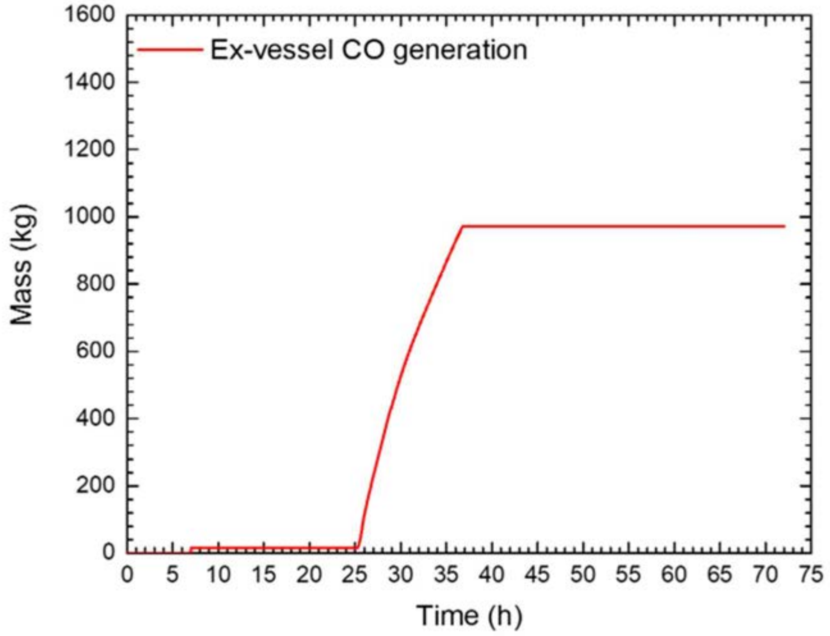

FIG. 42. MELCOR results: ex-vessel CO generation (base case).

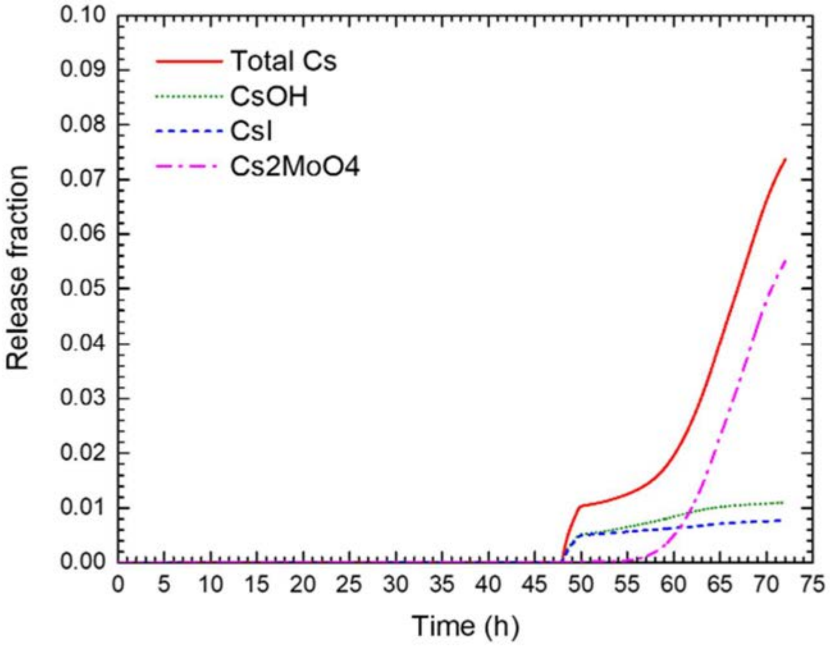

FIG. 43. MELCOR results: environmental release of Cs (base case).

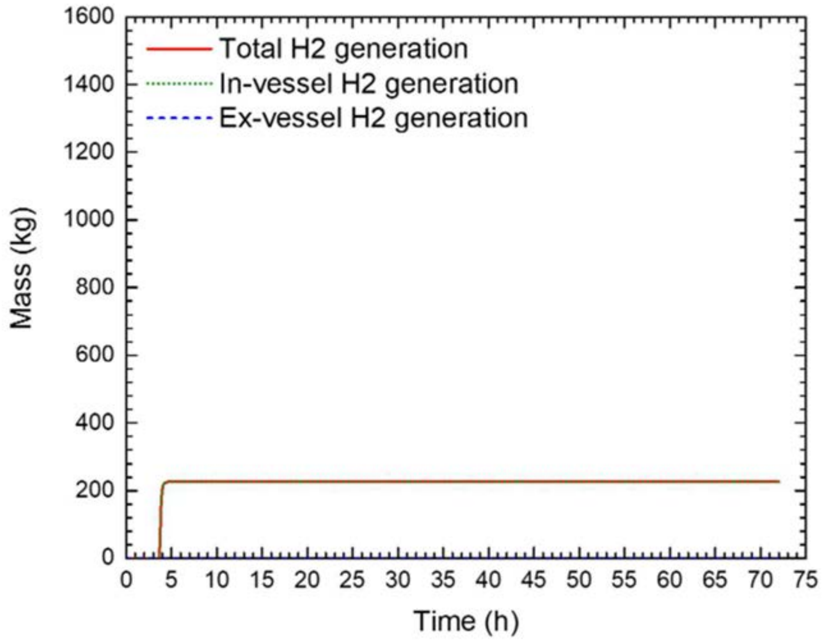

FIG. 44. MELCOR results: in-/ex-vessel H2 generation (case 1).

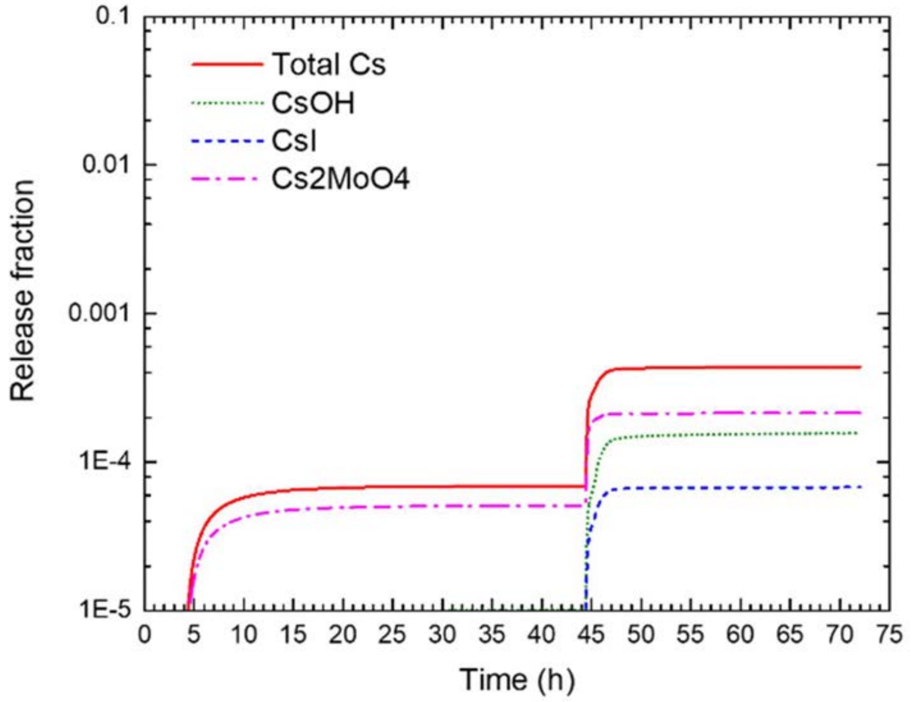

FIG. 45. MELCOR results: environmental release of Cs (case 1).

— *MAAP5 predictions (shown in Figs. 46–54)*: for the base case, MAAP5 predicted he similar trend of accident progression with MELCOR, but, for the timings of the key events after the failure of cladding (including FOMs 1–2) and FOMs 5–7, there were greater or lesser differences, as shown in Tables 21–22. While MAAP5 predicted somewhat later than MELCOR for the FOM 2 (RPV lower failure time), the containment failure (FOM 3) took place at almost the same time (44 h). Also, while both codes predicted a similar amount of hydrogen in the in-vessel (FOM 4), MAAP 5 predicted much larger amount of H_2 and CO than MELCOR in the ex-vessel (FOMs 5–6). This seems be mainly due to the difference of modeling schemes employed for the MCCI phenomena, related to closely the generation of the foregoing gases. Besides, there was a great difference between both codes in predicting the Cs release into the environment (FOM 7); MAAP5 predicted a double than that of MELCOR (5.7%). This also indicates that the fission product release and transport models employed both codes influenced such results.

For Cases 1 & 2, MAAP5 predicted similar trends of accident progressions with MELCOR after taking the relevant mitigation actions. Also, likewise MELCOR, Case 2 was much more effective mitigation strategy for the STSBO accident, compared to Case 1.

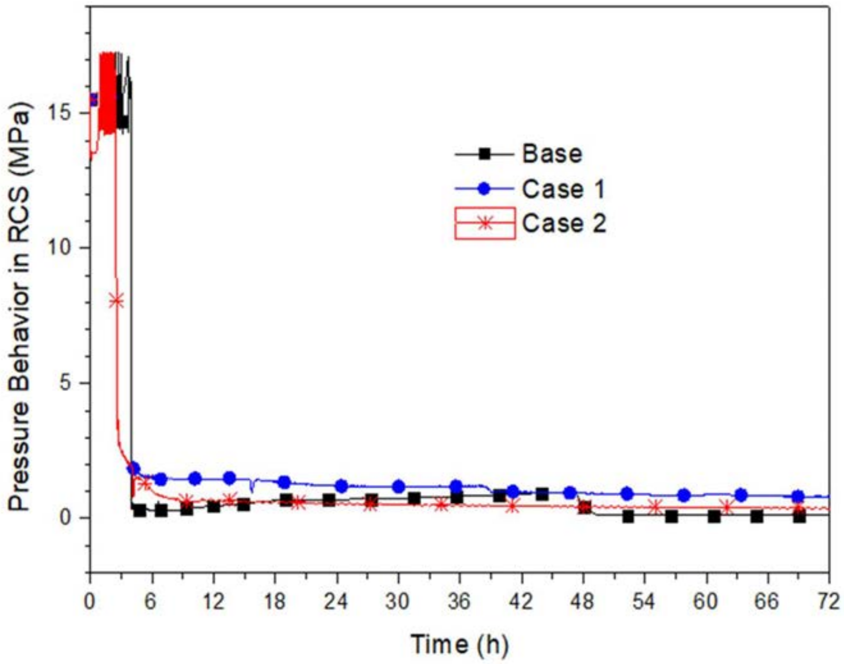

FIG. 46. MAAP5 results: RCS pressure.

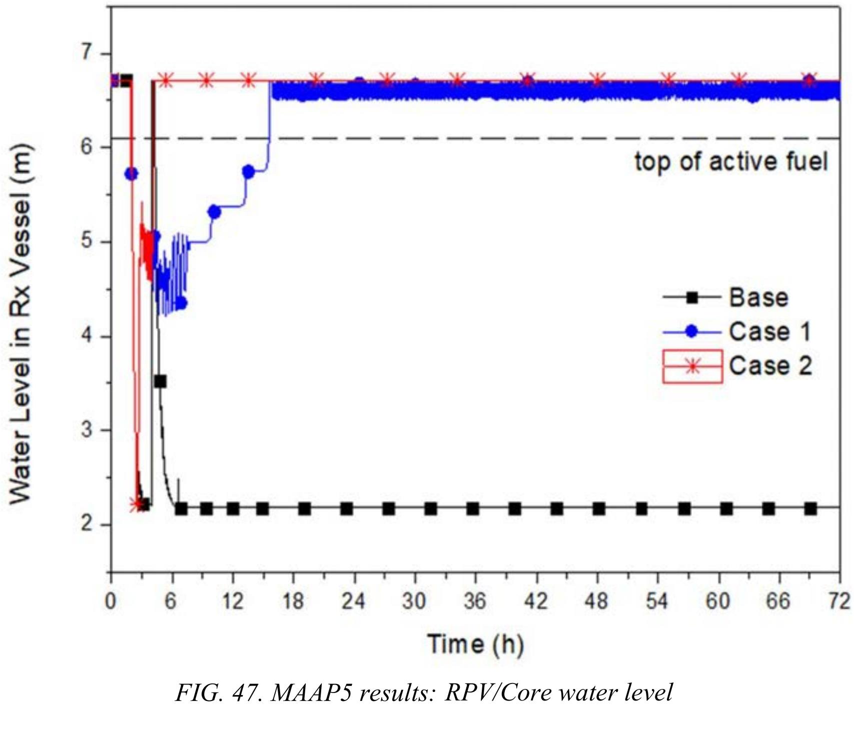

FIG. 47. MAAP5 results: RPV/Core water level

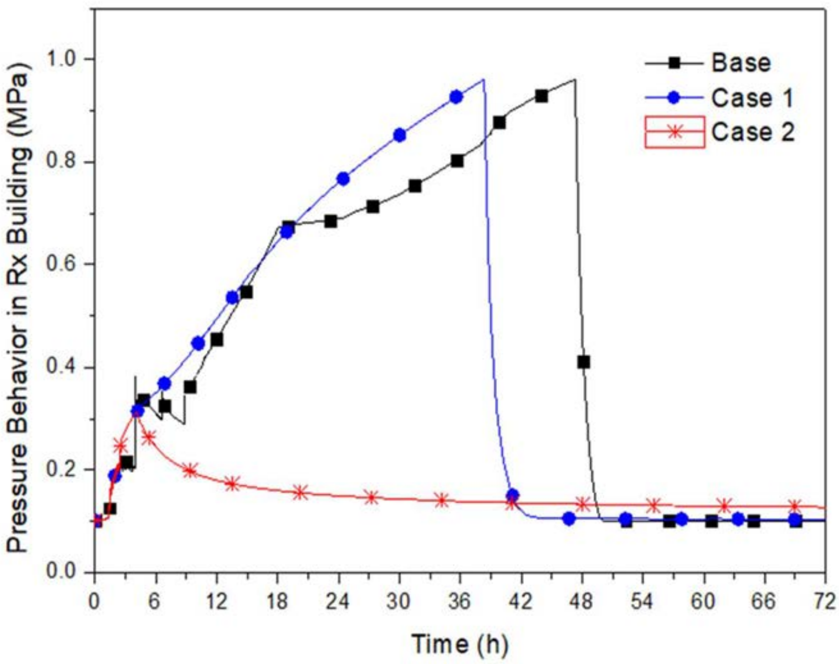

FIG. 48. MAAP5 results: containment pressure.

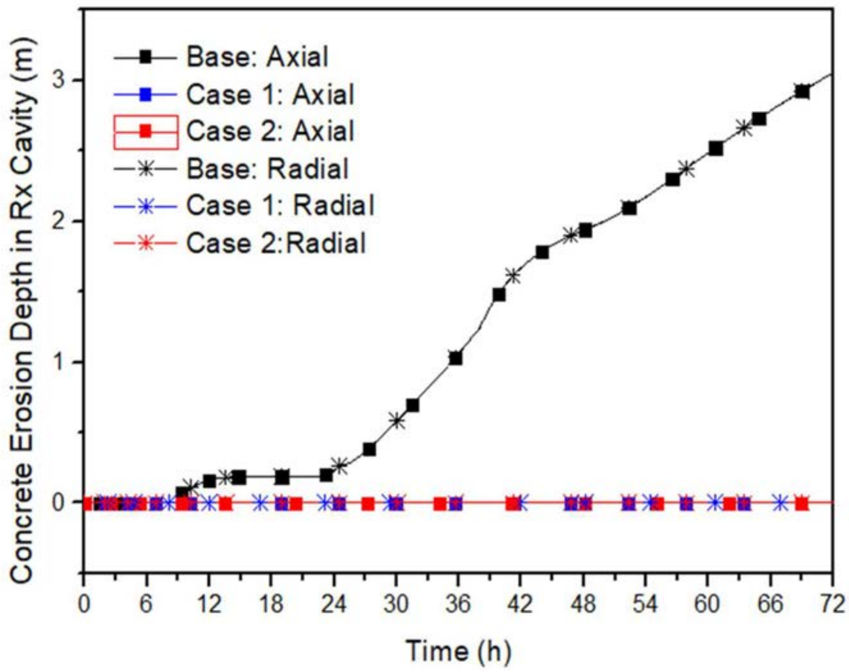

FIG. 49. MAAP5 results: concrete erosion by MCCI.

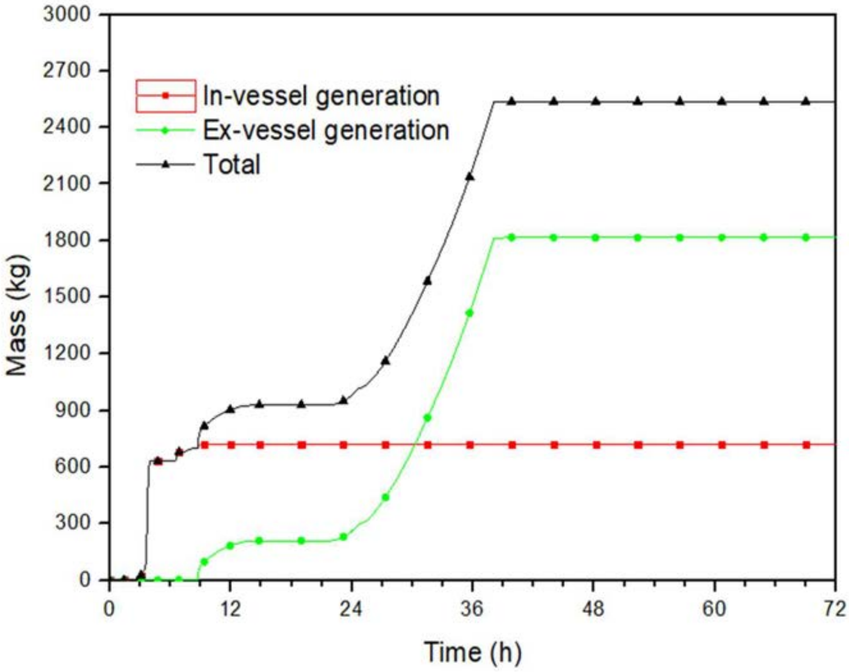

FIG. 50. MAAP5 results: in-/ex-vessel H_2 generation (base case).

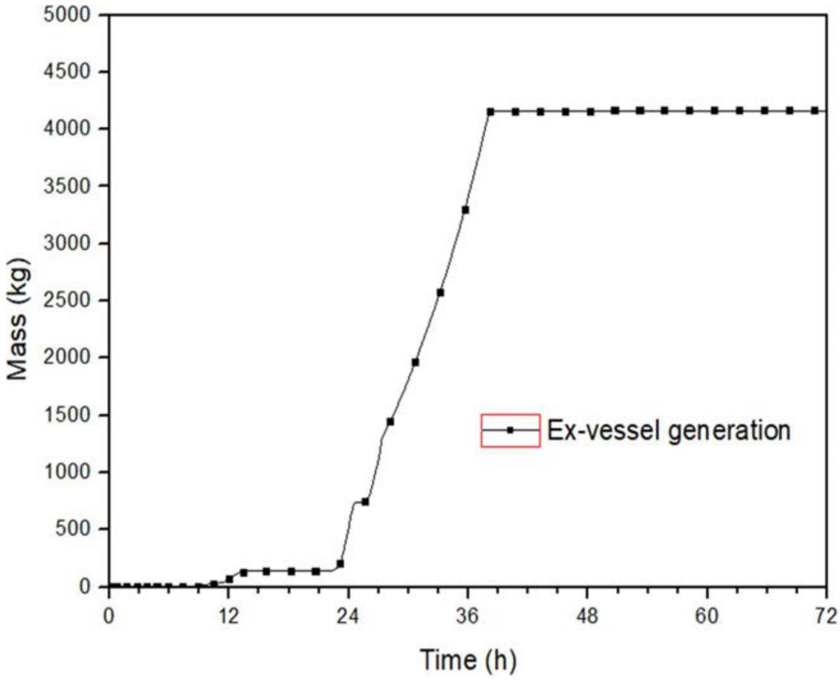

FIG. 51. MAAP5 results: ex-vessel CO generation (base case).

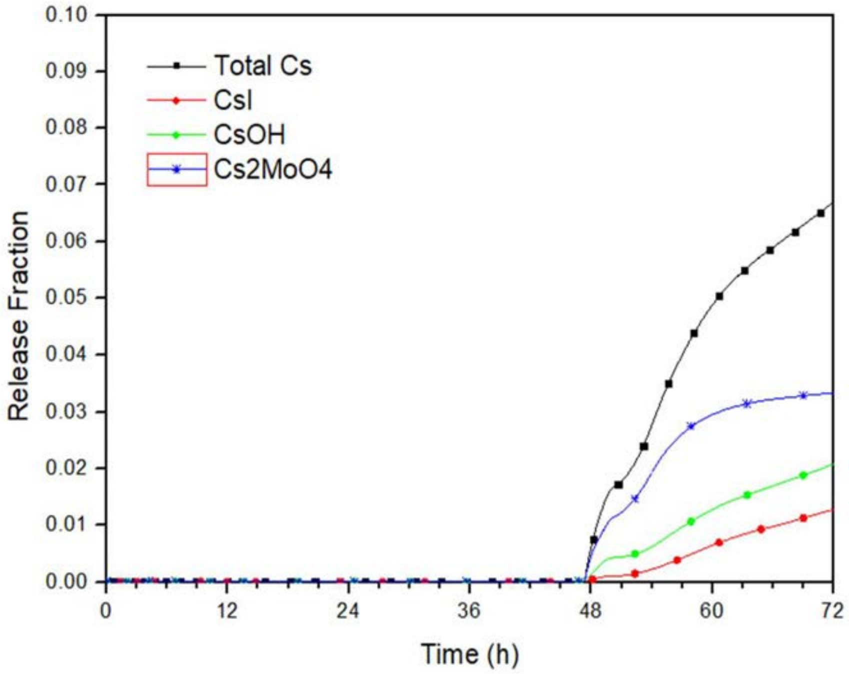

FIG. 52. MAAP5 results: environmental Cs release (base case).

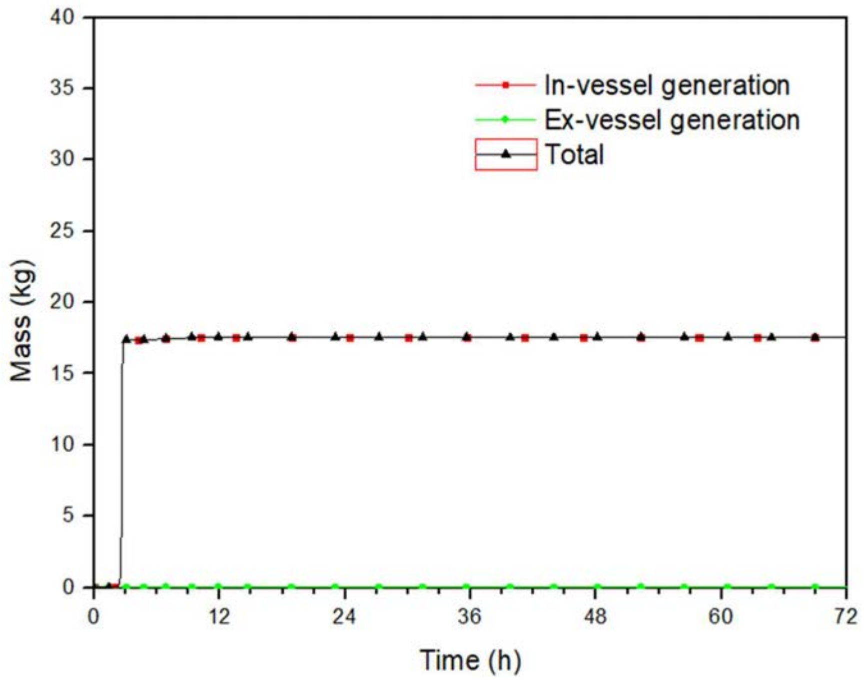

FIG. 53. MAAP5 results: in-/ex-vessel H_2 generation (case 1).

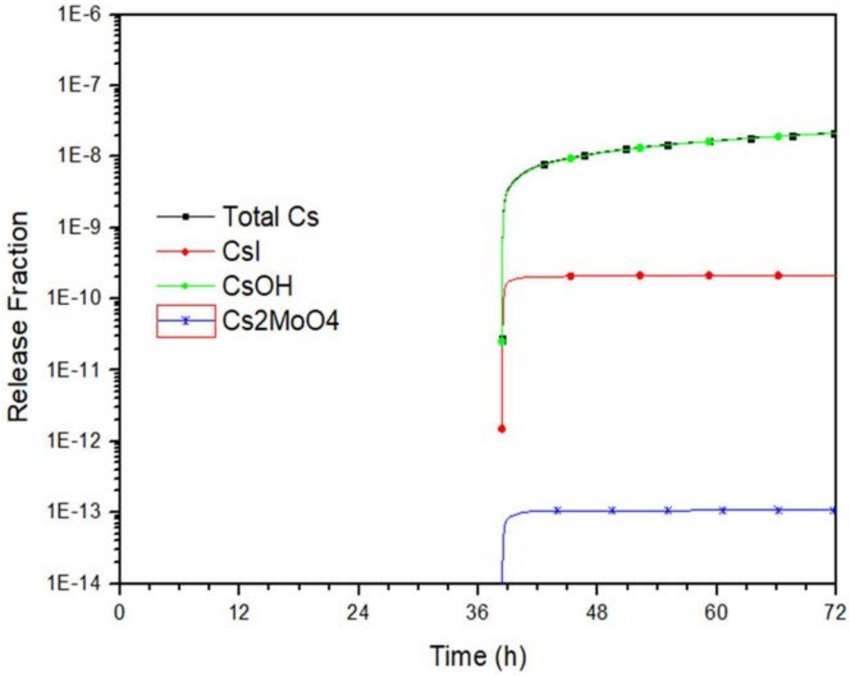

FIG. 54. MAAP5 results: environmental Cs release (case 1).

<u>Uncertainty and sensitivity analysis results</u>: for the three case scenarios, the random samples of 200 are simulated until 72 h after the initiation of the accident. The summary of results are as follows:

— *MELCOR uncertainty analysis results*: around 30% failed among the tested 200 samples, without sharing any specific tendency. The reason might be due to combinations of physically unreasonable inputs in the random sampling process and/or closely related to the minimum time steps as required for a numerical convergence. Thus, the failed runs were removed from the analysis of FOMs and, among the normal ones, the 100 samples were randomly taken for the final analysis.

  Tables 23 and 24 summarize mean values of the uncertainty results for the forgoing three cases, i.e., a base and two mitigations, as predicted by the MELCOR code.

  Figures 55–59 show the corresponding time trends and cumulative distribution functions (CDFs) for each relevant FOM, respectively. Tables 25 and 26 provide the corresponding statistical properties for each relevant FOM.

  The MELCOR analysis results show that mean values for the three cases were almost the same as the corresponding reference results as presented in Tables 21 and 22, until before taking dedicated mitigation actions. But, thereafter, each case scenario led to somewhat different trends with respect to the respective means. For example, some key events like the creep rupture of hot leg, failure of fuel cladding, failure of the RPV lower head (FOM 2), and in-vessel oxidation of Zr and steel (FOM 4), were observed depending on the uncertainty inputs employed for the present analysis. However, as shown in Table 21, such events are not predicted in the reference analyses for the two mitigations.

TABLE 23. KEY EVENT TIMINGS (MELCOR) (IN HOURS)

Events	**Uncertainty mean**		
	Base case	**Case 1**	**Case 2**
Reactor trip	0.0		
Open of MSSV	0.01		
Dryout of SGs	1.03	1.04	1.02
Open of PSV	1.40	1.41	1.38
Core uncover (**FOM 1**)	2.11	2.13	2.08
SAMG entry	2.44	2.46	2.40
Clad oxidation	2.47	2.99	2.40(3)
SDS valves open	n.a.	2.42	2.40
Cladding failure	2.52	3.53	3.77(4)
Hot leg rupture	3.27	4.11(1)	–
SIT injection	3.27	2.52	2.46
Two ADVs open	n.a.	4.00	–
SIT injection stop	3.35	2.65	7.06
EWI (RCS/SG)	n.a.	4.00	4.03
Support plate fail	6.31	–	–
RPV lower head failure (**FOM 2**)	7.30	– (2)	– (5)
Reactor building failure (**FOM 3**)	49.54	46.44	–

(1)64 samples with a mean of 4.11 h; (2)1 sample at 6.86 h; (3)54 samples; (4)17 samples; (5)4 samples with a mean of 5.55 h.

TABLE 24. COMBUSTIBLE GASES AND Cs RELEASE (MELCOR)

FOMs	**Uncertainty mean**		
	Base case	**Case 1**	**Case 2**
FOM 4 (kg)	445	191	(negligible)
FOM 5 (kg)	961	–	–
FOM 6 (kg)	1,301	–	–
FOM 7 (–)	0.0583	0.0039	8.66×10^{-4}(1)

(1)Cs release via the containment design leak rate: 16 samples, with 4 cases greater than 0.01.

TABLE 25. STATISTICS OF RELEVANT FOMs (BASE CASE)

FOMs	**5th percentile**	**Median**	**95th percentile**	**Standard deviation**	**Mean**
FOM 1 (h)	1.86	2.10	2.35	0.16	2.11
FOM 2 (h)	6.53	7.29	8.10	0.50	7.30
FOM 3 (h)	42.17	49.05	57.35	4.81	49.54
FOM 4 (kg)	374.0	440.0	533.0	53.0	445.0
FOM 5 (kg)	678.0	1,014	1,121	161	961
FOM 6 (kg)	874.0	1,383	1,547	240	1,301
FOM 7 (–)	0.0217	0.0613	0.0902	0.0221	0.0583

TABLE 26. STATISTICS OF RELEVANT FOMs (CASES 1 & 2)

FOMs	**Cases**	**5th percentile**	**Median**	**95th percentile**	**Standard deviation**	**Mean**
FOM 3 (h)	Case 1	37.9	47.7	55.8	5.93	46.4
FOM 4 (kg)	Case 1	118.3	195.0	261.2	42.0	191.1
FOM 7 (–)	Case 1	1.80×10^{-4}	8.59×10^{-4}	0.0166	0.00945	0.00392
	Case 2	–	–	1.01×10^{-6}	0.00456	8.66×10^{-4}

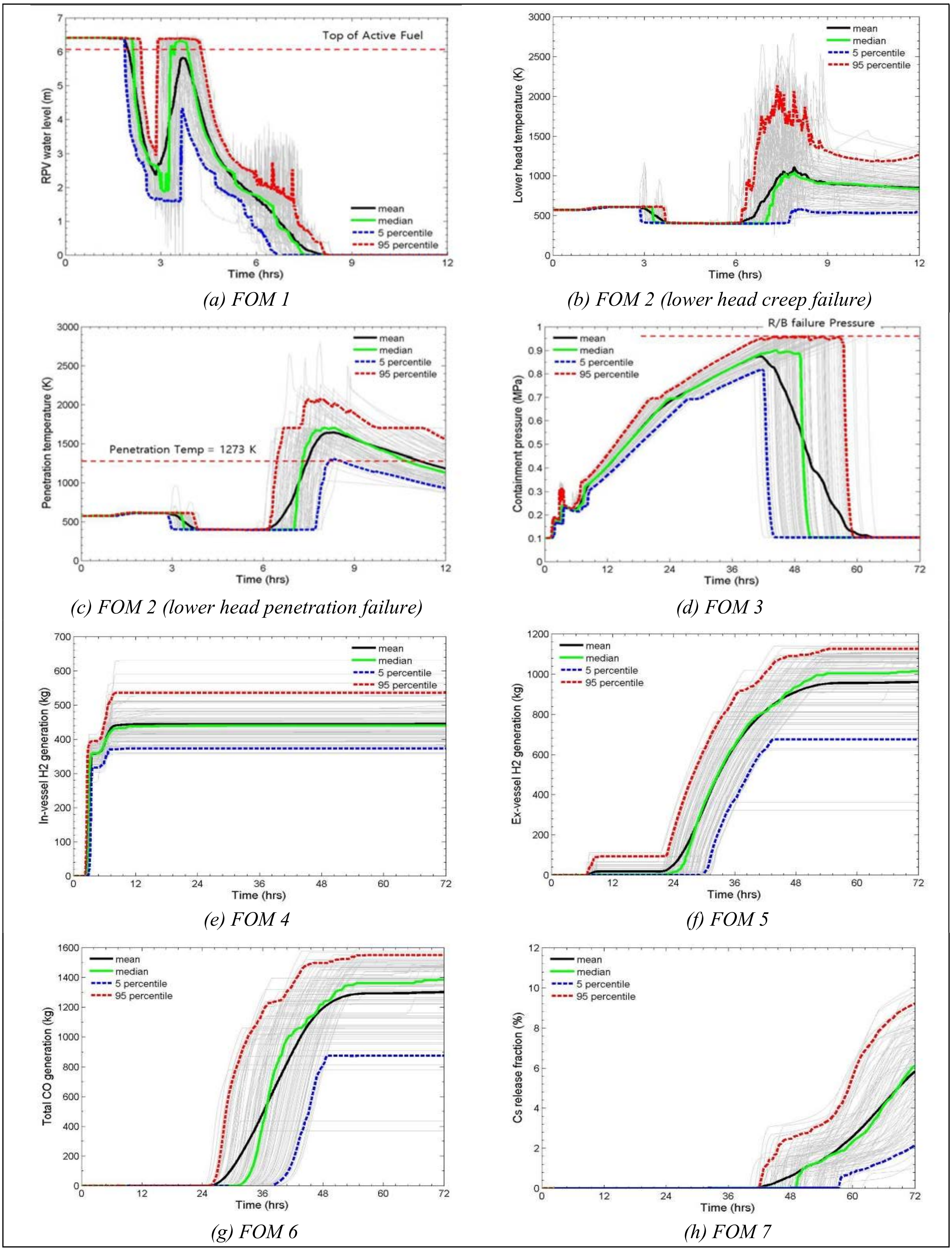

(a) FOM 1

(b) FOM 2 (lower head creep failure)

(c) FOM 2 (lower head penetration failure)

(d) FOM 3

(e) FOM 4

(f) FOM 5

(g) FOM 6

(h) FOM 7

FIG. 55. MELCOR uncertainty results (base case).

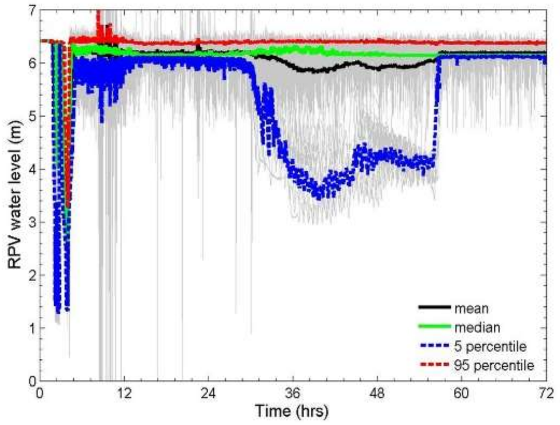

(b) FOM 1

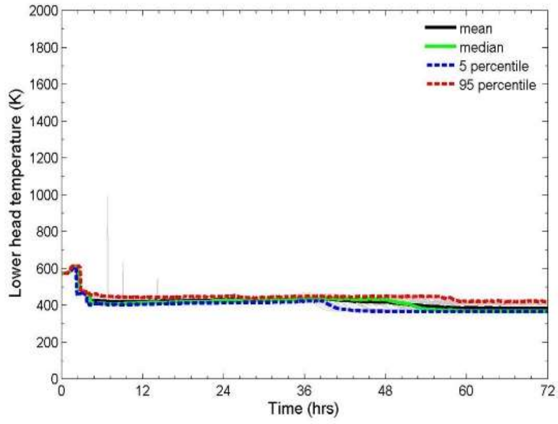

(c) FOM 2 (lower head creep failure)

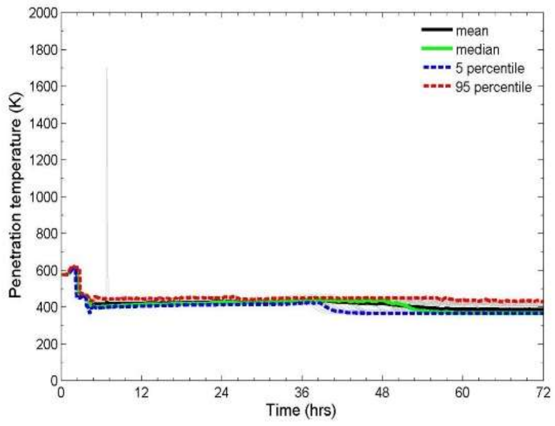

(d) FOM 2 (lower head penetration failure)

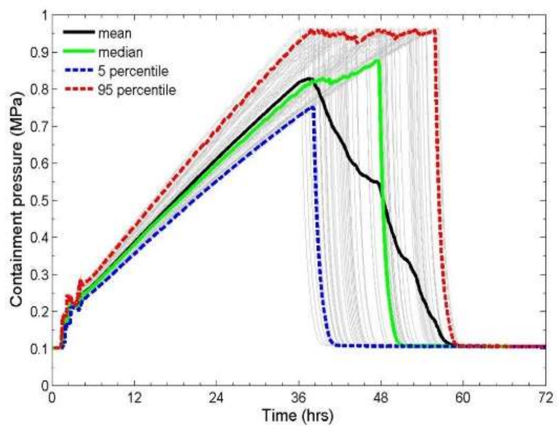

(e) FOM 3

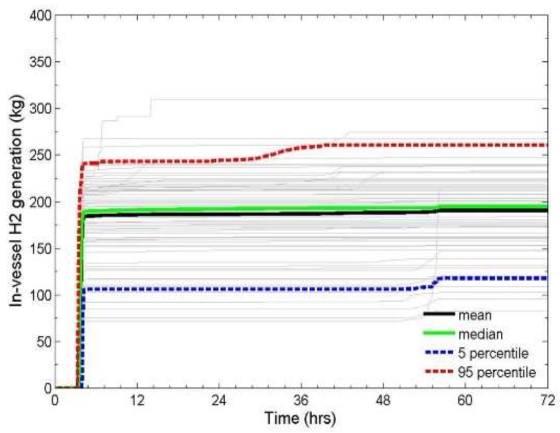

(f) FOM 4

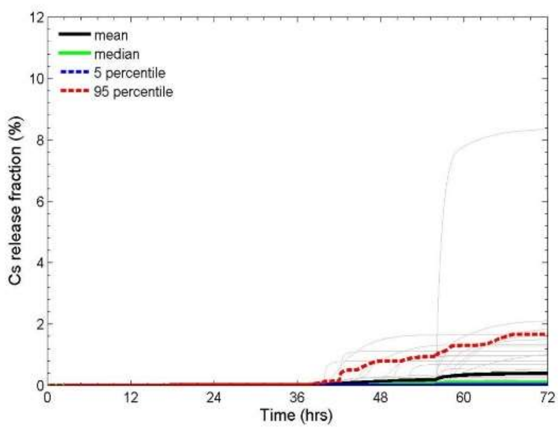

(g) FOM 7

FIG. 56. MELCOR uncertainty results (case 1).

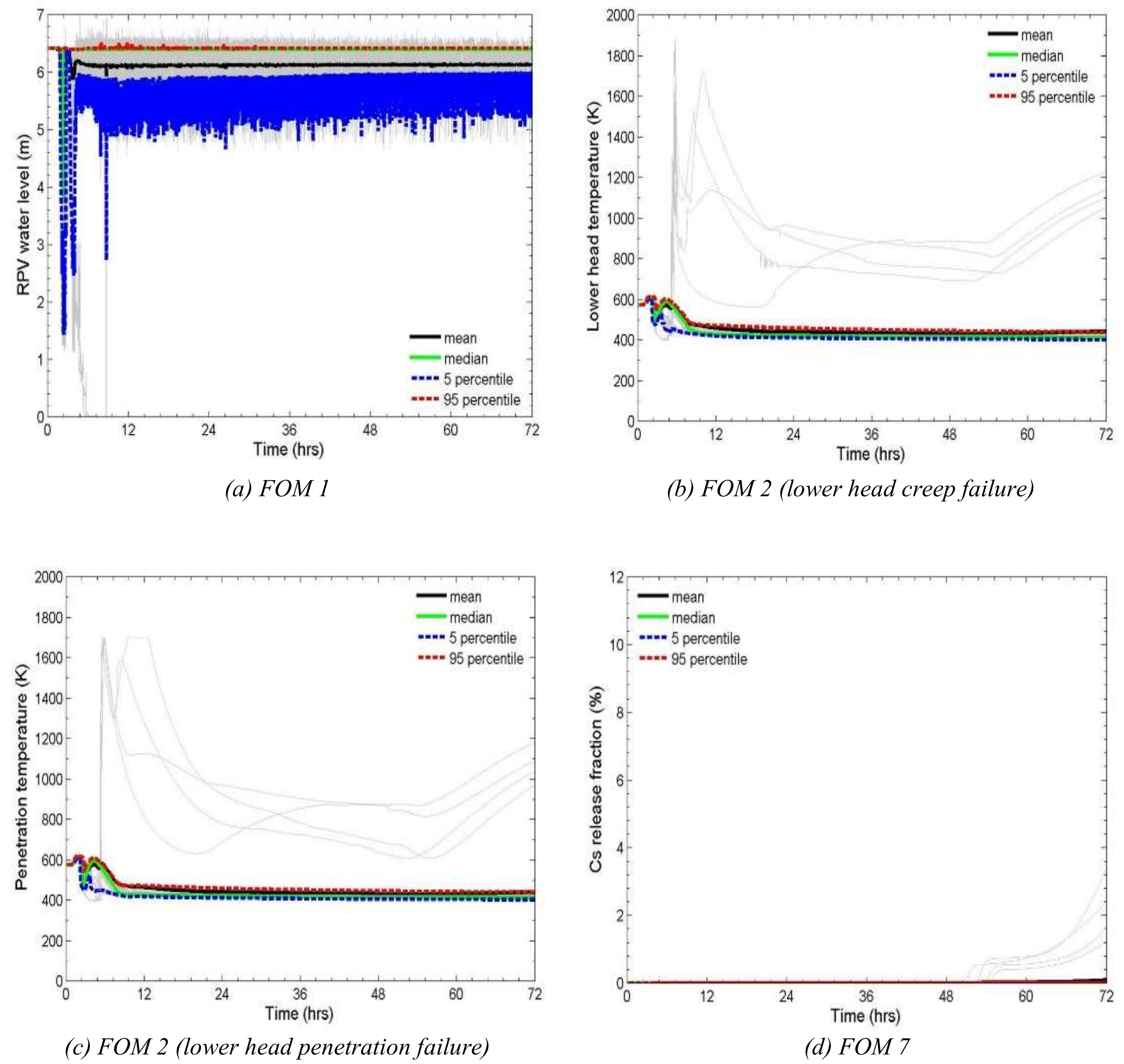

(a) FOM 1

(b) FOM 2 (lower head creep failure)

(c) FOM 2 (lower head penetration failure)

(d) FOM 7

FIG. 57. MELCOR uncertainty results (case 2).

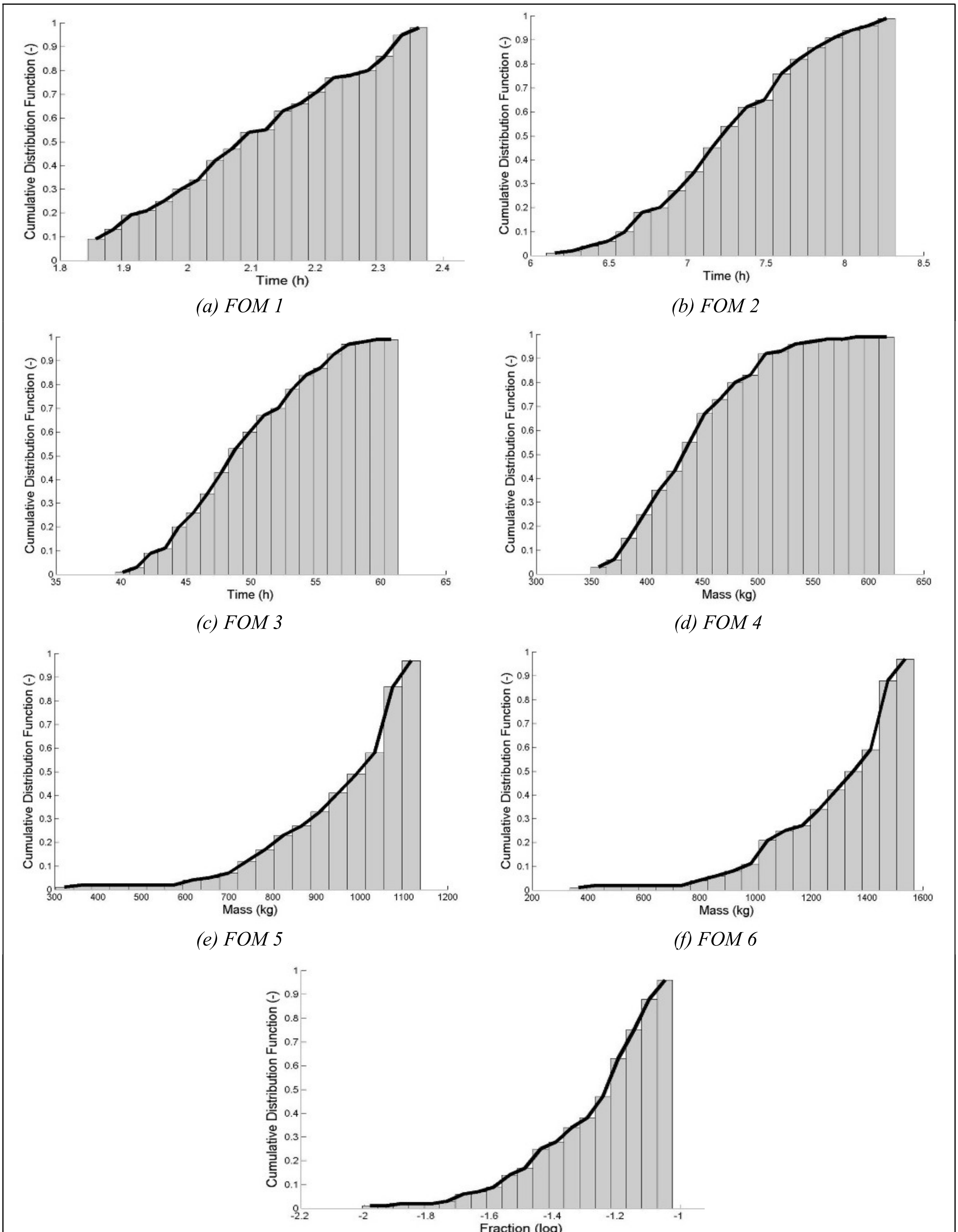

(a) FOM 1

(b) FOM 2

(c) FOM 3

(d) FOM 4

(e) FOM 5

(f) FOM 6

(g) FOM 7

FIG. 58. MELCOR uncertainty results (CDF, base case).

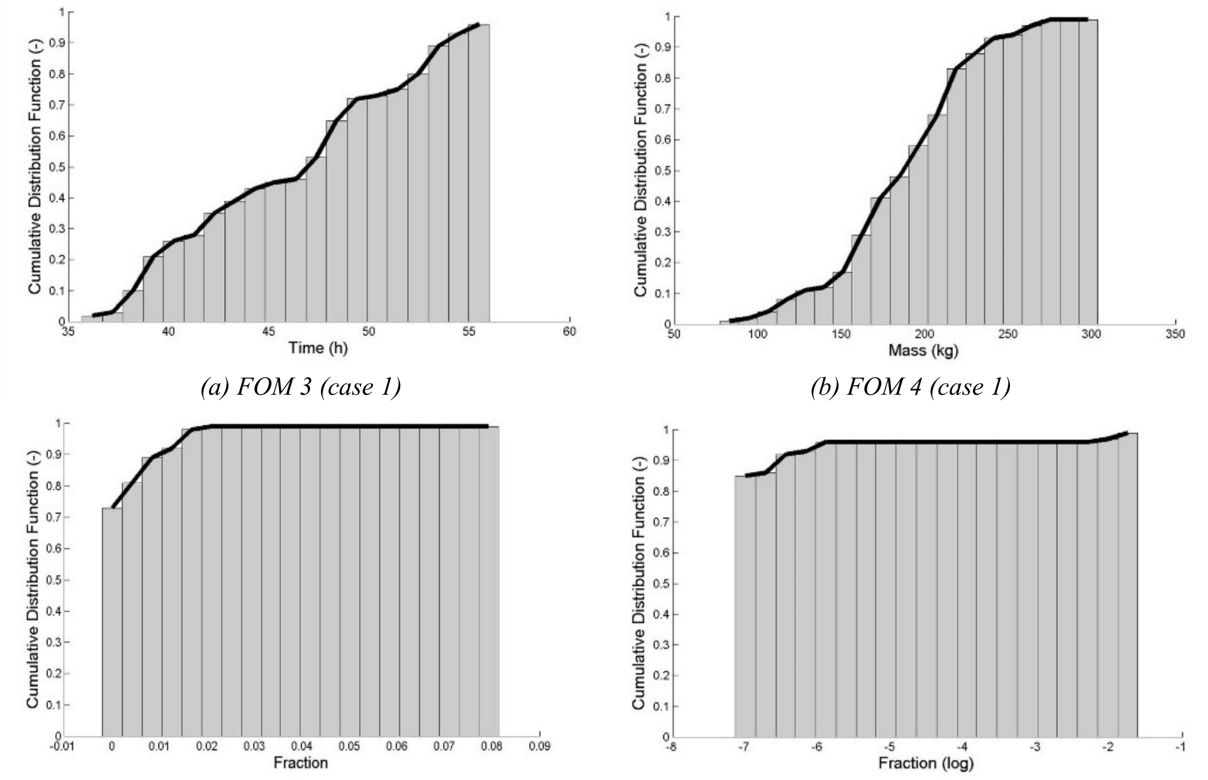

(a) FOM 3 (case 1)

(b) FOM 4 (case 1)

(c) FOM 7 (case 1)

(d) FOM 7 (case 2)

FIG. 59. MELCOR uncertainty results (CDF, cases 1 & 2).

- **MELCOR base case**: according to the first column of Table 23, the difference between the reference value (i.e., point estimate) and the mean value of the corresponding uncertainty results was negligible until before reaching the SAMG entrance point from the initiation of the accident, including FOM 1. Otherwise, the mean values for FOMs 2–3 were 0.5 to 1.5 h longer, compared to the reference cases (i.e., point estimates) of Table 21. According to Figs. 57 (b) and (c), the reference failure times (6.77 h and 47.94 h) for FOMs 1–2 correspond to the lower 20th and 45th percentiles in the relevant CDFs, respectively.

  In the case of FOMs 4–6, their mean values were estimated as 445 kg, 961 kg, and 1,301 kg, respectively. While the mean of FOM 4 slightly underestimates over the corresponding reference value (573 kg), the latter two FOMs are much greater than the reference values (658 and 972 kg) in Table 22. According to Figs. 57 (d)–(f), these reference values correspond to the upper 97th, lower 4th, and lower 10th percentiles in the relevant CDFs, respectively. The mean value (0.058) of FOM 7 is almost the same as the reference case (0.0571), whose value matches the lower 45th percentile of the relevant CDF in Fig. 57 (g).

- **MELCOR mitigation case 1**: although the dedicated operator action was taken in case 1 (i.e., SAG-3: RCS water level control using the EWI into it at approximately 4 h after the beginning of the STSBO), the hot leg creep rupture took place in 64 sample cases, as shown in Table 23, but its frequency was greatly reduced compared to the corresponding base case.

These hot leg creep ruptures in case 1 are mainly due to both thermal and pressure stress exerted to the RCS pressure boundary by both temperature and pressure peaks of 1,500–1,600 K and 2–4 MPa, which took place just after the mitigation action. For reference, the creep time of the hot leg was steeply decreased below hundreds or tens of seconds in these temperature and pressure peaks, consequently leading to the hot leg creep rupture during the short temperature peak. Regardless of the foregoing hot leg creep ruptures, the RPV failure (FOM 2) was observed in only 1 sample case, as shown in Table 23.

On the other hand, the dedicated mitigation action prolonged the steam generation in the core and, in turn, the steam released via the ruptured hot leg continuously increased the containment pressure. As a result, the mean containment failure time of 46.44 h (FOM 3) was estimated in case 1, 3 h faster than the reference case (49.54 h), whose value matches the median value of the relevant CDF in Fig. 58 (a).

With respect to FOM 4, Table 24 shows that a moderate amount of H_2 was generated in in-vessel (191 kg), slightly less than the reference case (226 kg), whose value matches the upper 86th percentile of the relevant CDF in Fig. 58 (b). The difference between the base case and case 1 mainly arises from the difference in time duration between the core uncovery and the injection of SIT water into the RCS: the longer exposition of the fuel cladding to in-vessel steam leads to the more oxidation and H_2 generation. Owing to the mitigation action by which the lower head failure did not occur, no combustible gas (H_2 and CO) were generated in the ex-vessel phase (FOMs 5 and 6). Whereas, due to faster failure of the containment than the reference case led to the mean value of 3.9×10^{-3} for FOM 7, one order greater than that of the reference case (3.6×10^{-4}), as shown in Table 22.

- **MELCOR mitigation case 2**: although the dedicated operator action was taken in case 1 (i.e., SAG-1: Steam generator water level control using the EWI into it at approximately 4 h after the initiation of the accident), unlike the case 1, the cladding failure occurred in 17 samples in case 2, as shown in Table 23. These cladding failures could be caused by the difference of SIT injection time and the uncertainty of decay heat. Also, differed from the case 1, no hot leg creep rupture was observed in case 2. On the other hand, the RPV lower head failure (FOM 2) was observed in 4 sample cases, while its integrity was maintained in the case 1 except for only 1 sample case.

  Owing to the dedicated action taken for heat removal of the reactor core via the steam generator secondary side in case 2, the reactor core continuously maintained a coolable state. As a result, the containment (FOM 3) maintained its integrity in case 2, while failed in most samples in case 1, as shown in Table 23.

  Table 24 shows that only a negligible amount of H_2 and CO generation (FOM 5 to FOM 6) was observed in the in-/ex-vessel in case 2. With respect to the environmental release of Cs (FOM 7), only a small amount of release via the design leakage of containment but not through its rupture was observed in case 2, with the mean value of 8.66×10^{-4}.

— *MELCOR sensitivity analysis results*: four sensitivity measures, Pearson and Spearman correlations coefficients PRCC, and SRRC, were estimated to investigate more influencing contributors on each FOM and relevant results are presented in Figs. 59 and 60. Except the Pearson correlation, the remaining three measures are based on non-parametric rank correlation and regression methods. Relating to the PRCC and SRRC, the input parameters having the R^2 value less than 0.5, were excluded in these figures, because the relevant regression performances were not enough to provide meaningful information. Fig. 61 summarizes the key contributors, having stronger correlations with each FOM than others, determined by a weighted average of meaningful sensitivity measures.

- **FOM 1 (core uncovery time, all the three cases):** because the dedicated mitigation actions (i.e., SAG-1 and SAG-3) are taken before the core uncover and core degradation, the influence of relevant uncertainty inputs on FOM 1 was similar in the three case scenarios. This is because FOM 1 is mainly influenced by relevant thermal hydraulics in the core as well as the decay heat until the core damage. Among them, the highest contributor on FOM 1 was SC3200_1 (proportional constant for decay heat calculation), having a very strong negative correlation with FOM 1. This is just because the larger SC3200_1 causes the coolant faster boiling and, in turn, the earlier core uncovery. FCELR and FCELA (related to the radial and axial radiative heat transfer between fuel cells) also somewhat affected the decrease of core water level and associated core uncover time, because the core heat is dissipated by the radiative heat transfer. But, since the relevant sensitivity measures were less than 0.1, their influence was minor for FOM 1.

- **FOM 2 (RPV failure time, base case only):** thanks to the dedicated mitigation actions, only a few number of RPV failures was observed in two mitigation cases, as shown in Figs. 60 and 61. Thus, the relevant sensitivity analysis was limited to only the base case. Among the uncertainty inputs influenced FOM 2, SC3200_1 is the most influential one, having a very strong negative correlation with FOM 2. This is because the RPV failure criteria employed in this study are closely related to the temperature of the lower head, the higher SC3200_1 causes an earlier RPV failure by the higher decay heat. HDPBN (heat transfer between the debris and the penetration) and COR_CHT_SS (candling heat transfer of steel parts in the core) were also additional contributors greatly influenced FOM 2. The larger HDPBN transfers the more heat to the penetration, consequently leading to its earlier failure. Also, the larger COR_CHT_SS could delay the failure time for the RPV since the relocation of molten corium and subsequent lower head heating are delayed by the event. TPFAIL (temperature criteria of the RPV failure) also somewhat influenced FOM 2 since the higher TPFAIL value, the longer time needs to reach the RPV failure temperature. SC1020_2 (parameter for the radial relocation speed of the molten corium) was the fifth important contributor to FOM 2 since the higher SC1020_2 quickly moves the molten corium to the radial direction and thus the axial relocation of the molten corium is delayed. The other uncertainty inputs have minor impact on FOM 3 or remains unclear.

- **FOM 3 (containment failure time, base and mitigation case 1)**: FOM 3 was observed only in the base and mitigation case 1, but the influence of relevant uncertainty inputs on FOM 3 differed each other, as shown in Figs. 59–61.

  Base case: the most influential contributor to FOM 3 was observed as SC3200_1 whose correlation with FOM 3 is negatively very strong. In the in-vessel phase, the higher decay heat generated more steam from the core in the in-vessel phase. Whereas the higher decay heat ablates the more concrete through the MCCI in the in-vessel phase, consequently leading to more non-condensable gases in the ex-vessel and, in turn, leading to an earlier failure of the containment. XHTFCL (heat transfer between the containment atmosphere and the concrete wall) was an additionally influenced contributor in base case. The higher XHTFCL more accelerates the heat transfer between the containment atmosphere and the concrete wall, thus delaying the pressure increment of the containment. CHI (aerosol dynamic shape factor affecting affects the sedimentation of the radioactive aerosol) also somewhat contributed to FOM 3, leading to the change of heat distribution. However, its effect is unclear due to the relatively small magnitude of relevant coefficient. The other uncertainty inputs have minor impact on FOM 3 or remains unclear.

Mitigation case 1: due to the dedicated mitigation action (SAG-3), the key contributors to FOM 3 slightly differed compared to the base case. Among the uncertainty input inputs employed, COR_CHT_SS and VFALL (the velocity of falling debris) was the two most influential contributors to FOM 3 but having a weak positive correlation. SC3200_1, SC1141_2 (core melt breakthrough candling parameter), and HDBPN were three inputs additionally influenced FOM 3 as shown in Fig. 61. Notably, the determination coefficient (R^2) of the regression models formulated for mitigation case 1 was less than 0.5, indicating that the formulated relationships are enough to explain the influence of relevant uncertainty inputs.

- **FOM 4 (H_2 generation in the in-vessel, base and mitigation case 1):** similar to FOM 3, FOM 4 was observed only in the base and mitigation case 1 and the influence of relevant uncertainty inputs on FOM 4 differed each other, as shown in Figs. 60–62.

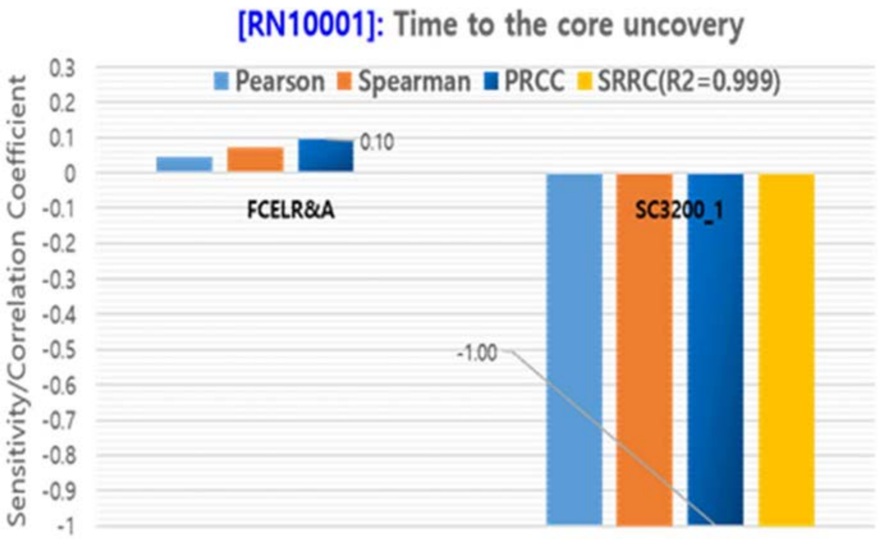

FIG. 60. (a) MELCOR sensitivity results (base case): FOM 1

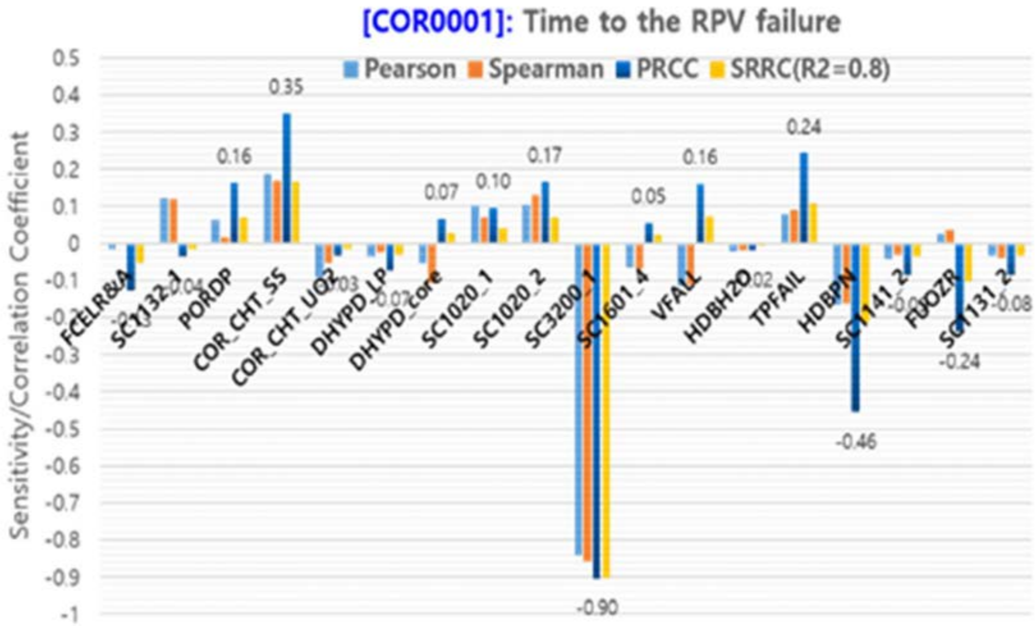

FIG. 60. (b) MELCOR sensitivity results (base case): FOM 2

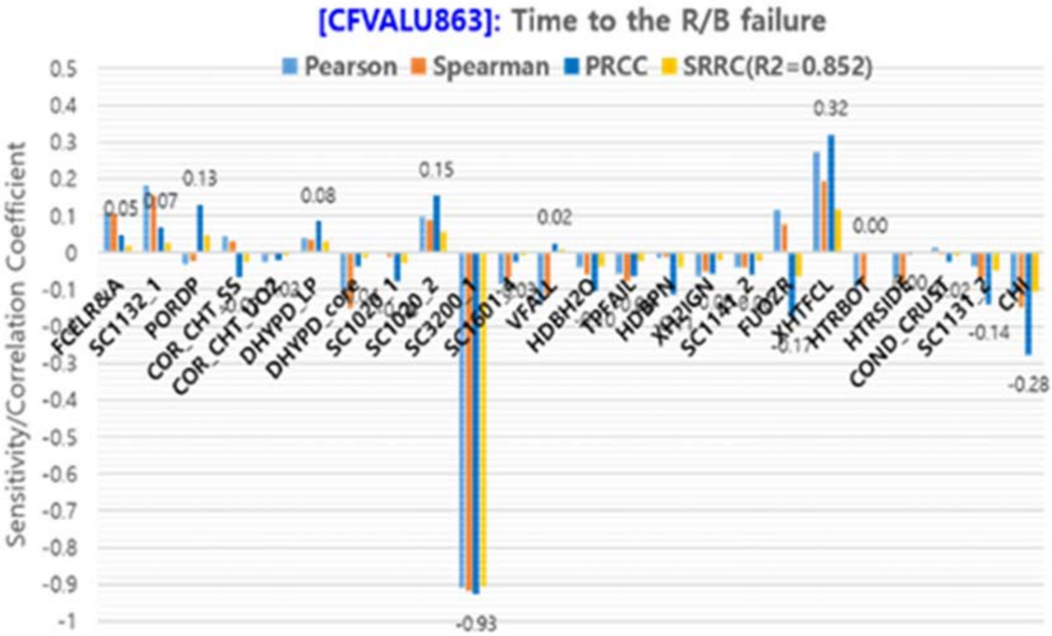

FIG. 60. (c) MELCOR sensitivity results (base case): FOM 3

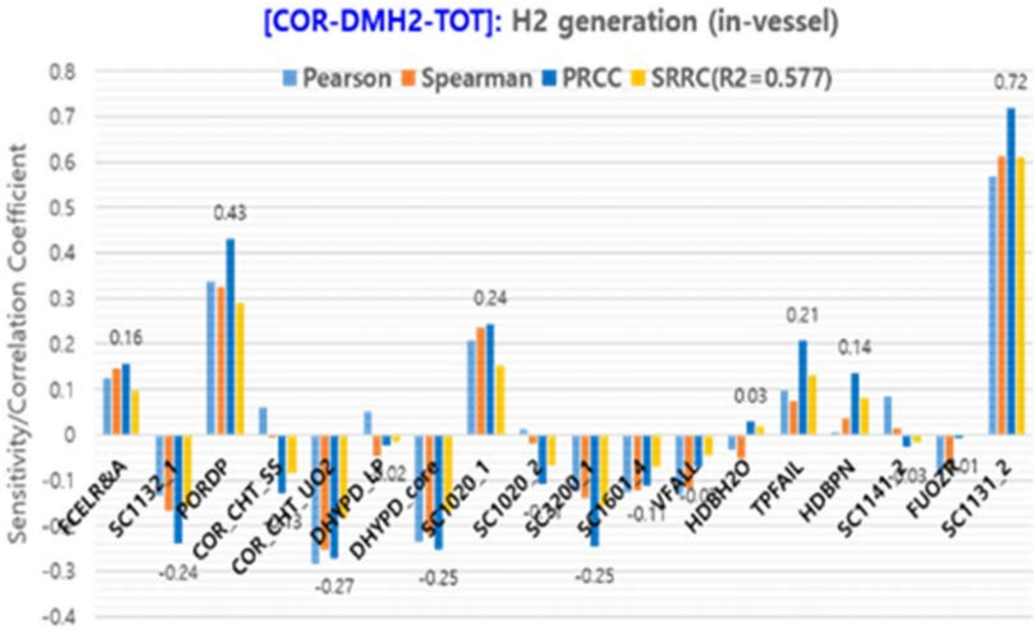

FIG. 60. (d) MELCOR sensitivity results (base case): FOM 4

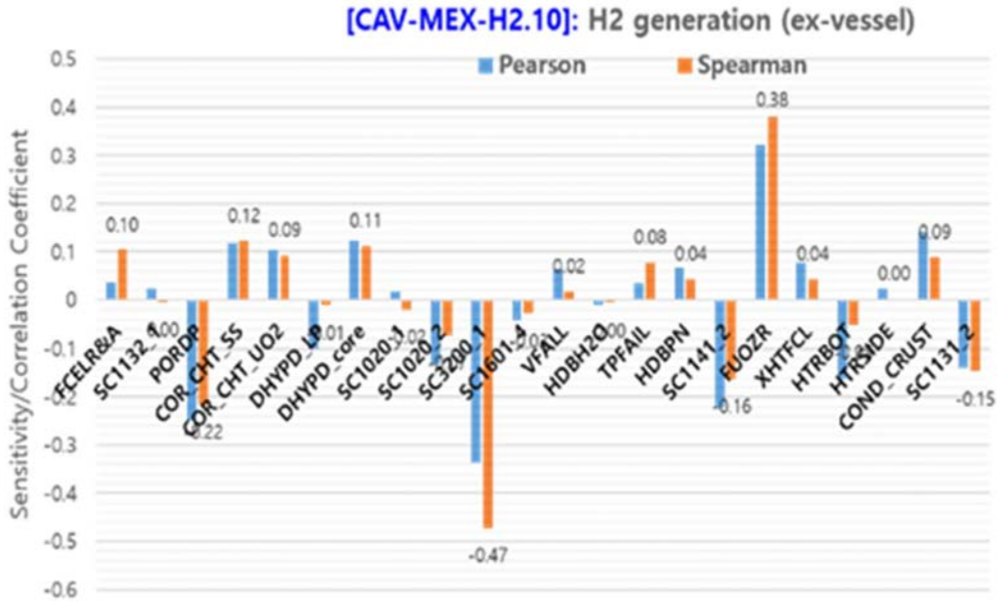

FIG. 60. (e) MELCOR sensitivity results (base case): FOM 5

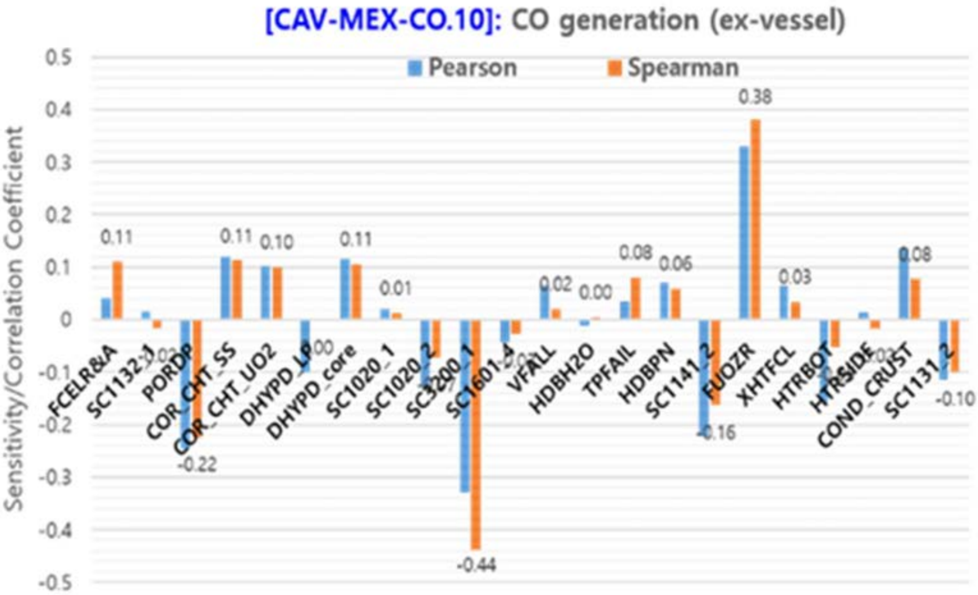

FIG. 60. (f) MELCOR sensitivity results (base case): FOM 6

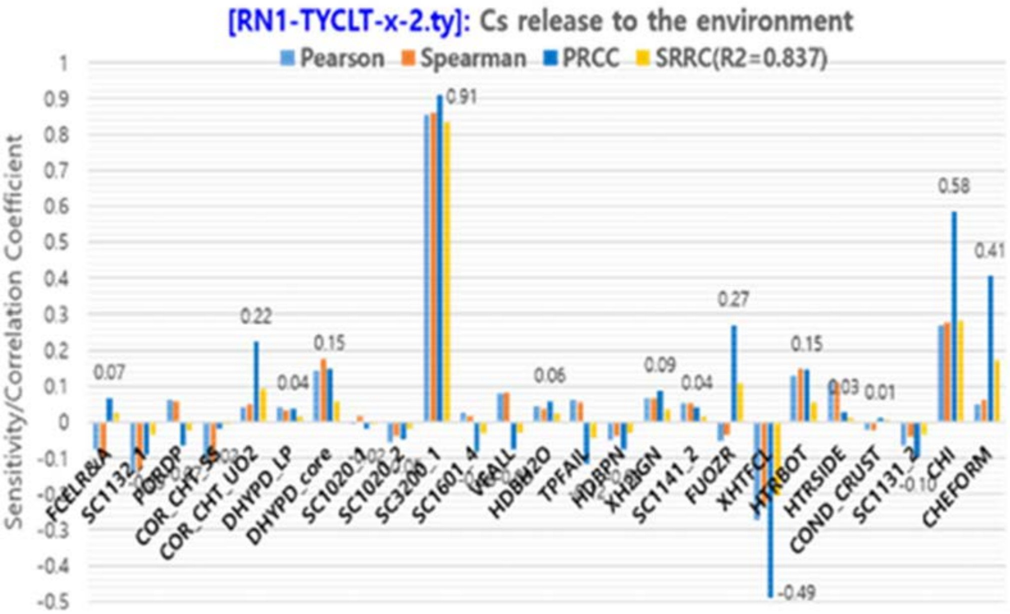

FIG. 60. (g) MELCOR sensitivity results (base case): FOM 7

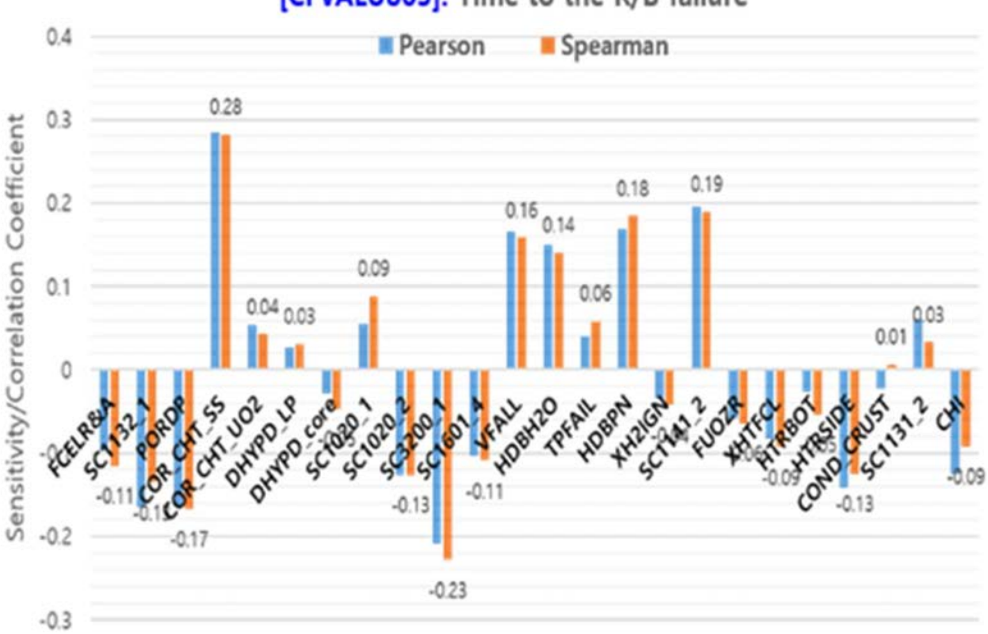

FIG. 61. (a) MELCOR sensitivity results: case 1, FOM 3

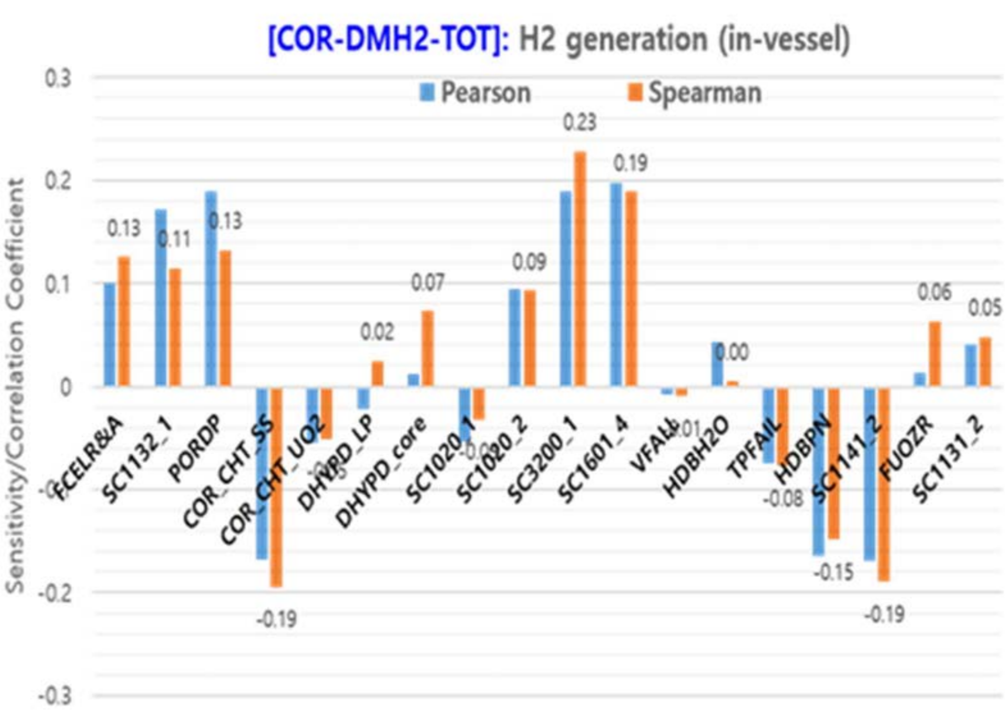

FIG. 61. (b) MELCOR sensitivity results: case 1, FOM 4

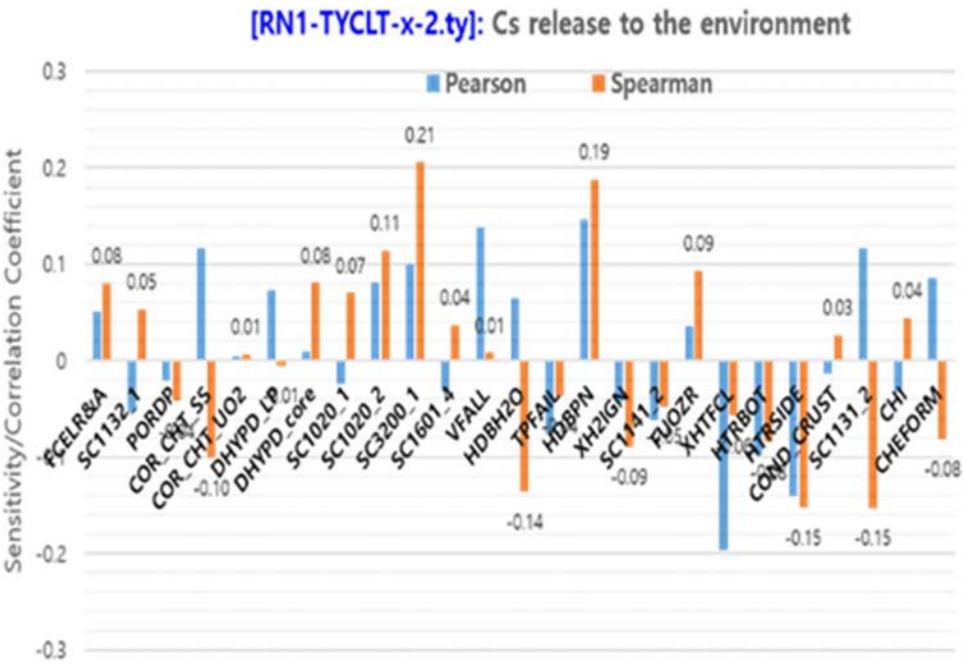

FIG. 61. (c) MELCOR sensitivity results: case 1, FOM 7

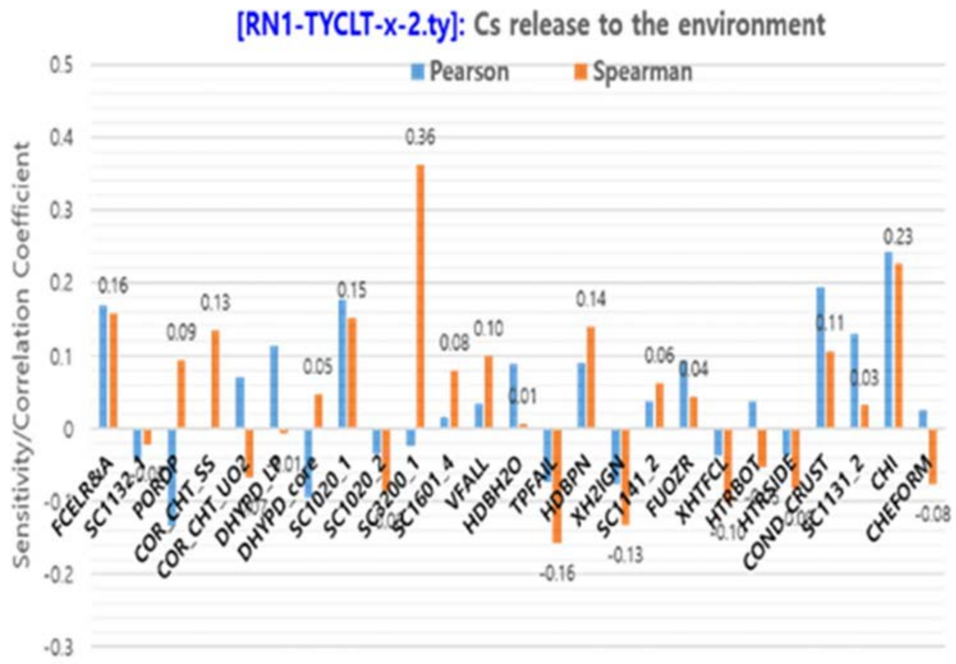

FIG. 61. (d) MELCOR sensitivity results: case 2, FOM 7

Base case: SC1131_2 (molten corium holdup parameter) was the most influential contributor, having strong positive correlation. When oxidized Zr cladding reaches above its failure temperature, the molten Zr is released from oxidized Zr cladding, and transformed fuel geometry reduces the area reacting with steam. Because the reaction area of the intact fuel geometry is greater, the higher SC1131_2 generates the more hydrogen, due to delay of the cladding failure time.

PORDP (porosity of the core debris) and COR_CHT_UO2 (candling heat transfer coefficient for the molten core material) were two inputs additionally influencing FOM 4, but having weak correlation with FOM 4. In general, the higher PORDP leads to larger surface area in the same volume, thus causing more oxidation by steam. Also, since the higher value of COR_CHT_UO2 leads to more heat transfer to fuel cladding in candling process, the molten corium is solidified more easily, consequently leading to flow area blockage.

DHYPD_core (equivalent diameter of the particulate debris in core region) somewhat influencing FOM 4, because the higher DHYPD_core lowers the area-to-volume ratio of debris, consequently leading to hydrogen generation from debris decreasing with reduced reaction area. The influence of SC1020_1 (radial relocation particulate debris speed) was observed, but its impact is lower compared to DHYPD_core.

Mitigation case 1: SC3200_1 is the most influential contributor, but having weak positive correlation. Its impact is mainly due to temporary core exposure between initial uncover of the core and its re-flood following SIT injection. The higher decay heat by the higher SC3200_1 causes earlier core exposure and higher cladding temperature, leading to accelerated oxidation. Influence of SC1141_2, SC1601_4 and HDBPN, which control the heat transfer process during the oxidation, was observed. Their impact is not clear since the relevant regression performance is not good due to low R^2 values.

FOMs 5 and 6 (ex-vessel H_2 and CO generation, base case only): these two FOMs being caused by ex-vessel MCCI, are greatly affected by the amount/thermal condition of molten debris released into the cavity and their cooling mechanism in the cavity. The SC3200_1, which affects the in-vessel molten corium conditions before the RPV failure, and FUOZR (local dissolution fraction of UO_2 in the molten Zr) were observed as two most influential contributors FOMs 5 and 6. Besides, PORDP and SC1141_2 were additionally influencing contributors. Figures 59 and 61 show that the in-vessel corium condition could affect the MCCI more significantly compared to cooling mechanism of molten core debris in ex-vessel. However, there remains much uncertainties.

- **FOM 7 (Cs release to the environment, all the three cases)**: FOM 7 is greatly affected by not only behavior of fission products but the containment failure time. Cs release into the environment was observed in all three case scenarios, but their amount differed; it was greatly lower in mitigation case 2 where the containment integrity was maintained.

  Base case: SC3200_1 was the most influential contributor, having strong positive correlation; the higher SC3200_1 leads to an earlier failure of the containment. Since the environmental release of Cs was also continuously progressed until 72 h, the earlier containment failure led to more Cs release. CHI and XHTFCL are two additional contributors influencing FOM 7, with each having positive and negative correlations. The lower XHTFCL causes more heat removal of containment gas, leading to late containment failure. Consequently, the higher CHI and lower XHTFL lead to more Cs release through late containment failure. Besides, CHEFORM (Cs fraction in the fuel forming Cs_2MoO_4) and DHYPD_core also influenced FOM 7, but their impact are relatively weak.

Mitigation case 1: since the RPV failed for only one sample, most Cs remains inside the RCS, thus behavior is mainly related to in-vessel phenomena. As a result, SC3200_1 was observed as the most influential contributor to FOM 7, but the relevant correlation with FOM 7 was lower than the base case. HDBPN, HTRSIDE, SC1020_2, and SC1131_2 was observed as four additional contributors in mitigation case 2, but their impact is insignificant and not clear because the relevant R^2 values are less than 0.3.

Mitigation case 2: notably, the containment did not fail in mitigation case 2, nevertheless a limited amount of Cs was released through the design leakage of the containment, as shown in Table 24. It is noted that only four samples led to RPV failure by the core degradation and only 16 samples are related to the environmental release of Cs through the containment. According to data points in Fig. 60 (d), SC3200_1, CHI, and SC1020_1 are observed as three most influential contributors to FOM 7 (Figs. 61 (d) and 62 (c)).

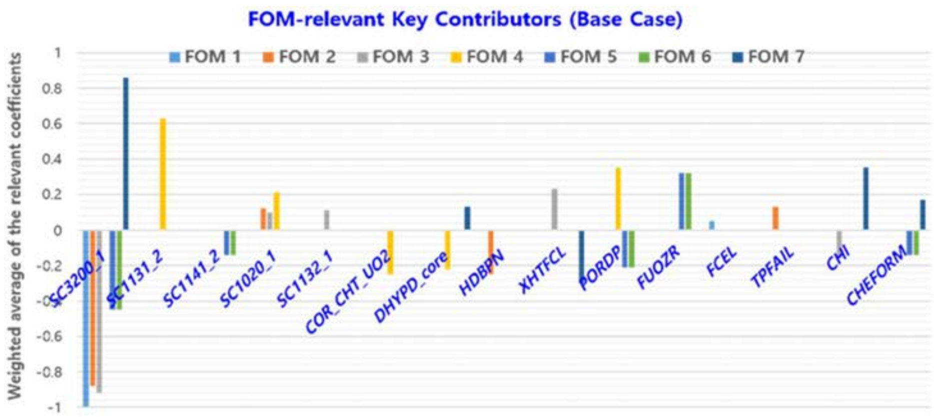

(a)

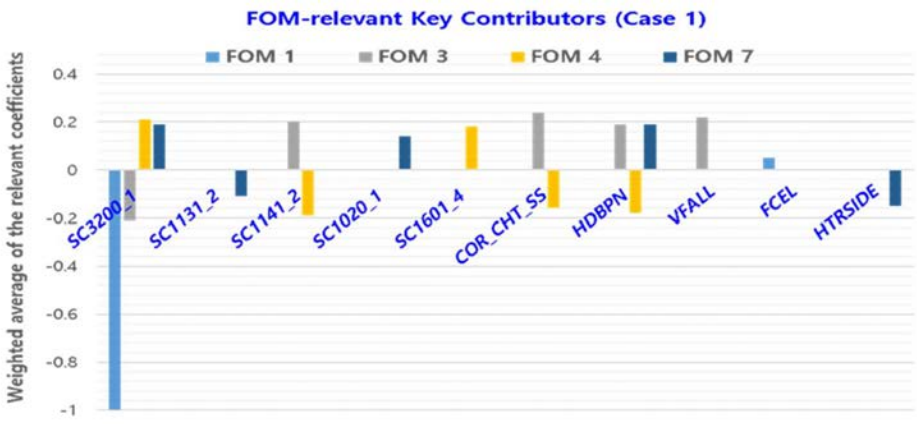

(b)

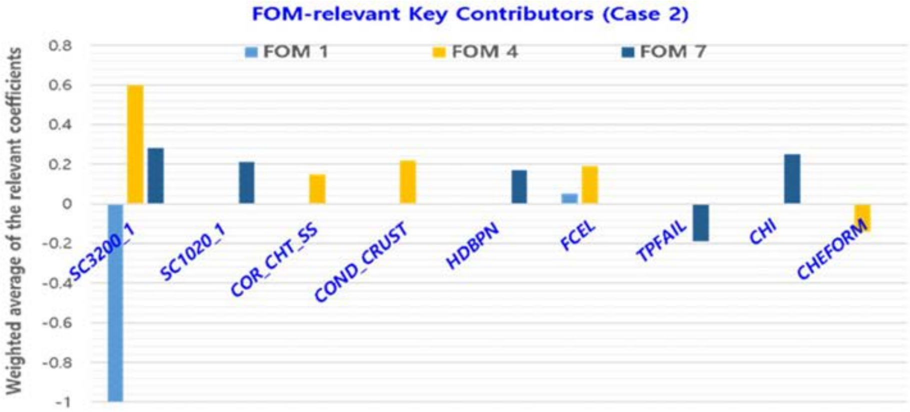

(c)

FIG. 62. MELCOR sensitivity results (key contributors): (a) base case, (b) case 1, (c) case 2.

— MAAP5 uncertainty analysis results: among the random samples of 200 tested until 72 h after the accident, the failed code runs were within 1% for the base case, without any failure in the two cases. Accordingly, the failed runs were removed from the analysis of FOMs and the remaining normal calculations ($N = 198$) were used for the final analysis.

As predicted by the MAAP5 code, Tables 27 and 28 summarize uncertainty mean values taken from the base and two mitigations. Figures 63–67 show the corresponding time trends and CDFs for each relevant FOM. Tables 29 and 30 provide the corresponding statistical properties for each FOM.

TABLE 27. KEY EVENT TIMINGS (MAAP5) (IN HOURS)

Events	Uncertainty mean		
	Base case	**Case 1**	**Case 2**
Reactor trip	0.0		
Open of MSSV	0.001		
Open of PSV	0.96		
Dryout of SGs	1.14		
Core uncover (**FOM 1**)	1.93		
Clad oxidation	2.11		
SAMG entry	2.28		
SDS valves open	n.a.	2.28	2.28
Cladding failure	2.34	2.32	2.32
Hot leg rupture	3.68	–	–
SIT injection	3.73	2.47	2.47
Two ADVs open	n.a.	n.a.	4.0
EWI (RCS/SG)	n.a.	4.98	4.05
SIT injection stop	3.78	14.28	4.11
Support plate fail	4.51	–	–
RPV lower head failure (**FOM 2**)	6.01	–	–
Reactor building failure (**FOM 3**)	42.72	34.61	–

TABLE 28. COMBUSTIBLE GASES AND Cs RELEASE (FOMs)

FOMs	**Uncertainty mean**		
	Base case	**Case 1**	**Case 2**
FOM 4 (kg)	480	240	238
FOM 5 (kg)	2,029	–	–
FOM 6 (kg)	4,535	–	–
FOM 7 (–)	0.0532	2.29×10^{-4}	–

TABLE 29. STATISTICS OF RELEVANT FOMs (BASE CASE)

FOMs	**5th percentile**	**Median**	**95th percentile**	**Standard deviation**	**Mean**
FOM 1 (h)	1.81	1.90	2.05	0.08	1.92
FOM 2 (h)	3.68	6.27	7.60	1.21	6.01
FOM 3 (h)	36.6	43.23	49.35	4.29	42.72
FOM 4 (kg)	358	474	610	67	480
FOM 5 (kg)	346	2,281	2,469	632	2,029
FOM 6 (kg)	856	5,096	5,423	1,409	4,535
FOM 7 (–)	9.89×10^{-3}	0.0501	0.104	0.0282	0.0532

TABLE 30. STATISTICS OF RELEVANT FOMs (CASES 1 & 2)

FOMs	**5th percentile**		**Median**		**95th percentile**		**Standard deviation**		**Mean**	
	Case 1	Case 2	Case 1	Case 2	Case 1	Case 2	Case 1	Case 2	Case 1	Case 2
FOM 3	36.6	–	43.23	–	49.35	–	4.29	–	42.72	–
FOM 4	33.0	33.0	249.0	248.0	351.0	350	93.0	92.0	240	238
FOM 7	4.44×10^{-8}	–	4.34×10^{-5}	–	9.54×10^{-4}	–	8.68×10^{-4}	–	2.29×10^{-4}	–

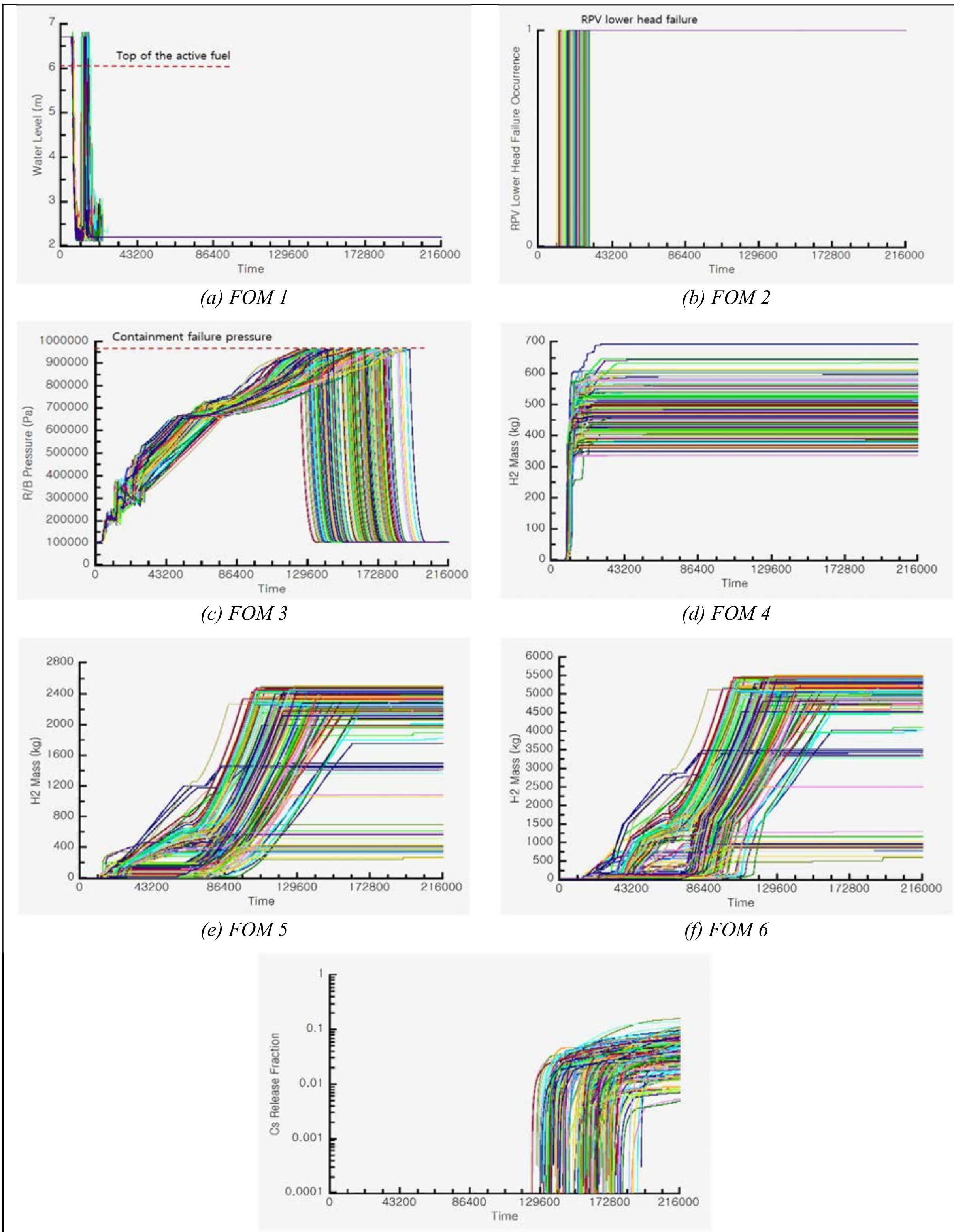

(a) FOM 1 (b) FOM 2

(c) FOM 3 (d) FOM 4

(e) FOM 5 (f) FOM 6

(g) FOM 7

FIG. 63. MAAP5 uncertainty results (base case).

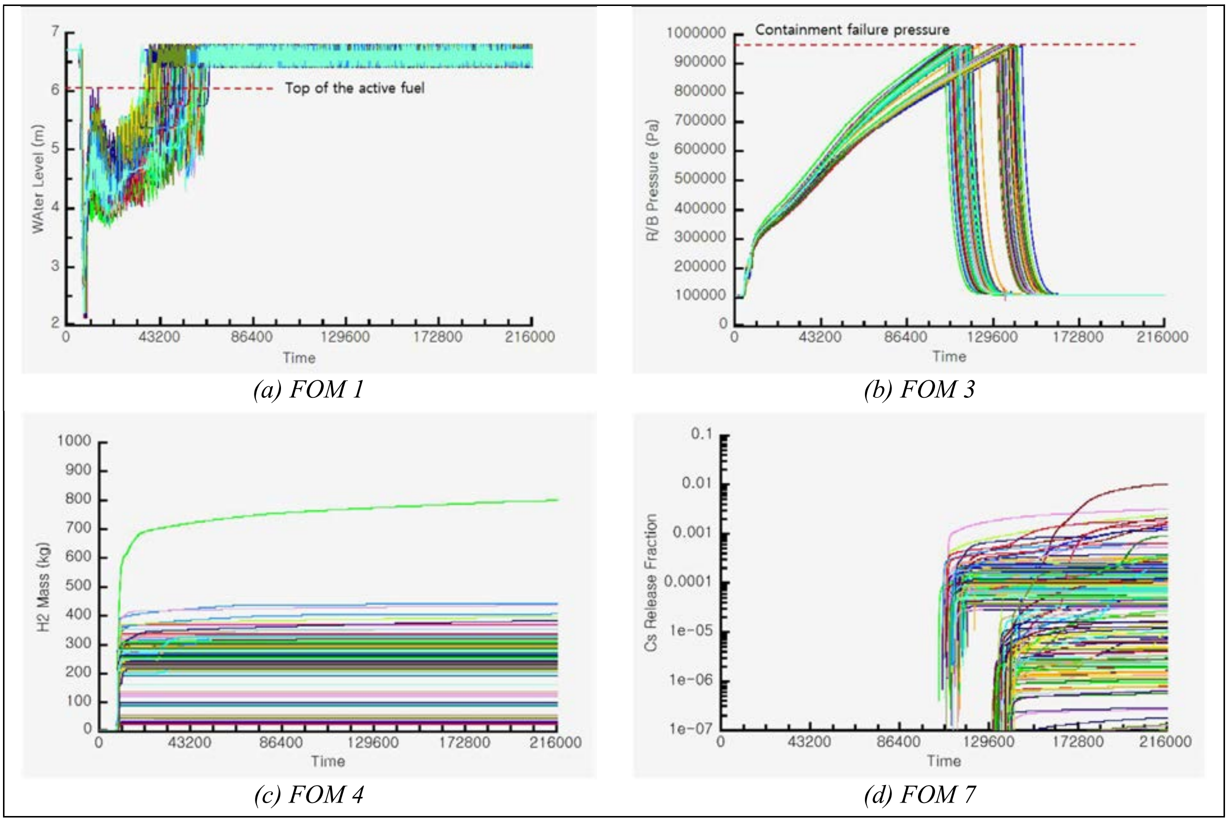

(a) FOM 1 (b) FOM 3
(c) FOM 4 (d) FOM 7

FIG. 64. MAAP5 uncertainty results (case 1).

The MAAP5 results show that, similar with MELCOR, the mean values for the three cases were almost the same as the corresponding reference results as presented in Tables 21 and 22, until before taking dedicated mitigation actions. After taking relevant mitigation actions, each case scenario led to somewhat different trends with respect to their means, More specifically, there were additional generation of H_2 in the in-vessel (FOM 4, cases 1 & 2) and the slight release of Cs into the environment (FOM 7, case 1), compared to the reference results in Table 22.

- **MAAP5 base case**: according to the first column of Table 27, there is no difference between the reference value (point estimate) and the corresponding mean value until before reaching the SAMG entrance point after the beginning of the accident, including FOM 1. Such a trend is very similar to MELOCR cases. Otherwise, the mean values for FOMs 2–3 were relatively less than reference cases, Table 21. The corresponding reference failure times (6.77 h and 44.44 h) match the 20th and 45th percentiles in the relevant CDFs, respectively (Figs. 66 (b) and (c)). Except for FOM 4, which slightly underestimated than reference case, the mean values for FOMs 5–6 are almost the same as the reference cases (Tables 22 and 28). The mean value of 0.053 estimated for FOM 7 matches half the reference case (0.107), the 95th percentile in the CDF of Fig. 66 (g).

  MAAP5 mitigation case 1: dedicated operator action taken in case 1 (i.e., SAG-3) did not cause the failure of the RPV lower head in case 1, but prolonged the steam generation in the core and, in turn, the steam released via the ruptured hot leg continuously increased the containment pressure. This trend is also very similar to the MELCOR case. As a result, the mean failure time of 34.61 h (FOM 3) was estimated in case 1, approximately 3 h faster than the reference case, whose value takes up the 85^{th} percentile in the relevant CDF in Fig. 66 (a).

Owing to the dedicated mitigation action taken in case 1, Table 28 shows that only a small amount of H_2 was generated in in-vessel (26 kg) (FOM 4), much less than the reference case (616 kg) and less than the 5^{th} percentile (~37 kg), as shown in Fig. 67 (b). Similar to the reference case, combustible gas (H_2 and CO) were not generated in the ex-vessel phase (FOMs 5 and 6). While the release fraction of Cs was negligible in the reference case, as shown in Table 22, the case 1 led to the mean value of 2.29×10^{-4} for FOM 7 (the environmental release of Cs), but whose impact is negligible as shown in Table 30 and Fig. 67 (c).

- **MAAP5 mitigation case 2**: dedicated mitigation action (i.e., SAG-1) taken to cool down the reactor core did not lead to failures of the RPV lower head and the reactor building (FOMs 2 and 3), as shown in Table 27. Whereas there was a moderate amount of H_2 generation (mean of 238 kg) in the in-vessel phase (FOM 4), which was almost the same as case 1, but much greater than the reference case (25 kg).

  The reference value of approximately 25 kg matches the 85^{th} percentile in the relevant CDF in Fig. 67 (d). Similarly, to case 1, there were no generation of combustible gases (FOMs 5 and 6) and no environmental release of Cs (FOM 7) in case 2.

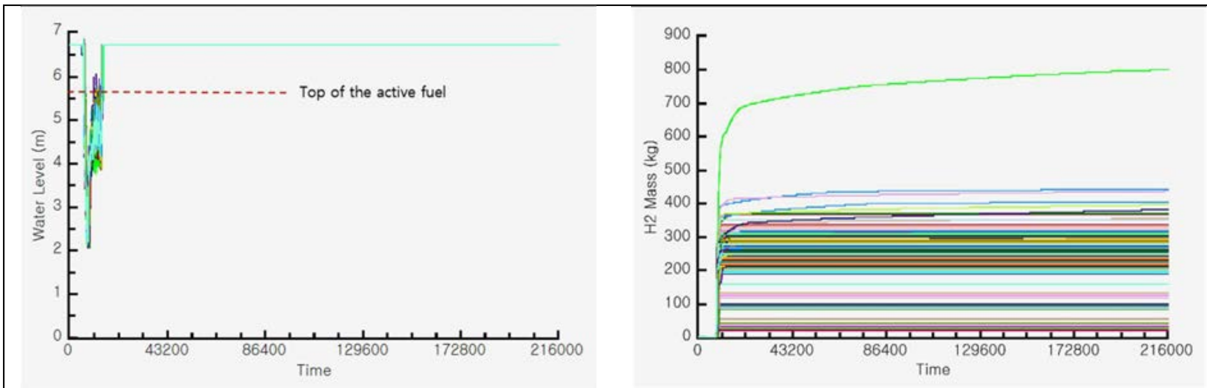

(a) FOM 1 *(b) FOM 4*

FIG. 65. MAAP5 uncertainty results (case 2): (a) FOM 1, (b) FOM 4

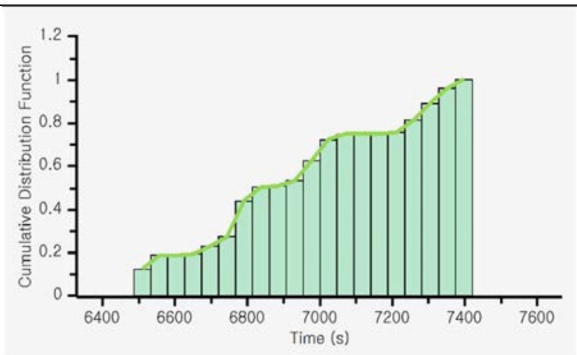

(a) FOM 1

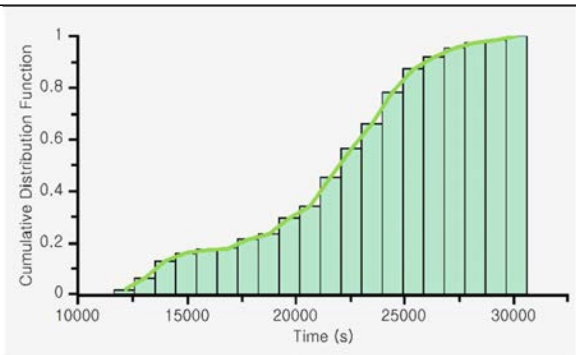

(b) FOM 2

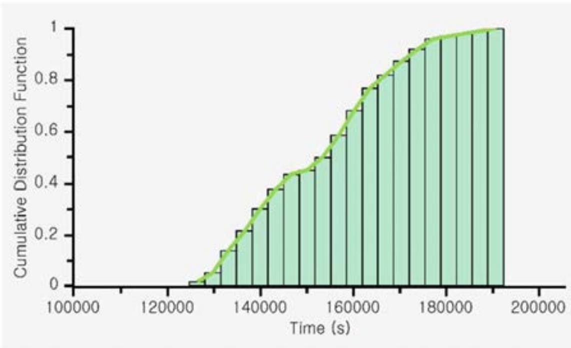

(c) FOM 3

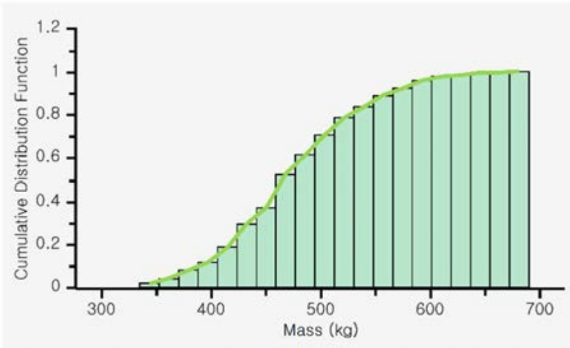

(d) FOM 4

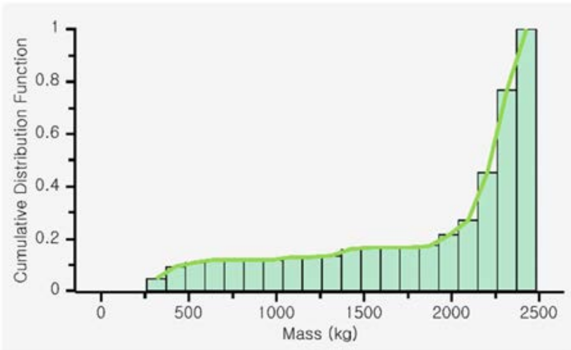

(e) FOM 5

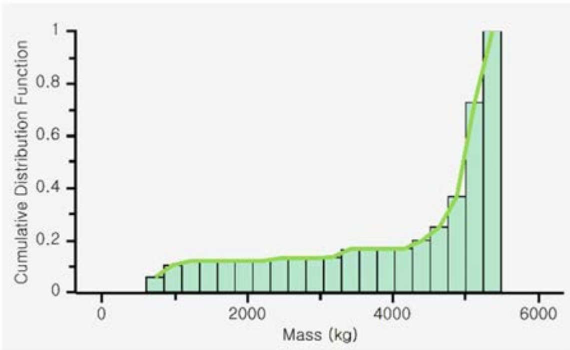

(f) FOM 6

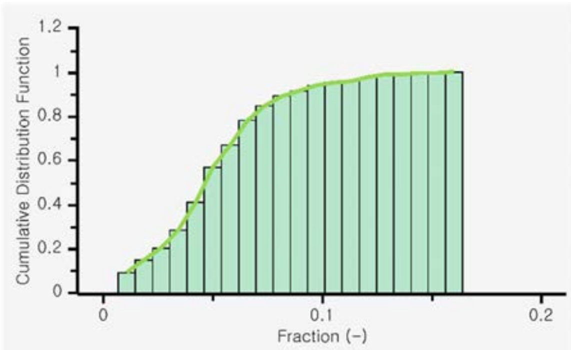

(g) FOM 7

FIG. 66. MAAP5 uncertainty results (CDF, base case).

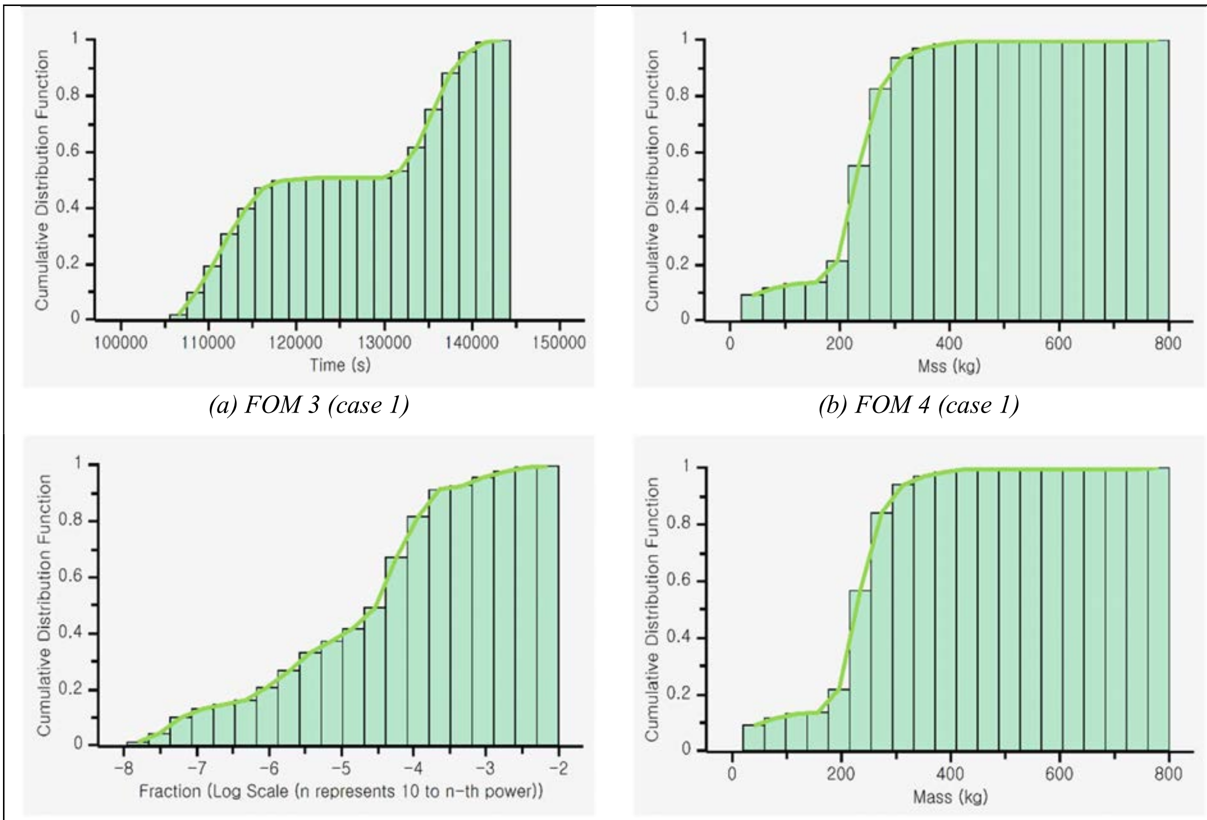

(a) FOM 3 (case 1) *(b) FOM 4 (case 1)*

(c) FOM 7 (case 1) *(d) FOM 4 (case 2)*

FIG. 67. MAAP5 uncertainty results (CDF, cases 1 & 2).

— *MAAP5 sensitivity analysis results*: similar to MELCOR, four sensitivity measures were estimated to investigate more influencing contributors on each FOM. Among the estimated sensitivity measures, the uncertainty inputs with $|r| \geq 0.05$ are presented in Figs. 68 and 69. As shown in the figures, the regression models formulated to estimate PRCC and SRRC did not provide a good performance for all case scenarios, i.e., $R^2 < 0.5$. Accordingly, the input parameters having the R^2 value less than 0.5, were excluded when determining the key contributors on each FOM, in the same way as the MELCOR analysis.

  On the other hand, differently from the MELCOR inputs, a few uncertainty inputs employed for the MAAAP5 analysis are not physical quantities, but flag variables being used to switch relevant models (or correlations) wherever required, providing no meaningful information for the estimated Pearson correlation. Accordingly, such a variable was screened out in the Pearson correlation analysis results. Whereas the nonparametric sensitivity approaches using the ordinal ranks can be made to estimate the remaining three sensitivity measures if they were arranged in order of higher (or lower) level of conservatisms, as implemented in this study.

  Figure 70 summarizes key contributors, having stronger correlations with each FOM than others, determined by the forgoing approach and a weighted average of relevant sensitivity measures.

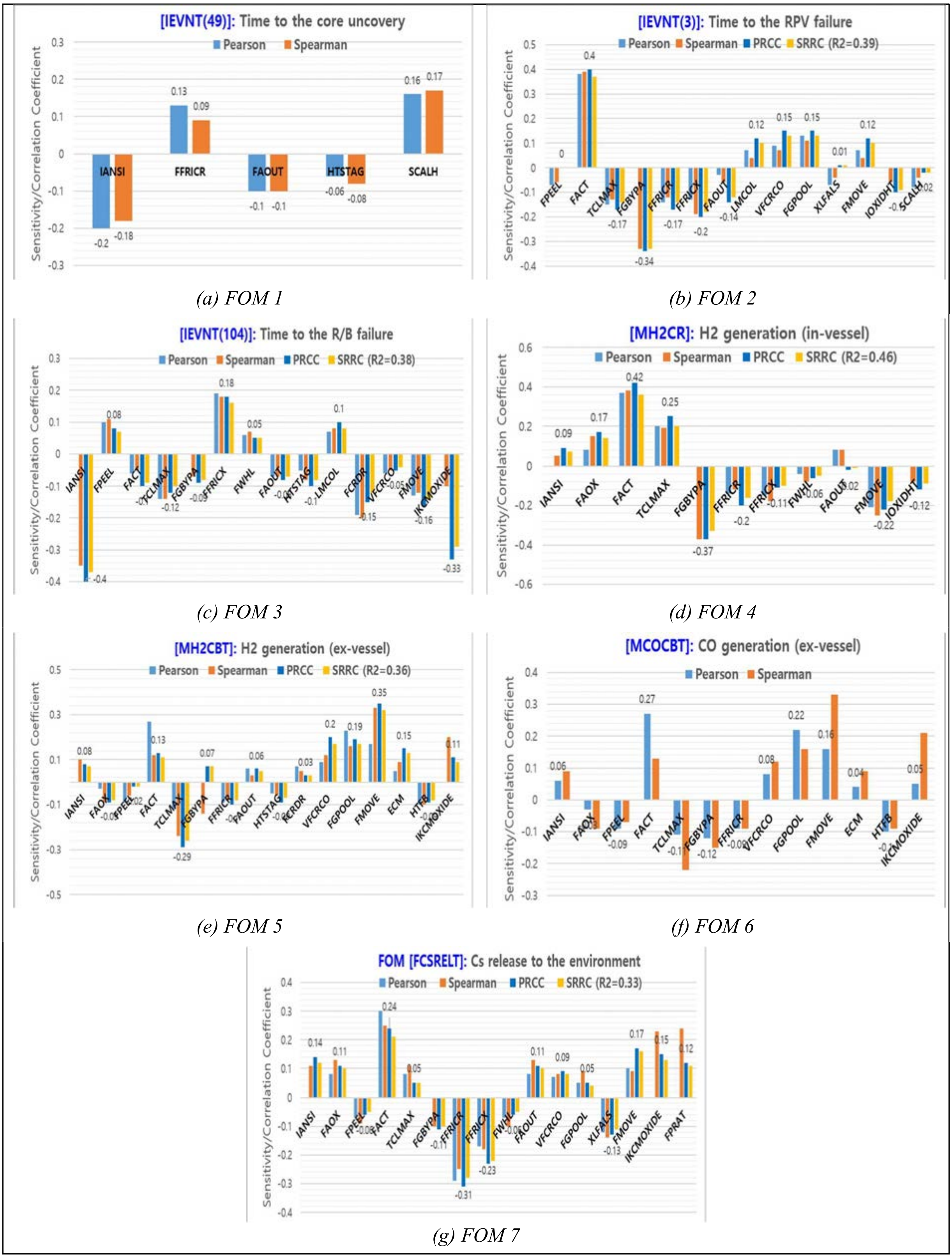

FIG. 68. MAAP5 sensitivity results (base case).

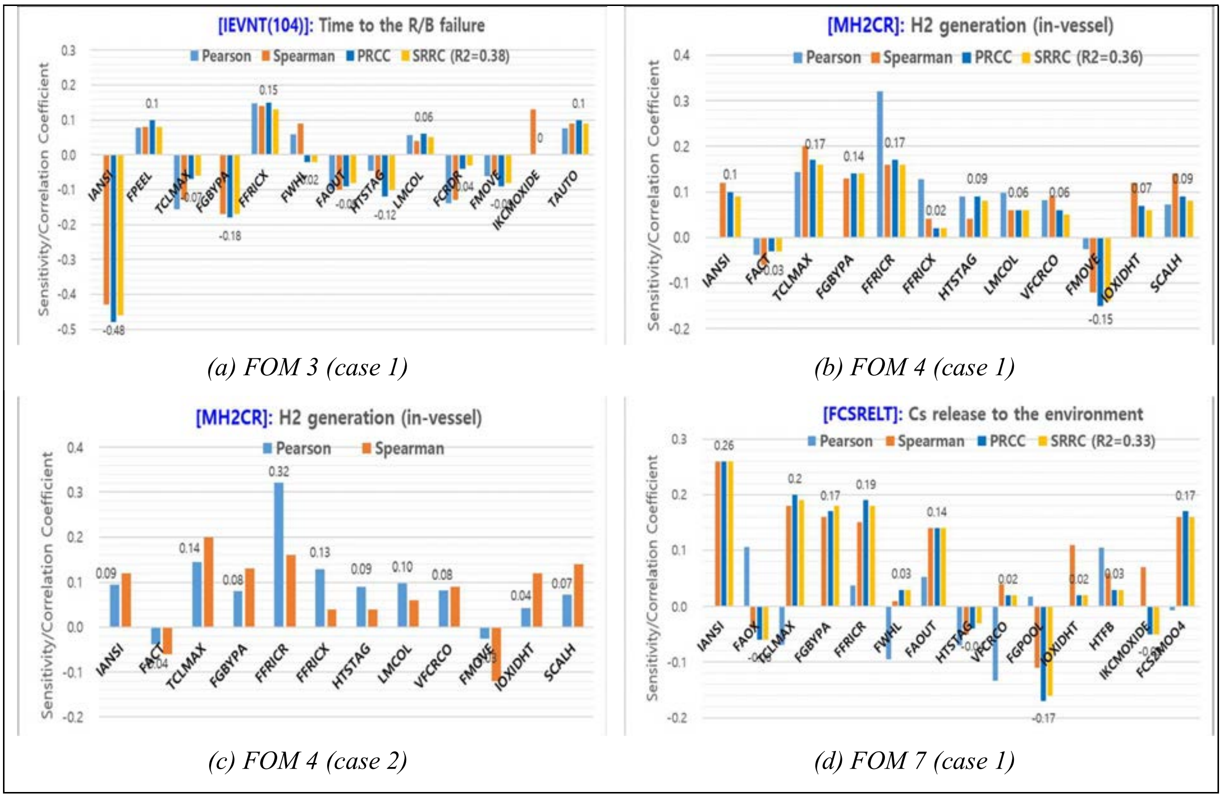

(a) FOM 3 (case 1) *(b) FOM 4 (case 1)*

(c) FOM 4 (case 2) *(d) FOM 7 (case 1)*

FIG. 69. MAAP5 sensitivity results (cases 1 & 2).

- **Base case**: as shown in Figs. 68 and 70, IANSI (related to the decay heat) more influenced only FOMs 1 and 2 than the rest; FACT (affecting the in-vessel cladding oxidation) greatly influenced most FOMs except for FOMs 1 and 3; FGBYPA (affecting the in-vessel cladding oxidation) influenced only FOMs 2 and 4; FMOVE (affecting the relocation of corium material) was the most dominant contributors on FOMs 4–6; TCLMAX (related to the failure temperature of a cladding) also greatly affected most FOMs except for FOMs 1 and 7; FGPOOL also influenced only FOMs 6 and 7. Contrary to expectation, FOM 7 was much more influenced by FACT (related to the hydraulic diameter of collapsed fuels) and FFRICR/FFRICX (related to the in-vessel natural circulation) than the other inputs related to the release and transport of the fission products (such as FCS2MOO4 employed to determine a fraction of Cs forming Cs_2MoO_4) except for FPRAT (related to the release of fission products). This indicates that the environmental release of Cs may be greatly affected by the in-/ex-vessel thermal-hydraulics after fission products in the fuel are released to the RCS.

- **Mitigation cases**: In case 1, IANSI and FFRICR additionally influenced FOM 7, compared to the base case, as shown in Figs. 69 and 70. Ut can be seen that in case 2, the dominant contributors to each relevant FOMs were limited to only a few inputs, such as IANSI, FFRICR, TCLMAX, and SCALH (related to the boiling heat transfer in the core). This is because the dedicated mitigation actions greatly reduced the ensuing accident progressions, consequently led to the synergetic effects on relevant FOMs to the same extent.

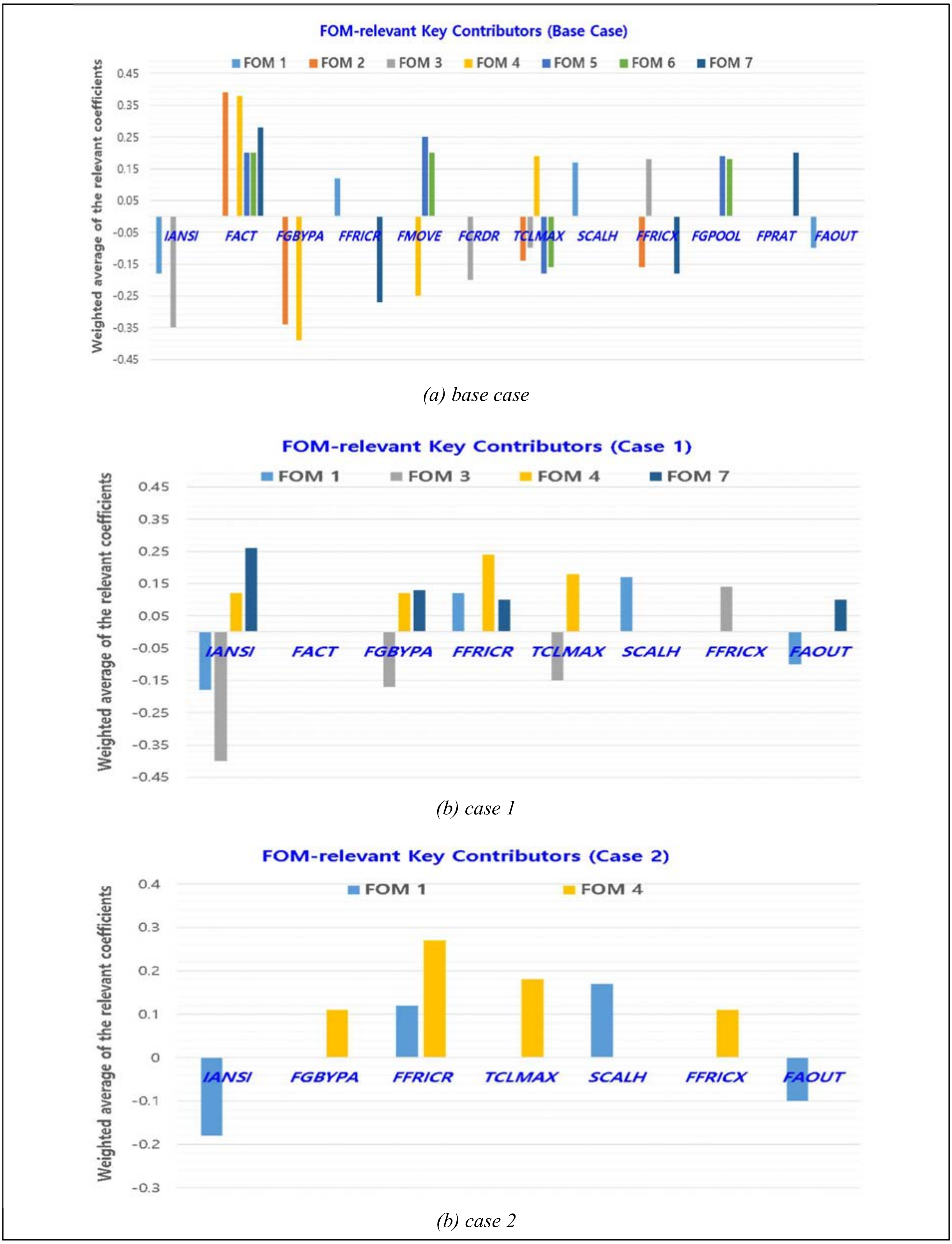

(a) base case

(b) case 1

(b) case 2

FIG. 70. MAAP5 sensitivity results (key contributors).

2.3.3.7. *Summary and conclusions*

In this study, a series of uncertainty and sensitivity analyses were performed for the STSBO of the OPR1000 plant, to characterize uncertainties addressed in various model inputs of the latest version of MELCOR and MAAP5 and to identify relevant key contributors influencing the FOMs of interest. For the purpose, three case scenarios, a base and two cases employing dedicated mitigation strategy, to explore their effect on the FOMs of interest, as summarized in Table 31.

TABLE 31. OPR1000 MITIGATION ACTIONS EMPLOYED IN THE STUDY

SAM	RCS pre-bleed via SDS	Feed & bleed operation
Case 1	Open two SDS valves at the SAMG entry condition[1]	· RCS injection by portable pump at 4 h after the accident
Case 2		· SG injection by portable pump at 4 h after the accident

For the analysis, a series of uncertainty inputs covering all the phases of severe accident progressions were employed for this study: 26 in the case of MELCOR and 29 in the case of MAAP5. Then, the uncertainties for each relevant FOMs were tested using the simple random samples of 200 per case scenario. But, the unexpected number of code crashes allowed for only a limited number of simulation results in the final analysis: 100 for MELCOR and 198 for MAAP5.

Based on the aforementioned approach, the uncertainty analysis results showed that the three reference cases led to almost the same trends until before taking operator actions for the dedicated mitigation, but, thereafter, each case scenario led to somewhat different trends each other. A suit of sensitivity and correlation analyses also showed that the contribution of uncertainty inputs to each relevant FOM differed, consequently provided a range of impacts on particular FOM. That is, a few input parameters much more influenced the uncertainties of relevant FOMs in one case scenario but did not necessarily have the impact of the same level in another scenarios. Uncertainty inputs having a very strong sensitivity/correlation over the various FOMs were limited to just a few inputs, and among them, the decay power was identified as one of the most important contributors over several FOMs. For both MELCOR and MAAP5, the dedicated mitigation measures played a great role in mitigating the consequences of accident for all the FOMs employed in this study, among them the Case 2 strategy was more effective than Case 1.

The followings summarize main sources of uncertainty resulted from the analysis and following lesson learned and best practices, which were obtained from the present study.

<u>*Main sources of uncertainty resulting from the analysis:*</u>

- For both MELCOR and MAAP5, the decay power multiplicative factor was the primarily important contributor over various FOMs of interest, compared to the rest;
- In the case of MELCOR, the failed code runs of around 30% might influence the relevant uncertainty results, but their impact is negligible in the case of MAAP5. The best way for resolving the code crash issue is to reduce their possibility through a fine tuning of relevant code models and/or by appropriately controlling the numerical time step below the minimum time step limit wherever effective.
- In the case of MAAP5, a few uncertainty inputs employed for the analysis, e.g., flag variables used to switch relevant models/correlations, might influence the relevant uncertainty results. While the

explicit involvement of such a type of uncertainty inputs provide much insights for the underlying code uncertainties, they may mask the influence of model parameters on each FOM or relevant correlation.

<u>Lesson learned and best practices:</u>

To reach more clear conclusions for the present study, more careful investigations are required, taking into account some constraints and limitations which could be arisen from the use of the highly complex severe accident codes such as MELCOR and MAAP5, as follows.

- To get more reliable results on the uncertainties of FOMs of interest, it is necessary to specify more relevant inputs influencing the FOMs and more relevant PDFs which could well characterize the underlying inputs uncertainties, including relevant distributional sensitivity analysis if available [41];
- To apply a statistical sampling-based uncertainty analysis, it is necessary to understand the underlying basis for relevant methods (such as SRS, LHS, and Wilks formula) in terms of their merits and disadvantages;
- To ensure a sufficient confidence of the analysis results, the influence of sample sizes on the uncertainties of FOMs of interest also needs to explore, if possible, so that mean and standard deviation of the relevant FOM converge with the number of samples;
- It is necessary to check the influence of possible code crashes and/or biases including outliers in the simulation results, as implemented in the present study;
- While not implemented in this study, it is necessary to investigate further the impact of plant nodalization schemes and the impact of modelling uncertainties (or correlations) employed by each code.

2.3.4. Korea Institute of Nuclear Safety (KINS)

The KINS based the accident analysis using as a reference plant the evolutionary PWR, APR1400 plant type. Description of this plant specifics, accident scenarios analysed, applied models and approaches, and summary of the results are provided in the following sections.

2.3.4.1. Motivation and objectives

The objective of this study is to evaluate the uncertainty involved in long-term corium coolability in containment during severe accidents when various SAM actions were applied. The objective can be achieved by the following evaluations on:

- Uncertainty in the predicted reactor cavity corium conditions in view of long-term corium coolability;
- Uncertainty in corium coolable mass/area and non-coolable mass/area;
- Uncertainty in the axial and radial ablation depths during MCCI.

In this work, the analysis focuses on the long-term cooling in the case of the pre-flooded reactor cavity, such as APR1400 [1] type NPP using two codes, MELCOR2.2 [2] and COOLAP [3]. The analysis procedures of the uncertainty analysis consist of three steps; (a) Ex-vessel condition evaluation based on the MELCOR analysis (b) the initial coolability of ex-vessel corium based on the COOLAP analysis, and (c) long-term coolability based on the MELCOR analysis.

The first step of the analysis provides the initial and boundary conditions of the accident progression in containment. The MELCOR2.2 uncertainty analysis is performed to obtain the uncertainty ranges of the parameters affecting to evaluate the limiting conditions of the corium spreading, MCCI as well as containment performance. In the second step, the thermal conditions of the discharged corium, evaluated from the first step, provide the input parameters of COOLAP. Subsequent analysis is performed to verify the assumptions of the coolable mass/area and non-coolable mass/area of the corium relocated into the reactor cavity at the initial stage. Finally, in the third step, the MELCOR2.2 analysis for the long-term containment performance with the given corium cooling conditions is carried out. The overall uncertainty analysis for the axial and radial ablation depths as the FOM using the uncertain parameters for the physical models, accident scenarios and accident management in the cavity package of MELCOR is conducted.

2.3.4.2. Description of the relevant plant

The APR1400 [1] is an evolutionary PWR, in which a reactor vessel is connected with two closed loops in parallel. Each loop has one steam generator, two RCPs, and a pressurizer. The reactor core fuelled with uranium dioxide pellets enclosed in fuel rods consists of 241 fuel assemblies that contain varying ^{235}U enrichments. The information presented herein pertains to one reactor unit with a thermal power, up to 4,000 MWt. Based on the reference design, the plant operates at an estimated gross electrical power output at a rated power of 1,425 MWe. This electrical output can vary depending on site-specific conditions. The APR1400 containment is a steel-lined and pre-stressed concrete structure that consists of a right circular cylinder with a hemispherical dome on a reinforced concrete common basement. There is no structural connection between the freestanding portion of the containment and adjacent structures other than penetrations and associated supports. The containment can be accessed through the personnel air locks, or by the equipment hatch. The detailed design parameters of the APR1400 plants are presented in Table 32.

TABLE 32. APR1400 PLANT DESIGN SPECIFICATION

Parameter	**Value**
Electric power (MWe)	1,400
Reactor power (MWt)	3,983
No. of loops/steam generator	2 / 2
No. of hot/cold legs	2 / 4
No. of RCPs	4
Seismic design	0.3g SSE (Safety Shutdown Erathquake)
Safety system characteristics	DVI (Direct Vessel Injection) IRWST (In-containment Refuel Water Storage Tank) FD (Fluidic Device) in SIT
No. of fuel assemblies in core	241
No. of fuel rods in an assembly	236

TABLE 32. APR1400 PLANT DESIGN SPECIFICATION (Cont.)

Parameter	Value
Primary/secondary pressure (MPa)	15.5/6.89
Hot leg/cold leg temperature (K)	597.0/563.7
RCP seal flow rate (liter/s)	1.325
RCS mass flow rate (kg/s)	20,991
Steam mass flow rate/SG (kg/s)	1130.2
SIT set pressure (MPa)	4.025
POSRV capacity (kg/s)	68.0 at 17.0 MPa
ADV capacity in secondary side (kg/s)	138.6 at 6.9 MPa

2.3.4.3. Accident scenarios and severe accident codes

The SBO with operator manual depressurization is selected as an accident scenario. At the time 0 s, the loss of offsite power (LOOP) occurs and simultaneously turbine and reactor are tripped. Although emergency diesel generators should start in a normal situation, in SBO, electric power in the plant from the generators are unavailable except a direct current power from the class 1E battery. Following the complete loss of the AC power, the RCP seals may lose their cooling support systems when the seal flow is lost. Component cooling water to the RCP thermal barrier heat exchanger may also be unavailable. The leakage of an RCS fluid through the RCP seals may occur without makeup capability which eventually leads to the core uncovering, core heat-up, and possibly core damage. Also, a let-down line is isolated, which consequently leads to the opening of the let-down relief valve, increasing the coolant loss until the RCS pressure decreases below the valve set-point pressure of 4.23 MPa. The design with the secondary side heat sink is available but the RCP seal leak leads to the need for station blackout simulations. However, the RCP seal leak scenario was not considered in this study since the RCP seal in APR1400 has a relatively stronger design than those in other PWR designs. Following the complete loss of an AC power and the reactor/RCP trip, the inventory loss through the pressurizer POSRV (Pilot Operated Safety Relief Valve) results in an active core uncovered leading to core damage. According to the emergency operating procedure, the accident management procedure should be activated just after the representative core exit temperature exceeds 1200°F. In an early stage of the accident management procedure, the operators should manually open the depressurization valve (emergency rapid depressurization valve) in the reactor coolant system to prevent the high pressure melt ejection and direct containment heating.

For the analysis of ex-vessel corium cooling associated with the SAM measures like the cavity pre-flooding in power plants, the present study utilizes the coupled analysis of MELCOR2.2 [2] and COOLAP [3]. The MELCOR code is used to predict the progression of severe accidents of the APR1400 plant. A lumped parametric code, COOLAP, is used to provide the initial condition for the following MCCI and long-term cooling analysis with consideration on the melt jet breakup and debris bed cooling. The stand-alone analysis of the debris bed coolability with a simple containment model was also employed to evaluate the containment pressurization. For reference, the detailed model description of the COOLAP code is shown in Fig. 71.

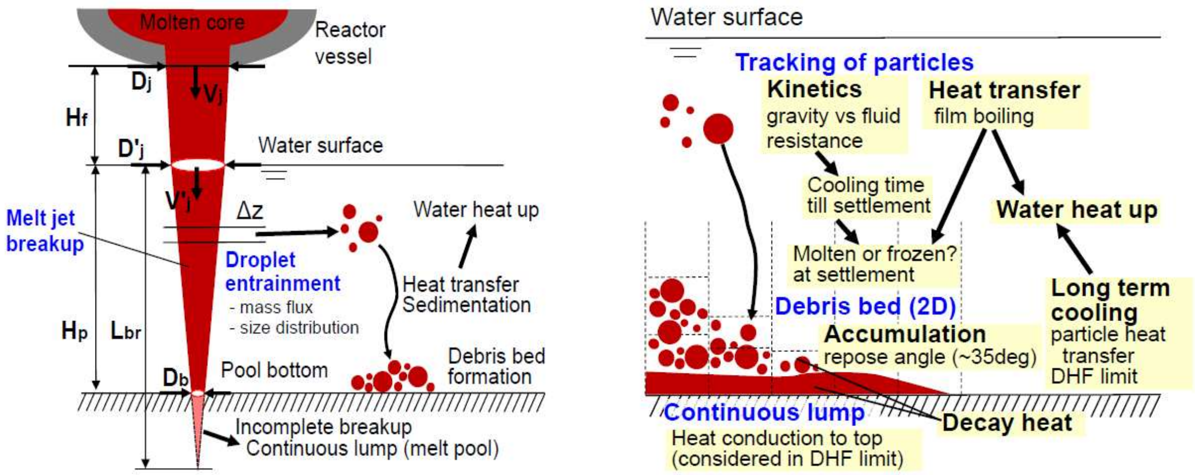

FIG. 71. Model schematics of the COOLAP code.

2.3.4.4. Plant modelling and nodalization

The MELCOR2.2 nodalization of the primary, secondary and containment systems used for the present study, are illustrated in Fig. 72. As shown in the figure, the MELCOR input for the APR 1400 plant is modelled with 65 control volumes, 130 flow paths, and 430 heat structures.

The RPV consists of 5 control volumes i.e., the downcomer, lower plenum, core channel, core bypass, and upper plenum. Each RCS loop has seven (7) control volumes i.e., one hot leg, steam generator U-tube hot side including steam generator inlet plenum, steam generator U-tube cold side including outlet plenum, two intermediate legs, and two cold legs.

The pressurizer is connected to the hot leg of loop A. The secondary side of a steam generator has two volumes in total, including a steam generator downcomer, and steam generator main volume including a steam dome.

The APR1400 plant has a large containment with a total free volume of 95,000 m^3. It is sub-divided into sub-compartments, which are simply modelled using 15 control volumes as follows:

1) Reactor Cavity (CV001);
2) Corium Chamber room (CV002);
3) Reactor Vessel Annulus (CV003);
4) In-containment refuelling water storage tank (CV004);
5) Steam Generator #2 Compartment (CV005);
6) Steam Generator #1 Compartment (CV006);
7) Pressurizer Compartment (CV007);
8) Upper Compartment A (CV008);
9) Upper Compartment B (CV080);
10) Dome (CV009);
11) Annulus A (CV010);

12) Annulus B (CV015);
13) HVT (Holdup Volume Tank) (CV011);
14) IRWST (CV012);
15) IRWST Sparger (CV013).

The reactor cavity has a free volume of 707.93 m^3 and the in-containment refuelling water store tank (IRWST) is located inside the containment, about 2,500 m^3 of water during normal operation. It plays a role as a primary heat sink for the discharge of POSRVs, as well as a water source for a safety injection pump, containment spray pumps (CSP), and cavity flooding system (CFS) during accident conditions. Several number of heat structures are taken for the containment wall, dome, basement, and internal structures in the containment.

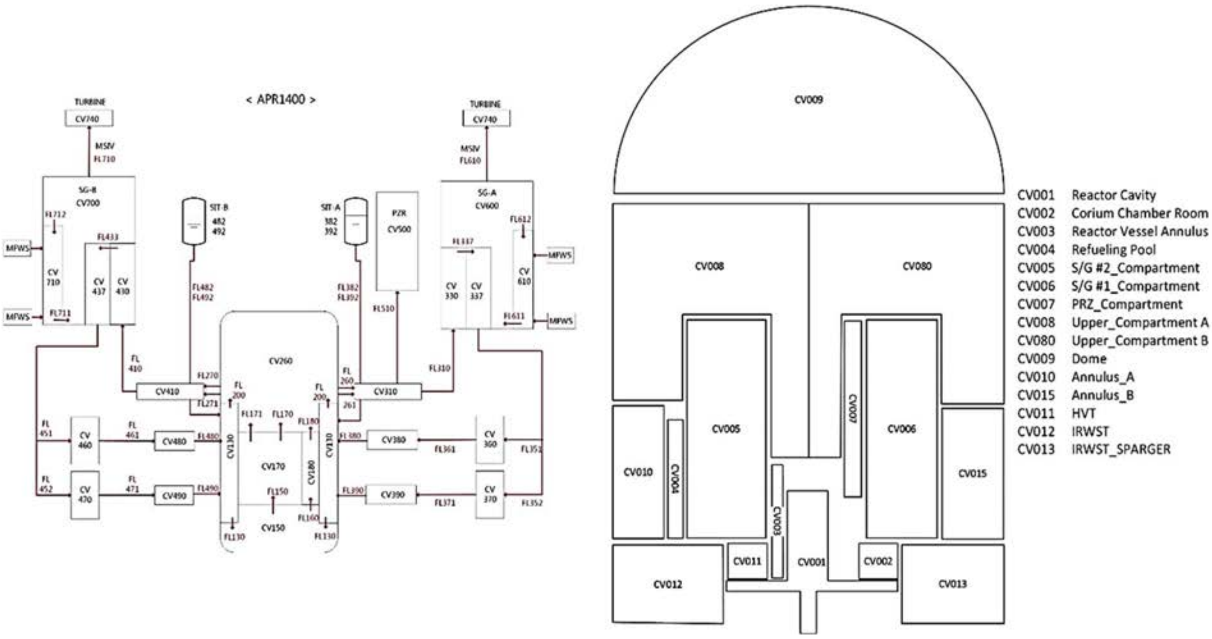

FIG. 72. APR1400 MELCOR nodalization.

2.3.4.5. Methodologies and tools for the uncertainty and sensitivity analysis

<u>Uncertainty analysis methodology:</u>

— MELCOR-SNAP methodologies: in this study, SNAP/DAKOTA [4] was used for MELCOR2.2 calculation and the schematic drawings of relevant job processing are given in Fig. 73.

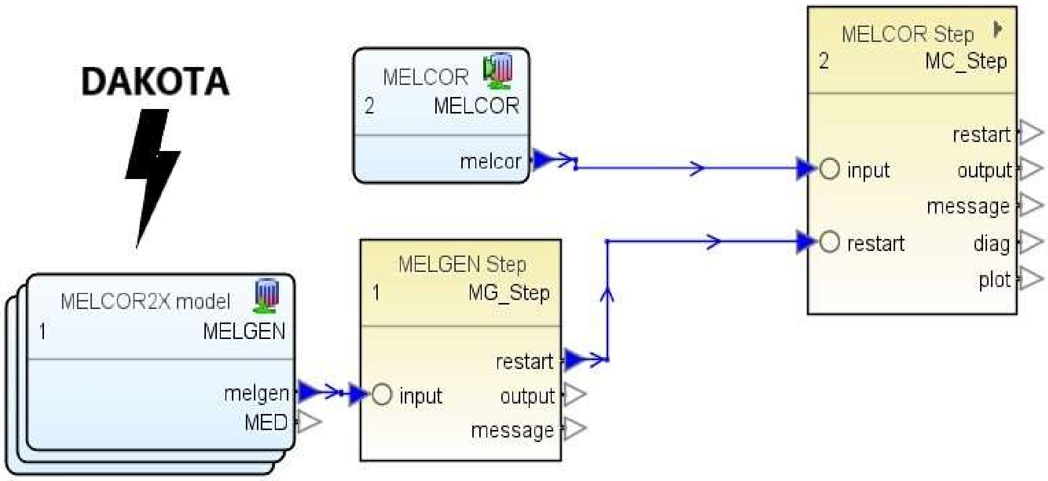

FIG. 73. SNAP/DAKOTA job processing.

— COOLAP-II methodologies: flow chart of the MELCOR-COOLAP coupled analysis is shown in Fig. 74. Two codes, COOLAP and MELCOR, were used in tandem and the data was transferred in only one direction. The analysis starts at the melt discharge from the bottom of the reactor vessel. The initial 1 h including the melt discharge, breakup, debris bed, melt lump formation and their cooling is simulated by COOLAP. The variables describing the state of the debris bed/melt lump and the containment thermos-hydraulic conditions, i.e., water level, temperature, pressure, etc. at the end of the COOLAP calculation are given to MELCOR to simulate the following 72 h, including the MCCI and containment pressurization.

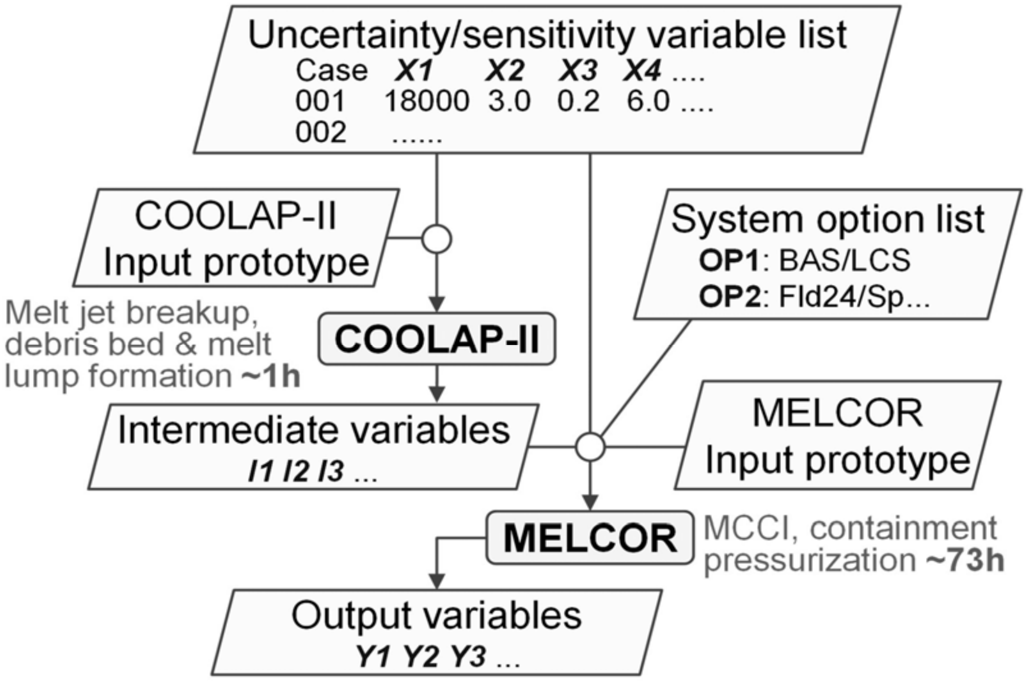

FIG. 74. Flow chart of the MELCOR-COOLAP coupled analysis.

The input variables for the two codes were separated into two parts, the fixed part and the uncertainty/sensitivity variables changed for specific analysis cases. The “Input prototype” includes the fixed part of input data and that describes most of the system definition and variables for which common values are used in all cases. The variables changed by cases are given in the “uncertainty/sensitivity variable list.” Those include the melt release conditions, water level at the reactor cavity, model parameters in the codes. A part of the MELCOR input data related to the system specification and the accident management action, i.e., the concrete type and the additional water supply, were also handled parametrically as system options OP1, and OP2. They were given as discrete set of variables rather than continuous values and fed to the MELCOR input by the “system option list.” A part of the COOLAP output was extracted and inserted into the MELCOR input as “intermediate variables.”

Sensitivity analysis methodology: in uncertainty analysis, correlations are useful because they can indicate a predictive relationship that can be exploited in practice. The following correlations are important for uncertainty analysis: (a) variables – FOM correlation, and (b) variables correlations associated with FOMs. Correlation is a statistical method that determines the degree of relationship between two different Variables. For the evaluation of correlation between two variables, first, the scatter plot and the scatter plot matrix show the association between two variables, and all pairwise scatter plots for many variables, respectively. Secondly, to calculate covariance, a measure of how much two variables change together, a covariance matrix measures the covariance between many pairs of variables. The correlation coefficient magnitude indicates the strength of the relationship between variables. When the association between the variables is linear, the product moment correlation coefficient describes the strength of the linear relationship. This is generally called the Pearson correlation coefficient. The correlation coefficient ranges from -1 to +1. Where, +1 indicates a perfect positive linear relationship, and -1 indicates a perfect negative linear relationship. While ‘0’ (Zero) indicates the variables are un-correlated and there is no linear relationship among them. When the association between the variables is not linear, a rank correlation coefficient describes the strength of association. This is generally called Spearman correlation coefficient. These correlation coefficients are from -1 to +1. A positive rank correlation coefficient describes the extent to which as one variable increases the other variable also tends to increase, without requiring that increase to be linear. If one variable increases, as the other tends to decrease, the rank correlation coefficient is negative. As the sensitivity measures between uncertain input variables and relevant FOM of interest, the present study utilizes the two correlation coefficients, i.e., Pearson correlation coefficients and Spearman rank correlation coefficients.

Uncertainty and sensitivity calculation scheme and relevant tools:

- SNAP description: symbolic nuclear analysis package (SNAP) [4] developed by SNL for the USNRC is a graphical user interface for simplifying the task of creating input files for the analytic codes such as MELCOR and helping to visualize code results. For uncertainty and sensitivity analysis, the SNAP provides an additional plugin program DAKOTA [4]. Using the DAKOTA plugin, the users can create the random samples or the Latin hypercube samples and combine them into the input data set for calculation of the specified code.
- COOLAP in-house uncertainty and sensitivity tool: COOLAP is coupled with an in-house program coded with the FORTRAN language based on the conventional theory for uncertainty and sensitivity analysis that includes the parameter sampling method based on the LHS method and the importance analysis.

Uncertain parameters and related probability distributions:

— MELCOR: in this study, the FOM of the uncertainty evaluation is reactor cavity ablation depth and all uncertainty parameters are selected in view of the FOM. The MELCOR cavity package is developed from CORCON/MOD3, and the models of aerosol generated by MCCI have been introduced. In this study, aerosols generated from MCCI are not considered and uncertainty analysis is mainly focused on the MCCI model. For the reference, it can be found that recent uncertainty studies on source terms in containment have been conducted by the USNRC and SNL [5–12]. The MCCI phenomena are treated by the CORCON model in MELCOR [7, 13].

Without overlying water, the corium is generally not coolable and MCCI occurs, producing large quantities of hydrogen as well as non-condensable CO and CO_2. However, in the presence of overlying water, such configuration ought to be coolable owing to water penetration into the crust and breakup of the insulating crust. In general, the CORCON model assumptions are such that quenching of core debris by overlying water in the cavity region can occur only if the debris layers are very thin because of the CORCON's modeling assumption that the crust is impenetrable to downward water intrusions. Significant thermal resistance offered by the surface crusts at the water interface severely limits heat transfer to the overlying water. This is illustrated in the following two figures. Firstly, the predicted debris temperature for the base CORCON modeling is shown in Fig. 75 (a): one with only the increased pool heat transfer coefficient, and another with both the increased pool heat transfer coefficient and the increased crust conductivity.

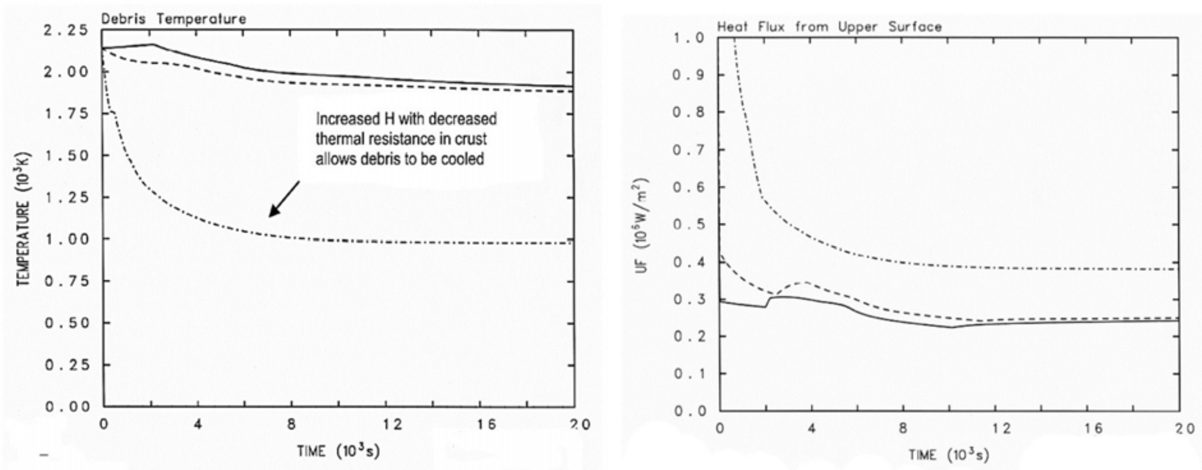

(a) *(b)*

FIG. 75. Default and modified CORCON analysis of MCCI in a Sequoyah cavity: (a) predicted cavity debris temperature, (b) predicted heat flux to the pool [7].

It can be seen that increasing pool heat transfer alone cannot increase the cooling rate but increasing the crust conductivity together with an increase in the pool heat transfer can produce debris cooling by overlying water. Second, the predicted heat flux rejected to the water for these cases is given in Fig. 75 (b). This allows the user to effectively control the heat flux rejected to the water pool and permits the possibility of cooling and mitigating the MCCI. SNL proposed to parameterize the heat flux rejected to the water by appropriate adjustment of the heat transfer coefficient, based on observations from experimental studies of MCCI (MACE: melt attack and coolability experiment) [6] or on projections of expected cooling behavior from other experts. A distribution of heat rejection ability can therefore represent uncertainties in this area of admittedly diverse opinion. Based on reviewing test data from the MACE program (SAND2014-2210) [6], SNL was characterizing heat rejection in term of the peak initial heat rejection rate observed in experiments.

Peak heat flux rejected in MACE tests range from 2,000–5,000 kW/m2; however, CORCON-predicted peak heat fluxes using default parameters can be significantly lower. CORCON-predicted heat rejection for 80 MT corium that is deeply flooded by water using the conductivity multipliers described earlier for several different values, as shown in Fig. 76 (a). Multipliers near 1 are typical of default CORCON application and result in peak heat fluxes of about 400 kW/m2. Whereas multipliers above 10 produce results that are more typical of those observed in MACE tests. The effect of the different heat rejection rates on corium cooling is shown in Fig. 76 (a). The distribution function prescribed for the characterization of ex-vessel corium cooling is shown in Fig. 76 (b). The distributions are specified so that the median of the distribution reflects the approximate division from configurations that are coolable and those that are not. This reflecting approximately the diversity of scientific opinion on this subject.

In OECD/NEA MCCI project [7], extensive MCCI experiments had been performed and the purpose was to carry out reactor materials experiments and associated analysis to achieve the following two technical objectives: (a) resolve the ex-vessel debris cooling issue by providing both confirmatory evidence and test data for cooling mechanisms identified in previous tests, and (b) address remaining uncertainties related to long-term 2D core-concrete interaction (CCI) under both wet and dry cavity conditions. In the MCCI, two corium cooling mechanisms were observed, and analytical models had been developed. Those models were implemented in CORQUENCH code [8] which had been developed in Argonne National Laboratory. Experimental assessments and validation show that the CORQUENCH code predicts the experimental results well. In 2017, the above two models were implemented in MELCOR2.2.

The MELCOR best practice [16] suggests that four parameters were related to boiling enhancement and oxide/metal/crust conductivities. In the recent MELCOR user's guide, the MELCOR developer team suggested that the boiling enhancement factor should be set 1.0 because of the implementation of water ingression and melt eruption models. Finally, the five parameters were selected as shown in Table 33 and described as follows.

TABLE 33. MELCOR UNCERTAINTY PARAMETERS

Parameters	Description
ZO	Axial coordinate of center of the ray system (geometry parameter)
COND.OX	Thermal conductivity multiplier of oxidic mixtures
COND.MET	Thermal conductivity multiplier of metallic mixtures
COND.CRUST	Thermal conductivity multiplier of crusts
3200-1	Multiplier for ANS decay heat curve

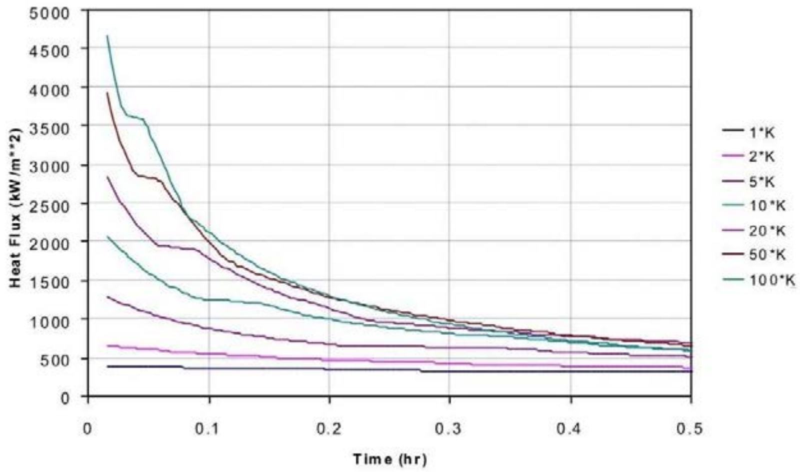

(a)

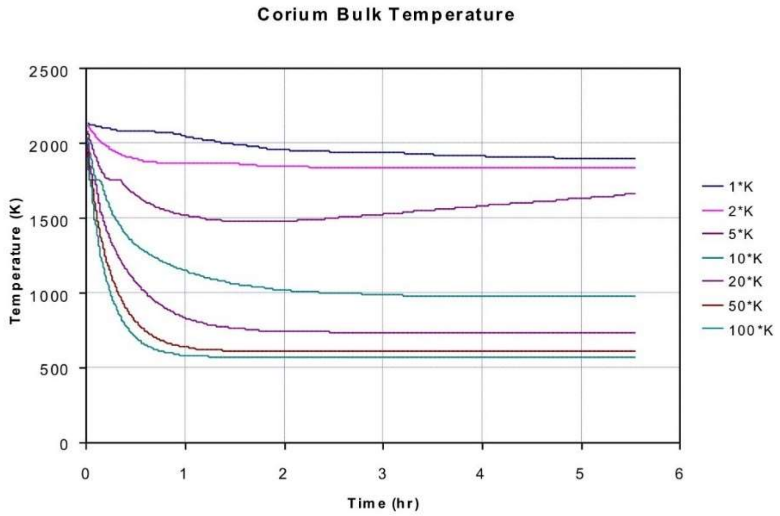

(b)

FIG. 76. Impacts of different values of the conductivity multiplier (concrete ablation temperature=1,650 K): (a) heat rejection (b) corium cooling (corium bulk temperature) [6].

- *ZO: axial coordinate of center of the ray system*: cavity package of CORCON or MELCOR adopts a unique feature called the ray-system as shown in Fig. 77. In this figure, RO is readily determined while ZO can be determined according to the axial centerline. Moreover, the lower ZO provides a more conservative prediction of the axial ablation depth, although MELCOR suggests that ZO would be in the cavity center location. The cavity center, 0.5, is the mean value, the lower bound 0.3, and the upper bound 0.7 and the distribution type is regarded as triangular.
- *COND.OX: thermal conductivity multiplier of oxidic mixtures [2]:* as already described, the heat transfer between the corium pool and coolant is governed by corium temperature and that is controlled by the thermal conductivity of three material groups. This parameter is thermal conductivity multiplier of oxidic layer. Distribution type cannot be specified, and triangular distribution is adopted. Mean value, 5.0 is adopted and this value is suggested in

MELCOR2.2 manual [2]. Low end value is 1.0 and high-end value is 10.0. High end value is that previous MELCOR version (1.8.6) best practice value.

- *COND.MET: Thermal conductivity multiplier of metallic mixtures [2]:* second material layer is metal layer, and this parameter also adopts triangular distribution. Mean value is 5.0 (MELCOR2.2 default value) and high/low end values are set to 1.0/10.0

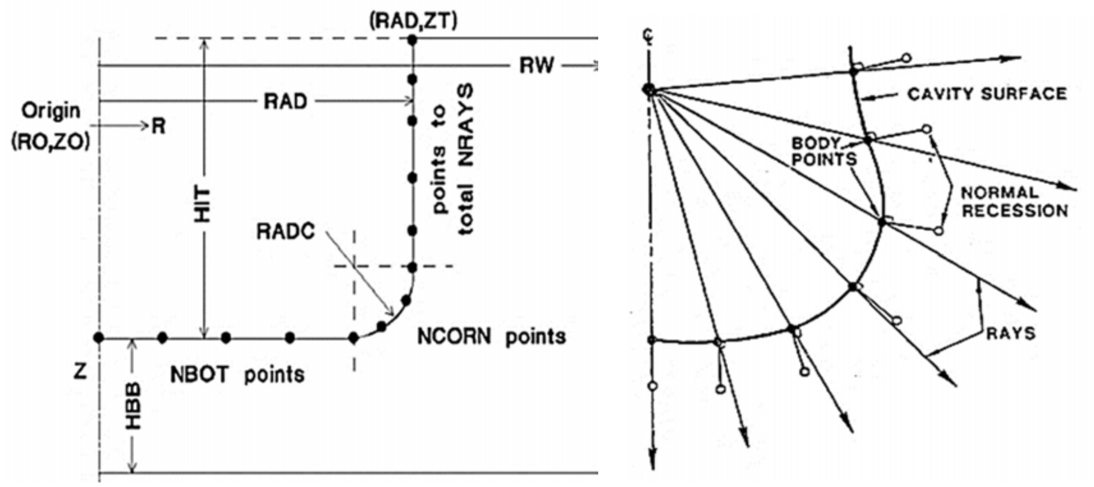

FIG. 77. CORCON coordinate system [2].

- *COND.CRUST: thermal conductivity multiplier of crusts [2]:* third material layer is crust and also adopts triangular distribution. As default mean value for MELCOR 2.2 is 1.0 and set to 1.2, as close as possible to default value. High/low end values are set to 1.0/5.0.
- *3200-1: multiplier for ANS decay heat curve [2]*: the ANS decay heat curve is adopted in MELCOR and the reference ANS decay heat model is ANSI/ANS-5.1-1979 [15]. The decay heat model distribution type is regarded as normal distribution and to get the distribution parameter, standard deviation, reference documents (ANSI/ANS-5.1-1994 [16], USNRC Research Information Letter 0202 [17]) shows the standard deviation of ANAI/ANS-5.1-1994 model and it is assumed that this value is in the same order of magnitude of that of ANAI/ANS-5.1-1979. This value will be updated.

In SNAP/DAKOTA, LHS is used, and the distribution type of the above variables is assumed as triangular. These variables are not clearly identified, and they have physical meaning. Thus, minimum and maximum values are adopted, and the default value is adopted as the most frequent value. If reactor vessel failure time is reduced, the decay heat level should be increased, and the decay heat uncertainty will be added to consider this uncertainty. The decay heat level is one of the most important parameters in view of ablation depth. For validation per Table 34 variable ranges, the validation analysis are performed using OECD/NEA MCCI CCI-2 experiment [7]. Two FOMs were selected, axial ablation depth and radial ablation depth. The 99 cases were selected and compared with experimental results as shown in Fig. 78. The results show that the experiment is located around the middle of the analysis results.

TABLE 34. MELCOR UNCERTAINTY VARIABLES FOR CAVITY PACKAGE

Variables	**Dist. Type**	**Min.**	**Mode (Mean)**	**Max.**	**Remarks**
ZO	Triangular	0.3	0.5	0.7	Normalized
COND.OX	Triangular	1.0	5.0	10.0	5.0[(1)]
COND.MET	Triangular	1.0	5.0	10.0	5.0[(1)]
COND.CRUST	Triangular	1.0	1.2	5.0	1.0[(1)]
3200-1	Normal	0.999	1.0	1.001	3.5×10^{-4} (SD)

[(1)] MELCOR2.2 default value

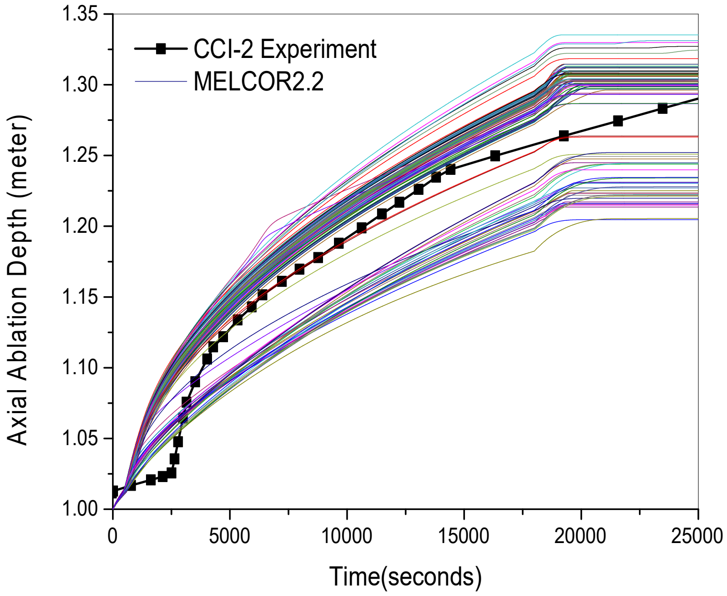

(a)

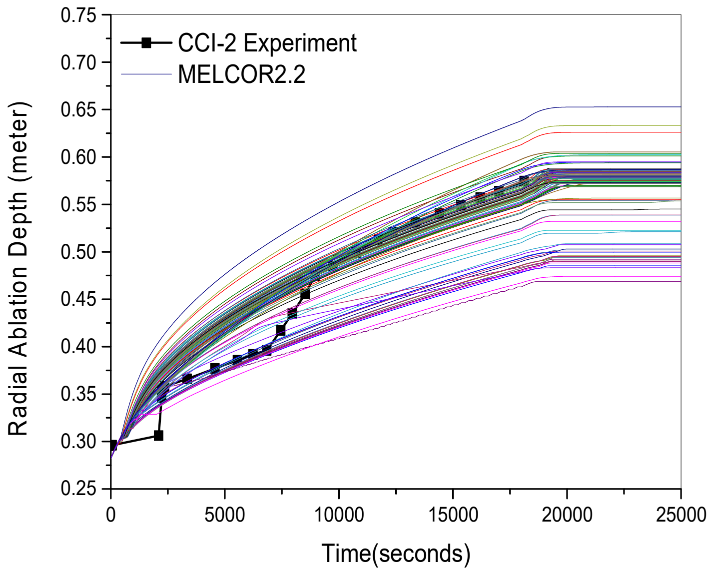

(b)

FIG. 78. CCI-2 MELCOR uncertainty analysis: (a) axial ablation depth, (b) radial ablation depth.

— *COOLAP-II*: the in-house COOLAP code was used for the uncertainty analysis to evaluate the ex-vessel phase of the severe accident after the melt discharge from the reactor vessel. For the analysis, the initial conditions such as the amount of the core melt in the lower head of the reactor vessel that falls into the reactor cavity, and the time of the reactor vessel failure are needed. The vessel failure time has a significant meaning as it provides the time from shutdown that determines the decay heat level. Severe accident analysis results for the model plant using the MELCOR analysis described in the previous section were used for such information.

The parameters considered in the COOLAP analysis are presented in Fig. 79. The definitions of each parameter and variable are shown in Table 35. At present, the selection of those parameters and variables as well as the uncertainty ranges and profile probability distribution functions by considering various plant-specific accident scenarios for the APR1400 like model plant have been performed. Except for a few model parameters, those parameter values depending on plant-specific accident scenarios are determined from the completed in-vessel MELCOR analysis.

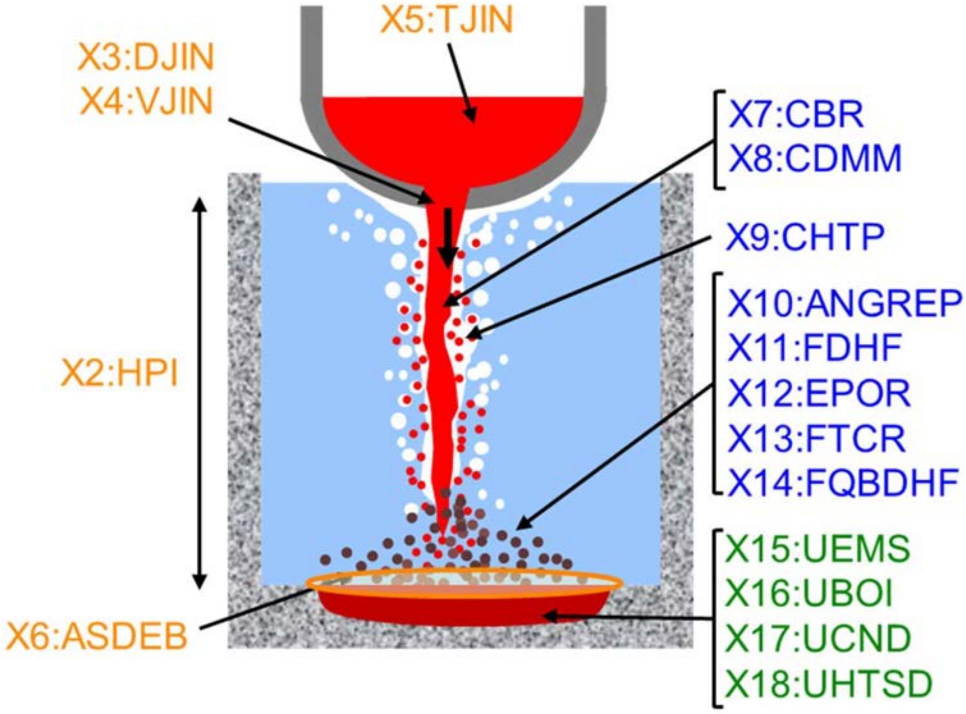

FIG. 79. Parameters for the sensitivity and uncertainty analysis of COOLAP.

The COOLAP code consists of the simplified models of corium jet breakup, debris bed formation and bed cooling. Prior to the plant analysis, those simplified models for the prototypic model plants should be validated. For this purpose, the simplified ex-vessel melt-jet discharging and thermo-hydraulic conditions assuming a severe accident in OPR1000 type nuclear power plant have been tested and compared with results with FCI mechanistic code like JASMINE (JAERI Simulator for Multiphase INteraction and Explosion) [20]. The JASMINE code was used for this validation since this code has two-dimensional FCI models with the similar jet break-up mechanism. The model parameters validated in the work has been used for the analysis for the APR1400 plants. In the following paragraph, the model parameter validation performed for the prototypic power plant, herein OPR1000, is described. Variables and parameters used for the COOLAP model validation are given in Table 36. The base case and a case with a shallow water pool as shown in Table 36 were selected up to simulate the melt jet breakup and sedimentation in the reactor cavity. The base case condition also corresponds to the typical values of the input variables in the plant analysis for model plants.

TABLE 35. DEFINITION OF VARIABLES AND PDFs OF COOLAP

Input variables			**PDFs**
Sensitivity Variables	X1	T0SD: Time after shutdown$^{(1)}$	
	X2	High pressure injection system: initial water pool depth	Uniform, 1.1 – 8.3
	X3	DJIN: Melt jet diameter^{*2}	X50$^{(1)}$=0.2, EF$^{(2)}$ = 2
	X4	VJIN: Melt jet velocity^{*3}	X50=6, EF = 2
	X5	TJIN: Melt jet T (liq.2670+ΔT)	X50=170, EF = 2 (Superheat)
	X6	ASDEB: Debris accumulate area	
Model Parameters	X7	CBR: Jet breakup length factor^{*4}	X50=1, EF = 1.5
	X8	CDMM: Particle size factor^{*4}	X50=1, EF = 1.5
	X9	CHTP: Heat transfer factor^{*4}	X50=2, EF = 2
	X10	ANGREP: Repose angle^{*5}	
	X11	FDHF: Deteriorating heat transfer factor	
	X12	EPOR: Debris bed porosity^{*6}	
	X13	FTCR: Merge criterion const.^{*4}	Uniform, 0 – 0.5
	X14	FQBDHF: Lump heat transfer limitation factor	
Model Parameters	X15	UEMS: Melt emissivity	
	X16	UBOI: Top boiling hot leg factor	
	X17	UCND: Melt conductivity factor	
	X18	UHTSD: Melt hot leg factor (side)^{*7}	

(1) Median of the lognormal distribution; (2) Error factor of the lognormal distribution.

TABLE 36. VARIABLES AND PARAMETERS IN COOLAP

Parameters	**Base case**	**Water Pool 2**
Melt material	UO_2/ZRO_2 (80/20)	
Melt jet diameter (m)	0.2	
Melt initial velocity (m/s)	6	
Melt initial temperature (K)	3010	
Cavity depth (m)	6.5	
Water pool depth (m)	5.9	3.1
Water temperature (K)	300	
Floor area (m^2)	80	
System pressure (MPa)	0.2	

To evaluate the model performance of prediction of melt debris during jet breakup, a relatively shallow water depth of 3.1 m compared to the value of the base case was considered. COOLAP model parameter settings are shown in Table 37. The result in the base case compared with the JASMINE is shown in Fig. 80.

The indexes for comparison are (a) the transferred heat from the melt, (b) the quench ratio (solidification basis), (c) the melt lump mass fraction and (d) the melt lump enthalpy. When the model parameters are set as same as JASMINE, the simplified model overestimated the heat transfer as observed in (a) and (b), while the mass fraction of the lump was in good agreement with JASMINE (c). The enthalpy of the lump was larger than the result of JASMINE (d). The lump enthalpy is assumed to be the liquidus point enthalpy and no heat removal was modelled, while JASMINE considers the heat transfer from the melt pool.

TABLE 37. COOLAP MODEL PARAMETER SETTINGS FOR APR1400

	Base Case	**Case 1**	**Case 2**	**Case 3**	**Case 4**
	JASMINE	$C_{htc}/4$	$C_{htc}/4$, deteriorating heat transfer	$C_{htc}/4$, merge T_{av}	$C_{htc}/4$, deteriorating heat transfer, heat transfer T_{lmp}
C_{htc} for particle	2.0	0.5	0.5	0.5	0.5
C_{htc} for debris bed	0.1	0.1	0.1	0.1	0.1
Deteriorating heat transfer limitation for debris bed			ON		ON
Particle merging criterion	~ T_{sf}	~ T_{sf}	~ T_{sf}	~ T_{av}	~ T_{sf}
Melt lump heat transfer					ON

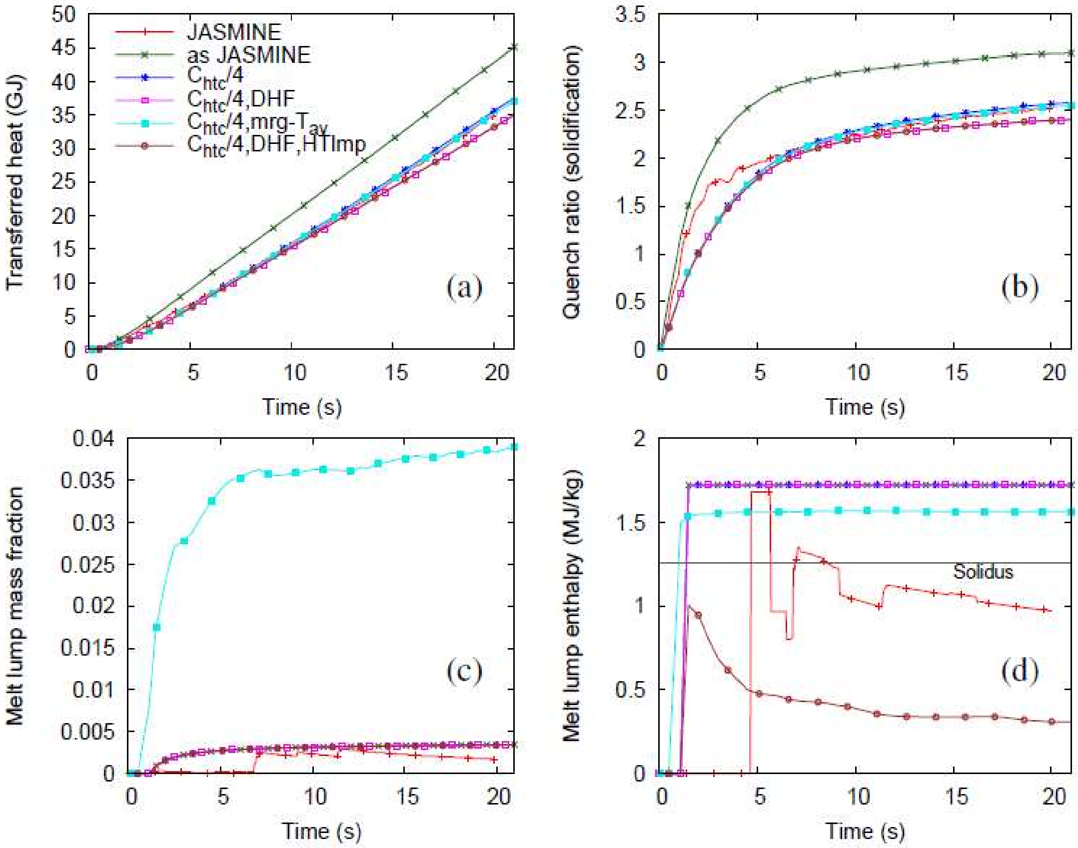

FIG. 80. Comparison of the evaluation of (a) heat transfer, (b) quenching ratio (solidification basis), (c) melt lump (pool) fraction, and (d) melt lump enthalpy evaluated by JASMINE and COOLAP for the base case.

Decreasing the heat transfer multiplier, C_{htc} for particles from 2.0 (recommended value for JASMINE based on simulation of experiments) to 0.5 in all the cases, the heat transfer decreased by ~15% and became close to the JASMINE results. Further a slight decrease occurred by applying the deteriorating heat transfer limit for the debris bed heat transfer (case 3). The change in the temperature criterion for the merge of particles into the lump, the case 3, showed a significant change of the lump fraction, from 0.3 to 4%. This change accompanied the decrease of lump enthalpy due to the addition of less hot melt into the lump. When the heat transfer model for the lump was applied, the case 4, the melt lump enthalpy significantly decreased (d), while other variables did not change.

The same comparison for the case with a shallow water pool, water pool 2 (3.1 m instead of 5.9 m in base case) is given in Fig. 81, in which a significant amount of melt pool formation was observed in the simulation by JASMINE. The dependence on the model parameters was similar to the base case. The model parameter setting as same as JASMINE resulted in an overestimation of the heat transfer (a, b) and underestimation of the lump (melt pool in JASMINE) formation (c). The modification of the parameters, i.e., reduced C_{htc} and application of deteriorating heat transfer limit, the Case 2, made a good agreement on the heat transfer (a, b), while it did not change the underestimation of the lump formation (c).

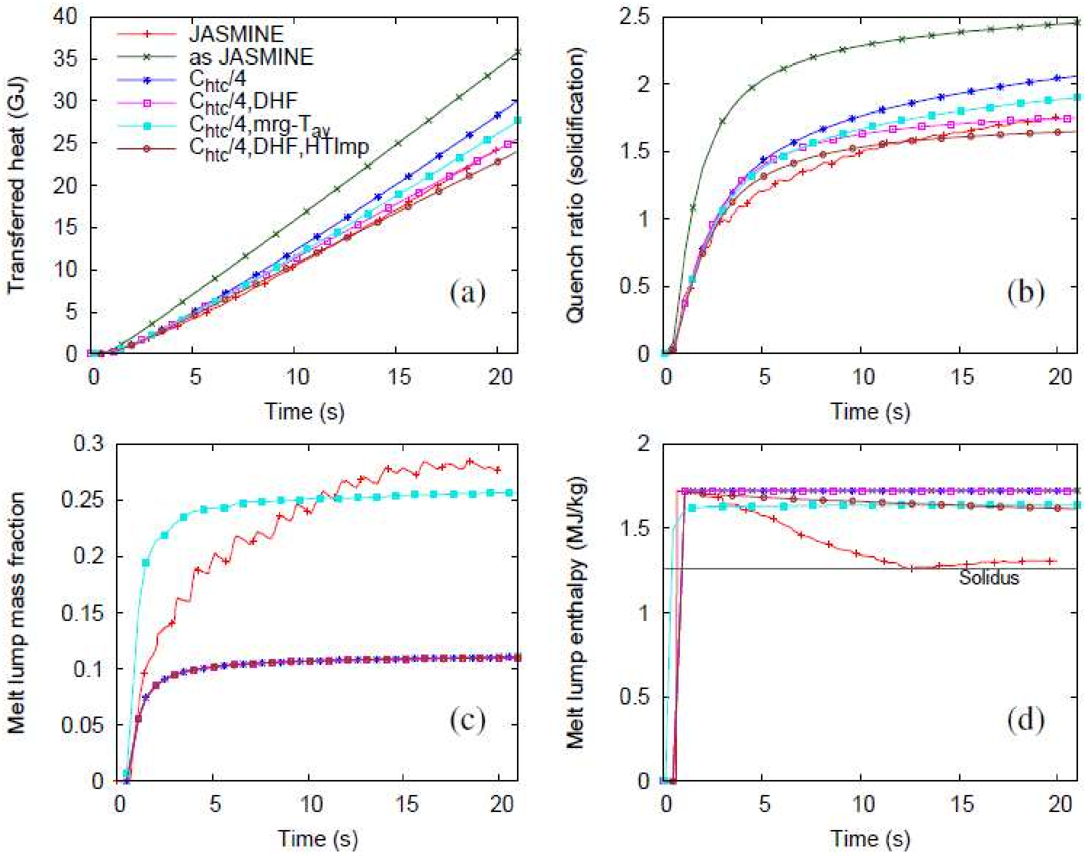

FIG. 81. Comparison of the evaluation of (a) heat transfer, (b) quenching ratio (solidification basis), (c) melt lump (pool) fraction, and (d) melt lump enthalpy evaluated by JASMINE and COOLAP for the shallow water case (water pool 2).

The alternative temperature criterion for the merge of particles into the lump, the case 3, showed a drastic increase of the lump fraction, 25%, which was like the JASMINE result (c). The melt pool model of JASMINE has 1D divided nodes in the radial direction and spatial temperature variation. It assumes locally that a group of particles in contact with the melt pool surface merge into the pool when either of the pool node or the particles are molten, determined by the surface or the average temperature criterion. The lump model of COOLAP has only one average temperature and such interaction with particles above is not considered. The merge of particles into the lump is determined by the temperature condition on the particles only. This difference explains that COOLAP estimates smaller amount of the melt lump even in the case if it uses the same temperature criterion as JASMINE.

The melt lump enthalpy was like the JASMINE result just after the formation of the lump, which was close to the liquidus point enthalpy. The JASMINE result showed decrease in the solidus point enthalpy in 12 s while COOLAP showed only a slight and slow decrease even in case 4 in which the heat transfer of the lump was considered. The melt lump heat transfer model of COOLAP only considers the internal heat conduction of the lump while the melt pool model in JASMINE considers boiling heat transfer at the surface. That can be the reason for the slow cooling in the COOLAP model. The melt pool model in JASMINE and the lump model in COOLAP are both rather crude and they lack realistic consideration for the boundary condition between the lump and the bottom of the debris bed. In the COOLAP model, however, the heat removal from the lump surface is compensated by the reduction of the heat removal capacity for the debris bed through the deteriorating heat transfer model. In other words, the limitation on the total cooling capacity of the debris bed and the underlining lump is given by the deteriorating heat transfer model, and this is an advantage of COOLAP over JASMINE.

Regarding the fraction of the continuous lump, the base case showed that the temperature criterion by T_{sf} gives a good agreement with JASMINE. While the water pool 2 case showed that the criterion by T_{av} gives a good agreement. This inconsistency leaves us a difficulty in making a recommendation on the choice for this option. For a reference, JASMINE is not well validated on the melt pool fractions. It was reported that JASMINE tends to overestimate the melt pool fraction compared with experimental results when the melt pool formation is significant. Thus, for this aspect, we need to further examine through many analytical cases, and comparisons with experimental data. In the present calculations, the merging of particle into the lump occurred only at the arrival of particles on the floor; no re-melt of debris particles was observed. For the COOLAP model validation, further comparison of overall indexes in a wide range of conditions were performed. A probabilistic analysis of the APR1400 ex-vessel melt jet breakup and cooling with JASMINE by varying eight input variables by the LHS method was reproduced by COOLAP for comparison in a wide range of conditions. It included a total valid case of 292. Input variables varied were: the factor for the jet breakup length, X7, the factor for the particle size, X8, the factor for particle heat transfer, X9, the factor for particle-pool merge criterion, X13, the melt initial temperature (X5), the melt jet diameter (X3), the melt jet release velocity (X4), and the water pool depth (X2) as shown

Three variations of calculation were performed with the LHS sets as same as that used for JASMINE. The variations are as discussed in the previous section including base case for JASMINE code values and the other four cases. The comparison between JASMINE and COOLAP for the quench ratio (solidification basis) (a), the melt lump fraction (b) and the ``molten pool index'' (c) as primary coolability indexes, is presented in Fig. 82. The molten pool index was proposed as an indicator of the significance of the melt lump in the molten state and defined by the ratio of the specific enthalpy of the melt lump and the specific enthalpy at the solidus point melt lump, multiplied by the melt lump mass fraction. The tendency of the results was like that observed in the previous sensitivity analysis: the base case shows overestimation of the heat transfer and underestimation of the melt lump (pool) production. Good agreement on the heat transfer is obtained by the cases with the reduced C_{htc} for particles. Regarding the melt lump production, the base case, and the Case 2, both using the original T_{sf} based merge criterion, show's smaller lump masses for many samples, especially in the right zone, while overestimations are seen in the small lump masses.

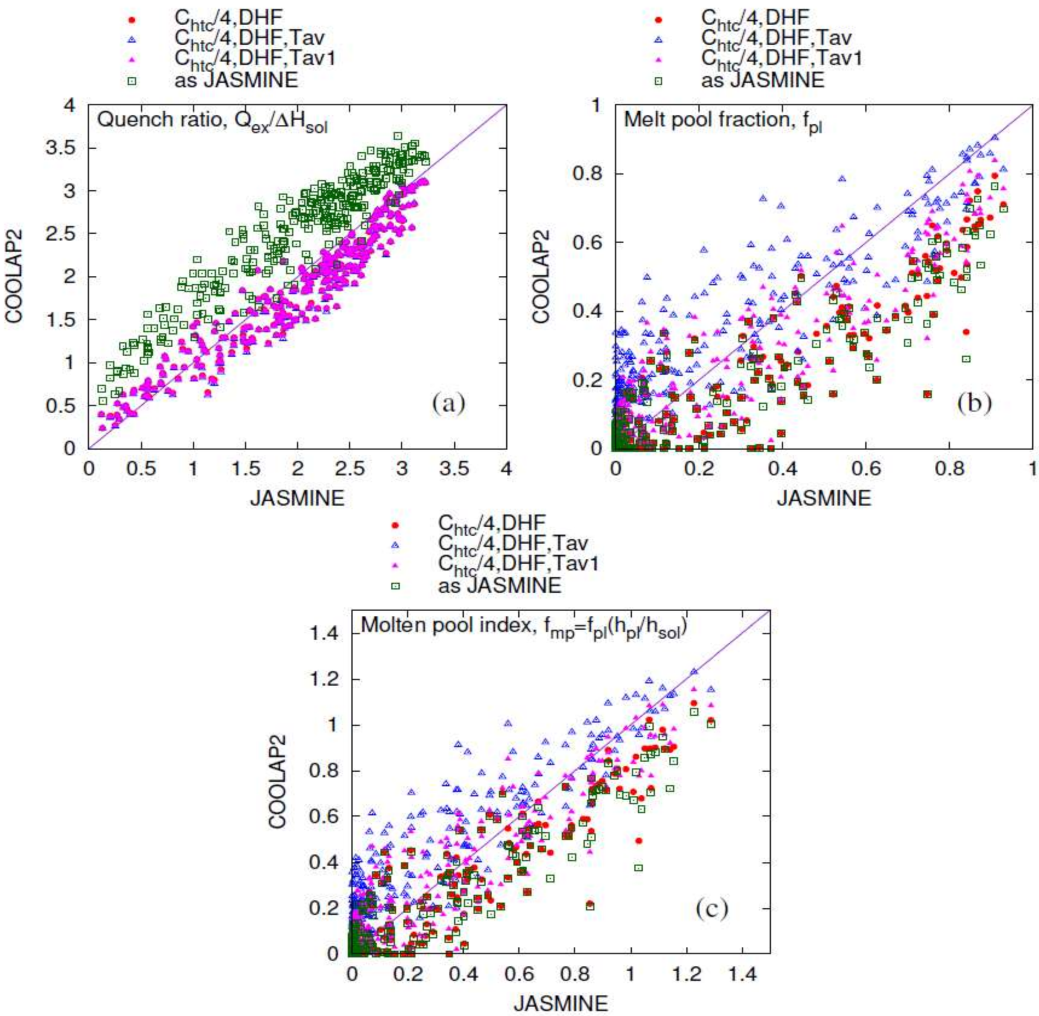

FIG. 82. Comparison of (a) the quench ratio (solidifaction basis), (b) melt pool fraction (c) melt pool index at 20 s evaluated by JASMINE code and (d) COOLAP for 300 random samples generated by LHS.

The change of the temperature criterion for the merge of particles to the T_{av} based one increases the melt lump production. The samples showing small fractions of the melt lump (e.g., <0.1) by JASMINE have larger lump masses by COOLAP. This overestimating trend becomes weaker in the right-hand side with larger melt lump fractions. With the original criterion with T_{sf}, the center of the scattering of COOLAP results in the low melt lump fraction zone is around the diagonal and it shifts to the right in the higher melt lump fraction zone. The case with the alternative T_{av} criterion also shows similar trend and the center of distribution is closer to the diagonal. Considering the reported JASMINE's overestimating tendency for the case of large melt lump fractions, these COOLAP results might be reasonable. The plot of the molten pool index (c) is less scattered than the one for the melt lump mass fraction (b). This index represents the enthalpy fraction in the melt lump and depicts its significance in terms of the cooling process. The three variations for the merge temperature criterion all show such a tendency in the comparison of plot (b) and (c). The results with the original T_{sf} criterion and the alternative T_{av} criterion distribute close to the diagonal.

For the brief discussion of the analysis conclusions, the modification from the JASMINE model parameter setting for the particle heat transfer as in the case 3 looks reasonable for COOLAP. The overall heat transfer behavior is not significantly affected by the change of the particle merge criterion. The large scattering in the comparison of the melt lump (pool) fraction with JASMINE indicates the large uncertainty in predicting this aspect. It shows a sensitivity to the temperature criterion for the merge of particles. Among the cases tested, using the average temperature criterion with the uncertainty range given by the merging criterion of 0-1 gives the closest results to the original JASMINE calculation with surface temperature criterion. COOLAP gives under-estimating and significantly overestimating trends against the JASMINE results with the original surface temperature-based criterion or the average temperature-based criterion, respectively. This is a purely analytical comparison and the JASMINE model itself has a significant uncertainty in the prediction of continuous melt lump production. Thus, further examination for the validity of COOLAP model is necessary by comparison with experimental data. Considering the realistic situation in a longer time span, the balance of the decay heat of the core debris and the cooling performance of the debris bed determines the overall debris behaviour. The initial division of the continuous lump and particulate debris might be prevailed by such factors.

2.3.4.6. Results

<u>*Results for the uncertainty analysis*</u>

To establish the full power steady state of APR1400, the initial conditions were adjusted including the pressurizer pressure, the steam pressure, the feed-water flowrate, and the feed-water temperature. The parameter values for the steady state condition in APR1400 are shown in Table 38.

TABLE 38. APR1400 STEADY STATE ANALYSIS RESULT

Parameter	Desired Value	Steady State Value
Reactor power (MW_t)	3,983	3,983
Primary pressure (MPa)	15.5	15.4
Secondary pressure (MPa)	6.89	6.86
Hot leg temperature (K)	597.0	598.2
Cold leg temperature (K)	563.7	563.2
RCS mass flow rate (kg/s)	20,991	20,433.5
Steam/Feed-water mass flow rate/SG (kg/s)	1,130.2/1,130.2	1,129.3/1,130.2

— *MELCOR analysis results*: an SBO is initiated by loss of AC power, followed by a reactor trip, RCP trip, main steam isolation valves closure, and main feed water trip. Following the SBO, besides the auxiliary feed water system, all safety systems required for core cooling and decay heat removal powered by AC power are unavailable. The operability of auxiliary feed water system depends on the battery capacity and water inventory of auxiliary feed water storage tanks. The APR1400 battery is designed to work for at least 8 h for all instrumentations, controls, and valves essential for the operation of turbine-driven pump. However, in this analysis, auxiliary feed water system is not considered. The RCP leakage is not considered because there could be large uncertainty in timing and the size of RCP seal leakage. All ECCSs are unavailable except for four SITs, which will automatically inject water into the reactor downcomer when the primary system pressure reaches 4.3 MPa.

The RCS pressure decreases after a reactor trip due to the reduction of the reactor power and coolant average temperature, as shown in Fig. 83. Simultaneously, four reactor coolant pumps are tripped, and natural circulation flow is established because the secondary side will act as a heat sink. Continuous heat input from the reactor coolant system makes the coolant level of the secondary side decline and finally the steam generator will dries out. The reactor coolant system flow starts to decrease as the steam generator coolant inventory decreases and the pressurizer pressure starts to increase. Finally, pressurizer pressure reaches 17.2 MPa and then causes an opening and closing of the POSRVs with the discharge of a two-phase mixture.

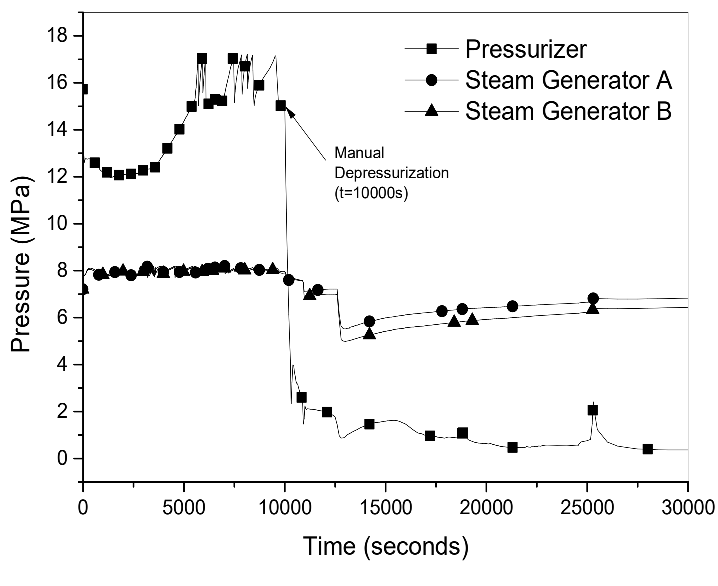

FIG. 83. Pressure behavior (short-term).

The continued discharge of a two-phase mixture from pilot operated safety relief valve (POSRV) finally results in a depletion of the water inventory in the core. Because the primary system pressure remains at a pressure around 17 MPa, higher than the set-point of the SITs, the water inventory in the reactor core cannot be recovered. The core liquid level decrease under active core and fuel rod temperature start to increase, as shown in Fig. 84. In accident management program, operator should actuate the manual depressurization device when the core exit thermocouple shows 933 K (1,200 ^{o} F). In Fig. 83, the core gas temperature reaches 933 K at 8,960 s and the assumption was made that operator opens POSRV manually at 10,000 s considering delay time to decide manual depressurization. Just after the POSRV opens, pressurizer pressure decreases rapidly, and four SITs start to inject into the core through the downcomer at 4.3 MPa. SIT coolant injection starts at 10,308 s and ends at 12,793 s. In Fig. 85, delivered coolant makes core water level recovered quickly, and fuel temperature decreases. After SIT injection is finished, coolant inventory in reactor vessel can maintain fuel temperature in a safe condition until the collapsed water level in core starts to decrease at 15,100 s.

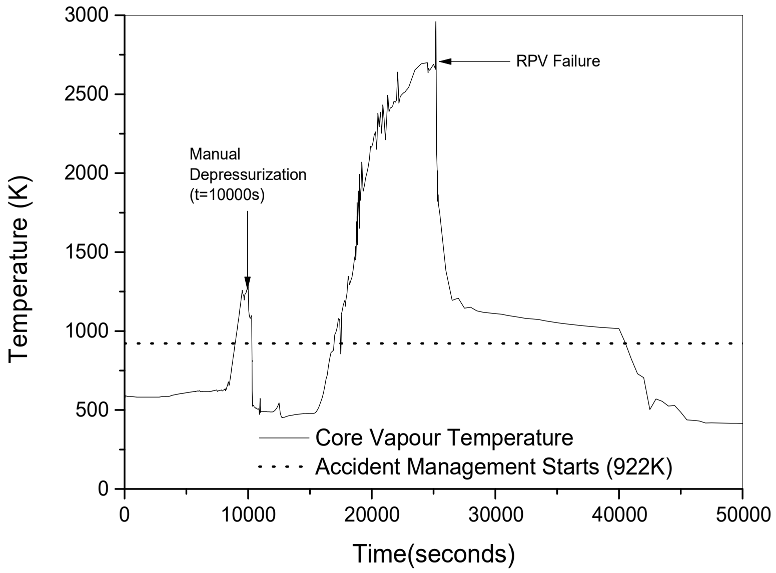

FIG. 84. Core gas temperature (short-term).

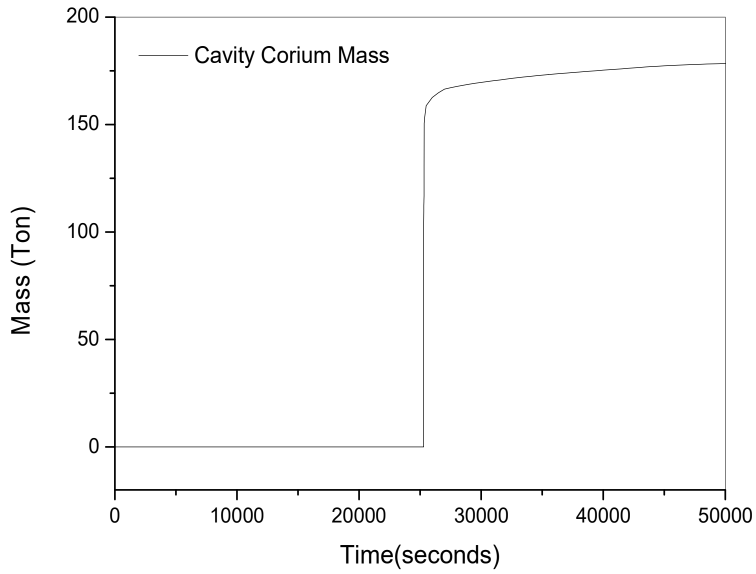

FIG. 85. Collapsed water level in the reactor core.

After active fuel is uncovered, fuel cladding temperature rapidly increase and increasing zirconium oxidation process accelerates fuel temperature as shown in Fig. 86 (a). This exothermic reaction accelerates fuel clad melting and eutectic formation with UO_2. As a result, core fuel temperatures increase, and particulate debris is formed in the degraded core cell. In Fig. 86 (b), core cell fuel temperatures disappeared, and particulate debris are appeared in the core cell. These particulate debris can be appeared, as particulate debris. MELCOR has a molten pool option, but the option is not used in this analysis due to errors. As a sequence, the fuel in the core is melted and the degraded cladding/fuel mixture in the core is relocated to the lower plenum. In Fig. 86 (b), core cell 101 to 105 is located in the lower head and 101 is corium cell just above the reactor vessel lower head structure. Thus, thick lines are 101 and 102 cell temperature, and two temperatures are maintained until 25,290 s. This time is the failure of the RPV lower head. All these events are summarized in Table 39.

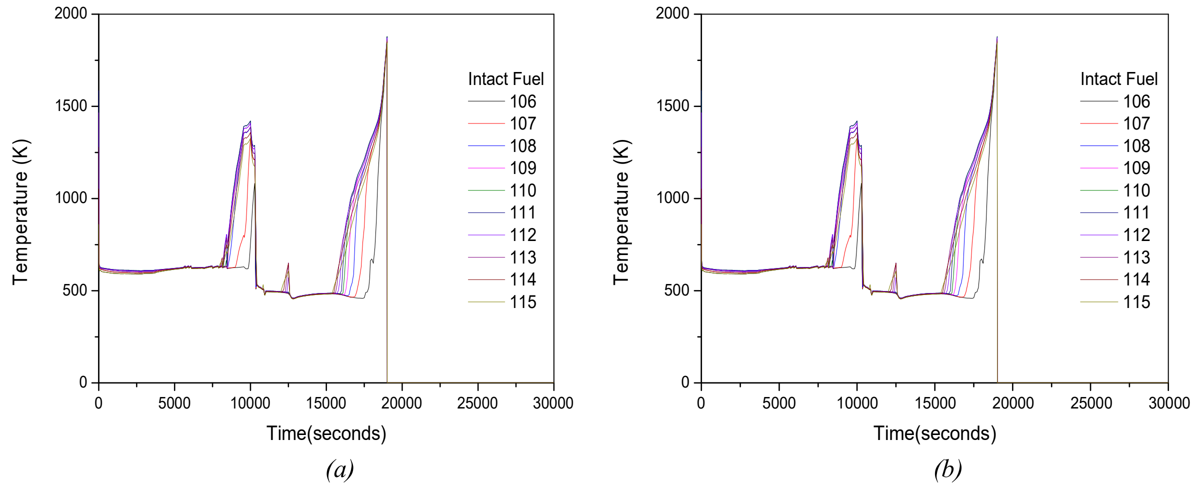

FIG 86. Fuel and particulate debris temperature in core ring1: (a) fuel temperature, (b) particulate debris

TABLE 39. SEQUENCE OF KEY EVENTS

Events	**Time (s)**
SBO Initiation	0.0
SG dryout	3,520
POSRV open at 17.2 MPa (2,500 psia)	5,700
Core uncovery	6,900
Core exit temperature reaches 933K	8,960
Manual depressurization starts	10,000
SIT Injection (start/stop)	10,308/12,793
Core dryout starts	15,100
RPV failure	25,290
Maximum corium mass relocated to cavity	26,500

After the reactor vessel lower head fails, corium inside the lower head is relocated to the reactor cavity which is flooded. The relocated amount of corium in the cavity is shown in Fig. 87 in which 170 tons of corium are relocated almost instantaneously. Small increase occurs until 60,000 s and the continuous relocation amount is less than 20 tons.

During corium discharge, coolant, steam, and hydrogen also discharged and hydrogen concentration in the reactor cavity shows a peak value, of about 80%. Figure 88 (a) shows the hydrogen concentration in reactor cavity and containment in short term and long-term behavior is shown in Fig. 88 (b). As shown in Fig. 88 (b), the hydrogen concentration in containment is much less than 4%, after the peak concentration occurs and inside reactor cavity is filled with steam/hydrogen mixture. This means that the combustion possibility in the reactor cavity can be ignored.

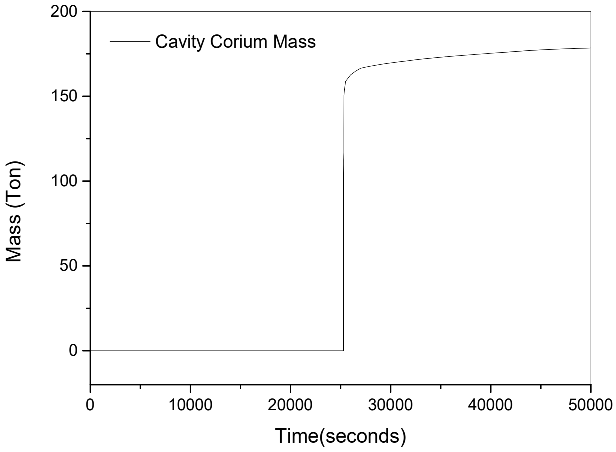

FIG. 87. Corium mass in reactor cavity.

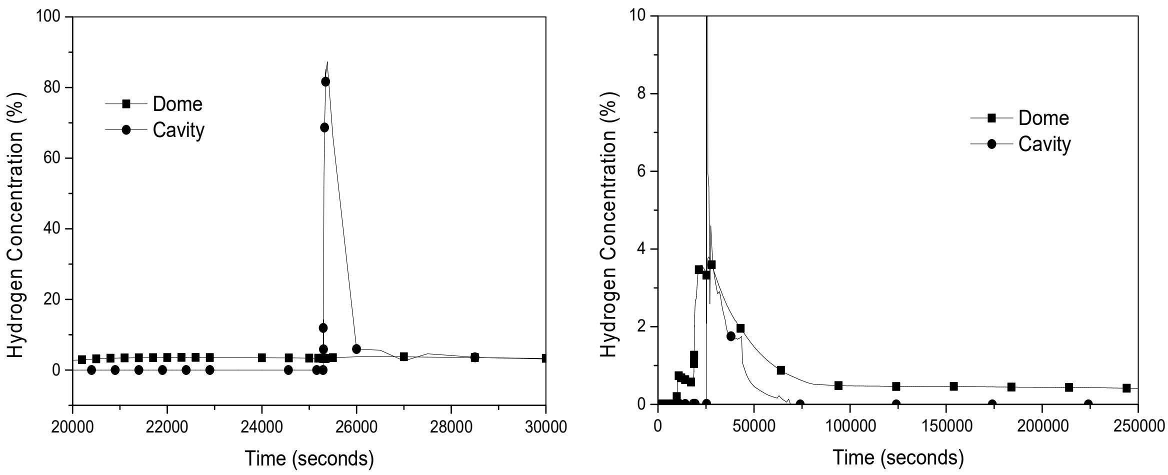

(a) *(b)*

FIG. 88. Hydrogen concentration in reactor cavity and containment dome: (a) short-term, (b) long-term

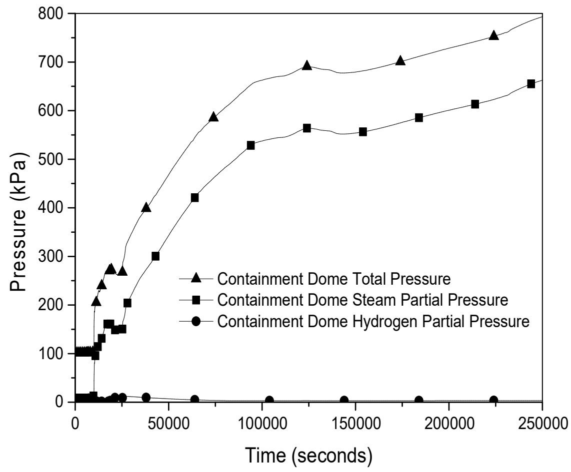

FIG. 89. Containment pressure.

In view of containment pressure, steam generated in the reactor cavity contributes to the pressure increase and in Fig. 89 containment total pressure is almost follows the same trend as steam partial pressure. Of course, the hydrogen partial pressure in the containment dome is very small and almost negligible. Containment dome gas temperature in Fig. 90 shows stable condition about slightly less than 440 K.

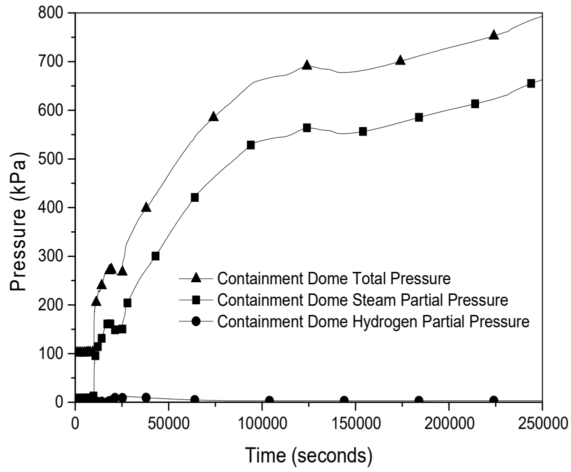

FIG. 90. Containment gas temperature

— *COOLAP analysis for MELCOR:* although there is a need to further validate the parametric approaches, the above validation results demonstrated the FCI calculation feasibility of the COOLAP code. As the MELCOR code cannot simulate the jet break-up mechanism that is involved in the case of the pre-flooded cavity condition, we estimated the melt lump mass fraction by the COOLAP calculation using the MELCOR results (at the time of RPV failure) as initial conditions and boundary conditions. The parameters used in the COOLAP calculation considering the in-vessel MELCOR results for the APR1400 design parameters are shown in Table 40.

TABLE 40. COOLAP-II INPUT PARAMETER BY THE MELCOR RESULTS

Parameter	Value
Reactor normal power (MW_t)	3,983
Vessel failure time (s)	25,290
Vessel height from cavity bottom (m)	7
Molten corium mass (ton)	171
Corium temperature (K)	2,600
Cavity water pool depth (m)	6.14
Cavity water temperature (K)	323.15
Cavity bottom area (m^2)	80
Containment pressure (MPa)	0.1

The vessel failure time determines the decay heat of corium during the FCI calculation. It should be noted that there are variables that cannot be determined by the MELCOR results/APR1400 design parameters among the parameters required for the COOLAP calculation. As shown in Table 43, the three variables, the melt initial diameter, the melt initial velocity and the jet break-up length model were considered the uncertainty parameters. In the melt initial diameter, a range greater than the median value (0.2 m) in Table 35 was established in the uncertainty analysis. In melt initial velocity with Bernoulli's equation, the pressure difference observed in the MELCOR results (~ 1.0 MPa) was included in the test matrix. The Epstein/Fauske and Saito model were used individually to calculate the jet break-up length (Table 42).

TABLE 41. COOLAP-II INPUT VARIABLES FOR UNCERTAINTY ANALYSIS

Variable	Value
Melt initial diameter (m)	0.2–0.6
Melt initial velocity (m/s)	6, Bernoulli's equation
Jet break-up length model	Epstein-Fauske, Saito

TABLE 42. BREAK-UP LEGNTH MODEL IN COOLAP-II

Model	Correlation
Epstein/Fauske	$\frac{L_{br}}{D_{j.l}} = 10(\frac{\rho_j}{\rho_l})^{0.5}$
Saito	$\frac{L_{br}}{D_{j.l}} = 2.1(\frac{\rho_j}{\rho_l})^{0.5}(\frac{v_{j.l}^2}{gD_{j,l}})^{0.5}$

In the COOLAP code, non-coolable corium can be generated in two ways. First, the corium can be directly generated from the melt jet when the jet break-up length is longer than the cavity water depth. Second, the corium can be generated from droplets which are not sufficiently cooled (Fig. 91). For the corium temperature of 2,600 K, most of debris droplets are sufficiently cooled hence the mass of non-coolable corium generated from droplets is negligible. In other words, non-coolable corium mass is only dependent on the break-up length. For this reason, the melt initial diameter and velocity are significantly important variables to determine the non-coolable corium mass.

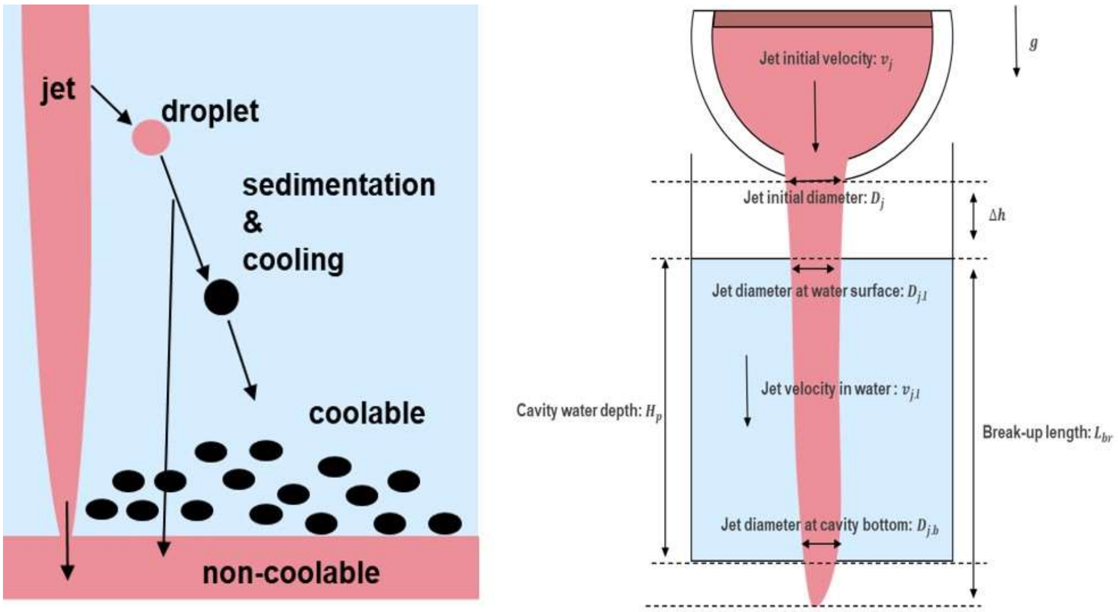

(a) *(b)*

FIG. 91. (a) non-coolable corium formation mechanism and (b) Jet figure in COOLAP-II. When jet break-up length is longer than cavity water level, non-coolable corium is directly generated.

The test matrix for the group 1 (Epstein-Fauske model) and the group 2 (Saito model) to estimate the reasonable melt lump mass fraction for the MELCOR-MCCI calculations is given in Table 43. The reference melt initial velocity (V0) is 6 m/s and the velocity in other cases are calculated based on the pressure difference through the Bernoulli equation. The range of 0.0 – 1.0 MPa included the observed pressure difference magnitude at the time of RPV failure with MELCOR. As shown in the V1 case, even in the absence of pressure difference (0.0 MPa), the initial melt velocity exists due to gravity.

TABLE 43.TEST MATRIX OF BOTH JET BREAK-UP MODELS (EPSTEIN-FAUSKE AND SAITO)

Case	Melt initial diameter (m)	Melt initial velocity or pressure difference (MPa)	Maximum jet break-up length (m)	
			Group 1	Group 2
V0	0.2 ~ 0.6	6 m/s	15.86	10.48
V1		0.0	15.93	10.69
V2		0.2	16.69	14.92
V3		0.4	16.94	18.19
V4		0.6	17.08	20.95
V5		0.8	17.15	23.39
V6		1.0	17.20	25.61

In the Epstein-Fauske model, the initial jet velocity affects the jet diameter at the water surface, $D_{j.l}$ as shown with:

$$D_{j.l} = D_j \left(1 + \frac{g\Delta h}{v_j^2}\right)^{-0.25} \quad (22)$$

The jet diameter at the water surface is smaller than the initial diameter because of gravitational acceleration and mass conservation. As the initial jet velocity increases, the difference between the initial diameter and the diameter at the water surface becomes smaller. It means that the effect of jet initial velocity on non-coolable corium mass gradually decreases as the velocity increases. For example, the difference between the mass fraction results of 0.0 and 0.2 MPa is much larger than the difference between the 0.8 and 1.0 MPa. When the break-up length is longer than the cavity water level, the jet diameter at the cavity bottom was determined by:

$$D_{j.b} = D_j\left(1 + \frac{g\Delta h}{v_j^2}\right)^{-0.25} - \frac{H_p}{10(\frac{\rho_j}{\rho_l})^{0.5}} \tag{23}$$

The results of group 1 (G1) according to the boundary conditions are shown in Fig. 92 (a). In the 0.2 m melt initial diameter condition, the break-up length is calculated to be lower than the cavity water level at all velocity cases, hence the non-coolable corium mass converges to zero. It should be noted that the mass fraction cannot exceed 0.3 under all velocity conditions even at the 0.5 m diameter condition which is more than twice the 0.2 m. The COOLAP results with the Epstein/ Fauske model suggest that a mass fraction of 0.3 is a reasonable value for MELCOR-MCCI calculation.

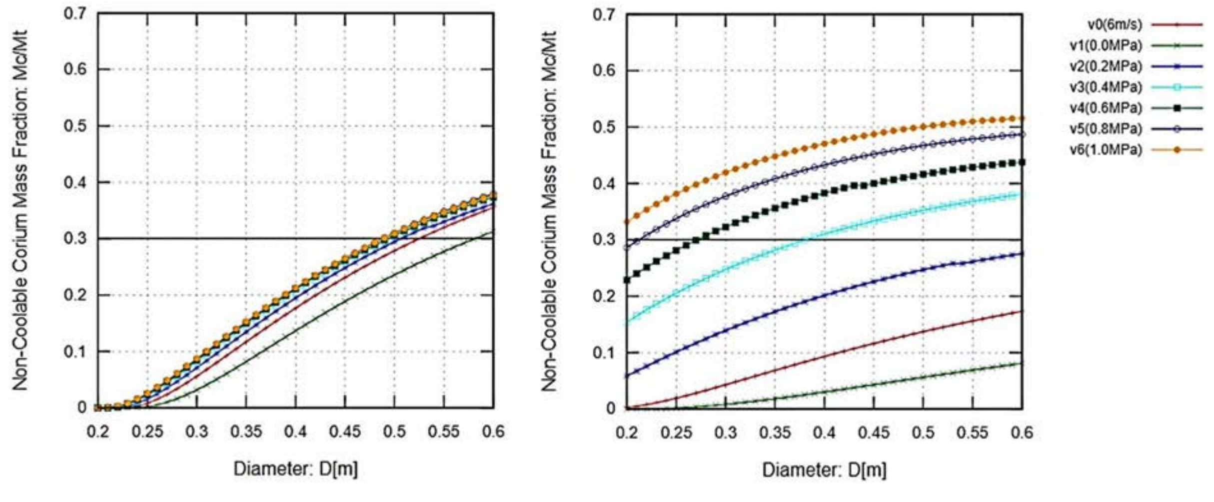

(a) (b)

FIG. 92. Calculated non-coolable corium mass fraction (melt lump mass fraction) according to the melt initial diameter and velocity, using COOLAP code: (a) G1, (b) G2

Unlike the Epstein/Fauske model, In the Saito model, jet diameter at cavity bottom is determined by:

$$D_{j.b} = D_j\left(1 + \frac{g\Delta h}{v_j^2}\right)^{-0.25} - \frac{H_p}{2.1(\frac{\rho_j}{\rho_l})^{0.5}\left(\frac{v_{j.l}^2}{gD_{j.l}}\right)^{0.5}} \tag{24}$$

As shown in Table 43, the initial jet velocity more dominantly affects the jet break-up length and the non-coolable mass fraction in this model. As shown in Fig. 92 (b), an increase in the mass fraction according to the pressure difference was more clearly observed. When the pressure difference reached 0.4 MPa, the mass fraction exceeded 0.3. However, the Saito model has not been validated with experimental results for a diameter range of 0.2 m or more. Also under the 0.2 m diameter condition, the mass fraction was nearly close to 0.3 even when the pressure difference reaches 1.0 MPa. As a result, the base non-coolable mass fraction for the MELCOR-MCCI calculation was determined as 0.3. The maximum break-up length according to the melt initial diameter and velocity is shown in Fig. 93. Because non-coolable corium mass is only dependent on break-up length in this corium temperature condition, the calculated break-up length shows a similar trend to that of the non-coolable corium mass fraction. The maximum break-up length at each initial velocity condition can be found in Table 44.

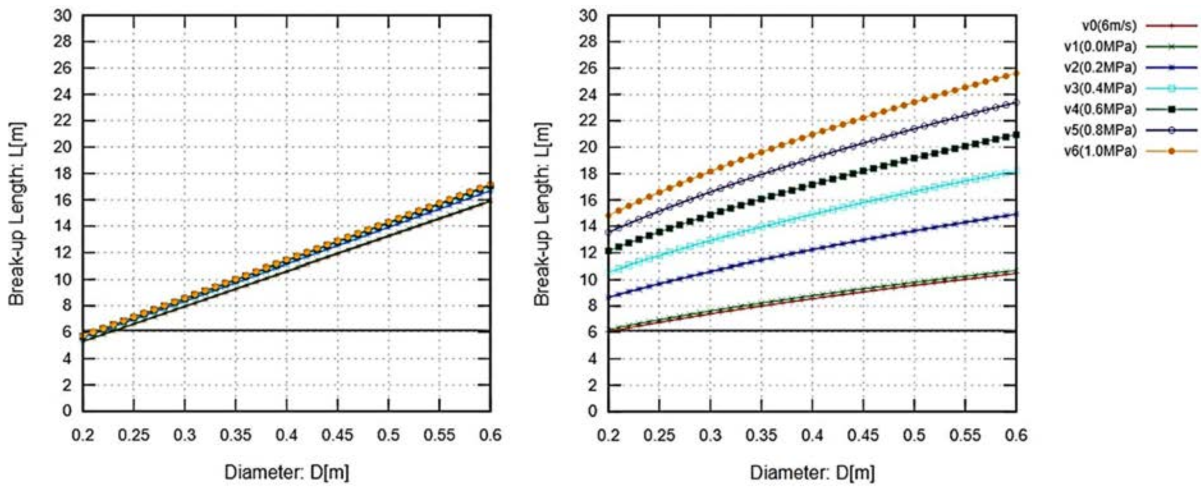

(a) *(b)*

FIG. 93. Maximum break-up length according to the melt initial diameter and velocity, using COOLAP code: (a) G1, (b) G2.

TABLE 44. IMPLEMENTATION OF TWO CAVITY MODELING FOR APR1400

Identification	**Cavity 1 (non-coolable)**	**Cavity 2 (coolable)**	**Remarks**
Area ratio (Area)	1 ($8m^2$)	9 ($72m^2$)	Fixed
Corium ratio 1 (CR-1)	3	7	Base case
Corium ratio 2 (CR-2)	2	8	Sensitivity
Corium ratio 3 (CR-3)	4	6	Sensitivity

It has been well recognized from the MELCOR analysis and experimental observations that the corium thickness is one of the most critical parameters for corium cooling. The relocated corium characteristics to determine the corium thickness depends largely on the presence of water in the cavity. Therefore, it is significant to evaluate the containment integrity mainly against the basemat ablation due to MCCI and containment over-pressurization due to corium cooling. However, the present MELCOR model has a limited model capability to evaluate those impacts of pre-existing water on corium cooling and MCCIs.

To overcome the limited capability of the present MELCOR code to handle the corium relocation with two different characteristics, like, melted and debris corium, the two-cavity model has been proposed in this analysis. The basic concept of the model is the physical division of the cavity volume of the model plant where the coolable (debris) and non-coolable (melted) corium is separately placed. In this analysis, the cavity area of the APR1400 design (80 m^2) is divided into the area ratios of the coolable and non-coolable corium depending on the COOLAP analysis results discussed in the previous section. If the ratio of 1 to 9 is considered, the cavity area of the non-coolable corium (Cavity 1) becomes 8 m^2 and coolable corium (Cavity 2) 72 m^2.

The next step of the treatment in MELCOR requires to define the corium transfer from the lower plenum to the cavity. It can be implemented in several ways using the transfer process package with the matrix input to evaluate the corium from in-vessel to the reactor cavity. In this process, it is important to evaluate the corium and cavity area ratios. For instance, the combination of the small cavity area with a large amount of corium indicates that the corium layer thickness in the cavity becomes thicker than one estimated in the one cavity model. For this analysis, Table 44 shows the corium ratios and the cavity area ratio chosen for uncertainty analysis. As described in the previous section of the COOLAP analysis, the base case of the corium ratio of 3:7 was achieved the vessel failure with the size of 0.5 m when the jet break-up model of Epstein-Fauske correlation is used. The results from the uncertainty analysis for CR-1 shows in Figs. 94 and 95. Both plots indicate that the reactor lower head failed at approximately 25,000 s after the accident initiation and pressure increased prior to the reactor pressure vessel failure due to manual depressurization through POSRV of the pressurizer in Fig. 95. Figure 94 shows the basemat ablation started at approximately 30,000 s and coolant flooded into the reactor cavity delayed the concrete ablation. Three specific cases show the basemat melt progression in the reactor cavity and containment failure due to pressurization. This result indicates that the containment cooling should be needed to maintain the containment integrity under severe accident conditions because the partial pressure of steam is almost 95% of the containment pressure.

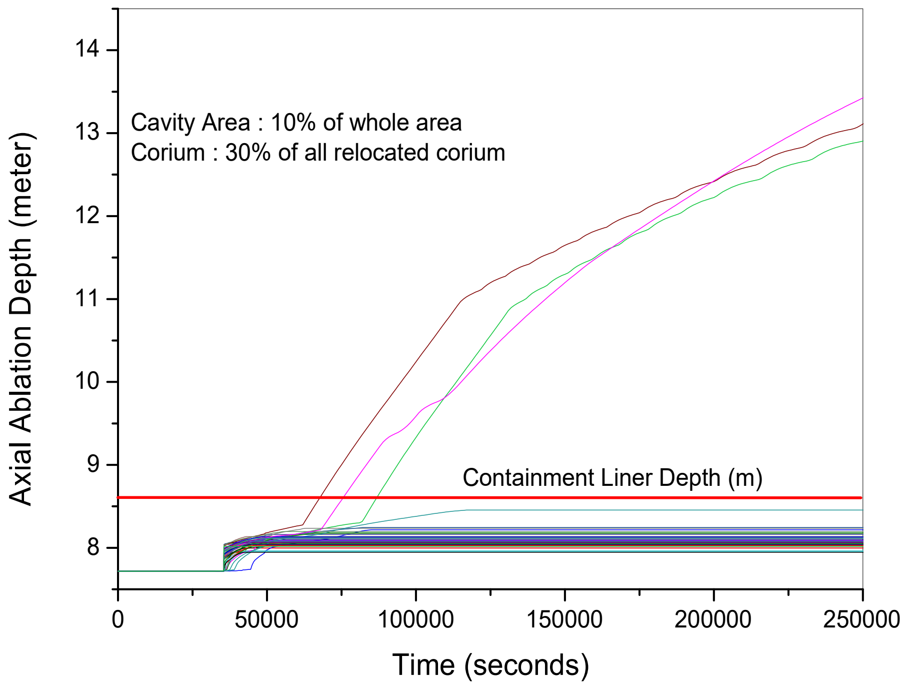

FIG. 94. Reactor cavity basemat axial ablation depth of CR-1 (3:7) uncertainty calculation.

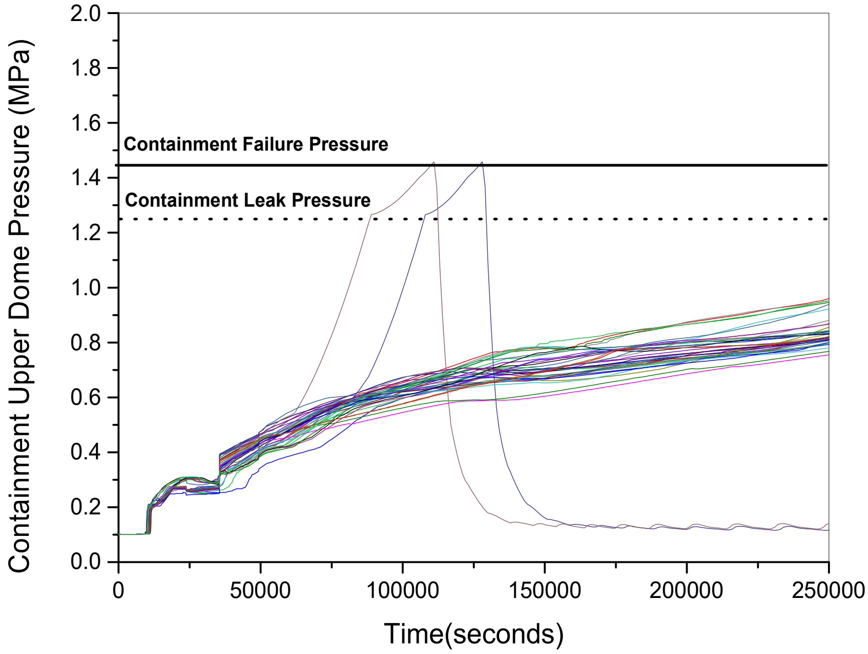

FIG. 95. Containment upper dome pressure in CR-1 (3:7).

Results for the sensitivity analysis

Besides the MELCOR calculation result of CR-1 as described in the previous section, other two cases, CR-2 and CR-3 for the sensitivity of the corium mass ratio of 2:8 and 4:6 at the area ratio of 1:9 was performed.

The CR-2 results as shown in Figs. 98 and 99 indicate that reactor cavity ablation occurred in only one case and the containment pressures of all sequences are maintained at a significantly lower level than the containment leak pressure expected from the effect of the low corium ratio. However, the CR-3 results with the corium mass ratio of 4:6 in the cavity area ratio of 1:9 shows that reactor cavity basemat ablation occurred in 18 out of 80 cases and the failure of the containment integrity occurred in 13 out of 80 cases due to pressurization (Figs. 100 and 101).

This analysis depicts that the evaluation of the corium relocation from the reactor vessel down to the cavity basemat in various cases of the existence of water in a reasonable manner plays a significant role in the determination of the consequence of the severe accident progression (termination and stabilization). To identify what is needed for the refinement of the analysis, the overall comprehensive uncertainty analysis considering the model, scenarios and severe accident management parameters is needed and will be performed in our new analysis platform with the coupled MELCOR-COOLAP codes.

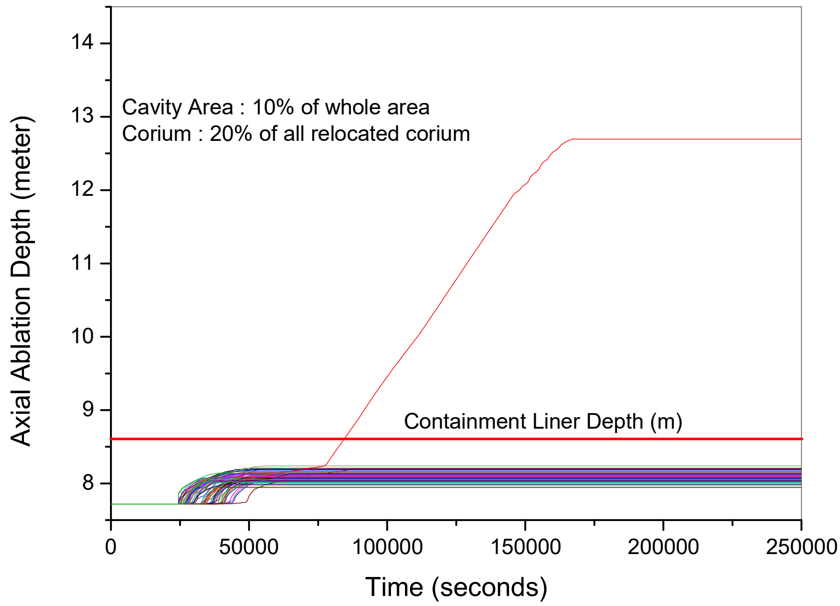

FIG. 98. Reactor cavity basemat axial ablation depth of CR-2 (2:8).

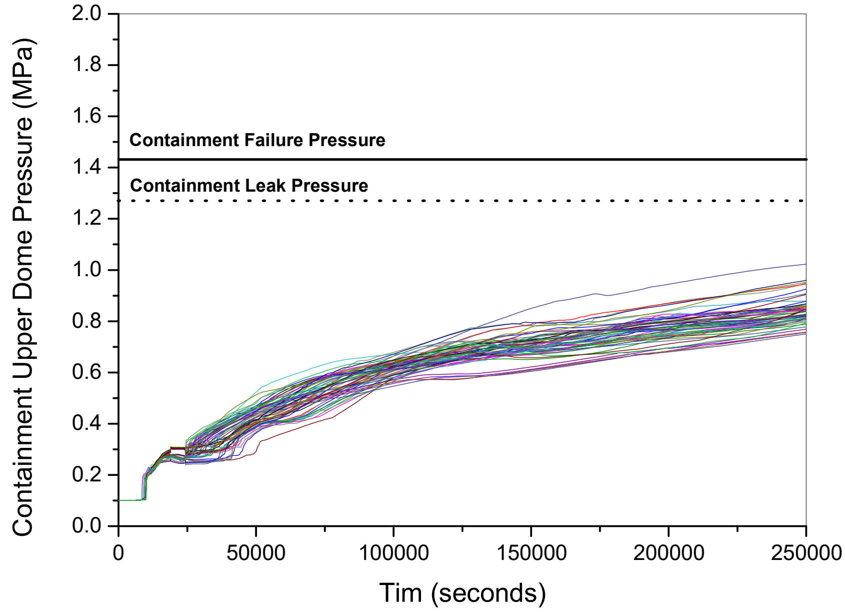

FIG. 99. Containment upper dome pressure in CR-2 (2:8).

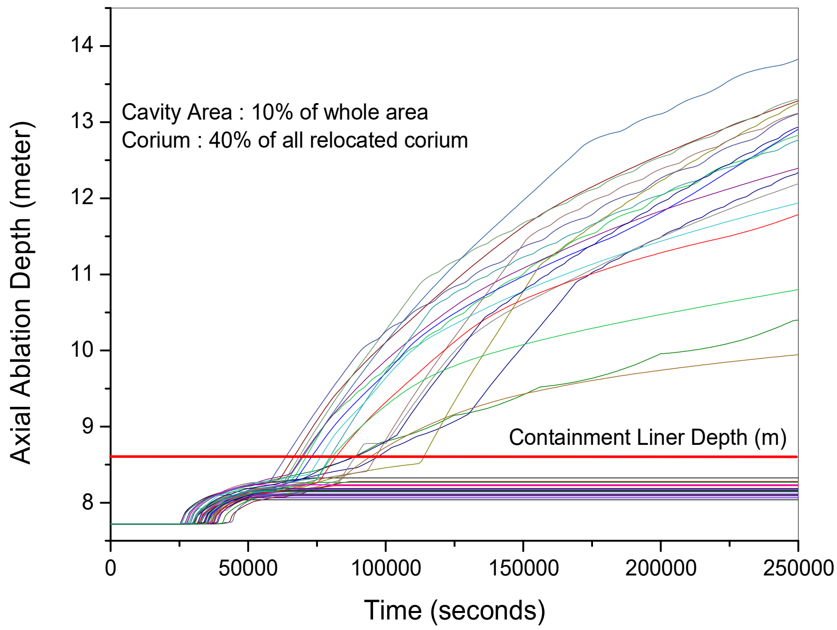

FIG. 100. Reactor cavity basemat axial ablation depth of CR-3 (4:6).

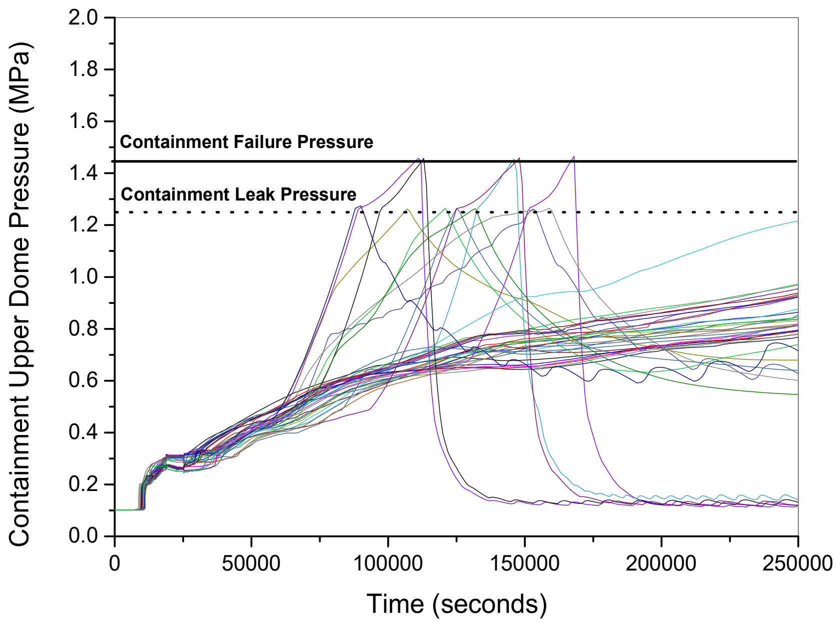

FIG. 101. Containment upper dome pressure in CR-3 (4:6).

2.3.4.7. Summary and conclusions

KINS and SNU have performed the join efforts to develop the analysis platform to evaluate the uncertainty analysis on severe accident risk associated with the corium relocation and cooling when the reactor cavity is in the wet conditions in prior to the reactor vessel failure. The platform is comprised of the coupling of MELCOR for the plant accident progression and COOLAP for corium relocation and cooling during the initial stage of reactor vessel failure.

A new two-cavity model was designed in MELCOR to accommodate separately the coolable and non-coolable corium in the reactor cavity. A new in-house parametric code, COOLAP, is used to define the specific initial conditions for a MELCOR analysis during long-term cooling.

The uncertainty and sensitivity analysis for the validation of the COOLAP model parameters to evaluate the base case for the MELCOR two cavity model analysis and for the containment integrity analysis due to MCCI and corium coolability have been performed and demonstrated its usefulness for extending the MELCOR analysis capacity.

Main sources of uncertainty resulting from the analysis

The main sources of uncertainty resulting from the analysis have been identified as below.

- Main sources of uncertainty are resulted from the limited understanding of physical phenomena associated with the problem addressed in this analysis, such as jet breakup model, debris size distributions, and debris formation and cooling as well as MCCI. However, it is uncertain at present whether those levels of uncertainty in physical models may be critical.
- Another main source of uncertainty is resulted from the wide combination of the parameters associated with the scenario and plant design specific accident progression. The scrutinization of those parameter uncertainty is needed.
- Currently, MELCOR two-cavity model is valid when non-coolable corium will be made in the center of reactor cavity if the location of vessel failure is center of vessel. In order to consider the vessel side failure, MELCOR two-cavity model cannot treat the side ablation in reactor cavity and the model might be modified.

Lesson learned and best practices

In this study, a new approach that investigates the uncertainty involved in the evaluation of the ex-vessel severe accident progression when the reactor cavity is in the wet conditions has been demonstrated. In this exercise, the following lessons are learned.

- For the evaluation of ex-vessel severe accident progression and containment integrity associated with the various reactor cavity conditions and corium relocation from the reactor vessel, MELCOR can provide the meaningful prediction if the code is adequately coupled with a model that is able to analyze the corium relocation process and corium coolability.
- The evaluation of the containment integrity associated with the ex-vessel coolability, MCCI and containment pressurization are largely related to the adequate models for the intermittent physical models related to reactor vessel failure modes, fuel coolant-interaction and corium cooling.
- However, the conventional uncertainty analysis provides a meaningful insight to identify key parameters and criteria associated with mitigating the accident consequences.
- For the best practices beyond the present study, the comprehensive uncertainty and sensitivity

analyses with the carefully selected parameters and their ranges of the physical models, accident scenarios and accident management procedures are needed and will be performed in the suggested analysis methodology.

2.3.5. Shanghai Jiao Tong University (SJTU)

The SJTU based the accident analysis using CNP600 as a reference plant. Description of this plant specifics, accident scenarios analysed, applied models and approaches, and summary of the results are provided in the following sections.

2.3.5.1. Motivation and objectives

Severe accident analysis of nuclear reactors has been a frontier issue concerned by nuclear industry and academia. Up to now, several severe accident analytical codes have been developed, which can simulate the complicated phenomena such as melting of reactor core, rupture of pressure vessel, hydrogen burning in containment, and interaction between melt and concrete. During the severe accidents, hydrogen burning or rapid deflagration may cause damage to equipment and systems, and even threaten the integrity of containment, causing significant amounts of radioactivity to release to the environment. Since the analytical results of hydrogen source term in the same sequence are different by using different codes, or even different by using the same code, the uncertainty of analytical results deserves further investigation.

The hydrogen source term for the 600 MWe PWR (CNP600) [38] under the severe accident of high pressure core melt initiated by an SBO is calculated, and the influence on the hydrogen source term under the mitigation measures to open the pressurizer relief valves are discussed. Methodology by using the MELCOR code with the LHS method is employed to predict the uncertainty of hydrogen source term. The 18 parameters which are in the models affecting the hydrogen generation are investigated to give the uncertainty of hydrogen with 120 runs. Pearson, Spearman, partial and partial rank correlation coefficients (PCC/PRCC) are used to do sensitivity analysis which the importance of the parameters is given.

The objective of this study is to investigate the uncertainty of hydrogen source term under SBO severe accident, and the influence of severe accident measures on the hydrogen source term for CNP600, so as to provide technical support for severe accident management.

2.3.5.2. Description of the relevant plant

The parameters of CNP600 are described in Table 45 [1].

TABLE 45. DESIGN PARAMETERS OF CNP600

Type	Parameter	Value
Reactor power	Power	1,930 MWt (600 MWe)
Reactor core	Diameter of equivalent core	2,670 mm
	Height of reactor core	3,658 mm
	Number of fuel assemblies	121
	Material of fuel	UO_2
	Enrichment of ^{235}U in fuel	1.9-3.1 wt%
	Material of fuel cladding	Zircaloy-4
	Array of fuel rod	17 × 17
	Absorber material	Ag-In-Cd
Primary system	Number of coolant loops	2
	Operating pressure of primary loop	15.5 MPa
	Temperature of coolant inlet	292.8°C
	Temperature of coolant outlet	327.2°C

2.3.5.3. Accident scenarios and severe accident codes

The severe accident scenarios initiated by SBO are analysed, in which it is assumed that all off-site AC power is lost, emergency diesel generators and turbine-driven auxiliary feed pump fails. The only water available to cool down the reactor core is the initial inventory of the reactor coolant system and steam generators, the pressurizer level control, RCP seal injection, active safety injection systems, motor-driven auxiliary feedwater system are unavailable. When the water level in the secondary side of steam generator side becomes low and finally dry out, the pressure in the primary loop gradually rises which reach the open set point of the pressure safety valve of the pressurizer. As the safety valve opens and closes, the coolant level in the primary loop decreases which induces the core exposed and melting. After the core exit temperature exceeds 650°C, the severe accident management guidelines is taken in action, in which the manual opening of the pressurizer safety valves can be adopted as the preferred measure to reduce the pressure in the primary loop. The influence of opening one safety valve, two safety valves and three safety valves on hydrogen generation is investigated respectively.

The MELCOR code, version 1.8.5 [2, 3], was used to analyse the hydrogen generation.

2.3.5.4. Plant modelling and nodalization

The plant model of CNP600 mainly includes primary and secondary loop, pressurizer, pressure relief tank and containment, which is described as follows:

— The reactor primary loop includes the pressure vessel, the reactor core and two circuits: one with pressurizer and the other without. As shown in Fig. 102, each circuit also includes hot and cold leg, steam generator, transition section, and main coolant pump and cold leg;
— The pressurizer is connected with one of hot legs, and also comprises a surge pipe and a pressure relief tank. The model of pressurizer includes three independent safety valves, which can be automatically opened or closed according to the setting value or manually opened/closed by the operator as required;
— The steam/water discharged from the safety valve is released into the pressure relief tank of the

pressurizer. When the pressure in the pressure relief tank exceeds a certain value, the bursting disc break and the fluid will be directly released from the pressure relief tank into the containment;

— The secondary loop includes the secondary side of the steam generator and the steam turbine system, and so on.

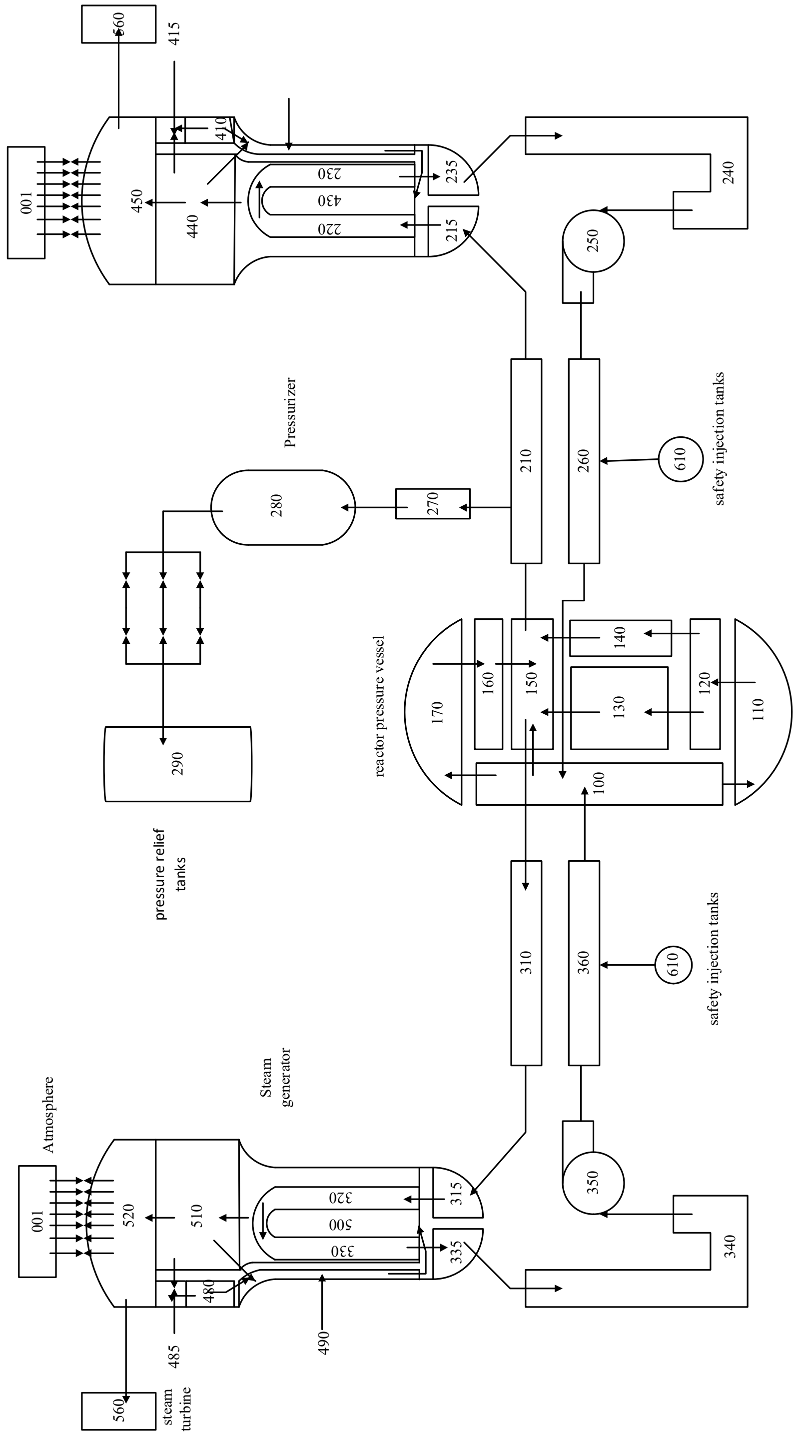

FIG. 102. CNP600 system node diagram.

The reactor core is divided into 4 rings in radial direction, 14 sections in axial direction, of which the core heating section is 4–13 sections. The normal operating power of the core is 1,930 MWt. The core nodes are shown in Fig. 103.

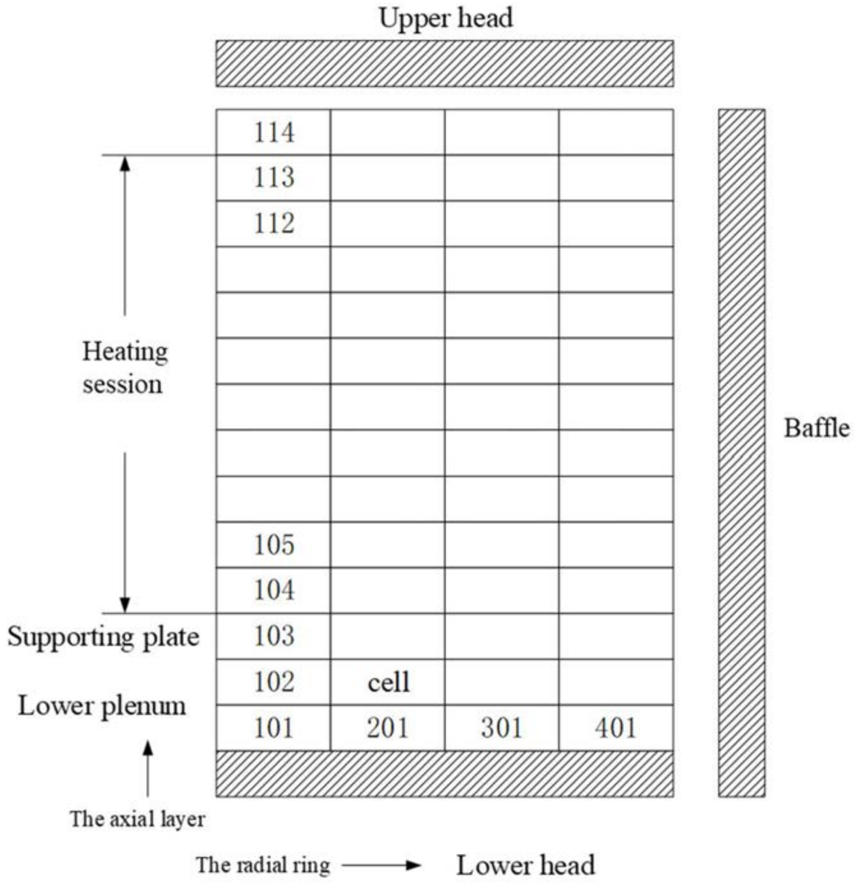

FIG. 103. CNP600 core node diagram.

2.3.5.5. Methodologies and tools for the uncertainty and sensitivity analysis

The used sampling technique LHS is designed to reconstruct the input parameter distribution by sampling with fewer iterations [38, 39]. The key to LHS is to stratify the input parameter probability distribution, which divides the cumulative curve into equal intervals on a cumulative probability scale (0–1.0), and samples are then randomly drawn from each interval of the input parameter distribution. However, in the analysis with many inputs and even more outputs, the sampling technique may be misleading in assessing the relationships between individual inputs and outputs [40].

Uncertainty analysis methodology: the number of simulations is determined based on the desired confidence level and the sampling methodology being applied and is independent of the input parameter number. Therefore, the minimum number of sampling number *N* required for 95% of the output distribution with 95% confidence in this study is determined to be 93 based on Wilks's formula [41]:

$$\beta = 1 - \gamma^N \tag{25}$$

Thus, 120 runs are conducted in this study. The data sets of hydrogen generation are extracted for all calculation, and the maximum and minimum, median, and 95% confidence intervals of uncertainty band (5th percentile/95th percentile) for the mass of hydrogen generation in-vessel and ex-vessel at different time is counted, to intuitively indicate the uncertain effect of hydrogen generation during severe accidents.

Sensitivity analysis methodology: four sensitivity analytical methods are employed, including Pearson and Partial correlation coefficients used to measure the linear relation between the parameters, and Spearman and Partial rank correlation coefficients used to measure the monotonic relation between the parameters [42]. The value of the correlation coefficients ranges from −1 to 1, and the greater the absolute value, the stronger the correlation is.

(1) Pearson simple correlation coefficient (Pearson)

A value of 1 indicates that the variables *X* and *Y* have a linear relationship, and *Y* increases with the increasing the *X*. The value of −1 is the opposite. When the correlation coefficient is 0, it means that there is no linear correlation between *X* and *Y*:

$$\rho_{XY} = \frac{cov(X,Y)}{\sigma_X \sigma_Y} \tag{26}$$

(2) Partial correlation coefficient

In multivariate correlation analysis, simple correlation coefficient may not actually reflect the correlation between *X* and *Y*, due to the complicated relationship, and may be affected by more than one variable. Partial correlation coefficient may be a better choice at this time. That is, the influence of other factors is not considered for the time being, and the closeness of the relationship between the two factors. For example, by controlling the variable X_2, the correlation between X_1 and *Y* is explored as follows.

$$r_{X_{1Y}|X_2} = \frac{r_{X_1Y} - r_{X_1X_2} r_{X_2Y}}{\sqrt{(1 - r_{X_1X_2}^2)(1 - r_{X_2Y}^2)}} \tag{27}$$

(3) Spearman rank correlation coefficient (Spearman)

The Spearman rank correlation coefficient is a non-parametric rank statistical parameter used to measure the strength of the connection between two variables. The i^{th} ($1 \le i \le N$) value of the input variable and the output variable are represented by X_i、Y_i, respectively. Sort *X* and *Y* (at the same time in ascending or descending order) to get two element ranking sets x and y, where the elements x_i and y_i are respectively the rank of X_i in *X* and the rank of Y_i in *Y*. The elements in the sets x and y are subtracted correspondingly to obtain a ranking difference set d, where $d_i = x_i - y_i$, $1 \le i \le N$. The correlation coefficient can be calculated by d as follows:

$$\rho = 1 - \frac{6 \sum d_i^2}{n(n^2 - 1)} \tag{28}$$

(4) Partial rank correlation coefficient

Partial rank correlation analysis, which considers the relationship between parameters on the basis of partial analysis, can carry out monotonicity analysis between parameters with the control of other variables.

Uncertainty and sensitivity scheme and relevant tool: the used sampling tool is MATLAB, a commercial mathematics software developed by MathWorks. Through MATLAB code, the LHS input set of parameters with three distribution form is realized by self-programming, which is then put into the code for calculation. The output results of hydrogen generation are extracted by Aptplot code, and the uncertain features are counted by the statistical analytical code SPSS (Statistical Package for the Social Sciences). The SPSS code includes several categories such as descriptive statistics, general linear model, correlation analysis, regression analysis, log-linear model etc., used to carry out the analysis of Pearson correlation, Spearman correlation and the partial correlation. The workflow between each tool is shown in Fig.104.

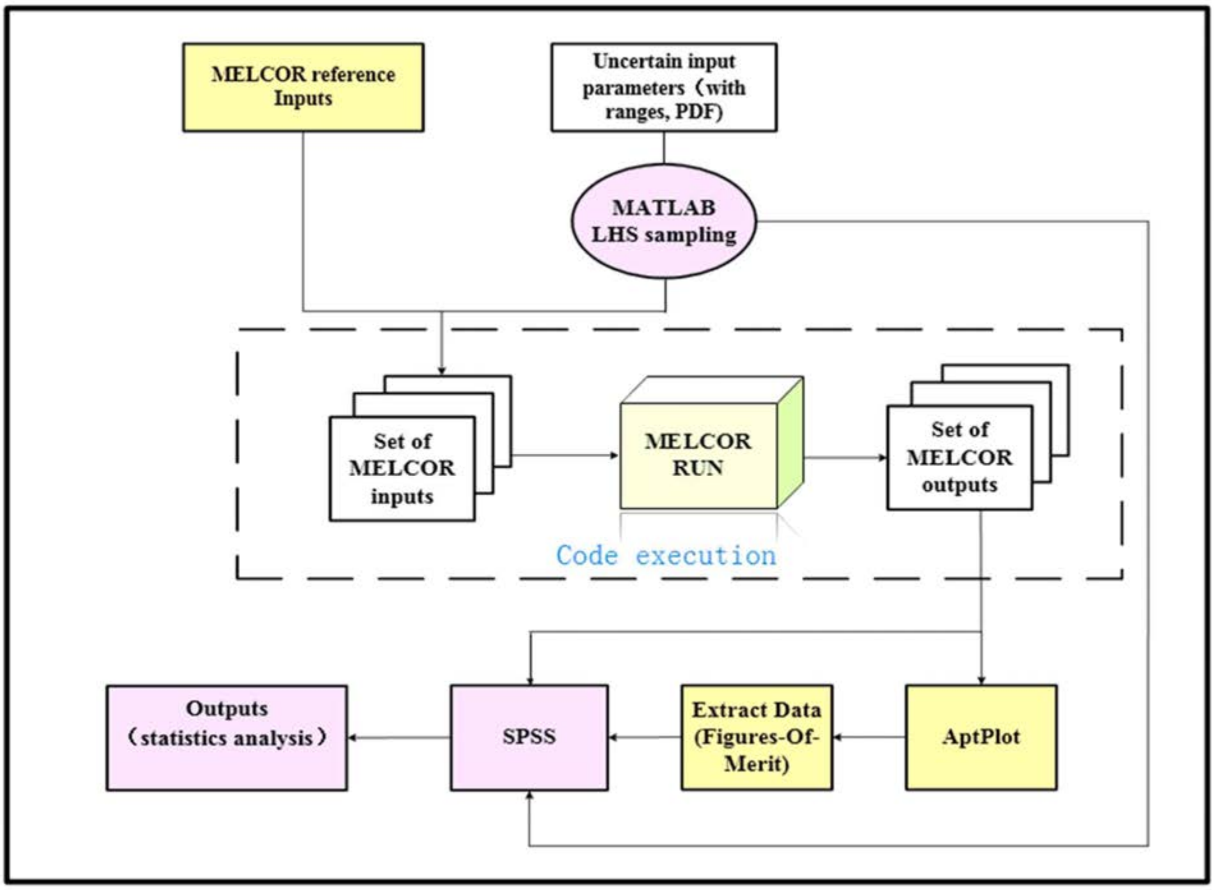

FIG. 104. Workflow of the CNP600 calculation uncertainty analysis.

Uncertain parameters and related probability distributions: the selection of the uncertain input parameters is based on the phenomena of the severe accident process as shown in Table 46, which can be divided into parameters related to the accident phenomenon inside and outside the vessel.

TABLE 46. INPUT PARAMETERS, THEIR RANGES AND DISTRIBUTIONS

Parameter	Description	Scope	Distribution
C1001(1,1)	Constant coefficients of zircaloy oxidation rate - constant coefficient of low temperature range	Mean: 29.6, Sigma: 2.96, 20.72 – 38.48	Normal
C1001(3,1)	Constant coefficients of zircaloy oxidation rate - constant coefficient of high temperature range	Mean: 87.9, Sigma: 8.8, 61.5 – 114.3	Normal
SC1131(2)	Maximum temperature of ZrO_2 allowed to hold up molten zirconium	Mean: 2400 K, Sigma: 50 K, 2,100 – 2,550 K	Normal
COR00005	Candling heat transfer coefficients	Mean: 8,000 W/m^2-K, Sigma: 2,400 W/m^2-K, 2,000 – 22,000 W/m^2-K	Normal
HDBH2O	Heat transfer coefficient for the heat transfer from dropping debris to molten pool in-vessel	Mean: 200 W/m^2-K, Sigma: 60 W/m^2-K, 125 – 400 W/m^2-K	Normal
CORijj04(DHYPD)	Equivalent diameter of particulate debris in core region	Mean: 0.01 m, Sigma: 0.004 m, 0.002 m – 0.05 m	Normal
CORijj04(DHYPD)	Equivalent diameter of particulate debris in lower plenum	Mean: 0.025 m, Sigma: 0.0075 m, 0.01 m – 0.06 m	Normal
SC1132(1)	Temperature to that oxidized fuel rod can endure without unoxidized zirconium in fuel cladding	Mean: 2,550 K, Sigma: 83 K, 2,400 K – 2,800 K	Normal
PORDP	Particulate debris porosity	Mean: 0.3, Sigma: 0.06, 0.12 - 0.48	Normal
SC1141(2)	Maximum flow rate of molten core material after breakthrough per unit width	0.1 kg/s - 2.0 kg/s, Mode: 0.2 kg/s	Triangular
TPFAIL	Penetration failure temperature or lower head failure temperature	Mean: 1273.5 K, Sigma: 127.3 K, 1,273 K – 1,600 K	Normal
FCELR	Radially outward radiative exchange factor from cell boundary to next adjacent cell	Mean: 0.1, Sigma: 0.03, 0.18	Normal
FCELA	Axially upward radiative exchange factor from cell boundary to next adjacent cell	Mean: 0.1. Sigma: 0.03, 0.02 – 0.18	Normal
Boiling	Enhancement treatment to boiling profile for heat transfer to covering coolant	Mean: 35, Sigma: 10, 5 – 100	Normal
HTRBOT	Debris-to-surface heat transfer treatment on debris bottom surface	Mode: 1, Min: 0.2, Max: 5	Triangular
HTRINT	Debris-to-surface heat transfer treatment at internal interfaces between layers of debris	Mode: 1, Min: 0.2, Max: 5	Triangular
HTRSIDE	Debris-to-surface heat transfer treatment on debris radial surface	Mode: 1, Min: 0.2, Max: 5	Triangular
POWER	Plant power	1930 MW_t ± 1%	Uniform

Phenomena in vessel mainly include the core melting, including zirconium alloy oxidation, cladding failure, melt condensation and relocation, melt candling and fuel rod collapse. The formation process of molten pool, including quenching of molten pool etc., and the penetration failure leads to the rupture of the reactor pressure vessel. The important model parameters related to the above phenomena are selected, and the introduction of specific parameters and the basis for selecting uncertain features are as follows:

(1) C1001(1,1) & C1001(3,1)

The rate and amount of hydrogen caused by oxidation reaction are important factors that affect the hydrogen concentration in containment.

The uncertainty of rate coefficient and exponential change of cladding oxidation model directly affects the uncertainty of hydrogen production. The default oxidation model in the code accords with parabolic growth rate law:

$$\frac{dw}{dt} = \frac{1}{2}\frac{K(T)}{W} \tag{29}$$

where w is the specific mass of cladding metal reacted in kg/m^2. The rate of growth factor is expressed as:

$$K(T) = Aexp\left[\frac{-B}{T}\right] \tag{30}$$

Generally, different values of A and B are applied in two discrete temperature ranges. In this study, the uncertainty of the rate coefficient A of Urbanic-Heidrich model in the range of low temperature and high temperature is considered. Based on the engineering judgment and uncertain study presented in [43], the uncertainty fluctuation range is 10%, which accords with the normal distribution.

(2) SC1131(2)

When the oxidized cladding breaks or fails, the zirconium alloy melts, repositions, new oxidized surfaces are created, and uncertainty about hydrogen production increases. The outer ZrO_2 shell maintains a default value of 2,400 K for the inclusion of the molten zirconium alloy in the code. According to the study by Gauntt et al., the melt easily breaks at lower temperatures under high hydrogen reduction conditions, and the Zr metal has a strong tendency to dissolve its oxides [44].

The temperature of the fuel rod collapse is generally considered to be about 2,500 K, so the oxidation cladding rupture temperature is unlikely to be above 2,500 K. In this study, considering the above conditions and the melting point temperature of zirconium, the parameters are varied in the range of 2,100–2,550 K, and the distribution form follows the corresponding normal distribution with the mean value of 2,400 K.

(3) COR00005

The series of parameters specifies the re-freezing heat transfer coefficient for each molten core material used in the candling model, thus affecting blocking trend, mainly of molten zirconium alloys and molten steel. The specific uncertainty range is selected as 2,000–22,000 W/m^2·K with reference to [44] and the uncertainty study per [45], subject to the normal distribution with the mean value of 8,000 W/m^2·K.

(4) COR00012

Upon the failure of support plate in reactor core in every one of radial rings, core debris falls to the lower head and transfers heat to the water. COR00012 is a falling debris quench model parameter characterizing the heat transfer coefficient for the heat transfer from dropping debris in the vessel to the lower head. Factors that affect heat transfer, such as boiling caused by adjacent particles, need to be reflected in the value of the heat transfer coefficient. In the large-scale simulation of melt relocation, an appropriate value of 100 W/m^2·K is obtained [44]. Based on the above investigation, this parameter is selected to obey the normal distribution with the mean value of 200 W/m^2·K, and the uncertainty range is 125–400 W/m^2·K.

(5) CORijj04 (Core area & lower plenum area)

The equivalent diameter of debris will influence the degree of cooling, oxidation and material migration of it. The equivalent diameter in the lower plenum is directly applied to the quenching model to calculate the dropping debris heat transfer area in pool after reactor core support plate fails. Given that the fuel pellet diameter of the fuel pellets is on the order of centimeters, an equivalent diameter of the particulate debris may be present between a few millimeters and centimetres [44]. In the SOARCA project study [46], the core area debris diameter was used to be 1 cm. Referring to the uncertainty study of hydrogen in SNL and in Tehran Institute of Nuclear Science and Technology, the particle diameter in the core is selected to obey the normal distribution with the mean value of 1cm, and the uncertainty range is 0.2 cm to 5 cm [44, 45]. For debris in the lower plenum region, by the time the debris material is relocated to it, the core material will likely have sintered or melted to form larger agglomerates [47, 48]. Therefore, the characteristic size will be larger than the size of the core region debris to the order of centimeters. Researchers of Sandia National Laboratory believed that if the debris were to be relocated in the form of a stream down the plenum, it might exhibit a characteristic size of about 5 cm. Therefore, reference is made to the study of the melt ejection initial diameter in the melt particle bed agglomeration and particle size distribution study [49, 50], determining that the debris diameter in the lower plenum region follow a normal distribution with a mean value of 2.5 cm, and an uncertainty ranging from 1 cm to 6 cm.

(6) SC1132(1)

The fuel rod collapse causes the release of molten zirconium, which affects the relocation and oxidation of the core material and increases the uncertainty of the hydrogen. Pontillon et al. in French Atomic Energy Agency performed the VERCORS experiment to investigate the effect of the UO_2-ZrO_2-FP interaction on the collapse temperature of irradiated fuel [51]. The temperature range of the fuel loss integrity is 2,400–2,600 K, which is lower than the unirradiated UO_2 melting point and the ZrO_2-UO_2 eutectic melting temperature. Therefore, the lower temperature limit of 2,400 K is selected based on the above experimental results. The upper temperature limit of 2,800 K is based on the eutectic melting point of UO_2/ZrO_2, and the collapse temperature follows the normal distribution with the mean value of 2,550 K.

(7) PORDP

The porosity of the debris affects heat transfer and surface area. Duc-hanh Nguyen, in the institute for radiological protection in Sao Paulo, and others used a granular approach to study the geometry of the debris beds which might form in the core of a nuclear power plant under the conditions of severe accident [50]. For loose debris beds, the porosity is about 0.41. The calculated tests showed that it is possible to reach a porosity ~0.32 in such an unfavorable situation for cooling. Combined with the uncertainty range adopted in the uncertainty analysis [10], the input parameter is determined to be normally distributed between 0.12 and 0.48 with a mean of 0.3.

(8) SC1141(2)

The molten core material breakthrough candling parameter determines the maximum flow rate of molten core material after breakthrough per unit width. The range of 0.1–2 kg/m·s is considered based on the SOARCA project [46]. Combined with the parameter distribution selected in the uncertainty analysis [52–

54] of severe accidents, the parameter is determined to be a triangular distribution and the value is the default value 0.2 kg/m·s.

(9) TPFAIL

The parameter is the failure temperature of the penetration of pressure vessel. The default value in the code is 1,273 K. Currently, the study on the uncertainty of the parameter is insufficient.

Based on the engineering judgment, it is considered that the failure temperature of the penetration part is generally not lower than 1,273K, and it is more inclined to the higher failure temperature. The parameter range is selected to be 1,273–1,600 K, which is subject to the normal distribution.

(10) FCELR/FCELA

The parameter is the radiation exchange factor in vessel, and Siemens' ranges for FECLR and FECLA are 0.01–0.25 and 0.02–0.3 [10], respectively. Based on the magnitude analysis as described in [44] on the parameter, it basically agrees with Siemens' opinion, and it is considered that the axial and radial radiation calculations should be equal. Therefore, based on the above investigation, the uncertainty range of the parameter is selected to be 0.02–0.18, which follows the normal distribution. In this study, the hydrogen generation outside the vessel is mainly derived from the oxidation reaction of metal melt with thermal decomposition gas of concrete in the MCCI stage.

The erosion of core debris to concrete is mainly thermal erosion. The heat source is decay heat and oxidation reaction heat, which are generated in the debris and transferred to different directions of the reactor cavity. The four parameters related heat transfer in cavity are considered.

(11) Boiling

The parameter affects the heat transfer between molten core material in cavity and the overlying coolant. Since the code does not consider the interaction between the overlying water and the molten debris, and according to the experimental study conducted by the Sandia National Laboratory in the USA, the default value of the code greatly underestimated the heat transfer capacity and the coolability of the melt ex vessel. Therefore, based on the uncertainty study by [45], the heat transfer factor is increased to the uncertainty range of 5–100, and the distribution form is selected as normal distribution to explore the effect of the uncertainty.

(12) HTRBOT/HTRINT/HTRSIDE

In the evaluation of concrete erosion, the heat transfer model from the molten core material to the molten pool surface is very important. The code provides several model parameters to meet the user's flexibility requirements, and the HTRBOT/HTRSIDE/HTRINT is divided into heat transfer multiplication factors for the molten debris to the bottom, radial, and debris layers. Based on the OECD MACE (Melt Attack and Coolability Experiment) experimental results, the code with default parameters underestimates the above heat transfer phenomena [55]. At the same time, based on the uncertainty judgment of the parameter in the sensitivity analysis with the OECD core-concrete interaction experiment described in [56], the parameter is selected to range from 0.2 to 5, and subject to triangular distribution.

(13) POWER

The nominal value of the thermal power of CNP600 is 1,930 MW_t. According to the power calibration study of the power plant, the uncertainty is determined to be ±1%.

2.3.5.6. Results

<u>*Steady-state results*</u>

A steady-state analysis was carried out with the calculation time of 5,000s. Some important parameters are listed in Table 47, including reactor power, average coolant temperature, pressurizer pressure, pressurizer water level, etc. Compared to the nominal value, the calculated parameters are within an error of no more than 1%.

TABLE 47. STEADY-STATE DEBUGGING RESULTS

Parameters	**Unit**	**Nominal value**	**Calculated value**	**Error, %**
Reactor power	MW	1,930.0	1,929.8	0.01
Mean coolant temperature	℃	310.0	308.0	0.65
Primary hot section temperature	℃	326.6	324.8	0.55
Primary cold section temperature	℃	293.0	291.2	0.61
Pressurizer pressure	MPa	15.5	15.49	0.65
Pressurizer water level (elevation)	m	18.47	18.41	0.33
Steam generator pressure	MPa	6.71	6.709	0.02
Steam generator water level (elevation)	m	22.839	22.845	0.03
Steam flow	kg/s	542.0	539.7	0.42
Containment pressure	Pa	1.01×10^5	1.011×10^5	0.10
Containment temperature	K	318.15	314.9	1.0

<u>*Reference case results*</u>

The accident sequence process of SBO with the failure of emergency feed water pump driven by steam turbine is shown in Table 48. At 0s, the accident occurs, and the water in steam generator secondary side is continuously evaporated to dryness due to emergency feed water pump failure. At about 4,500s, the pressure in the primary loop starts to increase, and reaches the set point of the pressurizer relief valve at about 4,718 s, as shown in Fig. 105. With the opening of the relief valve, the coolant in the primary loop begins to lose, and the core cooling deteriorates further. The zirconium water reaction starts at about 9,000 s, and the generated hydrogen and water vapor are discharged into the cold liquid water of the pressure relief tank through the pressure relief valve. The lower head fails at 16,780 s due to reaching the failure temperature of the penetration, and the pressure in the primary loop decreases rapidly to the set point of the safety injection tank. The water level of the RPV keeps dropping as shown in Fig. 106. At the end of calculation, a total of 344.21 kg of hydrogen is generated in the vessel, which is equivalent to the hydrogen production of 49.7%

zirconium-water reaction, as shown in Fig. 107. The maximum peak value of hydrogen generation in-vessel is 0.44 kg/s as shown in Fig. 108. After RPV fails, the high-temperature molten core material is injected into the reactor cavity and contacts with the cooling water dropped from the lower plenum, generating a large amount of high-temperature steam, and the molten core contacts with concrete to release hydrogen after the water in the cavity is consumed with the rate of about 0.01 kg/s as shown in Fig. 109. The cumulative hydrogen generation in cavity is shown in Fig. 110, and the total hydrogen output reaches the value of 100% zirconium water reaction at 51,300 s.

TABLE 48. SEQUENCE OF IMPORTANT EVENTS

Key event	Time/s
Accident occurs	0
Reactor shutdown	2
Core top uncovered	7,067
Core Zr-H_2O reaction begins	9,000
Failure of the lower head	16,780
SIT injection start	16,900
Calculation end	60,000

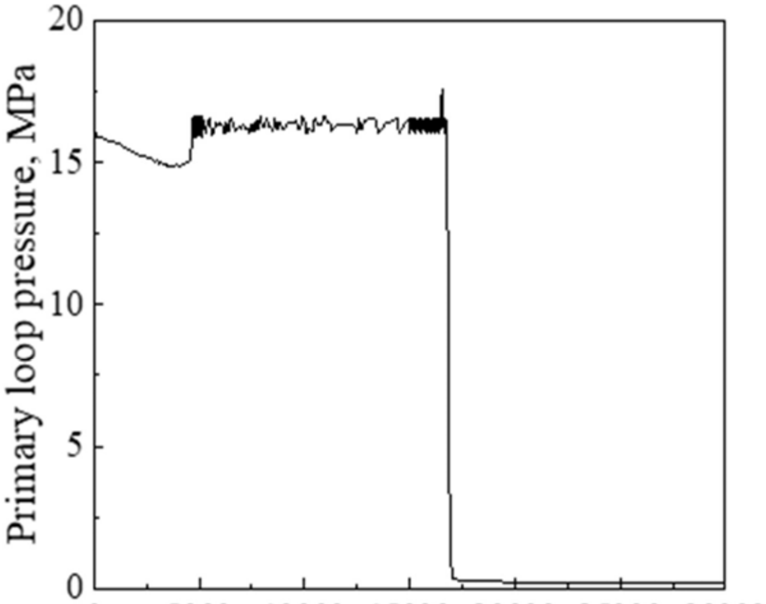

FIG. 105. Primary loop pressure.

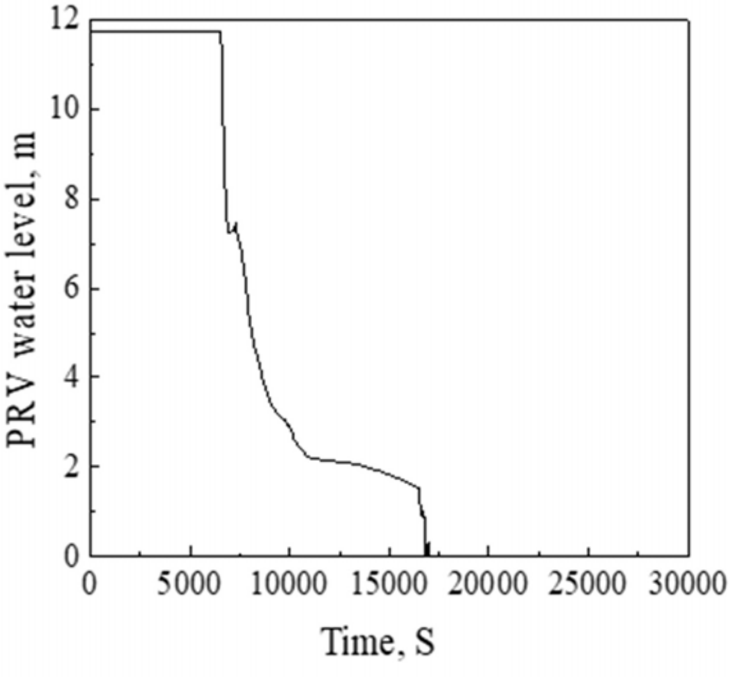

FIG. 106. PRV water level.

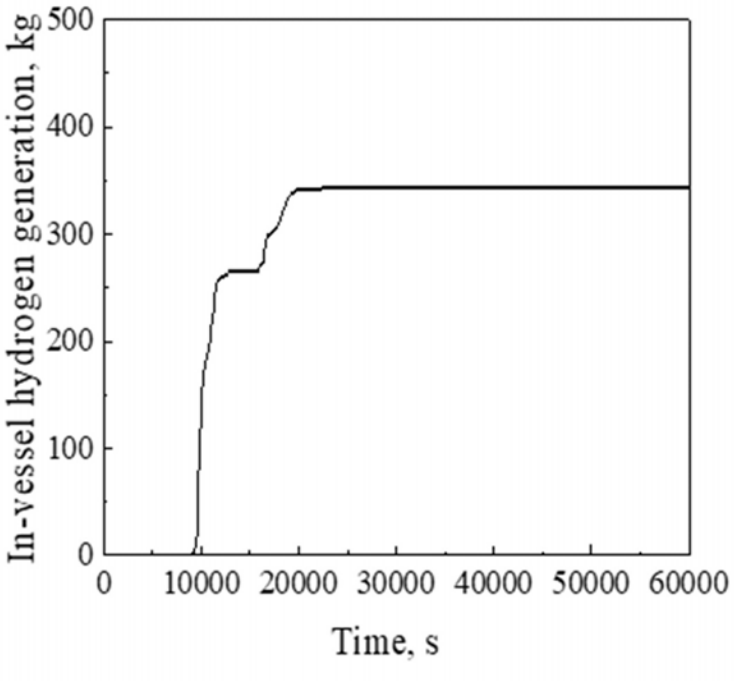

FIG. 107. In-vessel H_2 generation.

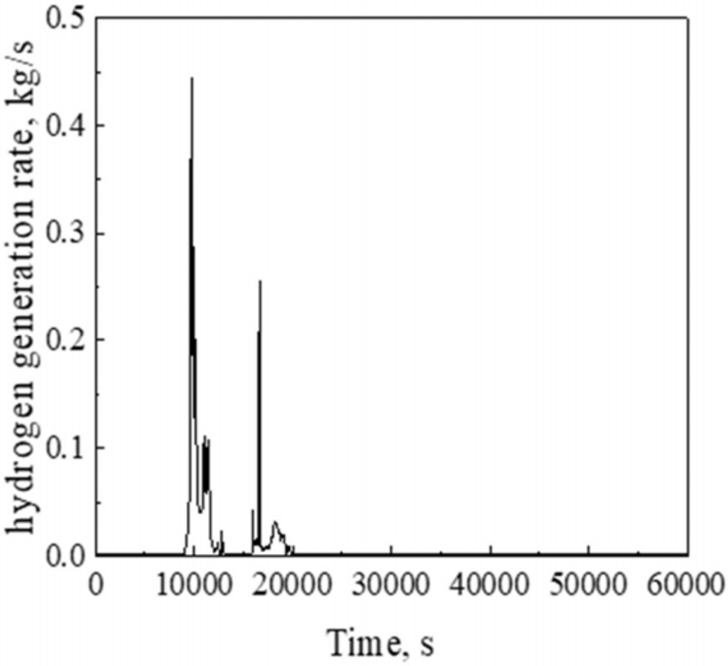

FIG. 108. H_2 generation rate in vessel.

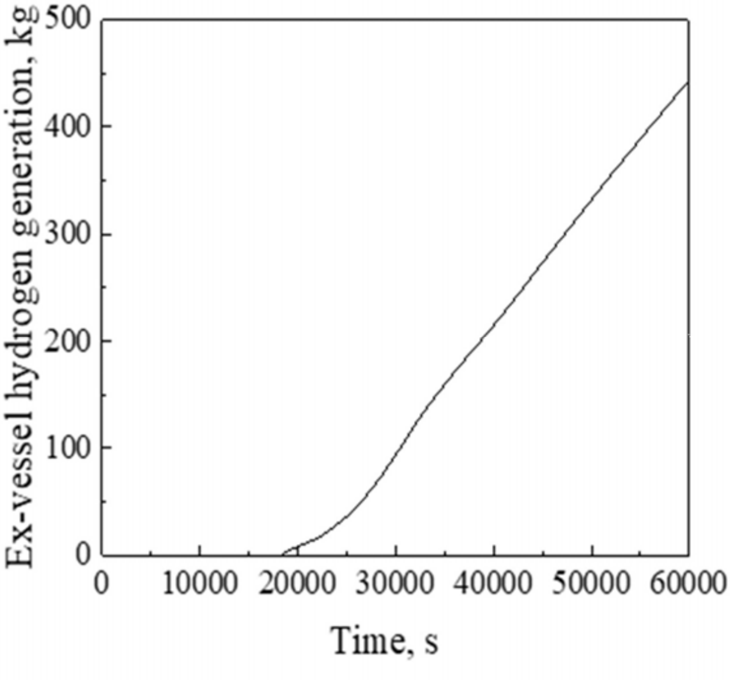

FIG. 109. Ex-vessel H_2 generation.

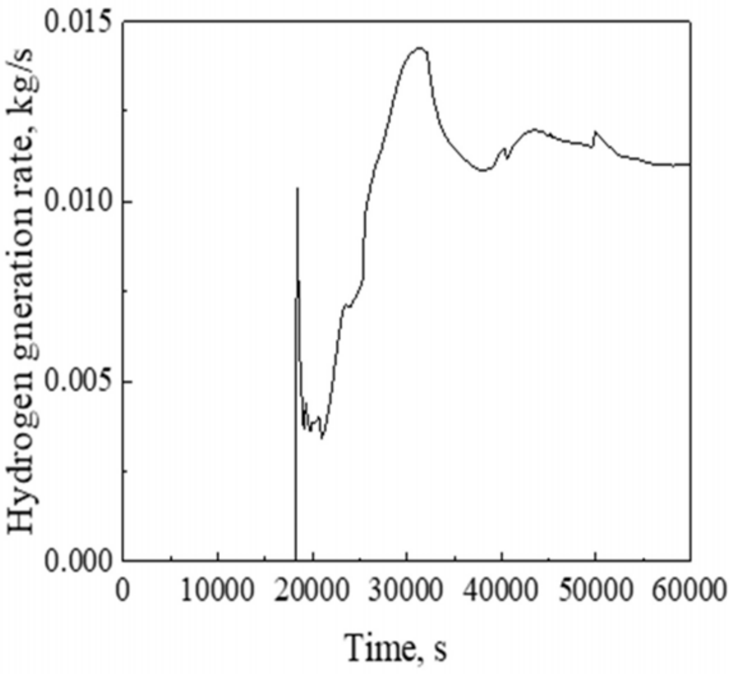

FIG. 110. H_2 generation rate ex vessel.

<u>Uncertainty analysis of hydrogen generation in vessel under high pressure core melt</u>

The results of uncertainty statistical analysis and probability density of hydrogen generation in vessel under high-pressure core melt severe accident of SBO are given in Fig. 111 where R^2 is used to characterize the fitting effect of the model, which means the larger the value is, the better the characterization effect of the statistical characteristics of the uncertainty of the hydrogen generation is. With the 90% confidence interval (5th/95th centile) as uncertainty band, the range of uncertainty for hydrogen production with no mitigation measure is 241−336kg, with a mean of 276 kg.

The sensitivity analysis results with significance test are shown in Fig. 112.

The study combines with a variety of correlation analysis methods to screen out important impact parameters. The importance of parameters is referred to Sheskin statistical study [57], and the correlation degree is divided into the following categories according to the correlation coefficient ($|r|$): $|r|\geq 0.7$, it could be considered as a high correlation; $0.3\leq|r|<0.7$ is regarded as moderate correlation; $0<|r|<0.3$ is regarded as low correlation. It can be concluded that the debris porosity and the temperature at which the fuel rod maintains its geometric shape have a relatively important impression on the hydrogen source term in the vessel under the high pressure core melt accident.

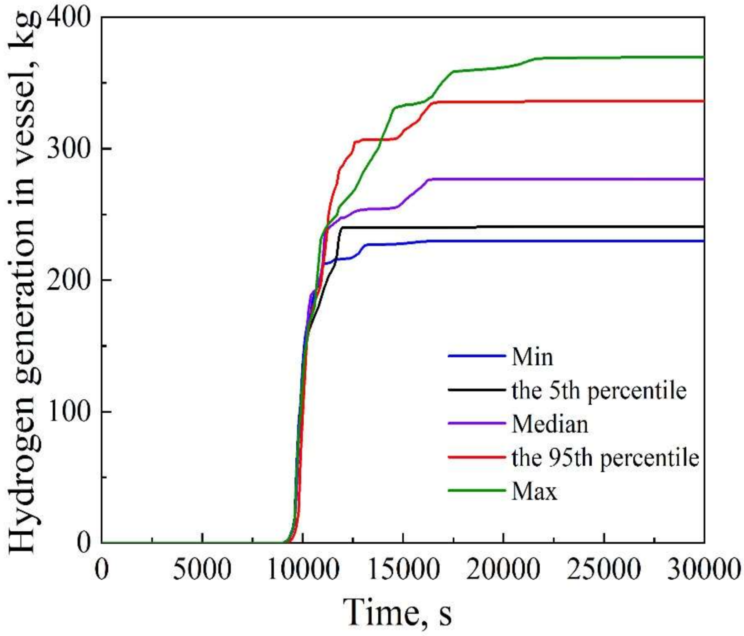

(a)

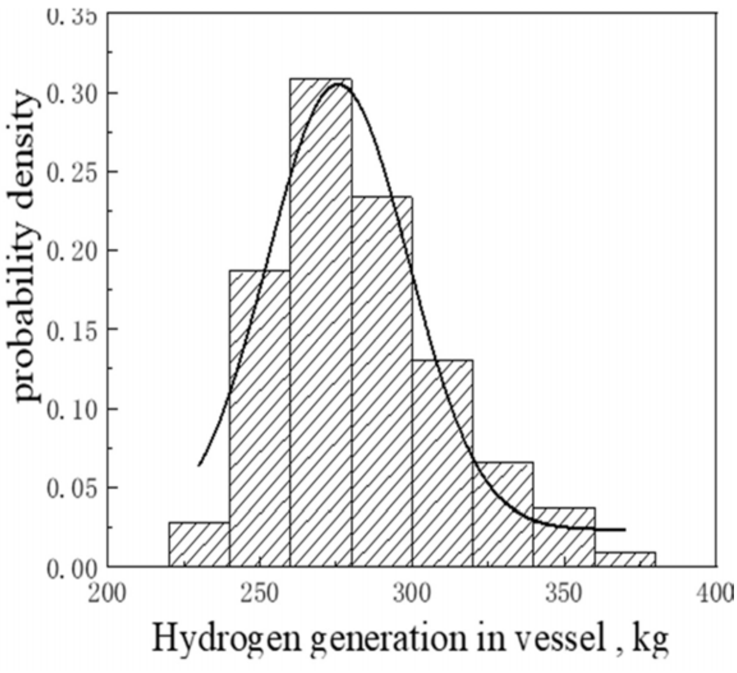

(b)

FIG. 111. No-mitigation condition, (a) uncertainty statistics of H_2 production in vessel, (b) PDF of H_2 production in vessel (mean: 276 kg, SD: 23kg, adjusted R^2=0.94).

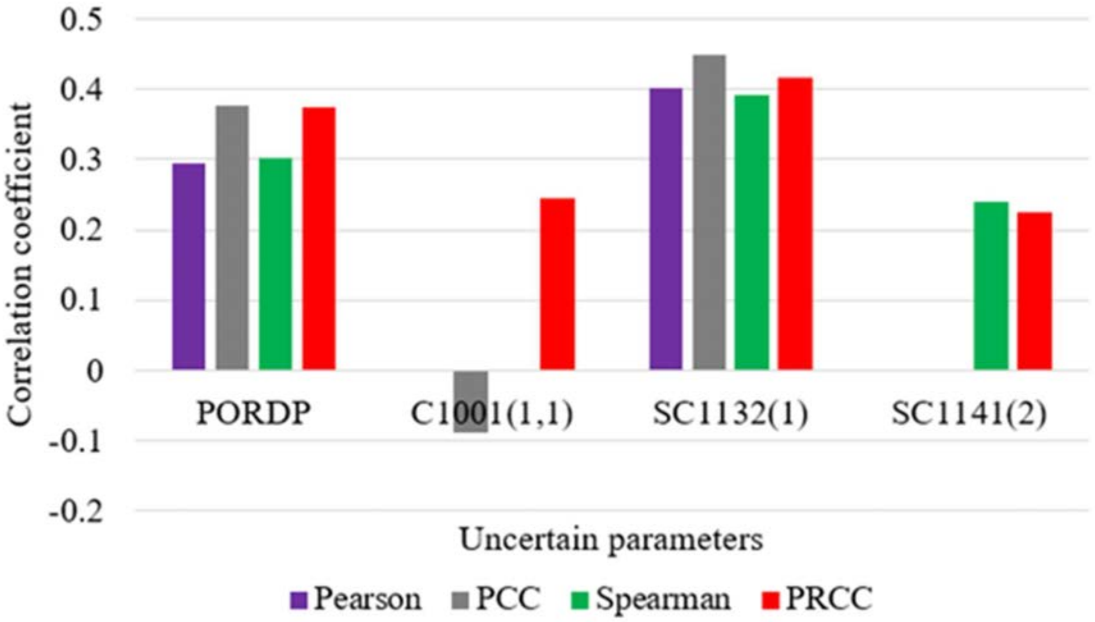

FIG. 112. Sensitivity analysis results without mitigation.

<u>Uncertainty analysis of hydrogen source term under pressure relief action of the pressurizer</u>

In order to explore the effect of the pressure relief measures on the uncertainty of hydrogen source term in vessel and ex vessel after the failure of RPV under low pressure, the measures to open one, two and three pressure relief valves were analysed. The results of uncertainty statistical analysis and probability density of hydrogen production in vessel with different pressure relief measures under the severe accident of SBO are shown in Figs. 113–115.

With opening of one relief valve, the hydrogen production uncertainty ranges from 252–488kg with the maximum mean of 368 kg; with opening of two relief valves, the hydrogen production uncertainty ranges from 237–331 kg with a mean of 282 kg; with opening of three relief valves, the hydrogen production uncertainty ranges from 210–261 kg with the minimum mean of 237 kg.

It can be concluded that opening of one relief valve significantly increases the uncertainty of hydrogen generation in vessel and increases the mean hydrogen generation by about 92 kg, compared to the no-mitigation accident condition; the uncertainty of hydrogen production with opening of two relief valves is comparable to that without mitigation; the mitigation measures taken to open three relief valves significantly reduces the hydrogen production in the reactor and the uncertainty.

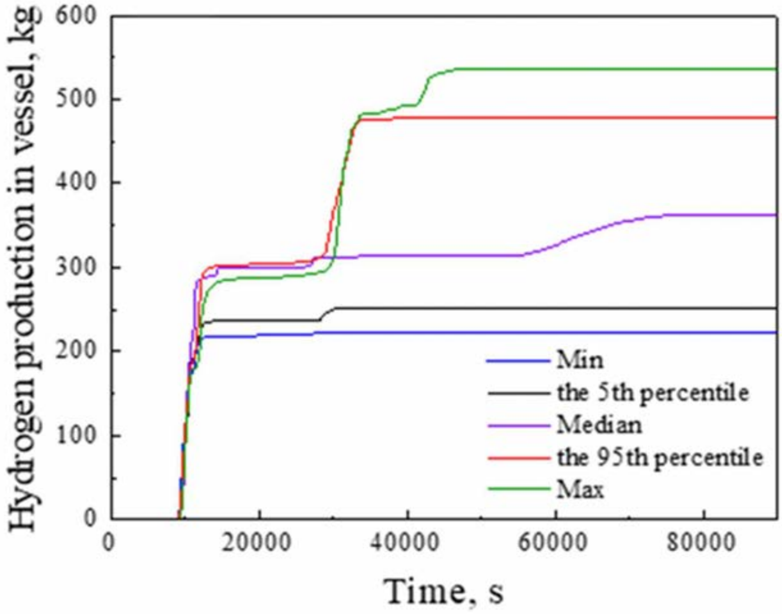

(a)

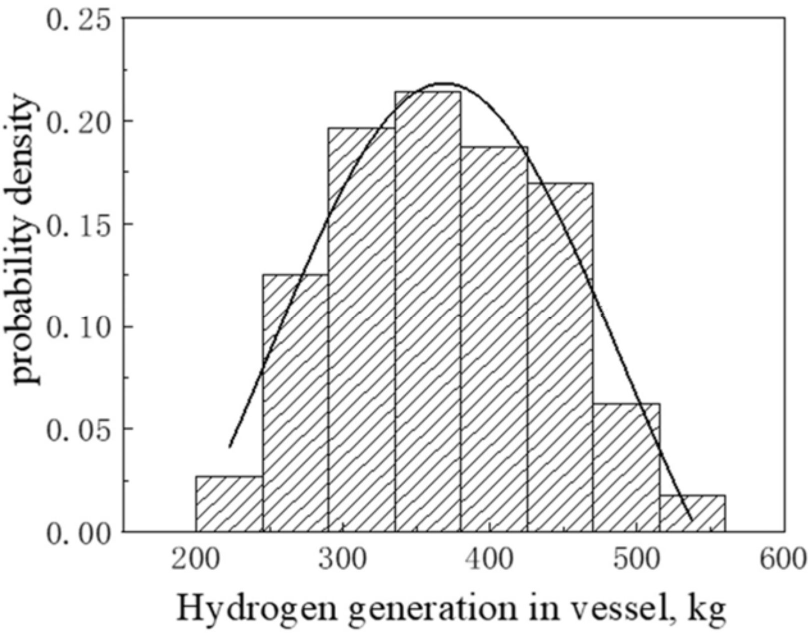

(b)

FIG. 113. Open one relief valve condition, (a) uncertainty statistics of H_2 production in vessel, (b) PDF of H_2 production in vessel (mean: 368 kg, SD: 120 kg, adjusted R2=0.94).

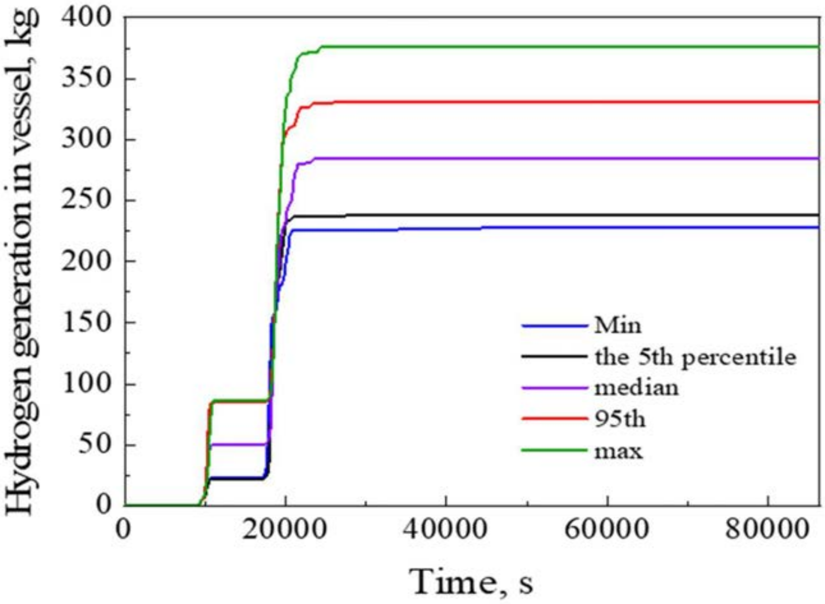

(a)

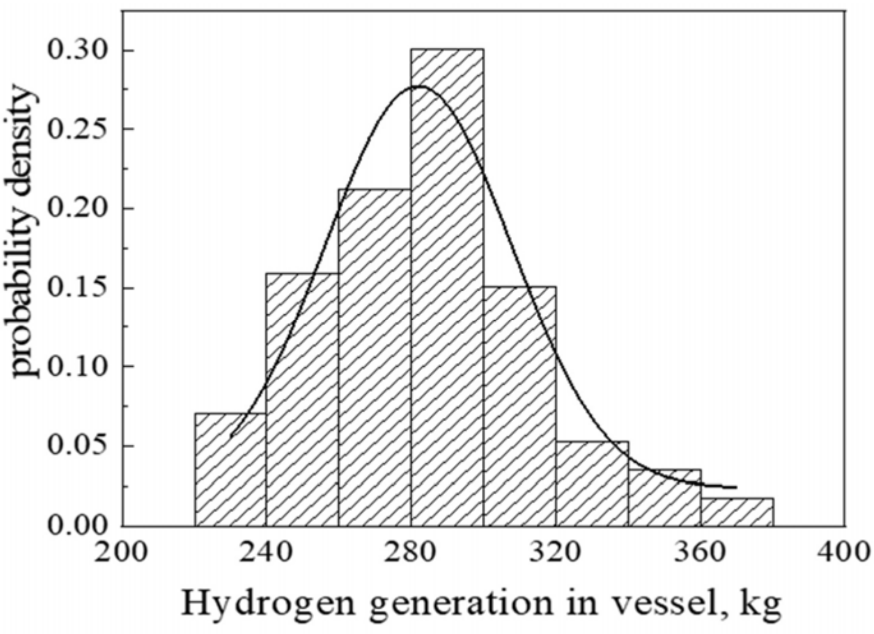

(b)

FIG. 114. Open two relief valve condition, (a) uncertainty statistics of H_2 production in vessel, (b) PDF of H_2 production in vessel (mean: 282 kg, SD: 26 kg, adjusted R^2=0.9).

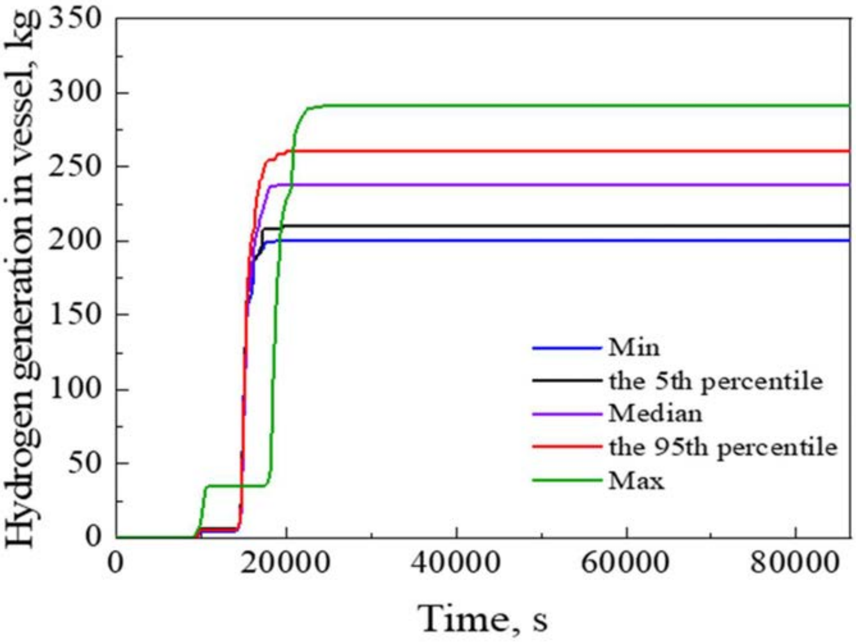

(a)

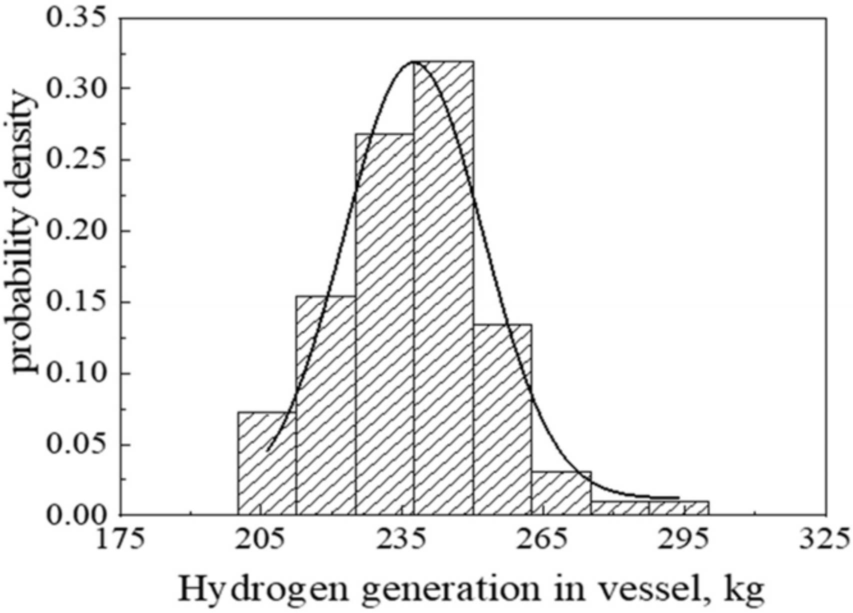

(b)

FIG. 115. Open three relief valve condition; (a) uncertainty statistics of H_2 production in vessel, (b) PDF of H_2 production in vessel (mean: 237 kg, SD: 15 kg, adjusted R^2=0.95).

The sensitivity analysis results after significance test for the hydrogen source term in vessel under different pressure relief conditions are given in Figs. 116–118. The results listed in Tables 46–49 are obtained by ranking the importance of the parameters that simultaneously shows correlation under different analysis methods. It can be seen that only a few uncertain parameters show correlation with the hydrogen source term in vessel; The maximum temperature of the oxidized fuel rod which can maintain the geometric shape when there is incompletely oxidized zirconium in the cladding exhibits a non-negligible positive correlation with respect to the hydrogen source term under both non-relief and pressure relief condition.

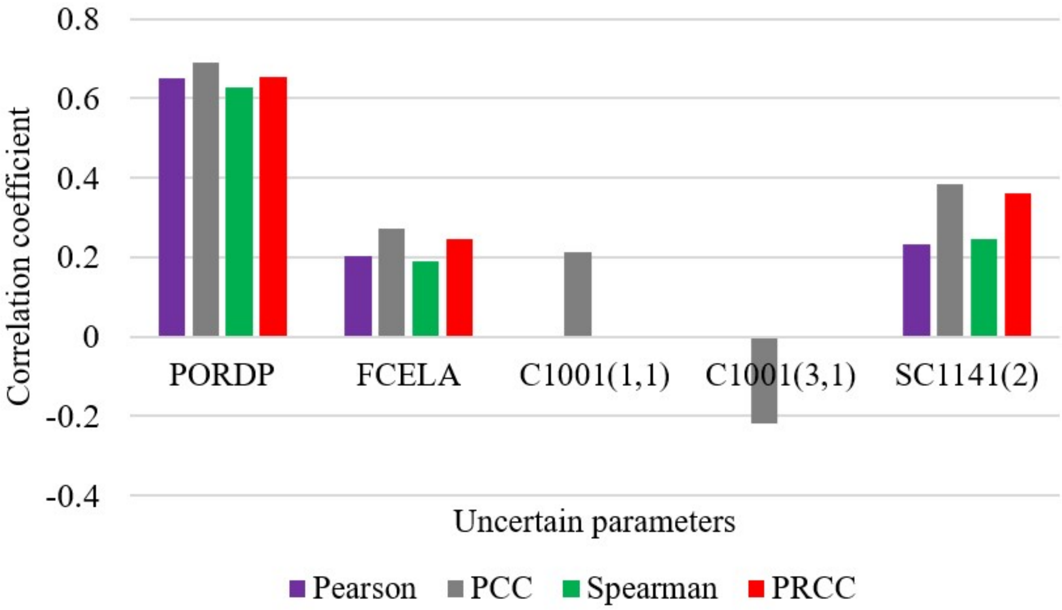

FIG. 116. Results of sensitivity analysis with opening one relief valve.

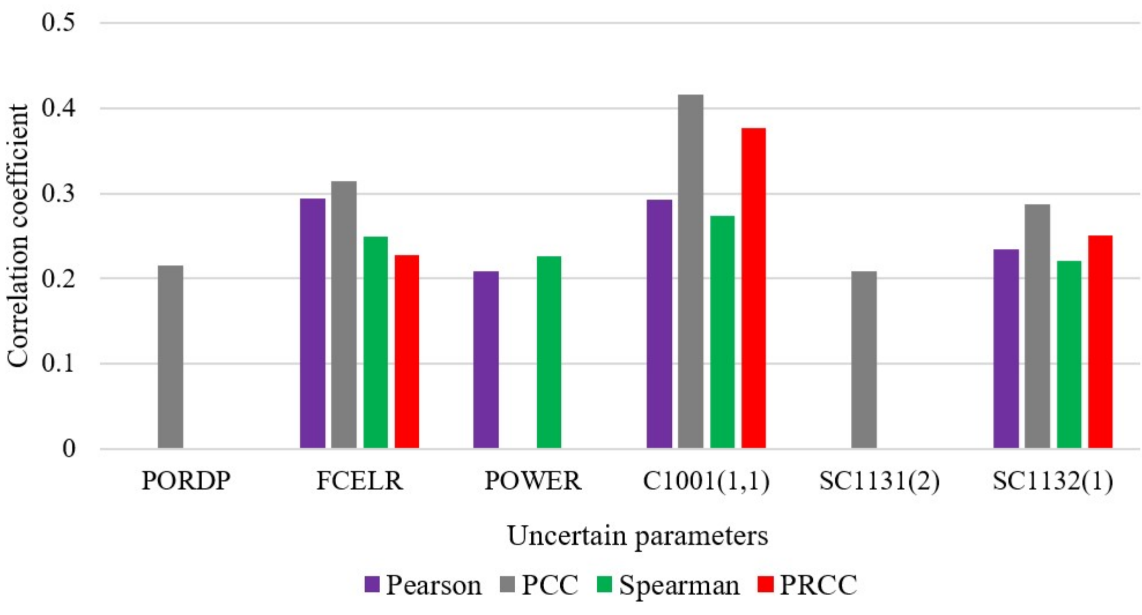

FIG. 117. Results of sensitivity analysis with opening two relief valves.

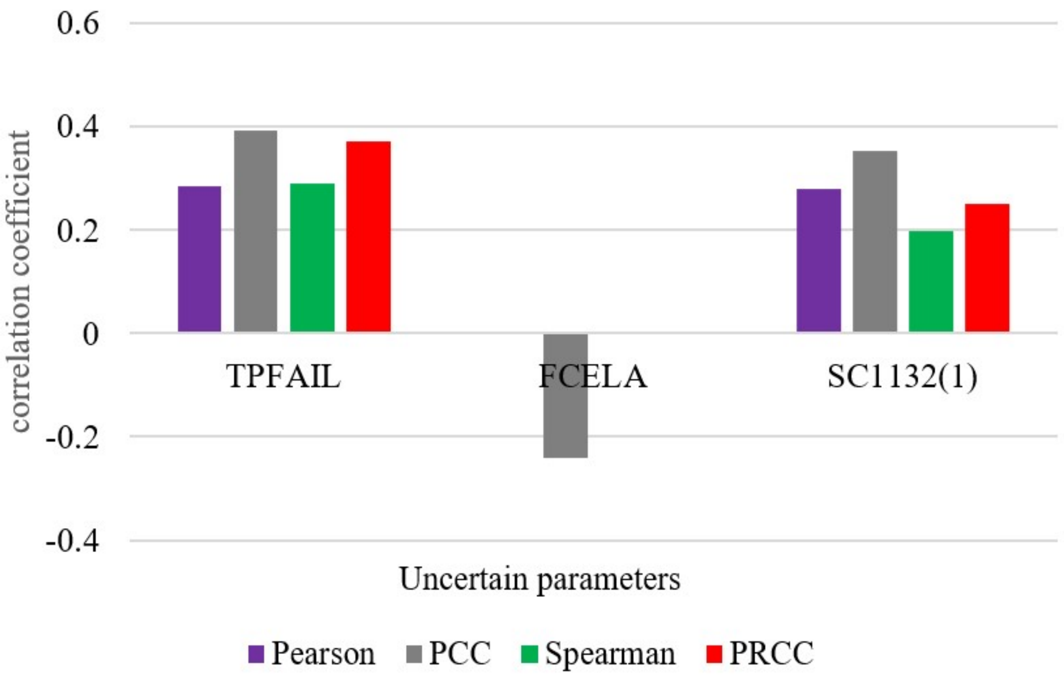

FIG. 118. Results of sensitivity analysis with opening three relief valves.

TABLE 49. IMPORTANCE ORDER OF PARAMETERS FOR H_2 ST IN VESSEL

Conditions	**Parameter importance ranking**		
	1	**2**	**3**
No mitigation	SC1132(1)	PORDP	/
Open one relief valve	PORDP	SC1132(1)	FCELA
Open two relief valves	C1001(3,1)	FCELA	SC1132(1)
Open three relief valves	TPFAIL	SC1132(1)	/

The results of uncertainty statistical analysis and probability density of hydrogen production ex vessel with different pressure relief conditions are given in Figs. 119–121.

With the opening of one relief valve, the hydrogen production uncertainty ranges from 435–658 kg, with the mean value of 543 kg; with the opening of two relief valves, the hydrogen generation uncertainty ranges from 585–808 kg with the mean value of 708 kg; with the opening of three relief valves, the hydrogen generation uncertainty ranges from 644–875 kg, with the highest mean production being 765 kg. Thus, under the condition of opening one relief valve, the failure time of the RPV is relatively late, and the hydrogen production in cavity is relatively small within 24 h after the accident. With the opening of more pressure relief valves, the pressure of the vessel is rapidly reduced, and the process of the reactor core accident is accelerated, and the hydrogen generation in the cavity within 24 h is increased. However, under different pressure relief measures, there is no significant difference in the uncertainty degree of hydrogen production, with the difference of the uncertainty band about 220 kg.

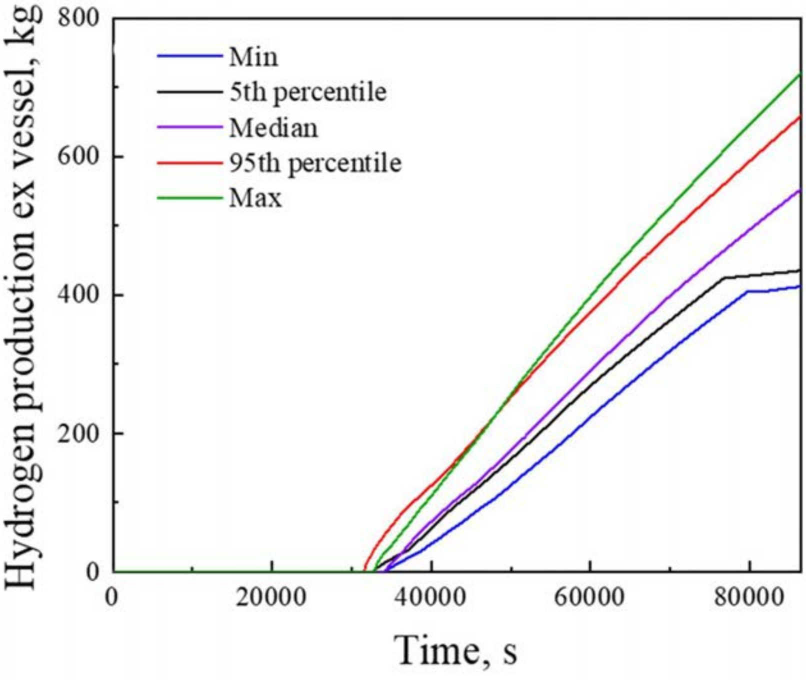

(a)

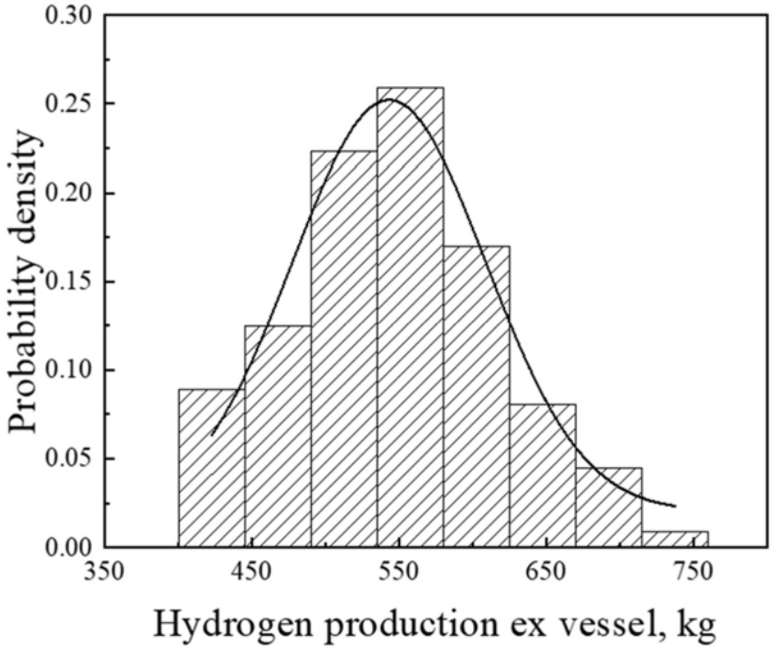

(b)

FIG. 119. Open one relief valve condition, (a) uncertainty statistics of H_2 production ex vessel, (b)PDF of H_2 production ex vessel (mean: 543 kg, SD: 65.5 kg, adjusted R^2=0.95).

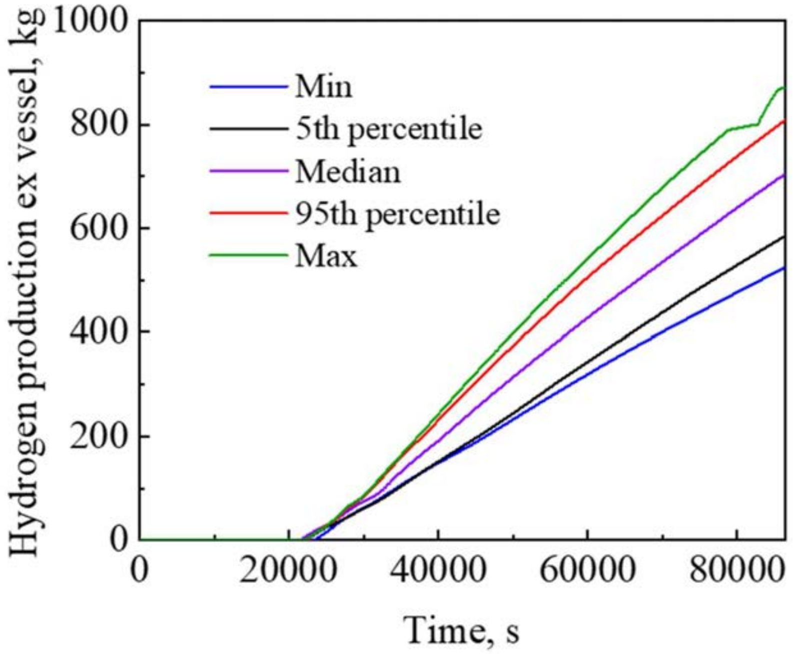

(a)

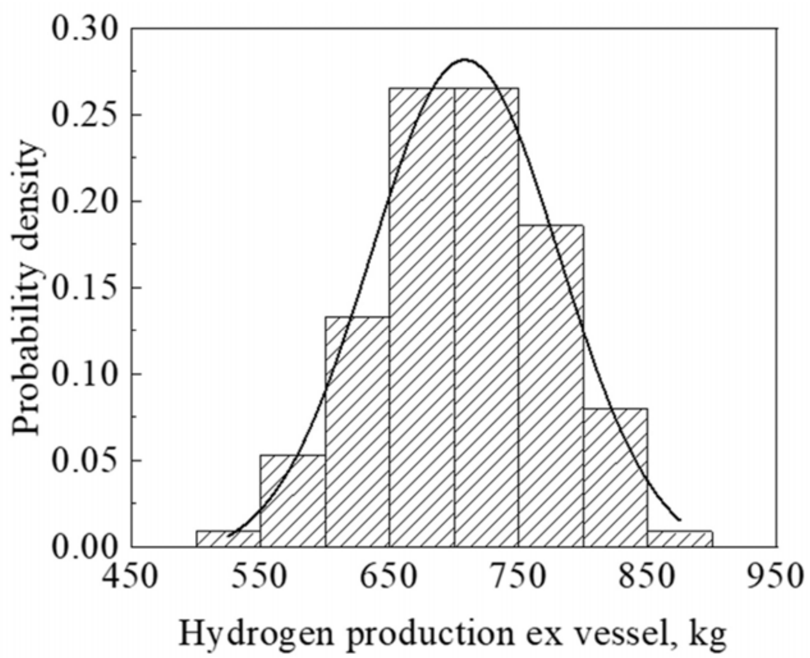

(b)

FIG. 120. Open two relief valves condition, (a) uncertainty statistics of H_2 production ex-vessel, (b) PDF of H_2 production ex vessel (mean: 708 kg, SD: 73 kg, adjusted R^2=0.99).

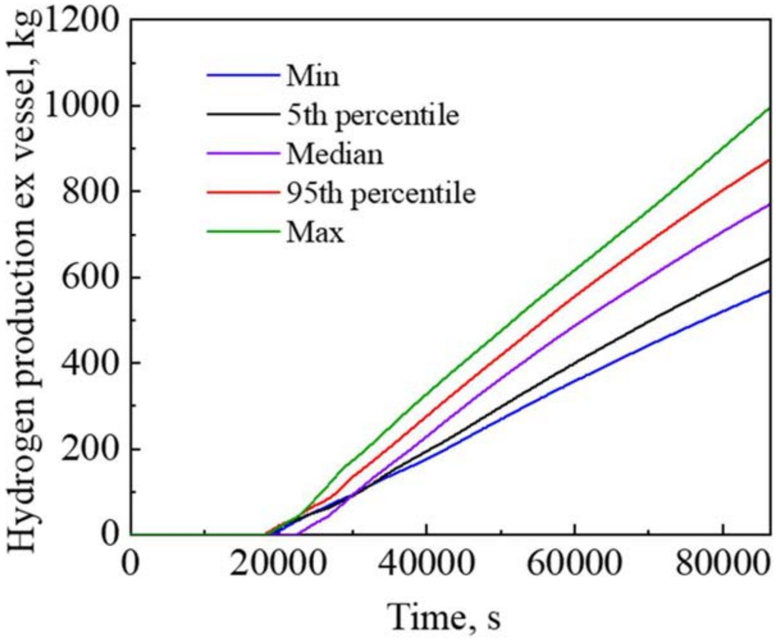

(a)

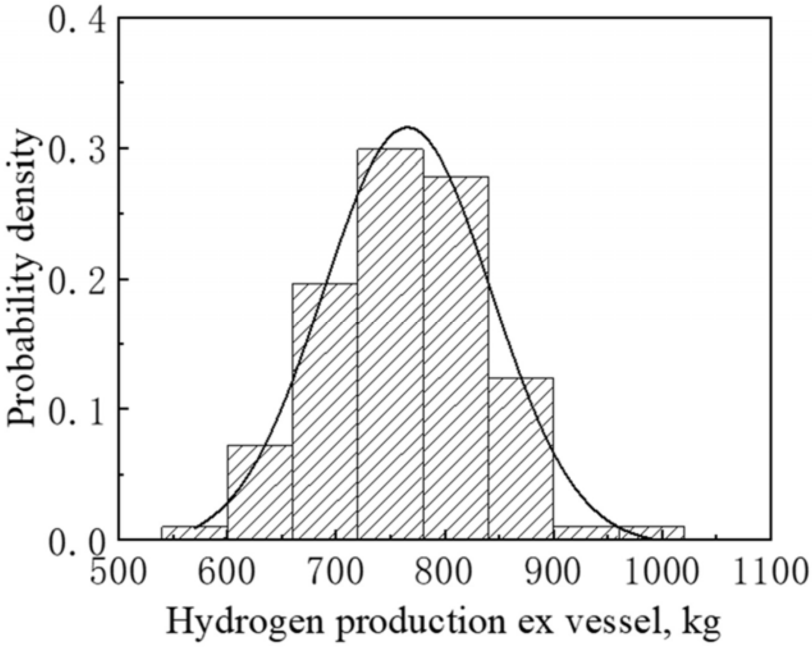

(b)

FIG. 121. Open three relief valves condition, (a) uncertainty statistics of H_2 production ex-vessel, (b) PDF of H_2 production ex vessel (mean: 765 kg, SD: 77 kg, adjusted R^2=0.99).

The sensitivity analysis results of hydrogen generation ex vessel under different conditions are shown in Figs. 122–124, and the uncertainty parameters in the top three of importance ranking are screened out, as listed in Table 50. It shows that under different pressure relief measures, the heat transfer coefficients in the radial and the bottom direction of the cavity always present the most important positive correlation effect on the hydrogen generation ex vessel. The porosity of the debris presents a moderate negative correlation effect when one pressure relief valve is opened, and the failure temperature of the penetration of the pressure vessel presents a moderate negative correlation effect when two and three pressure relief valves are opened.

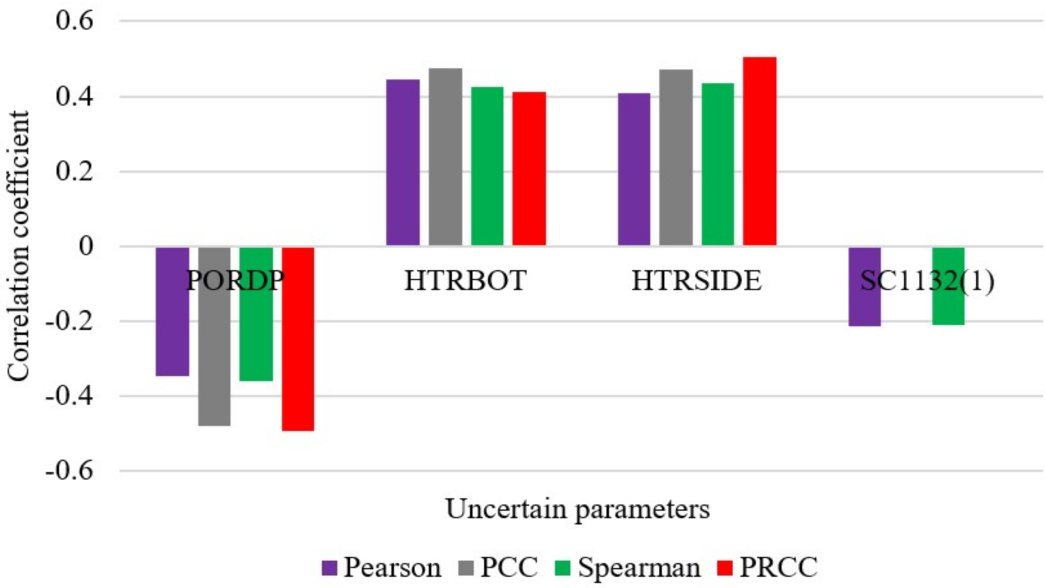

FIG. 122. Results of sensitivity analysis with opening one relief valve.

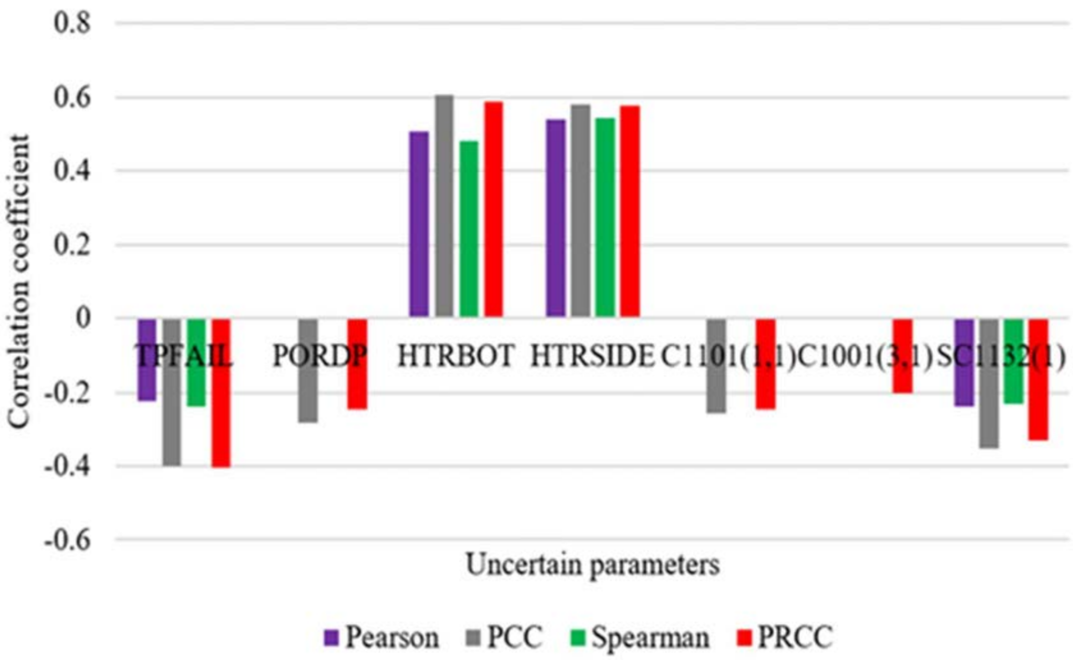

FIG. 123. Results of sensitivity analysis with opening two relief valves.

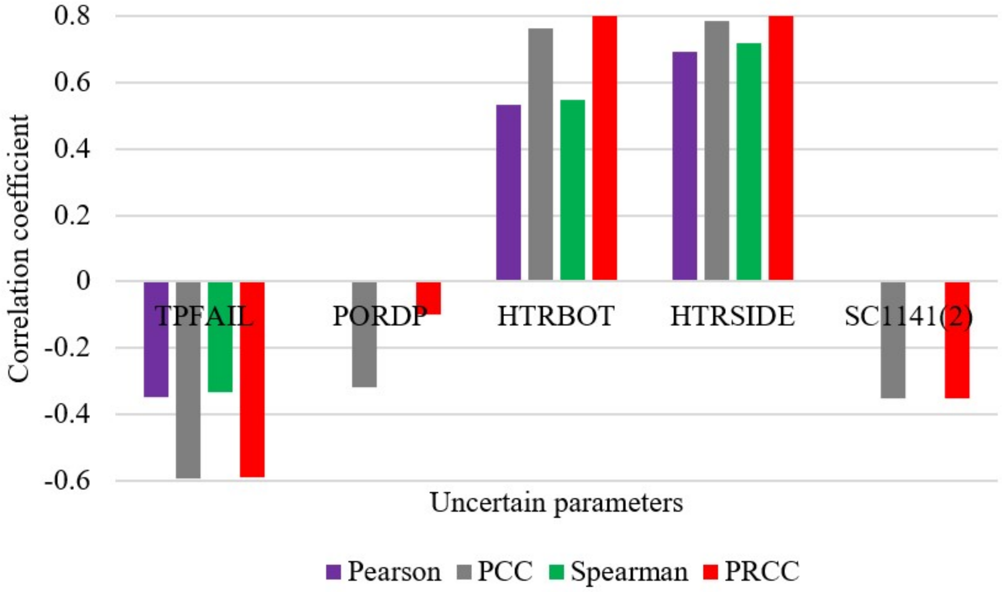

FIG. 124. Results of sensitivity analysis with opening three relief valves.

TABLE 50. IMPORTANCE OF PARAMETERS FOR EX-VESSEL H_2 GENERATION

Conditions	**Parameter importance ranking**		
	1	**2**	**3**
Open one relief valve	HTRSIDE	HTRBOT	PORDP
Open two relief valves	HTRSIDE	HTRBOT	TPFAIL
Open three relief valves	HTRSIDE	HTRBOT	TPFAIL

Influence of parameter distribution form on t hydrogen generation

The selected probability distribution of uncertainty parameters is generally based on experimental investigation and expert judgment. In order to investigate the influence of distribution form on the hydrogen generation, the parameter of the porosity of debris is selected with the mitigation of opening one relief valve as a case study. The distribution form is changed from the original normal distribution to the uniform distribution [58]. The results of uncertainty statistical analysis and probability density of hydrogen production in vessel under the uniform distribution of porosity are given in Figs. 125 and 126. The uncertainty of hydrogen generation in vessel ranges from 241–525 kg, which is equivalent to 35–76% of the hydrogen which is generated by the zirconium-water reaction. Compared with the case where the porosity is normally distributed, the uncertainty is slightly increased, and the average hydrogen production is increased by about 10 kg.

The results of the sensitivity analysis are presented in Figs. 127 and 128. Compared with the normal distribution form, the debris porosity in the uniform distribution form shows a stronger influence on the hydrogen source term, which reflects that the uncertainty of the distribution form of the model parameters has an influence on the hydrogen generation, and it is worthy of further study on the important model parameters.

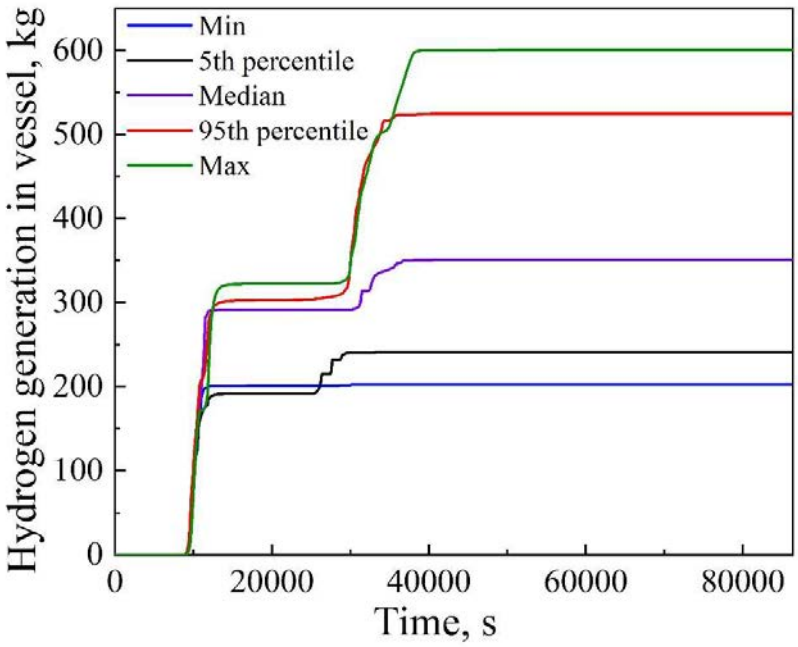

(a)

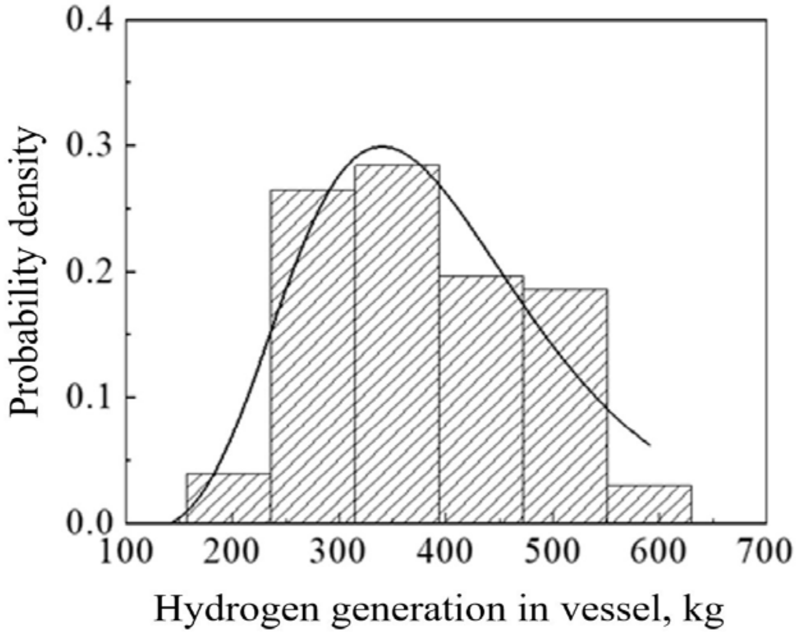

(b)

FIG. 125. Open one relief valve condition, (a) uncertainty statistics of in-vessel H_2 production, (b) PDF of in-vessel H_2 production (mean:377 kg, SD:0.362 kg, adjusted R^2=0.9).

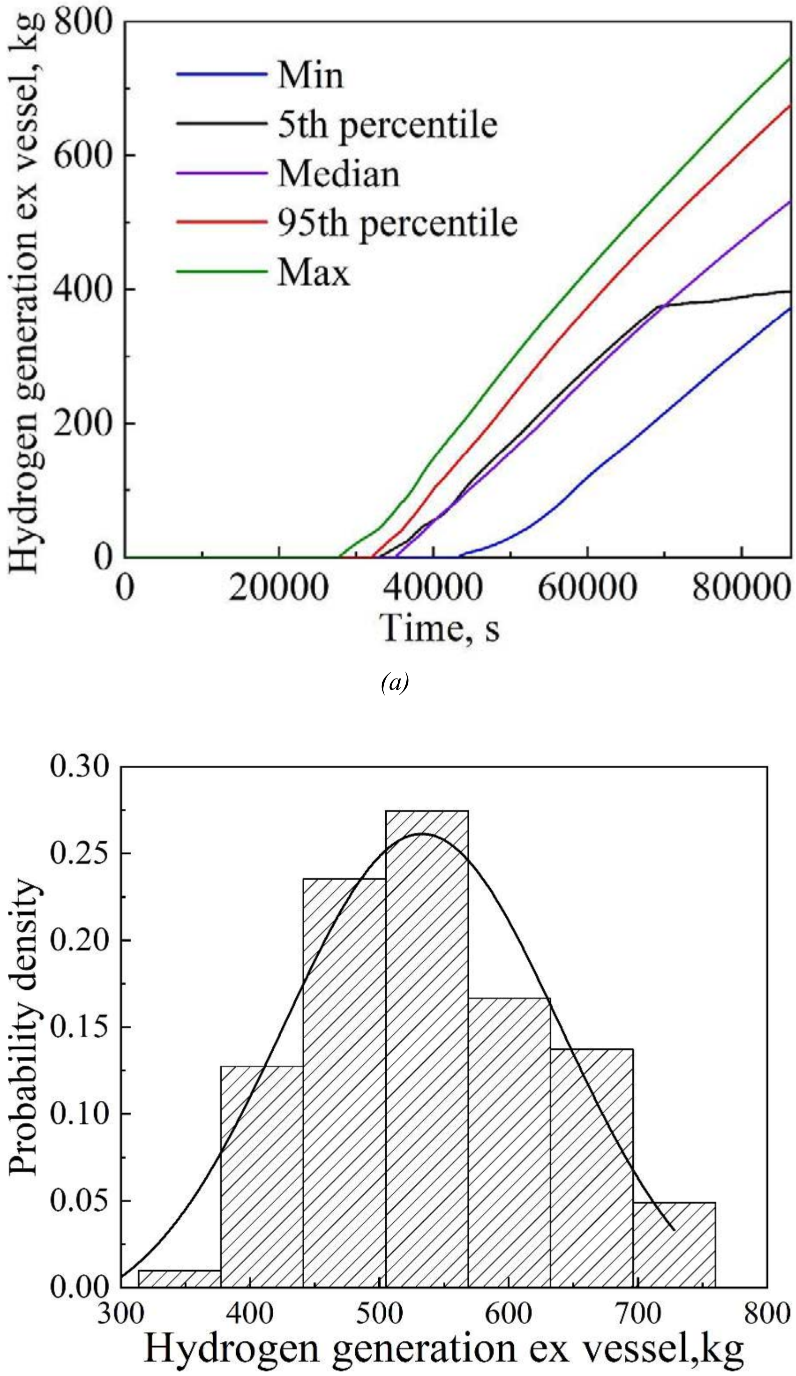

(a)

(b)

FIG. 126. Open one relief valve condition, (a) uncertainty statistics of ex-vessel H_2 production, (b) PDF of ex-vessel H_2 production (mean: 533 kg, SD: 107 kg, adjusted R^2=0.9).

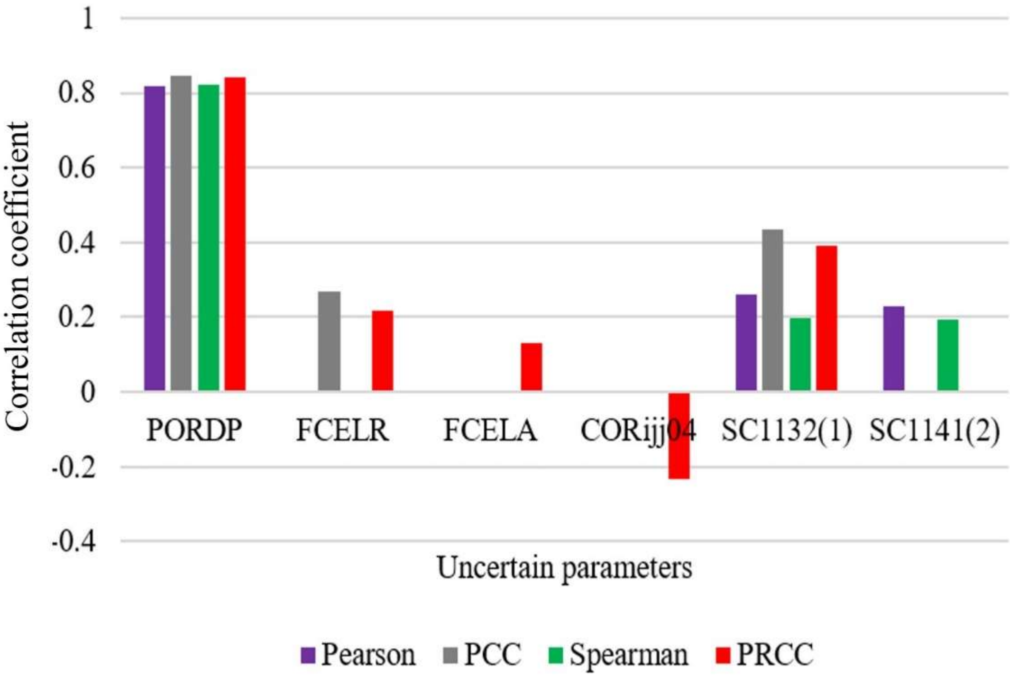

FIG. 127. Sensitivity analysis results in vessel with changing the distribution form of PORDP.

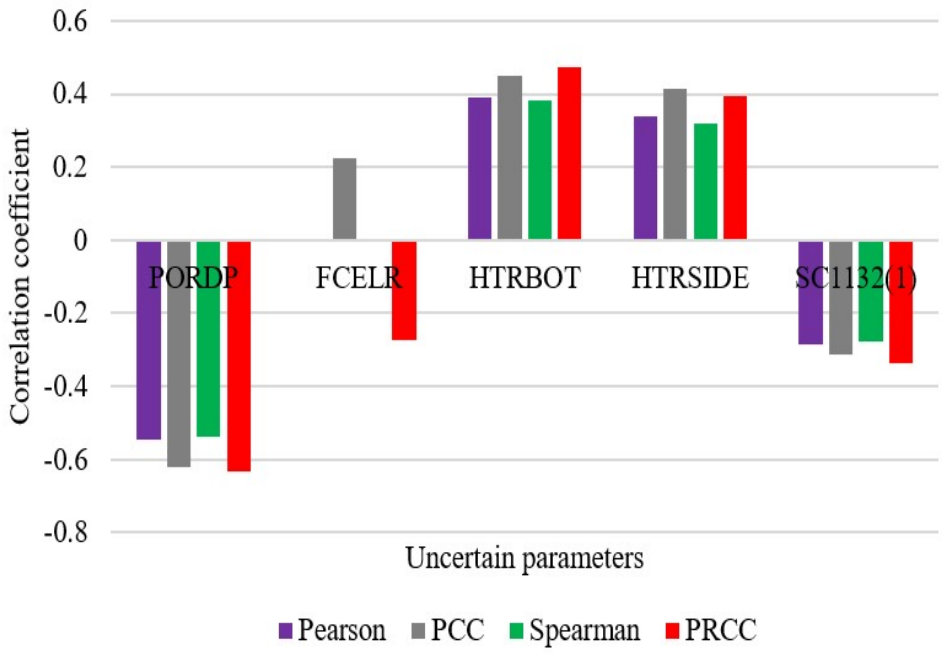

FIG. 128. Sensitivity analysis results ex vessel with changing the distribution form of PORDP.

2.3.5.7. Summary and Conclusions

The hydrogen generation is calculated for CNP600 under the severe accident of high pressure core melt initiated by SBO, and the influence of the selected model parameters and mitigation measures on the hydrogen generation and the uncertainty is investigated based on the LHS method. The uncertainty statistical results of hydrogen production are obtained and the important parameters are screened out. The main conclusions are as follows:

- In the severe accident of high pressure core melt with no mitigation measure, the uncertainty range of hydrogen production in vessel is 241–336 kg.
- The pressure relief measures have obvious influence on the hydrogen generation. With the opening of three relief valves, the hydrogen production mean value is 237 kg with uncertainty ranges from 210 kg to 261 kg, which is smaller than those in the cases with the opening of one relief valve and two relief valves.
- The probability distribution form of parameters will affect the uncertainty range and the sensitivity analysis results, which needs to be further studied.

Main sources of uncertainty resulting from the analysis

The uncertainty of the hydrogen production is from the distribution form and range of model parameters, and also the pressure relief measures of pressurizer have an influence on the hydrogen production and the uncertainty.

Lesson learned and best practices

- The uncertainty method based on LHS realizes the uncertainty analysis with small sampling sizes and the uncertainty distribution of hydrogen production is obtained under the severe accident of high pressure core melt initiated by SBO.
- The results of sensitivity analysis may be different with different sampling sizes, which needs to be further studied.
- It is necessary to reasonably select the sampling size when using LHS method and pay attention to the likelihood of being misleading of the sensitivity analysis results in a large analysis with many inputs.

2.3.6. University of Sharjah (UoS)

The UoS provided the accident analysis using APR1400 PWR plant as a reference one. Description of this plant specifics, accident scenarios analysed, applied models and approaches, and summary of the results are provided in the following sections.

2.3.6.1. Motivation and objectives

Sensitivity based [59–61] and Monte Carlo sampling based [62, 63] methods are extensively used in nuclear power and physics modelling and simulations [64–66]. These two methods are often used to estimate the parameter related uncertainties. The Monte Carlo uncertainty quantification is based on sampling the response of interest (RoI) with Monte Carlo random samples of the Parameters of Interest (PoI). This approach does not assume any functional form of the model, unlike the sensitivity based uncertainty quantification. Additionally, with Monte Carlo technique it is not possible to rate the parameters according to their importance in terms of the RoI uncertainty. There are studies based on the utilization of the subspace method to reduce the parameter space or the response space [61, 67–69].

The main objective of this exercise was to introduce computationally efficient parameter space analysis based uncertainty quantification technique [67, 69, 70], to rate the importance of the contributing parameters whenever Monte Carlo uncertainty quantification is used and sensitivity analysis is not available in the model, and to exemplify and test the proposed approach using the APR1400 power plant early response to an SBO. The applied approach is efficient as it does not require further sampling because the Monte Carlo samples used to evaluate the uncertainty in the integral parameter are used to assess differential contribution of each parameter's uncertainty in the integral uncertainty. The overarching goal of this approach is to equip analysts with computationally efficient method to estimate integral response uncertainties along with parameters' uncertainty contributions using Monte Carlo sampling technique.

2.3.6.2. Description of the relevant plant

APR1400 PWR is the plant design used throughout the verification and validation of algorithms proposed herein. Key parameters and reference plant conditions are summarized in Table 51.

TABLE 51. APR1400 PLANT REFERENCE OPERATIONAL PARAMETERS

Parameter	Value
Reactor power (%)	100
Electric Power (%)	100
Reactor power (MW_t)	3,981.4
Generating power (MW_e)	1,408.2
Boron concentration (PPM)	1,505.3
Reference temperature (°C)	309.1
Pressurizer pressure (Kg/m2)	157

2.3.6.3. Accident scenarios and severe accident codes

Accident scenario

The reference accident scenario is the SBO. In this scenario all AC power that feeds reactor systems is lost. It includes the failure of emergency diesel generators and the loss of offsite power during a turbine trip. In such a scenario, the APR1400 will operate its steam-driven turbine to power the emergency feed-water pumps and maintain water level in two steam generators. The APR1400 includes as well direct current power sources to power relays and valves of the main coolant cycle as well as safety systems in the reactor. The batteries also power the AC instrumentation and control systems, including safety consoles and radiation monitoring systems through inverters, which are used to control the feed-water steam-driven turbine [71]. Additionally, a gas turbine generator serves as an alternate AC source of power, capable of powering essential safety systems required to maintain sub-criticality and dissipate decay heat from the reactor and the spent fuel. The auxiliary feedwater system provides an independent safety related means of supplying feedwater to the steam generator(s) secondary side for removal of heat and prevention of reactor core uncovery during emergency phases of APR1400 operation. It is designed to be automatically or manually initiated, supplying feedwater to the steam generators for any event that resulted in the loss of normal feedwater and requires heat removal through the steam generators, including the loss of normal onsite and normal offsite AC power.

The gas turbine generator is designed to reach its rated voltage and frequency within 2 min. In the event of SBO, the gas turbine generator is started and manually connected to systems assuring safe shutdown, within 10 min. These systems include the safety injection pump, shutdown cooling pump, component cooling water pump, the motor driven feed-water pump, the spent fuel pool cooling pump, and the safety related batteries chargers. Successful mitigation of SBO requires the operator to manually connect these necessary systems from the main or remote control rooms [72]. An alternate AC source provides the power for equipment necessary to cope with SBO at least for 8 hours. For the diversity of emergency electrical power sources, the gas turbine type is selected for alternate AC source. It is connected to non-safety systems in the event of loss of offsite power. The on-site standby power is the most crucial for safety and should be available in any situation. The emergency diesel generators are available to provide on-site stand-by power. The reactor can also be AC powered by two mobile diesel generators or direct connection from a nearby power station.

<u>*Severe accident codes*</u>

3KEYMASTER [17], specifically developed to replicate the APR1400 design, is used. RELAP5 is used for thermal hydraulics calculations and NESTLE is used for neutronics calculations [73] to simulate the power plant in real time via 3KEYMASTER environment [17, 74].

2.3.6.4. Plant modelling and nodalization

The 3KEYMASTER simulator uses an adapted version of RELAP5 nodalized as illustrated in Fig. 129.

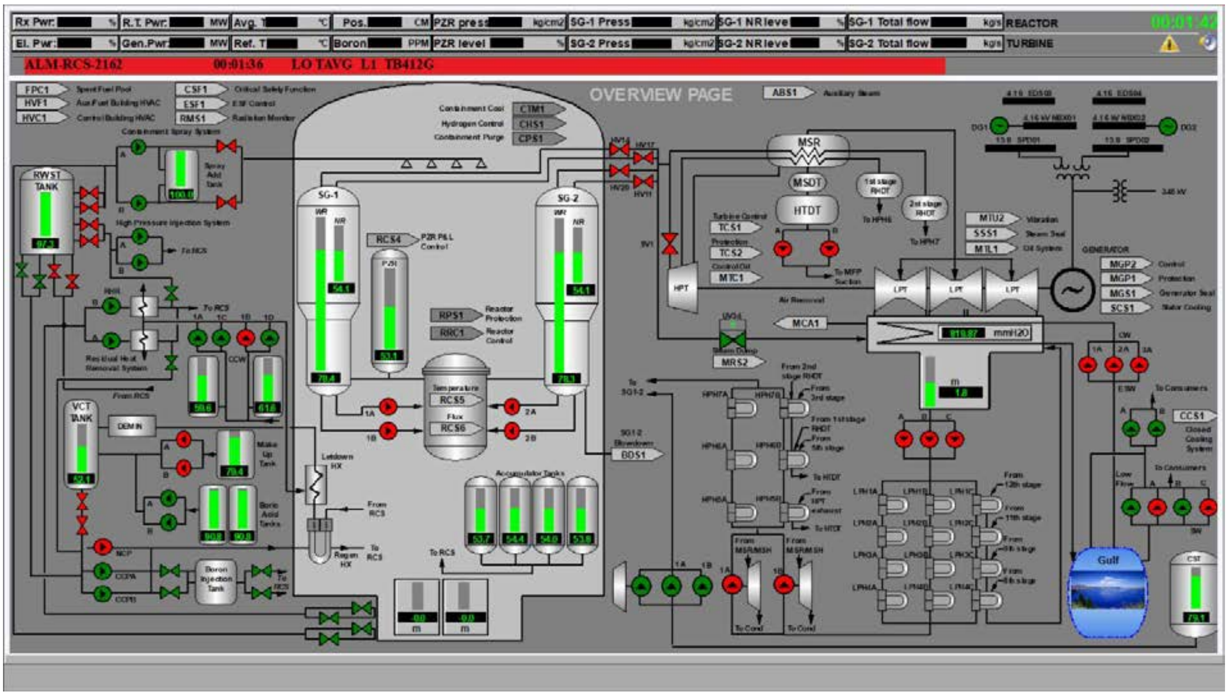

FIG. 129. APR1400 plant nodalization of the 3KEYMASTER simulator.

2.3.6.5. Methodologies and tools for the uncertainty and sensitivity analysis

The proposed technique relies on utilizing the Monte Carlo based uncertainty quantifications samples implicitly to estimate the first-order sensitivity coefficients while sampling the RoI. The method is explained and tested for neutronics calculations [70]. Assume a function *f,* which represents the relation between the RoI ($\bar{R}$) and the PoI $\bar{x}$:

$$\bar{R} = f(\bar{x}) \tag{31}$$

where $\bar{R} \in \mathbb{R}^m$ and $\bar{x} \in \mathbb{R}^n$. The number of model runs required to estimate the sensitivity coefficients using a forward approach is $\sim n$ and using the adjoint approach is $\sim m$. If the Monte Carlo based uncertainty quantifications uses *N* samples, then in the proposed approach the samples are used to estimate the first order sensitivity coefficients and individual uncertainty contributions of the model parameters. In the high dimensional parameter space *N* <<*n,* implying that these samples are not sufficient to estimate sensitivity coefficients; at least *n* samples are required. However, using the efficient subspace method [3], the parameters' space dimension can be reduced by means of active subspace analysis $\mathscr{s} \in \mathbb{R}^r$ where *r* << *n* is identified, providing that the parameter space can be reduced by projection on $\mathscr{s}$:

$$\bar{x}^{n\times1} = \sum_{i=1}^{n} \alpha_i \bar{u}_i^{n\times1} \approx \sum_{i=1}^{r} \alpha_i \bar{u}_i^{n\times1} = \mathbf{U}^{n\times r} \bar{\alpha}^{r\times1} \tag{32}$$

where $\mathbf{U}^{n\times r}$ is the matrix containing the basis of $\mathscr{s}$ with a dimension of $n \times r$; $\bar{\alpha}^{r\times1}$ is a vector containing coefficients that relate actual parameters' vector (i.e. $\bar{x}^{n\times1}$) to the projected space basis vector. Once projected on the space represented by matrix $\mathbf{U}^{n\times r}$, the original parameters' set can be replaced by reduced parameters' set $\bar{\alpha}^{r\times1}$. Therefore, the response variation ($\Delta\bar{R}^i$) can be written in terms of derivatives of the RoI with respect to reduced input variable ($\bar{\alpha}^{rx1}$) as follows:

$$\Delta\bar{R}^i = \bar{R}^i - \bar{R}^{ref} = \frac{\partial\bar{R}}{\partial\alpha_1}.\Delta\alpha_1^i + \cdots + \frac{\partial\bar{R}}{\partial\alpha_r}.\Delta\alpha_r^i = \mathbf{S}_{\frac{\mathrm{R}}{\alpha}}^{\mathbf{T}} \Delta\bar{\alpha}^i \tag{33}$$

where $\mathbf{S}_{\frac{\mathrm{R}}{\alpha}}^{\mathbf{T}}$ is the transpose of the sensitivity matrix of response R with respect to parameter vector α. With reference to Eq. (32), the vector $\Delta\bar{\alpha}^i$can be calculated using:

$$\Delta\bar{\alpha}^i = \mathbf{U}^{n\times r,\mathbf{T}} \Delta\bar{x}^i \tag{34}$$

where $\mathbf{U}^{nxr,\mathbf{T}}$ is the transpose of the basis vectors matrix $\mathbf{U}^{nxr}$ and $\Delta\bar{x}^i$ is the $\underline{i^{th}}$ snapshot of parameter vector $\bar{x}$ perturbation. The Monte Carlo based uncertainty quantifications entails collecting *N* response samples:

$$\mathbf{R} = [\bar{R}^1 | \ldots | \bar{R}^N] \tag{35}$$

$$\Delta\mathbf{R} = [\Delta\bar{R}^1 | \ldots | \Delta\bar{R}^N] \tag{36}$$

If $r<<n$ and $N \geq r$, then variations matrix ($\Delta\mathbf{R}$) can be used to formulate r linear equations with r unknowns (the sensitivity coefficients of the response $\bar{R}$ with respect to reduced parameters $\bar{\alpha}$ (i.e. $\boldsymbol{S}_{\underline{\underline{\bar{R}}}{\bar{\alpha}}}$)) where $\boldsymbol{S}_{\underline{\underline{\bar{R}}}{\bar{\alpha}}}$ is a vector if the problem has only one response of interest. Therefore, the matrix system of equations can be written as follow:

$$\Delta\mathbf{R} = \boldsymbol{S}^{T}_{\underline{\underline{\bar{R}}}{\bar{\alpha}}}\mathbf{A} \tag{37}$$

where

$$\mathbf{A} = [\Delta\bar{\alpha}^{1}| \dots |\Delta\bar{\alpha}^{r}]^{rxr}, \text{ and } \boldsymbol{S}_{\underline{\underline{\bar{R}}}{\bar{\alpha}}} = \left[\frac{\partial R_1}{\partial\bar{\alpha}}|\dots|\frac{\partial R_m}{\partial\bar{\alpha}}\right]^{r\times m} \tag{38}$$

The matrix $\mathbf{A}$ is a full rank matrix representing the reduced parameters' perturbations and therefore the sensitivity matrix can be computed as follow:

$$\boldsymbol{S}^{T}_{\underline{\underline{\bar{R}}}{\bar{\alpha}}} = \Delta\mathbf{R}\,\mathbf{A}^{-1} \tag{39}$$

Once determined, the sensitivity coefficients can be mapped to the original space (of the response $\bar{R}$ with respect to the actual parameters $\bar{x}$ (i.e. $\mathbf{S}_{\underline{\underline{\bar{R}}}{\bar{x}}}$)) using Eqs. (32) and (34) via:

$$\mathbf{S}_{\underline{\underline{\bar{R}}}{\bar{x}}} = \boldsymbol{S}_{\underline{\underline{\bar{R}}}{\bar{\alpha}}}\,.\,\mathbf{S}_{\underline{\underline{\bar{\alpha}}}{\bar{x}}} = \boldsymbol{S}_{\underline{\underline{\bar{R}}}{\bar{\alpha}}}\,.\,\mathbf{U}^{\mathbf{T}} \tag{40}$$

where $\mathbf{S}_{\underline{\underline{\bar{\alpha}}}{\bar{x}}}$ represents sensitivity of the reduced parameters with respect to the original parameter. Thus, the linearly estimated parameter (x_i) - related uncertainty in the j^{th} response R_j can be calculated as follow:

$$\sigma^2_{x_i\to R_j} = \left(\frac{\partial R_j}{\partial x_i}\right)^2 .\, \sigma^2_{x_i} \tag{41}$$

and the relative contribution of the i^{th} parameter in the integral uncertainty of the j^{th} response:

$$\partial_{x_i\to R_j} = \frac{\sigma^2_{x_i\to R_j}}{\sum_{i=1}^{n}\sigma^2_{x_i\to R_j}}. \tag{42}$$

The individual uncertainty (σ^2) contribution of each parameter x_i on the response R_j ($\sigma^2_{x_i\to R_j}$) in the Monte Carlo estimated integral uncertainty is estimated as follows:

$$\left(\sigma^2_{x_i\to R_j}\right)_{\text{Monte Carlo based uncertainty quantifications}} = \partial_{x_i\to R_j}\left(\sigma^2_{R_j}\right)_{\text{Monte Carlo based uncertainty quantifications}} \tag{43}$$

Identifying the active subspace $\mathcal{S}$: possible variations of the input parameters can be restricted to certain degrees of freedom which can help in reducing the dimensionality of the parameter space. By perturbing the cross sections, the parameter related uncertainty can be estimated and therefore the parameter variations are limited to those along the dominant uncertainty DoFs. The i^{th} covariance perturbation can be created with:

$$\Delta\bar{x}^i = \bar{x}^i - \bar{x}_{ref} = \mathbf{C}_{\bar{x}}\bar{\boldsymbol{\xi}}^i \tag{44}$$

where $\bar{\boldsymbol{\xi}}^i$ is a vector of normally distributed random independent values. From Eq. (44), the variations of the parameters' perturbations $\Delta\bar{x}^i$ are parts of the subspace spanned by the columns of matrix $\mathbf{C}_{\bar{x}}$ (the covariance matrix), therefore, the basis of this matrix ($\mathbf{U}_{\mathbf{C}_{\bar{x}}}^{nxn}$ in Eq. (45) is a basis for parameters' perturbations. In other words, the columns space of the covariance matrix is inclusive of parameters' perturbations. Thus, the parameters covariance matrix is symmetric and its SVD is obtained as follows:

$$\mathbf{C}_{\bar{x}}^{n\times n} = \mathbf{U}_{\mathbf{C}_{\bar{x}}}^{nxn}\boldsymbol{\delta}_{\mathbf{C}_{\bar{x}}}^{2}\mathbf{U}_{\mathbf{C}_{\bar{x}}}^{n\times n,T} \tag{45}$$

where $\mathbf{U}_{\mathbf{C}_{\bar{x}}}$ is the matrix of the orthonormal basis of the column space of matrix $\mathbf{C}_{\bar{x}}$, and $\boldsymbol{\delta}_{\mathbf{C}_{\bar{x}}}^{2}$ is a diagonal matrix of the corresponding singular values denoting the variances. If the covariance matrix is reducible, then the columns corresponding to extremely small singular values (diagonal of matrix $\boldsymbol{\delta}_{\mathbf{C}_{\bar{x}}}^{2}$) can be omitted from the basis with negligible error. The columns of matrix $\mathbf{U}_{\mathbf{C}_{\bar{x}}}$ form a basis of the reduced active subspace within the parameter space [i.e. matrix $\mathbf{U}$ in Eqs. (31) and (33)].

To confirm that the reduced subspace is representative of the parameters' variations, the following error upper bound estimate is computed for a range of subspace dimensions:

$$\epsilon_{upper}(r) = \mathbf{10}\sqrt{\frac{2}{\pi}}\ \mathbf{max}_{i=1,..p}\left\|(\mathbf{I}^{n\times n} - \mathbf{U}^{n\times r}\mathbf{U}^{r\times n,T})\Delta\bar{x}^{i^{n\times 1}}\right\|_2 \tag{46}$$

This upper bound ($\epsilon_{upper}(r)$) is guaranteed with a success probability of $P(r,p) = 1\text{-}10^{-p}$ where p is the number of extra snapshots used to compute that upper bound and $\Delta\bar{x}^i$ is the i^{th} snapshot of the parameters vector, [75].

Uncertainty and sensitivity calculation scheme and relevant tools

The following steps summarize the method used in this study:

(1) Using Eq. (14), reduced space basis is calculated;
(2) Determine Using Eq. (45) the suitable space dimension (r) is determined;
(3) Monte Carlo based samples are collected to quantify the uncertainty (**R**);
(4) Reduced parameters' perturbation matrix (**A**) is calculated;
(5) Using Eq. (38), sensitivity matrix $\boldsymbol{S}_{\frac{\bar{R}}{\bar{\alpha}}}$ is estimated;
(6) Using Eq. (39), sensitivity matrix is mapped from the reduced space to the original space;
(7) Once the sensitivity matrix is available ($\mathbf{S}_{\frac{\bar{R}}{\bar{x}}}$), the uncertainty contribution of each parameter can be rated according to Eq. (42).

ROMUSE [76] is used as an analysis tool in conjunction with reactor core simulators. Written in C++ it can perform various types of parameter perturbations with sensitivity analysis, uncertainty quantification, surrogate model construction and subspace analysis. Version 2.0 can be interfaced with DAKOTA code [77], providing to ROMUSE the access to various algorithms [72]. It also can be used in conjunction with reactor analysis codes such as reactor core simulators as well. ROMUSE can be utilized stand alone or interfaced with DAKOTA. Comprehensive uncertainty quantification studies performed with ROMUSE can be based one of these uncertainty quantification methods:

- Brute force Monte Carlo;
- Multi-physics Karhunen-Loeve expansion (utilizing the multi-physics efficient range finding algorithm in the case of coupled multi-physics codes);
- Surrogate based Monte Carlo.

Uncertain parameters and related probability distributions

The problem of interest is to estimate the contribution of cross sections in the estimated fuel temperature as a FOM. After the reactor, the generated heat is mostly decay heat, however the premise of this work is to assess if the cross sections pose any significant variation in the estimated fuel temperature. The 44groupcov covariance library is used for the cross sections uncertainty quantification [78, 79]. The library is comprehensive and provides data for total of 401 materials; it is based on various sources, including ENDF/B-VII, ENDF/-VI, and JENDL-3.3. Since the simulator package takes two group cross sections structure, the perturbations are mapped from the 44 groups onto the two groups. Therefore, each perturbation is performed on the 44 groups SCALE library being collapsed into two groups cross sections that are then fed onto 3KEYMASTER simulator.

2.3.6.6. Results

Reference case

The reactor thermal power is 3,981 MWt with a flow rate of 10,743 kg/s. In the case of SBO, reactor control rods will drop instantaneously to shut the reactor down causing thermal power to decrease sharply after 25 sec to ~255 MWt; this will cause a drop in fuel temperature from 590°C to 352°C. The heat generated in the core by fission products will start to decrease slowly, as the coolant flows between the reactor vessel and the steam generator. The SBO scenario is simulated for the first 85 min. The maximum tolerable pressure of 20 MPa is not exceeded. The flow rate in steam generator before SBO is 10,743 kg/s. The coolant starts to boil at 45 min causing two phase flow. After 45 min into blackout, the steam generators will dry out and no longer will have sufficient flow rate to remove the heat from the coolant. This is shown in Fig. 130. The temperatures of the hot and cold legs will increase until they reach the boiling temperature. The increase in temperature will cause the pressure in the primary loop to increase as well, which might lead to a rupture in the RCS pipes and initiate LOCA. As can be seen in Fig. 131, this will cause the fuel temperature to increase sharply. The fuel temperature will continue to increase until the fuel starts to melt down, which is around 1 h into the SBO. Figure 131 shows that maximum fuel temperature is ~800ºC; at this temperature the simulator stopped because it reached a simulation limit; this is where the cladding oxidation occurs, i.e. water metal reaction starts to become significant.

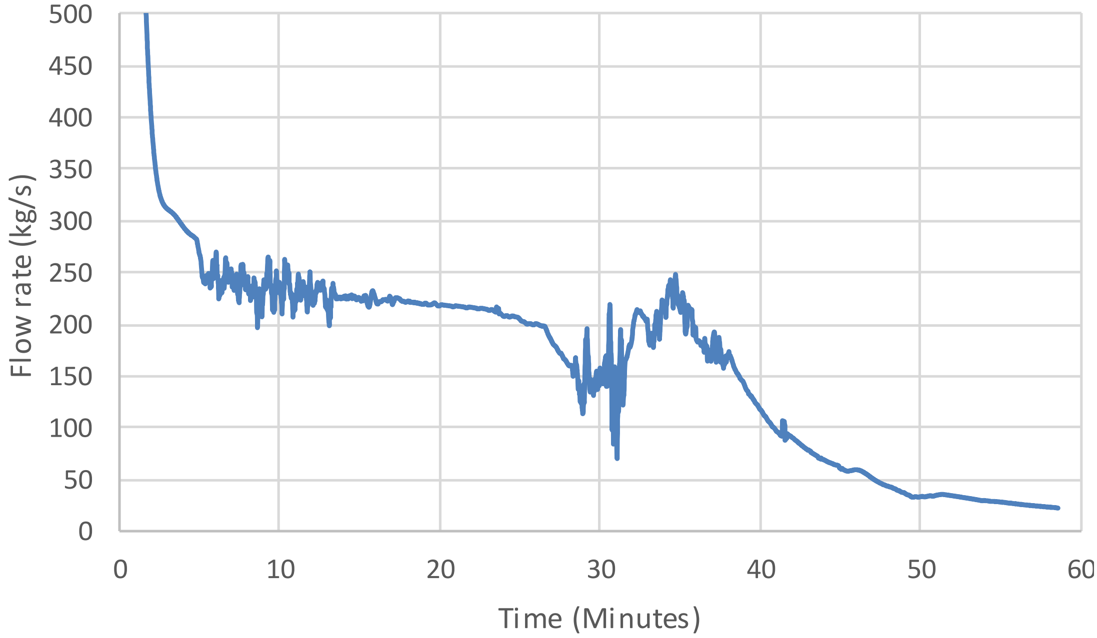

FIG. 130. Average flow rate per steam generator.

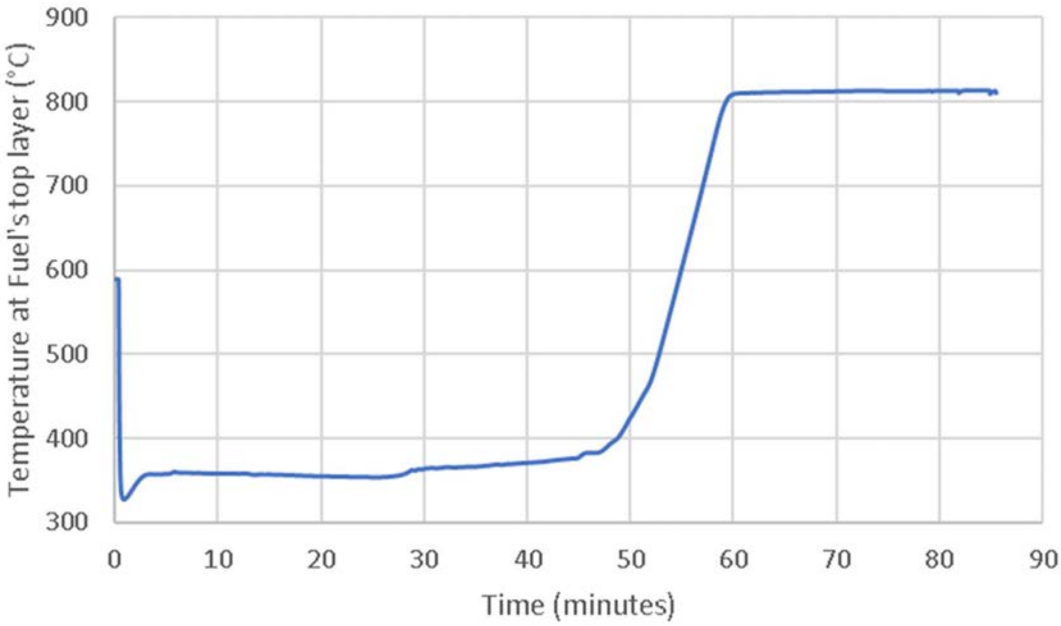

FIG. 131. Fuel temperature vs. time in case of SBO.

Uncertainty estimation of input parameters

The considered input parameters are the cross-sections of nuclear fuel only. The covariance data available in the 44groupcov library are used to create the i^{th} perturbations from the reference cross section vector as follow:

$$\Delta\bar{\Sigma}^i = \bar{\Sigma}^i - \bar{\Sigma}_{ref} = \mathbf{C}_{\bar{\Sigma}}\bar{\boldsymbol{\xi}}^i \quad (47)$$

Once generated, the cross-sections are mapped to the right structure and fed to the neutronics code. Given the available covariance data and material available in the 4 different mixtures available in the PLUS7 fuel assembly model, the total number of materials, reactions, energy groups parameters = 2,860. Using Eq. (44) the orthonormal basis of the covariance matrix is computed and used in Eq. (45) to determine the number of principal components (effective DoFs). The error upper bound decay to < 1% when 120 degrees of freedom are included. This means that with 120 model runs one can determine the overall uncertainty in the FOM and estimate the first order sensitivities of the reduced space ($\in \mathbf{R}^{120}$). Once determined, these first order sensitivities are mapped to the actual space ($\in \mathbf{R}^{2800}$) using Eq. (39).

<u>*Uncertainty estimation of output response*</u>

The response of interest is the fuel temperature as a function of time.

The cross sections related uncertainty in the fuel temperature over time are illustrated in Fig. 132. As shown in this figure, the standard deviation decays over time right after the reactor shutdown. This might be because the overall reactor heat becomes more and more dominated by decay heat while the fission related heat source becomes weaker overtime due to the shutdown. The Monte Carlo estimated uncertainty in the FOM for certain time steps is summarized in Table 52. The calculation scheme as outlined is then used to segment the overall uncertainty into the various cross-sections' uncertainty matrices available in the 44groupcov library (Table 53).

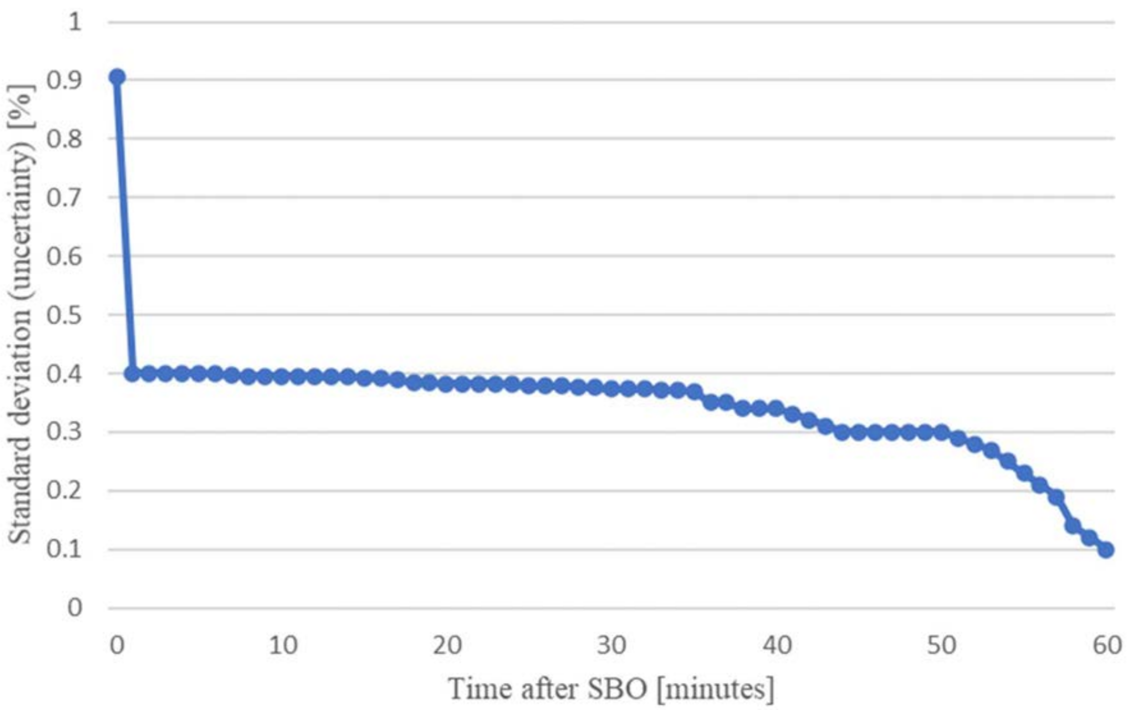

FIG. 132. Cross-sections related standard deviation in the fuel temperature.

TABLE 52. FOM UNCERTAINTY DUE TO CROSS SECTIONS ONLY

Time (min)	Reference Fuel Temperature (°C)	Standard deviation
0	590	0.9%
10	352	0.4%
30	363	0.4%
45	385	0.3%
50	414	0.3%
60	813	0.1%

TABLE 53. TOP CROSS SECTIONS CONTRIBUTING TO THE OVERALL FOM UNCERTAINTY BEFORE AND AT THE END OF THE SIMULATION

Time	Top 3 Contributors	% Contribution ($\Delta T/T_{ref}$)
Just before the SBO	$^{238}U(n, \gamma)$	0.41 %
	$^{235}U(\bar{\upsilon})$	0.35 %
	^{235}U(n,fission)	0.15 %
60 min after the SBO (once T_{max} is reached)	$^{238}U(n, \gamma)$	0.64 %
	$^{238}U(\bar{\upsilon})$	0.52 %
	^{238}U(n,fission)	0.23 %

2.3.6.7. Summary and Conclusions

In this study, an efficient principal component analysis based Monte Carlo uncertainty quantification scheme is used to assess the contribution of cross sections data in the uncertainty of fuel temperature. The proposed approach paves the way for the inclusion of large number of sources in uncertainty quantification practices in severe accidents analysis. The 3KEYMASTER simulator is used to simulate the APR1400 response to SBO. Since the 3KEYMASTER simulator uses a two group neutronics code, the perturbations were generated and collapsed to the right structure via SCALE6.1. Results indicate a minor contribution of the cross sections to FOM of interests; once differential contributions are realised using the principal component analysis, the uncertainties due to U^{238} uncertainty matrices increase importance in the overall fuel temperature uncertainty.

Main sources of uncertainty resulting from the analysis

Cross sections have a minor uncertainty effect on fuel temperature post shutdown (< 1%), as the fuel temperature increases, U^{238} cross sections uncertainty starts to be a major contributor to uncertainty.

Lesson learned and best practices

- Nuclear data cross sections result in a minor uncertainty in the fuel temperature after reactor shut down as a response to an SBO accident.
- Using principal component analysis and Monte Carlo sampling, analysts can determine the uncertainty in FOMs due to large number of input parameters efficiently.

2.3.7. National Atomic Energy Commission (CNEA)

CNEA developed the accident analysis using CAREM-like NPP model. Description of this plant specifics, accident scenarios analysed, applied models and approaches, and summary of the results are provided in the following sections.

2.3.7.1. Motivation and objectives

This analysis, based on a CAREM (Central Argentina de Elementos Modulares) like plant MELCOR model, is expected to contribute providing a knowledge basis associated to severe accident management guidelines development and possible implementation. The question to be answered in this context would be what is the time available for human actions and severe accident management programme initiation in case of severe accident. From a more general point of view, this study provides insights onto the best practices and possible methodology to be used for uncertainty and sensitivity calculations associated with severe accident codes applications [80], which in turns leads to a significant improvement in the quality of the severe accident analysis.

2.3.7.2. Description of the relevant plant

The study is applied to a CAREM-like NPP model, based on the CAREM-25 simplified and outdated design [80]. In this section, some of the main characteristics of the CAREM-25 NPP design are described. CAREM-25 is an integral type PWR with distinctive features that simplify the design and support the objective of achieving a higher level of safety compared with large NPP designs. Some of the design characteristics of CAREM-25 are integrated primary coolant system, self-pressurization, core cooling by natural circulation and in-vessel hydraulic control rod drive mechanisms. Other important characteristic is the actuation of passive safety systems during a grace period of 36 h. Due to this and to the presence of additional safety features with external coolant supply, the SBO event is intrinsically included into the CAREM-25 design basis, which strengthen the design in coping with extreme external events. Main design characteristics of CAREM-25 are presented in Table 54.

TABLE 54. GENERAL DESIGN CHARACTERISTICS OF CAREM-25

System/Component	Design Value
Core	Power = 100 MWt
Primary System	Pressure: 12.25 MPa Core inlet temperature: 284°C Core outlet, riser, and dome temp. ~ saturation = 326°C Mass flow rate: 410 kg/s
Secondary System	12 identical “mini helical” steam generator “once-through” type, secondary system in the tube side Secondary pressure: 4.7 MPa
Fuel	PWR Type fuel assembly with a hexagonal array Enrichment: 3.1%
Reactor Vessel	Height: 11 m Inner Diameter: 3.16 m Wall thickness: 0.123 m

Design internalization of defence in depth concept

Defence in Depth (DID) concept was internalized in CAREM-25 design since the conceptual engineering. It is the base for structures, systems and components safety classification, which in turns allows a clear assignation of requirements to systems important to safety. The applied DID concept includes clarification on multiple failure events, severe accidents and independence between levels. The adopted approach in CAREM-25 is briefly described as follows:

1) **Level 2**: control of abnormal operation and failures associated with the anticipated operational occurrences by means of enhanced process and control systems.
2) **Level 3:** control of events to avoid radiological releases and prevent escalation to core melt conditions.

   Design goals: to avoid fuel damage and departure from nucleate boiling, also in case of LOCA events, to keep the core covered and the RPV and containment pressure below design limits.

   Passive safety features of CAREM-25 make it possible the existence of a grace period (36 h) in which neither operator action nor electrical power supply is required to ensure the fulfillment of the fundamental safety functions. Taking into consideration this grace period, two different plant states are distinguished at this level from the safety point of view:

   - **Plant safe state**: plant state reached after the actuation of the safety systems during the grace period.
   - **Plant final safe state**: plant state reached with active safety systems, which operate after the grace period to carry the plant to conditions equivalent to cool shutdown.

   In order to address the clear differences between events with and without core melt and to explicitly consider multiple failure events without core melt as part of DID level 3, this level is subdivided in two sublevels:

   - **Sub-level 3A**: control of postulated single initiating events by the main line of protection. During the grace period (initial stage) this is done by means of the passive Safety Systems to reach the Plant Safe State. During the final stage after the grace period, the control in charge of the active Final Safe State Systems.
   - **Sub-level 3B**: control of postulated multiple failure events without core melt by the diverse line of protection. During the grace period (initial stage) and in case of failure of a safety system of the main line of protection, this is done by means of the passive safe state systems in order to reach the plant safe state. In case of failure of the final safe state systems of the main line of protection the extension of plant safe state systems of this sublevel actuate, by means of external supply, to extend the plant safe state.

3) **Level 4**: control of postulated core melt accidents to limit off-site releases, by means of the severe accident mitigation systems.

   Design goals: to retain the corium inside RPV, to avoid hydrogen detonations and to limit possible iodine releases.

Engineering safety features related to severe accidents mitigation systems

A brief description of CAREM-25 DID Level 4 (severe accident mitigation systems) engineering safety features is as follows.

— Hydrogen control system:

  This system consist of passive autocatalytic recombiners installed at different containment locations in order to limit hydrogen concentration to avoid possible deflagrations or detonations that could damage the containment.

— In-vessel corium retention:

  This system provides in-vessel melt retention by cooling the external surface of the RPV during the late phase of a severe accident. This is done by submerging the lower part of the vessel in water, injected by means of off-site fire engines. Diverse water sources are considered.

— Iodine suppression pool retention (pH increase):

  This system promotes the retention in the suppression pool water of the iodine released during a severe accident, in order to limit off-site releases. This is done by injecting an alkaline solution into the suppression pool water to increase its pH, thus preventing the formation of gaseous iodine.

2.3.7.3. *Accident scenarios and severe accident code*

The postulated severe accident scenario for the present analyses is mainly based on the following assumptions [80]:

— Loss of coolant accident due to the instantaneous double-ended guillotine rupture of a pipe of the passive residual heat removal system (PRHRS) connected to the RPV (pipe diameter 0.0381 m);
— Reactor shutdown at $t = 0$ s;
— Failure of all DID Level 2 and Level 3 heat removal and injection systems;
— RPV external cooling system success (DID Level 4, in-vessel melt retention).

Under these conditions, the general time progression of the severe accident in a CAREM-like reactor is expected to be the following:

— Pipe rupture: $t = 0$ h;
— Reactor shutdown: $t = 0$ h;
— Core uncovery (top of core): $t \sim 3$ h;
— Onset of core degradation: $t \sim 7$ h;
— Total core uncovery: $t \sim 8$ h;

— Core relocation to lower plenum: $t \sim 13$ h;
— RPV failure: does not take place due to external RPV cooling system actuation.

In addition to this, it is expected to get a large amount of the total zircaloy mass present in the core oxidized, due to the typical low heat up rate (lower than 0.1 K/s) because of the low power density of these integral type reactors. MELCOR 1.8.6 [2, 3] was considered in this work as the simulation tool to perform severe accident tests in both the uncertainty and parametric analysis considered.

2.3.7.4. Plant modelling and nodalization

The CAREM-like plant MELCOR model used for the present analysis is briefly described in this section. The primary system, the containment system and most of the safety important systems were included in this model. A simplified secondary system model was included as a boundary condition for the steady state operation.

Primary system model: the thermal-hydraulic nodalization for the integrated primary coolant system is shown in Fig. 133, where the main components are indicated, corresponding to the control volume hydrodynamics, flow path and heat structures MELCOR code packages. In this model, the core region is represented using one control volume (CV120) as well as the riser zone (CV130), the dome (CV140), the steam generators zone (CV160), downcomer (CV180) and finally the lower plenum (CV110). The volume CV125 represents the cooling channels inside core shroud structure and CV170 models the fluid region among steam generators. All relevant flow paths and solid structures were modelled using the corresponding MELCOR components.

Core model: the axial and radial core nodalizations implemented for the MELCOR core package are schematically presented in Figs. 134 and 135, respectively. The core package is mainly used to model core components heating, degradation and relocation processes along the progression of a severe accident, together with the oxidation processes and the consequent hydrogen production. A total of fourteen axial levels were implemented for the core and lower plenum regions (Fig. 133). Radial nodalization is consistent with the radial arrangement of fuel assemblies (Fig. 135). Axially, the lower plenum region was modelled using four levels, and seven levels were used for active core region.

The components included in this core model are the following:

— Fuel;
— Cladding;
— Control rods;
— Core shroud;
— Lower core support plate;
— Lower plenum structures.

Also, the core power was modelled using the MELCOR core package in conjunction with the decay heat package, implementing a radial and axial distribution of power.

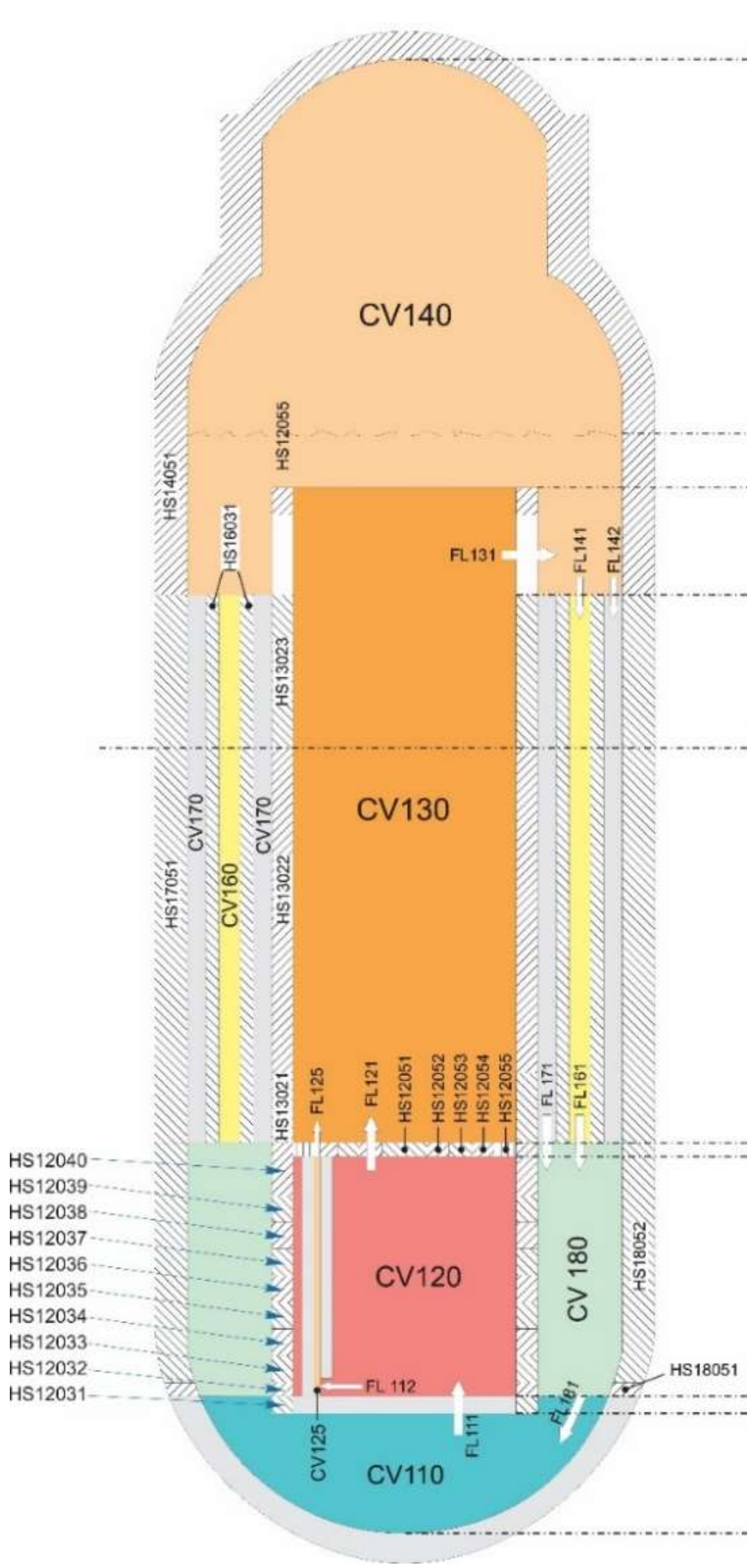

FIG. 133. MELCOR model nodalization for CAREM-like primary system.

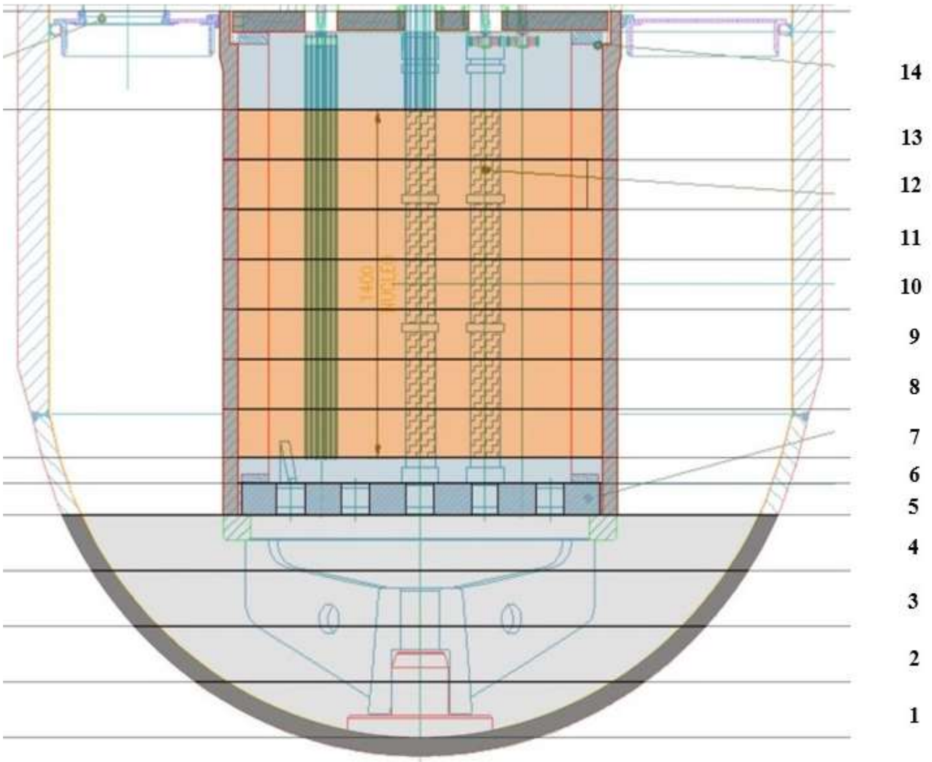

FIG. 134. MELCOR core model - axial nodalization.

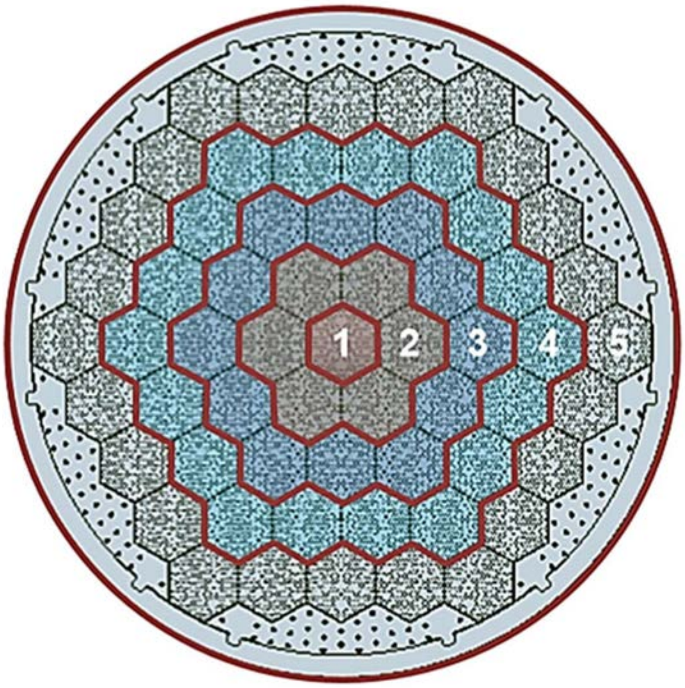

FIG. 135. MELCOR core model - radial nodalization.

Containment model: each of the containment rooms was represented in the MELCOR model using a separated control volume, and most of the interconnection between rooms were modelled using flow paths together with control functions. Most of the containment building structures were included in this model, represented using the heat structure MELCOR component. The corresponding nodalization is schematically presented in Fig. 136 where it can be distinguished between drywell and wetwell volumes as follows:

- Drywell rooms: CV900, CV901, CV902, CV910, CV960 and CV970. All of these rooms are interconnected through structural openings in floors, ceilings or walls;
- Suppression pool room: CV930;
- Passive residual heat removal system rooms: CV940 and CV950.

The ducts connect the drywell with the suppression pool, and the PRHRS rooms with the suppression pool, to mitigate possible containment over pressurization following an accident, using the suppression pool as containment final heat sink. All these connections were modelled using flow path MELCOR components.

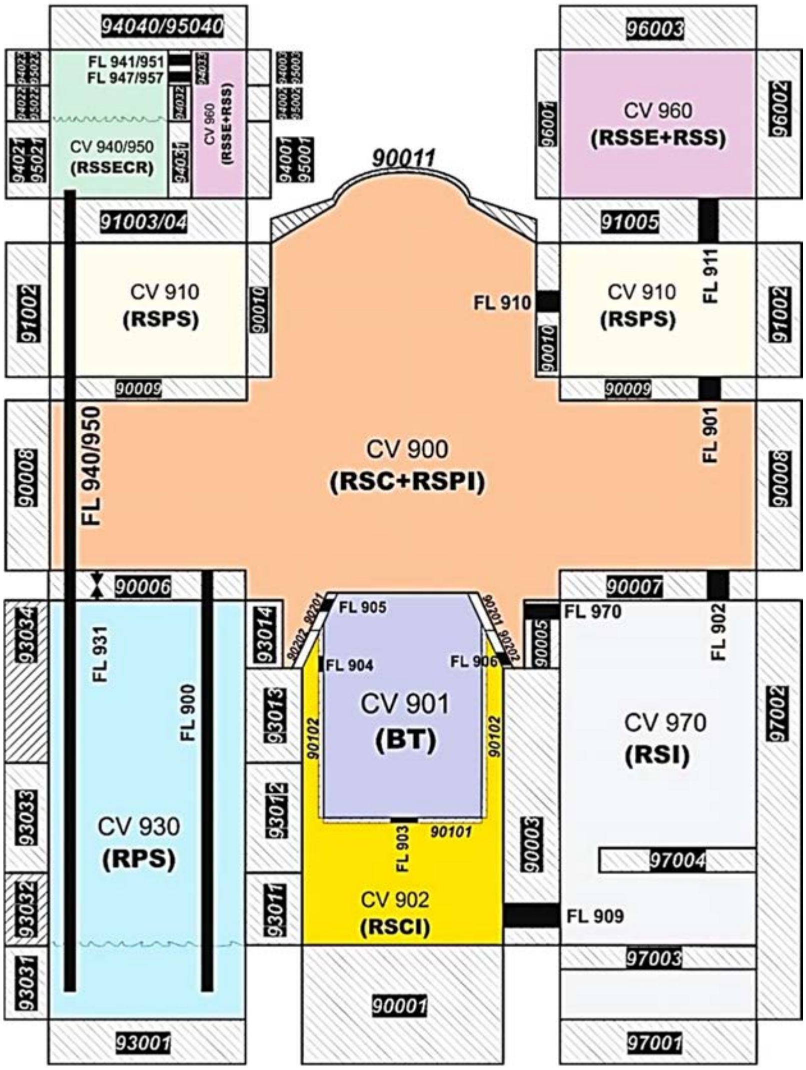

FIG. 136. MELCOR model nodalization for CAREM-like containment.

<u>*RPV external cooling model*</u>: this system was modelled in a very simplified way in MELCOR, taking into consideration just the required connections to implement the external water injection inside the thermal shielding structure surrounding the RPV. The external water is injected through FL907, taking the liquid from a boundary condition volume (CV903). Also, the connections to model the water drainage (FL903) and the steam release during the system actuation (FL904) were included as part of the containment model. The system nodalization is presented in Fig. 137.

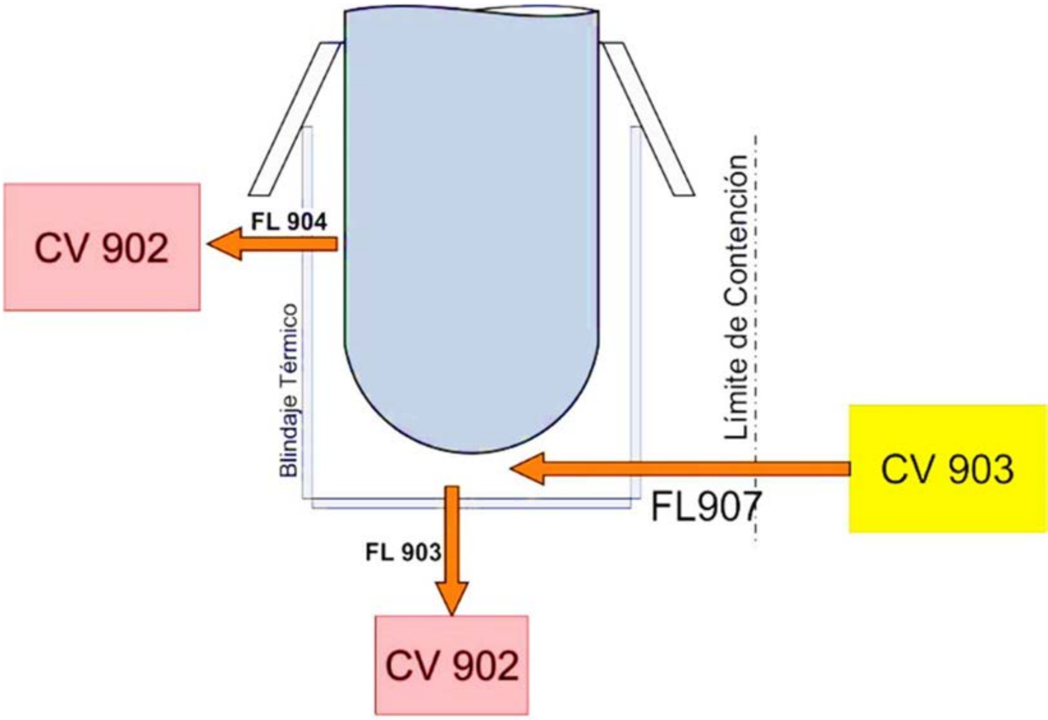

FIG. 137. MELCOR model nodalization for in-vessel melt retention system.

2.3.7.5. Methodologies and tools for the uncertainty and sensitivity analysis

The general methodology to be applied for this uncertainty analysis [80] is schematically presented in Fig. 138. The plant MELCOR model is firstly developed, adjusting the corresponding steady state and simulating different accident scenarios in order to verify the model behavior and the expected phenomena. After that, the key parameters affecting the defined FOM's are identified and selected for the following uncertainty analysis. For each of the selected parameter the corresponding range and probability distribution functions are defined. This process is done taking relevant previous uncertainty analysis with MELCOR code as a reference, together with expert judgement related to CAREM-like particular characteristics. This analysis is based on the application of Wilks' formula [81] to address a convenient number of population samples. In order to follow this approach, a minimum number of simulations is needed corresponding to the desired level of confidence in the results, sampling the variables affecting the defined FOM's. DAKOTA code is used as the calculation tool for sampling and managing the interface with the plant code, which in this case is MELCOR 1.8.6. Finally, after sampling and simulation process, DAKOTA is used for the post-processing of the results, calculating a range for the selected FOM and some sensitivity coefficients.

The FOM's chosen for the present uncertainty analyses are related to the timing of key events for the in-vessel severe accident progression. The selected FOM's are the following:

- Core uncovery time;
- Onset of core degradation time;
- Core relocation to lower plenum time.

All of these FOM's are directly related to the in-vessel phase of the severe accident and the estimation of a range for their values represents a relevant input for the development and implementation of possible strategies of the severe accident management program.

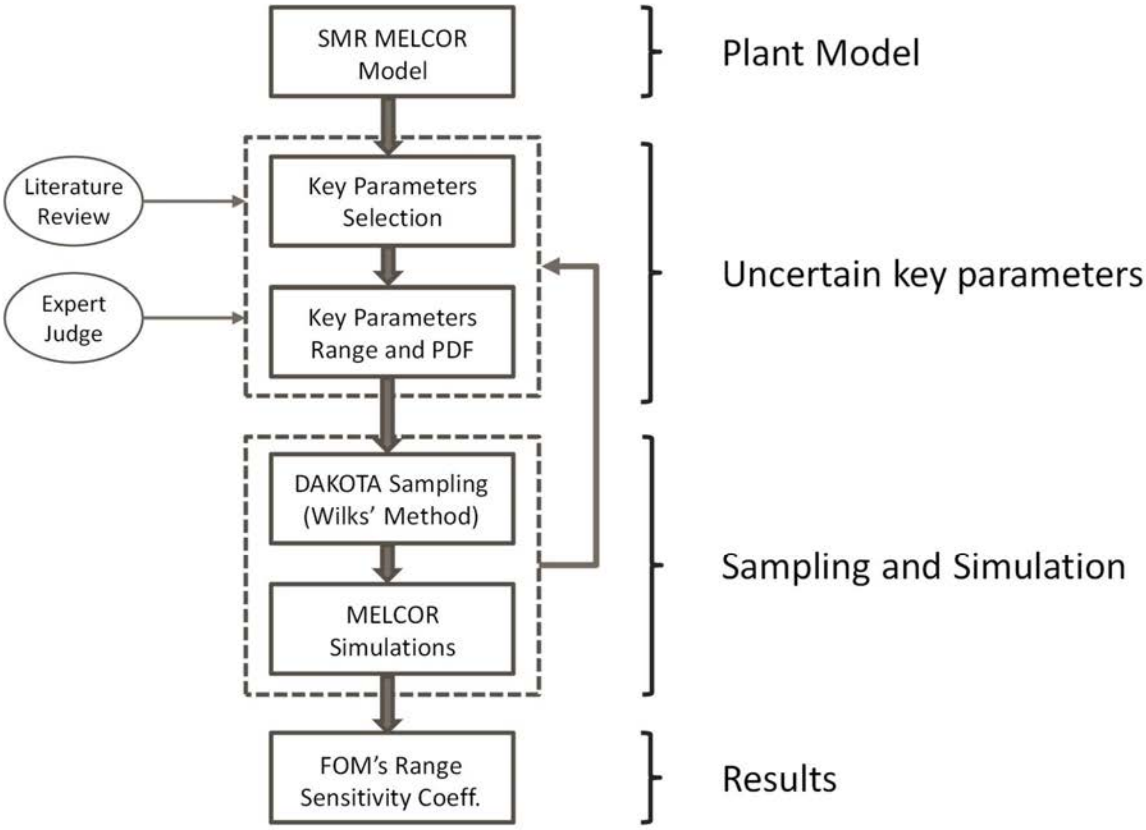

FIG. 138. General uncertainty analysis methodology.

<u>*Uncertainty and sensitivity calculation scheme with DAKOTA coupled to MELCOR code [80]*</u>

DAKOTA [82, 83] is a publicly licensed programmable interface to perform different kind of analysis related to a model, such as uncertainty, parametric or sensitivity studies. It can be coupled to a calculation code (e.g.: RELAP, MELCOR, etc.) to assess a dynamic environment in which one can easily manage huge quantities of simulations. In this work, Dakota 6.10 was considered to assess uncertainty and parametric analysis. In the next section, a Dakota input deck is fully descripted to assess an uncertainty analysis in case of coupling with the MELCOR code for performing severe accidents simulations. The mentioned input was the first formal approach to a complete uncertainty analysis and a solid basis to get knowledge and develop the later version of the work. A DAKOTA study [81, 82] to perform an uncertainty analysis is shown in Figs. 139 and 140, using DAKOTA coupled to the MELCOR calculation code.

A batch execution software called 'simulator_CRP_v2.bat' can be noticed in Fig. 139, acting as the 'analysis_driver' described in the previous sections to carry out the pre-processing, the execution of the calculation code and the post-processing. Coupling with the calculation code, construction of each input from a generic one with the parameters specified by DAKOTA and extraction of the responses from the code's output information is performed by the mentioned software. A loss of coolant event for an integral type reactor was modelled in the MELCOR input deck, locating the generic input files in a directory called ‘input’. As the input for MELCOR was distributed in several files, a master input was created in the mentioned folder, while the rest of the files were placed in the subdirectory 'R-I-F' of the folder 'input'. Since each of those files corresponds to a section of the generic input developed, marks of the type {V1}, {V2}, {V3}, etc. were located in the places that corresponds to the parameters with descriptors called V1, V2, V3, etc. in the input for DAKOTA. MELCOR executable files, pre-processing and post-processing files, as well as the previously mentioned ‘simulator_CRP_v2.bat’ file were included in the ‘templatedir’ folder.

```
environment
  tabular_data
    tabular_data_file 'data_CRP_v2.dat'
  output_file 'output_CRP_v2.out'
  error_file 'errors_CRP_v2.err'
  write_restart 'restart_CRP_v2.rst'

method
 id_method = 'UQ'
 sampling
   sample_type random
   wilks
     probability_levels = 0.95 0.95 0.95
     confidence_level 0.95
   seed = 9999
 response_levels  = 0.2 0.4 0.6 0.8
                    0.2 0.4 0.6 0.8
                    0.2 0.4 0.6 0.8
 distribution cumulative

interface
 failure_capture
    recover NaN NaN NaN
 fork
    asynchronous
      evaluation_concurrency 8
    analysis_driver = 'simulator_CRP_v2.bat'
    parameters_file = 'parameters.dat'
    results_file    = 'results.out'
    work_directory directory_tag
    copy_files = 'templatedir/*'
    named 'simu' file_save  directory_save
```

FIG. 139. Sections of the environment, method and interface of the input developed for DAKOTA.

```
# AM: Parameters regarding Accident Management
# PM: Parameters regarding Physical Models
# RM: Parameters regarding Relocation Models
# IC: Parameters regarding Integrity Criteria
variables
 lognormal_uncertain 3
    lower_bounds   1.0E-10   0.85   0.002
    upper_bounds   28800.0   1.2    0.05
    means          8103.1    1.0    0.045
    std_deviations 10621.78  0.1    0.0085
    descriptors    'AM_1'    'PM_1'  'RM_1'

 uniform_uncertain 5
    lower_bounds 0.01   0.02   26.64  0.0    100.0
    upper_bounds 0.25   0.3    44.4   1.0    1000.0
    descriptors  'PM_2' 'PM_3' 'PM_4' 'RM_3' 'RM_4'

 normal_uncertain 3
    means          2500.0 2400.0 0.4
    std_deviations 70.0   55.0   0.08
    descriptors    'IC_1' 'IC_2' 'RM_2'


# FOM-1: START OF CORE UNCOVERY
# FOM-2: START OF CORE DEGRADATION
# FOM-3: START OF RELOCATION TO LOWER PLENUM
responses
 response_functions 3
    descriptors 'FOM-1' 'FOM-2' 'FOM-3'
    no_gradients
    no_hessians
```

FIG. 140. Variable sections and input responses developed for DAKOTA.

For all the simulations to be carried out, new folders will be generated in the root directory called “simu.1”, “simu.2”, “simu.3”, etc., where the content of the 'templatedir' folder will be copied. It can be seen in the 'method' section of the DAKOTA input that an analysis of the type ‘Uncertainties Quantification’ is defined, using random sampling and the Wilks formula with the parameters of probability and confidence levels specified for the three responses that the study contains. Some generic probability levels are included in the mentioned section to condense the information from the response histograms.

The random sampling option selection was based on the extremely high computational cost associated to the addition of new simulations to a study already carried out using a LHS. In the case of an analysis with the LHS, new tests can be added using the 'refinement_samples' card but only doubling the number of original tests. In the event of errors during any of the simulations with the MELCOR code, it would not be feasible from a practical point of view to add new tests, so the study statistics could be compromised.

Using random sampling no problems like those are likely to be found since all the tests are considered independent and as many tests as necessary can be added to the study in the future to extend it. Repeatability in the test was reached by using a seed in the development with the value '9999'. That value can be modified, however, to any other integer, but it is kept unchanged when adding new tests to extend the study from a restart file.

In the 'variables' section it can be seen that a total of eleven variables with different probability distributions were used: three of them were assigned a lognormal distribution, five of them a uniform distribution and the last three parameters a normal distribution. Parameters and descriptors with their names were defined for them. Names were qualitatively divided into four groups taking into account the characteristic or origin of each variable, so the descriptors were named with the initials 'AM', 'PM', 'IC' and 'RM' (Accident Management, Physical Models, Integrity Criteria and Relocation Models, respectively).

In the 'responses' section, it can be noticed that the descriptors were presented for each of the three responses the study has, and the numerical calculation of Hessians or gradients is not requested. It is important to note that a significant increase in the number of required simulations (which could become considerable depending on the type of calculation) can be originated by those type of calculations in the responses section. Characteristic times in the dynamic of the severe accident are represented by responses in this scheme.

In the 'interface' section, eight processes were set to be launched simultaneously to speed up the analysis, according to an 8-CPUs computer. It can also be seen in the aforementioned section that the 'recover' option on the 'failure_capture' card was considered to discard responses in the statistics calculus if failures in the execution of the MELCOR code were presented.

The execution of the batch file 'postpro_PI.bat' by the software 'simulator_CRP_v2.bat' mentioned above is done in the post-processing stage. A legend in the output information that MELCOR writes to the console through some control function is searched by the post-processing batch file for each of the responses. For instance, for the first response called "FOM-1", this legend is "START OF CORE UNCOVERY", which corresponds to the message that a logical control function writes when activated. Time at which that message was written is taken when the batch file reads the mentioned caption from the shell data.

The time at which the core degradation starts and the time at which relocation to the lower plenum takes place are considered by the two remaining responses, respectively. Messages associated to those last responses will be looked for by the batch file in the post-processing stage.

Uncertain parameters and related probability distributions

After the development of the plant model, the key parameters affecting the defined FOM's are planned to be identified and selected in order to perform the intended uncertainty analysis.

(1) Methodology applied

The methodology applied for the identification and selection of parameters consists of the following steps:

— Initial identification of parameters

— Preliminary selection of parameters
— Multiple revisions of selected parameters
— Final list of selected parameters

Each of these steps are presented in the following titles.

(2) Initial identification of parameters

First, a general identification of possible parameters to be included in the analyses was performed. This was done considering at first all parameters of the different MELCOR code packages that could have any possible impact on FOM's. It is important to mention that model switches were not taken into account for the present uncertainty analyses. There are just a few parameters concerning model switches and their impact on FOM's that are not considered relevant.

The identified parameters were listed using a spreadsheet table whose format is shown in Table 55 specifying the MELCOR name of the general parameter, the corresponding MELCOR package, MELCOR card, and a brief description of its physical meaning and units. After that, two other columns were added to rank and select parameters according to their expected influence in FOM's values.

The physical importance indicator was defined in each case according to the criteria described in Table 56. The selected parameters for this first iteration were almost all parameters ranked with an index 3 using the explained physical importance indicator criteria.

TABLE 55. SPREADSHEET FORMAT FOR THE GENERAL IDENTIFICATION OF KEY PARAMETERS

MELCOR Parameter	MELCOR Package	MELCOR Card	Description	Units	Physical Importance Indicator	Parameter Selected
FCELR	COR	COR00003	Radiative exchange factor for radiation radially outward from the cell boundary to the next adjacent cell.	None	3	X
FCELA	COR	COR00003	Radiative exchange factor for radiation axially upward from the cell boundary to the next adjacent cell.	None	3	X
FLPUP	COR	COR00003	Radiative exchange factor for radiation from the liquid pool to the core components.	None	2	
....	....	....	....	....	....	....

(3) Preliminary selection of parameters

After the first general identification and selection of parameters, the specific model input parameters were put in more detail into the table and a total number of 83 parameters were selected and included in this detailed list.

After more exhaustive discussions about expected impact on FOM's, a detailed identification and selection of parameters was done where some physical importance indicators values were changed from the general selection list and a total of 8 parameters were selected.

TABLE 56. PHYSICAL IMPORTANCE INDICATOR CRITERIA

Physical Importance Indicator	
Value	**Expected influence in FOM's**
0	Negligible impact on FOM calculation
1	Low/indirect impact on FOM calculation
2	Medium/indirect impact on FOM calculation
3	High/direct impact on FOM calculation

(4) Multiple revisions of selected parameters

Several revisions of the selected parameters have been performed after the first detailed identification and selection step, adding comments in the last column of each table to explain the criteria used regarding changes. It is important to remark that in this step of the parameters' selection process, the criterion applied in several cases was based on sensitivity calculations using the developed plant MELCOR model.

Five parameters were added and three of them were excluded from the list, based on parametric studies. In addition to this, the resulting parameters were grouped in categories for a clearer presentation of the different kinds of parameters selected.

(5) Final list of selected parameters

A total number of 11 parameters were included in the final list of parameters selected for the following uncertainty analyses, as is shown in Table 57.

(6) Range and PDF for the selected parameters

The next step in the methodology proposed for the uncertainty analyses is a definition of the ranges and probability distribution functions for the selected parameters. To do this, an exhaustive literature review was conducted taking it as a basis, together with the expert judge criteria associated with CAREM-like design particular characteristics to apply to define the values as presented in Table 57.

TABLE 57. LIST OF SELECTED KEY PARAMETERS WITH THEIR RANGES AND PROBABILITY DISTRIBUTION FUNCTIONS

	Parameter	Units	Min	Max	PDF	Ref.	Comments
			Accident Management				
1	Delay in RPV external water injection time.	s	0	28800	LogNormal	Expert Judge, [84]	Mu: 8.5, Sigma: 1 (normal equivalent distribution). Human Factors are considered the main contributors to the uncertainty of this parameter. The effect of the uncertainties in other parameters are considered negligible.
			Physical Models				
2	Decay power multiplicative scale factor.	None	0.85	1.2	LogNormal	[85]	According to the work in previous CRP related to uncertainties.
3	Radiative exchange factor for radiation radially outward from the cell boundary to the next adjacent cell.	None	0.01	0.25	Uniform	[86]	
4	Radiative exchange factor for radiation axially outward from the cell boundary to the next adjacent cell.	None	0.02	0.30	Uniform	[87]	
5	Zircaloy Oxidation Rate Constant Coefficients - low temperature range constant coefficient	$kg^2/m^4.s$	26.64	44.4	Uniform	[88],[89], Expert Judge	Proposed Best-Estimate value in between Urbanic-Heidrick and Lemmon correlations. It was verified that it is possible to move from one correlation to the other modifying the leading coefficient, because proposed *Kp* shapes are very similar for $T < 1580^oC$.
			Integrity Criteria				
6	Temperature at which oxidized fuel rods can stand when unoxidized Zr is absent from the cladding.	K	2,400	2,800	Normal	[88]	Median value: 2,500K. Estimated standard deviation: 70 K.
7	Maximum ZrO_2 temperature permitted to hold up molten Zr	K	2,250	2,550	Normal	[88]	Median value: 2400K. Estimated standard deviation: 55K.
			Relocation Models				
8	Particulate debris equivalent diameter.	m	0.002	0.05	Log-normal	[88]	Median value: 0.045 m. Estimated standard deviation: 0.0085 m.
9	Porosity of particulate debris for all cells in axial level jj.	None	0.1	0.5	Normal	[88],[89]	Median value: 0.4. Estimated standard deviation: 0.08.
10	Fraction of channel volume denied to particulate debris by presence of fuel rods, FU and/or CL.	None	0.0	1.0	Uniform	Expert Judge	Complete range considered with uniform distribution, due to lack of knowledge.
11	Time constant for the radial relocation of solid material.	s	100	1,000	Uniform	[90]	

2.3.7.6. Results

Steady-state and reference case [1]

The simulation of the reference case for representing a SBLOCA and station blackout event with failure of all DID Level 2 and Level 3 heat removal and injection systems was performed using the described CAREM-like plant MELCOR model and implementing the postulated severe accident conditions presented. The reference case values chosen for the selected parameters are the ones indicated as 'Input Values' in Table 57. Before simulating the postulated severe accident, the normal plant operation steady state was calculated using the developed MELCOR model. The results obtained for some of the main plant characteristic variables are presented in Table 58.

TABLE 58. CAREM-LIKE STEADY STATE VALUES

Variable	Value
Total power (MW)	100
Primary system pressure (dome) (MPa)	12.25
Inlet core mass flow rate (kg/s)	420
Inlet core temperature (°C)	285
Outlet core temperature (°C)	325
Containment drywell pressure (MPa)	0.1
Containment drywell temperature (°C)	30
Suppression Pool temperature (°C)	30

As it was explained previously, the postulated severe accident scenario consists of a loss of coolant event with success of the core shutdown system and failure of all residual heat removal and injection systems, except for the external RPV cooling system after core degradation (in-vessel melt retention).

The evolution of the LOCA mass flow rate is shown in Fig. 141, which in turns leads to the primary system depressurization presented in Fig. 142, and the corresponding RPV level decrease shown in Fig. 143. Also, core active zone limits are indicated in Fig. 144. It is important to note from this figure the significant amount of liquid water above the core. This is a particular characteristic of this kind of reactor with integrated primary system, which delays core uncovery time in case of severe accident. Cladding temperature evolution for different axial positions of the central core ring is presented in Figs. 145 and 146 shows in more detail the cladding temperature at the top position. As it is indicated in this figure the fuel heat up rate is very low, about 0.07 K/s, which is also a particular characteristic of this type of reactor design, as a consequence of the low power density in core region. Considering this low heat up rate, it is expected a slow core degradation process, with a significant cladding oxidation. Core support plate temperatures are shown in Fig. 147 to identify the core plate failure time (about 13 h after initiating event). Finally, last two figures are related to the cladding oxidation process and the consequent hydrogen production. The evolution of total zircaloy mass and zirconium dioxide mass is shown in Fig. 148. From this figure it is possible to see that about 60% of the total initial zircaloy mass is oxidized during the in-vessel phase of the severe accident. The resulting hydrogen production evolution is shown in Fig. 148. The RPV lower head never fails during this simulation, due to the actuation of the external RPV cooling system.

The corresponding values for the FOM for the reference case simulation are presented in Table 59.

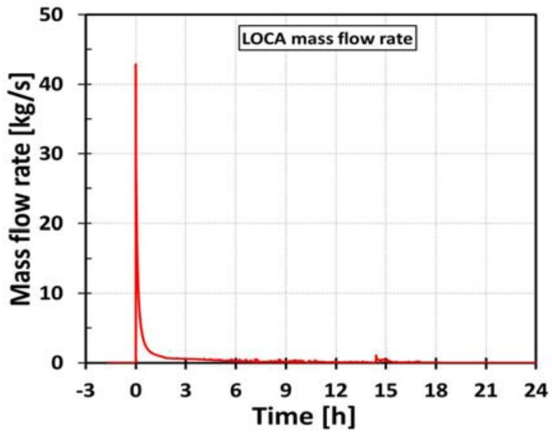

FIG. 141. LOCA mass flow rate evolution.

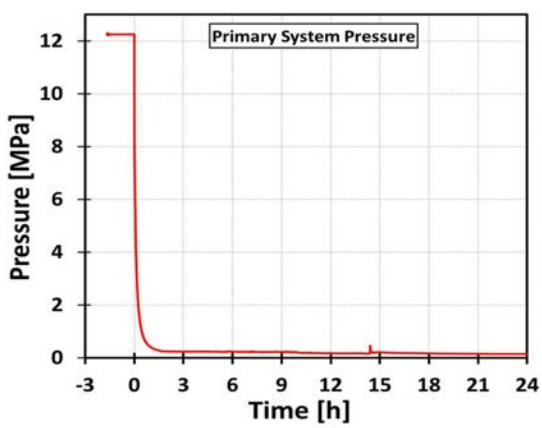

FIG. 142. Primary system pressure evolution.

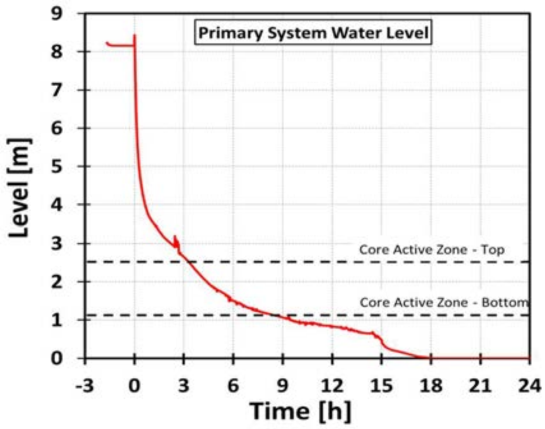

FIG. 143. RPV liquid level evolution.

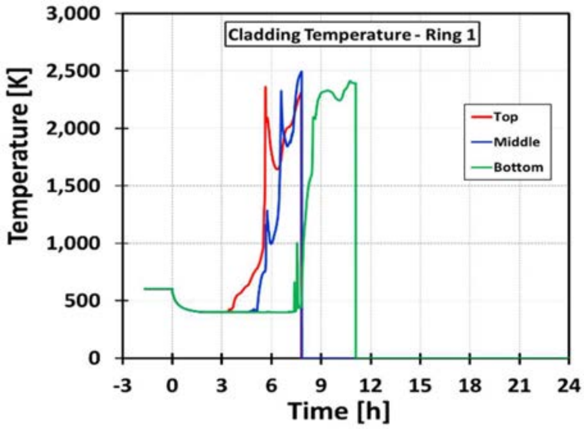

FIG. 144. Cladding temperatures evolutions for the core central ring.

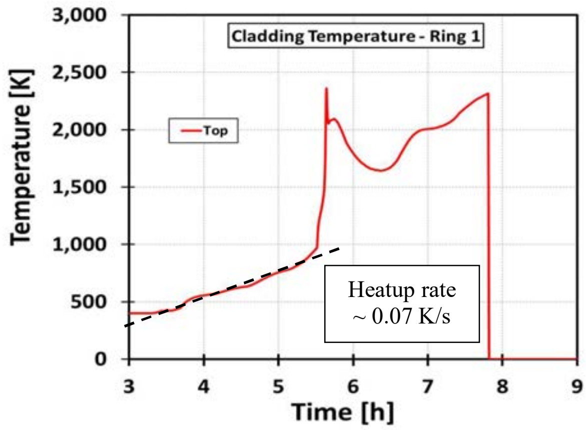

FIG. 145. Cladding temperature evolution for the top of core central ring.

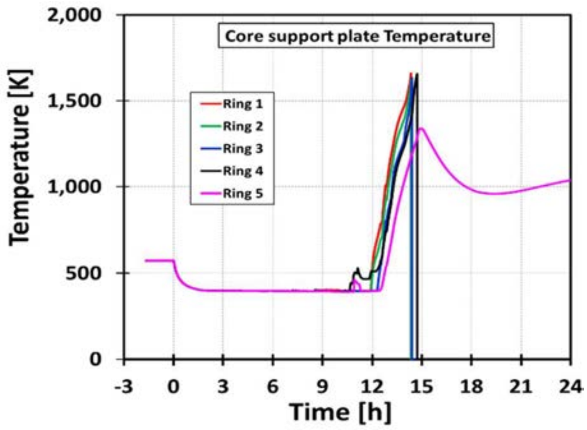

FIG. 146. Lower core support plate temperature evolution.

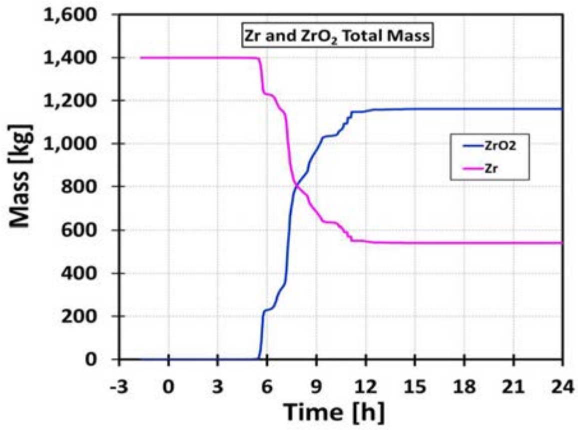

FIG. 147. Total mass of Zry and ZrO_2 evolutions.

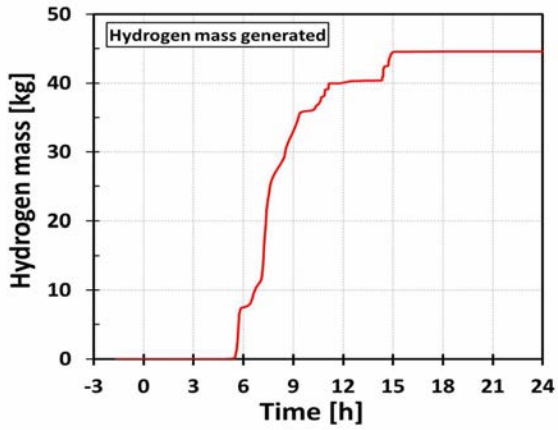

FIG. 148. Hydrogen production evolution.

TABLE 59. FOM VALUES FOR THE REFERENCE CASE (SBLOCA WITH DID LEVEL 2 AND LEVEL 3 SYSTEMS FAILURE)

FOM Variable	Value
Core uncovery (h)	3.3
Onset of core degradation (h)	5.5
Core relocation to lower plenum (h)	14.3

Core uncovery time was calculated from Fig. 143 as the time when water level reaches the core active zone top. The onset of core degradation was considered as the time when particulate debris first appears. Taking into account that the first debris material appears at the top central region of the core, Fig. 145 was used to calculate the onset of core degradation. In MELCOR, when the intact material is converted into particulate debris the corresponding component temperature is set to zero. This was used in Fig. 145 to find out the onset of core degradation time. Finally, the core relocation to lower plenum time was associated to the core support plate failure time. This was calculated from Fig. 147, taking into account again that after component failure its temperature falls down to zero.

Input deck developed for DAKOTA and plot variables

The input text file developed for DAKOTA to run the uncertainty scheme is shown in Fig. 149. It is highly based on the input deck explained previously, with small differences regarding the distribution's parameters of the 'variables' section to take into account the data presented in Table 57. Different parts of the input deck can be noticed in the file including all details about the scheme.

Some relevant MELCOR variables were added to the model by using the External Data File MELCOR package to obtain useful information to make plots after the analysis performed by DAKOTA. Water level, primary system pressure and temperature as well as hydrogen production were included.

```
environment
  tabular_data
    tabular_data_file 'data_CRP_v3.dat'
  output_file 'output_CRP_v3.out'
  error_file 'errors_CRP_v3.err'
  write_restart 'restart_CRP_v3.rst'

method
 id_method = 'UQ'
 sampling
  sample_type random
  wilks
   probability_levels = 0.05 0.1 0.15 0.2 0.3 0.4 0.5 0.6 0.7 0.8 0.85 0.9
0.95
                  0.05 0.1 0.15 0.2 0.3 0.4 0.5 0.6 0.7 0.8 0.85 0.9 0.95
                  0.05 0.1 0.15 0.2 0.3 0.4 0.5 0.6 0.7 0.8 0.85 0.9 0.95
   confidence_level 0.95
  seed = 9999
 distribution cumulative

# AM: Parameters regarding Accident Management
# PM: Parameters regarding Physical Models
# RM: Parameters regarding Relocation Models
# IC: Parameters regarding Integrity Criteria
variables
 lognormal_uncertain 3
  lower_bounds   1.0E-10   0.85   0.002
  upper_bounds   28800.0   1.2    0.05
  means          8103.1    1.0    0.045
  std_deviations 10621.78  0.1    0.0085
  descriptors    'AM_1'   'PM_1'  'RM_1'

 uniform_uncertain 5
  lower_bounds 0.01   0.02   26.64   0.0    100.0
  upper_bounds 0.25   0.3    44.4    1.0    1000.0
  descriptors  'PM_2'  'PM_3'  'PM_4'  'RM_3'  'RM_4'

 normal_uncertain 3
  lower_bounds   2400.0  2250.0  0.1
  upper_bounds   2800.0  2550.0  0.5
  means          2500.0  2400.0  0.4
  std_deviations 70.0    55.0    0.08
  descriptors    'IC_1'  'IC_2'  'RM_2'

interface
 failure_capture
  recover NaN NaN NaN
 fork
  asynchronous
   evaluation_concurrency 8
  analysis_driver = 'simulator_CRP_v2.bat'
  parameters_file = 'parameters.dat'
  results_file   = 'results.out'
  work_directory directory_tag
  copy_files = 'templatedir/*'
  named 'simu' file_save  directory_save

# FOM-1: START OF CORE UNCOVERY
# FOM-2: START OF CORE DEGRADATION
# FOM-1: START OF RELOCATION TO LOWER PLENUM
responses
 response_functions 3
  descriptors 'FOM-1' 'FOM-2' 'FOM-3'
  no_gradients
  no_hessians
```

FIG. 149. Input deck developed for DAKOTA to run the uncertainty scheme.

— *First batch of simulations [1]*: after developing the MELCOR and DAKOTA models and establishing the coupling between them, the first batch of 59 simulations were released. An 8-CPU computer was used to perform the analysis and 3.5 days were needed till the completion of the study. The parameter values selected after the sampling process and the values for the FOM's were successfully obtained. Failures were reported in twelve simulations out of fifty-nine after the first launching was concluded.
— *Second batch of simulations [1]*: of 12 simulations was launched after the first one was finished to get a total number of 59 simulations without errors. Incremental sampling was added to the initial input deck in order to extend the scheme with DAKOTA. An 8-CPU computer was used to perform the analysis and 1 day was needed till the completion of the study. The parameters adopted for the second batch of simulations and the FOM's values were successfully obtained.
— *Parameters' coverage map and failure rate [1]*: normalized coverage map for the parameters of the analysis is shown in Fig. 150 taken into account the simulations without errors in the MELCOR code execution. The proper map for the simulations with errors is shown in Fig. 151. After a carefully analysis of both maps, an appropriate coverage of the parameters' domain was noticed and no failure patterns were recognize

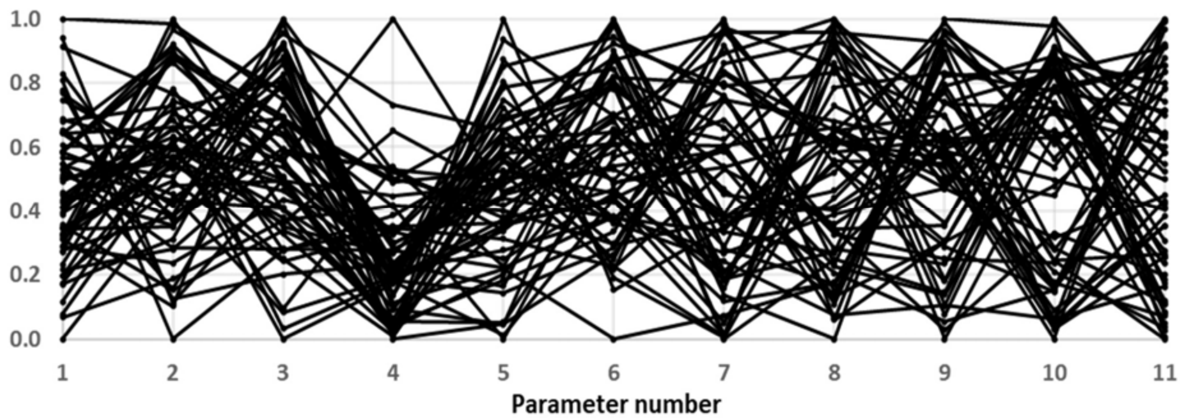

FIG. 150. Normalized parameters' coverage map for the simulations performed by DAKOTA without errors in the MELCOR code execution (reproduced from Ref. [1])

Failures on 12 simulations out of 71 were reported due to MELCOR errors during running, representing a failure rate of almost 17%. Errors raised were mostly a result of modelling issues in the bypass region of the core representation and will be taken into account for future model improvements.

— *Probability density functions of parameters*: three distinct types of mathematical functions were considered to represent the PDF's of the normalized parameters in the analysis, namely: lognormal, uniform and normal distributions. A dummy scheme was run in DAKOTA considering 1,000 samples for each PDF in order to verify that the shapes of the distributions were correct and that all the PDF's were properly defined.

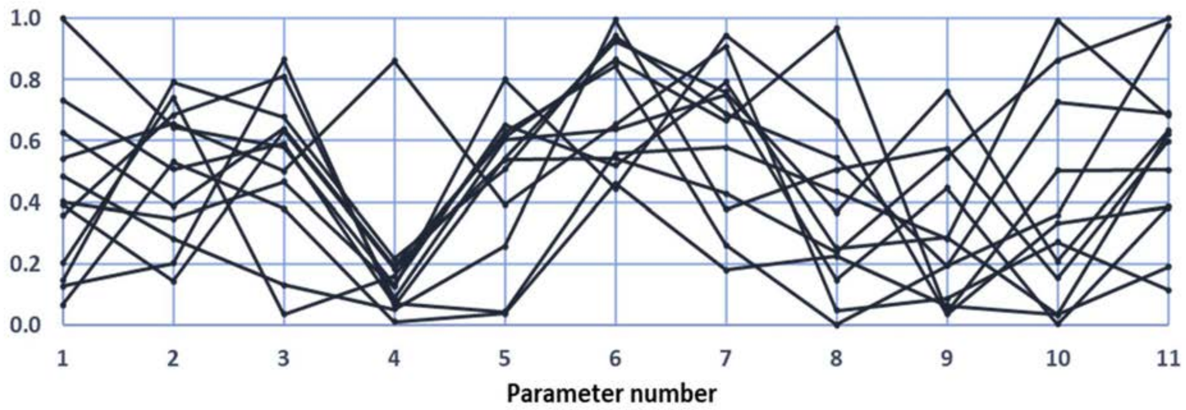

FIG. 151. Parameters' coverage map for the simulations performed by DAKOTA with errors in the MELCOR code execution.

— *Distribution and main statistics of FOMs [1]*: mean value, standard deviation, skewness and kurtosis[2] for the FOMs considered in the scheme are presented in Table 60. Dispersion of key times in the accident can be noticed as time progresses and more physical phenomena take place

TABLE 60. MAIN FOMs STATISTICS

Statistical variable	FOM-1	FOM-2	FOM-3
Mean (h)	3.36	5.77	13.6
Standard deviation (h)	0.29	0.47	1.46
Skewness	-0.204	0.403	0.411
Kurtosis	0.811	-0.517	-0.071

Maximum and minimum values for FOMs are shown in Table 61, where key times in the severe accident progression were obtained with a 95% probability level and 95% confidence level, meaning that key times selected are highly likely to fall between those limits under the assumptions made in the analysis.

TABLE 61. MAXIMUM AND MINIMUM VALUES FOR FOMs

Parameter	FOM-1	FOM-2	FOM-3
Maximum (h)	3.97	6.78	16.87
Minimum (h)	2.44	4.83	10.93

The probability density function and its corresponding cumulative distribution function are plotted for FOM-1 in Figs. 152 and 153, respectively. The statistical mode of the distribution for FOM-1 is placed at the left of the mean value (3.36 h).

[2] Kurtosis is a measure of the tailedness of a distribution.

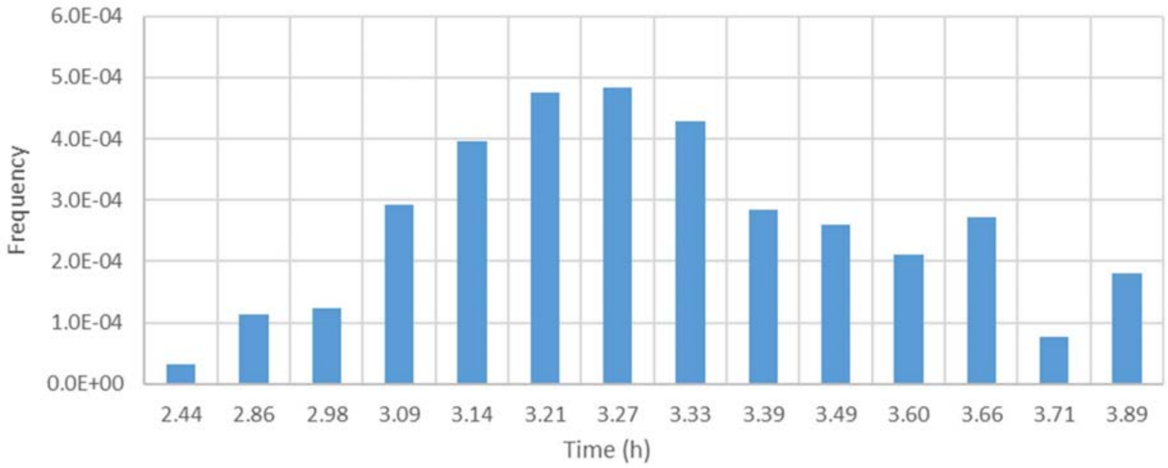

FIG. 152. Probability density function of FOM-1 obtained after running the scheme (reproduced from Ref. [1])

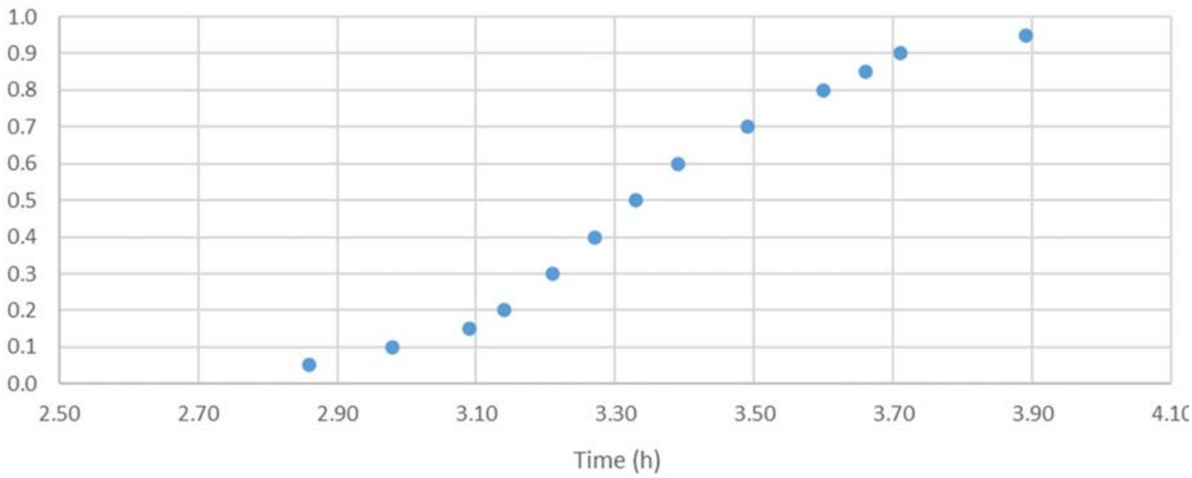

FIG. 153. Cumulative distribution function of FOM-1 obtained after running the scheme.

The probability density function and its corresponding cumulative distribution function are plotted for FOM-2 in Figs. 154 and 155, respectively.

The statistical mode of the distribution for FOM-2 is placed at the left of the mean value (5.77 h) and the standard deviation is greater than the one for FOM-1, as time goes by and the distributions for key times tend to flatten.

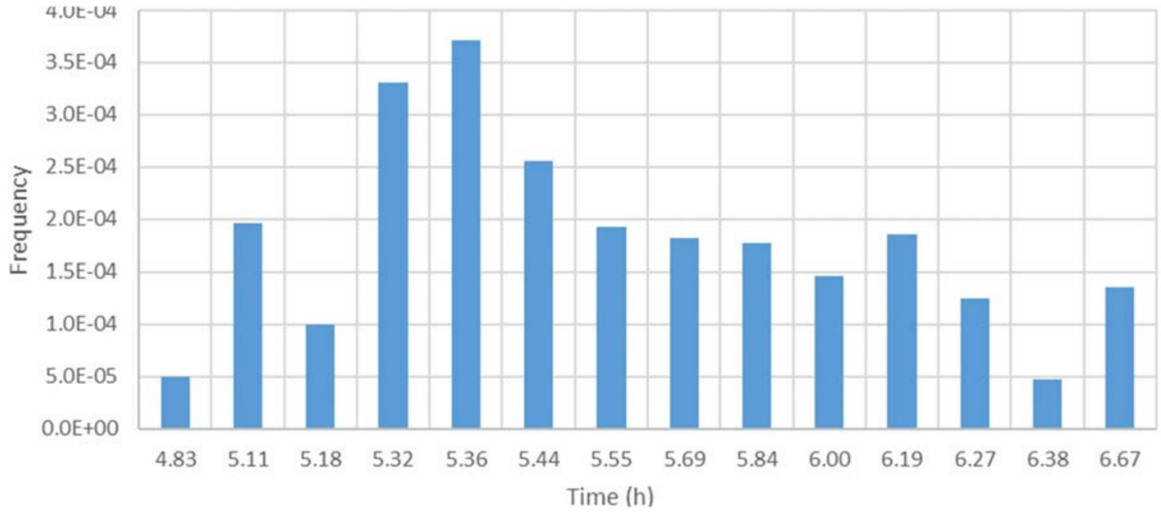

FIG. 154. Probability density function of FOM-2 obtained after running the scheme (reproduced from Ref. [1])

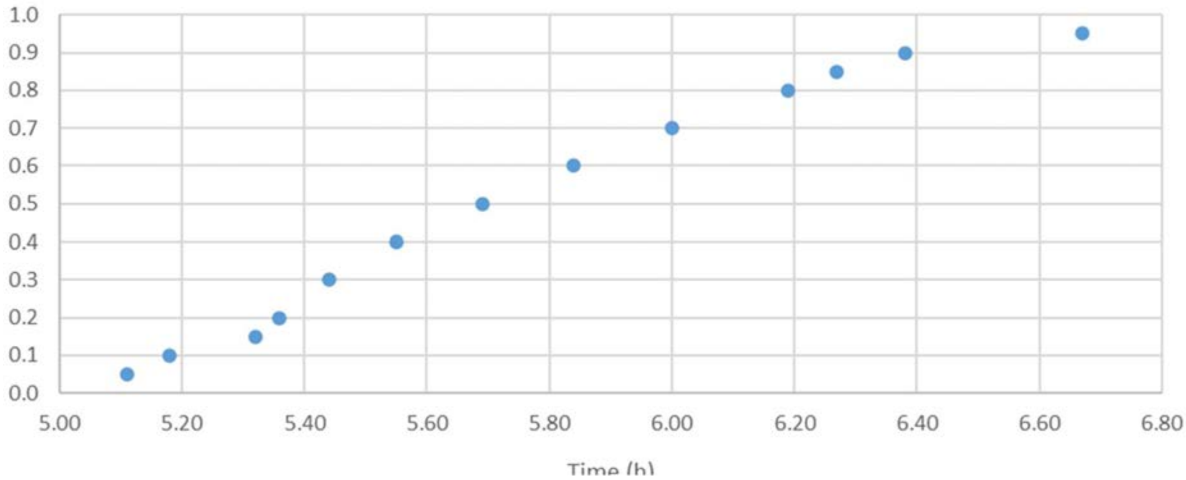

FIG. 155. Cumulative distribution function of FOM-2 obtained after running the scheme.

The PDF and its associated CDF are plotted for FOM-3 in Figs. 156 and 157, respectively.

The standard deviation for FOM-3 is greater than the one for FOM-2 since the dispersion of the distribution is larger and a more complex rising of the CDF is noticed.

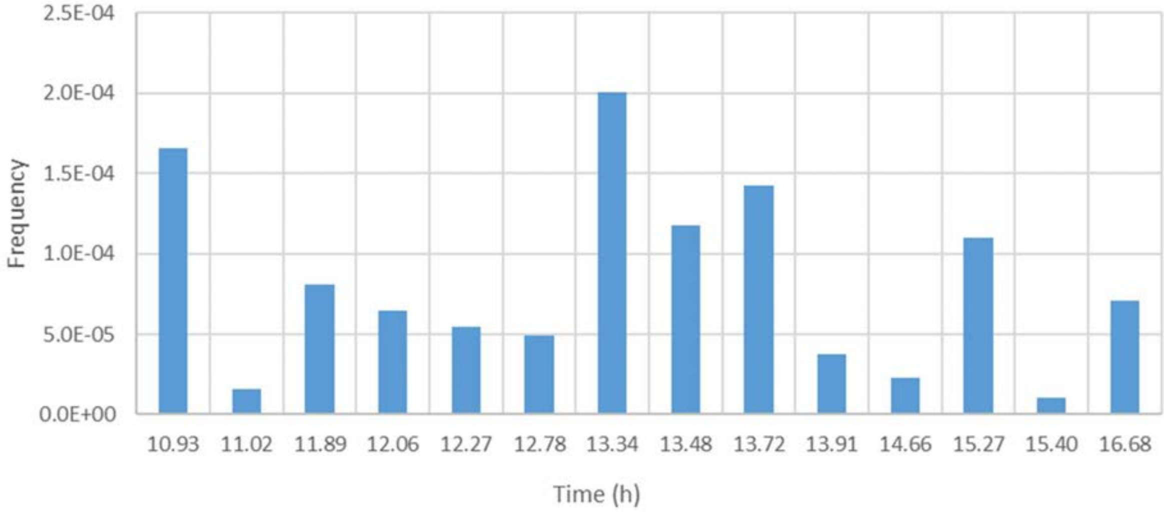

FIG. 156. Probability density function of FOM-3 obtained after running the scheme (reproduced from Ref. [1])

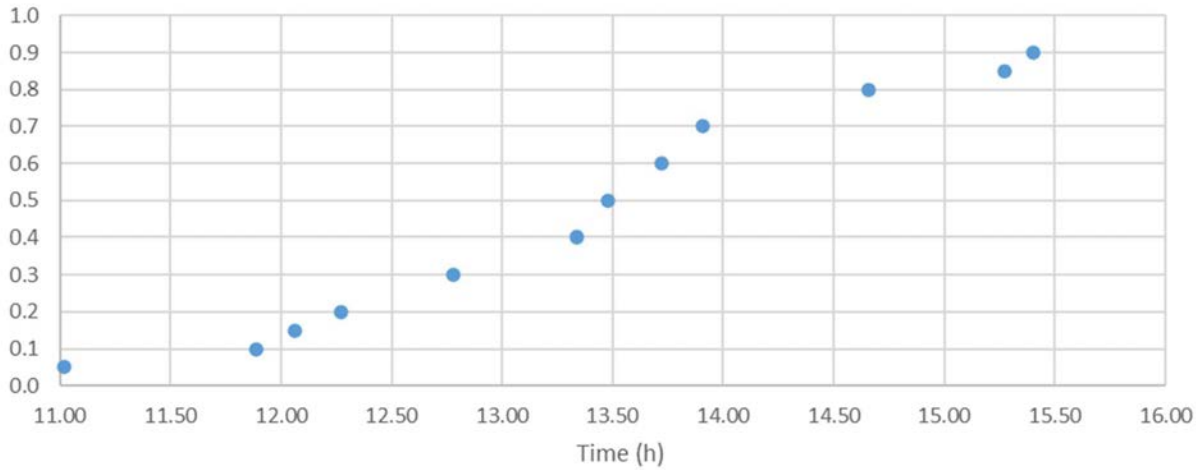

FIG. 157. Cumulative distribution function of FOM-3 obtained after running the scheme.

Dispersion of FOMs in the accident progression is shown in Fig. 158 where normalized FOMs are plotted. FOM-2 vs. FOM-1 scatter plot is less dispersed than FOM-3 vs. FOM-2 graph because more uncertainty sources are included as the accident advances.

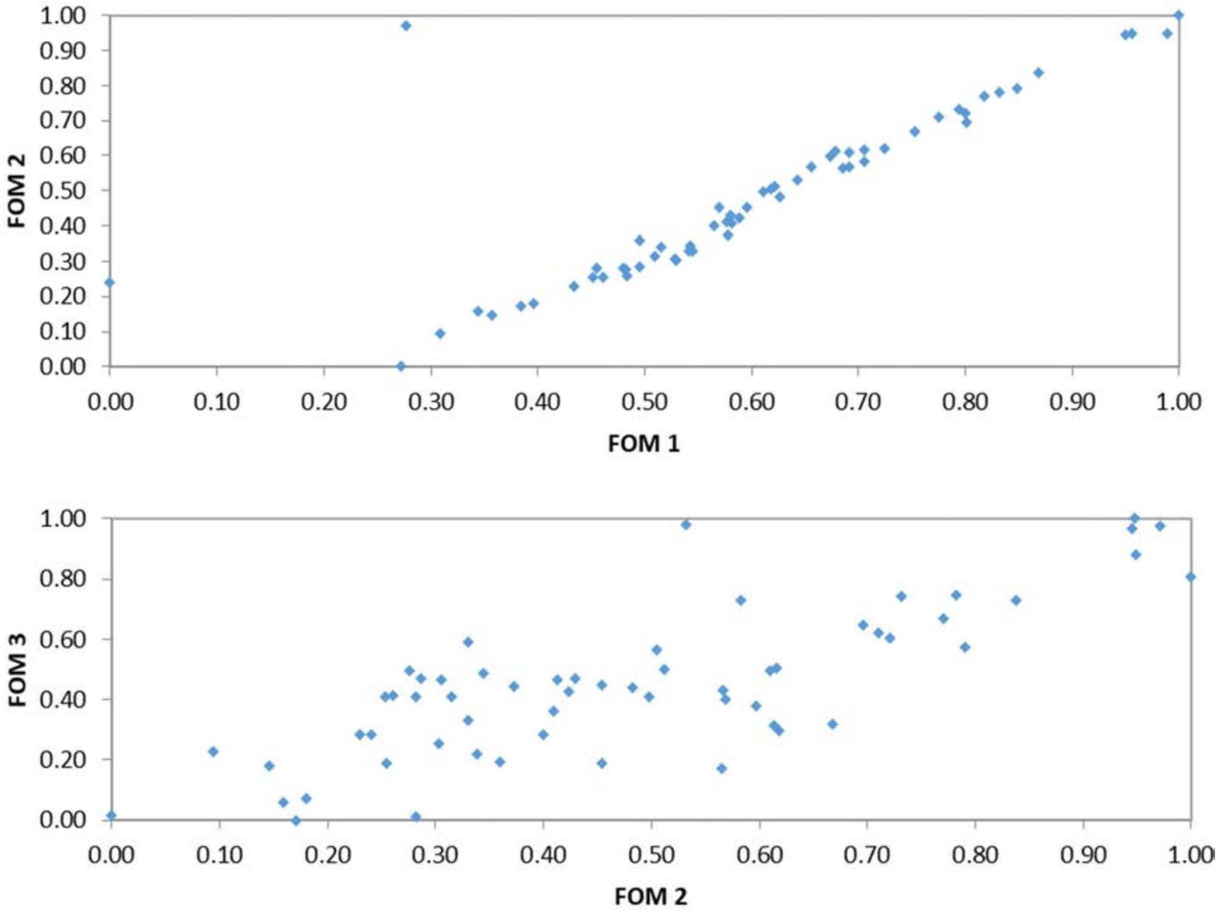

FIG. 158. Dispersion of FOM's in the accident as time progresses.

<u>*Sensitivity/correlation analysis [1]*</u>

— *Correlation matrices*: Simple correlation matrix among parameters and FOMs is shown in Table 62 and simple rank correlation matrix is shown in Table 63. Colors were used to mark the dependencies among the variables, where blue represents a high direct correlation and red represents a high inverse correlation. Partial correlation matrix and partial rank correlation matrix are shown in Tables 64 and 65, respectively, where the effect of linear correlation between parameters was fixed.

After examining the correlation matrixes, the most relevant dependencies were distinguished and are presented in Table 66 including a description of each relevant parameter and an interpretation of the correlations observed in relation to the MELCOR model.

Since FOM's were selected as key times in the accident progression, a high direct correlation can be noticed in the matrixes among them. Besides this trivial fact, all physical model parameters (PM_1 to PM_4) were considered more important than the others regarding their influence on the FOMs, and the most important one was individualized as the decay heat power multiplier (PM_1).

TABLE 62. SIMPLE CORRELATION MATRIX

	IC_1	IC_2	RM_2	AM_1	PM_1	RM_1	PM_2	PM_3	PM_4	RM_3	RM_4	FOM-1	FOM-2	FOM-3
IC_1	1.000													
IC_2	0.008	1.000												
RM_2	0.027	0.021	1.000											
AM_1	-0.068	0.022	0.058	1.000										
PM_1	-0.073	-0.014	0.001	-0.034	1.000									
RM_1	0.077	-0.006	-0.005	0.039	0.085	1.000								
PM_2	-0.097	0.008	-0.099	0.009	-0.061	-0.032	1.000							
PM_3	0.007	0.006	-0.079	-0.004	-0.021	0.069	0.027	1.000						
PM_4	0.041	0.014	-0.003	0.021	-0.011	-0.016	0.034	-0.074	1.000					
RM_3	-0.089	-0.033	0.022	-0.113	0.101	-0.009	-0.010	-0.115	-0.077	1.000				
RM_4	0.053	0.034	-0.004	-0.086	-0.033	-0.052	0.034	0.078	0.025	-0.056	1.000			
FOM-1	0.099	0.003	-0.024	0.068	-0.852	0.000	0.001	0.047	0.149	-0.098	0.116	1.000		
FOM-2	0.074	0.012	-0.003	0.011	-0.989	-0.095	0.102	0.098	-0.054	-0.099	0.009	0.827	1.000	
FOM-3	0.096	-0.015	0.088	0.043	-0.801	-0.085	0.421	-0.330	0.082	-0.059	-0.042	0.636	0.790	1.000

TABLE 63. SIMPLE RANK CORRELATION MATRIX

	IC_1	IC_2	RM_2	AM_1	PM_1	RM_1	PM_2	PM_3	PM_4	RM_3	RM_4	FOM-1	FOM-2	FOM-3
IC_1	1.000													
IC_2	0.024	1.000												
RM_2	0.014	-0.012	1.000											
AM_1	-0.069	-0.062	0.037	1.000										
PM_1	-0.048	0.022	0.061	-0.077	1.000									
RM_1	0.070	-0.014	0.038	0.046	0.097	1.000								
PM_2	-0.084	0.022	-0.097	-0.056	-0.060	-0.042	1.000							
PM_3	-0.027	0.011	-0.089	0.031	-0.084	0.096	0.015	1.000						
PM_4	0.057	0.010	-0.022	0.032	-0.019	0.006	0.046	-0.098	1.000					
RM_3	-0.110	-0.032	0.016	-0.125	0.028	0.021	-0.053	-0.139	-0.097	1.000				
RM_4	0.057	0.029	-0.021	-0.029	-0.024	-0.068	0.041	0.076	0.022	-0.102	1.000			
FOM-1	0.111	-0.030	-0.050	0.126	-0.915	-0.026	0.015	0.113	0.110	-0.009	0.083	1.000		
FOM-2	0.052	-0.035	-0.051	0.077	-0.992	-0.097	0.082	0.140	-0.061	-0.034	0.034	0.900	1.000	
FOM-3	0.151	-0.024	0.068	0.059	-0.746	-0.114	0.432	-0.328	0.127	-0.060	-0.033	0.655	0.730	1.000

TABLE 64. PARTIAL CORRELATION MATRIX

	FOM-1	FOM-2	FOM-3
IC_1	0.039	0.095	0.276
IC_2	-0.029	-0.012	-0.107
RM_2	-0.057	0.094	0.347
AM_1	0.094	-0.230	0.013
PM_1	-0.867	-0.995	-0.945
RM_1	0.148	-0.174	0.035
PM_2	-0.119	0.418	0.829
PM_3	0.058	0.610	-0.785
PM_4	0.278	-0.528	0.118
RM_3	0.029	0.013	-0.046
RM_4	0.184	-0.313	-0.209

TABLE 65. PARTIAL RANK CORRELATION MATRIX

	FOM-1	FOM-2	FOM-3
IC_1	0.163	0.167	0.394
IC_2	-0.022	-0.187	-0.042
RM_2	0.009	0.188	0.353
AM_1	0.155	0.042	0.099
PM_1	-0.924	-0.997	-0.923
RM_1	0.138	-0.069	-0.014
PM_2	-0.089	0.349	0.798
PM_3	0.114	0.547	-0.769
PM_4	0.249	-0.708	0.148
RM_3	0.126	-0.046	-0.169
RM_4	0.169	0.081	-0.157

TABLE 66. INTERPRETATION OF CORRELATION AMONG VARIABLES IN THE SCHEME FOR RELEVANT PARAMETERS

Variable	Comments	MELCOR parameter	Parameter description	Observations
FOMs	High level of correlation among FOMs	-	-	Key times are highly dependent among them.
PM_1	Strong inverse correlation with all FOMs	ARADCN	Decay power multiplicative scale factor	Higher decay power levels mean faster progressing accidents
PM_2	Highly correlated with FOM 3 and weekly correlated with FOM 2	FCELR	Radiative exchange factor for radiation radially outward from the cell boundary to the next adjacent cell	Higher levels of radial heat transfer delay relocation to lower plenum

TABLE 66. INTERPRETATION OF CORRELATION AMONG VARIABLES IN THE SCHEME FOR RELEVANT PARAMETERS (Cont.)

Variable	Comments	MELCOR parameter	Parameter description	Observations
PM_3	Highly correlated with FOM 2 (direct) and FOM 3 (inverse)	FCELA	Radiative exchange factor for radiation axially outward from the cell boundary to the next adjacent cell	Higher levels of axial heat transfer slow down core degradation but accelerate relocation to lower plenum
PM_4	Weekly correlated with FOM 2 (inverse)	C1001(1,1)	Zircaloy oxidation rate constant coefficients - low temperature range constant coefficient	Higher zircaloy oxidation rate accelerates the start of core degradation

— *Influence of relevant parameters on FOMs*: Scatter plots between relevant parameters and FOMs are shown in Fig. 159. Strong inverse correlation can be noticed between PM_1 and all the FOMs, as was stated in the previous section.

  Regarding PM_2 and PM_3, a slightly correlation can be viewed in relation to FOM-3 and no correlation is easily observed associated with PM_4. Multiple variable dependencies are difficult to be noted in one-dimension diagrams, except for the case of strong correlations, as one can see for the decay heat multiplier (PM_1).

— *Dynamics of relevant MELCOR model variables [1]*: some representative parameters of the accident progression can be observed in Figs, 160 and 161, where the primary system pressure, water level and vapor temperature are shown, respectively. Sudden depressurization at the early start of the event can be noticed, as a consequence of the postulated pipe failure, together with the primary water level decrease.

  Reference case evolutions are shown in Figs. 162 and 163 in red dashed lines located near the middle-zone of the complete set of simulations.

  Regarding the hydrogen generation during the accident, dynamic of the generation is shown for all simulations performed in Fig.163, where the reference case is presented in a red dashed line. Percentiles for the 10%, 50% and 90% values are also plotted in Fig. 163 just for clarification. By the end of the 24 h-time simulation period the hydrogen generated for the reference case is greater that the value for the 90% percentile of the complete set of simulations, showing a conservative-like election for the reference case parameters in relation to the mass of hydrogen generated.

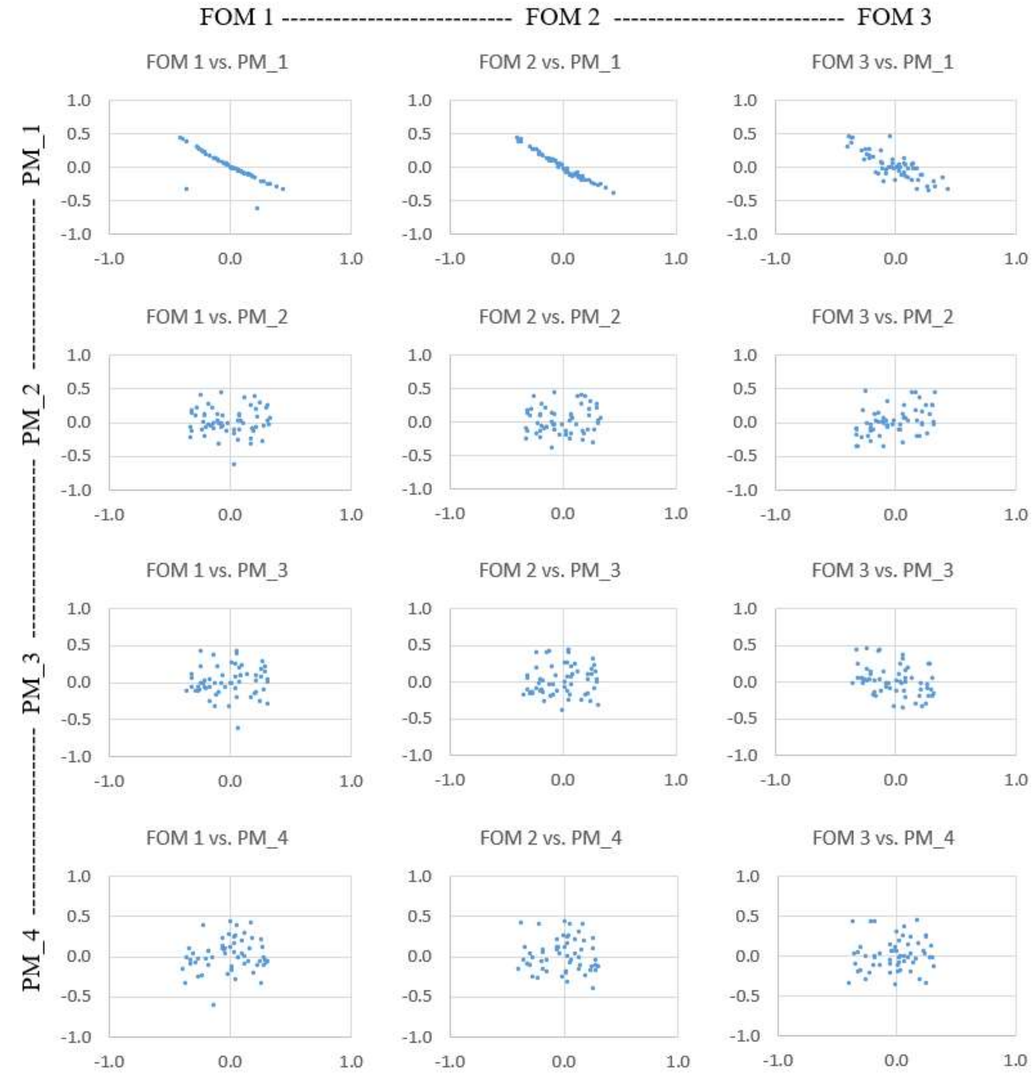

FIG. 159. Scatter plots between relevant parameters and FOMs.

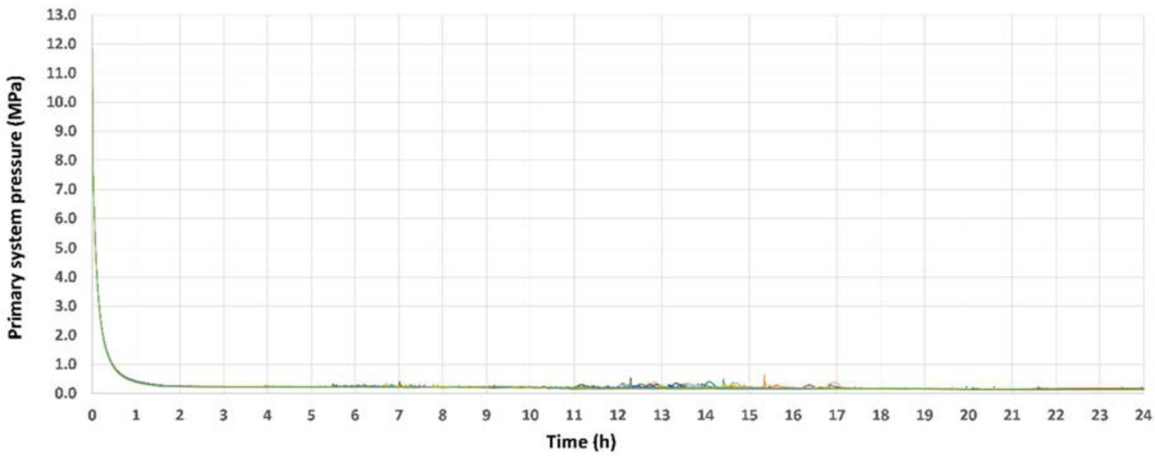

FIG. 160. Primary system pressure in the simulations.

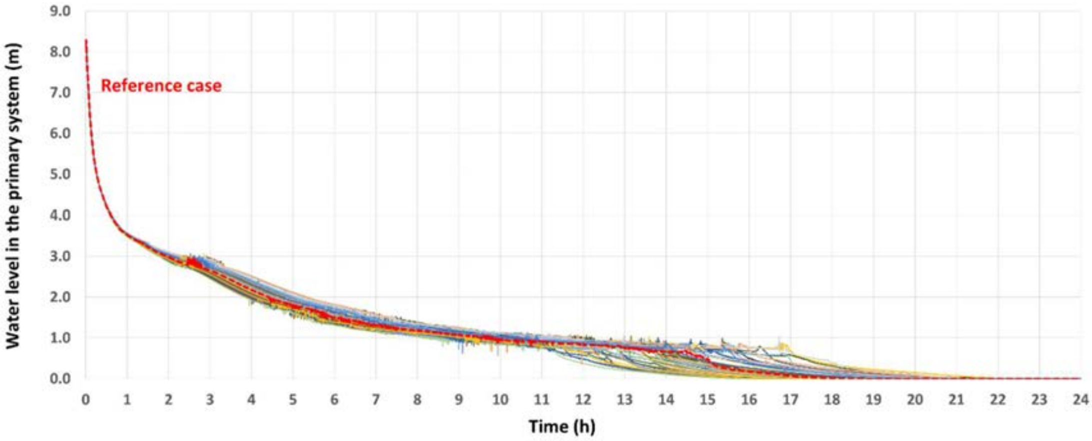

FIG. 161. Water level in the primary system in the simulations (reproduced from Ref. [1])

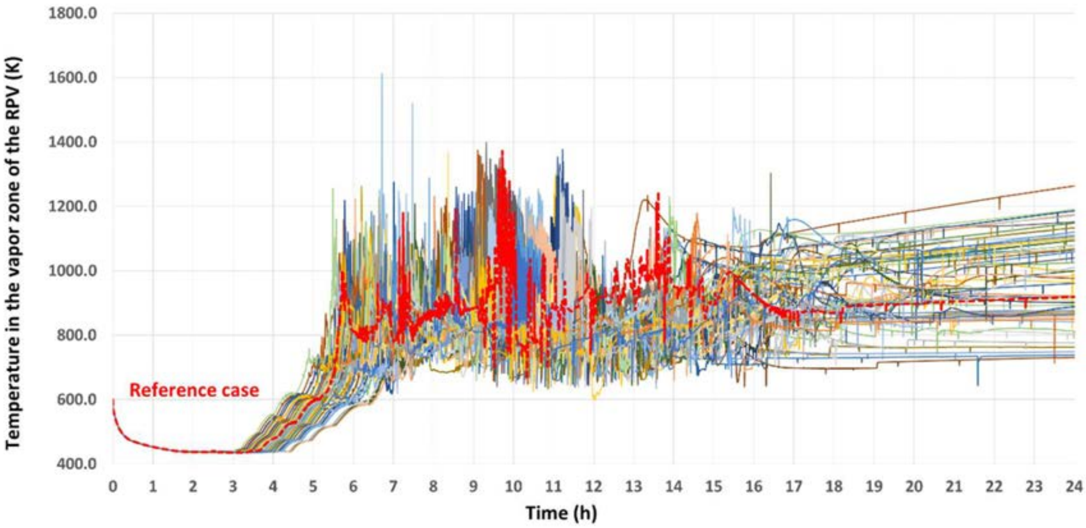

FIG. 162. Temperature in the vapor zone of the primary system for the simulations of the scheme performed (reproduced from Ref. [1])

Time evolution of the standard deviation and mean of hydrogen generated are shown in Fig. 164 for the simulations performed. As it can be observed, standard deviation rises up in a linear way till simulation time is about 6.5 h and then starts to stabilize while mean continues to increase.

The complex behaviour of hydrogen generation dispersion is mostly concentrated in the first 3–4 h after core degradation starts. The ratio standard deviation/mean is plotted in Fig. 165 as a measurement of the relative importance of the hydrogen dispersion. It can be noted that hydrogen dispersion starts to be insignificant after 8 h from the initiating event.

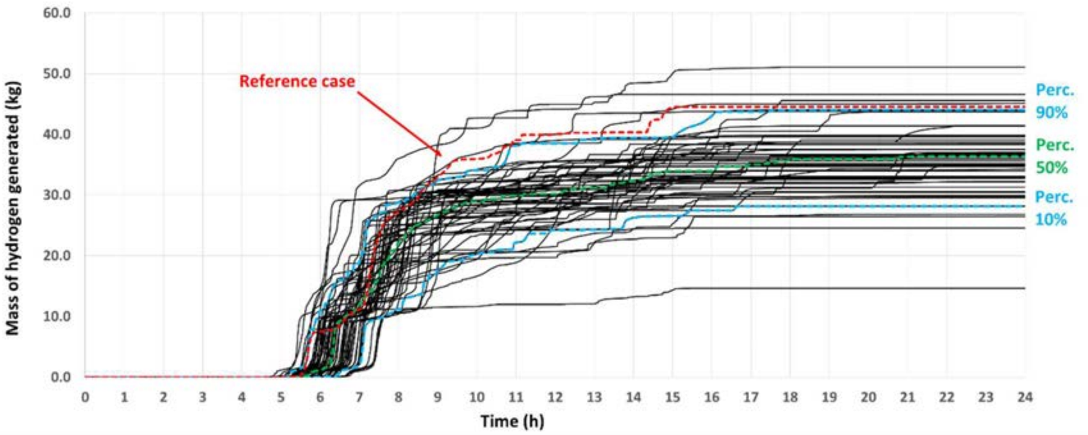

FIG. 163. Hydrogen generated for the simulations of the scheme performed (reproduced from Ref. [1])

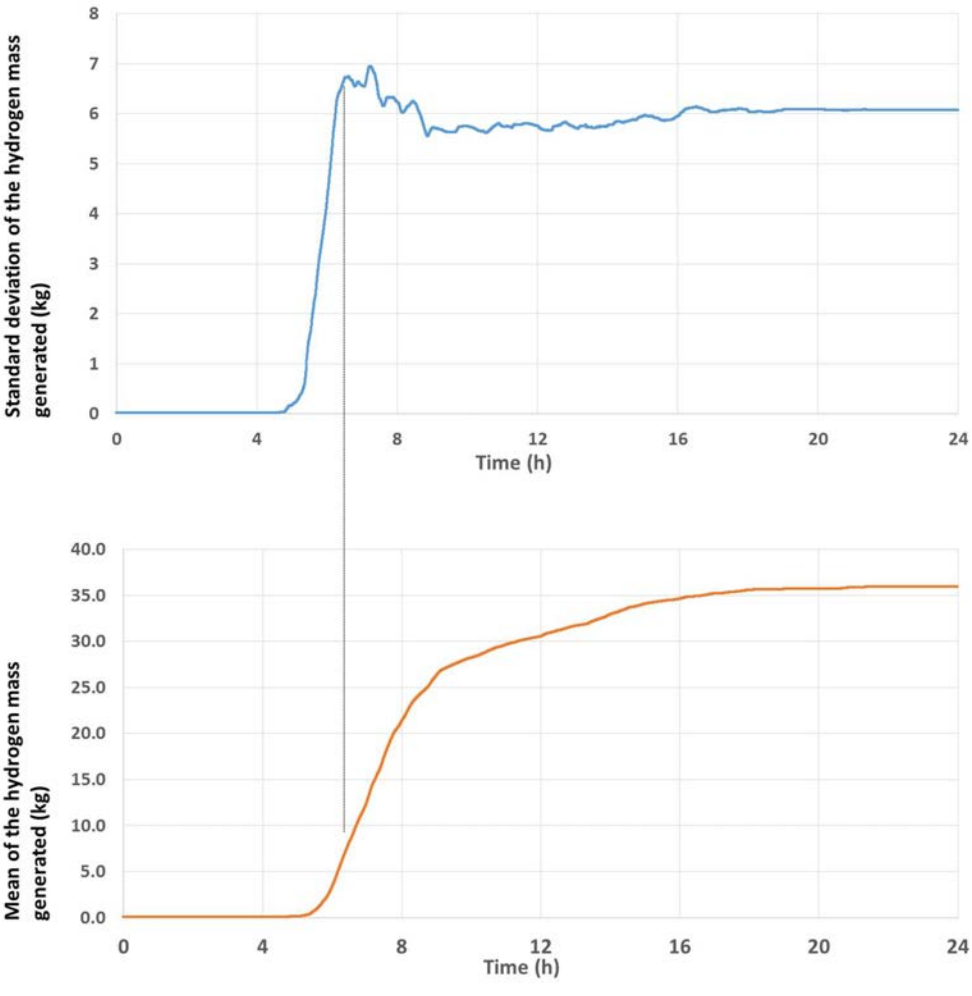

FIG. 164. Time evolution for the standard deviation and mean of the hydrogen generated in the simulations performed.

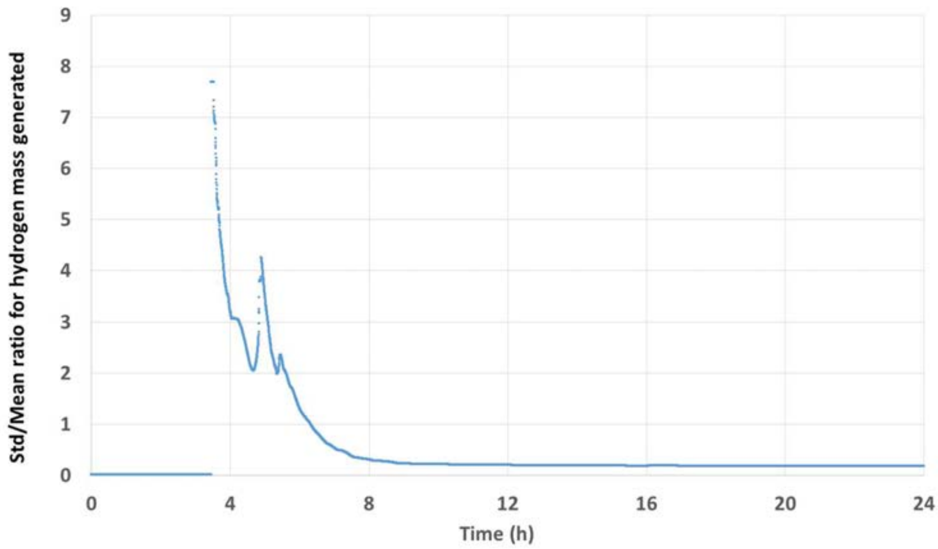

FIG. 165. Standard deviation/mean ratio for the hydrogen mass generated in the simulations performed.

— *Parametric scheme for relevant parameters [1]:* after four most important parameters were identified based on the uncertainty analysis (PM_1 to PM_4), a centered parametric DAKOTA scheme was performed in order to quantify the individual influence of each parameter on the selected figures of merit. A 'centered_parameter_study' method was used to perform the mentioned parametric simulations. The nominal value for each of the four most relevant parameters was chosen to be at the middle of each domain interval (i.e. (max+min)/2), while the remaining parameter values were left constant, with the same values they had for the reference case. In order to obtain 8 independent simulations per relevant parameter, a uniform grid was chosen for each of them with its nominal value as the centre of the grid. With the configuration descripted, a total number or 33 simulations were performed, including the one for the nominal values of the scheme. Main results of the parametric analysis are shown in Fig. 166 where dependencies between each FOM in seconds and relevant parameter is presented. Based on the mentioned plots, PM_1 is highly inversely correlated with all FOMs, while PM_2 has a strong direct correlation with FOM-3. PM_3 is slightly correlated with FOM-3 and no dependencies are noticed regarding PM_4. Normalized standard deviation of FOMs is shown in Table 67 for relevant parameters to take into account different amplitudes of variation and their impact on FOMs. In addition to the strong effects of PM_1 on all FOMs, the influences of PM_4 on FOM-2 and PM_3 on FOM-3 are also remarkable. Dynamics of hydrogen mass generated during the accident and vapor temperature in the primary system is shown in Figs. 167 and 168, respectively.

TABLE 67. NORMALIZED STANDARD DEVIATION OF FOMs FOR RELEVANT PARAMETERS

Parameter	FOM-1	FOM-2	FOM-3
PM_1	1.211	1.189	1.312
PM_2	0.000	0.003	0.100
PM_3	0.000	0.007	0.292
PM_4	0.000	0.043	0.100

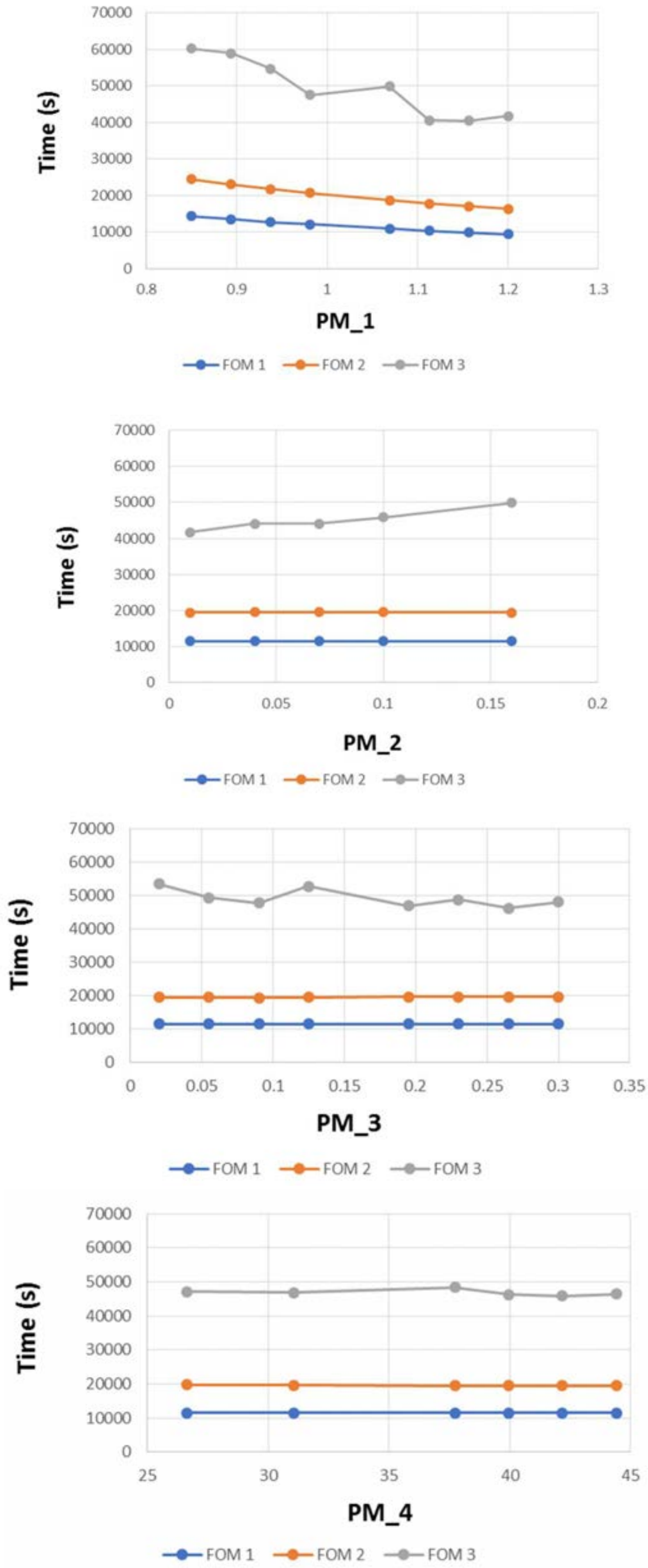

FIG. 166. Variation of FOMs with relevant parameters.

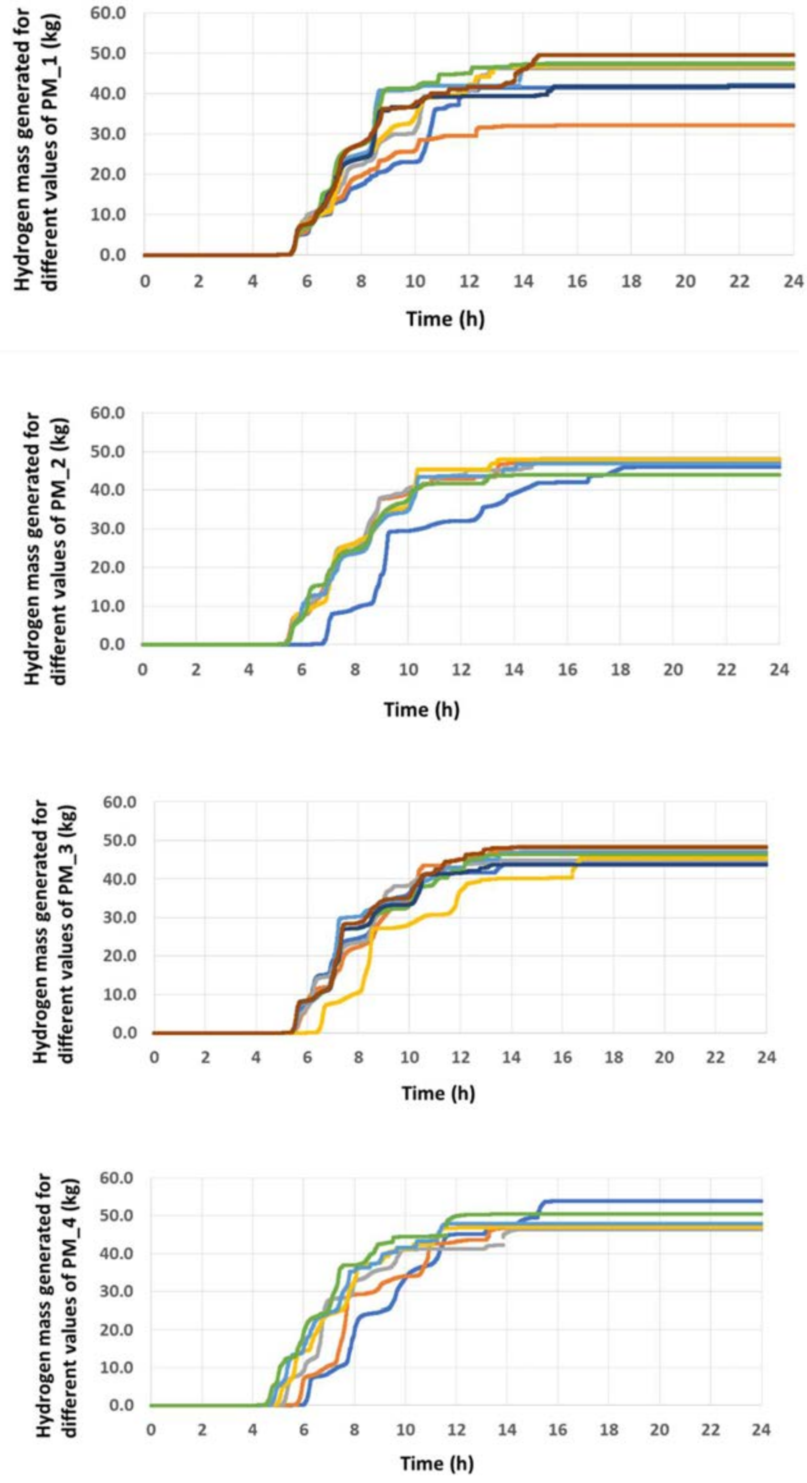

FIG. 167. Dynamics of hydrogen mass generated for performed parametric analysis.

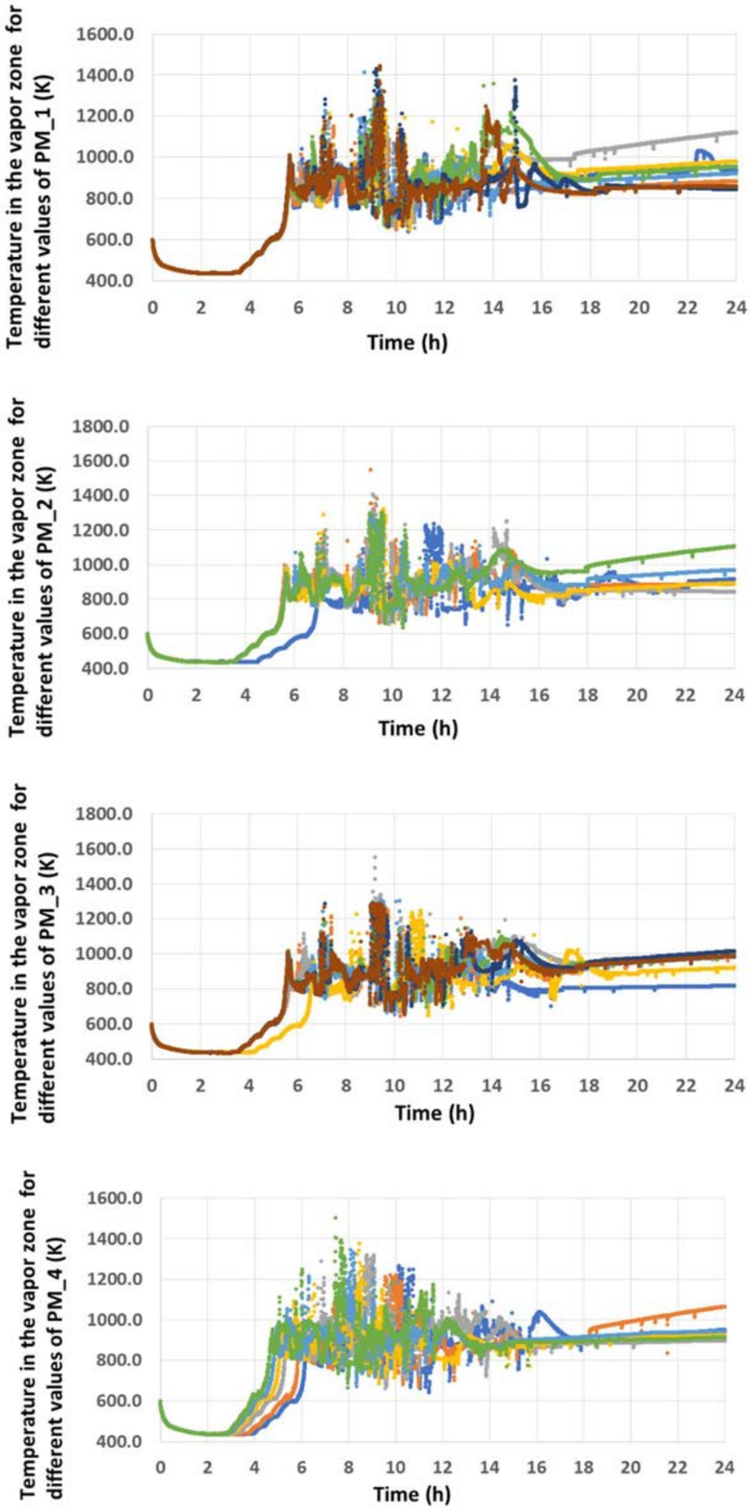

FIG. 168. Dynamic of vapor temperature in the primary system for performed parametric analysis.

A calculation to determine parameter's importance on these variables was performed normalizing standard deviation with total variation of relevant parameters and results are shown in Tables 68 and 69. In Table 68 the importance of PM_1 (decay power multiplicative scale factor) and PM_4 (zircaloy oxidation rate coefficient) in relation to hydrogen generation dispersion can be observed. Besides, in Table 69 the impact of variation by PM_1 and PM_4 on the mean and maximum value of vapor temperature in the primary system can be observed. In both these tables no important influence of PM_2 and PM_3 can practically be noticed on the variables taken into account.

TABLE 68. NORMALIZED STANDARD DEVIATION OF TOTAL HYDROGEN MASS GENERATED FOR RELEVANT PARAMETERS

PM_1	PM_2	PM_3	PM_4
1.00	0.05	0.06	0.32

TABLE 69. NORMALIZED STANDARD DEVIATION OF MAXIMUM AND MEAN VALUE OF VAPOR TEMPERATURE IN THE PRIMARY SYSTEM FOR RELEVANT PARAMETERS

Variable	PM_1	PM_2	PM_3	PM_4
Max	0.75	0.11	0.12	0.40
Mean	0.30	0.07	0.06	0.09

2.3.7.7. Summary and conclusions

During the first stage of this study, a MELCOR model for an integral type SMR was developed and an analysis was performed in order to identify relevant parameters and their probability distributions in the severe accident progression in relation to the FOMs selected. Proper identification and selection of relevant parameters is a key step for the uncertainty analysis. A comprehensive literature research together with the application of some engineering judgment was crucial to make progress at this stage.

In the second stage, a coupling interface between DAKOTA and MELCOR codes was successfully developed, including the analysis driver programming to generate MELCOR input decks and extract FOMs data from the MELCOR shell, and the failure capture strategy to consider MELCOR errors when simulations were run. As a first step for the coupling interface development, a simplistic approach was applied using a simple MELCOR model with only two control volumes and a simple configuration for the DAKOTA input deck. After that, complexity was added to the interface in a step-by-step process till having the coupling working as it was expected.

The third stage of the work was done by launching the simulations with DAKOTA in two different batches to take into account MELCOR errors. A high error rate was detected in that moment and a MELCOR model issue in the core region was later identified for future improvements.

The fourth stage of the work is related to the analysis, discussion, and presentation of results. Histograms and statistics of FOMs as well as scatter plots of parameters were considered in this point. Simple and simple rank correlation matrices were analysed from the output of DAKOTA, as well as partial and partial rank ones. Maximum and minimum key times were obtained for the FOMs taken into account, with both confidence and probability levels of 95%, according to the application of Wilks formula. Based on the results, the four most important parameters of the scheme were isolated. The most important parameters found correspond to the MELCOR physical model category. Relevant variables of the accident progression were plotted including the evolution of the reference case. It was noticed that the hydrogen generation for the reference case is slightly above the 90% percentile by the end of the simulation time and that main uncertainties regarding the hydrogen generation are focused on the first four hours since the start of core degradation.

The fifth and later stage was performed by launching a parametric analysis on the relevant parameters identified previously. The impact of each parameter on the selected FOMs and some other important variables was calculated. The decay heat multiplier parameter was found as the most important one in relation to the FOMs selected.

Main sources of uncertainty resulting from the analysis

MELCOR physical model parameters considered in the scheme were found to be the most important variables regarding the FOMs selected. Therefore, the most important sources of uncertainties in our scheme are decay power multiplicative scale factor (PM_1), radiative exchange factor for radiation radially/axially outward from the cell boundary to the next adjacent cell (PM_2 & PM_3) and low temperature range constant coefficient for zircaloy oxidation rate by water (PM_4). The decay power multiplicative scale factor was considered to be the most important one among the mentioned parameters.

Lesson learned and best practices

- Regarding the first part of the work, it is important to remark that extensive experience on severe accident modelling and analysis together with engineering judgment are required aspects for the identification and selection of relevant parameters. It is suggested to complement this with an exhaustive literature review. In addition to this, prior comprehension on the model behavior as well as familiarization with the model variables are considered relevant aspects to define and carry out the uncertainty analysis.
- A well-known confidence tool (e.g., DAKOTA) is suggested to be selected in order to perform the uncertainty study. Also, when there is no previous experience regarding the coupling between the uncertainty chosen tool and the simulation code, it is highly recommended to start considering simple models and interfaces for gaining experience meanwhile developing the scheme.
- After launching the simulations, it is recommended to analyze possible failure patterns from the parameters' coverage map related to simulations with errors, trying to identify the type of MELCOR error sources to better understand model behavior and to improve model robustness as well.
- After successfully identification of most relevant parameters, it is highly recommended to launch a parametric analysis in order to verify the direct impact of each parameter on selected FOMs.

2.3.8. Energy Software (ENSO)

The ENSO provided accident analysis based on an iPWR type plant. Description of this plant specifics, accident scenarios analysed, applied models and approaches, and summary of the results are provided in the following sections.

2.3.8.1. *Motivation and objectives*

ENSO contributed to the assessment of the uncertainty propagation in a long term SBO scenario postulated for an iPWR (SMR). The study aims at demonstrating the RELAP/SCDAPSIM capability to carry out a BEPU calculation of a Severe Accident scenario in a single sequence from operational conditions to RPV creep rupture. The expected outcomes of this study were to:

- Demonstrate the capability of the code to assess the plant availability of the iPWR design for a selected sequence of safety actions. Depending on the uncertainty of the input parameters at operational and DBA conditions, core damage will occur at different boundary conditions, which can affect to the final severe accident progression sequence;
- Assess the robustness of the iPWR design and safety systems, taking into account the publicly available data applied for the current model;
- Select severe accident parameters relevant to the iPWR long term SBO scenario;
- Perform a BEPU analysis including severe accident parameters;
- Identify potential limitations of the code during severe accident conditions;
- Assess the effect of the uncertainty in core damage phenomena for the selected set of severe accident input parameters.

2.3.8.2. *Description of the relevant plant*

The iPWR design used for generating RELAP/SCDAPSIM/MOD3.5 nodalization takes as reference some of the public available data of CAREM-25 reactor. Main features and references of the selected information are listed in Table 70. The design includes all the major components of a typical PWR primary system within the reactor pressure vessel (core, pressurizer, and steam generators). Thermal power is effectively removed by natural circulation for both nominal and shutdown conditions. The core heat transfer regime in the core is subcooled boiling, hence part of the vapor that is generated in the core is accumulated at the top of the vessel to passively pressurize the primary system. Heat exchangers are placed in 12 cylindrical risers at the downcomer region, with embedded coil tubes that heat counter current feedwater up to 30ºC of vapor superheating.

The selected iPWR design also includes different passive safety systems:

- Secondary shutdown system: high pressure gravity driven injection system with highly borated water. This system actuates if no rod insertion occurs after reactor scram signal;
- Emergency injection system (EIS): accumulator system that injects subcooled water when RPV pressure drops below 1.5 MPa;
- Passive residual heat removal system (PRHRS): ex-vessel heat exchanger that condensates the vapor of the RPV through horizontal tubes placed in a tank with 16 m^3 of subcooled water;
- PRV: passive control system to avoid pressures higher than 15 MPa in the RPV. This system also depressurizes the RPV if core dryout and vapor superheating is detected at the core exit temperature;
- External cooling system (ECS): Containment safety system that externally cools down the walls of the lower plenum under severe accident conditions. This system consists of an accumulator that fills with subcooled water a cavity placed below the RPV. The accumulator only injects the water with

core exit temperature signal associated to core dryout and vapor superheating.

TABLE 70. BASIC CAREM-25 SPECIFICATIONS

Parameter	**Value**
Thermal power	100 MWt
Pressure (primary/secondary)	12.25 / 4.7 MPa
Core inlet/outlet temperature	557 / 599 K
Mass flow rate	410 kg/s
Feedwater temperature	473 K
Number of steam generators (SG)	12 [91]
Number of coil tubes per SG	52 [91]
Length of coil tubes	35 m [92]
RPV height/diameter	11 / 3.2 m [93]
Assembly array	Hexagonal [94]
Number of fuel assemblies	61 [94]
Core active length	1.4 m [94]
Chimney height	4.6 m
Coolant volume	39 m^3
Secondary shutdown system volume	2 m^3
EIS volume	41 m^3 [95]
PRHRS tank volume	16 m^3

2.3.8.3. Accident scenarios and severe accident codes

Severe accident scenario

The severe accident scenario selected for simulation is a SBO with all the emergency systems fully available. This selection allows to assess how the uncertainty associated to the selected thermal hydraulic parameters affect the plant availability. In addition, due to the unique features of RELAPS/CDAPSIM (Best Estimate simulation in a single execution from operation to severe accident conditions) the selected conditions allow to analyze the effect of the severe accident input parameters in the timing and magnitude of relevant severe accident output parameters. The main events of the selected SBO scenario are shown in Table 71. The boundary conditions for the transient simulation are:

- SBO takes place at 5,000 s (SCRAM signal);
- Secondary system is isolated 5 s after SCRAM signal;
- PRHRS is automatically started with isolation signal;
- PRV operating conditions: open $P_{RPV} > 14.8$ MPa, close $P_{RPV} < 14.2$ MPa;
- PRV fully opened if core exit temperature > 628K;
- EIS injection if $P_{RPV} < 1.5$ MPa.

TABLE 71. iPWR STATION BLACKOUT EVENTS

Main events	RS35
Start of the transient (SoT), SCRAM signal	5,000 s
PRHRS fully opened	5,007 s
Feedwater stopped	5,008 s
Secondary system isolated	5,011 s
Loss of natural circulation (PRHRS tank empty)	13 h 34 min
PRV opened ($P_{RPV} > 14.8\ MPa$)	24 h 49 min
PRV depressurization (core exit temperature > 628K)	38 h 50 min
EIS started ($P_{RPV} < 1.5\ MPa$)	39 h 03 min
Core dryout	74 h 28 min
Oxidation	77 h 44 min
Ballooning rupture	77 h 50 min
Ceramic formation (U-Zr-O)	84 h 40 min
Core Slumping	91 h 26 min
Creep rupture	93 h

Severe accident codes

ENSO participates with RELAP/SCDAPSIM/MOD3.5 (RS3.5 for short) system code [96, 97] and its IUA module [98]. This code version contains two best-estimate codes: one to simulate the thermal-hydraulic phenomena (RELAP) and one to simulate the severe accident phenomena (SCDAPSIM). Both RELAP and SCDAPSIM are defined as *mechanistic* codes, as opposed to parametric, meaning that the codes contain realistic models to provide an accurate prediction of the behavior of a reactor. In other words, most of the user input information relates to plant data (geometry, materials, initial thermodynamic conditions), and not to parameters for the models (threshold values, time at which models are initiated).

Historically from 80s to mid-90s SCDAP/RELAP5 (RELAP/SCDAPSIM precursor) was designed to describe the overall RCS thermal hydraulic response and core behavior under normal operating conditions, under design basis and severe accident conditions. The code was used for TMI-2 [99] accident evaluation and core/vessel examination. It was the first to predict molten pool formation and relocation into lower plenum. Both SCDAP/RELAP5 and RELAP/SCDAPSIM has been continuously assessed against integral thermal and severe accident experiments including integrated uncertainty analysis. Model assessment and validation for LWRs and PHWRs started in the 90s. The code used publicly available data and reassessment results which include analysis of experiments performed in LOFT [100, 101], PHEBUS [102–104], PBF [105, 106], and CORA [107, 108] facilities. In the latest code versions, RELAP/SCDAPSIM [109] have improved modeling options developed and validated by the Innovative Systems Software and international collaborators through on-going severe accident research programs in Europe, Japan, and Korea including the influence of air ingression and water addition. RELAP/SCDAPSIM is currently used to support the design and analysis of integral thermal hydraulic experiments performed in French PHEBUS FPT [102–104] and German QUENCH [110, 111]. Furthermore, RELAP/SCDAPSIM has been used to perform first detailed calculations for Fukushima-Daiichi conditions and to support ongoing decommissioning research and development activities.

The SCDAPSIM portion of the code includes best-estimate models that describe the behavior of typical light and heavy water reactor core components during severe accident conditions including changes in core geometry associated with melting or water addition. SCDAPSIM includes burnup and transient fuel behavior models, and it incorporates mechanistic DBA fuel behavior models for fission product release, gap conductance, cladding ballooning and rupture, cladding oxidation, and embrittlement, as well as mechanistic severe accident core and vessel models to control element failure, metallic and oxide melt formation, and relocation. Other available severe accident models can simulate molten pool behavior and in-vessel melt retention. For LWR, RELAP/SCDAPSIM has detailed user-selectable reactor component models such as fuel rods, Ag-In-Cd and B_4C control rods, BWR control blade/channel boxes, electrically heated fuel rod simulators, and general core and vessel structures. For PHWR designs (including CANDU reactors), specialized horizontal components with different models and correlations are also available.

The SCDAPSIM portion is linked to expanded MATPRO material property correlations [98] which include air ingression and advanced cladding materials. Some of the materials included in the code are uranium, uranium dioxide, mixed uranium-plutonium, dioxide fuel, zircaloy cladding, zirconium dioxide, stainless-steel, stainless-steel oxide, silver-indium-cadmium alloy, cadmium, boron carbide, Inconel 718, U-Zr-O_2 mixture, fill gas mixtures, carbon steel, tungsten, tantalum. In addition, SCDAPSIM includes COUPLE porous media module [108, 112], which is used to simulate debris beds and lower core support structures (for LWRs/PHWRs). Some COUPLE features include the modelling of internal porosity and convective heat removal using the RELAP volumes for the boundary conditions. Oxidation with steam phenomena can be reproduced as well by COUPLE. With regards to the heat conduction phenomena in the lower plenum, a 2D finite element mesh is available. Additionally, a 1D model at crust boundary perimeter of the molten material is included. Finally, the COUPLE module for molten pool behavior of liquefied/molten U-Zr-O_2 mixture includes models to reproduce phenomena such transient natural circulation, interactions with surrounding wall and ex-vessel flooding.

The RELAP portion of the code calculates the overall RCS thermal hydraulic response, control system behavior, reactor kinetics, and the behavior of special reactor system components such as valves and pumps.

The current RS3.5 version is the first release with the new QUENCH/PARAMETER-experiment-driven SCDAP modelling improvements. The added modelling options include (a) an improved fuel rod gap conductance model, (b) improved models for the electrically heated fuel rod, (c) improvements to the shroud model, and (d) models to treat the influence of air ingression. The improved fuel rod simulator model now includes the option to model tantalum heater elements in addition to the tungsten heater elements historically used in the QUENCH and other European bundle experiments. The improved shroud models include enhanced user options to simulate some of the unique features of experimental facilities including options to better simulate the influence of the thermal-mechanical failure of the experimental shrouds during high temperature and quenching conditions. The air ingression modelling options account for the changes in the Zircaloy oxidation kinetics and the uptake of nitrogen due to the presence of air [113]. The new modelling also allows the user to input user defined SCDAP material properties as a table.

2.3.8.4. Plant modelling and nodalization

The iPWR RS3.5 input deck as shown in Fig. 169 was performed based on the specifications as described in previous section. Main features of the nodalization are:

— Number of hydrodynamic volumes: 301;
— Number of hydrodynamic junctions: 34;
— Number of heat structures: 221;
— Number of trips: 22;
— Number of control blocks: 16.

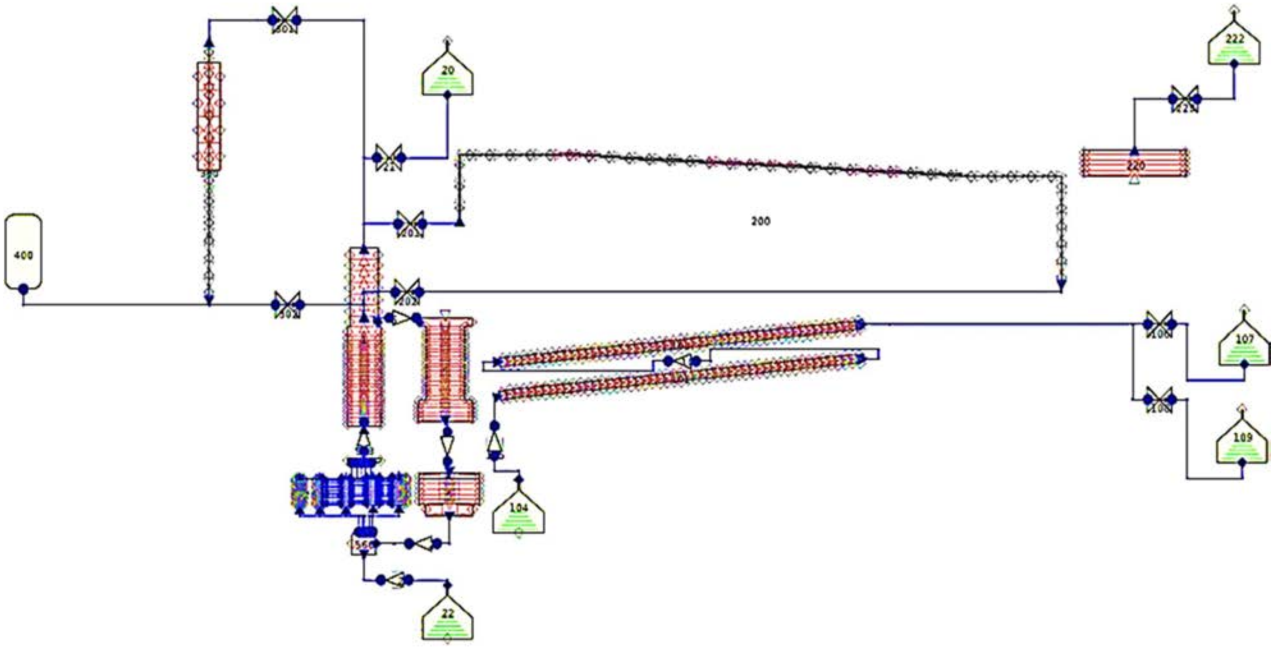

FIG. 169. Sketch of the RELAP5mod33 and RS3.5 nodalizations.

The number of control blocks and trips is greatly reduced because only one active system is defined for the feedwater. This system adjusts the RPV pressure to the set-point value. Otherwise, the different passive safety systems are also modelled: secondary shutdown system, EIS, PRHRS, PRV and ECS. In addition, the nodalization simulates the environmental heat losses at the top and the bottom of the RPV, as well as in the pipes of the passive safety systems. Heat transfer coefficients of the environment heat structures have been adjusted to obtain a total loss of energy equivalent to 0.1 % of the nominal power.

In regard to the fuel components, RS3.5 uses SCDAP components. Core region is divided in 4 fuel and 1 bypass parallel channels of 12 axial levels. Crossflow junctions are defined for the fuel channels and the number of rods and relative powers for each channel follows the distribution shown in Fig. 170 [114]. For SCDAP components, detailed fuel information is included (He mass and pressure, density, fuel composition, burnup) as well as specific components for simulating the guide thimbles and the radiation shielding. SCDAP components also include the simulation of the radiation heat transfer effects for the different fuel channels and their interaction with the radiation shielding, as well as a COUPLE module to simulate core slumping and debris bed heat exchange with the fluid and the walls of the lower plenum (see Fig. 171).

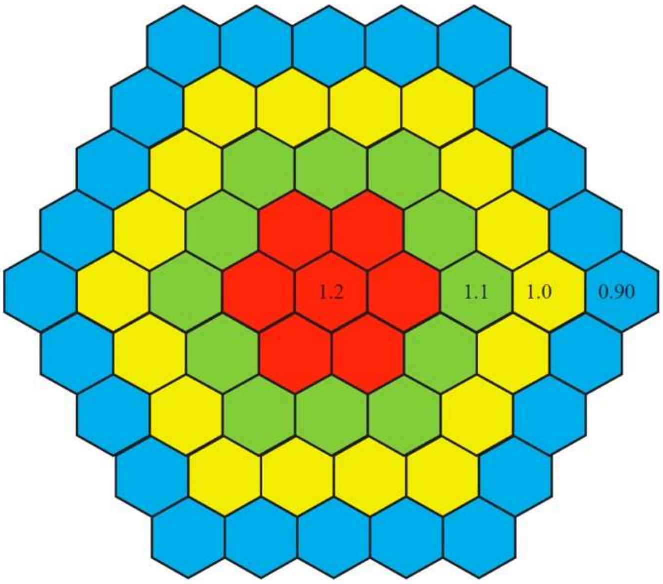

FIG. 170. iPWR radial power distribution.

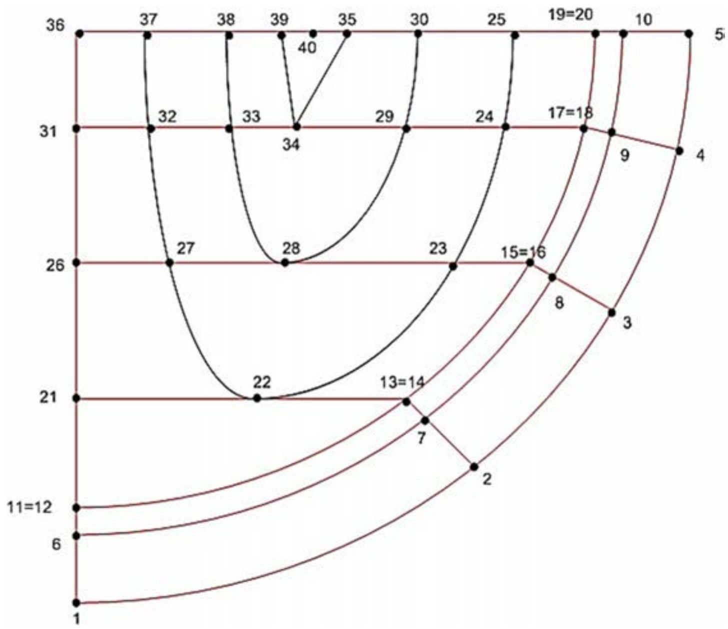

FIG. 171. COUPLE meshes for RS3.5 nodalization.

2.3.8.5. Methodologies and tools for the uncertainty and sensitivity analysis

The methodology employed to evaluate the performance of an SMR reactor under severe accident conditions combines the use of a best-estimate code with realistic assumptions on the initial and boundary conditions. This approach corresponds to Option 3 in IAEA classification [115], which corresponds to the BEPU methodologies.

Among the BEPU methodologies, ENSO has followed the statistical approach proposed by GRS [116]. This approach propagates the input uncertainty to the code results by running multiple calculations with the same input model, except for a set of selected input parameters, and is sketched in Fig. 172.

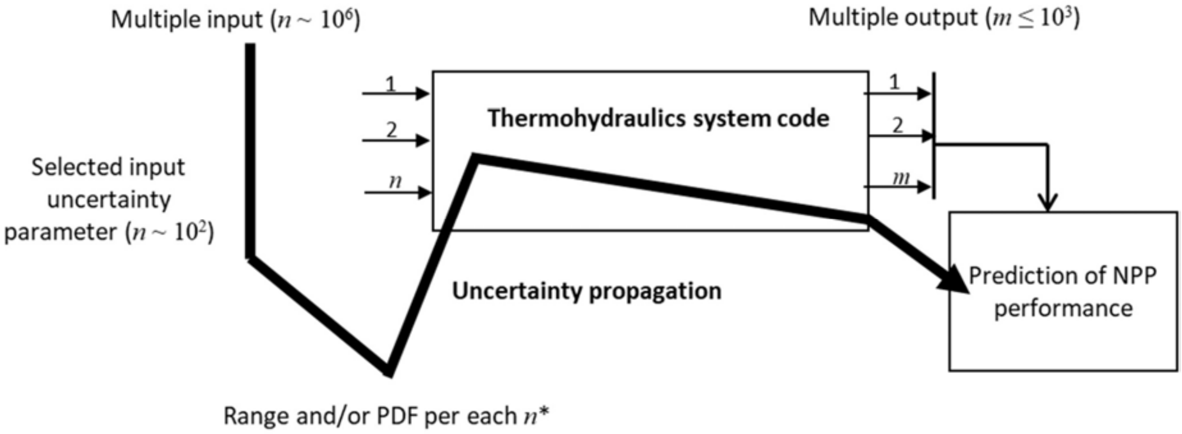

FIG. 172. BEPU approach: propagation of input uncertainties

The uncertainty associated to the selected parameters describes the imprecise knowledge of the actual value and does not refer to random variability. The sources of uncertainty considered are:

— Material properties;
— Initial and boundary conditions;
— Code correlations.

The uncertainty of the parameters is described with PDFs, and the values are sampled using the SRS technique.

The Wilks' formula determines the minimum number of code runs needed to generate a tolerance limit that estimates the specified percentile with the given confidence level. A relevant feature of the method is that the number of required code runs is independent of number of selected input parameters with uncertainty associated.

The form of the output uncertainty is a tolerance limit that estimates the selected percentile (typically 95%) with a certain confidence level (typically 0.95). The Wilks' formula can be applied at different orders, the higher the order the less impact of the sample size on the results. From a regulatory perspective, the 1st order seems to be preferred. However, following BEMUSE recommendations for Wilks' methodologies [117], the occurrence of code failures during the analysis may require increasing the order of application and thus the number of code calculations.

Information about the number of code runs calculated with the Wilks' formula for several percentiles, confidences and orders is provided in Table 72.

TABLE 72. WILK'S MINIMUM NUMBER OF CODE RUNS GIVEN PERCENTILE, CONFIDENCE AND ORDER

Percentile	Confidence	Order	Code runs
95%	0.95	1	59
95%	0.95	2	93
95%	0.95	3	124
95%	0.97	1	69
95%	0.97	2	105
97%	0.95	1	99
97%	0.95	2	157

The output values for the selected FOM are arranged in increasing order to proceed with ranks statistics. At 1st order the maximum value corresponds to the 95/95 tolerance limit, at 2nd order the second highest value corresponds to the 95/95 tolerance limit.

Uncertainty and sensitivity analysis scheme and relevant tool

The IUA module follows the BEPU statistical method proposed by GRS, based on the use order statistics and the Wilk's formula.

— *Introduction to the IUA Package of RS3.5:* the uncertainty evaluation capability is implemented as an alternative run mode to RELAP/SCDAPSIM, the uncertainty mode, which allows the automatic execution of an uncertainty analysis. A complete uncertainty analysis using RS3.5 code requires the execution of three consecutive phases, namely the "setup" phase, the simulation phase consisting of several executions, and the post-processing phase. Because of the large number of files involved in the uncertainty analysis, specific suffixes on file names are required.

  The setup phase generates the total number of sampled values, also called weights, and the required information to build the tolerance bounds during the post-processing phase. The weights are used to associate uncertainty to code parameters by applying them as multipliers to the base values. During this phase the code also computes the required number of code runs by using the Wilks' formula, or simply uses the value supplied by the user. The setup information is written on disk files, one for each simulation run, and another one for the post processing. The command line for executing the "setup" phase is:

  relap5o.exe -i smr_sbo.is -U setup

  The *U* field activates the uncertainty run mode and the setup specifies the first phase of the package. The input file name, *smr_sbo* in the example above, needs to be the same in all phases, and is also the given name for the output, the only difference being the file extension. The entered data in the setup input file is the data to compute the minimum required code runs from the Wilk's formula, the selected uncertainty parameters and their uncertainty characterization, and the base case input deck for checking process. The required suffix for the "setup" input file is "is". The output file will be *smr_sbo*.os (-o), the restart plot file will be *smr_sbo*.rs (-r), and the weight files will be *smr_sboNNNN*.w (-s). The number of weight files N_w, will be equal the number of uncertainty runs entered or determined during this phase and NNNN, written as a four-digit number with leading zeros, will range from 0001 through N_w.

The simulation phase consists of the base case run (best-estimate case with no input perturbation) and the set of uncertainty runs which have input and source variations. For each uncertainty run the code will read the base case nodalization *smr_sbo.i* and its corresponding weight file generated by the setup phase. The command line for executing the "simulation" phase is

relap5o.exe -i smr_sbo.i -U n

The required suffix for the simulation input file is *i* as it is the regular input file for the standard run mode. The number n indicates the run number and is 0 for the base case and is the run number for the uncertainty runs. The run number NNNN (four digits with leading zeros) will be appended to the name of the output and restart plot files, *smr_sboNNNN*.o *smr_sboNNNN*.r in the example. The weight file read during the NNNN runs will be *smr_sboNNNN*.w. To allow the simulation runs to be restarted from a restart-plot file (most likely containing stead-state results), the -r option can be entered and its file name and suffix could be *smr_sbo*.r but any other name and suffix could be used. The code does not modify the indicated restart-plot file but only copies it to *smr_sboNNNN*.r. The command line for executing a restart run from a unique restart-plot file is:

relap5o.exe -i smr_sbo.i -r stst.r -U n

From the above command, the code will generate *smr_sboNNNN*.o and *smr_sboNNNN*.r. The post-processing phase reads the restart-plot files written during the simulation phase from the base case and the uncertainty runs, and generates the rank and run matrices for the output quantities defined in the post-processing input file, *smr_sbo.ip* in the example. The required information in the post-processing input file are the output parameters using the minor edits, as well as the simulation run numbers to be used in the generation of the tolerance intervals. The command line for executing the post processing phase is:

relap5o.exe -i smr_sbo.ip -U postpr

The *postpr* field specifies the last phase of the uncertainty package and the required suffix for the post-processing input file is *ip*. The post-processing phase will generate rank- and run- based matrices files for each requested output parameter:

- The rank matrices contain the values for the output parameters sorted according to its rank and are used to determine the tolerance intervals.
- The run matrices contain the values for the output parameters for each run and are useful to identify the run number that generated a specific result that requires further analysis.

Each rank-based matrix is written to disk with the file name *smr_sboALFNUM*.m and each run-based matrix is written to disk with the file name *smr_sboALFNUM*.mruns, where ALF is the variable code (alphanumeric) and NUM is the parameter (numeric) of requested quantities. A graph containing the time history of the base result, the upper and lower bounds and the span between them will also be generated for each requested parameter. As for the other phases, the output file name is defined from the input file name and thus, for the example will be lbloca.op. The input and output files required and generated during a full application of the uncertainty package are sketched in Fig. 173.

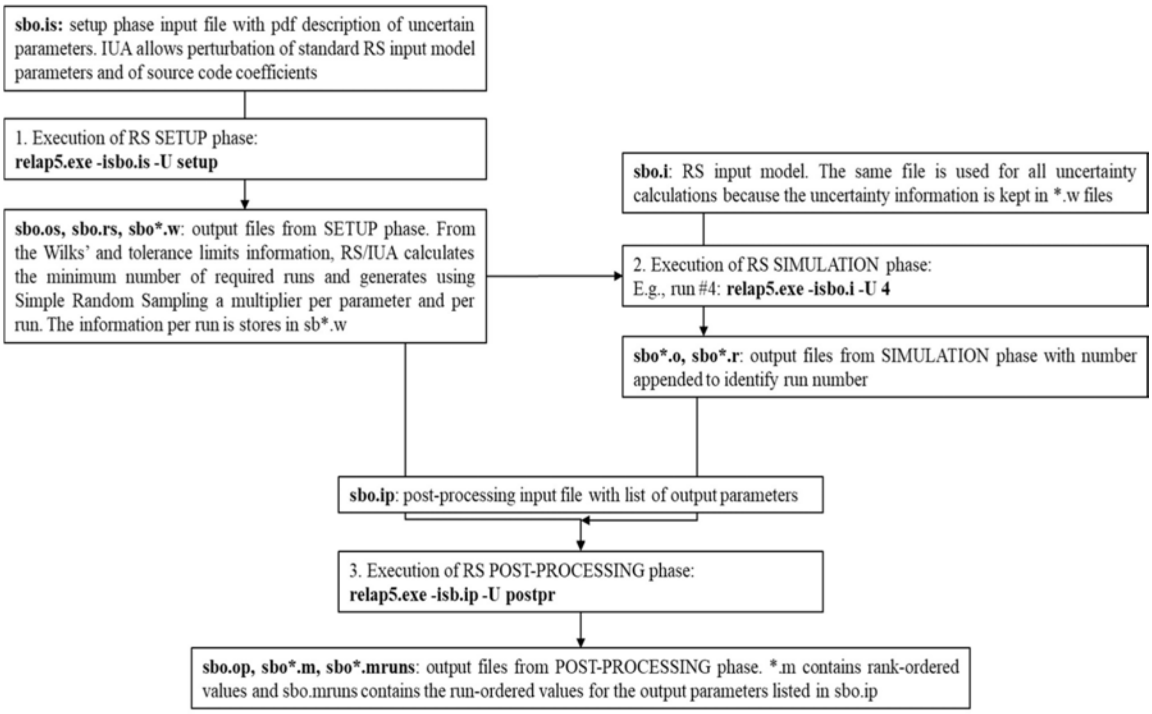

FIG. 173. RS/MOD3.5 IUA: phases, files and execution commands.

- *Uncertainty analysis using the IUA tool:* ENSO, a priori, will generate one-sided tolerance intervals from the first order with the typical characteristic values of 95/95 for the percentile and confidence. The selection of the one-sided 95/95 tolerance limit follows from the objective of evaluating the highest values of several quantities such as the cladding temperature and the mass of fission products released.
- *Uncertain parameters and related probability distributions:* the a priori set of selected uncertain parameters for the BEPU analysis is shown in Table 73 in which the global phenomenon, the specific probability distribution function describing their uncertainty, and the components affected are specified. The types of parameters selected for the analysis are related to:

  - Heat transfer coefficients and critical heat flux;
  - Interphase heat transfer;
  - Material properties;
  - Cladding behavior under severe accident conditions;
  - Radiation;
  - Core power;
  - Conditions for safety systems;
  - Natural circulation.

TABLE 73. LIST OF UNCERTAIN PARAMETERS FOR THE BEPU ANALYSIS

#	Phenomenon	Parameter		PDF(1)	Components	Reference(2)
01	Heat transfer across solid surfaces	Film boiling HTC to liquid	HT-1	U [0.74; 1.29]	RELAP heat structures (heat transfer to the secondary) and SCDAP components (core)	[118]
02		Film boiling HTC to vapor	HT-2	U [0.49; 3.43]		[118]
03		Nucleate boiling HTC - subcooled	HT-3	T [0.76; 0.86; 1.19; 1.43]		[119]
04		Nucleate boiling HTC - saturated	HT-4	U [0.35; 2.5]		[119]
05		Vapor single phase HTC	HT-5	N [1., 0.2]		EJ
06		Critical heat flux	CHF	N [1.; 0.18]		EJ
07	Interphase	Heat transfer global	IPH-1	U [0.27, 1.94]	Water fluid	[118]
08		Friction	IPH-2	U [0.75, 1.29]		[118]
09	Cladding behaviour under severe accident conditions	Zr oxidation rate and thickness	OXI	N [1,0., 075]	SCDAP fuel components	EJ
10		Rupture strain	SA-1	BE = 0.18, N [1., 0.1]		Code ranges
11		Temperature for failure of oxide shell	SA-2	BE=2500K, N [1, 0.1]		Code ranges
12	UO_2 properties	UO_2 thermal conductivity	MP-1	N/A		Code built-in
13		UO_2 heat capacity for T> 2830K	MP-2	N/A		Code built-in
14	Zr properties	Zr heat capacity	MP-3	N/A		Code built-in
15	Radiation	shroud thickness	SA-3	BE = 1.8 cm U [1.5, 3] cm	SCDAP shroud component	EJ [120]
16	Safety systems	EIS injection trip (pressure set-point)	BC-1	N 1 sigma = 2.24%	EIS	[119]
17		EIS and ECS temperature	BC-2	U [15, 35] ºC	EIS and ECS	EJ, See Note (1)
		PRHRS temperature		U [15, 35] ºC	PRHRS	EJ, See Note (1)
18		PRHRS area	DSG	N [1, 0.05]		EJ, See Note (2)
19	Reactor power	Steady state reactor power	BC-3	N 1., range [0.95, 1.05]	Core power table	[121]
20		Decay power factor (ANS79-3)	DP	LN [0.85, 1.2]		[121]
(17)	Natural circulation	Containment temperature	(BC-2)	BE=298.15 U [15, 35] Celsius	Environmental heat losses	EJ, See Note (1)

(1) BE = Best estimate, LN/N/U = Log normal/normal/uniform, T = Trapezoidal
(2) EJ = Expert judgment
Note (1) Estimated delta temperature due to season change
Note (2) Estimated uncertainty from design (ENSO)
HT: heat transfer; HTC: heart transfer coefficient; CHF: critical heat flux; IPH: interphase phenomena SA: severe accident; BC: boundary condition; MP: material property; DP: decay power; OXI: oxidation

The uncertainty of each parameter was taken from mainly three types of sources: previous studies, code built-in data, and expert judgment for the system components that were designed by ENSO when generating the iPWR nodalization.

2.3.8.6. Results

<u>*Steady state reference case*</u>

The comparison between the iPWR expected values and those obtained for the RS35 simulation is given in Table 74. The results show a close agreement with a maximum deviation of the 1% for the RPV mass flow rate. It is worth mentioning that RS3.5 does not include any special model to simulate helical tubes and the cylindrical geometry of RELAP5 have been used. This limitation could affect the primary to secondary heat transfer as reported by Hoffer et al. in [122]. As it can be observed in Table 75 core inlet temperatures are slightly underpredicted, and that is something to remark taking into account the high number of nodes used in the modelling of the coil tubes (102). Future code improvement needs to be focused on the implementation of specific RELAP5 coil tubes models, not only for improving the precision of the results but also the efficiency of the codes.

TABLE 74. iPWR STEADY STATE PARAMETERS

Parameter	**Units**	**Expected Value**	**RS35 SCDAP**	**Deviation (%)**
Thermal power	MWt	100.0	100.0	0.0
Primary pressure	MPa	12.25	12.25	0.0
Secondary pressure	MPa	4.7	4.7	0.0
Core inlet temperature	K	557.0	561.6	0.8
Core outlet temperature	K	599.0	599.3	0.0
RPV mass flow rate	kg	410.0	406.1	1.0
RPV collapsed liquid level	m	–	6.7	–
Secondary inlet temperature	K	473.15	473.15	0.0
Secondary outlet temperature	K	563.2	565.2	0.3
Secondary mass flow rate	kg/s	–	48.3	–

<u>*SBO transient analysis: DBA conditions*</u>

The timing of the main events simulated by the iPWR nodalization is shown in Table 71. Relevant phenomena associated with DBA conditions are shown in Figs. 174 and 175. Accident sequence starts with reactor shutdown and secondary system isolation. As a result, core power is suddenly reduced also affecting the pressure of the RPV (see Fig. 174 (a)).

At around 2 MW of core power, saturated conditions are achieved in all the system and pressure starts to increase because of the vapor generation. PRHRS system does not start to cooldown the RPV until decay power becomes lower than heat removed by PRHRS. At this time, two different circulations occur in the RPV (see Fig. 174 (b)): the natural circulation induced by the PRHRS and the circulation through the direct current heat exchangers.

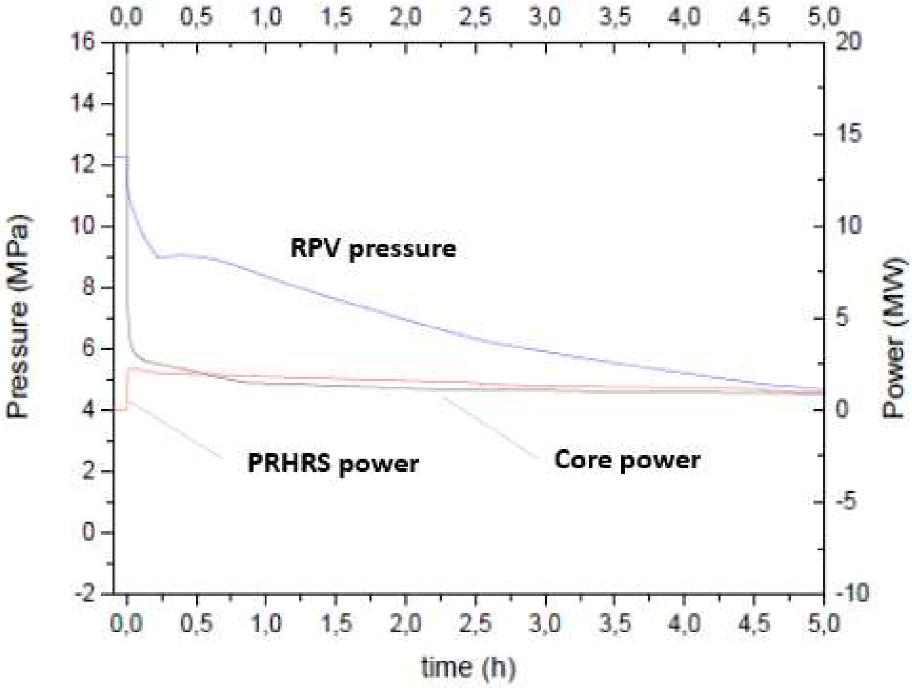

(a)

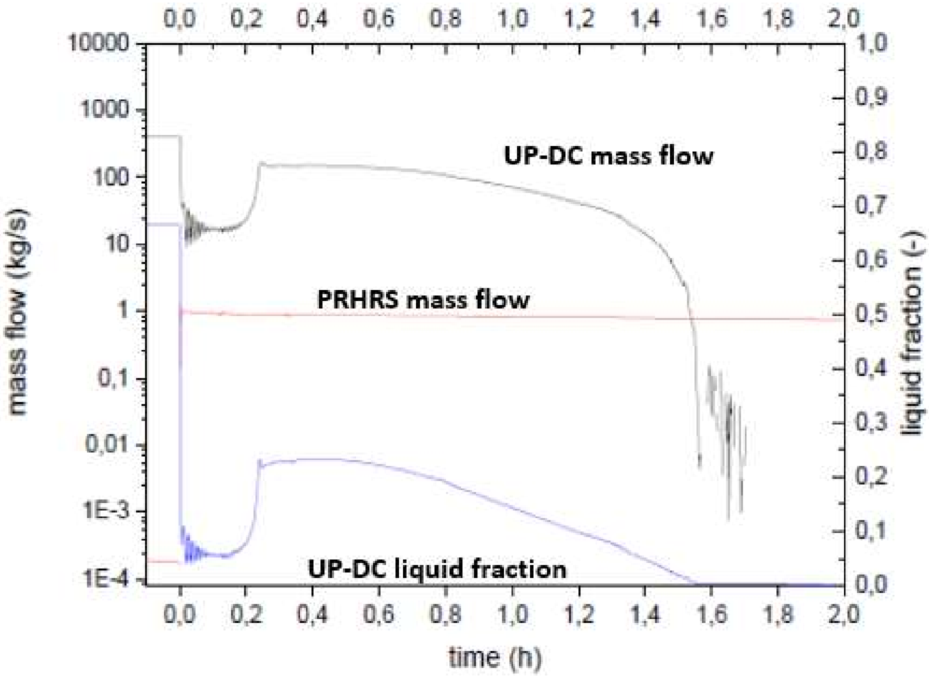

(b)

FIG. 174. Assessment of the SBO phenomena for DBA conditions I: (a) RPV vs core and PRHRS power, (b) RPV circulation vs PRHRS circulation

The one induced by the PRHRS results from the vapor accumulated at the top of the vessel that is condensed in the horizontal tubes of the PRHRS system. This circulation cools down the RPV for the first 12 h (see Fig. 171 (a)) until the PRHRS tanks are completely empty.

The circulation through the direct current heat exchangers is generated by liquid vaporization at the core and density differences. This circulation is kept until the swell level at the central chimney drops below the inlet of the direct current heat exchangers (see Fig. 175 (b)).

When natural circulation is (partially) lost, system pressures start to increase as shown in Fig. 175 (b) and liquid is expanded. At around 15 h, RPV circulation is recovered because swell level achieves again the connection to the direct current inlet. At this time, water that has been cooled at the bottom of the RPV by the environmental heat losses (see Fig. 175 (c)) is moved to the core, also reducing temperatures at chimney and the upper head. This phenomenon slows down the increase of pressure in the RPV and delays the opening of the PRVs until 24 h after the SoT (see Fig. 175 (d)).

With PRVs action, RPV mass inventory starts to reduce and at around 37 h after SoT, first core dry out occurs. Because ofthe core exit temperature signal, PRVs are fully opened, and system pressure is drastically reduced also enabling the initiation of the EIS (see Fig. 175 (e)).

The passive injection is extended for more than 8 h. It is worth mentioning that EIS needs more than 1 h to totally quench the core, and a maximum temperature of 840 K is reported.

After EIS injection, liquid levels are recovered in the RPV (see Fig. 175 (f)), and grace period is extended up to 74 h. In this sense, the selected iPWR design fulfills the 36 h grace period for SBO scenario of CAREM-25 design plus the extended 36 h grace period associated with the availability of EIS in loss of coolant conditions.

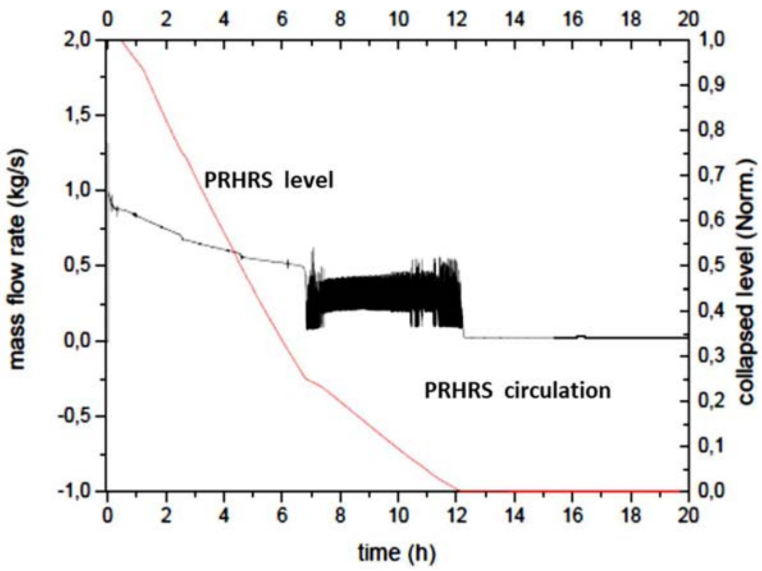

FIG. 175. Assessment of the SBO phenomena for DBA conditions II: (a) PRHRS circulation vs PRHRS level.

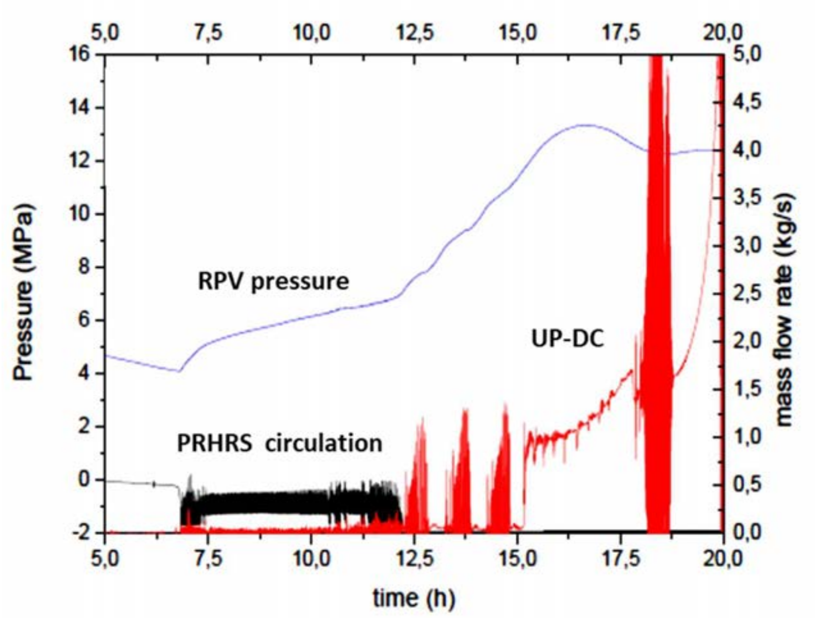

(b)

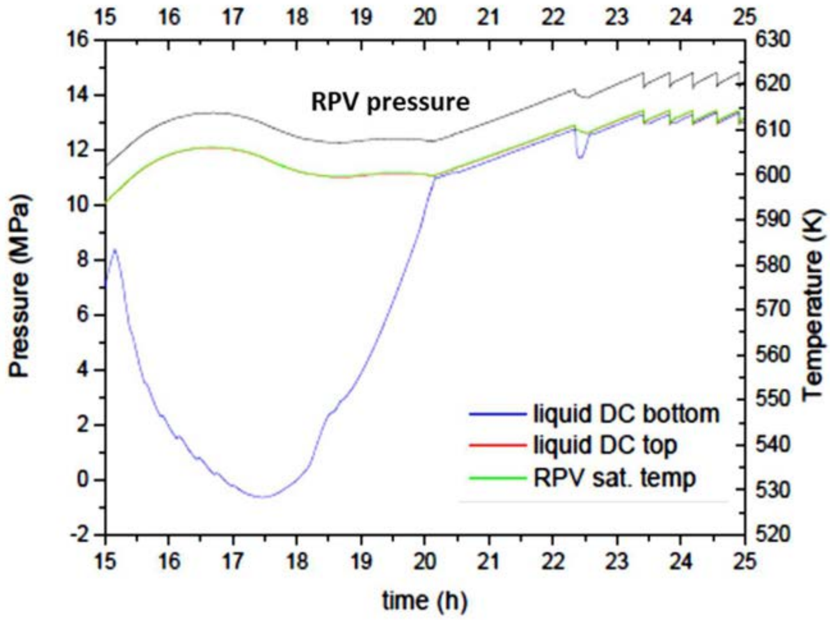

(c)

FIG. 175. Assessment of the SBO phenomena for DBA conditions II: (b) RPV pressure vs PRHRS and RPV circulation, (c) RPV pressure vs direct current temperature.

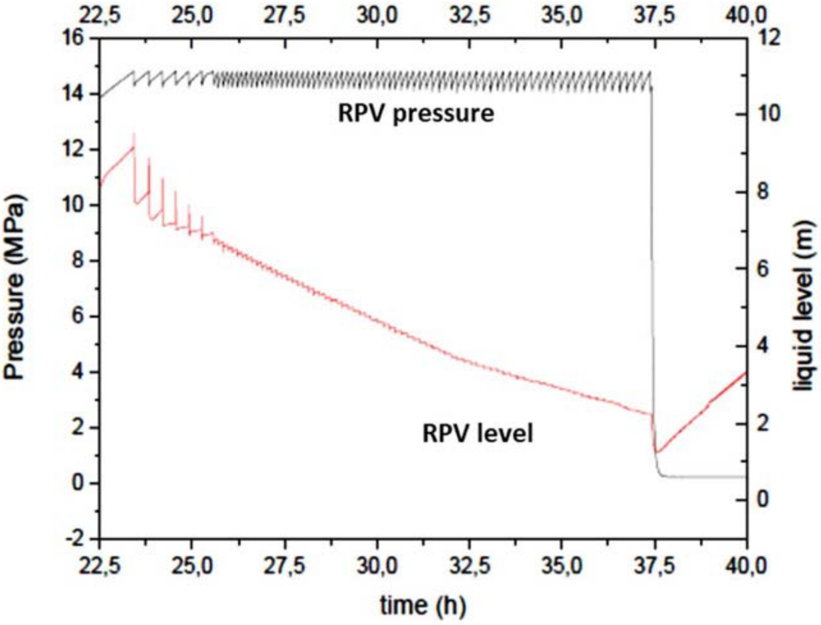

(d)

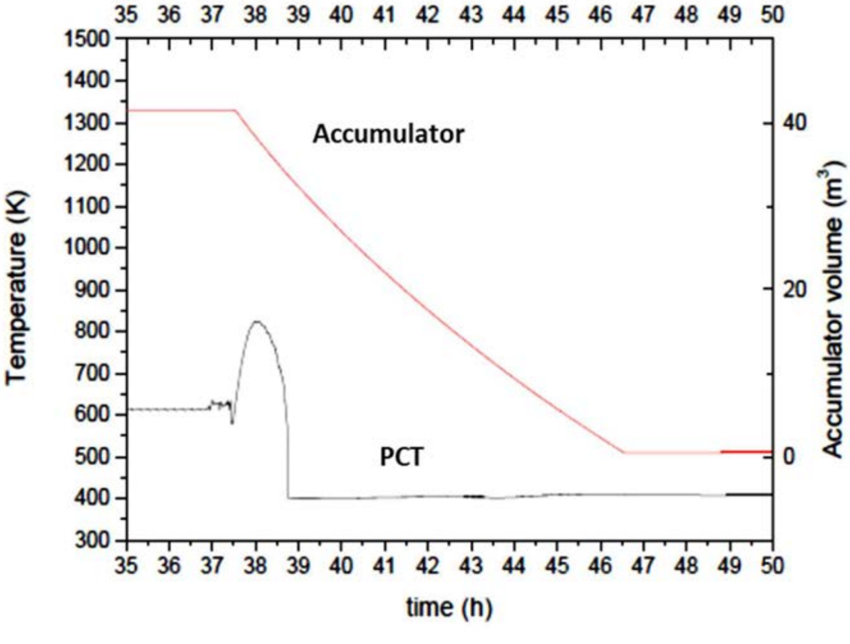

(e)

FIG. 175. Assessment of the SBO phenomena for DBA conditions II: (d) RPV pressure vs RPV level, (e) PCT vs EIS inventory.

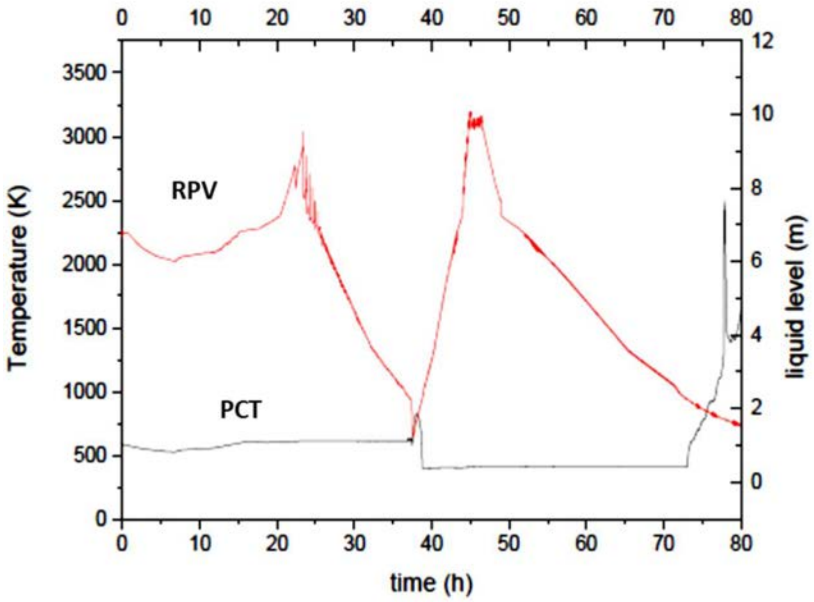

(f)

FIG. 175. Assessment of the SBO phenomena for DBA conditions II (f) RPV level vs PCT

<u>SBO transient analysis: severe accident conditions</u>

At around 74 h after the SoT, a second core dryout occurs (see Fig. 176 (a)). When cladding temperatures increase above1200K, oxidation starts with some spikes in the oxidation heat generation when temperatures achieve the 1,477K. Such peaks (approximately 400 kW) are equivalent to the 70% of the core decay power (569 kW). As result of this, PCT increases up to 2,400K causing ballooning and rupture, and finally the release of volatile and soluble fission products. This phenomenon will repeat subsequently at different core locations and heights as shown in Fig. 176 (b).

After fuel rupture, oxidation heat generation is interrupted and PCTs are reduced by radiation, convection and axial conduction to other materials and fluid. At around 85 h after the SoT, when PCTs achieve 2873 K, ceramic formation (U-Zr-O) occurs, and molten pool formation is observed (see Fig. 176 (c)).

Melted material is accumulated at the bottom of the core for 7 h, before core slumping occurs. The evolution of the lower plenum temperatures registered by COUPLE module when debris bed is placed at the bottom of the lower plenum is shown in Fig. 176 (d).

At 92 h after the SoT, the inner layer of the RPV wall is damaged, penetrating part of the debris bed and increasing the temperatures at the external layer. Finally, at around 95 h, external vessel wall is predicted to fail when temperatures on the outside layer are above 2,000 K. In this part of the simulation, results are not realistic as ex-vessel capabilities have not been included in the input nodalization. Hence, the simulation is considered as finished at 93 h after the SoT.

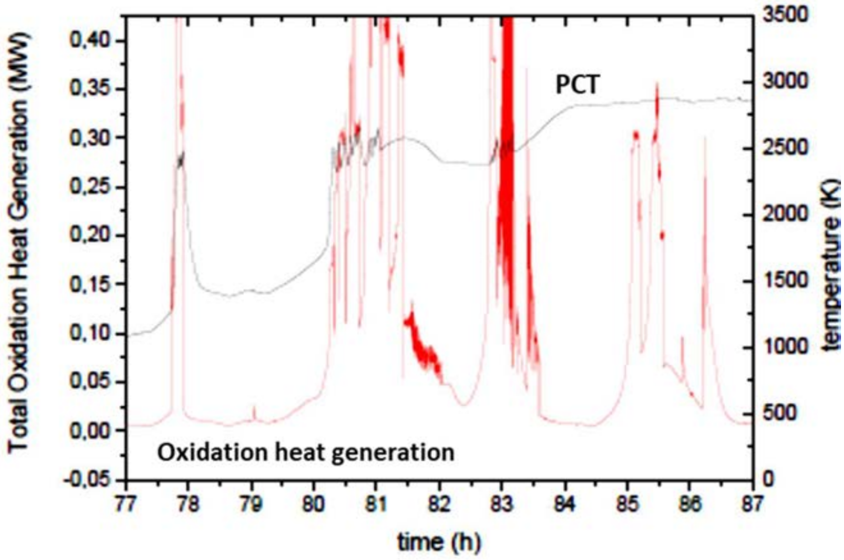

(a)

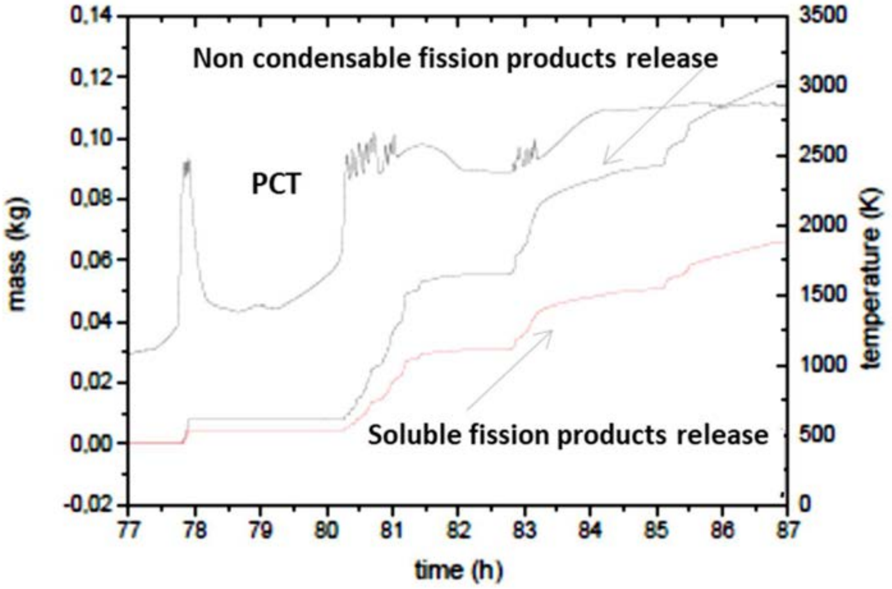

(b)

FIG. 176. Assessment of the SBO phenomena for severe accident conditions (a) PCT vs oxidation heat generation, (b) RPV circulation vs PRHRS circulation.

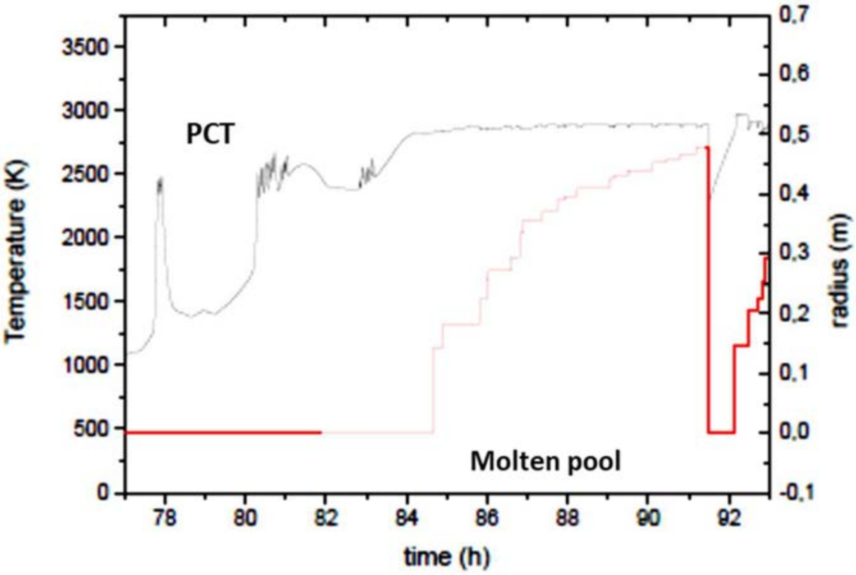

(c)

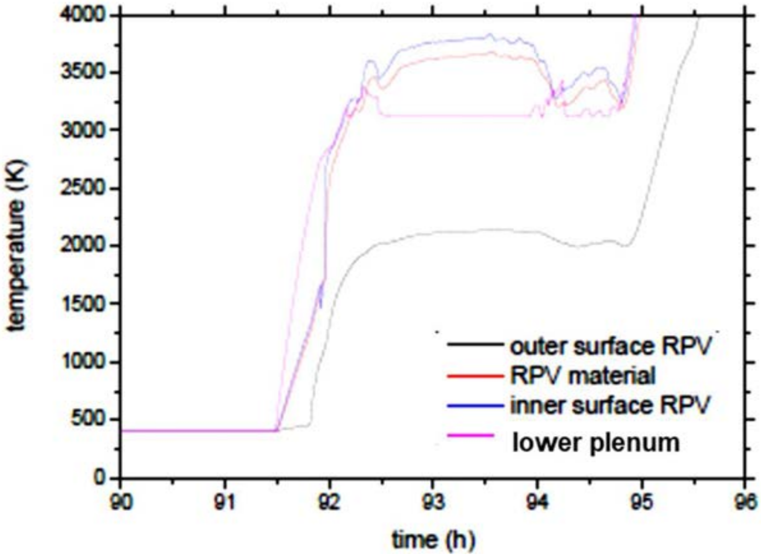

(d)

FIG. 176. Assessment of the SBO phenomena for severe accident conditions: (c) PCT vs molten pool radius, (d) temperatures in the lower plenum wall of the RPV.

<u>Uncertainty analysis</u>

The uncertainty analysis is carried out at first order of Wilks' formula to generate the 5th and the 95th percentile tolerance limits at a 0.95 confidence level, which requires 59 code runs.

The selected FOMs for the uncertainty analysis are the following:

O-1. Time when oxidation heat generation is greater than 0.1% of the nominal power by design (100

MW);

O-2. Time when $T_{cladding}$ is higher than ECCS acceptance criteria (1,477K);
O-3. Time$^{(*)}$ when cladding ruptures and fission product release occurs;
O-4. Time$^{(*)}$ when debris formation starts;
O-5. Time$^{(*)}$ when debris pool slumps to RPV lower plenum;
O-6. Time$^{(*)}$ when RPV creep rupture occurs;
O-7. Cumulative Hydrogen production until RPV creep rupture;
O-8. $T_{cladding}$ at which cladding ruptures and FP release occurs;
O-9. Cumulative non-condensable fission products released until RPV creep rupture;
O-10. Cumulative soluble fission products released until RPV creep rupture.

In the previous list, the time$^{(*)}$ for FOM O-3 to O-6 indicates a relative time to the $T_{cladding}$ exceeding the 1,477K (figure of merit O-2).

The analysis of the accident is divided in two parts. The first part analyses the effect of the input uncertainties to the plant availability and can be related to FOMs O-1 and O-2. The second part analyses the effect of the input uncertainty to the severe accident phenomena once core damage occurs and can be related to FOMs O-3, O-4, O-5, O-6, O-7, O-8, O-9 and O-10.

The calculations were stopped by a trip of creep rupture signal, and the maximum end time was set to 415,000 s. The calculation of the 59 cases with the perturbed input parameters resulted in:

- 1 failure during the steady state;
- 15 failures right after core slumping;
- 2 calculations reached end time without creep rupture;
- 1 calculation reached end time without core slumping nor creep rupture.

For a proper use of Wilk's formula all code runs need to terminate successfully and in the event of a code failure, it cannot be discarded, because the random nature of the sampling will be lost otherwise. In the event of code failures, however, they can be treated conservatively by assuming that their unknown result is the most adverse (extreme rank) and can therefore be discarded when going to applications of Wilk's formula at larger orders than first order. For instance, one code failure could be discarded at the second order application of Wilks' formula (93 code runs required) by assuming that rank 93 corresponds to the unknown value from the code failure and the 95/95 tolerance limit is estimated with rank number 92.

For the present analysis, due to the impracticability of repeating the 16 failures, all failures were re-executed by either reducing the time step (core slumping failures) or by broadening the bounds of the only active control of the reactor coolant system (secondary main feedwater). The repetition of the calculations using the same set of random input values, with the modifications indicated, lead to:

- Steady state failure, fixed;
- Four calculations fixed after core slumping, now reaches creep rupture.

Due to the number of cases that fail to reach creep rupture conditions or maximum end time, the uncertainty analysis with a quantitative estimation of the tolerance limits will be performed up to the core slumping. The considerations on the creep rupture will be qualitative.

Further analysis of the cases that fail to reach creep rupture conditions or maximum end time is required. The failure is due to water property error when debris material drops to lower plenum hydrodynamic component. The results of the uncertainty analysis are summarized in Table 75. From these results, it can be concluded that:

- The estimated time window of plant availability, calculated at the time at which the $T_{cladding}$ exceeds 1,477 K, is [38 h, 102.4 h], (O-1 and O-2). Both the base case (78 h) and the mean value (75 h) fulfill the ECCS acceptance criterion of CAREM design (72 h);
- The estimated time window at which cladding rupture occurs is [2.4, 5.2] minutes (O-3) after $T_{cladding}$ exceeds the acceptance criterion;
- The estimated $T_{cladding}$ window at which cladding rupture occurs is [2,180.2 K; 2,205.4 K], (O-8);
- The estimated time window at which debris formation starts is [5.5 h, 9.3 h] (O-4) after $T_{cladding}$ exceeds the acceptance criterion;
- The estimated time window at which the core slumping occurs (O-5) is [7.2 h, 19.1 h], excluding run # in which the core slumping never occurred;
- The estimated amount of H_2 generated is [22.7 kg, 32.3 kg] (O-7);
- The estimated mass of fission products release is [0.09 kg, 0.25 kg] of non-condensable and [0.05 kg, 0.14 kg] of soluble (O-9 and O-10, respectively).

TABLE 75. UNCERTAINTY ANALYSIS RESULTS

FOM	Units	Mean	Standard Deviation	Base Case	Lower Limit (perc 5/95)	Upper Limit (perc 95/95)
O-1	hr	75.4	10.8	77.8	38.0	102.4
O-2	hr	75.4	10.8	77.8	37.9	102.4
O-3	sec	178	32	173	142	314
O-4	hr	6.9	1.0	6.9	5.5	9.3
O-5	hr	13.4	2.7	13.7	7.2	19.1
O-6	hr	14.2	2.8	15.1	7.6*	20.4*
O-7	kg	27.4	2.5	26.2	22.7	32.3
O-8	K	2,196	5.0	2,194.8	2,180.2	2,205.4
O-9	kg	0.12	0.02	0.12	0.09	0.25
O-10	kg	0.07	0.01	0.06	0.05	0.14

*Qualitative only: cases with creep rupture

For the creep rupture, based on the set of # calculations that reach the creep rupture, the estimated time window at which the creep rupture occurs (O-6) is [7.6,20.4] h. The number of runs that reached the end time but in which the creep rupture never occurred is 14. To support the uncertainty analysis, the Pearson, Spearman and Kendall correlation coefficients for the input/output parameters and their corresponding significance values are calculated. The significance of the correlation coefficient is tested against the null hypothesis of no correlation, and the *p*-value measuring the probability of observing a correlation by chance is calculated from the Pearson, Spearman distribution and from the standard normal distribution (Kendall).

A potential correlation between the input and the output values is identified at the generally accepted significance value of 0.05.

The significance values for the three coefficients, and the potential correlations are highlighted in green are shown in Tables 76–78. The significance values are rounded and 0.00 indicates a value lower than 10^{-4} and not the exact 0.00. The correlation coefficients and the significance values for O-1 and O-2 (time at which the oxidation exceeds the 0.1% of the nominal power and at which the T_{cladding} exceeds the ECCS acceptance criterion) are practically the same and it therefore can be concluded that their analysis is equivalent. The same reasoning can be applied for O-9 and O-10 (FP release amount of non-condensable and soluble, respectively)

TABLE 76. SIGNIFICANCE OF PEARSON CORRELATION COEFFICIENTS

Pearson	HT-1	HT-2	HT-3	HT-4	HT-5	CHF	IPH-1	IPH-2	OXI	MP-1	MP-2	MP-3	SA-1	SA-2	SA-3	BC-1	BC-2	BC-3	DSG	DP
O-1	0.29	0.06	0.79	0.67	0.42	0.08	0.82	0.44	0.46	0.22	0.49	0.01	0.15	0.59	0.38	0.88	0.78	0.12	0.07	0.00
O-2	0.29	0.06	0.79	0.67	0.42	0.08	0.81	0.44	0.46	0.22	0.49	0.01	0.15	0.59	0.38	0.89	0.78	0.12	0.07	0.00
O-3	0.33	0.61	0.71	0.52	0.83	0.63	0.90	0.43	0.65	0.30	0.95	0.51	0.50	0.85	0.09	0.21	0.49	0.04	0.22	0.10
O-4	0.58	0.86	0.40	0.70	0.63	0.29	0.71	0.09	0.14	0.20	0.75	0.07	0.81	0.06	0.80	0.36	0.66	0.32	0.04	0.00
O-5	0.16	0.54	0.04	0.17	0.14	0.85	0.05	0.02	0.65	0.12	0.39	0.25	0.50	0.24	0.20	0.72	0.39	0.24	0.31	0.00
O-7	0.16	0.28	0.01	0.08	0.10	0.86	0.12	0.17	0.09	0.15	0.78	0.33	0.33	0.25	0.52	0.77	0.80	0.05	0.37	0.00
O-8	0.09	0.37	0.70	0.11	0.19	0.14	0.73	0.04	0.00	0.91	0.37	0.55	0.05	0.12	0.00	0.44	0.97	0.50	0.26	0.62
O-9	0.48	0.77	0.69	0.21	0.25	0.72	0.13	0.17	0.17	0.96	0.22	0.41	0.87	0.58	0.00	0.25	0.15	0.19	0.18	0.79
O-10	0.48	0.77	0.69	0.21	0.24	0.72	0.13	0.17	0.17	0.96	0.22	0.41	0.87	0.58	0.00	0.25	0.15	0.19	0.18	0.80

TABLE 77. SIGNIFICANCE OF SPEARMAN CORRELATION COEFFICIENTS

Spearman	HT-1	HT-2	HT-3	HT-4	HT-5	CHF	IPH-1	IPH-2	OXI	MP-1	MP-2	MP-3	SA-1	SA-2	SA-3	BC-1	BC-2	BC-3	DSG	DP
O-1	0.44	0.07	0.40	0.86	0.27	0.10	0.65	0.39	0.91	0.31	0.71	0.09	0.10	0.47	0.48	0.90	0.97	0.15	0.04	0.00
O-2	0.44	0.07	0.40	0.86	0.27	0.10	0.65	0.39	0.91	0.31	0.71	0.09	0.10	0.47	0.48	0.90	0.97	0.15	0.04	0.00
O-3	0.86	0.89	0.90	0.89	0.20	0.64	0.82	0.18	0.34	0.62	1.00	0.66	0.94	0.90	0.00	0.36	0.70	0.03	0.17	0.00
O-4	0.48	0.78	0.12	0.38	0.43	0.20	0.98	0.05	0.35	0.10	0.64	0.14	0.98	0.05	0.66	0.51	0.90	0.25	0.04	0.00
O-5	0.16	0.58	0.02	0.11	0.17	0.94	0.05	0.02	0.82	0.10	0.40	0.32	0.49	0.28	0.30	0.75	0.52	0.16	0.21	0.00
O-7	0.16	0.31	0.01	0.06	0.12	0.85	0.15	0.14	0.06	0.21	0.91	0.37	0.29	0.26	0.55	0.85	0.78	0.07	0.33	0.00
O-8	0.05	0.56	0.18	0.12	0.38	0.11	0.84	0.06	0.00	0.64	0.82	0.47	0.01	0.22	0.01	0.44	0.74	0.31	0.27	0.85
O-9	0.34	0.69	0.08	0.58	0.04	0.99	0.58	0.69	0.05	0.55	0.20	0.93	0.53	0.08	0.00	0.99	0.57	0.23	0.52	0.03
O-10	0.34	0.69	0.08	0.58	0.04	0.99	0.58	0.69	0.05	0.55	0.20	0.93	0.53	0.08	0.00	0.99	0.57	0.23	0.52	0.03

TABLE 78. SIGNIFICANCE OF KENDALL CORRELATION COEFFICIENTS

Kendall	HT-1	HT-2	HT-3	HT-4	HT-5	CHF	IPH-1	IPH-2	OXI	MP-1	MP-2	MP-3	SA-1	SA-2	SA-3	BC-1	BC-2	BC-3	DSG	DP
O-1	0.51	0.07	0.44	0.81	0.24	0.10	0.77	0.40	0.98	0.25	0.75	0.09	0.10	0.49	0.51	0.97	0.94	0.17	0.05	0.00
O-2	0.51	0.07	0.44	0.81	0.24	0.10	0.77	0.40	0.98	0.25	0.75	0.09	0.10	0.49	0.51	0.97	0.94	0.17	0.05	0.00
O-3	0.92	0.88	0.84	0.86	0.16	0.61	0.75	0.15	0.33	0.59	0.99	0.61	0.96	0.89	0.00	0.31	0.75	0.04	0.19	0.00
O-4	0.44	0.90	0.11	0.43	0.37	0.19	0.92	0.04	0.27	0.08	0.44	0.15	0.98	0.07	0.67	0.46	0.85	0.27	0.03	0.00
O-5	0.18	0.64	0.03	0.12	0.15	0.81	0.04	0.01	0.65	0.10	0.34	0.35	0.61	0.30	0.29	0.67	0.53	0.15	0.24	0.00
O-7	0.16	0.29	0.01	0.05	0.10	0.75	0.17	0.16	0.04	0.26	0.94	0.32	0.28	0.27	0.58	0.85	0.82	0.08	0.40	0.00
O-8	0.06	0.55	0.15	0.12	0.30	0.12	0.82	0.05	0.01	0.53	0.76	0.51	0.01	0.23	0.01	0.52	0.77	0.29	0.25	0.53
O-9	0.37	0.69	0.08	0.60	0.03	0.95	0.56	0.54	0.05	0.53	0.16	0.95	0.67	0.08	0.00	0.91	0.53	0.21	0.52	0.05
O-10	0.37	0.69	0.08	0.60	0.03	0.95	0.56	0.54	0.05	0.53	0.16	0.95	0.67	0.08	0.00	0.91	0.53	0.21	0.52	0.05

The results indicate the following:

1) *Decay power:* significance of three correlation coefficients, which is well below 0.05, indicates that the input value of the decay power influences both the plant availability (outputs O-1 and O-2) and the progression of the severe accident (outputs O-3, O-4, O-5, O-7, O-9, and O-10). However, the analysis of the results indicates that the primary output affected by de DP is O-2 and that this dependency is propagated to the other output parameters identified by the correlation coefficients. This dependency can be seen more clearly in the significance value of the correlation coefficients between the time when the design limit is achieved (O-2) and both

the sequence of the severe accident events (O-3, O-4, O-5) and the cumulative releases (O-7, O-9, O-10), as shown in Table 79. Because of the strong correlation between the decay power and the O-2, the rather large uncertainty on the DP can explain the large difference between the estimated 5/95 and 95/95 tolerance limits of 64h when compared to the reference design limit of 72h. Such dispersion is related to the uncertainty range of the decay power. This relation is shown in Fig. 177, which plots the decay power for the full set of runs. In that plot the cases with an O-2 time lower than the mean minus the standard deviation, 64.5h, are identified with the run number (6, 13, 15, 26, 37, 49, 55 and 58). The plot shows that most of them are those with highest values (the horizontal line indicates the decay power multiplier at 10%). On the other hand, the temperature associated to the fuel clad rupture (O-8) does not seem influenced by the decay power. This result seems reasonable given that it should depend on the material properties and how the energy is removed (by conduction, convection and/or radiation) and not on the actual amount of power.

TABLE 79. SIGNIFICANCE OF CORRELATION COEFFICIENTS BETWEEN O-2 AND THE OTHER OUTPUT PARAMETERS

O-#	Pearson Sig	Spearman Sig	Kendall Sig
O-3	0.61	0.00	0.00
O-4	0.00	0.00	0.00
O-5	0.00	0.00	0.00
O-7	0.00	0.00	0.00
O-9	0.16	0.47	0.92
O-10	0.42	0.02	0.03

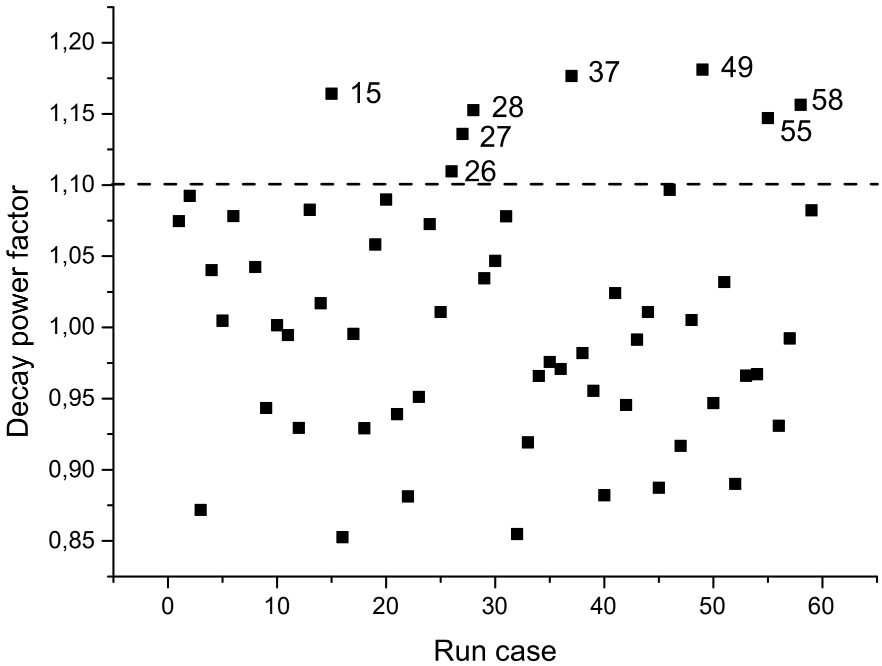

FIG. 177. Decay power for different run cases.

2) *Material properties (MP-1, MP-2, MP-3)*: material properties do not seem to have an influence on any of the output parameters. Only the Pearson correlation coefficients show a rather relevant significance, see for instance the correlation between MP-3 and O-2, and that seems to be an inconsistency because neither the Spearman nor the Kendall coefficients identify it. That can be explained from the fact that the Pearson coefficient is affected by the magnitude of the distance of each calculated value to the sample mean, but for the Spearman coefficient the information on the distances between sampled values is lost because all consecutive data (ranks) are equidistant [1]. This situation can lead to an unrealistic contribution of a single datapoint to the Pearson coefficient, and when this datapoint is removed from the analysis both the Pearson and the Spearman coefficients result in smaller correlation coefficients with no relevant significance. A numerical example of this behavior for the zircaloy heat capacity (input parameter MP-3) and the time at which the T_{cladding} exceeds the ECCS acceptance criterion (O-2) is presented:

   The calculated Pearson and Spearman correlation coefficients, along with the critical value above which the correlation can be considered significant are shown in Table 80.

TABLE 80. PEARSON AND SPEARMAN FOR O-2 AND MP-3

Pearson	0.321287
Spearman	0.224313
Critical value (0.5 significance, *N*=59)	0.256369

   The Pearson result suggests a relevant (linear) correlation, while the Spearman result does not identify any relevant (monotonic) correlation. This seems to be an inconsistency. Looking at the scatter plots in Fig. 178 it can be easily detected a single datapoint in the values plot that is significantly deviated from the O-2 bulk data (orange square in the left plot), and thus "far" from the mean value. However, this datapoint in the ranks plot (orange square in the right plot) cannot be as clearly differentiated from the bulk-data (ranks) as in the values case because the rank transformation locates the consecutive ranks at equidistant positions and the information on the distance between data is therefore lost.

   To test the effect of this particular data point, the correlation coefficients are re-calculated omitting this data point, and the results are shown in Table 81. It can be observed that both correlation coefficients are now below the critical value, and from these results the correlation between MP-3 and O-2 may be due to chance.

TABLE 81. PEARSON AND SPEARMAN FOR O-2 AND MP-3 WITHOUT RUN26

Pearson	0.230860
Spearman	0.184287
Critical value (0.5 significance, *N*=58)	0.258589

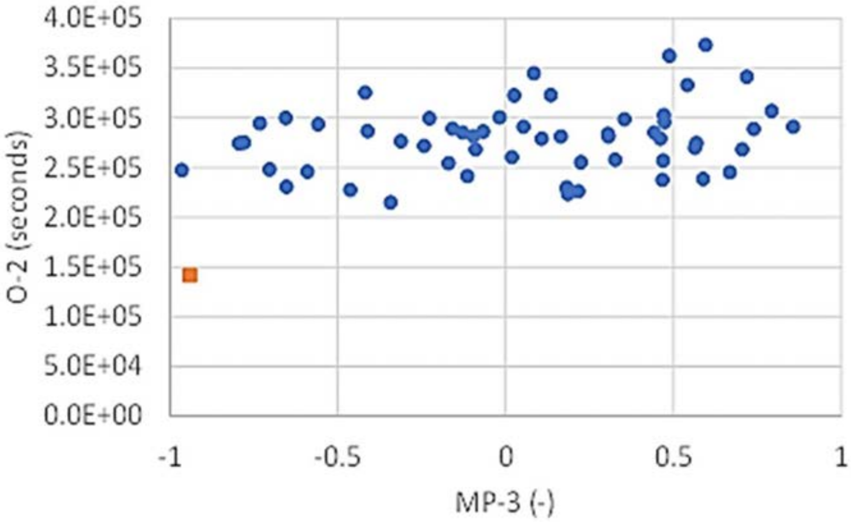

(a)

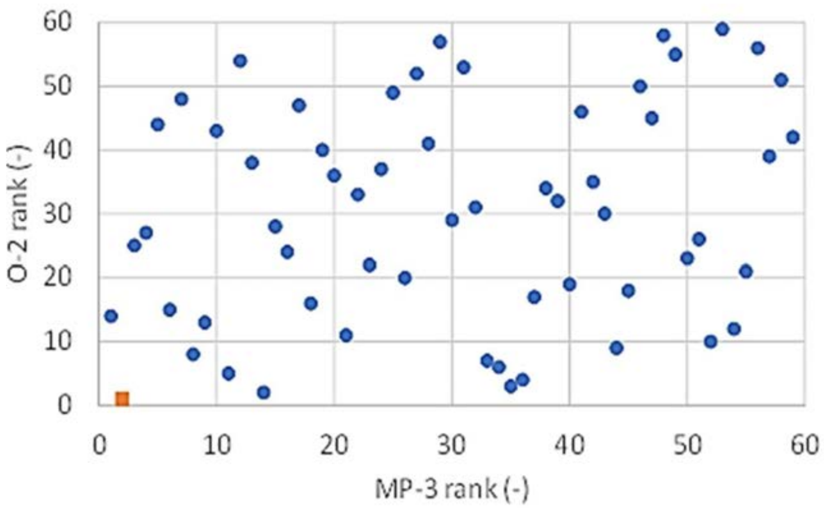

(b)

FIG. 178. (a) MP-3 vs O-2 values and (b) ranks.

The conclusion of the analysis is that, with the current data and results, the initial relevance indicated by Pearson coefficient can be dismissed.

3) *Heat transfer (HT-1, HT-2, HT-3, HT-4, HT-5):* significance of the heat transfer input parameters indicates a potential correlation with the progression of the severe accident (core slumping O-5, the cumulative production of H_2 O-7, and the cumulative release of FPs O-9 and O-10). Specifically, the subcooled nucleate boiling (HT-3) is identified by the three coefficients as relevant to the relative time of core slumping (O-5) and to the cumulative release of H_2 (O-7), and the single phase vapor (HT-5) is identified by the rank-based correlations as relevant to the cumulative release of fission products (O-9 and O-10). Also, the Spearman correlation is the only one that identifies the film boiling (HT-1) as relevant to the temperature at which cladding ruptures (O-8), and the Kendall correlation is the only one that identifies the saturated

subcooled (HT-4) as relevant to cumulative H_2 released (O-7)). However, the significances for the three correlations are rather similar and around the threshold of 0.05, and the conclusions on a relevant correlation need to be further analysed. In addition, for the temperature of cladding rupture O-8 the impact of the selected input uncertainty is not relevant as indicated by the small standard deviation (5K, see Table 75) and small distance between limits (25K, see Table 75). Among the identified heat transfer coefficients, it may be worth analysing in more detail the reason for identifying the subcooled boiling heat transfer (HT-3) relevant to the severe accident progression: during the severe accident progression, most of the time the debris material is accumulated at the support plate, and therefore the molten pool is mainly cooled by the boiling water accumulated in the core but also by the stagnant water in the lower plenum. This water is cooled by the ECS, hence a slight degree of subcooling can be expected as long as molten pool is stuck in the support plate.

4) *Oxidation*: influence of the oxidation correlations is clearly identified on the T_{cladding} when the cladding ruptures and on the hydrogen generation (O-8, and O-7, respectively). This correlation seems in accordance with the phenomena.
5) *Severe accident (SA-1, SA-2, SA-3):* significance of the severe accident parameters indicates a relevant influence on the cladding rupture (O-3 and O-8) and the cumulative release of fission products (O-9 and O-10). Specifically, the thickness of the shroud (SA-3) seems to be strongly correlated (significance $< 1.0\times10^{-4}$ for Spearman and Kendall correlations) with the fuel cladding rupture (O-3) and with the release of fission products (O-9 and O-10). This can be explained from the fact that in severe accident conditions, the shroud actuates as a radiation heat sink, and therefore the size of the structure should affect the time when fuel cladding fails as well as the amount of fission products and hydrogen generated. The influence of the fuel cladding rupture strain (SA-1) on the temperature at which the cladding rupture occurs (O-8) seems in accordance with the associated phenomena as well.
6) *Boundary condition parameters (BC):* correlation results indicate that the steady-state power (BC-3) is correlated with the relative time at which the fuel cladding rupture occurs (O-3) but shows no correlation with the T_{cladding} at which rupture occurs (O-8). Regarding the temperature output, the results for O-8 seem to be little affected by the uncertainty of the selected inputs as indicated by a standard deviation of only 5 K, a small value compared to the mean value (2,196 K) and to the distance between the tolerance limits (25 K), see Table 75. The conclusion for O-8 is that the T_{cladding} at which the rupture occurs is calculated by the specific code correlation and since it has not been included in the uncertain input parameters, the impact on O-8 of the uncertainty propagation is small. On the other hand, during the time interval defined by O-3 the heat removal by convection is lost and the variation of T_{cladding} mainly depends on the amount of energy stored in the fuel rod. Consequently, O-3 is correlated with the input parameters that influence the energy sources (BC-3 and DP). On the other hand, no relevant correlation is observed for O-2 and O-1 because both events are calculated relative to the start of the transient and Departure of Nucleate Boiling (DNB) does not take place for most of the time of the simulation (as shown in Table 74 the core dryout occurs at 74.5 h, and O-2 occurs at 77.8 h). From these results it can be concluded that the assessment of times relative to key events (or the assessment of time periods) are important because they do not drag the uncertainty propagated previously.
7) *Heat transfer area of the PRHRS (DSG):* correlation results indicate that the heat transfer area of the PRHRS is correlated with the plant availability and with the (relative) time at which

debris formation starts (O-4). Regarding plant availability, the rank-based correlation coefficients of DSG are significant with the time at which the T_{cladding} exceeds the ECCS acceptance criterion (O-2) and with the time at which the oxidation exceeds the 0.1% of the nominal power (O-1). The correlation with O-2 seems consistent because the condensation in the safety system can affect the collapsed level of the RPV and the timing of the core dryout. Regarding the potential correlation with O-4, it is not clear to the authors the effect of the DSG because the PRHRS is not active during the progression of the severe accident and therefore a priori, the apparent correlation is considered spurious. However, further analysis is advised. Finally, it is worth to mention that the uncertainty associated to this parameter (5%) is rather high compared the uncertainty of other design parameters because when building the SMR nodalization the authors did not find any reference about actual PRHRS designs, and therefore the surface areas were adjusted based on the PRHRS heat transfer versus RPV vessel correlation described in [6]. With the real data the uncertainty ranges for DSG need to be smaller and that would in turn reduce the impact on the plant availability.

8) *Interphase phenomena*: interphase heat transfer and friction seem to be correlated to the (relative) time at which core slumping occurs (O-5), as identified by the three correlation coefficients. Also, the effect of these input parameters is partially identified for the (relative) time of debris formation (O-4) and for the temperature at which cladding rupture takes place (O-8). As a general comment, since the interphase phenomena parameters determine the amount of vapor/liquid generated at the interphase and because during the severe accident progression there is a two-phase mixture and the evolution of the vessel empty is slow, it seems reasonable to have some type of dependence. However, further assessment is advised. Finally, the input parameters that have not been identified by any correlation at a significance level of 0.05 are heat transfer coefficient to vapor for the film boiling correlation (HT-2), the critical heat flux, the material properties (MP-1, MP-2), the pressure set-point of the EIS and the seasonal temperature variability of the containment, the EIS, the ECS and the PRHRS (BC-1 and BC-2), and the temperature for failure of oxide shell (SA-2). Looking at the overall results, however, the strong correlation coefficients of the decay power with most of the output parameters indicates a probable masking effect. It seems therefore advisable to review the uncertainty of the decay power and the calculation of other sensitivity measures such as the partial correlation coefficients, in which the effect of the rest of the sensed variables is minimized. In addition to this general recommendation, the authors suggest to further analyze the built-in uncertainty for the material properties because a priori there was some expected correlation with the outputs, and finally regarding the pressure and temperature boundary conditions (BC-1 and BC-2), although the result of no correlation seems reasonable for this scenario and reactor design, it is advised to keep such parameters for future analysis.

2.3.8.7. Summary and conclusions

An iPWR reactor has been modelled with RS3.5, including the core and safety systems that play an important role in an SBO long-term scenario (PRHRS, PRV, EIS and ECS). Due to the lack of data, the iPWR model is not based on a real design and some of the components (PRHRS) and control systems (main feedwater in secondary system) had to be defined by the authors to fulfill the nominal conditions and acceptance criterion of a reference design (CAREM-25 reactor).

The simulation of an iPWR extended Station Blackout scenario for low pressure core damage sequences has been simulated with success using RELAP/SCDAPSIM/MOD3.5 code. The analysis of the calculation results allowed identifying and understanding the key phenomena and events expected during the scenario such as natural circulation, PRHRS heat removal, RVs actuation, core exit temperature depressurization, EIS injection, core dryout, fuel rods oxidation, fuel rods ballooning and rupture, fission products release, hydrogen generation, debris formation, molten pool accumulation, core slumping and creep rupture.

An uncertainty analysis of the extended SBO scenario using the statistical BEPU propagation method based on the Wilks' formula has been also completed. The selection of the input parameters with uncertainty associated was based on the analysis of the reference calculation. A group of 20 parameters including boundary and initial conditions, material properties and code correlation was selected. The propagation of the uncertainties consisted in the re-execution of the reference case using 59 sample values of the selected input parameters. Ten scalar quantities have been assessed by estimating the 5/95 and 95/95 tolerance limits, as well as their mean and standard deviation. In addition, the Pearson, Spearman and Kendall correlation coefficients between the selected inputs and outputs have allowed to determine which of the input parameters had a strong influence on the selected output parameters. In the following subsections the main outcomes of the assessment are summarized.

During the performance of the project, the capabilities of the uncertainty analysis package integrated in RS3.5 have been extended by making available the built-in uncertainty of some MATPRO correlations, by adding code correlations for fluid-to-wall heat transfer and interphase phenomena, and by allowing the analysis of scalar quantities (output).

The *main sources of uncertainty identified* are:

- The correlation of the decay power with the plant availability outputs (O-1, O-2) is strong and is propagated to the severe accident outputs. The rather large uncertainty of the decay power may be masking the effect of other influential input parameters and it is therefore recommended to review the uncertainty definition of decay power, as well as the calculation of other sensitivity measures such as the partial correlation coefficients, which measures the strength of an association between two variables while removing the effect of the rest;
- The correlation of the shroud thickness (SA-3) is particularly strong with the fuel cladding rupture (O-3 and O-8) and with the release of fission products (O-9 and O-10). It is recommended to update the value and uncertainty of SA-3 with referenced design data, which is not available at the time the analysis is performed;
- The correlation of the oxidation correlations and rupture strain (SA-1) also seem to have an impact on the progression of the severe accident;
- The heat transfer parameters seem to play an important role in the severe accident progression during the cooling of the molten pool;
- The correlation of the area of the PRHRS (DSG) with the plant availability is significant, but it may be due to the rather large uncertainty associated. It is therefore advised to update the value and uncertainty of DSG with referenced design data, which is not available at the time the analysis is performed;
- The correlation of the interphase phenomena with the severe accident progression is also identified as significant. Given the two-phase nature of the fluid during the long-term empty of the RPV, it

seems reasonable to have some degree of correlation. However, further analysis of the uncertainty ranges as well as of the specific parameters representing the interphase phenomena is advised;

— The effect of the boundary conditions, the material properties and the critical heat flux is not significant. However, it is advised to maintain these parameters in future uncertain analysis and review the built-in uncertainty for the material properties.

Lesson learned and best practices are:

— With regards to the FOMs, it is advisable to carefully select between relative and absolute times to avoid dragging the effect of uncertainties to posterior events. This is specially recommended for severe accident scenarios, in which the plant availability and the severe accident progression can have different influential parameters. It is also important to take into account that the cumulative release of fission products as well as the cumulative generation of H_2 are also affected by the uncertainty propagated from the DBA conditions.

— Regarding the correlation coefficients, the Kendall formulation is advisable because it seem less dependent to singular datapoints than the Spearman calculations. In addition, it is advisable to calculate other type of sensitivity coefficients such as the partial correlation coefficients to try avoiding masking effects of strong correlations.

3. SUMMARY AND CONCLUSIONS

3.1. SUMMARY

According to the proposed methodologies for the uncertainty and sensitivity analysis in the framework of the IAEA CRP I3103, the PWR and SMR group carried out separately the planned tasks, including (a) plant modelling and nodalizations (b) simulation of the reference cases, and (c) assessment of the uncertainty and sensitivity through a coupling of the relevant severe accident codes with the corresponding uncertainty and sensitivity quantification tools. The followings summarize main results and relevant insights gained through the plant application exercises for several dedicated severe accident codes and uncertainty and sensitivity analysis methodologies applied to the PWR and SMR types of plants.

3.1.1. Large-scale PWRs

<u>DNPER:</u> for an SBO accident scenario of the K-2 NPP (ACP1000) plant, the MELCOR 1.8.6 simulations of N = 2,548 (SRS) were carried out using uncertain parameter values sampled randomly with 95% probability and 95% confidence level of the relevant PDFs. An in-house tool, DST, was used for the uncertainty quantification. Pearson, Spearman, and Kendall correlations were applied as part of the sensitivity analysis. The sensitivity analysis results, which was determined by using a weighted average of the relevant correlation coefficients, showed that the uncertainty spectrums of relevant FOMs provided more appropriate safety threshold as compared to conservative model and assumptions. The sensitivity results suggested that uncertain parameters exert their influence at different timing and their effects vary in magnitude.

<u>ENRRA:</u> for a LBLOCA scenario without control rod insertion of the German-type KWU-PWR plant (1300 MWe), an advanced method based on the SVD/UT and LRA/UT algorithms was introduced to reduce the

computation time required by a random sampling like Monte Carlo. Relevant PCTs were calculated using ATHLET, and the reactivity coefficients and relevant covariance matrix were computed using SCALE6.2. The plant application results showed that the difference between the reactivity input and sample means calculated using the proposed sampling algorithms is much smaller than the SRS, where the difference between the relative standard deviation in the PCT calculated by the three sampling techniques is due to the non-linearity of the calculating model.

KAERI: for a STSBO of the OPR1000 plant, three reference case scenarios, a base and two cases employing dedicated mitigation strategies were employed for the uncertainty analysis. DAKOTA (MELCOR) and MOSAIQUE (MAAP5) were used as tools for the uncertainty quantification. Among the tested MELCOR2.2 and MAAP5.05 simulations of $N = 200$ (SRS), a high failed run was observed in the MELCOR simulations. The uncertainty results showed that the three reference cases led to almost the same trend until before taking operator actions for the dedicated mitigation, but, thereafter, each case scenario led to somewhat different trends each other. Pearson and Spearman correlations, PRCC, and SRRC were applied as part of the sensitivity analysis. The sensitivity analysis results, which were determined by using a weighted average of the relevant correlation coefficients, showed that a few uncertainty inputs much more influenced the uncertainties of relevant FOMs in one case scenario but did not necessarily have the impact of the same level in another case scenarios.

KINS: for an SBO accident with operator manual depressurization of the APR1400 plant, the coupled analysis of MELCOR2.2 and COOLAP was carried out to evaluate uncertainties associated with the corium relocation and cooling when the reactor cavity is in the wet conditions in prior to the vessel failure. With the approach, a new two-cavity model was designed for MELCOR to accommodate separately the coolable and non-coolable corium in the reactor cavity. The COOLAP program was used to define specific initial conditions for the MELCOR analysis during long-term cooling. The uncertainty analysis was based on the sample simulation of $N = 300$ (LHS) and DAKOTA was used as a tool for the uncertainty quantification. A simple parametric approach (i.e., one-at-a-time) was applied as part of the sensitivity analysis.

SJTU: for an SBO accident of the CNP600 plant, the hydrogen source term analysis was carried out using MELCOR 1.8.5, and the influence of the mitigation measures (opening of the PSVs) on each relevant FOM were discussed. A plant model mainly includes primary and secondary loop, pressurizer, pressure relief tank and containment. The uncertainty analysis was performed through the simulation of the samples of $N = 120$ (LHS), and time trends and relevant PDFs for the in-/ex-vessel H_2 generation (FOMs) were presented as part of the uncertainty results. The uncertainty results showed that the pressure relief measures as taken for accident mitigation had obvious influence on the hydrogen source term. Pearson and Spearman correlation coefficients, PCC, and PRCC were calculated as part of the sensitivity analysis.

UoS: for an SBO accident of the APR1400 plant, an efficient PCA-based Monte Carlo uncertainty quantification scheme was introduced to assess contribution of nuclear data cross-sections to the uncertainty of fuel temperature. The proposed approach paves the way for the inclusion of large number of sources in uncertainty quantification practices in severe accidents analysis. The 3KEYMASTER simulator was used to simulate the plant's response following the SBO accident, using the cross-sections as it main uncertainty input. The analysis results indicated a minor contribution of the cross-sections to the FOM of interest. The process was completed with 120 model runs instead of 2800 that would have been required if the proposed algorithm.

3.1.2. SMR (iPWR)

CNEA: for a LOCA scenario of an iPWR (CAREM-like SMR), the MELCOR 1.8.6 simulations of $N = 59$ (SRS) were carried out for the unceratinty analysis. The number of simulations is based on the application of Wilks formula with both confidence and probability levels of 95% (N = 59). DAKOTA was used as a tool for the uncertainty quantification. Pearson and Spearman correlations were applied as part of the sensitivity analysis. The sensitivity analysis results showed that the most relevant parameters affected the defined FOMs correspond to the MELCOR physical model category and the decay heat multiplier was the most important among them.

ENSO: for an extended SBO scenario of an iPWR (CAREM-like SMR), the RELAP/SCDAPSIM/MOD3.5 simulations of $N = 59$ (SRS) were carried out for the unceratinty analysis. As like the CNEA, the number of simulations is based on the minimum sample size required for one-side Wilks tolerance limit, 95%/95%. The IUA package was used as a tool for the uncertainty quantification. The plant application mainly focused on plant availability, calculated at the time at which cladding temperature exceeds 1,477K and on severe accident phenomena after a core damage. The uncertainty analysis results indicated that it is necessary to carefully select between relative and absolute times to avoid dragging the effect of uncertainties to posterior events. The Pearson, Spearman and Kendall correlation analysis results, which was applied as part of the sensitivity analysis, showed that it is advisable to calculate other type of sensitivity coefficients such as the partial correlation coefficients to try avoiding masking effects of strong correlations.

3.2. CONCLUSIONS

According to the CRP framework for the uncertainty and sensitivity analyses, the eight partners, all the partners, who participated in the exercises of PWR and SMR types, have successfully implemented their own planned tasks. The relevant FOM's range was well estimated, and the most impacting parameters were identified per each partner. Nevertheless, a deeper understanding of several aspects is still required to ensure the applicability of the utilized approaches in the context of severe accident analyses, and to advance the current framework for uncertainty and sensitivity analyses, *for example*:

— Specify more relevant inputs influencing FOMs of interest to get more robust results on their uncertainties and more relevant PDFs which could well characterize the underlying uncertainties of given input parameters;
— Check the influence of uncertainty sources related to plant nodalization schemes and/or code-specific modelling approaches (e.g., different sub-models and correlations employed by each code);
— Check the influence of sample sizes applied for the uncertainty analysis in terms of how many statistical samples are enough to ensure a confidence for the analysis results, if possible, so that mean and standard deviation of the relevant FOM converge with the number of samples;
— Check the influence of possible code crash (failed code run) and/or biases including outliers in simulation results, being often observed in the sampling-based uncertainty analyses;
— Explore sensitivity measures less dependent to singular data points (e.g., Kendall formulation) and to avoid masking effects of strong correlations which indicate the strength of an association between two variables while removing the effect of the rest (e.g., PCC and/or PRCC);
— Understand the limitation of linear regression and correlation-based sensitivity measures employed by most of the CRP partners, and explore the other types of sensitivity measures characterizing

non-linear relationships between input and response variables as the possible alternative;
- Together with this, possible alternative uncertainty analysis methods need to be further investigated.

REFERENCES

[1] IAEA, Approaches and Tools for Severe Accident Analysis for Nuclear Power Plants, IAEA Safety Reports Series No. 56, IAEA, Vienna (2000).

[2] Gauntt, R.O., Cole, R.K., Erickson, C.M., Gido, RIG, Gasser, R.D., Rodriguez, S.B., Young, M.F., MELCOR Computer Code Manuals, Vol. 1: Primer and Users' Guide, Version 1.8.6, NUREG/CR-6119 (Rev. 3), SAND 2005-5713, Sandia National Laboratories, Albuquerque, NM, USA (2005).

[3] Gauntt, R.O., Cole, R.K., Erickson, C.M., Gido, RIG, Gasser, R.D., Rodriguez, S.B., Young, M.F., MELCOR Computer Code Manuals, Vol. 2: Reference Manuals, Version 1.8.6, NUREG/CR-6119 (Rev. 3), SAND 2005-5713, Sandia National Laboratories, Albuquerque, NM, USA (2005).

[4] Humphries, L.L., Beeny, B.A., Gelbard, F., Louie, D.L., Phillips, J., MELCOR Computer Code Manuals, Vol. 1: Primer and Users' Guide, Version 2.2, SAND2017-0455, Sandia National Laboratories, Albuquerque, NM, USA (2017).

[5] EPRI, Modular Accident Analysis Program Version 5.04 EPRI Product ID 3002007340, Vol. 1–4, Electric Power Research Institute (EPRI), USA (2016).

[6] ATHLET, ATHLET Programmer's Manuals, *GRS-P-1,* Vol. 2, No. 7 (2017).

[7] TRAMBAUER, K., Coupling methods of thermal-hydraulic models with core degradation models in ATHLET-CD, Nuclear Engineering — ICONE6 (Proc. 6th Int. Conf. San Diego, CA) (1998).

[8] RELAP5 Code Development Team, RELAP5/MOD 3.3 Code Manual, Vol 1–8, NUREG/CR-5535/Rev1 (2010).

[9] Allison, C.M., Hohorst, J.K., Role of RELAP/SCDAPSIM in nuclear safety, *Science and Technology of Nuclear Installations,* (March 2010).

[10] SCDAP/RELAP5 Development Team, SCDAP/RELAP5/MOD3.2 Code Manual, Vol. 1–5, NUREG/CR-6150, INEL-96/0422 (July 1998).

[11] Jacquemain, D., Bourdon, S., de Braemaeker, A., Barrachin, M., *Final report FPT-1*; Saint-Paul-lez-Durance, France (2000)

[12] Sepold, L., et al., Experimental and Computational Results of the QUENCH-06 Test (OECD ISP-45). Report FZKA-6664. Karlsruhe, Germany (2004).

[13] Hering, W., Homann, C., Lamy, J.-S., Miassoedov, A., Schanz, G., Sepold, L., Steinbrück, M., Comparison and Interpretation report of the OECD International Standard Problem no.45 Exercise (QUENCH-06). Report FZKA-6722, Forschungszentrum Karlsruhe, Germany (2002).

[14] ORNL, SCALE: A Comprehensive Modeling and Simulation Suite for Nuclear Safety Analysis and Design, ORNL/TM-2005/39, Available from Radiation Safety Information Computational Center at Oak Ridge National Laboratory (ORNL) as CCC-785, USA (2011).

[15] SCALE, SCALE 6.2.2 Manual, Getting started with SCALE 6.2.2 (2017).

[16] Wieselquist, W.A., Lefebvre, R.A., and Jessee, M.A., SCALE Code System, ORNL/TM-2005/39, Version 6.2.4, Oak Ridge National Laboratory, Oak Ridge, TN, USA (2020).

[17] 3KEYMASTER Platform Product Sheet, Frederick, Western Services Corporation, Maryland, USA (2016).

[18] Moriyama, K. et al. Parametric Model for Ex-Vessel Melt Jet Breakup and Debris Bed Cooling, Nuclear Engineering — ICONE26 (Proc. 26th Int. Conf. London, England) (2018).

[19] Wilks, S. S., Statistical prediction with special reference to the problem of tolerance limits, *Ann Math Stat,* **13**(4), pp. 400–409 (1942).

[20] Cleff, T., Exploratory Data Analysis in Bussiness and Economics (An introduction using SPSS, STAT

and Exce), *Exploratory Data Analysis in Bussiness and Economics (An introduction using SPSS, STAT and Exce)*, Springer.
[21] USNRC, State of-the-Art Reactor Consequences Analysis (SOARCA) Report, NUREG/CR-7110, U.S. Nuclear Regulatory Commission (USNRC), Washington, D.C. (2012).
[22] USNRC, Fukushima Daiichi Unit 1 Uncertainty Analysis – Preliminary Selection of Uncertain Parameters and Analysis, SAND2014–1170, Sandia National Laboratories, Albuquerque, NM, USA (2014).
[23] Luo, H., Quantified PIRT and Uncertainty Quantification for Computer Code Validation, OREGON State University (2013).
[24] Ganutt, R.O., Kalinich, D.A., et al., MELCOR Simulation of Severe Accident at the Fukushima 1F1 Reactor, Proceedings of 2012 ANS Winter Meeting & Nuclear Technology Expo, San Diego, CA, USA (Nov. 2012).
[25] Ganutt, R.O., Kalinich, D.A., et al., Fukushima Daiichi Accident Study, SAND2012-6173, Sandia National Laboratraries: Albuqueque, NM, USA (2012).
[26] Abdel-Khalik, H., & al., e. Reduced order modeling for nonlinear multicomponent models. International Journal for Uncertainty Quantification, 2(4), 341–336 (2012).
[27] McKay, M. , & et. al. A comparison of three methods for selecting values of input variables in the analysis of output from a computer code. Technometrics American Statistical Association, 21(2), 239-245 (1979).
[28] Sobol, I. (1993). Sensitivity estimates for nonlinear mathematical models. Mathematical Modelling and Computational Experiments, 1, 407–414 9 (2013).
[29] Janssen, H. Monte-Carlo based uncertainty analysis: Sampling efficiency and sampling convergence. Reliability Engineering and System Safety, 109, 123–132.
[30] Eckart, C., & Young, G. The approximation of one matrix by another of lower rank. *Psychometrika,* 1(1936).
[31] Wan, E., & Merwe, R. The Unscented Kalman Filter. *Wiley Publishing* (2001).
[32] Xiaoqin, Z., & al. SVD based Kalman particle filter for robust visual tracking. SVD based Kalman particle filter for robust visual tracking (2008).
[33] Tsyganova, J., & Kulikova, M. SVD-based Kalman Filter Derivative Computation. *IEEE Transactions on Automatic Control*, 62(9), 4869–4875 (2007).
[34] Press, W. H., & al. Numerical Recipes 3rd Edition, The art of scientific computing. *Cambridge University Press*, 3 edition (2007).
[35] Cacuci, D. G. Sensitivity and Uncertainty Analysis, Theory, Vol. 1. *Chapman & Hall/CRC*, Boca Raton (2003).
[36] Foad, B., & Takeda, T. Sensitivity and Uncertainty Analysis for UO_2 and MOX Fueled PWR Cells. *Annals of Nuclear Energy*, 75, 595–604 (2015).
[37] Guo, L, Cao, X. Sensitivity Analysis of Hydrogen Source Term under LB-LOCA severe accident in Nuclear Power Plant, *Nuclear Power Engineering*, **28**(5), pp. 69–74 (2007).
[38] Itoh, H, Zheng, X, Tamaki, H., et al, Source term uncertainty analysis: probabilistic approaches and applications to a BWR severe accident, *Mechanical Engineering Journal*, **2**(5):15–00032 (2015).
[39] Balakrishnan, N, Colton, T, Everitt, B, et al., Latin Hypercube Sampling, Wiley StatsRef: Statistics Reference Online (2014).
[40] Helton, J,C,, Davis, F.J., Johnson, J.D, A comparison of uncertainty and sensitivity analysis results obtained with random and Latin hypercube sampling, *Reliability Engineering & System Safety*, **89**(3),

pp. 305–330 (2005).
[41] Wilks, S.S., Determination of Sample Sizes for Setting Tolerance Limits, *Annals of Mathematical Stats*, **12**(1), pp. 91-96 (1941).
[42] Marino, S, Hogue, I.B, Ray, C.J., et al., A methodology for performing global uncertainty and sensitivity analysis in systems biology, *Journal of theoretical biology*, **254**(1), pp. 178–196 (2008).
[43] Itoh, H., Zheng. X., Tamaki. H., et al., Influence of in-vessel melt progression on uncertainty of source term during a severe accident, 22nd International Conference on Nuclear Engineering (ICONE), American Society of Mechanical Engineers, V006T15A002-V006T15A002 (2014).
[44] Gauntt, R.O., Bixler. N.E., Wagner, K.C., An uncertainty analysis of the hydrogen source term for a station blackout accident in Sequoyah using MELCOR 1.8.5, SAND2014-2210, Sandia National Laboratories Letter Report to USNRC (2002).
[45] Gharari, R., Kazeminejad, H., Kojouri, N.M., et al., Application of a severe accident code to the sensitivity and uncertainty analysis of hydrogen production in the WWER1000/V446, *Annals of Nuclear Energy*, **152**:108018 (2021).
[46] Ross, K., Phillips, J., Gauntt, R.O., Wagner, K., MELCOR best practices as applied in the state-of-the-art reactor consequence analyses (SOARCA) project, US Nuclear Regulatory Commission, Office of Nuclear Regulatory Research (2014).
[47] Kudinov, P., Davydov. M. Development and validation of conservative-mechanistic and best estimate approaches to quantifying mass fractions of agglomerated debris, *Nuclear Engineering and Design*, **262**, pp. 452–461 (2013).
[48] Kudinov, P., Karbojian, A., Tran, C.T., et al.. Agglomeration and size distribution of debris in DEFOR - A experiments with Bi2O3-WO3 corium simulant melt, *Nuclear Engineering and Design*, **263**, 284–295 (2013).
[49] Magallon, D., Characteristics of corium debris bed generated in large-scale fuel-coolant interaction experiments, *Nuclear Engineering and Design*, **236**(19–21), pp. 1998-2009 (2006).
[50] Nguyen, D.H., Fichot, F., Topin, V., Investigation of the structure of debris beds formed from fuel rods fragmentation, *Nuclear Engineering and Design*, **313**, pp. 96–107 (2017).
[51] Pontillon, Y., Malgouyres, P., Ducros, G., et al., Lessons learnt from VERCORS tests: Study of the active role played by UO2–ZrO2–FP interactions on irradiated fuel collapse temperature, *Journal of Nuclear Materials*, **344**(1–3), pp. 265–273 (2005).
[52] Sergey, Galushin, Pavel Kudinov, Analysis of the effect of MELCOR modelling parameters on in-vessel accident progression in Nordic BWR, *Nuclear Engineering and Design*, **350**, pp. 243-258 (2019).
[53] Choi, W., Kim, T., Jeon, J., et al., Effect of Molten Corium Behavior Uncertainty on the Severe Accident Progress, *Science and Technology of Nuclear Installations*, **2018**, (2018).
[54] Galushin, S., Kudinov, P., Sensitivity and uncertainty analysis of the vessel lower head failure mode and melt release conditions in Nordic BWR using MELCOR code, *Annals of Nuclear Energy*, **135**:106976 (2020).
[55] Park, S.Y., Park, J.H., Kim, S.D., et al., Evaluation of upward heat flux in ex-vessel molten core heat transfer using MELCOR, No. JAERI-CONF–2000–015, Japan (2000).
[56] Jung, W.H., Hwanga, B., Park, H.S., et al., Simulation of CCI experiments for the sensitivity analysis with MELCOR 2.2, Transactions of the Korean Nuclear Society Autumn Meeting Yeosu, Korea (October 2018).
[57] Sheskin, D.J., Handbook of Parametric and Nonparametric Statistical Procedures. CRC Press, Florida,

USA (2004).
[58] Rao, R.S., Kumar, A., Gupta, S.K., et al., Uncertainty and sensitivity analysis of TMI-2 accident scenario using simulation based techniques, *Nuclear Engineering and Technology*, **44**(7), 807-816 (2012).
[59] Smith, R.C., Uncertainty quantification: theory, implementation, and applications. Siam; 2013 Dec 2 (2013).
[60] Cacuci, D.G., Second-order adjoint sensitivity analysis of a general ratio of functionals of the forward and adjoint fluxes in a multiplying nuclear system with source, *Annals of Nuclear Energy*. **135**:106956 (2020).
[61] Abdel-Khalik, H.S., Bang, Y., Wang, C., Overview of hybrid subspace methods for uncertainty quantification, sensitivity analysis, *Annals of Nuclear Energy*. **52**, pp. 28-46 (2013).
[62] Yamamoto, A., Kinoshita, K., Watanabe, T., Endo, T., Kodama, Y., Ohoka, Y., Ushio, T., Nagano, H., Uncertainty quantification of LWR core characteristics using random sampling method, *Nuclear Science and Engineering*. **181**(2), pp.160-74 (2015).
[63] Giles, M. Monte Carlo Methods for Uncertainty Quantification, Lecture from the KU Leuven Summer School on Uncertainty Quantification (2013).
[64] Avramova, M.N., Ivanov, K.N., Verification, validation and uncertainty quantification in multi-physics modeling for nuclear reactor design and safety analysis, *Progress in Nuclear Energy*, **52**(7), pp. 601-14 (2010).
[65] Metwally, W.A., Alawad, A.S., Khuwaileh, B.A., On the over-conservatism of the 5% depletion uncertainty rule in spent fuel criticality analyses, *Annals of Nuclear Energy*, **125**, pp. 1-1 (2019)
[66] Arbanas, G., Williams, M.L., Leal, L.C., Dunn, M.E., Khuwaileh, B.A., Wang, C., Abdel-Khalik, H., Advancing inverse sensitivity/uncertainty methods for nuclear fuel cycle applications. *Nuclear Data Sheets*. **123**, pp. 51-56 (2015).
[67] Abdel-Khalik, H.S., Turinsky, P.J., Jessee, M.A., Efficient subspace methods-based algorithms for performing sensitivity, uncertainty, and adaptive simulation of large-scale computational models, *Nuclear Science and Engineering*, **159**(3), pp. 256-72 (2008).
[68] Constantine, P.G., Dow, E., Wang, Q., Active subspace methods in theory and practice: applications to kriging surfaces, *SIAM Journal on Scientific Computing*, **36**(4):A1500-24 (2014).
[69] Foad, B., Yamamoto, A., Endo, T., Efficient uncertainty quantification for PWR during LOCA using unscented transform with singular value decomposition, *Annals of Nuclear Energy*, **141**:107341 (2020).
[70] Khuwaileh, B.A., Said, Z., Differential parameters uncertainty estimation via a principal component analysis -based Monte Carlo sampling approach: IRT-4M fuel type as a case study, *Journal of Nuclear Science and Technology*, **58**(9), pp. 984-991, DOI: 10.1080/00223131.2021.1899996 (2021).
[71] Advanced Reactors Information System (ARIS): Advanced power reactor 1400 MWe (APR1400), Report No. 83 (2011).
[72] KEPCO/KHNP, APR1400 Design control document tier 2, Chapters 1-8, Korea Electric Power Corporation (KEPCO); Korea Hydro & Nuclear Power Co., Ltd. (KHNP) (2014).
[73] Turinsky, P.J., Al-Chalabi, R.M., Engrand, P.H., Sarsour, H.N., Faure, F.X., Guo, W.E., NESTLE: Few-group neutron diffusion equation solver utilizing the nodal expansion method for eigenvalue, adjoint, fixed-source steady-state and transient problems. EG and G Idaho, Inc., Idaho Falls, ID; Los Alamos National Lab., NM, USA (June 1994 Jun).
[74] Zvirin, Y., A review of natural circulation loops in pressurized water reactors and other systems, *Nuclear Engineering and Design*, **67**(2), pp. 203-225 (1982).

[75] Halko, N., Martinsson. P.G., Tropp, J.A., Finding structure with randomness: Probabilistic algorithms for constructing approximate matrix decompositions, *SIAM review*, **53**(2), pp. 217-88 (2011).

[76] Khuwaileh, B., Williams, B., Turinsky, P., Hartanto, D., Verification of reduced order modeling based uncertainty/sensitivity estimator (ROMUSE), *Nuclear Engineering and Technology*, **51**(4), pp. 968-976 (2019).

[77] Adams, B.M., Coleman, K., Gilkey, L.N., Gordon, N., Hooper, R., Khuwaileh, B.A., Lewis A., Maupin, K., Smith, R.C., Swiler, L.P., Turinsky, P.J., User guidelines and best practices for casl vuq analysis using Dakota, Los Alamos National Lab. (LANL), Los Alamos, NM, USA (Oct. 2017).

[78] Rearden, B.T., Mueller, D.E., Uncertainty quantification techniques of SCALE/TSUNAMI. *Transactions of the American Nuclear Society*, **104**:371 (2011).

[79] Rearden, B.T., SAMS: Sensitivity Analysis Module for SCALE, SCALE 6.1 Manual. ORNL/TM-2005/39, Oak Ridge National Laboratory, USA (2009).

[80] Ilardo, P.H., et al., Development of Uncertainty and Sensitivity Approaches for the Analysis of Severe Accidents in a Small Modular Reactor, International Conference on Topical Issues in Nuclear Installation Safety: Strengthening Safety of Evolutionary and Innovative Reactor Designs, Vienna, Austria (2022).

[81] Wilks, S.S., Statistical prediction with special reference to the problem of tolerance limits, *Ann Math Stat,* 13(4), pp. 400–409 (1942).

[82] SNL, DAKOTA, A Multilevel Parallel Object-Oriented Framework for Design Optimization, Parameter Estimation, Uncertainty Quantification, and Sensitivity Analysis: Version 6.10 User's Manual, SAND2014-4633, Sandia National Laboratories, Albuquerque, NM, USA (2019).

[83] SNL, DAKOTA, A Multilevel Parallel Object-Oriented Framework for Design Optimization, Parameter Estimation, Uncertainty Quantification, and Sensitivity Analysis: Version 6.10 Reference Manual, SAND2014-5015, Sandia National Laboratories, Albuquerque, NM, USA (2019).

[84] Kim, J., et al., Human and organizational factors for multi-unit probabilistic safety assessment: Identification and characterization for the Korean case, *Nuclear Engineering and Technology,* **51**(1), pp. 104-115 (2019).

[85] IAEA, Progress in Methodologies for the Assessment of Passive Safety system Reliability in Advanced Reactors, IAEA-TECDOC-1752, International Atomic Energy Agency (IAEA), Viena, Austria (2014).

[86] Kim, J., et al., Human and organizational factors for multi-unit probabilistic safety assessment: Identification and characterization for the Korean case, *Nuclear Engineering and Technology,* **51**(1), pp. 104-115 (2019).

[87] IAEA, Progress in Methodologies for the Assessment of Passive Safety system Reliability in Advanced Reactors, IAEA-TECDOC-1752, International Atomic Energy Agency (IAEA), Viena, Austria (2014).

[88] Gauntt, R.O., et al., Uncertainty Analyses Using the MELCOR Severe Accident Analysis Code, Workshop proceedings evaluation of uncertainties in relation to severe accidents and level-2 probabilistic safety analysis, Aix-en-Provence, France (2007).

[89] SNL, An Uncertainty Analysis of the Hydrogen Source Term for a Station Blackout Accident in Sequoyah Using MELCOR 1.8.5, SAND2014-2210, Sandia National Laboratories, Albuquerque, NM, USA (2014).

[90] Choi, W., et al., Effect of Molten Corium Behavior Uncertainty on the Severe Accident Progress, *Science and Technology of Nuclear Installations,* **Vol. 2018**:5706409 (2018).

[91] Comisión Nacional de Energía Atómica, Proyecto CAREM, Proc. Revista de la CNEA, (number 67-68), (2017).
[92] Boselli, A., et al., CAREM25. Proyecto CAREM, Proc. Comisión Nacional de Energía Atómica, (2018).
[93] IAEA, Advances in Small Modular Reactor Technology Developments. 2020 Edition, 20-02510E (2020).
[94] Markiewicz, M., Fuel Element Design for the CAREM-25 reactor, Proc. Symposium Small Modular Reactors for Nuclear Power (2014).
[95] Aramayo, C.F., Analisis de transitorios de pérdida de refrigerante en reactores integrados para el soporte de un sistema de inyección, Master's thesis, Centro Atómico Bariloche. Instituto Balseiro. Comisión Nacional de Energía Atómica. Universidad Nacional de Cuyo (2018).
[96] Freixa, J. et al., Revisiting ISP-13 with RELAP/SCDAPSIM/MOD3.5 using core SCDAP components. NURETH16-13462 (2015).
[97] Madokoro, H. et al., Assessment of RELAP/SCDAPSIM/MOD3.5 against the BWR core degradation experiment CORA-17, NUTHOS10-2846 (2014).
[98] Allison, C.M. et al., QUENCH-06 experiment post-test calculations and Integrated Uncertainty Analysis with RELAP/SCDAPSIM/MOD3.4 and MOD3.5, ICONE26-81912 (2018).
[99] T. M. Howe, C. M. Allison, G. P. Marino, "Initial SCDAP Predictions of the TMI-2 Event," 10th Water Reactor Safety Research Meeting, Gaithersburg (October 1982).
[100] E.W. Coryell (prepared by), "Summary of Important Results and SCDAP/RELAP5 Analysis for OECD LOFT Experiment LP-FP-2", NUREG/CR-6160 (April 1994).
[101] D. C. Mecham, prepared by EPRI, OECD LOFT Test LP-FP-2, Code Comparison Report, vol. I: Thermal-Hydraulic Comparisons, OECD LOFT-T-3811 (February 1990).
[102] P. von der Hardt et al. "Nuclear Safety Research: The PHEBUS FP Severe Accident Experimental Programme", Nuclear Safety, 35 (2) (1994).
[103] Salem, C. Allison, J. Hohorst, T. Le Bao, "Integrated Uncertainty Analysis of the PHEBUS FPT-0 Experiments using RELAP/SCDAPSIM/MOD3.4 with IUA Option", Proceedings of ERMSAR 2019, March 18-20, Prague, Czech Republic (2019).
[104] J. K. Hohorst, C. M. Allison, "An Assessment of RELAP/SCDAPSIM/MOD3.4 Using the Phebus FPT-2 Bundle Heating and Melting Experiment", Proceedings of the ICAPP-05, Seoul, Korea (May 2005).
[105] D. Knipe, S. A. Ploger, and D. J. Osetek, PBF Severe Fuel Damage Scoping Test - Test Results Report, NUREG/CR-4683, EGG-2413 (August 1986).
[106] D. A. Petti, C. M. Allison, et al., "Results from the Power Burst Facility Severe Fuel Damage Test 1-4", Proceedings of the International ENS/ANS Conference on Thermal Reactor Safety, Avignon, pp. 2313-2324 (October 1988).
[107] P. Hofmann, S. Hagen, L. Sepold, G. Schanz, Knowledge on core degradation phenomena obtained by the CORA program (1986-1993) and resulting remaining uncertainties", Proceedings of Quench Meeting, Karlsruhe (2014).
[108] Standard Problem 31: Summary of UK Blind Calculations of the CORA – 13 Melt Progression Experiment using the SCDAP/RELAP5 Code" AEA Reactor Services Report, AEA RS 5225 (January 1992).
[109] Allison, C.M. et al., Role of RELAP/SCDAPSIM in Nuclear Safety, *Science and Technology of Nuclear Installations*, **2010**: ID 425658 (2010).

[110] Gerova, G. et al., Quench Analysis Using RELAP/SCDAPSIM/MOD3.5, Bulgarian Nuclear Society (BNS) TRANSACTIONS **22**(1), 3-12 (2017).

[111] Hohorst, J. et al., Re-assessment of RELAPSCDAPSIMMOD3x using Historical Integral Experiments, Proceedings of the TopSafe 2017, February 12 – 16, Vienna, Austria (2017).

[112] Pericas, R., Allison C.M, Hohorst, J.K., RELAP/SCDAPSIM Fukushima related activities. The 17th International Topical Meeting on Nuclear Reactor Thermal hydraulics, NURETH-17, September (2017).

[113] Fernandez-Moguel, L., et al., Analysis of QUENCH-10 and -16 air ingress experiments with SCDAPSim3.5. http://dx.doi.org/10.1016/j.anucene.2012.08.030. *Annals of Nuclear Energy*. **53**, 202-212 (2013).

[114] Setiawan, M.B., et al., Evaluation of radionuclide inventory in the CAREM-25 small modular reactor, AIP Conference Proceedings, 2180 (1), pp. 020009 (2019).

[115] IAEA, Best Estimate Safety Analysis for Nuclear Power Plants: Uncertainty Evaluation, IAEA Safety Reports Series No.52 (2008).

[116] Glaeser, H., et al., GRS Method for Uncertainty and Sensitivity Evaluation of Code Results and Applications, *Science and Technology of Nuclear Installations*, **2008**: ID798901 (2008).

[117] OECD/NEA/CSNI, BEMUSE Phase VI report Status report on the area, classification of the methods, conclusions and recommendations, NEA/CSNI/R(2011)4 (2011).

[118] Freixa, J., et al., Testing methodologies for quantifying physical models uncertainties. A comparative exercise using CIRCE and IPREM (PREMIUM), *Nuclear Engineering and design*, **305**, 653-665 (2016).

[119] Wickett, T. et al., Uncertainty Methods Study for advanced Best Estimate thermal hydraulic code applications, Technical Report NEA/CSNI/R(97)35, Vol.2 (1988).

[120] https://www.nrc.gov/reactors/operating/ops-experience/baffle-former-bolts.html

[121] IAEA, Progress in Methodologies for the Assessment of Passive Safety System Reliability in Advanced Reactors. Results from Coordinated Research Project, IAEA-TECDOC-1752, IAEA, Vienna (2014).

[122] Hoffer, N.V., et al., Modeling a Helical-coil SteamGenerator in RELAP5-3D for the Next Generation Nuclear Plant, INL/EXT-10-19621 (2011).

LIST OF ABBREVIATIONS

APR1400	Advanced Power Reactor 1400 MWe
ATHLET	Analysis of THermal-hydraulics of LEak and Transients
BEPU	Best Estimate Plus Uncertainty
CAREM	Central Argentina de Elementos Modulares (Argentine Modular Power Plant)
CDF	Core Damage Frequency (or Cumulative Distribution Function)
CNEA	National Atomic Energy Commission
CRP	Coordinated Research Project
CsI	Cesium Iodide
DAKOTA	Design Analysis Kit for Optimization and Terascale Applications
DBA	Design Basis Accident
DNPER	Directorate of Nuclear Power Engineering-Reactor
ECCS	Emergency Core Cooling System
ENRRA	Egypt Nuclear and Radiological Regulatory Authority
ENSO	Energy Software
EWI	Emergency/External Water Injection
FOM	Figure Of Merit
IAEA	International Atomic Energy Agency
iPWR	integral Pressurized Water Reactor
IUA	Integrated Uncertainty Analysis
KAERI	Korea Atomic Energy Research Institute
KINS	Korea Institute of Nuclear Safety
LBLOCA	Large Break Loss of Coolant Accident
LHS	Latin Hypercube Sampling
LOCA	Loss of Coolant Accident
LRA	Low Rank Approximation
LWR	Light Water Reactor
MAAP	Modular Accident Analysis Program
MCCI	Molten Corium-Concrete Interaction
MELCOR	Methods of Estimation of Leakages and Consequences of Releases
NPP	Nuclear Power Plant
OPR1000	Optimized Power Reactor 1000 MWe
PAEC	Pakistan Atomic Energy Commission
PCC	Partial Correlation Coefficient
PDF	Probability Density Function
PRCC	Partial Rank Correlation Coefficient

PSA	Probabilistic Safety Assessment (or Parameter Space Analysis)
PSV	Pressurizer Safety Valve
PWR	Pressurized Water Reactor
RCP	Reactor Coolant Pump
RCS	Reactor Coolant System
RELAP	Reactor Excursion and Leak Analysis Program
RPV	Reactor Pressure Vessel
SAG	Severe Accident Guideline
SAM	Severe Accident Management/Mitigation
SAMG	Severe Accident Management Guideline
SBO	Station Black Out
SCALE	Comprehensive Modeling and Simulation Suite for Nuclear Safety Analysis Design
SCDAP	Severe Core Damage Analysis Package
SCDAPSIM	Severe Core Damage Analysis Package SIMulator
SCRAM	Safety Control Rod Axe Man
SDS	Safety Depressurization System
SJTU	Shanghai Jiao Tong University
SMR	Small Modular Reactor
SNAP	Symbolic Nuclear Analysis Package
SOARCA	State of Art Reactor Consequence Analysis
SRRC	Standardized Rank Correlation Coefficient
SRS	Simple Random Sampling
STSBO	Short-term Station Black Out
SVD	Singular Value Decomposition
UAE	United Arab Emirate

CONTRIBUTORS TO DRAFTING AND REVIEW

Ahn, Kwang-Il	KAERI (Republic of Korea)
Ali, Shaukat	DNPER/PAEC (Pakistan)
Borai, Basma F.	ENRRA (Egypt)
Cao, Xuewu	SJTU (China)
Cho, Yong-Jin	KINS (Republic of Korea)
Gabrielli, Fabrizio	KIT (Germany)
Garcia, Juan Matias	CNEA (Argentina)
Jevremovic, Tatjana	International Atomic Energy Agency
Khuwaileh, Bassam	University of Sharjah (UAE)
Ilrado, Pablo Hernan	CNEA (Argentina)
Luxat, David	SNL (USA)
Mascari, Fulvio	ENEA (Italy)
Pericas, Raimon	ENSO (Spain)
Rehman, ur Haseeb	International Atomic Energy Agency

Research Coordination Meetings (RCMs)

1st RCM, EVT1803724, IAEA Headquarters, Vienna, Austria, 14–17 October, 2019.

2nd RCM, EVT1903891, IAEA Headquarters, Vienna, Austria, 20–22 October, 2020.

3rd RCM, EVT2004045, IAEA Headquarters, Vienna, Austria, 8–10 November, 2021.

4th RCM, EVT2103131, IAEA Headquarters, Vienna, Austria, 7–10 November, 2022.

IAEA
International Atomic Energy Agency

No. 26

ORDERING LOCALLY

IAEA priced publications may be purchased from the sources listed below or from major local booksellers.

Orders for unpriced publications should be made directly to the IAEA. The contact details are given at the end of this list.

NORTH AMERICA

Bernan / Rowman & Littlefield

15250 NBN Way, Blue Ridge Summit, PA 17214, USA
Telephone: +1 800 462 6420 • Fax: +1 800 338 4550
Email: orders@rowman.com • Web site: www.rowman.com/bernan

REST OF WORLD

Please contact your preferred local supplier, or our lead distributor:

Eurospan Group

Gray's Inn House
127 Clerkenwell Road
London EC1R 5DB
United Kingdom

Trade orders and enquiries:

Telephone: +44 (0)176 760 4972 • Fax: +44 (0)176 760 1640
Email: eurospan@turpin-distribution.com

Individual orders:

www.eurospanbookstore.com/iaea

For further information:

Telephone: +44 (0)207 240 0856 • Fax: +44 (0)207 379 0609
Email: info@eurospangroup.com • Web site: www.eurospangroup.com

Orders for both priced and unpriced publications may be addressed directly to:

Marketing and Sales Unit
International Atomic Energy Agency
Vienna International Centre, PO Box 100, 1400 Vienna, Austria
Telephone: +43 1 2600 22529 or 22530 • Fax: +43 1 26007 22529
Email: sales.publications@iaea.org • Web site: www.iaea.org/publications

23-05301E

International Atomic Energy Agency
Vienna